

***An integrated study of Quaternary  
sedimentary processes on the eastern slope  
of the Porcupine Seabight, SW of Ireland***

*Een geïntegreerde studie van Kwartaire sedimentaire processen  
langs de oostelijke helling van de Porcupine Seabight,  
ten zuidwesten van Ierland*

***David Van Rooij***

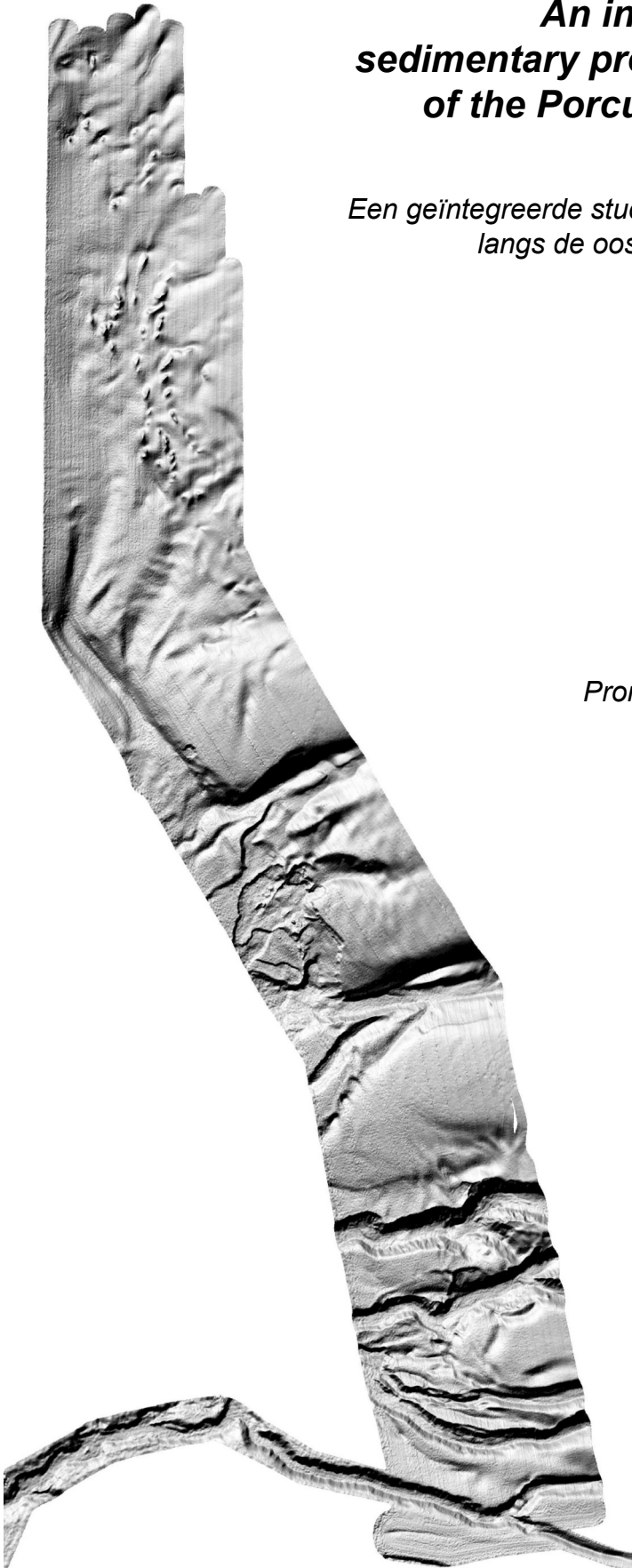
*Promotor: Prof. Dr. Jean-Pierre Henriët*



***Faculteit Wetenschappen***  
*Vakgroep Geologie en Bodemkunde*  
*Renard Centre of Marine Geology*

*Proefschrift voorgelegd tot het behalen  
van de graad van Doctor in de  
Wetenschappen, Geologie*

*Academiejaar 2003-2004*



***An integrated study of Quaternary  
sedimentary processes on the eastern slope  
of the Porcupine Seabight, SW of Ireland***

*Een geïntegreerde studie van Kwartaire sedimentaire processen  
langs de oostelijke helling van de Porcupine Seabight,  
ten zuidwesten van Ierland*

***David Van Rooij***

*Promotor: Prof. Dr. Jean-Pierre Henriët*



***Faculteit Wetenschappen***  
*Vakgroep Geologie en Bodemkunde*  
*Renard Centre of Marine Geology*

*Proefschrift voorgelegd tot het behalen  
van de graad van Doctor in de  
Wetenschappen, Geologie*

*Academiejaar 2003-2004*

## **Copyright**

The author and the promoter give the authorization to consult and copy parts of this dissertation for personal use only. Any other use is limited by the laws of Copyright, particularly concerning the obligation to mention the source when reproducing parts of this dissertation.

De auteur en de promotor geven de toelating dit doctoraatswerk voor consultatie beschikbaar te stellen en delen ervan te kopiëren voor persoonlijk gebruik. Elk ander gebruik valt onder de beperkingen van het auteursrecht, in het bijzonder met betrekking tot de verplichting uitdrukkelijk de bron te vermelden bij het aanhalen van de resultaten uit deze scriptie.

Gent, April 2004

The author  
David Van Rooij

The supervisor  
Prof. Dr. Jean-Pierre Henriët

## Acknowledgements

Starting a PhD is a task that should not be taken lightly. In many ways, this 4 years adventure can be compared with a now very well known epic story written by J.R.R. Tolkien. In “The Lord of the Rings”, a certain Frodo takes on the challenge in fulfilling a large project, knowing he will face many ordeals... which he will overcome through personal strength, helped by the supervision of Gandalf and by a large fellowship of local and foreign “specialists”... From October 1999 to this very moment, I was able to rely upon such a similar fellowship, without which this manuscript wouldn’t be half of what it is now. Therefore, I would like to express my gratitude to the following fine people;

And as in all great stories, everything starts with a wise man... who has sent me on adventures before, such as facing the dangers of the untameable ocean on a rusty foreign ship and revealing the mysteries of mountain rivers (and testing the stability of my shoulder joint). After a period of re-sourcing in Bretagne, he offered me the possibility of undertaking a fellowship to study contourites and other sediment properties. Within that period, I could always rely upon my personal “Gandalf”, to give me good advice in dark times, to let me independently do my own research, to help in into contact with other specialists and with sometimes a little “magic”. Jean-Pierre, I would like to thank you for these 4 wonderful years and for all the beautiful opportunities you offered me. Without any doubt, this wouldn’t have been possible without the financial support of the IWT Flanders, which I would like to thank for having confidence in me.

During this fellowship, I could always rely upon the staff, personnel and students who stayed or still are at the RCMG. However, there are a few persons for whom I developed a special kind of appreciation. From the early beginning, Maarten Vanneste taught me lots of tips and tricks and still is a permanent source for scientific and personal advice. Second of all, I would like to honour Willem “Wimpie” Versteeg for his continuous geophysical support, which was indispensable during the many campaigns. I will also very much miss our frequent discussions about science and life. Another very special person is Marc(ske) Faure Didelle, the “RCMG sunshine”, for helping me through all administrative trouble, for being there (except when telephoning) for all kinds of discussion, mainly about “life science”. Finally, without the help of the past and present RCMG “Advanced Technical Personnel”, there wouldn’t have been a single seismic trace... but they were also important for the solving of any kind of logistic problems and the sometimes very weird (Gamma?) kind of humour that cheered us up. More specifically, I would like to thank the omnipresent Koen “Keun” De Rycker, Peter “Omer” Vandamme and Jeroen Vercruysse.

I also appreciated the fine cooperation with Veerle Huvenne, who started at the same time revealing the secrets of the Porcupine Seabight. I enjoyed very much the discussions we had during those 4 years, and her straight-on (engineers) approach. And from Veerle it is no big step to her soulmate Anneleen (I will never forget the amount of laughter they both produced...). Anneleen, I know you suffered a lot with me and my “cruel jokes”... from the start of your MSc thesis, on board of the several boats and then again during the first years of your PhD.

A special word of thanks goes out to something that dwelled together with me in my office(s) during these 4 years... for the (pseudo-)scientific discussions, the silly jokes, the Yorki and Cantus sessions, the sing-along sessions and even, for being a team-mate in sport... Thanks Rob!

I would also like to thank Marc "Tist" De Batist for his good advice, passing through interesting papers, scientific discussions...

Furthermore, from 1997 to now, I have witnessed the RCMG grow to a full-sized research centre with lots of people coming and going: Maarten, Pieterke, Stephanie, Tom, Yannickske, Ben, Els, Vera, Geert(jeeeh), Samuel, Franske, Wim, Jeroen, Tine, Davy, Pol De Reiger, Lieven, Mieke, Sylvia, Abdelito, George, Pieter, Jeffrey, Irina, Babs, Catherine... and all the other ones I forgot... they did not only contributed to enjoyable (scientific) discussions, but were always prepared for a chat, practical jokes... And of course, I would like to pay a special tribute to the members of the "Delhaize-raid gang".

Since the realisation of this study was largely dependant of the results of some large campaigns, I would also like to thank the efforts of the captains and crews of all the expeditions on board of R/V Belgica and R/V Marion Dufresne.

For a lot of things, I was very happy that I could count on the professional help of a lot of people from outside the RCMG. First of all, I would like to thank everybody from the paleontology department for the support they gave when I came around to play with my mud and sand samples to look at the forams: Stephen Louwey, Jacques Verniers, Sabine Van Cauwenberghe and Nelly Reynaert. Likewise, I appreciated very much the possibility to use the facilities of the Marine Biology section for the grainsize analyses, for which I would like to thank Magda Vinckx, Ann Van Reusel, Dirk Van Gansebeke and Danielle Schram.

Outside Ghent University, I would like to thank Dominique Blamart from the LSCE in Gif-sur-Yvette (France) for introducing me into the work on the MD99-2327 core, and for being a fine colleague, advisor and friend for this period. Heloise Leclaire (LSCE, France), Barbara Donner (RCOM Bremen) and Mike Kaminski (UCL London) introduced me into the world of foraminiferal analyses. A large part of the work on MD99-2327 was performed in cooperation with the UCC Cork by Andrew Wheeler and Max Kozachenko. I also would like to thank Thomas Richter for helping me deciphering the paleoceanographic signals in this core, and for the fruitful discussions. A special word of gratitude goes out to the people from Université Bordeaux I, for the SCOPIX analyses and the professional help on board of R/V Marion Dufresne: Jean-Louis Turon, Sébastien Zaragosi, Michel Cremer, Joël Saint-Paul and Olivier Weber. Finally, I have been in touch with lots of excellent people who helped me around and gave me good advices: Peter Croker, Vik Unnithan, Pat Shannon, Nick McCave, Jean-Claude Faugères, Henk de Haas, Tjeerd Van Weering, Laurent Labeyrie, Jean-Claude Duplessy, Gérard Auffret, Bernard Dennielou, Neil Kenyon, Joachim Schönfeld, Martin Stoker and many others.

On the other hand, it has to be acknowledged that not only scientific support was needed to survive this deep-sea exploration journey. Fortunately, there were lots of fine people to accompany me for sports, the weekly quiz, movies, parties or for a good talk. I especially would like to thank Wendy for introducing me into the badminton-world again and for being such a good friend. Furthermore, I would like to thank the very good company of Maarten, Peter, Tom, Saskia, Gert, Sofie,

Annelies, Ivan, Jo, Bernard, Dirk, Cornui, Wouter, Herr Geerinckx, Yoeri, Wim DW, Peter, Andy, Beuwb Imke, Patricia, Elisabeth and certainly Stef & Karin.

A special, unusual word of appreciation goes out to the fine craftsmen responsible for the brewery of the delicious Trappist beers and distillery of the high-quality whiskeys that accompanied me in the late hours of the redaction of this work...

But all of this would mean nothing without the continuous support and friendship of Tom, Truus, Gunther, Marieke, Vincent and Katrien. Also Philippe, Jan and Mark certainly belong here for keeping in touch!

A very big “thank you” goes out to Pascale and Lode, certainly for their support during these last few months, to keep me running (literally and figuratively) and the delicious veggie-food.

I am forever indebted to my two wonderful parents... You haven’t seen me a lot these last months, but I’ll never forget all the large efforts you made to help me through this and for keeping encouraging me.

Last, and certainly not the least... Noukie, you gave me the spirit finishing this PhD. Since the time we have met, you have become an essential part of my life, which I wouldn’t trade for the anything in the world...

In order to finish with a final Lord of the Rings quote: “Well, here at last, dear friends, on the shores of the Sea comes the end of our fellowship in Middle Earth”

Thank you, good night!

David  
April 2004

## Abstract

A wide range of geophysical and sedimentological investigations on upper slope sediments of the eastern Porcupine Seabight, SW of Ireland, allowed to evaluate the local importance of bottom currents throughout the Upper Paleogene to recent times, as well as the influence of, and interplay with other deep-water sedimentary processes.

The tools available for this study mainly allowed to focus on the nature and characteristics of the Quaternary deposits of seismic unit U1, but also documented buried Middle Eocene to Pliocene sediment drifts and sediment waves. A Late Pliocene erosional event (RD1) created a highly irregular discontinuity, observed from the northern part of the Belgica mound province towards the southern Gollum channel and Goban Spur. During this event, the basis of all major channels was created. They remained to be major current pathways, although their seismic characteristics suggest that the vigour of these currents seems to have decreased. The local Quaternary sedimentary environment has been dominated by a dynamic bottom current environment and by the paleotopography of the underlying unit U2. In the Belgica mound province, this unique geographic and hydrodynamic setting was responsible for the deposition of several sediment and contourite drifts. South of the Belgica mounds, the evolution and construction of the flanks of the broad Kings channels is seen to be influenced by downslope flowing currents. It is thought to be affected by periodic turbidite currents, possibly already weakened by northward flowing bottom currents. The main Gollum channel system shows similarities with a submarine fan channel system. The channel deposits are predominantly turbidites and mass-wasting deposits. This study also strengthens the idea that this system is located directly downstream of a (still undiscovered) feeding glacial fluvial system located on the Irish mainland shelf.

A SE to NW transect of five long cores demonstrates the variability and distribution of British-Irish Ice Sheet (BIIS) sourced IRD in the Porcupine Seabight. Two cores located on the eastern slope almost exclusively contain BIIS-sourced material. Six ice-rafting events (IRE) were described and can be compared with the North Atlantic Heinrich Events. These regional events carry a very strong BIIS signature with mainly sands originating from Devonian and Carboniferous sandstones. The abundance of the IRD record shows a millennial-scaled disintegration of the BIIS from 25 ka onwards with distinct ice-rafting pulses about 17.4 and 15 ka BP. Moreover, all cores from the Belgica mound province show that the glacial deposits are muddy contourites in which several peak current episodes could be distinguished. More specifically, a core located on the small mounded contourite drift contains an amplified record of this bottom current variability. The presence of a massive sandy contourite between 1500 and 2625 cm suggests that during interglacial times the bottom current regime is similar as the present day situation. A similar conclusion was drawn from a core within one of the Gollum channel heads. During glacial times (especially during the last glacial maximum), turbidity currents were active due to a lowered sea-level. These fine-grained turbidites were deposited in a hemipelagic background sediment with IRD. During interglacial times, reversing bottom currents were active in this channel, creating muddy-silty contourites or even reworking the glacial turbidite deposits.

## Samenvatting

Een multidisciplinair geofysisch en sedimentologisch onderzoek van sedimenten gelegen langs de bovenste helling van de oostelijke Porcupine Seabight, ten zuidwesten van Ierland, stond toe om het lokale belang van bodemstromingen sinds het Boven Paleogeen, evenals de invloed van en het samenspel met andere diepwater sedimentaire processen, te evalueren.

De middelen beschikbaar voor deze studie stonden hoofdzakelijk toe om het onderzoek toe te spitsen op de aard en de eigenschappen van de Kwartaire afzettingen van de seismische eenheid U1, maar illustreerden ook de aanwezigheid van Midden Eoceen tot Pliocene sedimentdriften en sedimentgolven. Een Laat Pliocene erosieve gebeurtenis was verantwoordelijk voor de vorming van een onregelmatige discontinuïteit, waarneembaar van het noordelijkste gedeelte van de Belgica mound provincie naar de zuidelijke Gollum Kanalen en Goban Spur. Deze erosie zorgde voor het insnijden van de basis van alle belangrijke kanalen, dewelke belangrijke paden van stromingen bleven, hoewel hun seismische karakteristieken suggereren dat de intensiteit van deze stromingen zou zijn afgenomen. De lokale Kwartaire sedimentaire omgeving werd sterk beïnvloed door dynamische bodemstromingen en door de paleotopografie van de onderliggende eenheid U2. In de Belgica mound provincie droeg deze unieke setting toe tot het afzetten van verschillende sediment- en contourietdriften. Ten zuiden van de Belgica mounds werd de evolutie en opbouw van de brede Kings kanalen dan weer hoofdzakelijk beïnvloed te zijn door hellingafwaartse stromingen. Deze waarschijnlijk periodische turbidietstromingen, werden waarschijnlijk al afgezwakt door noordwaarts vloeiende bodemstromingen. Het belangrijke Gollum Kanalen systeem vertoont gelijkenissen met submariene fan kanalen systemen. De afzettingen in deze kanalen zijn hoofdzakelijk turbidieten en afglijdingen.

Een zuidoost-noordwest doorsnede aan de hand van vijf lange kernen illustreert de variabiliteit en de verdeling van *ice-rafted* zand (IRD) afkomstig van de Brits-Ierse ijskap (BIIS) in het studiegebied. Twee kernen langs de oostelijke helling vertonen bijna uitsluitend BIIS materiaal. Er werden zes *ice-rafting* gebeurtenissen (IRE) beschreven die vergeleken kunnen worden met de Noord Atlantische Heinrich Events. Deze regionale gebeurtenissen dragen een zeer sterk BIIS kenmerk met hoofdzakelijk zanden afkomstig van Devoon en Carboon zandstenen. De variaties in het IRD gehalte tonen een millenium-schalige desintegratie van de BIIS vanaf 25 ka met uitgesproken pulsen rond 17.4 en 15 ka BP. Daarenboven bevatten alle kernen van de Belgica mound provincie modderige contourieten, afgezet tijdens glacialen, in dewelke enkele episodes kunnen herkennen van sterkere stromingen. Meer specifiek bevat een kern in een kleine contouriet drift een versterkt signaal van de variabiliteit van deze bodemstromingen. De aanwezigheid van een zandige contouriet tussen 1500 en 2625 cm suggereert dat tijdens interglacialen het bodemstromingsregime gelijkaardig is aan de hedendaagse situatie. Een gelijkaardige conclusie werd getrokken uit een kern van de Gollum kanalen. Tijdens ijstijden (meer bepaald tijdens het Laatste Glaciaal Maximum), waren er hoofdzakelijk turbidietstromingen actief door een verlaagde zeespiegel. Deze fijnkorrelige turbidieten werden afgezet in een hemipelagische achtergrond met IRD. Tijdens interglacialen waren omkerende bodemstromingen actief, verantwoordelijk voor de afzetting van modderige-siltige contourieten of zelfs herwerking van de glaciale turbidietafzettingen.



## **Table of contents**

<b>1. Introduction</b> .....	1
1.1 Scientific rationale .....	1
1.2 Research strategy .....	4
1.3 Project framework .....	6
1.4 Definition of morphologic features .....	7
1.4.1 Belgica mound area .....	8
1.4.2 Kings channels area .....	11
1.4.3 Gollum channel area .....	12
<b>2. Geological and environmental setting</b> .....	17
2.1 Geological setting .....	17
2.1.1 Basin development .....	17
2.1.1.1 Economic basement and pre-rift sedimentation .....	17
2.1.1.2 Permo-Triassic early rifting phase .....	19
2.1.1.3 Lower Jurassic quiet period .....	19
2.1.1.4 Middle and Upper Jurassic crustal extension .....	19
2.1.1.5 Post-rift structure of the Porcupine basin .....	22
2.1.2 Post-rift thermal subsidence .....	23
2.1.2.1 Cretaceous transition .....	24
2.1.2.2 Paleocene-Eocene deltaic sedimentation .....	25
2.1.2.3 Oligocene-Neogene deep-marine environment .....	26
2.1.2.4 Introduction to the Quaternary sedimentary environment .....	27
2.1.3 Hydrocarbon exploration .....	28
2.1.3.1 Exploration history .....	28
2.1.3.2 Source rocks and reservoirs .....	28
2.1.3.3 Exploration potential .....	29
2.2 Hydrographic setting .....	30
2.2.1 Water masses and properties .....	30
2.2.2 Current circulation .....	30
2.2.3 Current enhancement .....	32
2.2.4 Bottom current observations .....	33
2.3 Cold-water coral banks along the NW European margin .....	37
2.3.1 Ecology of cold -water corals .....	37
2.3.2 Coral banks along the Irish margin .....	38
2.3.2.1 The Belgica mounds .....	38
2.3.2.2 The Hovland mounds .....	40
2.3.2.3 The Magellan mounds .....	41
2.3.2.4 The Pelagia mounds .....	43
2.3.2.5 The Logachev mounds .....	45
2.3.2.6 The Darwin mounds .....	46
2.3.2.7 Other reported mound and cold-water coral occurrences .....	46
2.3.3 Clues toward genesis and development .....	47
2.3.3.1 Environmental and ecologic control .....	47
2.3.3.2 “Internal” geological control and the influence of seepage .....	48

<b>3. Material and methodology</b> .....	57
3.1 Geophysical data .....	57
3.1.1 2D seismic data .....	57
3.1.2 Bathymetric data .....	60
3.1.3 Side-scan sonar data.....	60
3.2 Sedimentological data.....	63
3.2.1 Overview of available core data .....	63
3.2.2 Multi-sensor core logger data.....	65
3.2.3 Visual sediment properties .....	67
3.2.4 CORTEX XRF.....	67
3.2.5 SCOPIX radiography .....	68
3.2.6 Sediment properties .....	68
3.2.6.1 Physical properties .....	69
3.2.6.2 Coarse sand fraction $F_{150}$ .....	69
3.2.6.3 Biostratigraphy and isotopic analysis .....	69
3.2.6.4 Sedimentation and accumulation rates .....	71
3.2.6.5 Thin sections .....	72
3.2.7 Grainsize analysis .....	72
3.2.7.1 Coulter LS230 .....	73
3.2.7.2 Malvern MasterSizer 2000.....	73
3.2.7.3 Coulter LS130 .....	73
<b>4. The offshore record of BLS variability</b> .....	79
4.1 Current state-of-the-art of Heinrich events .....	79
4.1.1 An introduction to Heinrich Events <i>sensu strictu</i> .....	80
4.1.2 Provenance of HE.....	82
4.1.3 HE along the NW European margin .....	85
4.2 The IRD record in the Belgica mound province .....	87
4.2.1 Ice-rafting events in MD99-2327.....	91
4.2.1.1 IRE1.....	91
4.2.1.2 IRE2.....	91
4.2.1.3 IRE3.....	91
4.2.1.4 IRE4.....	94
4.2.1.5 IRE5.....	94
4.2.1.6 IRE6.....	94
4.2.2 IRE characteristics versus HL characteristics.....	94
4.2.2.1 Magnetic susceptibility .....	97
4.2.2.2 Ice-Rafted Debris .....	97
4.2.2.3 Calcium values and color .....	99
4.2.2.4 Foraminifers and $\delta^{18}\text{O}$ stable isotopes .....	101
4.2.2.5 Density.....	101
4.3 A SE to NW transect in PSB .....	101
4.3.1 Kings channels (MD01-2449).....	101
4.3.1.1 IRE1 (315-410 cm).....	103
4.3.1.2 IRE2 (662-911 cm).....	103

4.3.1.3 IRE3 (1115-1185 cm).....	104
4.3.1.4 IRE4 (1245-1645 cm).....	104
4.3.1.5 IRE5 (1787-1977 cm).....	104
4.3.2 Magellan mound province (MD01-2452).....	108
4.3.2.1 Core description and time frame .....	108
4.3.2.2 Last glacial ice-rafting events .....	108
4.3.3 Connemara (MD01-2453 & MD01-2457).....	109
4.3.3.1 Core description and time frame .....	111
4.3.3.2 Last glacial ice-rafting events .....	111
4.3.4 Sedimentation rates in PSB .....	111
4.4 Discussion .....	112
4.4.1 Patterns of IRD distribution in PSB .....	112
4.4.2 Implications for BIIS variability .....	113
4.5 Summary .....	116
<b>5. A stratigraphic framework for the eastern Porcupine Seabight .....</b>	<b>123</b>
5.1 Rationale.....	123
5.2 Brief geological overview of Goban Spur .....	125
5.3 DSDP leg 80 .....	128
5.3.1 Site 548 .....	128
5.3.1.1 Unit 1.....	128
5.3.1.2 Unit 2.....	129
5.3.1.3 Unit 3.....	129
5.3.1.4 Unit 4.....	130
5.3.1.5 Unit 5.....	130
5.3.1.6 Units 6, 7 and 8 .....	130
5.3.2 Site 549 .....	131
5.3.3 Sites 550 and 551 .....	131
5.4 Seismic stratigraphic control of DSDP site 548.....	132
5.4.1 The sea floor .....	132
5.4.2 Unit G1.....	132
5.4.3 Unit G2.....	134
5.4.4 Unit G3.....	137
5.4.5 Units G4 and G5.....	137
5.5 A Cenozoic stratigraphic framework .....	138
5.5.1 RD5: Lower Paleocene .....	138
5.5.2 RD4: Middle Eocene .....	138
5.5.3 RD3: early Late Oligocene.....	140
5.5.4 RD2: early Middle Miocene .....	140
5.5.5 Quaternary events.....	141
5.5.5.1 RD1: Late Pliocene .....	141
5.5.5.2 The Middle Pleistocene Revolution.....	143
5.6 Summary .....	144

<b>6. Seismic stratigraphy of the Belgica mound province &amp; Quaternary sedimentary processes</b> .....	149
6.1 Some morphological aspects .....	149
6.2 Units U4 and U3; markers of sediment drift development .....	159
6.2.1 Unit U4.....	159
6.2.1.1 Seismic characteristics and distribution.....	166
6.2.1.2 A Late Paleogene sediment drift initiation .....	166
6.2.2 Unit U3.....	167
6.2.2.1 Seismic characteristics and distribution.....	167
6.2.2.2 RD2 discontinuity.....	181
6.2.2.3 Early Neogene sediment wave fields .....	181
6.3 Unit U2 and the Belgica mounds.....	183
6.3.1 Seismic characteristics and distribution .....	183
6.3.2 RD1 discontinuity .....	191
6.3.3 Belgica mounds .....	191
6.3.4 Influence of the Late Pliocene environment on mound growth.....	195
6.4 Quaternary sedimentary processes .....	196
6.4.1 General features, facies and distribution.....	196
6.4.2 Alongslope channels.....	200
6.4.2.1 Arwen channel.....	200
6.4.2.2 Celeborn-Galadriel channels .....	201
6.4.2.3 Discussion .....	212
6.4.3 Depositional features around mounds .....	212
6.4.3.1 Geophysical evidence .....	212
6.4.3.2 Core evidence .....	215
6.4.3.3 Discussion .....	220
6.4.4 Small mounded drifts.....	221
6.4.4.1 Seismic and morphologic features .....	223
6.4.4.2 Sedimentary characteristics .....	226
6.4.4.3 Late Quaternary variability of the hydrodynamic environment .....	229
6.4.4.4 A special case: the Enya mound drift .....	234
6.4.4.5 Consequences for the regional sedimentary history .....	240
6.5 Summary .....	243
<b>7. Structure and development of the Gollum channel system</b> .....	253
7.1 The Kings channels .....	255
7.1.1 Aragorn channel .....	256
7.1.2 Theoden channel.....	257
7.1.3 Boromir channel and Denethor area .....	258
7.1.4 Clues for the development of KCS.....	259
7.2 The Gollum channels.....	270
7.2.1 The Bilbo channel .....	270
7.2.2 The Frodo channel .....	273
7.2.3 Secondary channels in between the Bilbo and Frodo channels .....	287
7.2.4 Clues for the recent sedimentary history; core MD01-2464 .....	287
7.2.4.1 Fine-grained turbidites .....	290
7.2.4.2 Contourites .....	290

7.2.4.3 Hemipelagites with IRD.....	293
7.2.4.4 Last glacial sedimentary processes in the Bilbo channel .....	294
7.2.5 Sedimentary processes of the Gollum channels.....	294
7.3 Summary .....	295
<b>8. Summary and conclusion.....</b>	<b>299</b>
8.1 Main results .....	299
8.1.1 Geophysical characterization of Neogene-Quaternary deposits.....	299
8.1.2 A study of paleoclimatic and paleoceanographic changes .....	300
8.1.3 A sedimentological study of recent and interglacial deposits .....	301
8.2 Conclusion .....	302
8.3 Future perspectives .....	303
8.3.1 Advanced understanding of PSB paleoceanography.....	303
8.3.2 Fine-tuning of the Cenozoic margin stratigraphy.....	304
8.3.3 Quaternary sedimentary processes .....	304
8.3.4 On the origin of the coral banks .....	305
<b>Uitgebreide Nederlandse samenvatting .....</b>	<b>307</b>



## List of figures

### Chapter 1: Introduction

1.1	General overview map of the north Atlantic margin off Irish western Ireland.	3
1.2	Combined GEBCO bathymetric map with shaded relief multibeam bathymetry (Beyer et al., 2003) inset, indicating the newly named morphologic features within the Belgica mound province.	9
1.3	Combined GEBCO bathymetric map with shaded relief multibeam bathymetry (Beyer et al., 2003) inset, indicating the newly named morphologic features within the Kings channel region.	10
1.4	Combined GEBCO bathymetric map with shaded relief multibeam bathymetry (Beyer et al., 2003) inset, indicating the newly named morphologic features within the Gollum channel system.	10

### Chapter 2: Geologic and environmental setting

2.1	Sketch map of the Porcupine Seabight illustrating the main structural elements after Naylor & Shannon (1982), Ziegler (1982), Shannon (1991), Moore & Shannon (1995) and Reston et al. (2001).	18
2.2	Generalized tectonosedimentary maps illustrating the development of the Irish offshore sedimentary basins (Shannon, 1991).	20
2.3	Generalized stratigraphy, tectonic history and relative sea-level changes in the Porcupine Basin after Ziegler (1982), Shannon (1991), Moore & Shannon (1992), Moore & Shannon (1995) and McDonnell & Shannon (2001).	21
2.4	Geological profile showing the plays of the southern Porcupine Basin (Spencer & MacTiernan, 2001)	23
2.5	Overview of known near-bottom current measurements, the predicted occurrence of enhancement due to internal tides and the assumed general circulation after Pingree & Le Cann (1989), Rice et al. (1990) and White (in press).	31
2.6	Compilation of the water stratification along a NE-SW bathymetric transect within the Porcupine Seabight, with indication of the major hydrographic interactions (Hargreaves, 1984; Rice et al., 1990; Rice et al., 1991; White, in press)	32
2.7	ROV images collected on board R/V Polarstern on the AWI Bremerhaven coordinated cruise ARK XIX/3a in June 2003. These images were made available through courtesy of IFREMER.	35
2.8	Main mound provinces along the NW European margin after Huvenne (2003).	38
2.9	Sparker section through a large Belgica mound and the buried foot of an adjacent mound (Henriet et al., 2003).	39
2.10	Trend map of Propeller mound within the Hovland mound province. The blue colours indicate the moats and the depressions (De Mol, 2002).	40
2.11	High-resolution 2D seismic profile across the Magellan mound	42

province (Huvenne et al., 2003).	
2.12 Perspective view of a portion of 30 kHz sonograph draped over a digital terrain model of a large carbonate mound on the northern Porcupine Bank margin (Kenyon et al., 2003).	43
2.13 Airgun seismic profiles across Pelagia coral banks (Akhmetzhanov et al, 2003).	44
2.14 Irregularly shaped clusters of mounds and a single mound at the slope edge within the Logachev mounds (Van Weering et al, 2003b).	45
2.15 Generalized model of mound province development under different evolutionary scenarios (Kenyon et al., 2003).	48

### Chapter 3: Material and methodology

3.1 Overview map of the very high-resolution single-channel reflection seismic profiles acquired by the RCMG during the Porcupine-Belgica campaigns from 1997 to 2003 with R/V Belgica.	59
3.2 Overview of available morphologic data with the GEBCO bathymetry background, the extent of the Polarstern ANTVXII/4 data (2000) and the TOBI 2002 and TTR7 ORETECH side-scan sonar data.	61
3.3 Overview map of available Calypso, gravity and boxcore data.	64
3.4 A typical Geotek multi-sensor core logger split/whole-core configuration as used during the MD114 and MD123 campaigns on board R/V Marion Dufresne (after <a href="http://www.geotek.co.uk">http://www.geotek.co.uk</a> )	66
3.5 Planktonic foraminiferal species assemblages and ranges in the five major faunal provinces (Boersma, 1998).	70

### Chapter 4: The offshore record of BIIS variability

4.1 Reconstruction of the North Atlantic Ocean during the last glaciation with the location of the North Atlantic surface currents and Polar Front between the Last Glacial Maximum and the Early Holocene. Modified after Ruddiman et al. (1977), Bond et al. (1992), Chapman & Maslin (1999), Grousset et al. (2001), Siegert (2001) and Auffret et al. (2002).	80
4.2 Characteristics of the Heinrich Layers, demonstrated by data from core MD95-2002, Meriadzek Terrace, Celtic Margin (Auffret et al., 2002).	82
4.3 Comparison of $\delta^{18}\text{O}$ and percentages of <i>N. pachyderma</i> s. in two ocean sediment cores from the North Atlantic, with the $\delta^{18}\text{O}$ record from the GRIP ice core (Bond et al., 1993).	85
4.4 $^{87}\text{Sr}/^{86}\text{Sr}$ ratios versus $^{143}\text{Nd}/^{144}\text{Nd}$ ratios, expressed as $\varepsilon_{\text{Nd}}(0)$ (Grousset et al., 2001).	84
4.5 Abundances of lithic grains, detrital carbonate, volcanic glass and quartz grains in coarse sediments (> 150 $\mu\text{m}$ ) from core SU90-09 (Grousset et al., 2001).	86
4.6 Location of studied cores in the Porcupine Seabight, with respect to the position of the Irish components of the British-Irish Ice Sheet during the Last Glacial Maximum. Modified after Bowen et al. (2002)	87

	and Holland (2001).	
4.7	Lithological content and chronostratigraphy of core MD99-2327.	98
4.8	Detail of the lithological content and chronostratigraphy of the glacial part of core MD99-2327, with special attention to the occurrence of the IRE.	90
4.9	Grainsize characteristics and coarse fraction of core MD99-2327.	92
4.10	Grainsize distribution curves of several IRE intervals observed in core MD99-2327.	93
4.11	Paleoenvironmental proxies based on the content of planktonic foraminifers in core MD99-2327.	95
4.12	SCOPIX X-ray visualizations of the 6 IRE intervals; (a) IRE1, (b) IRE2, (c) IRE3, (d) IRE4a, (e) IRE4b and 4c, (f) IRE5 and (g) IRE6.	96
4.13	Downcore variation in planktonic foraminiferal faunal composition in core MD99-2327.	98
4.14	Thin section slides of IRD in plain polarized light (left) and with crossed polars (right). (a) Sandstone with badly rounded quartz; (b) Basalt with large, elongate feldspar phenocrysts; (c) Inferred metamorphic rock (granite?) with chlorite and muscovite, cross-cut by quartz veins and (d) angular quartz sandstone.	100
4.15	Detail of lithological characteristics and physical properties of core MD01-2449.	102
4.16	Correlation of core MD01-2449 with MD-992327.	104
4.17	Grainsize distribution curves of several IRE intervals observed in core MD01-2449.	106
4.18	SCOPIX X-ray visualizations of specific intervals observed in core MD01-2449.	107
4.19	Physical properties of core MD01-2452.	109
4.20	Correlation of core MD01-2453 with MD01-2457.	110
4.21	Sedimentation rates of the 5 studied cores in the Porcupine Seabight.	112
4.22	Linear sedimentation rates and total fluxes over the last 100 ka BP within core MD99-2327.	113

## Chapter 5: A stratigraphic framework for the eastern Porcupine Seabight

5.1	Morphologic elements of the Goban Spur margin with the location of the DSDP Leg 80 sites and the RCMG very high-resolution seismic profiles, after de Graciansky & Poag (1984)	124
5.2	Regional tectonic setting of Goban Spur (Dingle & Scrutton, 1979)	125
5.3	Schematic geologic section across Goban Spur showing sites drilled during DSDP Leg 80 (de Graciansky & Poag, 1984)	127
5.4	Geologic interpretation of seismic profile OC202 crossing site 548 (de Graciansky et al., 1985).	129
5.5	Geologic interpretation of seismic profile CM10 where it crosses site 549 (de Graciansky et al., 1985)	130
5.6	Interpretation of NW-SE oriented profile P010501.	133
5.7	Interpretation of NE-SW oriented profile P010502.	134
5.8	Zoom on the clinoforms observed on profile P010502, as well as in DSDP profile OC202.	135
5.9	Detailed location map of the RCMG very high-resolution lines	136

	P010501 and P010502 with indication of the most important seabed features and location of the channels cut formed by the lower boundaries of unit G1 and G2.	
5.10	Correlation of DSDP site 548 with the seismic stratigraphy and overview of the major unconformities, after de Graciansky & Poag (1984), Stoker <i>et al.</i> (2001) and McDonnell & Shannon (2001).	139
5.11	Detail of the Pliocene-Pleistocene time scale (Berggren <i>et al.</i> , 1995)	142

## **Chapter 6: Seismic stratigraphy of the Belgica mound province & Quaternary sedimentary processes**

6.1	General setting of study area, with indication of all used profiles. The profiles in red highlight the locations of the general overview profiles.	150
6.2	P000665: Overview profile on the northern edge of the study area, illustrating the typical seismic facies and discontinuities.	151
6.3	P980521: Overview profile featuring two mounds and sediment drift properties.	152
6.4	P980519: Overview profile, featuring a single mound on an eroded surface above sigmoidal deposits and the onlap of units U3 and U4 on their lower boundaries.	153
6.5	P010521: Overview profile along the eastern upper slope of the Porcupine Seabight, with a surface and buried mound and a heavily eroded unit U2.	154
6.6	Multibeam bathymetry map illustrating the diversity of morphologies in the Belgica mound province.	155
6.7	Interpretation and legend of the TOBI side-scan sonar and AWI bathymetry data sets in the Belgica mound province (Huvenne <i>et al.</i> , submitted).	157
6.8	(a) Side-scan sonar profile, illustrating the diverse seabed features surrounding the Belgica mounds, (b) detail of figure 6.8a with echosounder profile illustrating the lensoid geometry of a sand sheet.	158
6.9	Facies distribution of unit U4, with positions of significant profiles.	159
6.10	P000665a: Detailed profile of the special configuration of units U3 and U4.	160
6.11	P980519a: Detailed profile focussing on the onlap and upslope progradation on the lower boundary of unit U3.	161
6.12	P980525: NNW-SSE profile across a broader part of the Arwen channel.	162
6.13	P000665b: Detail of profile P000665 underneath the Celeborn channel.	163
6.14	P000662: Profile across a wider and shallower part of the Celeborn channel.	164
6.15	P010520: Detail of a profile located on the upper slope of the study area.	165
6.16	P010521a: Detail of profile P010521 with special attention on the subunits within U3.	168
6.17	Facies distribution of unit U3, with positions of significant profiles.	169
6.18	P010529: Detailed profile of ENE prograding sigmoidal deposits within unit U3, underneath the main axis of the Arwen channel.	170

---

6.19	P000660: Detailed profile indicating the clear SSE progradation as observed on alongslope profiles.	171
6.20	P030509: Profile located in a flat area in between to mound ridges with an extremely thin Unit U1 due to intensified current action.	172
6.21	P980547: Alongslope overview profile, illustrating the variability of especially units U2 and U3.	173
6.22	P970531a: Overview profile illustrating the complex sigmoidal deposits in unit U3, as well as the heavily eroded upper part of unit U2.	174
6.23	P970533: Overview profile illustrating the variability of units U1 and U2.	175
6.24	P000658: Detailed profile along a giant single mound, overlying a wide variety of SSE prograding sigmoidal units within unit U3.	176
6.25	P010531a: Profile illustrating the eastern flank of the Celeborn channel.	177
6.26	P030531: Profile across the Enya mounds, illustrating a very thick unit U2 with several high-amplitude reflectors.	178
6.27	P010511c: Continued profile along the axis of the Arwen channel. Unit U3 shows northwards prograding sigmoidal units.	179
6.28	P980521: Detail of the sediment drift levee and its associated moat channel.	180
6.29	Upslope migrating sediment waves under a westward flowing bottom current in the Cilician basin, Northeastern Mediterranean (Ediger <i>et al.</i> , 2002).	182
6.30	Distribution of unit U2, the mounds and the steep scarp, created by the RD1 erosion event, as observed on the seismic profiles.	184
6.31	P980551: Alongslope overview profile featuring the large variability in thickness of unit U2.	185
6.32	P030525: N-S oriented profile across the Enya mounds, showing sigmoidal deposits in unit U3 and a thick unit U2.	186
6.33	P010521b: Detail of the upper slope part of profile P010521, illustrating the change in seismic facies and dip within unit U2.	187
6.34	P030524: N-S oriented profile across the Enya mounds, showing a thick unit U2.	188
6.35	P000661: Profile on the western levee of the Arwen channel. Unit U3 has been eroded and filled up with the transparent unit U2.	189
6.36	P99009a: Profile at the southern extremity of the study area. Unit U2 is relatively thick and shows several high-amplitude reflections.	190
6.37	P980523: Profile across the Arwen channel and a single mound, rooted on a scarp in unit U3.	192
6.38	P970536: Profile across a typical Belgica mound, rooted on a remnant of the unit U2.	193
6.39	P980549: Alongslope overview profile through a composite mounds and a single mound, rooted on the acoustically transparent unit U2.	194
6.40	P010521c: Detailed part of profile P010521, illustrating the seven different sections as observed in the small mounded drift at the centre of the Belgica mound province.	197
6.41	P970533a: Detailed section of profile P970533, illustrating the different 7 sections characteristic of the central part of the Belgica	198

	mound province, based upon changes in seismic facies.	
6.42	Positions of profiles illustrating the general characteristics of unit U1 and detailed profiles illustrating the alongslope channels.	199
6.43	P980503: Profile across the Arwen channel and its levee unit.	202
6.44	P970533: Profile across the deepest part of the Arwen channel, which cuts very deeply into unit U3.	203
6.45	P980506: Profile across the Arwen channel and its eastern flank. Unit U2 is heavily incised and shows converging high-amplitude reflectors.	204
6.46	P980507: Profile across the Arwen channel and its western flank.	205
6.47	P010511b: Profile along the main axis of the Arwen channel with major mass wasting deposits within the main channel thalweg.	206
6.48	P980519b: Detail of profile P980519 across the Arwen channel and its drift levee.	207
6.49	P980513: Profile across a broad Arwen channel with a rough and diffuse seafloor.	208
6.50	P010531b: Profile across the southern part of the Celeborn channel.	209
6.51	P010533: Profile across the Celeborn channel with mass-wasting deposits intercalated with an intra-channel levee.	210
6.52	Positions of cores and significant profiles on a multibeam background, illustrating the location, morphology and characteristics of the small mounded drift in the Belgica mound province.	211
6.53	P010523: Profile along the northern edge of the small mounded drift.	213
6.54	P010507: Detailed seismic profile across the core site of MD99-2327 and Bbc00-0606 on the eastern flank of a small mounded drift at the foot of a large mound.	214
6.55	Physical properties and grainsize characteristics of core ENAM-9901	217
6.56	Physical properties and grainsize characteristics of core ENAM-9905	218
6.57	Physical properties of core MD01-2450.	219
6.58	3D sketch illustrating the possible function of the gullies flanking the mound.	220
6.59	Surface 3D map of the northern part of the small mounded drift with position of core MD99-2327.	221
6.60	ESE-WNW oriented 3.5 kHz sub-bottom profiler line over the coring site MD99-2327 with inset of a 410 kHz side-scan sonar image with sand waves (RRS Discovery 248, courtesy of A. Wheeler, UCC, Ireland).	222
6.61	P980509: Profile across the small mounded drift in the central Belgica mound province. The mounded drift morphology is installed between the foot of a buried mound and a scarp in the flank of unit U2.	224
6.62	P970539: Profile across a typical drift mound of the Belgica mound province.	225
6.63	Lithological content and chronostratigraphy of core MD99-2327.	227
6.64	X-ray facies of core MD99-2327.	228
6.65	Five point moving average of the CORTEX XRF Ca, Fe and Si values in core MD99-2327.	229
6.66	Sedimentary processes and paleoceanographic interpretation of core MD99-2327.	230

6.67	Sedimentary parameters of core MD99-2327.	231
6.68	Special characteristics of the Enya drift system, with positions of the three Enya mounds, pockmarks, U2 scarp, the cut-and-fill scarp, drift mound crest and trough.	235
6.69	P030531: Detailed profile of unit U1 in the Enya mound province. The geometry of unit U1 is comparable with the one of a drift mound.	236
6.70	P030524: Detailed profile of unit U1 in the Enya mound province. The reflector configuration between the two mounds is mounded.	237
6.71	P030525: Detailed profile over the Enya mound province. The northern side of the Enya mound is flanked by very clear moats and the reflectors show a subtle mounded geometry.	238
6.72	TOBI side-scan sonar detail of a set of pockmarks, in the south of the Belgica mound province (Huvenne, 2003).	239
6.73	Reconstruction of the depositional evolution, in an idealised SW-NE section, of the small confined contourite drift in relationship with the growth of a coral bank.	242
6.74	Reconstruction of the depositional history in an ideal NE-SW profile.	244

## Chapter 7: Structure and development of the Gollum channel system

7.1	Overview map and location of the Kings channel system (KCS) and the Gollum channel system (GCS) with indication of the inferred Gollum deep-sea fan.	253
7.2	Schematic block diagram of the middle reaches of the Gollum Channel based on interpretation of side-scan sonar imagery (Wheeler <i>et al.</i> , 2003).	254
7.3	(A) Shaded bathymetry from EM12 swath data; (B) Interpretation of the swath bathymetry, 3.5 kHz profile and backscattering data, in terms of major sedimentary features (Akhmetzhanov <i>et al.</i> , 2003).	255
7.4	Shaded relief bathymetry map of the Kings channel area, highlighting the morphological features.	256
7.5	Location map of the used seismic profiles and core in the Kings channel area.	257
7.6	P99009b: Cross-section along the Aragorn and Faramir channel.	260
7.7	P99007b2: Alongslope profile across the upper reaches of the Aragorn and Faramir channels.	261
7.8	P010509: Cross-section across the upper reaches of the broad Theoden channel.	262
7.9	P99007: Profile across the upper southern flank of the Theoden channel, showing an incised unit U2.	263
7.10	P99007b1: Profile east of the Boromir channel head.	264
7.11	P010510a: Profile along the northwestern flank of the Boromir channel.	265
7.12	P010510b: Downslope running profile along the axis of the Boromir channel into the Denethor area.	266
7.13	P99010b: Downslope section across the Denethor area with a scarp and several debris flow deposits.	267
7.14	P010511a: Downslope section of the Aragorn channel, at the start of the Arwen channel and at the foot of a steep scarp.	268

7.15	Shaded relief bathymetry map of the northern two Gollum channel heads; Bilbo and Frodo, highlighting the morphological features.	270
7.16	Location map of the used seismic profiles and core in the Gollum channel area.	271
7.17	P010507: cross-section through the Bilbo and Frodo channels. Both have been incised into unit U2.	274
7.18	P030537b: profile along the southern flank of the Bilbo channels along its upper reaches.	275
7.19	P99006: downslope profile along the main upper axis of the Bilbo channel.	276
7.20	P010505: cross-section through the Bilbo and Frodo channels.	277
7.21	P010503: cross-section through the Bilbo and Frodo channels.	278
7.22	P030537a: downslope profile along the lower axis of the Bilbo channel, illustrating an important break in the thalweg.	279
7.23	P030533b: cross-section through the Bilbo channel and the intra-channel area.	280
7.24	P030533: profile along the northern flank of the Bilbo channel, cross-cutting a large depression.	281
7.25	P030535: cross-section through the Bilbo and Frodo channels.	282
7.26	P99005a: cross-section through the Bilbo and Frodo channels, this time with a leveed expression of both channels.	283
7.27	P99002: cross-section through the Bilbo channel with clear sediment levees.	284
7.28	P99003: lowermost cross-section of the Bilbo channel featuring large mass-wasting deposits.	285
7.29	P030509: profile along the intra-channel area, cross-cutting secondary channels with turbidite deposits on the channel floor.	286
7.30	Physical properties of core MD01-2464.	288
7.31	Grainsize characteristics of core MD01-2464.	289
7.32	Grainsize distribution curves of specific locations in core MD01-2464.	291
7.33	SCOPIX X-ray visualizations of specific intervals observed in core MD01-2464.	292
7.34	Existing vertical facies models of (1) coarse-grained turbidites, (2) classic turbidites (also known as the Bouma sequence), and (3) fine-grained turbidites, according to Shanmugam (2000).	293

## List of acronyms and abbreviations

		Definition or context on page:
AABW	Antarctic Bottom Water	30
ARb	Bulk accumulation rate	72
AWI	Alfred-Wegener-Institut für Polar- und Meeresforschung	60
BIIS	British-Irish Ice Sheet	2
BMP	Belgica mound province	1
CORTEX	XRF core scanner (NIOZ)	67
D-O	Dansgaard-Oeschger event	82
DSDP/ODP	Deep Sea Drilling Project/Ocean Drilling Project	5
EC-FP5	European Commission Fifth Framework Programme	6
ECOMOUND	EC-FP5 project studying the environmental controls on mound formation along the European margin	6
ENAM 2	European North Atlantic Margin project; quantification and modeling of large-scale sedimentary processes and fluxes	7
ENAW	Eastern North Atlantic Water	30
F <sub>150</sub>	Coarse sand fraction with a grainsize superior to 150 µm	69
FIS	Fennoscandian Ice Sheet	80
GCS	Gollum Channel System	253
GEBCO	General Bathymetric Chart of the Oceans	8
GEOMOUND	EC-FP5 project studying the internal (geo) controls of mound formation along the European margin	6
GIS	Greenland Ice Sheet	85
GRIP	Greenland Ice Core Project	85
HAR	High amplitude reflector	132
HE	Heinrich Event	80
HL	Heinrich Layer	80
HMP	Hovland mound province	4
IFREMER	Institut Français de Recherche pour l'Exploitation de la Mer	8
IGCP 432	International Geological Correlation Programme project 432, Contourite Watch	7
IHO	International Hydrographic Commission	60
IIS	Icelandic Ice Sheet	80
IMAGES	International Marine Past Global Changes Study	7
IOC	Intergovernmental Oceanographic Commission	60
IRD	Ice-rafted debris	68
IRE	Ice-rafting event	87
KCS	Kings Channel System	257
L*	Luminosity	67
LIS	Laurentide Ice Sheet	79
LSCE	Laboratoire des Sciences du Climat et de l'Environnement	65
LSR	Linear sedimentation rate	71
LSW	Labrador Sea Water	30
MDCS	Madeira Distibutary Channel System	295
MIS	Marine Isotope Stage	70
MMP	Magellan mound province	4
MOW	Mediterranean Outflow Water	30

MPB	Main Porcupine Basin	22
MPR	Middle Pleistocene Revolution	142
MS	Magnetic Susceptibility	66
MSCL	Multi-Sensor Core Logger	65
N(E)ADW	North(east) Atlantic Deep Water	30
NACW	North Atlantic Central Water	30
NIOZ	Royal Netherlands Institute for Sea Research	63
NPS	Percentage of <i>N. pachyderma</i> (s.) relative to the total of planktonic foraminifers	70
NSW	Norwegian Sea Water	30
PCE	Peak Current Event	226
PSB	Porcupine Seabight	1
RCMG	Renard Centre of Marine Geology	4
ROV	Remotely Operated Vehicle	4
SCOPIX	Digital X-ray imaging system (Université Bordeaux I)	68
SDS	Percentage of <i>N. pachyderma</i> (s.) relative to the abundance of <i>N. pachyderma</i> (s.) and <i>N. pachyderma</i> (d.)	70
SEC	Shelf Edge Current	30
SOC	Southampton Oceanography Centre	60
STRATAGEM	EC-FP5 project studying the stratigraphic development of the glaciated European margin	6
TOBI	Towed Ocean Bottom Instrument (SOC)	4
TTR	Training Through Research campaign (IOC)	60
TWT	Two-Way Travel time	57
UPR	Upper Pleistocene Revolution	142

## Chapter I: Introduction

### 1.1 Scientific rationale

The scientific interest in sedimentary systems where bottom currents play a key role has strongly developed since the progressive movement of the petroleum industry towards deep-water domains (Stow & Mayall, 2000; Stow *et al.*, 2002a; Rebesco & Stow, 2001). Turbidite systems have always received a special attention due to their large reservoir capacities (Stow & Johansson, 2000; Bouma, 2000; Shanmugam, 1997). However, recent studies show that the importance of contourite deposits may not be underestimated. Both turbidite (downslope) and contourite (alongslope) currents can create well-sorted, coarse-grained deposits, as well as fine-grained varieties (Stow & Mayall, 2000; Stow & Piper, 1984; Gonthier *et al.*, 2003). However, their geophysical characteristics can be very similar and are often the origin of (very expensive) misinterpretations (Viana *et al.*, 1998; Faugères *et al.*, 1999). Moreover, the lithological difference between hemipelagites, turbidites and contourites can be very subtle. Some deposits can be attributed a mixed turbiditic and contouritic origin, which can be observed, for example, in deep-sea fan systems (Massé *et al.*, 1998; Gonthier *et al.*, 2003).

Research on this topic has been ongoing since the late 60's, but there still is a necessity to develop criteria to distinguish contourites from other deep-water deposits (Stow & Johansson, 2000; Stow *et al.*, 2002a; Shanmugam, 2000; Rebesco & Stow, 2001). Moreover, every year, partly due to recent technological developments, other and smaller-scaled varieties of these deposits are reported (Faugères *et al.*, 1999; Rebesco & Stow, 2001). Also of great importance is to try to understand the link between climate, bottom water circulation and the sediment drift depositional process, although this does not always seem to be straightforward (Faugères & Stow, 1993; Rebesco & Stow, 2001). Studies of deep-water contourite and turbidite systems necessitate a multi-disciplinary approach, because these deposits can not be interpreted unambiguously on base of one single technique alone (Faugères *et al.*, 1999). A more challenging problem is the discrimination of both turbiditic and contouritic processes in mixed systems.

Such interplay of sedimentary processes seems to be present on the eastern slope of the Porcupine Seabight (PSB)(Fig. 1.1). This Mesozoic basin southwest of Ireland is enclosed by four shallow platforms and hence forms a small bight along the North Atlantic margin. Only in the southern part of this basin, a relatively small opening towards the deeper Atlantic basins is present. Because of this special location and its particular geological setting, the intense bottom currents, which make part of the "Global Conveyor Belt", do not seem to enter the basin. Hydrologic models and some current measurements, however, suggest the presence of enhanced bottom current flow in a limited zone within a depth interval of 500 to 1000 m (White, in press; New *et al.*, 2001; Rice *et al.*, 1991). In recent times, the Porcupine Basin has gained interest because of the presence of special deep-water habitats (Henriet *et al.*, 1998; De Mol *et al.*, 2002; Huvenne *et al.*, 2003; Wheeler *et al.*, in press). As such, a province of coral banks on the eastern slope was discovered and described as the Belgica mound province (BMP). Preliminary studies already suggested that the geometry of the most recent deposits in this province seemed to

be under influence of bottom currents of variable intensity. It is proposed that the sediments embedding the mounds are sediment drifts (De Mol *et al.*, 2002; Henriët *et al.*, 2003).

According to the current state-of-the-art, Stow *et al.* (2002a) defined **sediment drift** as a general term for a sediment accumulation, of no definitive or unique geometry, that has experienced some current control on deposition. It is thus not restricted to bottom current deposits. The sediments deposited by or significantly altered by the action of bottom currents are defined as **contourites**. A wide range of contourite facies can be recognized from muddy to gravel-lag facies, and of all different compositions depending on the sediment supply system. **Contourite drifts** are thus sediment drifts formed principally (though not necessarily exclusively) by bottom currents. Various authors consider these sediment drifts as ideal targets for paleoceanographic and paleoclimatologic studies (Joseph *et al.*, 2002; Llave *et al.*, 2001; Rebesco & Stow, 2001; Bianchi & McCave, 2000; McCave *et al.*, 1995; Stow & Lovell, 1979). A better understanding of the functioning of these sediment drifts may also imply a better insight in the possible relationship between the coral banks and such drift systems. However, within the Porcupine Seabight, very little is known about the regional Quaternary paleoceanography, mainly by a lack of long, high-resolution drilling records. Still, this basin is located in an ideal proximal position for the study of the evolution and the variability of the Irish component of the British-Irish Ice Sheet (BIIS). At present, available information is largely based on on-land work (Bowen *et al.*, 2002; Dowling & Coxon, 2001; McCabe *et al.*, 1998) and from work in basins and slopes north (Knutz *et al.*, 2002; Richter *et al.*, 2001; Armishaw *et al.*, 2000) and south of Ireland (Auffret *et al.*, 2002; Zaragosi *et al.*, 2001; Grousset *et al.*, 2000; Scourse *et al.*, 2000; Hall & McCave, 1998; Auffret *et al.*, 1996).

Further towards the southern part of the Seabight, located between the shelfbreak and the Porcupine Abyssal Plain, the Gollum channel system was discovered by Berthois & Brenot (1966) and further described by Kenyon *et al.* (1978). Kenyon (1987), Rice *et al.* (1991) and Wheeler *et al.* (2003) already described the important role of turbidites and slumps in this canyon system. However, its genesis, and its past and current functioning is not well-known. This channel system may have been an important source of detritic input into the Porcupine Basin during glacial lowstands.

On the eastern slope of the PSB, two kinds of sedimentary environment are suggested to be present at a relatively close distance. On the one hand, there is a hemipelagic sedimentation influenced by bottom currents (sediment drift), on the other hand, within the Gollum channel system, mainly turbidite currents and other mass wasting processes dominate the sedimentation. Therefore, it is necessary to study and understand the depositional processes and the interaction between them, using both sedimentological and geophysical techniques. The Porcupine Basin offers an ideal laboratory for this purpose.

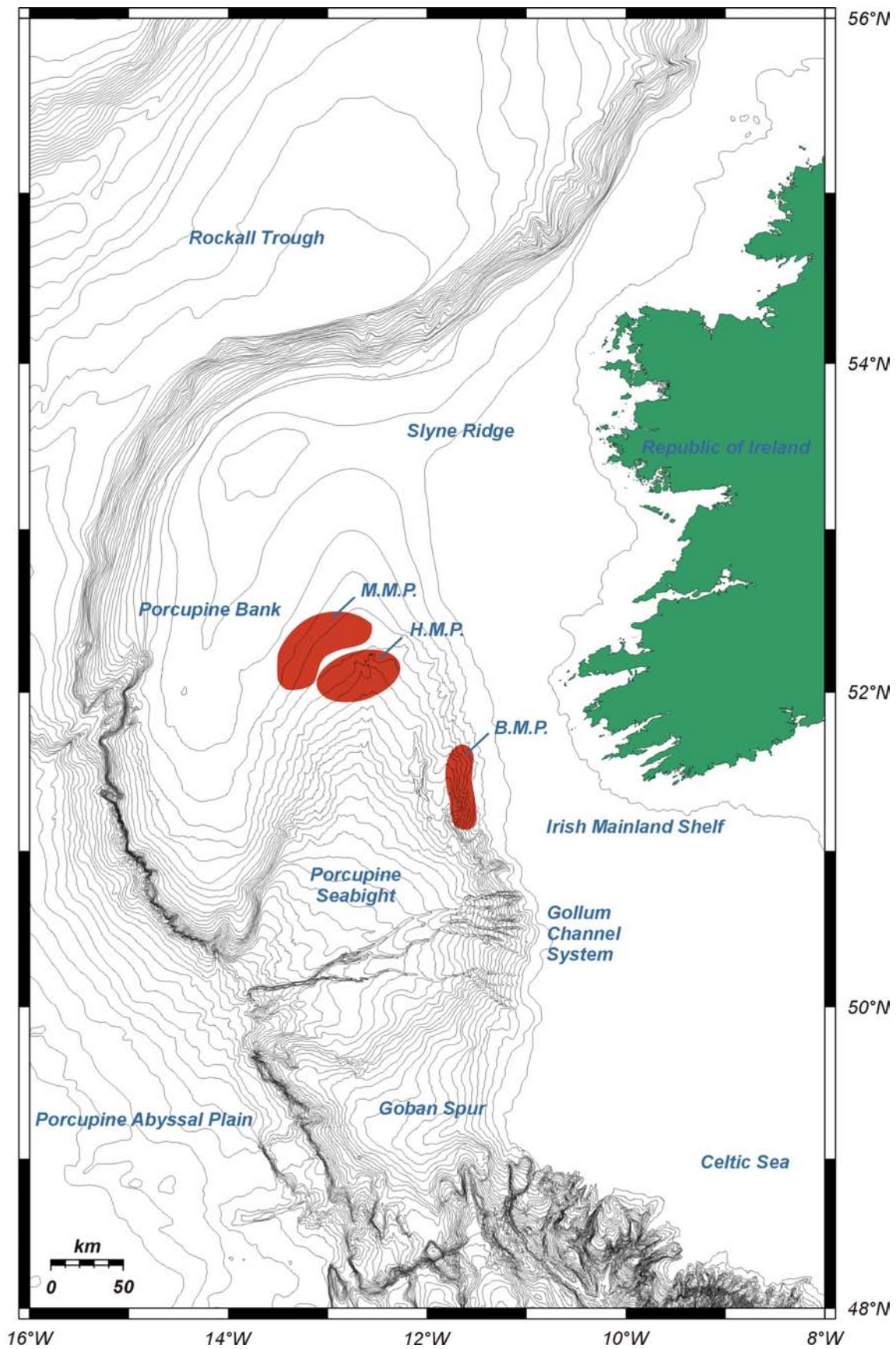


**Figure 1.1:** General overview map of the north Atlantic margin off Irish western Ireland. Contour intervals are drawn every 100 m. B.M.P.: Belgica mound province, H.M.P.: Houland mound province, M.M.P.: Magellan mound province.

## 1.2 Research strategy

Within the Renard Centre of Marine Geology (RCMG), a significant attention has already been paid onto the study of the cold- and deep-water coral banks and associated sedimentary processes. This has resulted in several M.Sc. theses with varying emphasis: stratigraphy (Van Rooij, 1998; Pillen, 1998; Van Herreweghe, 1999), geophysics (Galanes-Alvarez, 2001; Gwilym, 2002; Hinsinger, 2002), biostratigraphy (Mertens, 2002; Cornilly, 2003), sedimentary processes (Lekens, 2000; Nys, 2002; Van Landeghem, in prep.) and paleomagnetism (Foubert, 2002). Furthermore, within the last two years, two Ph.D. projects have been completed within the framework of PSB coral bank studies, each study addressing a specific aspect of the character, structure and evolution of the three mound provinces within the Porcupine Seabight (Fig. 1.1): Belgica mound province (BMP), Magellan mound province (MMP) and Hovland mound province (HMP).

A first complete study of the three mound provinces was performed by De Mol (2002) focussing on their morphology, seismic facies, sedimentology, biology and oceanography. This multidisciplinary study evaluated the role of hydrocarbon seeps and oceanography in the genesis of the coral banks using very high-resolution single channel reflection seismic profiles, gravity cores, grab samples and some detailed side-scan sonar imagery. A multi-step model with a start-up, catch-up, keep-up & give-up phase was proposed in order to explain the development of these large deep-water coral banks in relationship with current speed and sedimentation rates.

Huvenne (2003) made a spatial and statistical geophysical analysis of the Magellan mound province using a unique combination of both industrial 3D and academic 2D seismic data. An important topic addressed in this study was the relationship between the coral banks and the surrounding oceanographic and sedimentary processes. This was partly studied through observations of the present-day appearance of the mounds and the surrounding seabed using TOBI side-scan imagery and the Remotely Operated Vehicle (ROV) Victor. This new dataset also included the Belgica and Hovland mound provinces and shed some new light on the interpretations of De Mol (2002).

This present study is complementary to the former ones and aims to evaluate the importance of bottom currents within the Neogene to Quaternary evolution of the eastern slope of the Porcupine Seabight, as well as the influence of, and interplay with other deep-water sedimentary processes such as turbiditic ones. Moreover, the presence and location of the coral banks offer a unique opportunity to study the behaviour of enhanced bottom currents, as well as their impact on sedimentation, in areas with an irregular bathymetry. As suggested by many authors involved with contourite studies these processes will be studied on different scales using a wide range of methods and techniques (Faugères *et al.*, 1999; Rebesco & Stow, 2001; Stow *et al.*, 2002a). More specifically, this research project has 4 main focuses:

1. **Geophysical characterization of Neogene-Quaternary deposits** on the eastern slope of the Porcupine Seabight. Very high-resolution single-channel seismic reflection profiling, multibeam bathymetry and high-resolution side-scan sonar imagery has been used to study the *geometry* and *construction* of the sediment body around, and its *interaction* with the Belgica mounds. A detailed Neogene-Quaternary stratigraphy will be proposed and linked with

regional and world-wide *tectonic* and *paleoceanographic* changes. As well, the *structure, functioning* and *evolution* of the Gollum channel system will be investigated and coupled to the evolution and stratigraphy of the Belgica mound province.

2. **A sedimentological study of recent glacial and interglacial deposits** will further investigate the *nature, characteristics* and *short-term variability* of a variety of sedimentary processes in the Belgica mound province (contourites) and the Gollum channel system (turbidites). For such purposes, giant Calypso piston cores, boxcores and gravity cores were acquired on strategic places in the study area.
3. **A study of paleoclimatologic and paleoceanographic changes** will try to assess how the functioning of the BIIS was archived in the sedimentary record and in which way this and other world-wide *paleoclimatologic* events influenced the sedimentary environment and dynamics. Therefore, the availability and applicability of some well-known *paleoceanographic markers* and proxies will be *evaluated* and *reassessed* in order to facilitate the construction of an appropriate core stratigraphy.
4. **A Late-Cenozoic development model of the eastern Porcupine Seabight** will be proposed, integrating the results of the three previous topical points. This model will try to shed some more light on the “early days” of the mound genesis and through a comparative study it will enable to better fathom the nature, origin and evolution of the deposits in the Seabight. In this way, it will help assessing the uniqueness of this sedimentary environment.

Throughout this thesis, all consecutive chapters will focus on a part or on one of the four main goals. In order to set the stage, *chapter 2* will give a brief overview of the geological and hydrographic setting of the Porcupine Basin. Also the main results of the work on large deep-water coral banks along the Irish margin will be presented. The large variety of material, techniques and methods used in this study will be treated in *chapter 3*. Because it is of a great importance to define and use a correct stratigraphic framework for as well the sedimentological as seismic stratigraphy part, *chapters 4* and *5* will respectively discuss and propose the most suitable framework for this particular region. More specifically, *chapter 4* will discuss the influence of the proximity of the British-Irish Ice Sheet (BIIS) on the applicability of the Heinrich Layers as a tool for relative datations. This also allows to gain more insight in the variability and destabilisation history of the BIIS. *Chapter 5* will propose a chronostratigraphic framework based on the occurrence of hiatuses and unconformities observed on very high-resolution single-channel reflection seismic profiles over DSDP site 548 on Goban Spur (de Graciansky *et al.*, 1984) and which will be integrated with the existing knowledge of regional and world-wide oceanographic events. This will be applied in *chapter 6*, where the seismic stratigraphy of the BMP will be described and discussed. This chapter will also focus on the Quaternary sedimentary processes, as observed in cores and profiles, illustrated through a set of case studies. *Chapter 7* will deal with the structure and development of the Gollum channel system. The general model of the Late-Cenozoic development of the eastern Porcupine Seabight will be presented in *chapter 8*, along with an overview of the main results, the paleoceanographic implications and a final conclusion.

### 1.3 Project framework

This research project has been funded through a specialisation grant of the *Institute for the encouragement of Innovation through Science and Technology in Flanders* (IWT), but it also frames within a variety of other European and worldwide projects.

Due to its close link with the deep-water coral banks, this study is directly related to several projects which are grouped in the *European Commission Fifth Framework Programme* (EC-FP5) under the *Ocean Margin deep-water Research Consortium* (OMARC):

- **GEOMOUND** (2000-2003) focussed on the *geological evolution* of giant, deep-water carbonate mounds in the Porcupine Basin and southeast Rockall Basin. Its objectives included the production of a systematic inventory of recorded giant mound occurrences along the NW European margins, documenting morphologies, structural associations, patterns and temporal relationships which might identify the underlying geological control point on the genesis of mounds and on their sustained and episodic growth. Also the occurrence of these mounds was tested on their diagnostic value as potential indicators for *hydrocarbons* and for *fluid expulsion* events. Therefore, a model was developed for the fluid migration paths and processes which might have fuelled surface venting in the mound provinces. The RCMG was responsible for the coordination of this project.
- **ECOMOUND** (2000-2003) tried to define the *environmental controls* and processes involved in the development and distribution of carbonate mounds on the NW European continental margin. This project aimed to establish the relationship between carbonate mound biota and recent *water mass characteristics* and *dynamics*, as well as with the *sedimentological properties* of the surrounding seabed. In this way, it allowed a better understanding of environmental factors and their variability. RCMG was a full partner of this project.
- **STRATAGEM** (2000-2003) tried to address the problem of a lack of a regional approach to the *stratigraphic development of the glaciated European margin*. This project focused on the definition of sedimentary packages on the margin from Ireland to Norway and to produce a unified stratigraphic framework for the mid-Cenozoic to Recent using seismic profiling and cores. It also produced a geological model for the evolution of the margin. Although RCMG was not involved in these projects, the research strategy of this present thesis closely links to the objectives of STRATAGEM and will try to tie the evolution of the PSB to their geological model.

These three projects have been concluded by now and are publishing their results. The results of the GEOMOUND and ECOMOUND projects are to be published in a book entitled “Modern Carbonate Mound Systems: A window to Earth History”, edited by the respectively project coordinators Prof. Dr. J.-P. Henriët (RCMG) and Prof. Dr. C. Dullo (GEOMAR). The STRATAGEM project has already published most of its results and is publishing a stratigraphic atlas.

Within the framework of coral bank studies, this research project also related to the **GOA project** (1999-now) of Ghent University “*Porcupine-Belgica: Carbonate*

*Mud Mounds and Cold Water Reefs; Deep Biosphere – Geosphere coupling*". This study assists the GOA project to determine a spatial and temporal relationship in between the "carbonate sequences" and the drift deposits.

A part of this study also lies in the continuation of the objectives of the past European Commission-supported **ENAM II** project (1996-1999). Among the primary objectives were (1) a quantification of large-scale sedimentary processes, (2) the determination of late Quaternary oceanographic conditions with a focus on meltwater events governing the sediment fluxes and (3) the relationship between cryospheric, oceanographic and sedimentary processes. The main results of this project were published in a special edition of *Marine Geology* (Volume 188, issues 1-2, pages 1-248, August 2002) and in a combined STEAM-ENAM atlas of side-scan sonar and seismic images (Mienert & Weaver, 2003).

In order to foster a greater international dialogue and to stimulate more focussed research concerning the contourite problem, an International Geological Correlation Programme (IGCP) named **Contourite Watch** (Project 432) was launched in 1998 (until 2003). Through the organisation of meetings, workshops and newsletters this project aimed to improve the current knowledge and understanding of contourite systems. The results of the project were also published as a Geological Society Memoir (Stow *et al.*, 2002b).

An essential part of the studied core material was obtained and analysed within the framework of the international **IMAGES** programme. This international marine past global changes study was initiated to respond to the challenge of understanding the mechanisms and consequences of climatic changes using oceanic sedimentary records. One of the driving thoughts of IMAGES is that individual research does not longer seem to be sufficient because the acquisition of the required, long sediment cores in high sedimentation rate areas is expensive, and the proper study of such cores demands the use of multiple tools and large numbers of measurements.

#### **1.4 Definition of morphologic features**

A study concerning Quaternary contouritic and turbiditic processes involves the description of many positive and negative morphologies. Previous studies using multibeam bathymetry and side-scan sonar imagery already clearly indicate that the eastern slope of the Porcupine Seabight contains many eye-catching features including channels, canyons, scarps and mounds (Beyer *et al.*, 2003; Huvenne, 2003). It is particularly hard to refer to such features without giving them an appropriate name.

This is why some particular and highly investigated mounds have already received a name like Thérèse, Moira, Challenger or Enya. As a standard procedure, large coral bank provinces were given the name of the research vessel which firstly mapped these structures. In this way, the Porcupine Seabight received a Magellan mound province and a Belgica mound province (Henriet *et al.*, 1998; De Mol *et al.*, 2002; Huvenne *et al.*, 2003). Within the Rockall Trough, the Darwin (Masson *et al.*, 2003; Wheeler *et al.*, in press), Logachev and Pelagia mounds (Kenyon *et al.*, 2003; van Weering *et al.*, in press; Wheeler *et al.*, in press) were discovered during campaigns with respectively similarly named ships. One exception is the Hovland

mound province, named after the author who firstly described these features and related them to gas migration (Hovland *et al.*, 1994; Henriot *et al.*, 1998; De Mol *et al.*, 2002).

However, according to Kenyon & Hunter (1998) most of the features along the entire northeast Atlantic margin were given names of “heroic and positive places, tribes and characters”, following the nomenclature of Roberts (1975). Indeed, names like Feni (Roberts & Kidd, 1979; Dowling & McCave, 1993; Richter *et al.*, 2001), Gardar (McCave *et al.*, 1980; Manley & Caress, 1994; Bianchi & McCave, 2000), Barra (Armishaw *et al.*, 2000; Knutz *et al.*, 2002), Eirik (Stow & Holbrook, 1984), Bjorn (Bianchi & McCave, 2000) and even King Arthur (Dingle & Scrutton, 1979) are nowadays linked with very well known sediment drifts, deep-sea fans, canyons and channels. One of the very first features discovered in the Porcupine Seabight, and probably the only one which was given a name, was a channel system discovered by Berthois & Brenot, (1966). This system was further studied by Kenyon *et al.* (1978), who named it “after a particularly unpleasant creature in J.R.R. Tolkien’s book “The Lord Of The Rings””; Gollum. Within the course of this study, the same book regained attention through the release of three subsequent motion pictures (*The Fellowship of the Ring*, 2001; *The Two Towers*, 2002; *The Return of the King*, 2003). Because a multitude of characters and places are appearing in Tolkien’s world, it is a very grateful source of names that can be given to deep-sea features.

In order to pay tribute to this great writer and to follow the nomenclature tradition, the most prominent features discussed in this study were attributed appropriate names from “The Lord Of The Rings” (Figs. 1.2, 1.3 and 1.4). The following overview lists these new names, with their location and brief descriptions. A more detailed description of these features will be given in chapters 6 and 8.

#### 1.4.1 Belgica mound area

This area features a multitude of morphologic features like mounds and downslope running gullies (Fig. 1.2). However, already on the standard GEBCO bathymetry several south-north channels have been observed. The names of four of these channels will be referring to the most important Elves of “The Lord Of The Rings”. Most of these channels are relatively steep and deep in the south, while they broaden and shallow towards the north.

The **Galadriel channel** is located between 12°10’W, 12°00’W, 51°20’N and 51°45’N (respectively the western, eastern, southern and northern boundaries) in water depths from 800 to 1400 m. This approximately 50 km long channel has a maximum width of 5 km and depth of 200 to 300 m. The main direction is south-north, but is composed in a gently N190° oriented part in the north and a N150° oriented part in the south.

The deepest part of the Galadriel channel is shared with the **Celeborn channel**, located between 12°08’W, 11°59’W, 51°19’N and 51°37’N in water depths from 900 to 1400m. This approximately 30 km long channel has a maximum width of 5 km and depth of 200 to 300 m. The overall orientation of Celeborn is N195°.

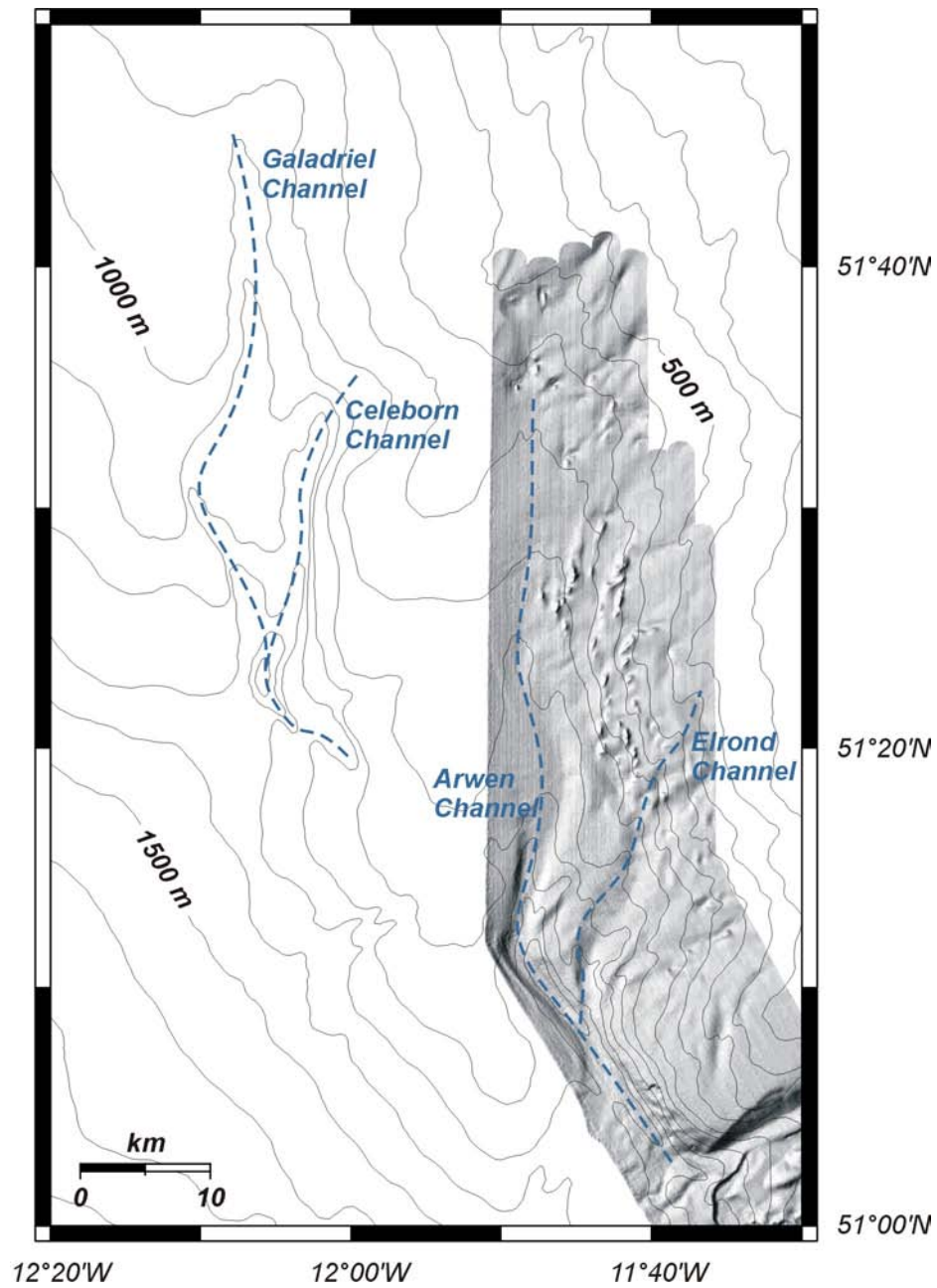


**Figure 1.2:** Combined GEBCO bathymetric map (contour intervals are drawn every 100 m) with shaded relief multibeam bathymetry (Beyer et al., 2003) inset, indicating the newly named morphologic features within the Belgica mound province.

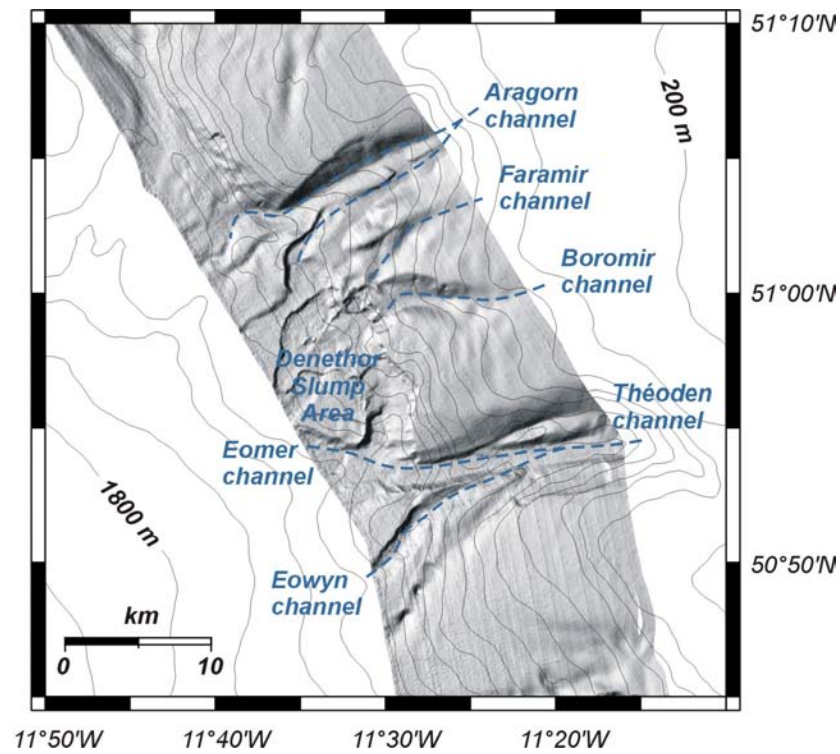


**Figure 1.3:** Combined GEBCO bathymetric map (contour intervals are drawn every 100 m) with shaded relief multibeam bathymetry (Beyer et al., 2003) inset, indicating the newly named morphologic features within the Kings channel region.

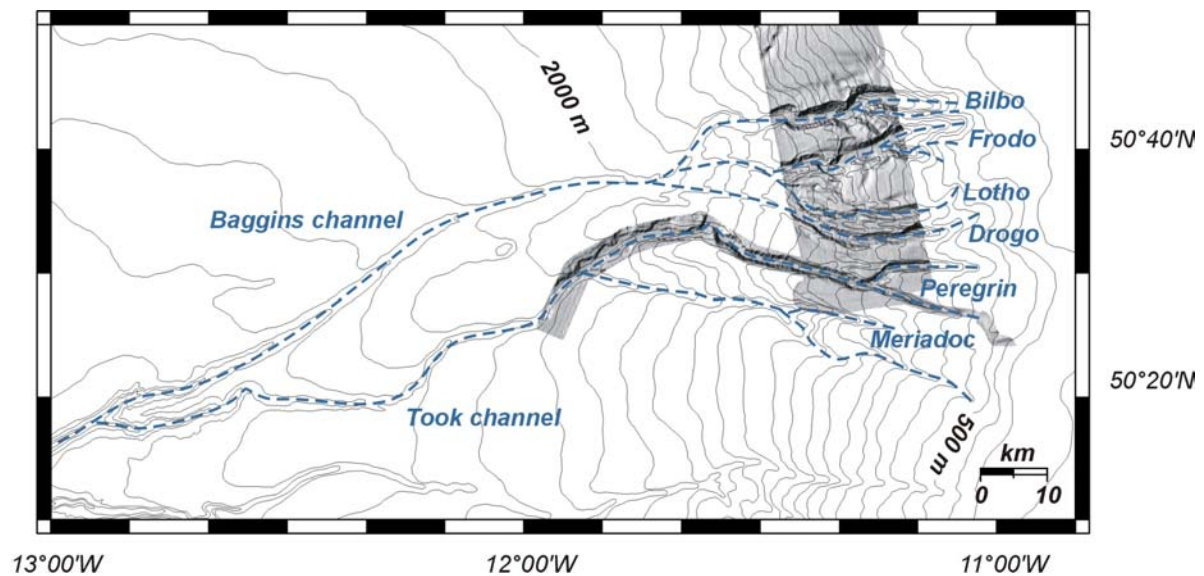


**Figure 1.4:** Combined GEBCO bathymetric map (contour intervals are drawn every 100 m) with shaded relief multibeam bathymetry (Beyer et al., 2003) inset, indicating the newly named morphologic features within the Gollum channel system.

The largest and most pronounced channel is the **Arwen channel**, located between 11°51'W, 11°36'W, 51°00'N and 51°40'N in water depths from 500 to 1500 m. This channel is approximately 65 km long, sometimes up to 7 km wide and up to 400 m deep. At its maximum depth, it is characterized by very steep flanks and a marked change in orientation from N-S to N135°.

The **Elrond channel**, which is located between 11°46'W, 11°35'W, 11°07'N and 51°25'N, is less pronounced than the Arwen channel, in which it ends. This channel is relatively shallow (50 m) and can be found in water depths from 300 to 1400 m. It has a roughly N195° orientation.

#### 1.4.2 Kings channels area

Although these channels were originally assigned as the northernmost branches of the Gollum channels (Kenyon *et al.*, 1978), newly acquired data described in this thesis clearly distinguishes them from the typical Gollum channels in the south (Fig. 1.3). Because of their size and sometimes dramatic characteristics, they are named after important Kings and Princes.

The northernmost channel is called the **Aragorn channel**, located between 11°40'W, 11°20'W, 51°00'N and 51°08'N, in water depths ranging from 300 to 1400 m. In general, this large channel is 20 km long, 5 km wide and approximately 350 m deep. Its orientation bears N240°, which also is the general trend of the other channels in this area. A N240° elongated mound divides the channel into two parallel running branches. At its deepest part, it coincides with the southernmost expression of the Arwen channel.

The **Faramir channel** is a smaller feature located between 11°33'W, 11°22'W, 51°00'N and 51°05'N on the upper slope from 300 to 1000 m. Its length approximates 10 km. It is only 1 km wide and has a negative relief of about 50 m. The net orientation also ranges N240°. The **Boromir channel** features similar characteristics as its brother channel (Faramir), although the orientation is different (N260°).

Both Faramir and Boromir channels converge in a large area (approximately 100 km<sup>2</sup>) with dramatic incisions: the **Denethor (slump) area**. It is located between 11°40'W, 11°27'W, 50°53'N and 51°03'N in water depths ranging from 800 to 1500 m.

A second large channel is formed by the **Théoden channel system**, diverging into two branches; **Eomer** to the north and **Eowyn** to the south. They are located between 11°40'W, 11°10'W, 50°48'N and 50°56'N in water depths ranging from 200 to 1600 m. The upper Théoden branch is about 10 km long, 8 km wide and up to 500 m deep. At its deepest point, the N270° orientation is maintained by the Eomer channel, which continues over 20 km. Théoden has a width of 3 to 4 km. The Eowyn channel, on the other hand, has an orientation of N235°, but it also continues for about 20 km with a width of about 2 km.

### 1.4.3 Gollum channel area

The Gollum channel system was earlier described as tributary channel system incising the upper slope of the south-eastern Porcupine Seabight (Berthois & Brenot, 1966; Kenyon *et al.*, 1978; Kenyon, 1987). It converges into one main channel, the Gollum channel, which ends into the Porcupine Abyssal Plain (Figs. 1.1 and 1.4). Our study zooms further into the northern branch on the upper slope, which has been mapped with multibeam bathymetry (Beyer *et al.*, 2003). Here, we describe two branches and their composing channels, located between 13°00'W, 10°50'W, 50°10'N and 50°50'N.

The Baggins branch is composed of four smaller channels that converge into the Baggins channel: Bilbo, Frodo, Lotho and Drogo (from north to south). All of these upper slope channels have a net N270° orientation and have a length of about 40 km before they converge. On average, they are 3 to 4 km wide and can be up to 300 m deep. The Baggins channel continues for about 90 km in a N245° direction. It still can be up to 3 km wide and its depth can vary from 100 to 300 m.

The **Took branch** only comprises two channels: **Peregrin** and **Meriadoc**. Their main orientation is N280°, although the Peregrin channel earlier adopts the orientation of the Took (and also Baggins) channel: N245°. Both Peregrin and Meriadoc have a maximal width of 2 km and can be up to 150 m deep. The **Took channel** has the same characteristics as the Baggins channel, although it is a few kilometres shorter and has a larger sinuosity.

## References

- Armishaw, J. E., Holmes, R. W. & Stow, D. A. V. (2000) The Barra Fan: A bottom-current reworked, glacially-fed submarine fans system. *Marine and Petroleum Geology*, **17**, 219-238.
- Auffret, G. A., Pujol, C., Baltzer, A., Bourillet, J. F., Müller, C. & Tisot, J. P. (1996) Quaternary sedimentary regime on the Berthois Spur (Bay of Biscay). *Geo-Marine Letters*, **16**, 76-84.
- Auffret, G. A., Zaragosi, S., Dennielou, B., Cortijo, E., Van Rooij, D., Grousset, F. E., Pujol, C., Eynaud, F. & Siegert, M. (2002) Terrigenous fluxes at the Celtic margin during the last glacial cycle. *Marine Geology*, **188**, 79-108.
- Berthois, L. & Brenot, R. (1966) Existence d'une flexure continentale parcourue par un réseau hydrographique, au Sud-Ouest de l'Irlande. *Comptes Rendus de l'Académie des Sciences Paris, Série II a*, **263**, 1297-1299.
- Beyer, A., Schenke, H. W., Klenke, M. & Niederjasper, F. (2003) High resolution bathymetry of the eastern slope of the Porcupine Seabight. *Marine Geology*, **198**, 27-54.
- Bianchi, G. G. & McCave, I. N. (2000) Hydrography and sedimentation under the deep western boundary current on Björn and Gardar Drifts, Iceland Basin. *Marine Geology*, **165**, 137-169.
- Bouma, A. H. (2000) Coarse-grained and fine-grained turbidite systems as end member models: applicability and dangers. *Marine and Petroleum Geology*, **17**, 137-143.
- Bowen, D. Q., Phillips, F. M., McCabe, A. M., Knutz, P. C. & Sykes, G. A. (2002) New data for the Last Glacial Maximum in Great Britain and Ireland. *Quaternary Science Reviews*, **21**, 89-101.
- Cornilly, W. (2003) Paleoenvironmental study of Heinrich Layers in the Porcupine Seabight; A case study of the Magellan Mound Province. M.Sc. thesis, Marelac. *Ghent University*, Gent, 39 pp.
- de Graciansky, P. C., Poag, C. W., Cunningham, R., Loubere, P., Masson, D. G., Mazzullo, J. M., Montadert, L., Müller, C., Otsuka, K., Reynolds, L. A., Sigal, J., Snyder, S. W., Townsend, H. A., Vaos, S. P. & Waples, D. (1984) *Initial Reports of the Deep Sea Drilling Project*, **80**. U.S. Government Printing Office, Washington.
- De Mol, B. (2002) Development of coral banks in Porcupine Seabight (SW Ireland): A multidisciplinary approach. Ph.D. thesis, Department of Geology and Soil Science. *Ghent University*, Gent, 363 pp.
- De Mol, B., Van Rensbergen, P., Pillen, S., Van Herreweghe, K., Van Rooij, D., McDonnell, A., Huvenne, V., Ivanov, M., Swennen, R. & Henriët, J.-P. (2002) Large deep-water coral banks in the Porcupine Basin, southwest of Ireland. *Marine Geology*, **188**, 193-231.
- Dingle, R. V. & Scrutton, R. A. (1979) Sedimentary succession and tectonic history of a marginal plateau (Goban Spur, Southwest of Ireland). *Marine Geology*, **33**, 45-69.
- Dowling, L. A. & Coxon, P. (2001) Current understanding of Pleistocene temperate stages in Ireland. *Quaternary Science Reviews*, **20**, 1631-1642.
- Dowling, L. M. & McCave, I. N. (1993) Sedimentation on the Feni Drift and late Glacial bottom water production in the northern Rockall Trough. *Sedimentary Geology*, **82**, 79-87.
- Faugères, J.-C. & Stow, D. A. V. (1993) Bottom-current-controlled sedimentation: a synthesis of the contourite problem. *Sedimentary Geology*, **82**, 287-297.
- Faugères, J.-C., Stow, D. A. V., Imbert, P. & Viana, A. R. (1999) Seismic features diagnostic of contourite drifts. *Marine Geology*, **162**, 1-38.
- Foubert, A. (2002) Een paleomagnetische studie met zeer hoge resolutie op Calypso-kernen in Porcupine Seabight, ten zuidwesten van Ierland. M.Sc. thesis, Department of Geology and Soil Science. *Ghent University*, Gent, 151 pp.
- Galanes-Alvarez, H. (2001) A pseudo 3D very high resolution seismic study of the Thérèse mound, Porcupine Basin, offshore SW Ireland. M.Sc. thesis, School of Ocean Sciences. *University of Wales, Bangor*, 114 pp.
- Gonthier, E., Faugères, J.-C., Viana, A. R., Figueiredo, A. G. & Anschutz, P. (2003) Upper Quaternary deposits on the Sao Tomé deep-sea channel levee system (South Brazilian Basin): major turbidite versus contourite processes. *Marine Geology*, **199**, 159-180.

- Grousset, F. E., Pujol, C., Labeyrie, L. D., Auffret, G. A. & Boelaert, A. (2000) Were the North Atlantic Heinrich events triggered by the behavior of the European ice sheets? *Geology*, **28**(2), 123-126.
- Gwilym, O. (2002) The integration of high resolution 2D seismic data with industrial scale 3D seismic data using seismic attribute analysis. M.Sc. thesis, School of Ocean Sciences. *University of Wales*, Bangor, 62 pp.
- Hall, I. R. & McCave, I. N. (1998) Glacial-interglacial variation in organic carbon burial on the slope of the N.W. European Continental Margin. *Progress in Oceanography*, **42**, 37-60.
- Henriet, J.-P., De Mol, B., Pillen, S., Vanneste, M., Van Rooij, D., Versteeg, W., Croker, P. F., Shannon, P. M., Unnithan, V., Bouriak, S., Chachkine, P. & The Porcupine-Belgica 97 Shipboard Party. (1998) Gas hydrate crystals may help build reefs. *Nature*, **391**, 648-649.
- Henriet, J.-P., Van Rooij, D., Huvenne, V., De Mol, B. & Guidard, S. (2003) Mounds and Sediment Drift in the Porcupine Basin, West of Ireland. In: *European margin sediment dynamics: side-scan sonar and seismic images* (Ed. by J. Mienert and P. P. E. Weaver), Springer-Verlag, Heidelberg, 217-220.
- Hinsinger, V. (2002) Analyse et définition d'un module d'investigation sous-marine proche du fond. M.Sc. thesis. *Ensieta*, Brest, 49 pp.
- Hovland, M., Croker, P. F. & Martin, M. (1994) Fault-associated seabed mounds (carbonate knolls?) off western Ireland and north-west Australia. *Marine and Petroleum Geology*, **11**(2), 232-246.
- Huvenne, V. A. I. (2003) Spatial geophysical analysis of the Magellan carbonate build-ups and the interaction with sedimentary processes: key to a genetic interpretation? Ph.D. thesis, Department of Geology and Soil Science. *Ghent University*, Gent, 285 pp.
- Huvenne, V. A. I., De Mol, B. & Henriet, J.-P. (2003) A 3D seismic study of the morphology and spatial distribution of buried coral banks in the Porcupine Basin, SW of Ireland. *Marine Geology*, **198**, 5-25.
- Joseph, L., Rea, D. K., van der Pluijm, B. A. & Gleason, J. D. (2002) Antarctic environmental variability since the late Miocene: ODP Site 745, the East Kerguelen sediment drift. *Earth and Planetary Science Letters*, **201**, 127-142.
- Kenyon, N. H. (1987) Mass-wasting features on the continental slope of Northwest Europe. *Marine Geology*, **74**, 57-77.
- Kenyon, N. H., Akhmetzhanov, A. M., Wheeler, A. J., van Weering, T. C. E., de Haas, H. & Ivanov, M. K. (2003) Giant carbonate mud mounds in the southern Rockall Trough. *Marine Geology*, **195**, 5-30.
- Kenyon, N. H., Belderson, R. H. & Stride, A. H. (1978) Channels, canyons and slump folds between South-West Ireland and Spain. *Oceanologica Acta*, **1**(3), 369-380.
- Kenyon, N. H. & Hunter, P. (1998) Physiography of the Porcupine Seabight. In: *Cold water carbonate mounds and sediment transport on the Northeast Atlantic margin* (Ed. by N. H. Kenyon, M. K. Ivanov and A. M. Akhmetzhanov), UNESCO, Paris, IOC Technical Series, **52**, 22-23.
- Knutz, P. C., Jones, E. J. W., Austin, W. E. N. & van Weering, T. C. E. (2002) Glacimarine slope sedimentation, contourite drifts and bottom current pathways on the Barra Fan, UK North Atlantic margin. *Marine Geology*, **188**, 129-146.
- Lekens, W. (2000) Een studie van de driftsedimentatie in het Porcupine Bekken. M.Sc. thesis, Department of Geology and Soil Science. *Ghent University*, Gent, 93 pp.
- Llave, E., Hernandez-Molina, F. J., Somoza, L., Diaz-del Rio, V., Stow, D. A. V., Maestro, A. & Alveirinho Dias, J. M. (2001) Seismic stacking pattern of the Faro-Albufeira contourite system (Gulf of Cadiz): a Quaternary record of paleoceanographic and tectonic influences. *Marine Geophysical Researches*, **22**, 487-508.
- Manley, P. L. & Caress, D. W. (1994) Mudwaves on the Gardar Sediment Drift, NE Atlantic. *Paleoceanography*, **9**(6), 973-988.

- Massé, L., Faugères, J.-C. & Hrovatin, V. (1998) The interplay between turbidity and contour current processes on the Columbia Channel fan drift, Southern Brazil Basin. *Sedimentary Geology*, **115**, 111-132.
- Masson, D. G., Bett, B. J., Billet, D. S. M., Jacobs, C. L., Wheeler, A. J. & Wynn, R. B. (2003) The origin of deep-water, coral-topped mounds in the northern Rockall Trough, Northeast Atlantic. *Marine Geology*, **194**, 159-180.
- McCabe, A. M., Knight, J. & McCarron, S. (1998) Evidence for Heinrich event 1 in the British Isles. *Journal of Quaternary Science*, **13**(6), 549-568.
- McCave, I. N., Lonsdale, P., Hollister, C. D. & Gardner, W. D. (1980) Sediment transport over the Hatton and Gardar contourite drifts. *Journal of Sedimentary Petrology*, **50**(4), 1049-1062.
- McCave, I. N., Manighetti, B. & Beveridge, N. A. S. (1995) Circulation in the glacial North Atlantic inferred from grain-size measurements. *Nature*, **374**, 149-152.
- Mertens, K. (2002) Ruimtelijke en temporele patronen in paleoproductiviteit van kalkschalig nannoplankton en diatomeeën langs NE-Atlantische continentale randen. M.Sc. thesis, Department of Biology. *Ghent University*, Gent, 186 pp.
- Mienert, J. & Weaver, P. P. E. (2003) *European margin sediment dynamics: side-scan sonar and seismic images*. Springer-Verlag, Heidelberg, 305 pp.
- New, A. L., Barnard, S., Herrmann, P. & Molines, J.-M. (2001) On the origin and pathway of the saline inflow to the Nordic Seas: insights from models. *Progress in Oceanography*, **48**, 255-287.
- Nys, M. (2002) Onderzoek van de sedimentaire transit in het Gollum Canyon System in Porcupine Seabight, ten zuidwesten van Ierland. M.Sc. thesis, Department of Geology and Soil Science. *Ghent University, Belgium*, Gent, 85 pp.
- Pillen, S. (1998) Detailkartering en seismische analyse van de Magellan-mounds in het Porcupine Bekken, ten zuidwesten van Ierland. M.Sc. thesis, Department of Geology and Soil Science. *Ghent University*, Gent, 89 pp.
- Rebesco, M. & Stow, D. A. V. (2001) Seismic expression of contourites and related deposits: A preface. *Marine Geophysical Researches*, **22**(5-6), 303-308.
- Rice, A. L., Billet, D. S. M., Thurston, M. H. & Lampitt, R. S. (1991) The Institute of Oceanographic Sciences Biology programme in the Porcupine Seabight: background and general introduction. *Journal of the Marine Biological Association of the United Kingdom*, **71**, 281-310.
- Richter, T. O., Lassen, S., van Weering, T. C. E. & de Haas, H. (2001) Magnetic susceptibility patterns and provenance of ice-rafted material at Feni Drift, Rockall Trough: implications for the history of the British-Irish ice sheet. *Marine Geology*, **173**, 37-54.
- Roberts, D. G. (1975) Marine geology of the Rockall Plateau and Trough. *Phil. Trans. Roy. Soc. A*, **278**, 447-509.
- Roberts, D. G. & Kidd, R. B. (1979) Abyssal sediment wave fields on Feni Ridge, Rockall Trough: long-range sonar studies. *Marine Geology*, **33**, 175-191.
- Scourse, J. D., Hall, I. R., McCave, I. N., Young, J. R. & Sugdon, C. (2000) The origin of Heinrich layers: evidence from H2 for European precursor events. *Earth and Planetary Science Letters*, **182**, 187-195.
- Shanmugam, G. (1997) The Bouma Sequence and the turbidite mind set. *Earth-Science Reviews*, **42**(4), 201-229.
- Shanmugam, G. (2000) 50 years of the turbidite paradigm (1950s-1990s): deep-water processes and facies models-a critical perspective. *Marine and Petroleum Geology*, **17**, 285-342.
- Stow, D. A. V., Faugères, J.-C., Howe, J. A., Pudsey, C. J. & Viana, A. R. (2002a) Bottom currents, contourites and deep-sea sediment drifts: current state-of-the-art. In: *Deep-Water Contourite Systems: Modern Drifts and Ancient Series, Seismic and Sedimentary Characteristics* (Ed. by D. A. V. Stow, C. J. Pudsey, J. A. Howe, J.-C. Faugères and A. R. Viana), Geological Society, London, *Memoirs*, **22**, 7-20.

- Stow, D. A. V. & Holbrook, J. A. (1984) North Atlantic contourites: an overview. In: *Fine Grained Sediments, Deep-Water Processes and Facies* (Ed. by D. A. V. Stow and D. J. W. Piper), Geological Society, London, Special Publication, **15**, 245-256.
- Stow, D. A. V. & Johansson, M. (2000) Deep-water massive sands: nature, origin and hydrocarbon implications. *Marine and Petroleum Geology*, **17**, 145-174.
- Stow, D. A. V. & Lovell, J. B. P. (1979) Contourites: Their Recognition in Modern and Ancient Sediments. *Earth-Science Reviews*, **14**, 251-291.
- Stow, D. A. V. & Mayall, M. (2000) Deep-water sedimentary systems: New models for the 21st century. *Marine and Petroleum Geology*, **17**, 125-135.
- Stow, D. A. V. & Piper, D. J. W. (1984) Deep-water fine-grained sediments: facies models. In: *Fine Grained Sediments, Deep-Water Processes and Facies* (Ed. by D. A. V. Stow and D. J. W. Piper), Geological Society, London, Special Publication, **15**, 611-646.
- Stow, D. A. V., Pudsey, C. J., Howe, J. A., Faugères, J.-C. & Viana, A. R. (2002b) *Deep-Water Contourite Systems: Modern Drifts and Ancient Series, Seismic and Sedimentary characteristics*. Geological Society, London, Memoirs, **22**, 464 pp.
- Van Herreweghe, K. (1999) Sequentiestratigrafie met hoge-resolutie seismiek van de Belgica-Mounds zone in het Porcupine Bekken, ten zuidwesten van Ierland. M.Sc. thesis, Department of Geology and Soil Science. *Ghent University*, Gent, 76 pp.
- Van Landeghem, K. (in prep.) Een multidisciplinaire study van het Gollum kanalen systeem. M.Sc. thesis, Department of Geology and Soil Science. *Ghent University*, Gent.
- Van Rooij, D. (1998) Sequentie-stratigrafie met hoog-resolutie-seismiek aan de rand van de Keltische Zee en het Porcupine Bekken, ten zuidwesten van Ierland. M.Sc. thesis, Department of Geology and Soil Science. *Ghent University*, Gent, 103 pp.
- van Weering, T. C. E., Andersen, H. L., van Breukelen, M., Croker, P. F., Grehan, A., de Haas, H., Kouvaev, I., Mienis, F., Norbert, F., Olu-Le Roy, K., Shannon, P. M., de Stigter, H. C., Taberner, C., Vonhof, H. & Wheeler, A. J. (in press) Carbonate mounds in margin settings: is the present the key to the past? In: *Modern Carbonate Mound Systems: A window to Earth History* (Ed. by J.-P. Henriët and C. Dullo), Springer-Verlag, Heidelberg.
- Viana, A. R., Faugères, J.-C. & Stow, D. A. V. (1998) Bottom-current-controlled sand deposits - a review of modern shallow- to deep-water environments. *Sedimentary Geology*, **115**, 53-80.
- Wheeler, A. J., Beyer, A., Freiwald, A., de Haas, H., Huvenne, V. A. I., Kozachenko, M. & Olu-Le Roy, K. (in press) Morphology and Environment of Deep-water Coral Mounds on the NW European Margin. In: *Modern Carbonate Mound Systems: A window to Earth History* (Ed. by J.-P. Henriët and C. Dullo), Springer-Verlag, Heidelberg.
- Wheeler, A. J., Kenyon, N. H., Ivanov, M. K., Beyer, A., Cronin, B., McDonnell, A., Schenke, H. W., Akhmetzhanov, A. M., Satur, N. & Zaragosi, S. (2003) Canyon Heads and Channel Architecture of the Gollum Channel, Porcupine Seabight. In: *European margin sediment dynamics: side-scan sonar and seismic images* (Ed. by J. Mienert and P. P. E. Weaver), Springer-Verlag, Heidelberg, 183-186.
- White, M. (in press) The hydrographic setting for the carbonate mounds of the Porcupine Bank and Sea Bight. In: *Modern Carbonate Mound Systems: A window to Earth History* (Ed. by J.-P. Henriët and C. Dullo), Springer-Verlag, Heidelberg.
- Zaragosi, S., Eynaud, F., Pujol, C., Auffret, G. A., Turon, J.-L. & Garlan, T. (2001) Initiation of the European deglaciation as recorded in the northwestern Bay of Biscay slope environments (Meriadzek Terrace and Trevelyan Escarpment): a multi-proxy approach. *Earth and Planetary Science Letters*, **188**, 493-507.

## Chapter II: Geological and environmental setting

### 2.1 Geologic setting

The Porcupine Seabight can be considered as an amphitheatre-shaped embayment in the Atlantic Irish shelf, off the southwestern coast of Ireland (Fig. 1.1). It has a triangular shape with the longest side (320 km) oriented roughly north-south. It widens from approximately 65 km in the north, up to 100 km in the south. The water depth gradually increases from 200 m in the northeast, to 3000 m in the southwest, where the seafloor slopes down to the Porcupine Abyssal Plain to depths of 4000 m. The main slope gradient of the Porcupine Seabight averages about 0.5°. Slightly steeper slopes are encountered in the eastern part, varying from 1.7° near the Gollum channel system up to 4.0° near the Kings channels.

The Seabight is enclosed by 4 shallow platforms (Figs. 1.1 and 2.1): Porcupine Bank and Porcupine Ridge on the western side, Slyne Ridge in the northeast, the Irish Mainland Shelf in the east and the terraced Goban Spur in the south (Naylor & Shannon, 1982). The only opening towards the Porcupine Abyssal Plain lies between the Porcupine Bank and Goban Spur. The Porcupine Seabight is the surface expression of the underlying deep sedimentary Porcupine Basin, which is a failed rift of the proto-North Atlantic Ocean, filled in with a 10 km thick series of Mesozoic and Tertiary sediments (Masson & Miles, 1986; Moore & Shannon, 1991).

In the following sections, the geological development of the basin will be reviewed, focussing on the dominating tectonic and sedimentary processes. The basin evolution can be summarized in three major steps: a Paleozoic *syn-rift phase*, a predominantly Jurassic *rifting episode* and a Late Cretaceous to recent *thermal subsidence period*. Because the hydrocarbon exploration within the Porcupine Basin contributed largely to the understanding of its geology, a review is provided of the exploration history, the major source rocks and the significance of hydrocarbons in the Porcupine Basin.

#### 2.1.1 Basin development

Like most of the Irish and British offshore basins, the development of the Porcupine Basin started under a tensional structural regime of an opening North Atlantic Ocean (Naylor & Shannon, 1982). During an entire rifting period of probably 30 to 40 Ma, three rifting episodes are known for the Porcupine Basin; (1) Permo-Triassic, (2) Middle to Late Jurassic and (3) Early Middle Cretaceous (Johnston *et al.*, 2001; Reston *et al.*, 2001).

##### 2.1.1.1 Basement and pre-rift sedimentation

Before the opening of the Atlantic, the future Porcupine Basin area was located in a central position of the super-continent of Pangaea (Johnston *et al.*, 2001). The bounding shallow crystalline basement platforms (Fig. 2.1) are composed of Precambrian and Lower Paleozoic metamorphic rocks, forming a continental crust of approximately 30 km thickness (Naylor & Shannon, 1982; McCann *et al.*, 1995a).

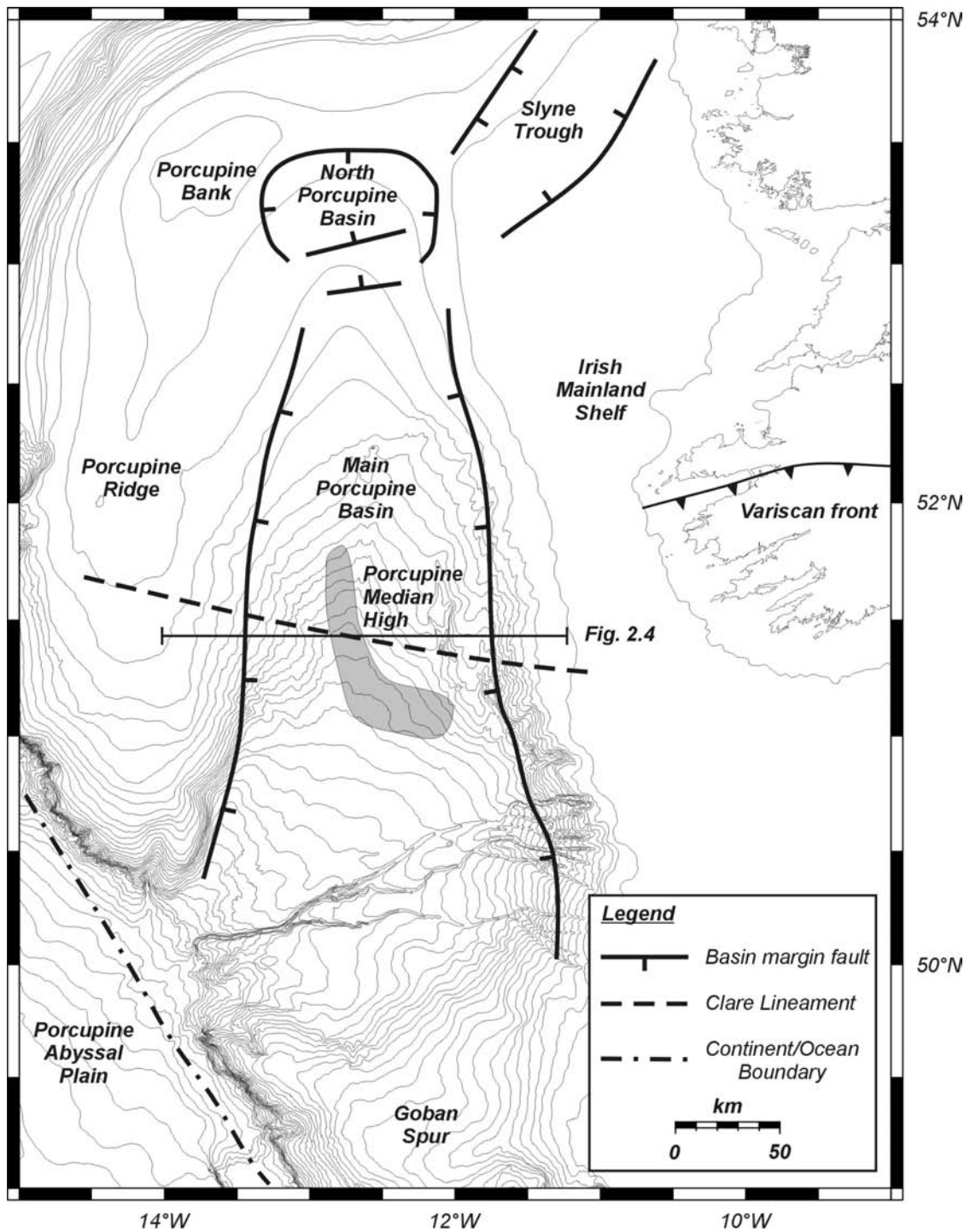


**Figure 2.1:** Sketch map of the Porcupine Seabight illustrating the main structural elements after Naylor & Shannon (1982), Ziegler (1982), Shannon (1991), Moore & Shannon (1995) and Reston et al. (2001).

Because the greater part of the basin is located north of the main Variscan deformation front, it has known a lesser degree of metamorphism than time-equivalent rocks of the southern basins (Naylor & Shannon, 1982; Shannon, 1991).

The pre-rift succession commences with probably Devonian clastic sediments, overlain with Lower Carboniferous (Dinantian) carbonates and clastics. The Upper Carboniferous rocks feature deltaic to shallow-marine deposits with Westphalian coal-bearing sandstones and shales and possibly Stephanian redbed sandstones (Naylor & Shannon, 1982; Ziegler, 1982; McCann *et al.*, 1995a).

#### **2.1.1.2 Permo-Triassic early rifting phase**

During this period (Fig. 2.2), a first minor east-west regional extension regime is inferred by the development of a series of small rift basins (Shannon, 1991; Moore & Shannon, 1992; Moore & Shannon, 1995). The fault trends predominantly exhibit NE-SW directions as a result of the reactivation of both Caledonian and Variscan structural lineaments (Johnston *et al.*, 2001).

The lowest Mesozoic deposits were interpreted by Naylor & Shannon (1982) as early rift-valley continental sediments, which can have a thickness of over 2 km. According to McCann *et al.* (1995a) they unconformably overlie Carboniferous strata. Within Permian times, predominantly fluvial and lacustrine sedimentation took place with non-marine mixed clastic deposits and evaporites (Fig. 2.3). Triassic sediments contain non-marine to marine facies (Ziegler, 1982; Shannon, 1991).

#### **2.1.1.3 Lower Jurassic quiet period**

The Lower Jurassic (Lias) is characterized by a tectonic tranquil period and a relative sea level rise, resulting in a marine sedimentary environment (Shannon, 1991). Lower Jurassic deposits are not found over the entire basin, but could comprise limestones and rare organic-rich shales with sandstones (Fig. 2.3). Triassic and Liassic strata are almost always absent, with an exception in the extreme north of the basin (Ziegler, 1982; Naylor & Shannon, 1982; Spencer & MacTiernan, 2001).

#### **2.1.1.4 Middle and Upper Jurassic crustal extension**

At the end of the Lower Jurassic period, the *Middle Kimmerian* rifting phase marked an increase of tectonic events in the Arctic, Atlantic and Thetys rift systems. Especially in the Atlantic domain, it was responsible for the acceleration of crustal extension and the onset of sea floor spreading. This major tectonic event was apparently accompanied by a renewed eustatic lowering of the sea-level and can be held responsible for the erosion of a large part of the Triassic and Liassic deposits (Fig. 2.3) (Ziegler, 1982; Naylor & Shannon, 1982).

Subsequently, during the Middle Jurassic the extension changed from NE-SW to E-W (Fig. 2.2). As a consequence, the small Permo-Triassic rift basins became redundant and the basin took on its present north-south alignment (Shannon, 1991; McCann *et al.*, 1995a). During this main rift phase faulting was extensive with predominant large faults, particularly along the eastern and western margins. The orientations are mainly parallel to the basin margins, although more variability is encountered in the north (McCann *et al.*, 1995b).

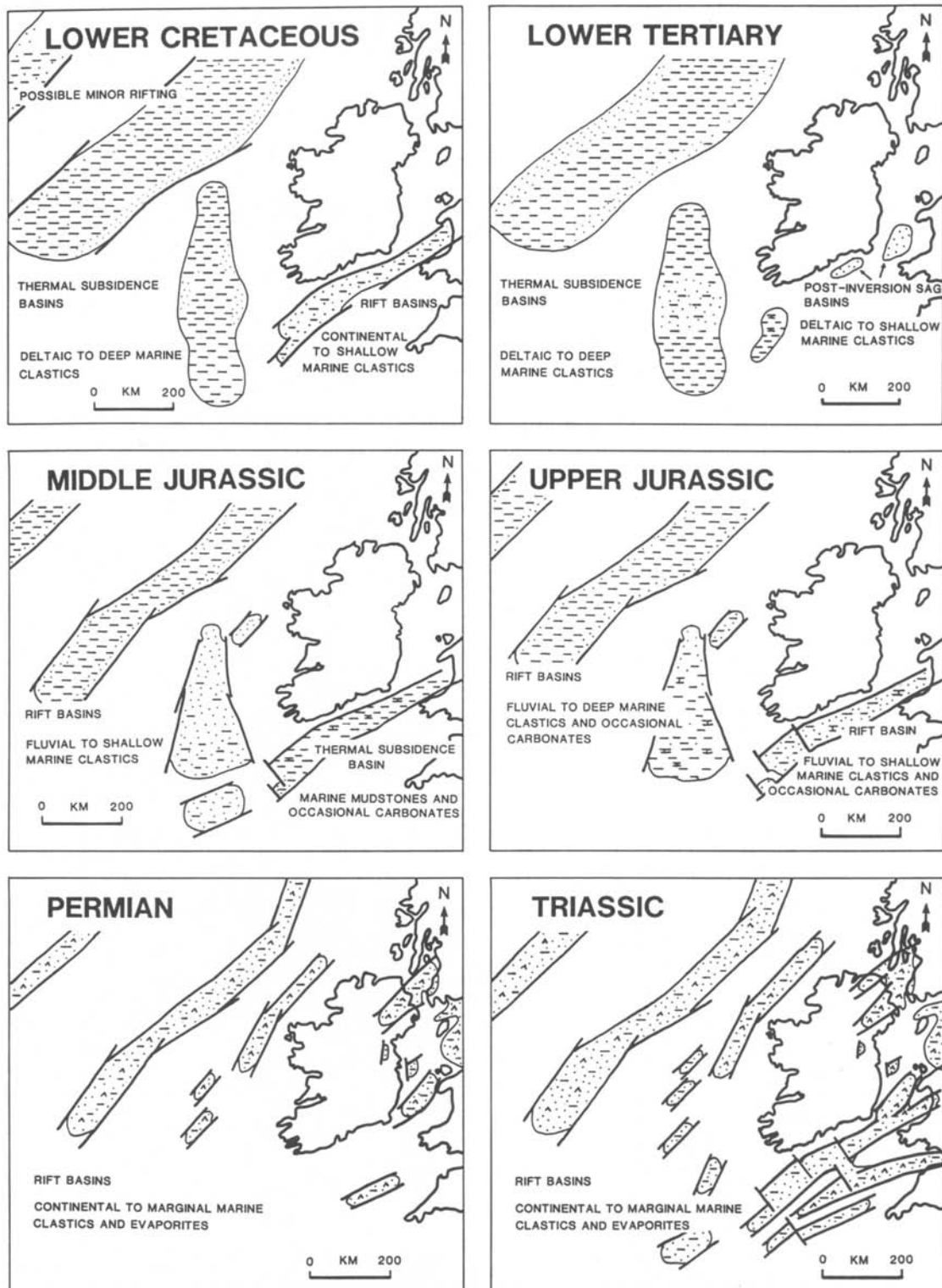


**Figure 2.2:** Generalized tectosedimentary maps illustrating the development of the Irish offshore sedimentary basins from Permian to Lower Tertiary times. The thick lines indicate fault control on the basin development (Shannon, 1991).

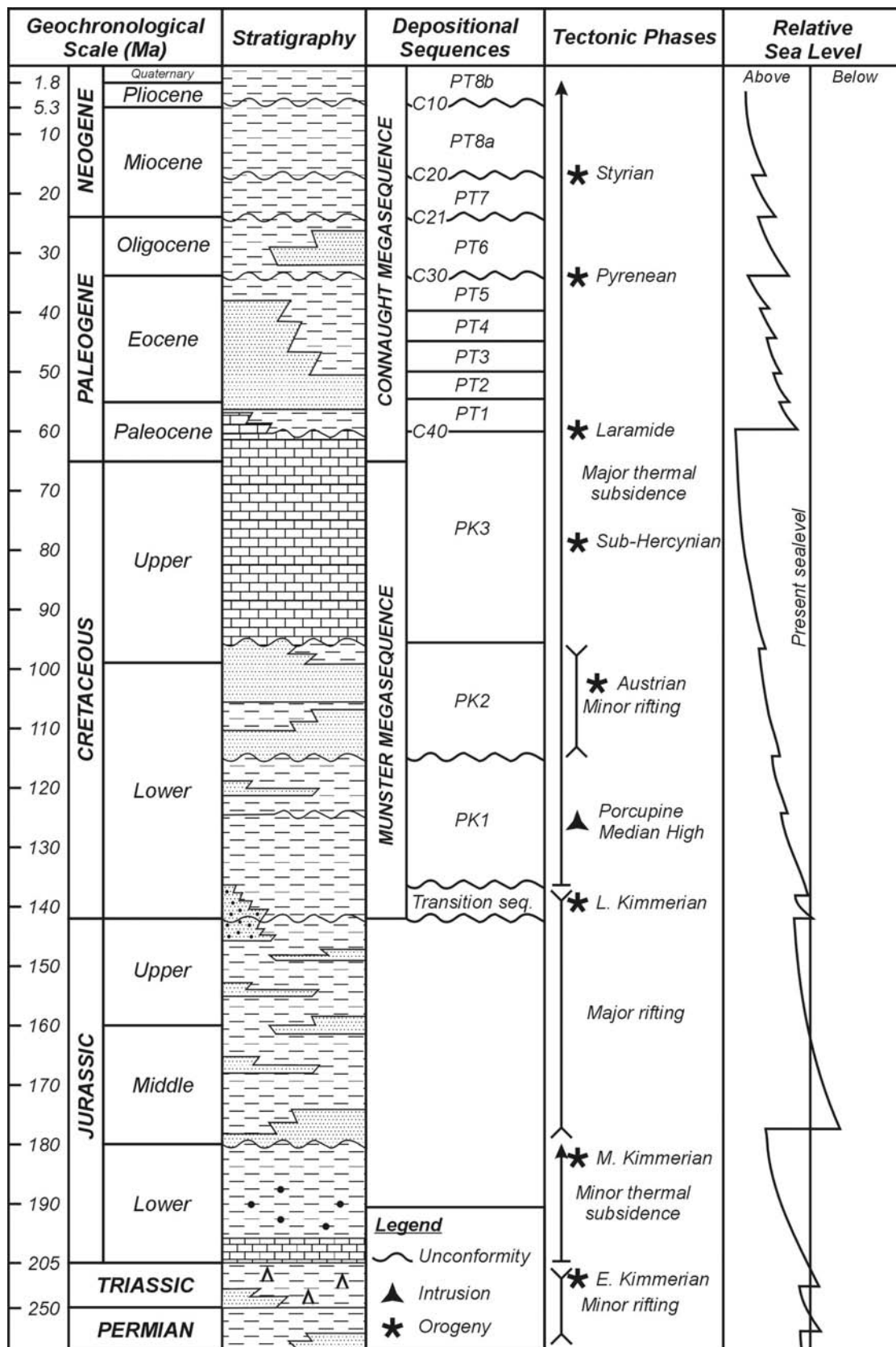


**Figure 2.3:** Generalized stratigraphy, tectonic history and relative sea-level changes in the Porcupine Basin after Ziegler (1982), Shannon (1991), Moore & Shannon (1995) and McDonnell & Shannon (2001).

Middle Jurassic fluvial claystones and minor sandstones might lie unconformably over earlier deposited strata and can be considered as products of this major rifting episode. The sandstones are more likely to be found near the margins, grading southwards into deltaic and marine deposits like marine shales and carbonates (Naylor & Shannon, 1982; Shannon, 1991).

During the Upper Jurassic, differential subsidence was responsible for the transition of a continental to a shallow marine sedimentary environment in the Porcupine Basin (Naylor & Shannon, 1982). These transgressive sediments, with rapidly varying facies, accumulated (onlap) on the symmetrical, block-faulted structure of the Porcupine Basin (Fig. 2.4), clearly observed in the north (Spencer & MacTiernan, 2001). According to McCann *et al.* (1995a) shallow-marine fans and scarp deposits were developed close to the basin margins, while within the centre of the basin deep-water sand-rich mass flow deposits can be found interdigitating with the background hemipelagic sedimentation. The uppermost Jurassic strata (Tithonian) show the effect of a last rifting phase with more movement on the edges of the basins and on intrabasinal fault blocks (Shannon, 1991). These continuous series were topped by an unconformity of latest Jurassic age, due to the *Late Kimmerian* tectonic phase.

### **2.1.1.5 Post-rift structure of the Porcupine Basin**

At the start of the Cretaceous, the general structure of the Porcupine Basin could be compared with a rift structure prior to break-up (Reston *et al.*, 2001). Its specific failed rift structure, showing a typical *steer's head profile* (Fig. 2.4), allowed the deposition of up to 10 km of sediments during the Mesozoic and Cenozoic (Moore & Shannon, 1991). In contrast with most other Irish offshore basins, the Porcupine Basin has a north-south trend, oblique to both Caledonian and Variscan structural trends. The newly formed oceanic crust is relatively thin from about 5 km to as little as 2 km and is more pronounced in the southern end (Naylor & Shannon, 1982; Masson & Miles, 1986; Shannon, 1991; McCann *et al.*, 1995a). Apart from some ash-fall tuffs, no syn-rift igneous rocks have been drilled in the Porcupine Basin. Therefore, no direct evidence is found for any syn-rift igneous activity within the basin (Reston *et al.*, 2001).

The deep margins of the Porcupine Basin are characterised by rotated fault blocks, formed as extensional features during the crustal extension (Fig. 2.4). Most of the normal faults encountered in the basin have a NW-SE and N-S to NE-SW trend. The NW-SE faults are parallel with the ocean-continent transition SW of the PSB, related to the Early Cretaceous North Atlantic rifting period. The other faults, which are more dominant in the Main Porcupine Basin (MPB), are similar to those of the former Permo-Triassic basins. It is suggested this was due to the reactivation of the early Mesozoic trends during a final Early Cretaceous rifting event. However, these faults are not considered to be extending deeply into the crust and most of them can be classified as tectonic growth faults (Masson & Miles, 1986; Shannon, 1991; Bailey *et al.*, 2003).

Two structural features seem to influence the post-rift sedimentation. An east-west ridge located at 53°N separates the Main Porcupine Basin from the smaller North Porcupine Basin (Fig. 2.1). This fault-bounded platform has been associated with a geothermal anomaly, suggesting relatively recent movement facilitating fluid passage from the depth. This structure was thought to be active during both

Carboniferous and Late Cretaceous times (Naylor & Shannon, 1982; Shannon, 1991; Moore & Shannon, 1992). A second structural feature is recognized by a break within the gravimetric and magnetic data as a NW-SE trending line at about 51°30'N within the MPB (Shannon, 1991; McCann *et al.*, 1995a). This break has been called the *Clare Lineament* and is believed to be the continuation of the adjacent North Atlantic Charlie Gibbs Fracture Zone (Naylor & Shannon, 1982). South of this lineament, the main Cenozoic units seem to be indicating a uniform subsidence and sedimentation along the main basin axis. In the north, the sedimentary succession is considerably thinner. Naylor & Shannon (1982) attribute this to the large “trapdoor” function of the Main Porcupine Basin, which has a greater down-faulting and resulting sedimentary infill.

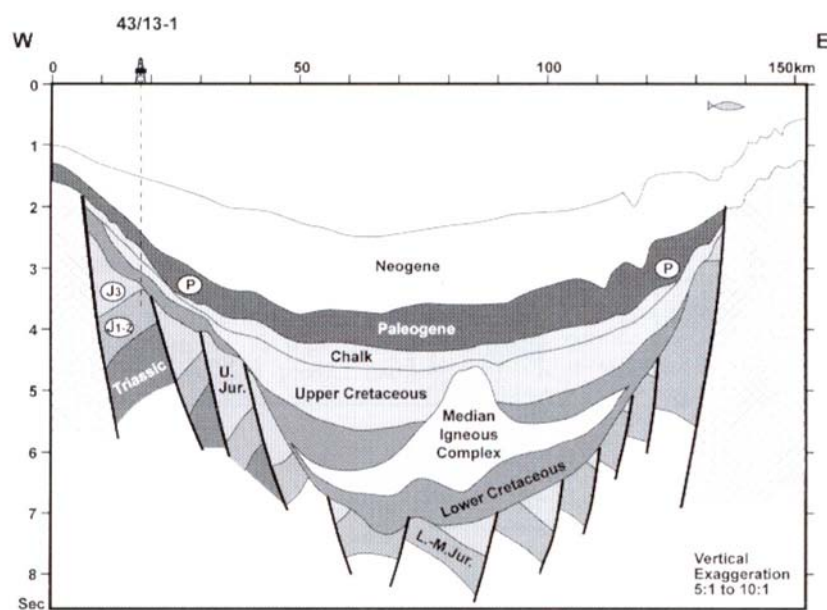


**Figure 2.4:** Geological profile showing the plays of the southern Porcupine Basin. See figure 2.1 for location. The hydrocarbon plays are identified with a letter; P, Paleocene; J3, Upper Jurassic; J1-2 Lower-Middle Jurassic (Spencer & MacTiernan, 2001).

### 2.1.2 Post-rift thermal subsidence

After the main Jurassic rifting phase, the Cretaceous marked the start of a period of thermal subsidence within the Porcupine Basin (Figs. 2.2 and 2.3). During this episode a large number of faults with a small individual throw were generated. Their distribution is interpreted in terms of a normal thermal subsidence combined with basin margin uplift and an accelerated basin centre subsidence due to ridge-push effects in the Atlantic (McCann *et al.*, 1995b). The sediments that were deposited during this period are of Cretaceous to Recent age and can have a thickness in excess of 5 km (Naylor & Shannon, 1982; Masson & Miles, 1986). During most of this period a marine sedimentation environment was present and the overall Tertiary deposits are broadly found to onlap upon the margins of the basin (Moore & Shannon, 1991; McDonnell & Shannon, 2001).

The increased climatologic and plate-tectonic reorganizations since the Paleogene also had their consequences on the deep-water circulation and the

sedimentation within the North Atlantic basins and the Porcupine Basin. Most of the post-rift sediments are dominantly sandstones and shales, influenced by frequent sea-level fluctuations. In contrast to the Celtic Sea Basins, the Lower Paleocene deposits of the Porcupine Basin only underwent a minimal inversion influence caused by the Alpine Orogeny (Naylor & Shannon, 1982; Stow, 1982; Masson & Miles, 1986; Shannon, 1991).

Moore & Shannon (1992) recognise 12 sequences during this post-rift period, grouped into two megasequences; the Cretaceous *Munster megasequence* and the Tertiary *Connaught megasequence* (Fig. 2.3). A more detailed study of the Connaught megasequence was performed by McDonnell & Shannon (2001), correlating the Tertiary stratigraphy of the Porcupine Basin with the Rockall Trough, in accordance with Stoker *et al.* (2001).

### 2.1.2.1 Cretaceous transition

The Cretaceous succession, up to 4 km thick, is subdivided into three sequences **PK1**, **PK2** and **PK3**, all preceded by a **Transition sequence** (Fig. 2.3). The faults within these sequences are predominantly north-south trending and are broadly distributed around the north-south axis (McCann *et al.*, 1995a). Faulting generally decreased with time through the Cretaceous (Moore & Shannon, 1995).

A major rifting pulse within the Lower Cretaceous, referred to as the *Late Kimmerian* tectonism, affected the entire NW European and Arctic-North Atlantic rift system. It preceded the Lower Cretaceous onset of sea-floor spreading between the Azores and the Charlie Gibbs Fracture Zones. This pulse was accompanied by a significant eustatic sea-level fall (Haq *et al.*, 1987) and gave rise to a regional unconformity that is largely of submarine nature (Ziegler, 1982). As in many of the Irish offshore basins, the base of the Cretaceous is marked by this undulatory unconformity where marine strata are found to onlap upon Jurassic sequences (Shannon, 1992). The contemporaneous **Transition Sequence** however, is only found in some confined subbasins of the MPB, filled with clastic fans (Moore & Shannon, 1992).

The Lower Cretaceous deposits belong to the **PK1 Sequence** and are still deposited on the wedge-shaped subbasins (Masson & Miles, 1986; Moore & Shannon, 1992). In the northern part of the MPB, these deposits are northwards-onlapping deep-sea sandstones on the Late Kimmerian unconformity (Fig. 2.2). A sea-level fall was responsible for the development of an emergent platform with shale and sandstone series on the surrounding slope due to the erosion of this platform (Naylor & Shannon, 1982). These series are observed as southward prograding deltas and fan-deltas, found along the northern, southeastern and southwestern margins of the basin (Moore & Shannon, 1992).

Within the Lower Cretaceous sedimentary succession, Masson & Miles (1986) reported the presence of a large igneous body north of 51°N (Figs. 2.1 and 2.4). It is marked by an axial gravity high and a negative magnetic anomaly. Therefore, it has been attributed a high-density, basic igneous composition. The morphology of this feature on deep seismic profiles indicated this might be a volcanic ridge, hence called the *Porcupine Median Volcanic Ridge* with a suggested age of Early Aptian or older (Shannon, 1991; Moore & Shannon, 1992). However, recent interpretations consider a non-volcanic origin, suggesting this ridge might be related to mantle

serpentinization effects (Spencer & MacTiernan, 2001). Reston *et al.* (2001) proposed the more neutral term of *Porcupine Median High*.

During the Upper Cretaceous, first pulses of early actual North Atlantic sea-floor spreading were assumed. Paleogeographically, the Porcupine Basin was adjacent to Orphan Knoll, Flemish Cap and Goban Spur. All of these basins had a similar Mesozoic sedimentation history. The initiation of the spreading occurred according to Naylor & Shannon (1982) south of the Charlie Gibbs Fracture Zone (along the Newfoundland-Porcupine sector). Later on, the spreading migrated northwards along the Labrador-Rockall sector. During middle Upper Cretaceous times, spreading along the North Atlantic Newfoundland-Porcupine axis resulted in the start of the separation of the Porcupine Basin and the Rockall Trough from the eastern North American basins (Naylor & Shannon, 1982).

The Albian **PK2 sequence** is affected by a minor rifting pulse that started within the Late Aptian (Shannon, 1991; Moore & Shannon, 1995). During this rifting period, faults were more localised and concentrated in the north of the basin, with predominant N-S orientations (McCann *et al.*, 1995b). According to McDonnell & Shannon (2001) the basin flank uplift occurred in response to regional extension and sea-floor spreading between the Bay of Biscay and Newfoundland. This local uplift of the basin margins produced a regressive period with an outer shelf deltaic sedimentation environment (Moore & Shannon, 1991; Moore & Shannon, 1992). The deltaic facies was well-developed along the northern and southeastern margins of the basin with locally sand-rich deltas and associated beach complexes (McCann *et al.*, 1995a). Some deep marine turbidites and mass-flow deposits, together with clastic fans associated with fault scarps, were described by Moore & Shannon (1992). While the basal boundary of this sequence is relatively flat, its upper boundary (Base Chalk) is erosive in places, especially towards the southeastern and southwestern margins (Moore & Shannon, 1995). In these times, MPB was still separated from the Northern Porcupine Basin by an east-west trending horst block.

The onset of the Upper Cretaceous **PK3 sequence** was characterized by a further relative sea-level rise. Early PK3 deposits feature offshore sandstone bars, followed by a northward thinning and onlapping outer shelf to slope sequence of carbonates (Naylor & Shannon, 1982). This contains the chalk facies that was deposited over almost the entire NW European margin. Some evidence of chalk turbidites was found along the margins of the MPB (Moore & Shannon, 1992). Along the southwestern and southeastern margins of the basin, Moore & Shannon (1995) recognised the presence of biohermal reef build-ups. Moreover, some features on reflection seismic profiles suggest the presence of strong bottom currents. After the deposition of the chalk facies, the seafloor is considered to have been relatively flat. An estimated thickness of 600 m is inferred on the margins, while 1000 m could be observed in the centre (Naylor & Shannon, 1982; McDonnell & Shannon, 2001).

#### **2.1.2.2 Paleocene-Eocene deltaic sedimentation**

The transition from Upper Cretaceous to Lower Paleocene is characterized by a high-amplitude reflector, known as the *Top Chalk* reflector, defined as **C40** by McDonnell & Shannon (2001). It marks the change from the carbonate to clastic deposition (Shannon, 1992). In general, the Paleocene succession is more mud dominated, whereas the main coarse clastic input occurred in the Middle Eocene to earliest Late Eocene times (McDonnell & Shannon, 2001).

The Paleocene-Eocene can be subdivided into 5 sequences **PT1** to **PT5** (Fig. 2.3). Within PT1 to PT4, every sequence is characterized by a southerly prograding complex deltaic event overlain by marine transgressive deposits (Moore & Shannon, 1992). According to Shannon (1992), the fans are located towards the edges of the basin, deposited in times of eustatic fall or lowstand. These deposits can be built up from north to south along the axis of the MPB, but also from west to east (fault-related). The deltas typically display sandy topsets and shale-dominant fore- and bottomsets (Naylor & Shannon, 1982). This gave way for deeper marine strata in the south with shales and sandstones interpreted as submarine fan turbidites and contourites (Shannon, 1991; McCann *et al.*, 1995a).

The controls on the relative rises and falls in sea level are dominantly due to the North Atlantic plate tectonic regime. A Late Paleocene tensional pulse affected the North Sea area and the Atlantic shelves of Scotland and Ireland and preceded sea-floor spreading in areas north of Charlie Gibbs Fracture Zone. This *Laramide pulse* was associated with a major sea-level fall, inducing drastic paleogeographic changes in Western and Central Europe (Ziegler, 1982). Furthermore, a significant phase of rapid basin subsidence was shown for the Eocene. This could be an effect of the sea floor spreading within the Greenland Sea. This ridge-push effect could produce non-faulted basin margin uplift and provides sediment source areas and rapid basin subsidence (Moore & Shannon, 1992).

The Upper Eocene is marked by a further sea level rise, with the development of offshore bar sandstones (Naylor & Shannon, 1982). The Late Eocene **sequence PT5**, differs from previous sequences in a deep-marine mudstone facies. No prograding wedges are observed, suggesting a tranquil deep water sedimentation environment (Moore & Shannon, 1992).

A major basin-wide unconformity has been developed in the latest Eocene to Early Oligocene time and has been correlated with the designated **C30** event in the Rockall Trough described by Stoker *et al.* (2001). This unconformity marks the start of the onset of a deep-water sedimentation and the establishment of regional contour-hugging bottom currents (McDonnell & Shannon, 2001).

### **2.1.2.3 Oligocene-Neogene deep-marine environment**

Within the Late Paleogene and the Neogene, a passive uplift of the Norwegian, British and Irish landmasses was very important in shaping the present day Atlantic margin. Although the origin of this uplift remains unclear, it probably resulted in the enhancement of contour currents, causing local erosion and deposition and the increased probability of sedimentary slide and slumps. Therefore, the overall Oligocene and Neogene sedimentation is characterized by an alongslope transport and redepositional processes yielding contourite siltstones and mudstones and (hemi)pelagic deep marine sediments, caused by a combination of differential basin subsidence and regional sea level and paleoclimate changes (McDonnell, 2001; Spencer & MacTiernan, 2001; Bailey *et al.*, 2003). Moore & Shannon (1992) subdivided the Eocene to Oligocene sediments into three sequences **PT6** to **PT8** (Fig. 2.3), which were further described by McDonnell (2001).

Moore & Shannon (1991), Moore & Shannon (1992) and McCann *et al.* (1995a) describe frequent sediment slumping during the Oligocene and Miocene, especially within sequences **PT6** and **PT7**. Many faults, related with syn-

sedimentary slumping, have been observed on a Middle Miocene horizon within the southern part of the MPB. Among the many possible causes of these instabilities, it is suggested that the rapid basin subsidence together with the high sedimentation rates built a relatively unstable sediment pile. Slumping could be triggered by reactivation of the syn-rift faulting system, or by a sea-level fall.

The base of the **PT6 sequence** is characterized by the high-amplitude continuous **C30** reflector, while the top reflector is the erosive base Miocene **C21** reflector. Within this Oligocene succession, a reworked Eocene microfauna has been described, suggesting shelfal incision or reworking by bottom currents. These Oligocene deposits are interpreted as a sediment drift (Shannon, 1992; McDonnell, 2001). Moore & Shannon (1991) also report submarine canyon development in the Oligocene.

Within **sequence PT8**, a slope-parallel sediment drift is described within the SE of the basin. The **C20** reflector, which forms the lower boundary of PT8, is related with a relative sea-level fall and is noticeably erosive in the south of the basin (McDonnell & Shannon, 2001). This intensified scouring may be related with intensified bottom current activity elsewhere in the North Atlantic (Stoker *et al.*, 2002). It is thought that this current flowed in a counter-clockwise direction.

The youngest unconformity mapped in the Porcupine Basin is correlated with the Early Pliocene **C10** event described by Stoker *et al.* (2001) in the Rockall Basin. This event is considered as nucleation site for present-day coral banks (McDonnell & Shannon, 2001; De Mol *et al.*, 2002).

#### **2.1.2.4 Introduction to the Quaternary sedimentary environment**

Prior to the start of the EC-FP5 projects studying the cold and deep-water coral banks, little was known concerning the Quaternary evolution of the PSB. The recent sedimentation is mainly pelagic to hemipelagic, although (probably reworked) foraminiferal sands can be found on the upper slope of the eastern continental margin (Rice *et al.*, 1991). The main sediment supply zone is probably located on the Irish and Celtic shelves, while the input from the Porcupine Bank seems to be rather limited (Rice *et al.*, 1991). In contrast to the slopes of the Celtic and Armorican margins, which are characterised by a multitude of canyons and deep-sea fans (Kenyon *et al.*, 1978; Zaragosi *et al.*, 2000; Auffret *et al.*, 2002), the east-west oriented Gollum channels are the only major downslope sediment transfer system located on the south-eastern margin of the Seabight (Kenyon *et al.*, 1978; Tudhope & Scoffin, 1995; Wheeler *et al.*, 2003) which discharges directly into the Porcupine Abyssal Plain (Akhmetzhanov *et al.*, 2003). Rice *et al.* (1991) and Wheeler *et al.*, (2003) suggest that the present-day channels are inactive. Although Akhmetzhanov *et al.* (2003) report a subtle expression of a channel-levee system, there is little evidence of a deep-sea fan. According to Rice *et al.* (1991) sediments may have been reworked and redistributed in drift deposits by strong bottom currents sweeping the Porcupine Abyssal Plain.

According to Games (2001) and Mathys (2001), the upper slope of the northern PSB bears the presence of predominantly north-south trending ploughmarks on several levels within the Quaternary sedimentary succession. Also smaller ploughmarks are observed and interpreted as the Quaternary abrasion of the continental shelf caused by floating ice grounding on the sea bed. An abundance

of pockmarks is also apparent on the sea bed of this area. Within some of these Connemara pockmarks, an associated fauna of the cold-water coral *Lophelia sp.* has been observed (Games, 2001). Together with *Madrepora sp.*, *Lophelia sp.* is found along the entire NW European margin, manifested by coral patches to giant coral banks. A more comprehensive review of the geology and ecology of these coral banks, within and outside the Porcupine Seabight is presented in a separate section below.

### **2.1.3 Hydrocarbon exploration**

#### **2.1.3.1 Exploration history**

Since the early 1960's there has been an enormous increase in geological knowledge resulting from investments by exploration companies, related to the discovery of hydrocarbons in Irish Mesozoic to Tertiary basins. The exploration of the deeper British and Irish basins only started after the major oil discoveries in the North Sea about 1969. First seismic reconnaissance campaigns within the Porcupine Basin were carried out in 1971. In 1976 the first exploration licenses were granted by the Irish government for the Porcupine Basin. A first well was drilled in 1977 by Shell at a water depth of 482 m (Naylor & Shannon, 1982). By 1978, already 15 wells had been drilled offshore Ireland (Croker & Shannon, 1995). Since the mid 80's, two to six wells have been drilled each year in the Irish offshore sector (Croker & Shannon, 1995). Most of these wells have been drilled in the northern region of the Porcupine Basin (Moore & Shannon, 1995). However, as the results of the exploration in the Irish basins turned out to be rather disappointing, already by the early 1990's the exploration within most of the Irish basins had slowed down (Shannon *et al.*, 2001). Due to the 'Merger mania' during the mid-nineties, the enlarged companies gained a renewed interest in the deep water Irish Atlantic margin basins (Shannon *et al.*, 2001). In 2001, the main focus of exploration activity was concentrated in the Porcupine and other deep basins west of Ireland. Although the potential of the Irish frontier basins is still generally recognized by the industry, Ireland is at a disadvantage in having relatively unproven deep water plays. Other so-called major exploration risks are the lack of information on likely reservoirs in the southern Porcupine Basin, which only can be proven when wells are drilled (Spencer & MacTiernan, 2001).

#### **2.1.3.2 Source rocks and reservoirs**

Naylor & Shannon (1982) suggested the oil-bearing structures of the Porcupine Basin are likely to be complex and small to moderate in size, by world standards. The oldest reservoir-quality sandstones can be found in Upper Carboniferous fluvio-deltaic deposits (Croker & Shannon, 1995).

The best known reservoirs are good-quality, but very complex Jurassic sandstones. They possibly contain the best source and reservoir horizons, since the burial depth of the organic-rich shales might be sufficient to generate hydrocarbons (Naylor & Shannon, 1982). The nature of these Middle and Upper Jurassic sandstones is fluvial to shallow marine. Also deep marine turbidites within Upper Jurassic to Lower Cretaceous strata are considered as possible reservoirs. Other reservoirs can be found in Lower Cretaceous and Lower Tertiary fluvio-deltaic deposits and Lower Tertiary turbidites. Numerous caprock opportunities are

encountered at the Carboniferous, Permo-Triassic, Jurassic, Cretaceous and Tertiary levels (Croker & Shannon, 1995).

However, most of the exploration has been carried out in the northern Porcupine Basin. The majority of the wells (26) have been drilled in the northern Porcupine Basin, compared to only one in the south. The southern part of the basin exhibits a large unknown for the existence of plays and reservoirs, while over the entire basin the reservoir distribution remains a challenge. Possibly interesting reservoirs for the south Porcupine Basin could be the inferred aeolian Permo-Triassic sandstones (Croker & Shannon, 1995; Johnston *et al.*, 2001). Future exploration should focus on Tertiary and Cretaceous levels on the basin flanks (Spencer & MacTiernan, 2001).

### **2.1.3.3 Exploration potential**

Most of Ireland's offshore basins with proven petroleum systems contain hydrocarbons located in Jurassic sandstones in late Jurassic fault traps (Moore & Shannon, 1991; Spencer & MacTiernan, 2001). According to Croker & Shannon (1995) some thick Jurassic sandstone intervals within the Porcupine Basin have proven to be oil reservoirs and thus are considered as a major exploration target (Fig. 2.4). Accordingly, most of the exploration drilling has been directed at the Jurassic tilted fault blocks in the north. The very complex Connemara Field has such a trap and contains oil in modest and poorly connected Upper Jurassic sandstones. However, many accumulation and migration features such as pockmarks, 'bright' reflectors and gas chimneys have been reported within the Cenozoic succession of Connemara Field (Spencer & MacTiernan, 2001; Games, 2001). Although this discovery contained an estimate of 195 million barrels of oil, Shannon *et al.* (2001) call the results of the appraisal drilling on oil disappointing.

A second interesting target is the Lower Cretaceous sequence, which also seems to be buried deeply enough to act as both source and reservoir. Hydrocarbons (oil) have been found in Lower Cretaceous deltaic to deep marine sandstones (Croker & Shannon, 1995; Spencer & MacTiernan, 2001). According to Croker & Shannon (1995) and Naylor & Shannon (1982) the Carboniferous coal-bearing strata are thought to have a potential for the generation of gas. Although some Tertiary units may contain high quality reservoir sandstones, they are considered thermally immature and seem to lack adequate capping sediments and sealing traps (Croker & Shannon, 1995).

Despite a promising exploration prospect, the water depths and the hostile environmental conditions still are considered as major obstacles for hydrocarbon exploitation and production within the Porcupine Seabight (Naylor & Shannon, 1982). Although a significant hydrocarbons presence has been encountered, a commercially significant discovery has yet to be made since only three of the 26 exploration wells have proven oil flow (Johnston *et al.*, 2001; Spencer & MacTiernan, 2001).

## 2.2 Hydrographic setting

### 2.2.1 Water masses and properties

The present-day identification of the water masses in the Porcupine Seabight has mainly been performed by Hargreaves (1984) and Rice *et al.* (1991) (Fig. 2.5). These mostly local observations were confirmed by New *et al.* (2001) through modelling. The stratification was extensively reviewed by White (in press), who distinguishes two broad categories of water masses within the basin; *upper water* from 0 to 1200 m and *deeper water* below (Fig. 2.6). The upper water can be grouped in *Sub Polar Mode Water* (SPMW), derived of *North Atlantic Central Water* (NACW), which has sources in the western Atlantic Ocean and the Mediterranean. A permanent thermocline is found from 600 up to 1400 m over which the temperature decreases from 10°C to 4°C. A seasonal thermocline is formed at about 50 m depth.

Within the upper 700 m, the NACW shows a slightly elevated salinity at about 100 m, decreasing below 320 m (Hargreaves, 1984). The responsible water mass is considered as a saline, winter mode water, formed by strong cooling of water masses NW of Spain. This winter cooling makes the *Eastern North Atlantic Water* (ENAW) more dense and saline than NACW. It is carried northwards along and adjacent to the NE Atlantic margin (White, in press).

Below, Hargreaves (1984) recognized a local salinity maximum and oxygen minimum at a depth of 950 m. A small secondary maximum was found at 1140 m. This is the *Mediterranean Outflow Water* (MOW), which is observed between 700 and 1200 m (White, in press). It has a varying influence on the upper layer water masses through deep convective mixing in winter months. According to New *et al.* (2001), the poleward spreading of the MOW occurs in a reasonably steady boundary undercurrent from the Gulf of Cadiz, as far as the Porcupine Seabight. Further progress northward is considered as less certain.

The deeper water below the MOW is characterized by the presence of water masses derived from the *Labrador Sea Water* (LSW) from 1200 to 1800 m (Hargreaves, 1984). At about 1900 m, the temperature and salinity values indicate the characteristics of dense Scotland-Iceland overflow, being the *North East Atlantic Deep Water* (NEADW) with contributions of *Norwegian Sea Water* (NSW) and weakly influenced by Antarctic Bottom Water (Hargreaves, 1984; Rice *et al.*, 1991; White, 2001).

### 2.2.2 Current circulation

White (2001) considers the general circulation to be influenced by two main circulation systems of the North Atlantic Ocean. The *North Atlantic Current* turns to the northwest, while against the continental margin itself, a predominantly poleward flowing slope current is present (Pingree & Le Cann, 1989). This is an *Eastern Boundary Current* which comprises the warm and saline *Shelf Edge Current* (SEC) at its upper levels. Below, the MOW and deep ocean re-circulation are flowing.

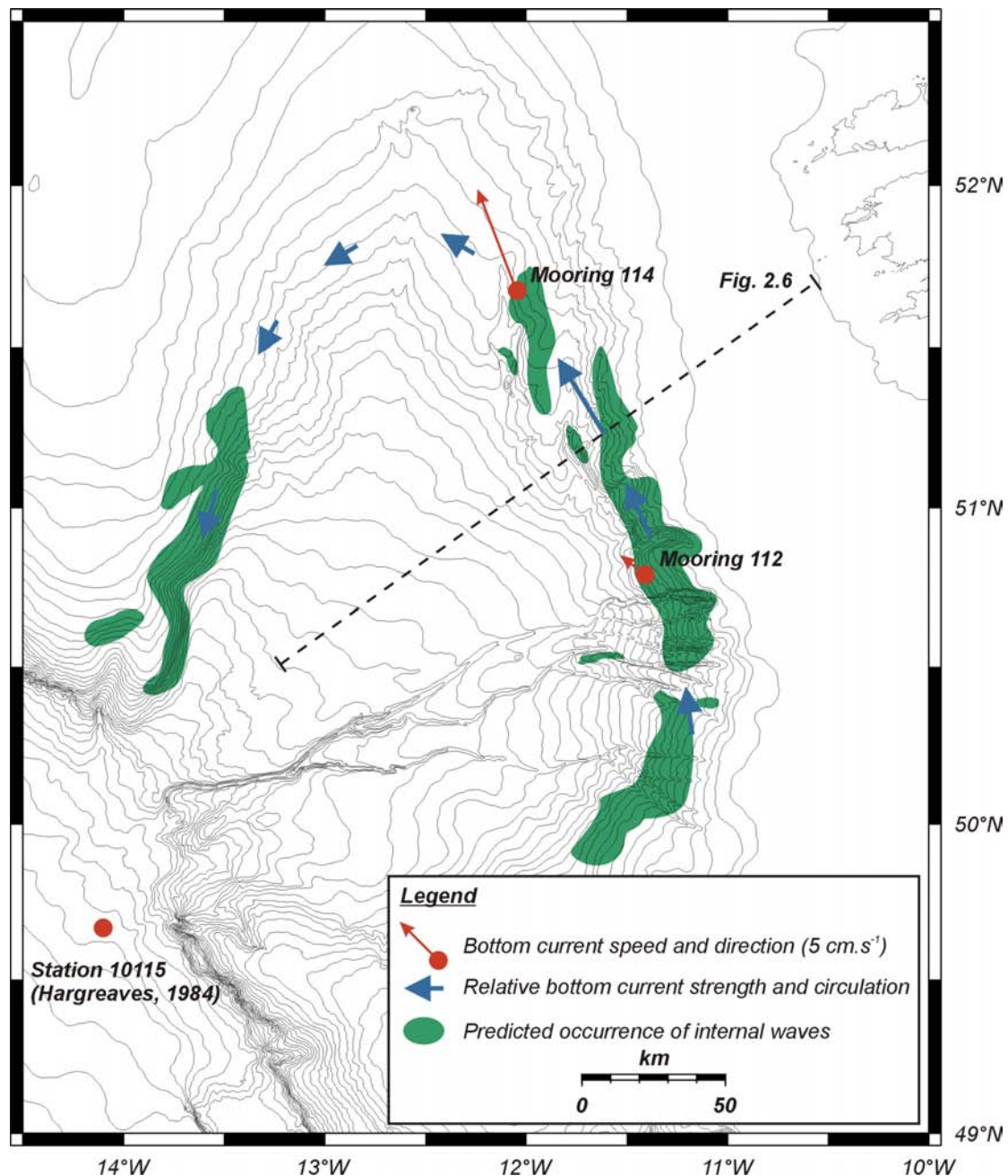


**Figure 2.5:** Overview of known near-bottom current measurements (red arrows, after Pingree & Le Cann (1989)), the predicted occurrence of enhancement due to internal tides (green areas, after Rice *et al.* (1990)) and the assumed general circulation (blue arrows, after White (*in press*)). The hydrographic transect presented in figure 2.6 is also indicated.

The SEC is known to be present along the eastern North Atlantic slope, from the Iberian margin to the Norwegian Sea (Pingree & Le Cann, 1989; Pingree & Le Cann, 1990; Rice *et al.*, 1991; New *et al.*, 2001; White, 2001). The SEC carries warm and saline upper-layer ENAW waters over the mid slope in the top 400 to 500 m (New *et al.*, 2001). Within the Bay of Biscay and the Celtic Sea, it seems to exist between the shelf break and the 1000 m isobath with current flows to a depth of 600 m with typical velocities from 5 (Biscay) to 30 cm.s<sup>-1</sup> (Rockall Trough) (Sherwin & Taylor, 1987; White & Bowyer, 1997).

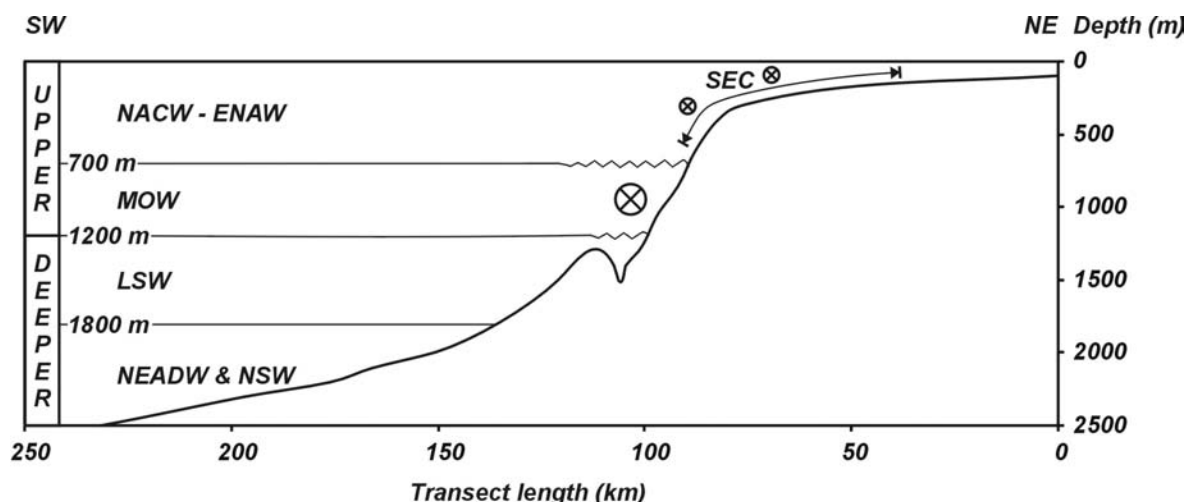


**Figure 2.6:** Compilation of the water stratification along a NE-SW bathymetric transect along the Porcupine Seabight, with indication of the major hydrodynamic processes, after Hargreaves (1984), Rice et al. (1990), Rice et al. (1991) and White (in press).

Within the Porcupine Seabight, a mean poleward current is less readily observed, except in the near-bottom current meters on the eastern flank (Fig. 2.5). Here, currents are predicted to be strongest at the mid-slope at about 500 to 600 m. These bottom currents are strongly steered by the bottom topography. Mean flows of this predominant cyclonic circulation are varying in between 2 to 5  $\text{cm}\cdot\text{s}^{-1}$  and even up to 10  $\text{cm}\cdot\text{s}^{-1}$  within the Belgica mound province (White, in press). At the northern end of the Seabight, the currents are relatively weaker, also with evidence of topographic steering of the flow towards an anticlockwise pattern around the northern slope (White, 2001).

### 2.2.3 Current enhancement

On the eastern slope of the Porcupine Seabight, within the Belgica mound province, the water mass characteristics seem to be more influenced by the presence of the MOW (White, in press). Pingree & Le Cann (1990) describe moorings in relatively deep water between 900 and 1000 meter, displaying strong bottom residual currents (Fig. 2.5). Also Rice *et al.* (1990) report currents, rarely exceeding a speed of about 15  $\text{cm}\cdot\text{s}^{-1}$  at a height of 1 m above the seafloor. However, within the mound zone, currents are supposed to be generally greater than 15  $\text{cm}\cdot\text{s}^{-1}$  for about 10% of the time (White, in press).

Pingree & Le Cann (1989), Pingree & Le Cann (1990) and Rice *et al.* (1991) have recorded strong **semidiurnal** to **diurnal tidal variations** in current speed and direction at several locations. During winter months from December to February, maximum poleward values are recorded for this current. From March, however, the flow characteristics change considerably with a full reversal from April to May. It is clear there is a strong **seasonal response** with a poleward flow during winter and spring, while during summer and autumn, the flow turns towards the equator. Moreover, the closer to the seabed, the stronger the mean currents, which seem to be more persistent and alongslope, due to the topographic control. In these lower, near-bottom layers, the reversal and any significant weakening, however, are not very pronounced (White *et al.*, 2000).

Another very important process responsible for the enhancement of the slope current is related to the generation of **internal tides** (Pingree & Le Cann, 1989). The internal tide is an internal wave with tidal period, generated by the interaction of tidal currents, water stratification and bottom topography. Modelling suggests such a density-driven current enhancement seems to be confined to the slope regions. This effect occurs on locations where the slope of the ray path of the tidal waves is exceeded by the slope of the seafloor. The greatest enhancement is to be expected near the upper boundaries of the interacting water masses, where mixing will occur (Sherwin & Taylor, 1987; Pingree & Le Cann, 1989; Huthnance *et al.*, 2001).

Rice *et al.* (1990) and De Mol *et al.* (2002) have suggested that the condition for reflecting internal waves is met at a depth between 500-1000 m. The greatest enhancement of currents is expected to appear on the eastern flank of the Seabight, where the upper boundary of enhancement runs along the 500 m contour, down to 1000 m at the northern and southern ends (Fig. 2.5). Here, one can expect near-bottom currents estimated at 15-20 cm.s<sup>-1</sup> at the eastern flank and 5-10 cm.s<sup>-1</sup> along the western flank. This complex system of enhanced currents has also been predicted by hydrodynamic modelling (New *et al.*, 2001).

#### 2.2.4 Bottom current observations

Although many authors inferred the presence of strong residual bottom currents within the Porcupine Seabight, there still are very few current measurements which can quantify the actual speed and orientation of these currents. On the other hand, since the boost in research on deep-water carbonate mounds, a wealth of seafloor observations is available from side-scan sonar imagery and ROV video footage.

Kenyon (1986) already reported sand transport on the shelf around the British Isles based on long-range side-scan sonar imagery. These sandy bedforms were observed in a variety of kinds on most of the upper slope south of Ireland.

Chachkine & Akhmetzhanov (1998), Kenyon *et al.* (1998) and Wheeler *et al.* (2000) identified current-induced bedforms like barchan sandwaves, sand ribbons and obstacle marks on high resolution side-scan sonar imagery on the eastern slope of the Porcupine Seabight. Some of these bedforms indicate that the peak current can reach a considerable speed up to 100 cm.s<sup>-1</sup> or even more. These current traces seem to go round the mounds in a south-north direction, following the depth contours. Moreover, a comparative textural analysis of side-scan sonar imagery by Huvenne *et al.* (2002) between the eastern and northern PSB around large coral banks described by De Mol *et al.* (2002), clearly demonstrates that the sediments of the Belgica mound province are rougher, with sediment mobility features that are not present in the more northern Hovland mound province. This may confirm the hydrographic theory predicting the strongest currents on a limited zone of the eastern slope of the PSB.

During the R/V Polarstern campaign ARK XIX/3a with the robotic submersible VICTOR6000, visual evidence was found of a strong hydrodynamic regime associated with the Belgica mound area (Figs. 2.7 a-f). The presence of gravels and boulders is very common (Figs. 2.7 a, d and e). Some of them are colonized by *Bathylasma* sp. barnacles, indicating strong currents. Other areas are characterized by patchy distributions of dropstones on an unrippled or rippled

seabed (Figs. 2.7 a-e). Sandwaves and superimposed ripples were observed on the ROV microbathymetry, indicating strong northward currents up to  $65 \text{ cm.s}^{-1}$  (Figs. 2.7 b, c d and f). The different orientations of some ripples are attributed to the influence of tidal currents. Also, long N-S lineated features with a length up to 250 m can be caused by strong currents of about  $150 \text{ cm.s}^{-1}$  (Foubert *et al.*, in press).

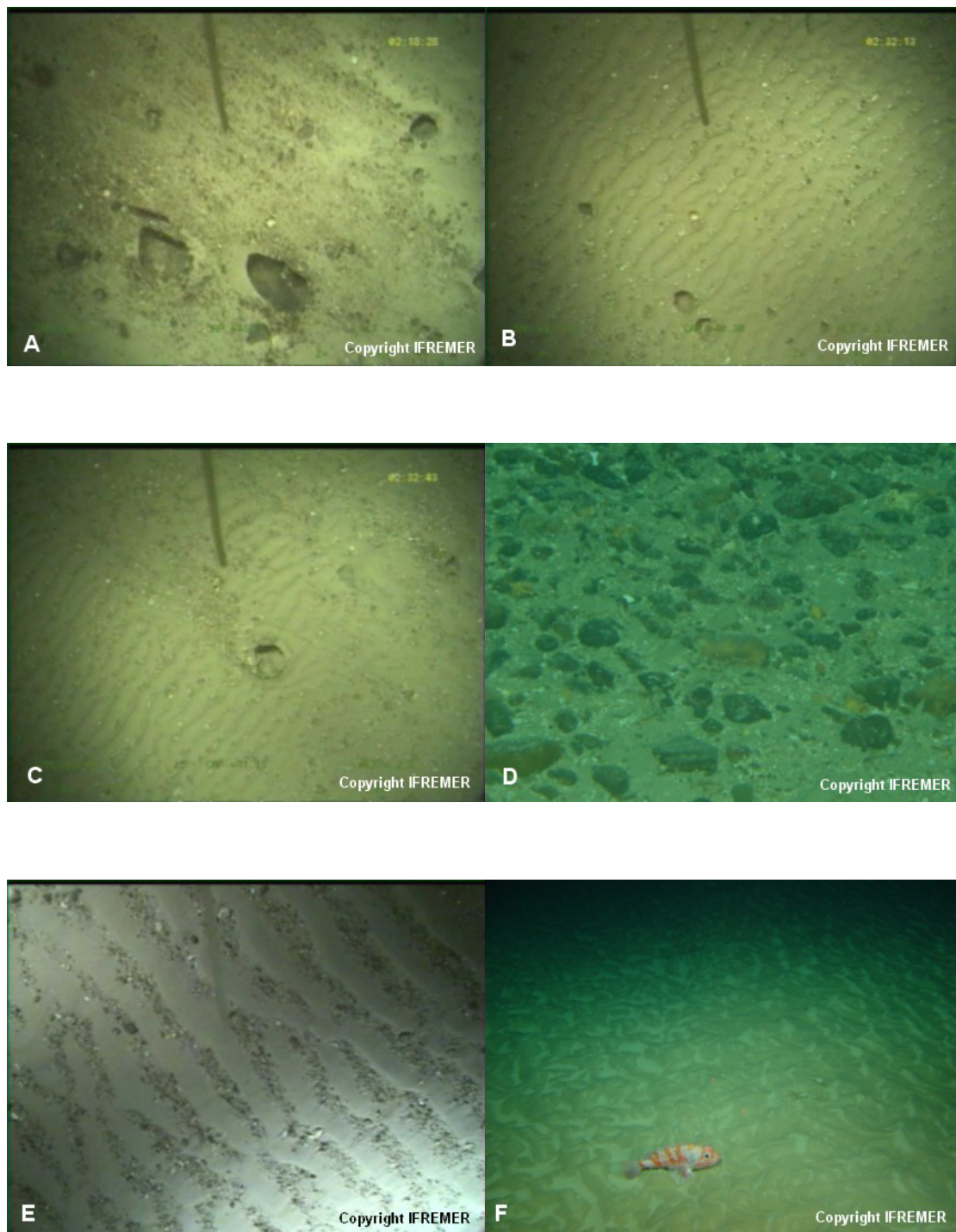


**Figure 2.7:** ROV images collected on board R/V Polarstern on the AWI Bremerhaven coordinated cruise ARK XIX/3a in June 2003. These images were made available through courtesy of IFREMER. Figures A-F illustrate the very strong hydrodynamic environment within the Belgica mound province. A, patchy distribution of dropstones on an unrippled seabed; B, rippled seabed with dropstones; C, rippled seabed with dropstones and obstacle marks around a boulder; D, a boulder-dominated seabed; E, current ripples filled up with dropstones; F, irregularly rippled seabed with a Redfish (Foubert et al., in press).

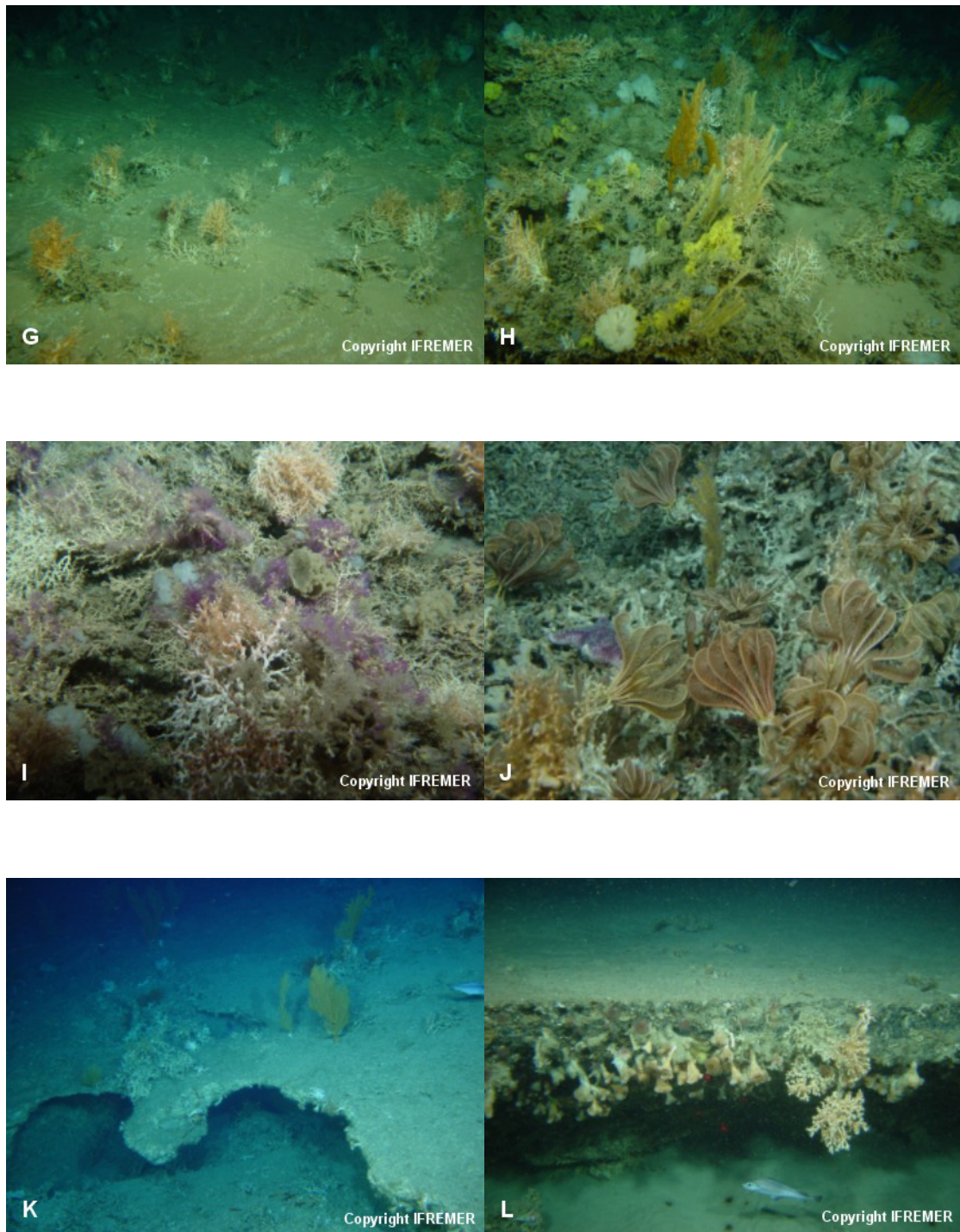


**Figure 2.7 continued:** Figures G to L illustrate the different ecologies, faunas and substrates as observed along the Irish margin coral banks. G, patchy distribution of live corals (*Madrepora oculata* and *Lophelia pertusa*) on a rippled sand (BMP); H & I, live coral coverage on top of the Galway mound with associated sponges (BMP); J, Crinoids and *Lophelia* corals on the Twin mounds (BMP); K, colonized hardground within the Pelagia mounds; L, scarp with live *Lophelia* and *Desmophyllum* corals on the Scarp (Pelagia) mounds (Foubert et al., in press; Wheeler et al., in press-a).

### 2.3 Cold-water coral banks along the NW European margin

The first observation of deep-water corals along the Irish margin was reported as result of the expedition of the *HMS Porcupine*. 75 years later, Le Danois (1948) revisited the Porcupine Seabight and named the “massifs coralliens”. However, it lasted until 1994 when Hovland *et al.* (1994) discussed the presence of carbonate knolls associated within gas seepage in the northern Porcupine Seabight, to boost research on deep- and cold-water corals. By this time, in 2004, numerous research campaigns and several large programmes as ACES, GEOMOUND and ECOMOUND mapped and studied the distribution of these corals, responsible for the formation of giant seabed mounds. Within the RCMG, especially the Porcupine Seabight mounds received much attention and were discussed extensively in the Ph.D. dissertations of De Mol (2002) and Huvenne (2003). A brief review is given on the ecology, location, characteristics and genetic hypotheses of these coral banks. Because the present study is framed around and within the Belgica mound province and tries to add to the present knowledge, these features are not discussed in too much detail.

#### 2.3.1 Ecology of cold-water corals

The principal framework builder in the deep-water coral structures is the scleractinian *Lophelia pertusa*, jointly with *Madrepora oculata*, *Desmophyllum dianthus* and *Dendrophyllia cornigera* (Figs 2.7 g-j). Unlike tropical scleractinians, they do not possess a symbiotic relationship with algae and are therefore not restricted to the photic zone (Frederiksen *et al.*, 1992; Rogers, 1999; Wheeler *et al.*, in press-b). Associated to these corals, also other fauna such as sponges, bryozoans, octocorals, hydrozoans and polychaetes were found (De Mol *et al.*, 2002; Wheeler *et al.*, in press-a).

These organisms have a global distribution and can be observed on special locations on the open shelf, fjord settings and upper slope environments, meeting several basic requirements which enable coral larvae settling and subsequent coral growth (Henrich *et al.*, 1995).

Generally, these aphotic corals have been found in water depths from 52 to 2000 m within a temperature range between 0 and 13.6 °C. They are also associated with a relatively **high salinity** (from 31.85 to 35 ‰) and with an **oxygen minimum zone** where levels as low as 3.64 ml O<sub>2</sub>/l can be attained (Hovland *et al.*, 1994; De Mol *et al.*, 2002; White, in press).

The quantity of dissolved oxygen content plays an important role in the **nutrient provision**. If no oxygen is added to the system, it is consumed through decomposition of organic matter, which offers an increased availability of digested food for the corals. This organic matter can be sourced from within the photic zone or it could be related to a chemosynthetic food chain based on bacteria that feed on seeping hydrocarbons or gas hydrates (De Mol, 2002; Bailey *et al.*, 2003).

These corals can be found in regions with **strong bottom currents**, which also are required to protect the coral framework from burial (De Mol, 2002). This is why these suspension feeding communities are frequently observed in areas of internal waves on shelf and slope (Frederiksen *et al.*, 1992; Henrich *et al.*, 1995).

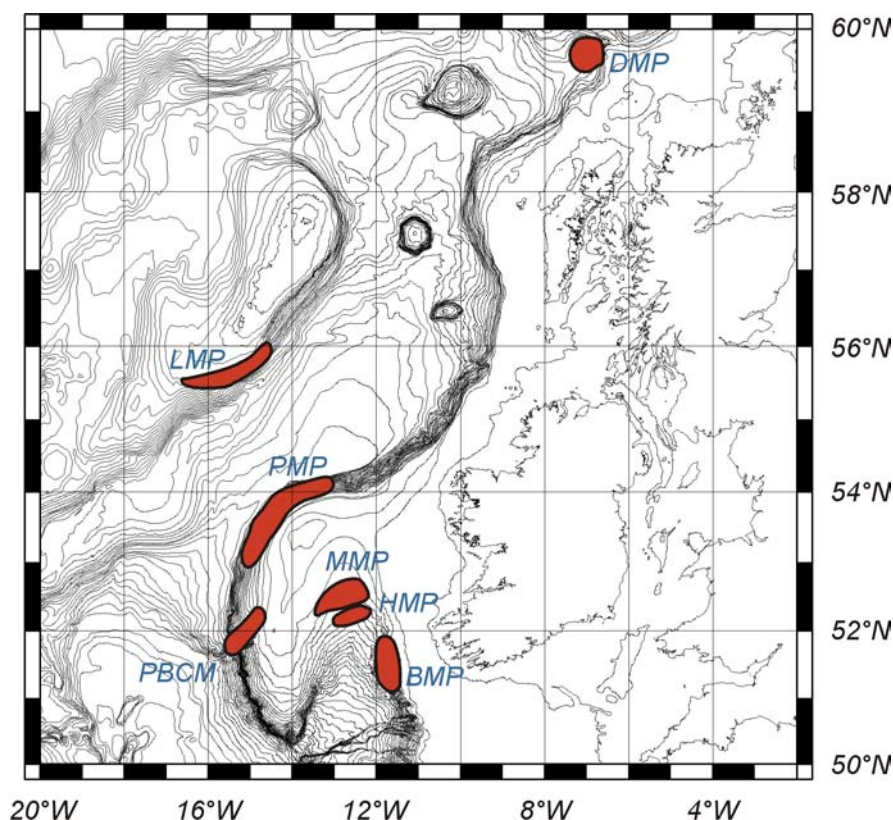


**Figure 2.8:** Main mound provinces along the NW European margin. Contour intervals (GEBCO) are drawn every 100 m. BMP: Belgica mound province, DMP: Darwin mound province, HMP: Hovland mound province, LMP: Logachev mound province, MMP: Magellan mound province, PMP: Pelagia mound province, PBCM: Porcupine Bank Canyon mounds after Huvenne (2003).

In addition, the corals require a suitable **hard substrate** for anchorage to assure they are not swept away by the strong currents (Figs. 2.7 g, k and l). The substrate may be provided by a hardground, moraine ridges, outcrops, dropstones, boulders and even pipelines and oil rigs (De Mol *et al.*, 2002). On the other hand, the strong near-bottom currents can also be responsible for the creation of a coarse seafloor (Huvenne *et al.*, 2002-a).

### 2.3.2 Coral banks along the Irish margin

Within the EC-FP5 projects on coral banks, the most prominent and largest mound provinces have been located along the Irish Atlantic margin within large hydrocarbon provinces and regions of strong bottom currents. In this section, a brief review of their main characteristics is presented along a SE-NW transect along the western Irish offshore basins (Fig. 2.8)

#### 2.3.2.1 The Belgica mounds

The Belgica mounds were first described as barrier reefs with ponded sediments, rooted on an “enigmatic” transparent layer, cut by a prominent erosion surface, which was later attributed an intra Pliocene age (Henriet *et al.*, 1998; De Mol *et al.*, 2002; Van Rooij *et al.*, 2003). However, towards the northern edge of the province, the mounds seem to root directly on sigmoidal depositional units (Fig. 2.9). Up to now, no internal structure has been observed (Henriet *et al.*, 2003).

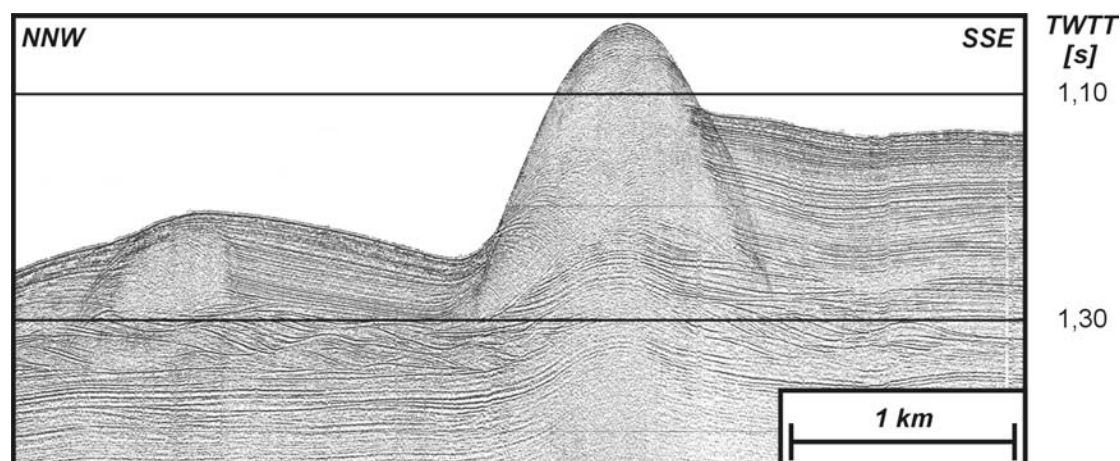


**Figure 2.9:** Sparker section through a large Belgica mound and the buried foot of an adjacent mound. Both mounds directly root on a horizon with sigmoidal depositional units (Henriet *et al.*, 2003).

They occur on the eastern slope of the Porcupine Seabight between 500 and 1100 m over a distance of 20 km (Fig. 2.8). Detailed mapping with multibeam bathymetry and very-high resolution seismic profiling allowed the observation of 42 outcropping and 22 buried mounds. Huvenne *et al.* (2003) estimated the mound density at 1 mound per 7 km<sup>2</sup>. The shape of the mounds is in general asymmetric, appearing conical on seismic profiles, with inferred slopes of 10 up to 30° on their northwest sides. The surface expression however mostly shows a N-S elongation due to sediment accumulation on the flanks. Larger mounds are observed to merge into ridge structures, while smaller mounds mostly occur as single and conical structures. The buried mounds have an average height of about 50 ms TWT (approximately 46 m) with a maximum of 160 ms TWT (148 m). They are generally covered with about 40 ms TWT (32 m) of sediment. The surface mounds are higher and broader with about 150 ms TWT (140 m) of height. They can reach heights of about 50 m to 150 m above the seabed. The mean width of the mounds varies from about 700 m (between 250 to 1100 m) for buried mounds and 1100 m (from 500 to 2200 m) for surface mounds. The average length varies from 1 to 3.5 km. The most developed mounds are found in the central part of the province, while the smallest mounds are observed in the southern part of the province (De Mol *et al.*, 2002; De Mol, 2002; Beyer *et al.*, 2003).

According to De Mol *et al.* (2002) and Van Rooij *et al.* (2003) well-developed moats are rarely found, however the mounds are flanked by channels, gullies and typical sediment tails. Moreover, Wheeler *et al.* (in press-a) report benthic current features including barchan dunes, seabed striations, comet marks, gravel ridges and sediment waves (Figs. 2.7 a-f). These features indicate a close association with currents. White (in press) confirms the water mass characteristics of this mound province are influenced by the MOW, introducing currents of 15 cm.s<sup>-1</sup>, which are a likely threshold for re-suspension of surface sediment.

A video transect across the mounds shows a lateral and vertical biozonation. Living coral zones are observed at the steep exposed flank of the mounds, with a higher biodiversity (De Mol, 2002).

In the vicinity of these mounds, smaller mounds were observed which could represent an early stage of the mound development. These Moira mounds can be up to 5-10 m high and 15 to 40 m across (Wheeler *et al.*, in press-a). They include

isolated examples, but they can also be present in clusters. They occur in areas of active sand transport on rippled sand sheets (Foubert *et al.*, in press; Wheeler *et al.*, in press-c).

### 2.3.2.2 The Hovland mounds

Hovland *et al.* (1994) first described these mounds on the northern Porcupine Basin (Fig. 2.8) as carbonate knolls and compared them to NW Australian counterparts. Due to the presence of underlying hydrocarbon reservoirs and faulting, they considered their origin to be closely linked to hydrocarbon seepage.

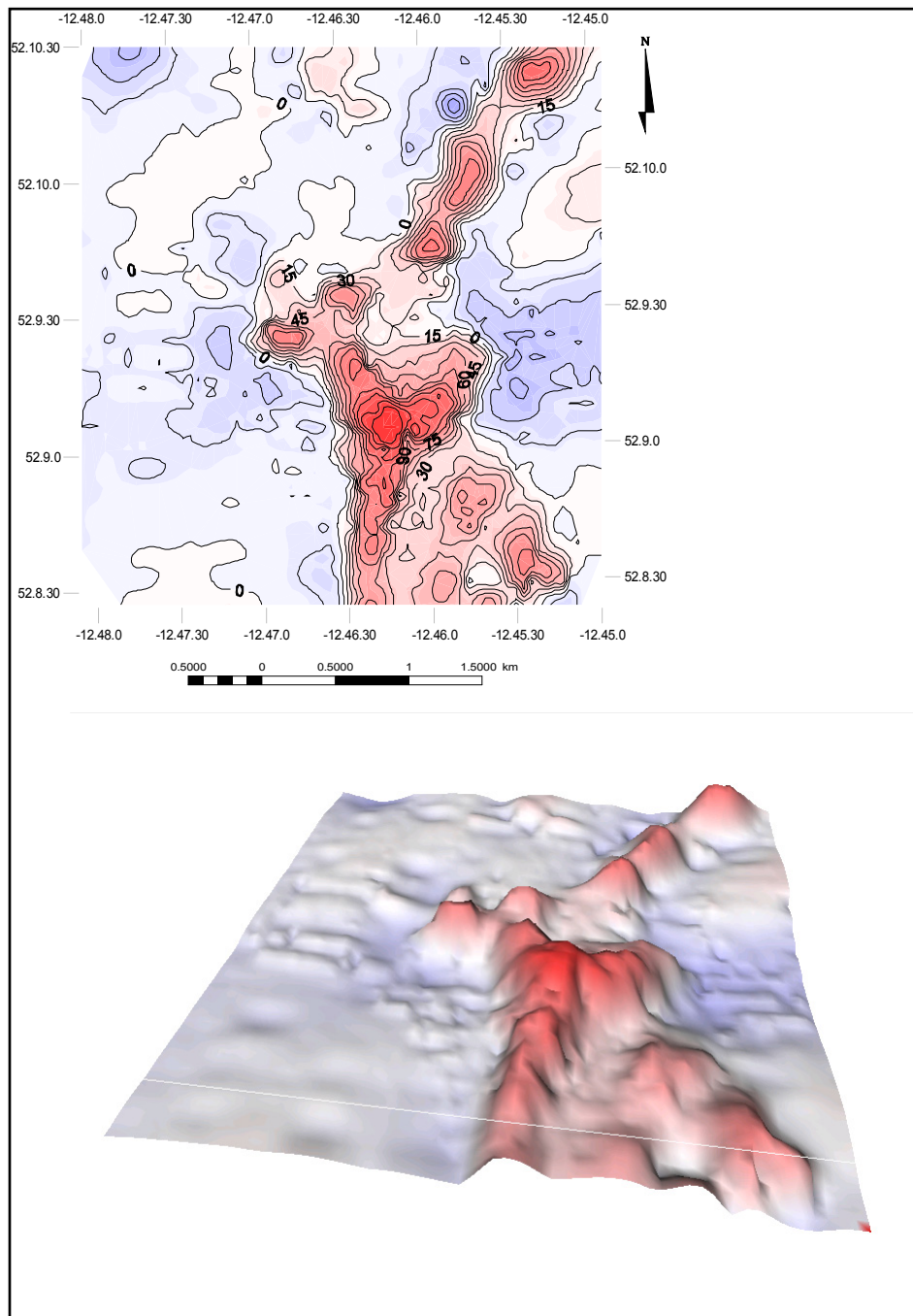


**Figure 2.10:** Trend map of Propeller mound within the Hovland mound province. The blue colours indicate the moats and the depressions. The red colours represent the elevation above and below the virtual base line of the mound (De Mol, 2002).

The base of the mounds is poorly imaged, but they probably root on an erosion surface of Late-Pliocene to Pleistocene age, constituting the youngest boundary of a cut-and-fill system. This system is a large erosional depression, around which the mounds are clustered (De Mol *et al.*, 2002).

Henriet *et al.* (2001) and De Mol (2002) consider them to be clustered in an area of 375 km<sup>2</sup> in water depths of 400 and 1100 m. A total of 14 outcropping and 25 buried mounds (in the NE sector) have been observed. The mound density was estimated at 1 mound per 10 km<sup>2</sup> by Huvenne *et al.* (2003). The bathymetry of the central part of the province is compared to a relatively steep amphitheatre-shaped depression, which is composed of four N-S oriented branches. The surface mounds have a mean width of 1300 m and a height of 215 ms TWT. The tallest mounds appear around the current scoured depression. The slope of these mounds can be up to 25°. Moats are observed to occur on all sides of the mounds, but they are not symmetrical. Side-scan sonar imagery however indicates that several mounds have an elongated shape, with lengths varying from 1700 up to 5000 m and widths of 450 to 1200 m. Most of the mounds have sharp ridges with several summits, while others consist of multiple mound structures and some small mounds are lined up, as if they represent half-buried mound ridges (Fig. 2.10). The overall direction of these ridges varies greatly (De Mol, 2002; De Mol *et al.*, 2002; Wheeler *et al.*, in press-a).

On-mound cores are intensively bioturbated and their matrix is dominated by nanofossil ooze and terrigenous clastic components. They also contain biodetritric material like shells and echinoderm spines. Throughout the cores, *Lophelia* and *Madrepora* are found, but also *Desmophyllum* (De Mol *et al.*, 2002).

Within the moats surrounding the mounds, De Mol (2002) described coarser sediment, rock fragments and slumped coral fragments near the seabed. Core material suggests that the coral concentration seemed to be high during warmer periods as the Holocene. Living corals have been observed on the upper slopes of the mounds, where they form a living rim. Also the flanks facing these depressions and the stoss sides are more densely colonized by living corals. The leeward sides are dominated by sediments.

Compared with the seabed features encountered in the Belgica mound province, the HMP seafloor is much smoother and less characterized by intense bottom currents (Huvenne *et al.*, 2002). On the other hand, the presence of sedimentary ridges, spurs and moats does suggest a (paleo?) north-south directed current (Wheeler *et al.*, in press-a).

### **2.3.2.3 The Magellan mounds**

These mounds were firstly discovered during an industrial 2D campaign by M/V Svitzer Magellan in 1996 and the subsequent R/V Belgica campaign in 1997 (Henriet *et al.*, 1998; Pillen, 1998). It is a crescent-shaped province in water depths of about 600 m, matching the isobaths of the NW part of the PSB, covering an area of approximately 1400 km<sup>2</sup> (Fig. 2.8). They are separated from the Hovland mounds by a broad moundless belt (Henriet *et al.*, 2001).

The Magellan mounds also are characterized by an acoustically transparent facies, buried beneath an approximately 50 m thick layer of drift sediments. Their average height approximates 62 m and they have an average width of 340 on 415 m.

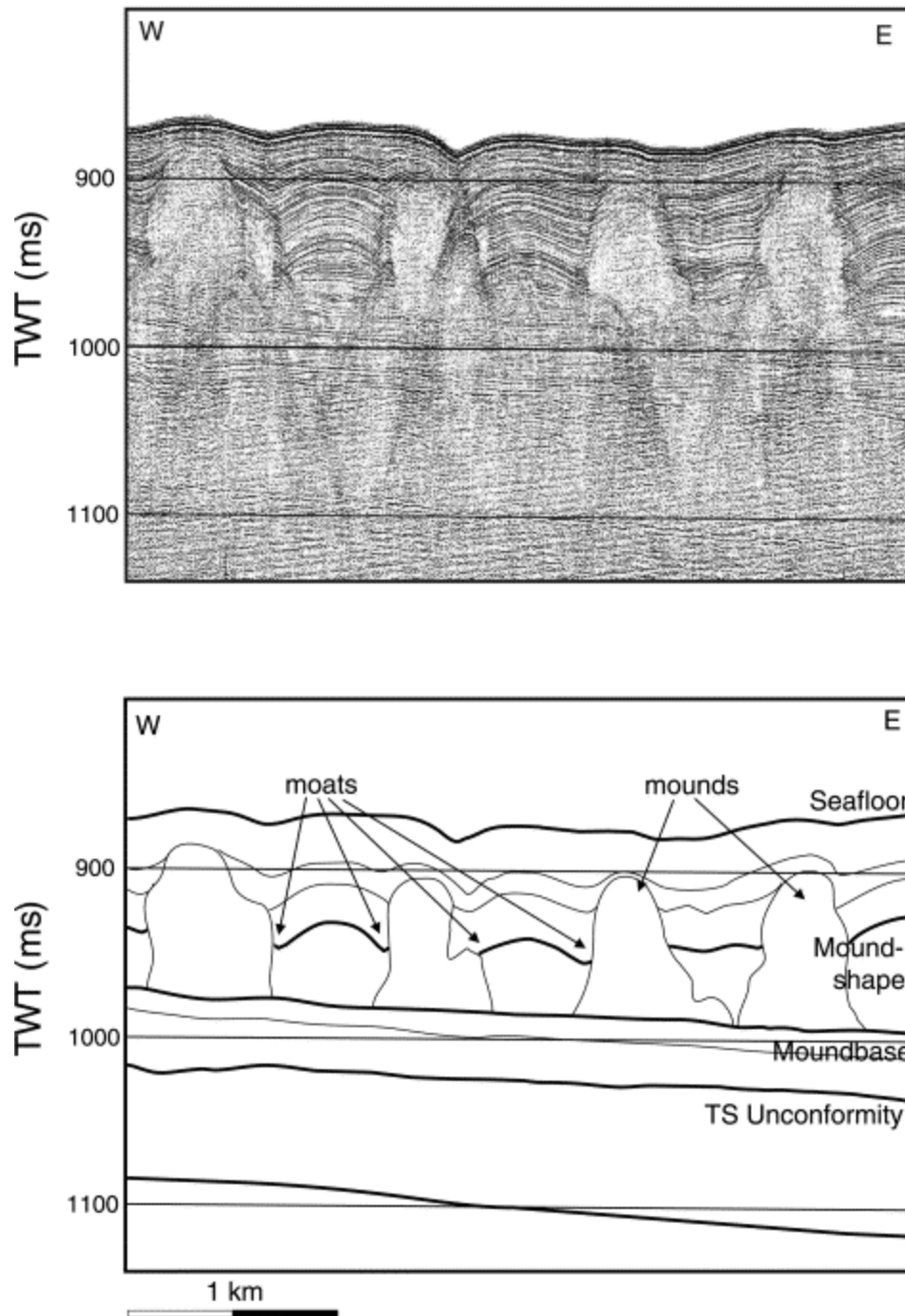


**Figure 2.11:** High-resolution 2D seismic profile across some Magellan mounds. The mounds appear as acoustically transparent zones between the seabed and the moundbase reflector. The depressions in the reflections adjacent to the mounds are interpreted as moats, caused by current scouring (Huvenne *et al.*, 2003).

The shape of these mounds predominantly is vertical and stock-like with a convex, often wider top (Fig. 2.11). Huvenne *et al.* (2003) did not observe any ring structures, earlier suggested by Henriët *et al.* (1998), which could be explained by the very close spacing of the mounds. The mounds are outlined by abrupt reflection terminations of the embedding strata. The larger mounds are found at the western boundary, where at least three of them are observed to extend to the present sea bed. Towards the northern part of the province, they decrease in size (Henriët *et al.*, 2001; De Mol *et al.*, 2002; Huvenne, 2003).

Huvenne (2003) performed an automated and manual mapping on a combination of industrial 3D and academic 2D data. 387 mounds were found spread over an area of 320 km<sup>2</sup>. They are considered as extremely numerous with a density of 1.22 mounds per km<sup>2</sup>. An extrapolation suggests up to 1700 mounds in the entire province. They are not believed to be lined up or occurring in specific patterns. A small slope plastered drift indicates a bottom current controlled sedimentation before mound initiation. The base of the Magellan mounds is also associated with a N-S elongated, bipolar moat, suggesting the influence of N-S reversing currents.

Along the mound base, a large number of smaller inferred coral accumulations is inferred, suggesting a spatially extensive start-up phase after which only a limited number of mounds continued development. They all root onto the same reflector, suggesting a common start-up phase. Although McDonnell & Shannon (2001) inferred an Early Pliocene C10 age for this mound base, various observations within the PSB suggest the equivalent C10 age is more likely located at the base Quaternary. A chaotic horizon underlying these mounds was interpreted by Huvenne *et al.* (2002b) as a slab slide that only partly underlies the Magellan province. The presence of this slide did not seem to have influenced the location of the Magellan mound province (Huvenne *et al.*, 2003). Additionally, no convincing spatial correlation between the different fault packages below the mounds and the mounds was found by Huvenne *et al.* (in press), strongly suggesting a past oceanographic control.

#### 2.3.2.4 The Pelagia mounds

The Pelagia mound province is located in the SE Rockall Trough on the Porcupine Bank, between 500 and 1000 m (Fig. 2.8). Some deeper mounds are observed at a depth of 1200 m. They occur downslope of a significant zone of iceberg ploughmarks and upslope of submarine canyons and slope failures.

These mounds are isolated, single and relatively small seabed features with a maximum length of 1000 to 2000 m and a height of 50 to 350 m above a relatively flat seabed (van Weering *et al.*, 2003b). Generally, their shape is irregular and

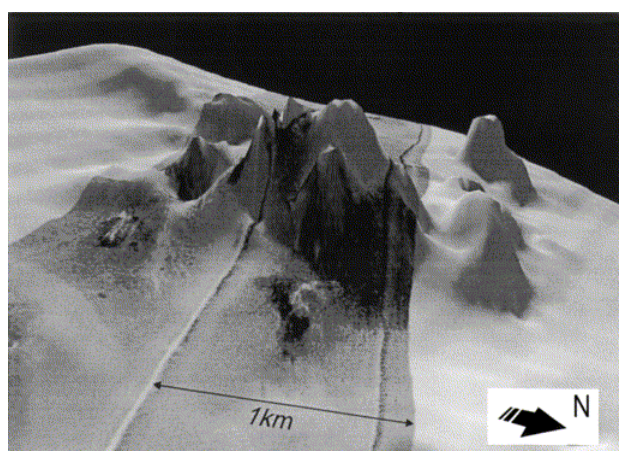


**Figure 2.12:** Perspective view of a portion of 30 kHz sonograph draped over a digital terrain model of a large carbonate mound on the northern Porcupine Bank margin. The image shows the complex, multi-peaked morphology of the Pelagia mounds. Vertical exaggeration is 1:10 (Kenyon *et al.*, 2003)

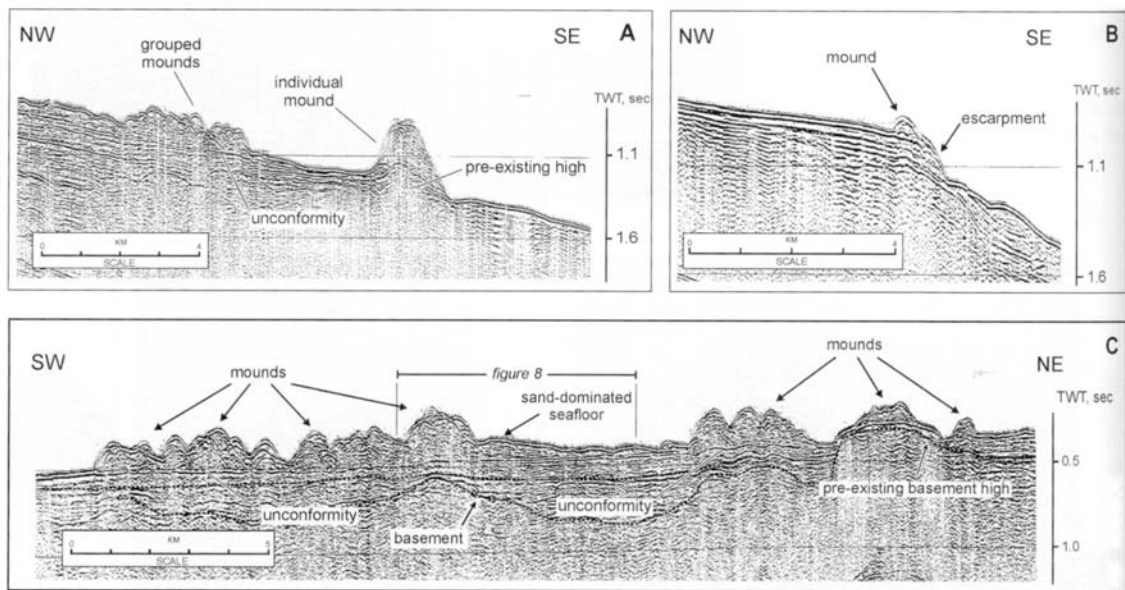


**Figure 2.13:** Airgun seismic profiles across the Pelagia coral banks. (A) the large mound is built up to 350 m above a pre-existing high in the acoustic basement; (B) the isolated mound is located on the edge of a 130 m high escarpment; (C) alongslope profile showing clusters of mounds rooted above a well-marked unconformity or growing from the top of a local basement high (Akhmetzhanov et al., 2003).

asymmetrical, from circular to elongate, but also clusters of mounds are observed (Figs. 2.12, 2.13). Acoustically, they are characterized by a chaotic internal structure. They root on an unconformity. Most of the mounds have relatively steep slopes up to 30 or 45°. At their NE side, sediment accumulations are found and moats on the SW side, suggesting current influence. This is also confirmed by side-scan sonar and video observations of mobile sand sheets, gravels and boulders. Seabed sampling yielded small amounts of living corals, foraminiferal ooze, shells and dead coral fragments. In one core, a marl of up to 80% carbonate is found. Coral colonization is restricted to the top of the mounds. Underwater TV observations suggest the corals mostly inhabit the very top of the mound, while the slopes are covered with mud. Video observations show the presence of carbonate hardgrounds of up to 15 cm thickness below the coral cover directly below and at summits of the mounds (Figs. 2.7 k and l). Van Rooij *et al.* (2001) also reported diagenetic hardgrounds, which were found to be very hard to penetrate during gravity coring. On these hardgrounds, but also on a number of scarps and rock outcrops, some small coral settlements were found (Akhmetzhanov *et al.*, 2003; van Weering *et al.*, 2003a; van Weering *et al.*, 2003b; Kenyon *et al.*, 2003; Wheeler *et al.*, in press-b).

This region of the SE Rockall Trough slope is dominated by a strong northerly to north-easterly directed semidiurnal tidal bottom current of up to 50 cm.s<sup>-1</sup>. In addition to this poleward contour current, enhanced currents due to internal waves are observed (van Weering *et al.*, 2003a; van Weering *et al.*, 2003b; Kenyon *et al.*, 2003).

### 2.3.2.5 The Logachev mounds

In the SW Rockall Trough, the Logachev mounds are located on the upper slope between 500 and 1200 m, aligned in a narrow zone sub-parallel to the slope (Fig. 2.8).

These mounds can be recognized as massive bodies with a chaotic internal structure, incorporated in an acoustically well-stratified uppermost package. Their dimensions are highly variable from single pinnacles to 350 m above the seabed with a diameter of 2 to 3 km or in clusters with a diameter up to 6 km (Fig. 2.14). Some of these ridges can have a length of up to 15 km, separated from each other by valleys and gullies, aligned with their longest axis perpendicular or at a high angle with the bathymetric contours. Sonographs shows closely spaced mounds, some conical, some ridge-like and less than 100 m high. Upslope, the mounds become less high and become gradually buried with a thin sedimentary cover. The relief between the mounds is filled with layered carbonate debris. The inter-mound areas are clearly flat-floored and have a very sandy lithology. Sand waves and comet marks indicate this sand is being transported to the S or SW at inferred speeds of 40 to 50 cm.s<sup>-1</sup>. Sampling indicates mostly grey foraminiferal oozes, broken branches of corals, including living species, coral and shell debris. There also is an associated fauna of sponges and polychaetes. The tops of the mounds are covered with an extremely dense and thriving fauna of ahermatypic cold-water corals and associated benthic fauna. Crinoids are extremely abundant here. The mounds all seem to have grown from the Early Pliocene C10 unconformity. Seismic profiling indicates the presence of a highly reflective (basaltic?) basement with an irregular and possibly faulted upper surface, covered with a 60 to 130 m thick sedimentary sequence. Multiple hardgrounds were also observed, outcropping at and below the mound summits. Multibeam and video data suggest a terraced morphology with the fronts colonized by the corals (van Weering *et al.*, 2003a; van Weering *et al.*, 2003b; Kenyon *et al.*, 2003; Wheeler *et al.*, in press-a).

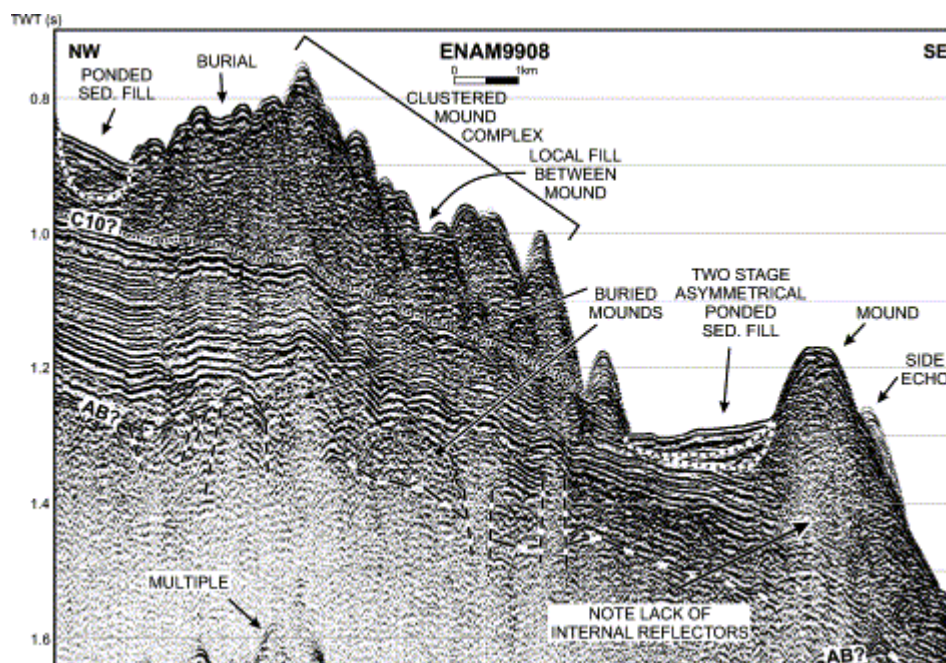


**Figure 2.14:** Irregularly shaped cluster of mounds and a single mound at the slope edge within the Logachev mounds. An unconformity below the mounds has been tentatively correlated with reflector C10 of Stoker *et al.* (2001). AB is an irregular and faulted acoustic basement (Van Weering *et al.*, 2003b).

### 2.3.2.6 The Darwin mounds

These mounds are located in the northern Rockall Trough and are closely associated to a 3000 km<sup>2</sup> large field of pockmarks lying south of the mounds. They occur in water depths between 900 and 1600 m. There has been a low sedimentary input since the end of the last glaciation and within the Holocene there has been a dominant redistribution of older sediments. This has resulted in a relatively smooth, polished sea floor. The Darwin mounds have a typical diameter up to 75 m and can be up to 5 m high. Sometimes they are associated with a distinctive tail-like feature, which is elongated in a S to SW direction, suggesting a high influence of benthic currents. High side-scan sonar backscatter suggests biological colonies or coarse sediment accumulations around the mounds.

The sediments of the pockmark field are more muddy compared to the Darwin mound facies, which are closely associated with the contourite sand. Because these mounds are primarily composed of sand and the biological debris only is a minor constituent, they are not considered as typical carbonate mounds. They were built by a non-biological process. The relationship with the pockmarks could be that these non-biological mounds were created by fluid escape. This fluid escape enables sand movement towards the surface where it provides anchor points for the corals. This is not possible within the pockmark field, where subsurface sand is absent (Masson *et al.*, 2003).

### 2.3.2.7 Other reported mound and cold-water coral occurrences

The Irish offshore basins are not the only location along the NW European margin where cold-water corals are located. Among the best known massive occurrences of *Lophelia* are the reefs along the Scandinavian margin, of which more than 407 locations are known. Henrich *et al.* (1995) discuss coralline algal reefs developed along the Norwegian current, protected on the inner shelf. They are most abundant on the continental shelf along the upper slope of the margin and along many flanks of the deep mid-shelf troughs in a bathymetric range of 200 to 400 m. Pleistocene glaciogenic processes provided a broad array of suitable hard substrata for the corals; ploughmarks, moraines and boulders. Despite the large occurrences, only few sites have been studied in detail. The best known study to date is the Sula Reef Complex (Wheeler *et al.*, in press-b)

Other *Lophelia* observations are made around the Faeroe Island shelf banks within bathymetric intervals of 200 to 700 m (Frederiksen *et al.*, 1992; Henrich *et al.*, 1995).

More to the south, Plets (2002) infers the presence of *Lophelia* mounds on Galicia Bank, west off Portugal. Henriët *et al.* (2002) reported deep-water corals on authigenic carbonate crusts within the Gulf of Cadiz also. Finally, very-high resolution deep-tow seismic profiles and multibeam bathymetry suggest the presence of mound-like features on an escarpment west of an important mud volcano province offshore Morocco (Van Rooij *et al.*, 2002).

### 2.3.4 Clues towards genesis and development

The coral banks along the Irish margin display several common features that might give clues for their genesis and development. First of all, they are always associated with past or present elevated *near-bottom currents*. The corals are most of the time attached on a *hard substrate*, which could be rocks or boulders, but more important is the close relationship with *hardgrounds* or *unconformities*. The initiation of *mound growth* always started from such an unconformity and is *relatively fast* and *simultaneous* within the same province, which is remarkably *well-delineated*. The occurrence of these mound provinces always seems to be within the vicinity of underlying Jurassic *hydrocarbon reservoirs* and often nearby seabed features indicate *seepage*. Especially the latter has been subject to a lot of discussion and controversy concerning the role these hydrocarbon provinces play(ed) in the mound history.

In any case, it is clear that throughout the different phases of mound genesis and development, several factors will have played an important role. The only problem is that, up to now, there still is a hiatus in our knowledge concerning initial mound nucleation. Although the juvenile Moira mounds could be a present-day example of proto-mounds, there is a great need for drilling through the mound base. Until that time, the history of mound development can be explained by a locally influenced blend of two major control factors; the ecologic and environmental control (as evaluated by the EC FP5 projects ECOMOUND & ACES) and the internal, geological control (studied by the GEOMOUND project).

#### 2.3.4.1 Environmental and ecologic control

Most authors relate the presence of the cold- and deep-water coral with associated strong bottom currents (with or without internal tidal effects). Local morphologic and hydrographic characteristics make mound sites attractive for deep-sea coral settling and growth, implying that benthic currents and a favourite settling ground are intrinsic to the growth of the mounds (De Mol *et al.*, 2002; Huvenne *et al.*, 2002; Wheeler *et al.*, in press-b). The framework building capacity of *Lophelia* is a major advantage which enables it to grow upwards into the water column. In doing so, *Lophelia* can feed in faster flowing waters, thus increasing food flux. Colonies that have grown to their maximum elevation eventually keel over and provide an elevated platform for new growth, or they may become supported by sediment trapped within the coral framework (Wheeler *et al.*, in press-a).

A first generalized model of mound evolution, including most of the environmental and ecological factors, was proposed by Kenyon *et al.* (2003) and illustrated in figure 2.15. Most of the mounds are rooting on a well-marked unconformity, representing a major change of sedimentary environment, due to the onset of a bottom-current dominated depositional regime. It is very common that coral patches develop on a coarse current-swept sea floor which provides an ideal hard settling ground (Huvenne *et al.*, 2002). This could also explain the scattered presence of smaller patches, as observed at the Moira mounds, where corals are found to be colonizing sand ripples (Foubert *et al.*, in press). The large N-S elongated moats along the mound base of the Magellan mounds strongly suggest a climatic control through bottom current action. The weakening of these currents towards recent times is thought to be responsible for the final burial of these mounds (Huvenne *et al.*, 2003).

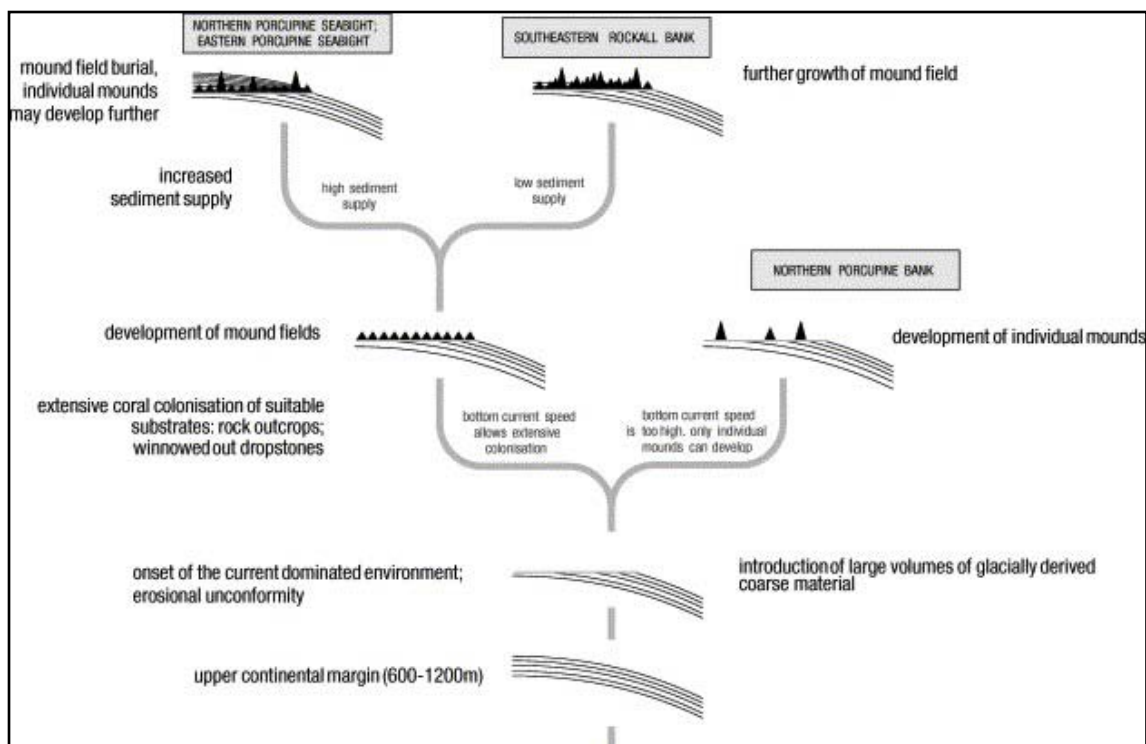


**Figure 2.15:** Generalised model of mound province development under different evolutionary scenarios (Kenyon *et al.*, 2003).

Also the water masses exert a major influence on the occurrence of corals. Especially the MOW within the Belgica mound province is responsible for enhanced currents often exceeding  $15 \text{ cm}\cdot\text{s}^{-1}$  which are a likely threshold for re-suspension of surface sediment in the NE Atlantic margin (White, in press). The density of the mounds is found to be dependent of the current regime, which might explain the lower density of the Pelagia mounds. A current speed which is too high can also limit food availability and can hinder initial coral settlement. Instead, large mounds were formed on pre-existing rocky outcrops (Kenyon *et al.*, 2003). Additionally, it is thought that the larvae of these azooxanthellate corals were introduced into the NE Atlantic through MOW, starting from a source area in the Mediterranean (De Mol *et al.*, 2002).

Another intervening factor recognized by Kenyon *et al.* (2003) seems to be the sedimentation rate, being responsible for the partial burial of the Belgica mounds and the complete burial of the Magellan mounds, while the Logachev mounds are preserved due to relatively low sedimentation rates.

However, despite the wide distribution of suitable environmental factors and substrates along the European margin, many of them are apparently not colonised (Wheeler *et al.*, in press-a). According to Masson *et al.* (2003), it appears that a lack of attachment points is not the main or sole control point on the local occurrence of absence of corals.

#### 2.3.4.2 “Internal” geological control and the influence of seepage

According to Bailey *et al.* (2003), the coral forming organisms require a combination of factors in order to grow. Except for the strong bottom currents and the required firm substrate the corals require a nutrient source, which could be in

the form of a chemosynthetic food chain based on bacteria that feed on escaped hydrocarbons or gas hydrates. Hovland *et al.* (1994) related the Hovland mounds to focused seepage because high average interstitial methane concentrations were observed at and near the mounds. Moreover, they seem to occur above deep-seated faults, suggesting tectonic control of fluid focusing and migration. This process was also invoked by Henriët *et al.* (1998). The presence of the relatively nearby Connemara field with evidence of shallow gases and pockmarks assisted this hypothesis. The Magellan mounds are observed above a deformed layer which was related by Henriët *et al.* (2001) to a large sea-bed failure, caused by interglacial destabilization of gas hydrate layers. A model was proposed for the Hovland mound region, with a more catastrophic event, related to episodic fluid venting of the underlying reservoirs.

However, pore fluid analysis and carbon isotopes from shallow cores on the Hovland mounds have failed to find evidence for hydrocarbon or methane (Henriët *et al.*, 2001). According to De Mol (2002) the present level of hydrocarbon evidence within the Hovland-Magellan province is extremely low, implying there is no evidence of petroleum seepage on any scale, although micro-seepage could not be excluded. Bailey *et al.* (2003) and Huvenne *et al.* (in press) did not observe a clear spatial relationship between faults and either buried or seabed mound provinces in the northern part of the Porcupine Basin. The same is observed at the Logachev and Pelagia mound provinces which are also located above hydrocarbon reservoirs (van Weering *et al.*, 2003b), but no interference or mediation from hydrocarbon seepage is observed (Kenyon *et al.*, 2003). Furthermore, *Lophelia* banks also occur in other regions independently of proven hydrocarbons seeps (De Mol *et al.*, 2002).

Henriët *et al.* (2001) suggest this paradox can be solved by invoking a short-lived 'triggering' control of mound nucleation, which may have been of internal (seep) origin, followed by relaying growth controls, probably from external fluxes. However, this can only be proven by deep drilling.

Another possibility could be microbial mediation within the initial development stage, as has been observed in Paleozoic mounds. Such processes can favour mineral precipitation and stabilize mineral frameworks to provide anchorage and protection. Microbial mediation in crust or hardground might have enhanced the chances for the corals to settle and trigger mound growth. But again, the presence of internal fluids (CH<sub>4</sub> or H<sub>2</sub>S) is needed (Henriët *et al.*, 2002).

Also van Weering *et al.* (2003b) feel the need of invoking a supplementary control stimulating the corals to settle, on top of the oceanographic control, which can stimulate coral thriving after settling. In both Rockall provinces, the role of hydrocarbon seepage is ruled out. However, both provinces are located above acoustic basement rocks. In this case, the initial coral settling could have been attracted by escaping pore-water fluids of unknown origin. They can possibly be related to cooling of volcanic sediments extruded after initial formation of the Rockall Trough.

Although the origin of the Darwin mounds also is related to fluid escape (porewater) and pockmarks, it is clear that fluid escape alone is not sufficient to support coral colonies (Masson *et al.*, 2003).



## References

- Akhmetzhanov, A. M., Kenyon, N. H., Ivanov, M. K. & Cronin, B. (2003) The Continental Rise West of Porcupine Seabight, Northeast Atlantic. In: *European margin sediment dynamics: side-scan sonar and seismic images* (Ed. by J. Mienert and P. P. E. Weaver), Springer-Verlag, Heidelberg, 187-192.
- Auffret, G. A., Zaragosi, S., Dennielou, B., Cortijo, E., Van Rooij, D., Grousset, F. E., Pujol, C., Eynaud, F. & Siegert, M. (2002) Terrigenous fluxes at the Celtic margin during the last glacial cycle. *Marine Geology*, **188**, 79-108.
- Bailey, W., Shannon, P. M., Walsh, J. J. & Unnithan, V. (2003) The spatial distributions of faults and deep sea carbonate mounds in the Porcupine Basin, offshore Ireland. *Marine and Petroleum Geology*, **20**, 509-522.
- Beyer, A., Schenke, H. W., Klenke, M. & Niederjasper, F. (2003) High resolution bathymetry of the eastern slope of the Porcupine Seabight. *Marine Geology*, **198**, 27-54.
- Chachkine, P. & Akhmetzhanov, A. M. (1998) Subbottom currents on the Porcupine Margin study by side-scan sonars. In: *Geosphere-biosphere coupling: Carbonate Mud Mounds and Cold Water Reefs* (Ed. by B. De Mol), UNESCO, Paris, IOC Workshop Report, **143**, 30.
- Crocker, P. F. & Shannon, P. M. (1995) The petroleum geology of Ireland's offshore basins: introduction. In: *The Petroleum Geology of Ireland's Offshore Basins* (Ed. by P. F. Crocker and P. M. Shannon), Geological Society, London, Special Publication, **93**, 1-8.
- De Mol, B. (2002) Development of coral banks in Porcupine Seabight (SW Ireland): A multidisciplinary approach. Ph.D. thesis, Department of Geology and Soil Science. *Ghent University*, Gent, 363 pp.
- De Mol, B., Van Rensbergen, P., Pillen, S., Van Herreweghe, K., Van Rooij, D., McDonnell, A., Huvenne, V., Ivanov, M., Swennen, R. & Henriët, J.-P. (2002) Large deep-water coral banks in the Porcupine Basin, southwest of Ireland. *Marine Geology*, **188**, 193-231.
- Foubert, A., Beck, T., Wheeler, A. J., Opderbecke, J., Grehan, A., Klages, M., Thiede, J., Henriët, J.-P. & the Polarstern ARK-XIX/3a shipboard party. (in press) New view of the Belgica Mounds, Porcupine Seabight, NE Atlantic: Preliminary Results from the Polarstern ARK-XIX/3a ROV cruise. In: *Deep-water Corals & Ecosystems* (Ed. by A. Freiwald and J. M. Roberts), Springer-Verlag, Heidelberg.
- Frederiksen, R., Jensen, A. & Westerberg, H. (1992) The distribution of the scleractinian coral *Lophelia pertusa* around the Faro Islands and the relation to internal tidal mixing. *Sarsia*, **77**, 157-171.
- Games, K. P. (2001) Evidence of shallow gas above the Connemara oil accumulation, Block 26/28, Porcupine Basin. In: *The Petroleum Exploration of Ireland's Offshore Basins* (Ed. by P. M. Shannon, P. Haughton and D. Corcoran), Geological Society, London, Special Publication, **188**, 361-373.
- Haq, B. U., Hardenbol, J. & Vail, P. R. (1987) Chronology of Fluctuating Sea Levels Since the Triassic. *Science*, **235**, 1156-1166.
- Hargreaves, P. M. (1984) The Distribution of Decapoda (Crustacea) in the open ocean and near-bottom over an adjacent slope in the northern North-East Atlantic Ocean during Autumn 1979. *Journal of the Marine Biological Association of the United Kingdom*, **64**, 829-857.
- Henrich, R., Freiwald, A., Betzler, C., Bader, B., Schäfer, P., Samtleben, C., Brachert, T. C., Wehrmann, A., Zankl, H. & Kühlmann, D. H. H. (1995) Controls on Modern Carbonate Sedimentation on Warm-temperate to Arctic Coasts, Shelves and Seamounts in the Northern Hemisphere: Implications for Fossil Counterparts. *Facies*, **32**, 71-108.
- Henriët, J.-P., De Mol, B., Pillen, S., Vanneste, M., Van Rooij, D., Versteeg, W., Crocker, P. F., Shannon, P. M., Unnithan, V., Bouriak, S., Chachkine, P. & The Porcupine-Belgica 97 Shipboard Party. (1998) Gas hydrate crystals may help build reefs. *Nature*, **391**, 648-649.
- Henriët, J.-P., De Mol, B., Vanneste, M., Huvenne, V., Van Rooij, D. & the "Porcupine-Belgica" 97, 98 and 99 shipboard parties (2001) Carbonate mounds and slope failures in the Porcupine Basin: a

- development model involving past fluid venting. In: *The Petroleum Exploration of Ireland's Offshore Basins* (Ed. by P. M. Shannon, P. Haughton and D. Corcoran), Geological Society, London, Special Publication, **188**, 375-383.
- Henriet, J.-P., Guidard, S. & the ODP "Proposal 573" Team (2002) Carbonate mounds as a Possible Example for Microbial Activity in Geological Processes. In: *Ocean Margin Systems* (Ed. by G. Wefer, D. S. M. Billet, D. Hebbeln, B. B. Jorgensen, M. Schlüter and T. C. E. van Weering), Springer-Verlag, Berlin Heidelberg, 439-455.
- Henriet, J.-P., Van Rooij, D., Huvenne, V., De Mol, B. & Guidard, S. (2003) Mounds and Sediment Drift in the Porcupine Basin, West of Ireland. In: *European margin sediment dynamics: side-scan sonar and seismic images* (Ed. by J. Mienert and P. P. E. Weaver), Springer-Verlag, Heidelberg, 217-220.
- Hovland, M., Croker, P. F. & Martin, M. (1994) Fault-associated seabed mounds (carbonate knolls?) off western Ireland and north-west Australia. *Marine and Petroleum Geology*, **11**(2), 232-246.
- Huthnance, J. M., Coeho, H., Griffiths, C. R., Knight, P. J., Rees, A. P., Sinha, B., Vangriesheim, A., White, M. & Chatwin, P. G. (2001). Physical structures, advection and mixing in the region of Goban Spur. *Deep-Sea Research II*, **48**, 2979-3021.
- Huvenne, V., Blondel, P. & Henriet, J.-P. (2002a) Textural analyses of sidescan sonar imagery from two mound provinces in the Porcupine Seabight. *Marine Geology*, **189**, 323-341.
- Huvenne, V. A. I., Croker, P. F. & Henriet, J.-P. (2002b) A refreshing 3-dimensional view of an ancient sediment collapse and slope failure. *Terra Nova*, **14**, 33-40.
- Huvenne, V. A. I. (2003) Spatial geophysical analysis of the Magellan carbonate build-ups and the interaction with sedimentary processes: key to a genetic interpretation? Ph.D. thesis, Department of Geology and Soil Science. *Ghent University*, Gent, 285 pp.
- Huvenne, V. A. I., Bailey, W., Shannon, P. M., Naeth, J., di Primio, R., Henriet, J.-P., Horsfield, B., de Haas, H., Wheeler, A. J. & Olu-Le Roy, K. (in press) The Magellan mound province in the Porcupine Basin. In: *Modern Carbonate Mound Systems: A window to Earth History* (Ed. by J.-P. Henriet and C. Dullo), Springer-Verlag, Heidelberg.
- Johnston, S., Doré, A. G. & Spencer, A. M. (2001) The Mesozoic evolution of the southern North Atlantic region and its relationship to basin development in the south Porcupine Basin, offshore Ireland. In: *The Petroleum Exploration of Ireland's Offshore Basins* (Ed. by P. M. Shannon, P. Haughton and D. Corcoran), Geological Society, London, Special Publication, **188**, 237-263.
- Kenyon, N. H. (1986) Evidence from bedforms for a strong poleward current along the upper continental slope of northwest Europe. *Marine Geology*, **72**, 187-198.
- Kenyon, N. H., Akhmetzhanov, A. M., Wheeler, A. J., van Weering, T. C. E., de Haas, H. & Ivanov, M. K. (2003) Giant carbonate mud mounds in the southern Rockall Trough. *Marine Geology*, **195**, 5-30.
- Kenyon, N. H., Belderson, R. H. & Stride, A. H. (1978) Channels, canyons and slump folds between South-West Ireland and Spain. *Oceanologica Acta*, **1**(3), 369-380.
- Kenyon, N. H., Ivanov, M. K., Akhmetzhanov, A. M. & New, A. L. (1998) The current swept continental slope and giant carbonate mounds to the West of Ireland. In: *Geosphere-biosphere coupling: Carbonate Mud Mounds and Cold Water Reefs* (Ed. by B. De Mol), UNESCO, Paris, IOC Workshop Report, **143**, 24.
- Le Danois, E. (1948) *Les profondeurs de la mer*. Payot, Paris, 303 pp.
- Masson, D. G., Bett, B. J., Billet, D. S. M., Jacobs, C. L., Wheeler, A. J. & Wynn, R. B. (2003) The origin of deep-water, coral-topped mounds in the northern Rockall Trough, Northeast Atlantic. *Marine Geology*, **194**, 159-180.
- Masson, D. G. & Miles, P. R. (1986) Structure and Development of Porcupine Seabight Sedimentary Basin, Offshore Southwest Ireland. *The American Association of Petroleum Geologists Bulletin*, **70**(5), 536-548.

- Mathys, M. (2001) Hoge-resolutie geofysische studie van gasmigratie in oppervlakkige mariene sedimenten ter hoogte van olie- en gasreservoirs, Porcupine Bekken (SW Ierland). M.Sc. thesis, Department of Geology and Soil Science. *Ghent University*, Gent, 157 pp.
- McCann, T., Shannon, P. M. & Moore, J. G. (1995a) Fault patterns in the Cretaceous and Tertiary (end syn-rift, thermal subsidence) succession of the Porcupine Basin, offshore Ireland. *Journal of Structural Geology*, **17**(2), 201-214.
- McCann, T., Shannon, P. M. & Moore, J. G. (1995b) Fault styles in the Porcupine Basin, offshore Ireland: tectonic and sedimentary controls. In: *The Petroleum Geology of Ireland's Offshore Basins* (Ed. by P. F. Croker and P. M. Shannon), Geological Society, London, Special Publication, **93**, 371-383.
- McDonnell, A. (2001) Comparative Tertiary basin development in the Porcupine and Rockall Basins. Ph.D. thesis, Department of Geology. *University College Dublin*, Dublin, 201 pp.
- McDonnell, A. & Shannon, P. M. (2001) Comparative Tertiary stratigraphic evolution of the Porcupine and Rockall basins. In: *The Petroleum Exploration of Ireland's Offshore Basins* (Ed. by P. M. Shannon, P. Haughton and D. Corcoran), Geological Society, London, Special Publication, **188**, 323-344.
- Moore, J. G. & Shannon, P. M. (1991) Slump structures in the Late Tertiary of the Porcupine Basin, offshore Ireland. *Marine and Petroleum Geology*, **8**, 184-197.
- Moore, J. G. & Shannon, P. M. (1992) Palaeocene-Eocene deltaic sedimentation, Porcupine Basin, offshore Ireland—a sequence stratigraphic approach. *First Break*, **10**(12), 461-469.
- Moore, J. G. & Shannon, P. M. (1995) The Cretaceous succession in the Porcupine Basin, offshore Ireland: facies distribution and hydrocarbon potential. In: *The Petroleum Geology of Ireland's Offshore Basins* (Ed. by P. F. Croker and P. M. Shannon), Geological Society, London, Special Publication, **93**, 345-370.
- Naylor, D. & Shannon, P. M. (1982) *The Geology of Offshore Ireland and West Britain*. Graham & Trotman Ltd., London, 161 pp.
- New, A. L., Barnard, S., Herrmann, P. & Molines, J.-M. (2001) On the origin and pathway of the saline inflow to the Nordic Seas: insights from models. *Progress in Oceanography*, **48**, 255-287.
- Pillen, S. (1998) Detailkartering en seismische analyse van de Magellan-mounds in het Porcupine Bekken, ten zuidwesten van Ierland. M.Sc. thesis, Department of Geology and Soil Science. *Ghent University*, Gent, 89 pp.
- Pingree, R. D. & Le Cann, B. (1989) Celtic and Armorican slope and shelf residual currents. *Progress in Oceanography*, **23**, 303-338.
- Pingree, R. D. & Le Cann, B. (1990) Structure, strength and seasonality of the slope currents in the Bay of Biscay region. *Journal of the Marine Biological Association of the United Kingdom*, **70**, 857-885.
- Plets, R. (2002) Onderzoek van sedimentstabiliteit langs de Iberische continentale rand: Galicia Bank en epicentrale zone van de aardbeving van Lissabon. M.Sc. thesis, Dept. of Geology and Soil Science. *Ghent University, Belgium*, Gent, 114 pp.
- Reston, T. J., Pennell, J., Stubenrauch, A., Walker, I. & Perez-Gussinye, M. (2001) Detachment faulting, mantle serpentinization, and serpentinite-mud volcanism beneath the Porcupine Basin, southwest of Ireland. *Geology*, **29**(7), 587-590.
- Rice, A. L., Billet, D. S. M., Thurston, M. H. & Lampitt, R. S. (1991) The Institute of Oceanographic Sciences Biology programme in the Porcupine Seabight: background and general introduction. *Journal of the Marine Biological Association of the United Kingdom*, **71**, 281-310.
- Rice, A. L., Thurston, M. H., & New, A. L. (1990) Dense aggregations of a hexactinellid sponge, *Pheromena carpenteri*, in the Porcupine Seabight (northeast Atlantic Ocean). *Progress in Oceanography*, **24**, 179-196.
- Rogers, A. D. (1999) The biology of *Lophelia pertusa* (LINNAEUS 1758) and other deep-water reef-forming corals and impacts from human activities. *International Reviews of Hydrobiology*, **84**(4), 315-406.

- Shannon, P. M. (1991) The development of Irish offshore sedimentary basins. *Journal of the Geological Society of London*, **148**, 181-189.
- Shannon, P. M. (1992) Early Tertiary submarine fan deposits in the Porcupine Basin, offshore Ireland. In: *Basins on the Atlantic Seaboard: Petroleum Geology, Sedimentology and Basin Evolution* (Ed. by J. Parnell), Geological Society, London, Special Publication, **62**, 351-373.
- Shannon, P. M., Corcoran, D. & Haughton, P. (2001) The petroleum exploration of Ireland's offshore basins: introduction. In: *The Petroleum Exploration of Ireland's Offshore Basins* (Ed. by P. M. Shannon, P. Haughton and D. Corcoran), Geological Society, London, Special Publication, **188**, 1-8.
- Sherwin, T. J. & Taylor, N. K. (1987) Modelling Internal Tide Processes Around the North-west European Shelf Edge. *Advances in Underwater Technology, Ocean Science and Offshore Engineering*, **12**, 263-278.
- Spencer, A. M. & MacTiernan, B. (2001) Petroleum systems offshore western Ireland in an Atlantic margin context. In: *The Petroleum Exploration of Ireland's Offshore Basins* (Ed. by P. M. Shannon, P. Haughton and D. Corcoran), Geological Society, London, Special Publication, **188**, 9-29.
- Stoker, M. S., Nielsen, T., van Weering, T. C. E. & Kuijpers, A. (2002) Towards an understanding of the Neogene tectonostratigraphic framework of the NE Atlantic margin between Ireland and the Faroe Islands. *Marine Geology*, **188**, 233-248.
- Stoker, M. S., van Weering, T. C. E. & Svaerdborg, T. (2001) A mid- to late Cenozoic tectonostratigraphic framework for the Rockall Trough. In: *Petroleum Exploration of Ireland's offshore basins* (Ed. by P. M. Shannon, P. Haughton and D. Corcoran), Geological Society, London, Special Publication, **188**, 411-438.
- Stow, D. A. V. (1982) Bottom currents and contourites in the North Atlantic. *Bull. Inst. Géol. Bassin d'Aquitaine*, **31**, 151-166.
- Tudhope, A. W. & Scoffin, T. P. (1995) Processes of sedimentation in Gollum Channel, Porcupine Seabight: submersible observations and sediment analyses. *Transactions of the Royal Society of Edinburgh: Earth Sciences*, **86**, 49-55.
- Van Rooij, D., Blamart, D. & Unnithan, V. (2001) Cruise Report MD123-Géosciences: Leg 2, part GEOMOUND. RCMG, Gent.
- Van Rooij, D., Huvenne, V. A. I., Moerkerke, G. & Henriët, J.-P. (2002) Cruise Report Belgica 02/12 CADIPOR, Gulf of Cadiz. RCMG, Gent.
- van Weering, T. C. E., de Haas, H., Akhmetzhanov, A. M. & Kenyon, N. H. (2003a) Giant Carbonate Mounds along the Porcupine and SW Rockall Trough Margins. In: *European margin sediment dynamics: side-scan sonar and seismic images* (Ed. by J. Mienert and P. P. E. Weaver), Springer-Verlag, Heidelberg, 211-216.
- van Weering, T. C. E., de Haas, H., de Stigter, H. C., Lykke-Andersen, H. & Kouvaev, I. (2003b) Structure and development of giant carbonate mounds at the SW and SE Rockall Trough margins, NE Atlantic Ocean. *Marine Geology*, **198**, 67-81.
- Wheeler, A. J., Beck, T., Thiede, J., Klages, M., Foubert, A., Grehan, A., Berov, D., Beyer, A., Brennan, C., Buldt, K., Dabrowski, P., Devanathan, V., Dorschel, B., Gault, J., Guinan, J., Gutt, J., Hall-Spencer, J., Kozachenko, M., Kroker, R., Kulaksiz, S., Möller, H.-J., Monteys, F. X., Pfannkuche, O., Pokorna, M., Rathlau, R., Roberts, J. M., Sharma, P., Sumoondur, A. D., Thomsen, L., Tseu, G., Unnithan, V. & Wilson, M. (in press-a) Deep-water Coral Mounds on the Porcupine Bank, Irish Margin: Preliminary Results from the Polarstern ARK-XIX/3a ROV cruise. In: *Deep-water Corals & Ecosystems* (Ed. by A. Freiwald and J. M. Roberts), Springer-Verlag, Heidelberg.
- Wheeler, A. J., Bett, B. J., Billet, D. S. M. & Masson, D. (2000) Very high resolution side-scan mapping of deep-water coral mounds: surface morphology and processes affecting growth. *EOS Transactions*, **81**(48), A0007.

- Wheeler, A. J., Beyer, A., Freiwald, A., de Haas, H., Huvenne, V. A. I., Kozachenko, M. & Olu-Le Roy, K. (in press-b) Morphology and Environment of Deep-water Coral Mounds on the NW European Margin. In: *Modern Carbonate Mound Systems: A window to Earth History* (Ed. by J.-P. Henriot and C. Dullo), Springer-Verlag, Heidelberg.
- Wheeler, A. J., Kenyon, N. H., Ivanov, M. K., Beyer, A., Cronin, B., McDonnell, A., Schenke, H. W., Akhmetzhanov, A. M., Satur, N. & Zaragosi, S. (2003) Canyon Heads and Channel Architecture of the Gollum Channel, Porcupine Seabight. In: *European margin sediment dynamics: side-scan sonar and seismic images* (Ed. by J. Mienert and P. P. E. Weaver), Springer-Verlag, Heidelberg, 183-186.
- Wheeler, A. J., Kozachenko, M., de Haas, H., Huvenne, V. A. I., Masson, D. G. & Olu-Le Roy, K. (in press-c) Hydrodynamically Influenced Small Deepwater Reefs (Moirra Mounds) in the Porcupine Seabight, NE Atlantic. In: *Modern Carbonate Mound Systems: A window to Earth History* (Ed. by J.-P. Henriot and C. Dullo), Springer-Verlag, Heidelberg.
- White, M. (2001) Hydrography and physical dynamics at the NE Atlantic margin that influence the deep water cold reef ecosystem. Dept. of Oceanography, NUI, Galway, Ireland.
- White, M. (in press) The hydrographic setting for the carbonate mounds of the Porcupine Bank and Sea Bight. In: *Modern Carbonate Mound Systems: A window to Earth History* (Ed. by J.-P. Henriot and C. Dullo), Springer-Verlag, Heidelberg.
- White, M. & Bowyer, P. (1997) The shelf-edge current north-west of Ireland. *Annales Geophysicae*, **15**, 1076-1083.
- White, M., Raine, R. & Bowyer, P. (2000) Slope current dynamics and variability west of Ireland. Martin Ryan Marine Science Institute, NUI, Galway, Ireland.
- Zaragosi, S., Auffret, G. A., Faugères, J.-C., Garlan, T., Pujol, C. & Cortijo, E. (2000) Physiography and recent sediment distribution of the Celtic Deep-Sea Fan, Bay of Biscay. *Marine Geology*, **169**, 207-237.
- Ziegler, P. A. (1982) *Geological Atlas of Western and Central Europe*. Shell Internationale Petroleum Maatschappij B.V., Amsterdam, 130 pp.



## Chapter III: Material and methodology

While De Mol (2002) and Huvenne (2003) focussed on the characterisation and spatial analysis of the coral banks in the Porcupine Seabight, this study will try to emphasize the various aspects and record of the temporal and environmental changes since Middle Cenozoic times. This requires a wide range of methodologies, because the variety of deposits that can be encountered on this scale can not be interpreted unambiguously based on a single survey technique (Stow *et al.*, 2002; Rebesco & Stow, 2001; Faugères *et al.*, 1999). In this chapter, an overview of the available geophysical and sedimentological data will be presented together with a discussion about their acquisition and processing.

All maps illustrating this thesis were mainly generated using the *Generic Mapping Tools* (GMT) freeware (Wessel & Smith, 1991) and *Golden Software Surfer* version 8.

### 3.1. Geophysical data

The most important source of “in-depth” geophysical information are the 2D seismic profiles acquired by the RCMG. Morphological and recent depositional processes were interpreted from the available multibeam, subbottom profiler and side-scan sonar data. It is evident that some of these data were already discussed by De Mol (2002) and Huvenne (2003), but within the framework and the objectives of this research project they were processed, interpreted and applied in a different way, so they form complementary data sets.

#### 3.1.1 2D seismic data

From 1997 up to 2003, the RCMG organised 6 seismic campaigns with R/V Belgica to the Porcupine Seabight, SW off Ireland. Here, about 1500 km of single-channel reflection seismic data was collected over the study area. Figure 3.1 displays those which have been used for this study. Most of these data were acquired with a SIG surface sparker source and recorded with a single-channel surface streamer, both towed with an offset of approximately 20 to 25 m behind the ship at about of 0.5 to 1 m below the sea surface. Only a few profiles used for this study were acquired with a 15 cubic inch watergun, in a deeptow 4-channel configuration during the Porcupine-Belgica 2000 campaign.

These data were recorded digitally on board with the *ELICS Delph 2* system and already underwent a basic bandpass filtering. At the end of each campaign, the *ELICS* data was merged with the navigational GPS data into the standard SEG-Y format. The technical specifications of these data are displayed in table 3.1.

In general, the standard vertical resolution of sparker data varies between 0.4 to 1 m, while those from watergun data varies from 0.6 to 1.7 m. Most of these parameters and characteristics have been calculated and discussed by De Mol (2002). The acoustic penetration of the sparker source ranges from 400 (average) to 800 (maximal) ms two-way travel time (TWT). The deeptow configuration yielded a penetration between 100 to 200 ms TWT.

<b>Campaign</b>	<b>1997</b>	<b>1998</b>	<b>1999</b>	<b>2000</b>	<b>2000</b>	<b>2001</b>	<b>2003</b>
<i>Source</i>	Sparker	Sparker	Sparker	Sparker	Watergun	Sparker	Sparker
<i>Energy</i>	500 J	500 J	500 J	500 J	140 bar	500 J	500 J
<i>Sampling frequency</i>	5 kHz	4 kHz	4 kHz	8 kHz	5 kHz	8 kHz	5 kHz
<i>Shot interval</i>	2-3 s	2-3 s	2.5-4 s	2-3 s	2.5 s	3 s	3 s
<i>Record length</i>	1-2.5 s*	2.8 s	2-3.5 s	2.5 s	2 s	2.75 s	2-2.5 s
<i>Tow speed</i>	2-4 kn	2-4.7 kn	3-4.5 kn	2.3-3.7 kn	2.2-2.7 kn	2-4.1 kn	0.3-3.3 kn
<i>Delph bandpass</i>	150 Hz Highpass	200 Hz – 3 kHz	200 Hz – 3 kHz	100 Hz – 10 kHz	60 Hz – 10 kHz	60 Hz – 20 kHz	200 Hz – 2 kHz

**Table 3.1:** Technical specifications of the seismic acquisition parameters used during the subsequent RCMG campaigns with R/V Belgica in the Porcupine Seabight. (\*) Some of the data acquired during the 1997 campaign were recorded with a delay.

The obtained network of profiles is organised in a general N60° orientation, running perpendicular to the slope (Fig. 3.1). The distance between adjacent profiles amounted to about 3 km. Only a limited number of long, alongslope (N155°) lines have been acquired. During later campaigns, lines were acquired in other directions in order to make a detailed survey of a specific area or to obtain information on special features.

As a next step, a thorough quality control was made of all profiles acquired in the study area. One of the main selection criteria was the penetration depth, signal-to-noise ratio and stratigraphic significance. After this selection, the profiles were digitally processed with *Landmark PROMAX* software on a *SUN* workstation. Due to the different recording settings and weather conditions of each campaign, a different work flow was used in order to enhance the quality of the profiles. Generally, the data processing involved a first, broad-window *Butterworth* bandpass filter (200 Hz with a 24 db/oct slope and 2000 Hz with a 36 db/oct slope), *minimum phase predictive deconvolution* (with a 20 ms window), followed by a second *Butterworth* bandpass filter (250 Hz with a 24 db/oct slope and 700 Hz with a 36 db/oct slope). Additionally, a *true amplitude recovery* (Porcupine-Belgica 1998, 1999 and 2001) or an *automatic gain control* (Porcupine-Belgica 2003) was applied. Some of the profiles were also swell-filtered using the method described by Huvenne (2003) or with the swell-filter newly developed by P. Staelens (RCMG, Ghent University).

Subsequently, the profiles were plotted on 55 cm wide paper and covered with transparency foil for the interpretation and location of unconformities, as well as for the temporal and spatial study of sedimentary processes. Due to the relatively large “mesh” size of the obtained network and the scale and complexity of the sedimentary packages encountered in the study area, a digital and automated mapping was not performed, because it would oversimplify the obtained data. Moreover, this has already been performed and described by De Mol (2002) using data from the 1997, 1998, 2000 and 2001 campaigns. On the other hand, the latter method does not allow displaying the location of specific structures and morphologic features.

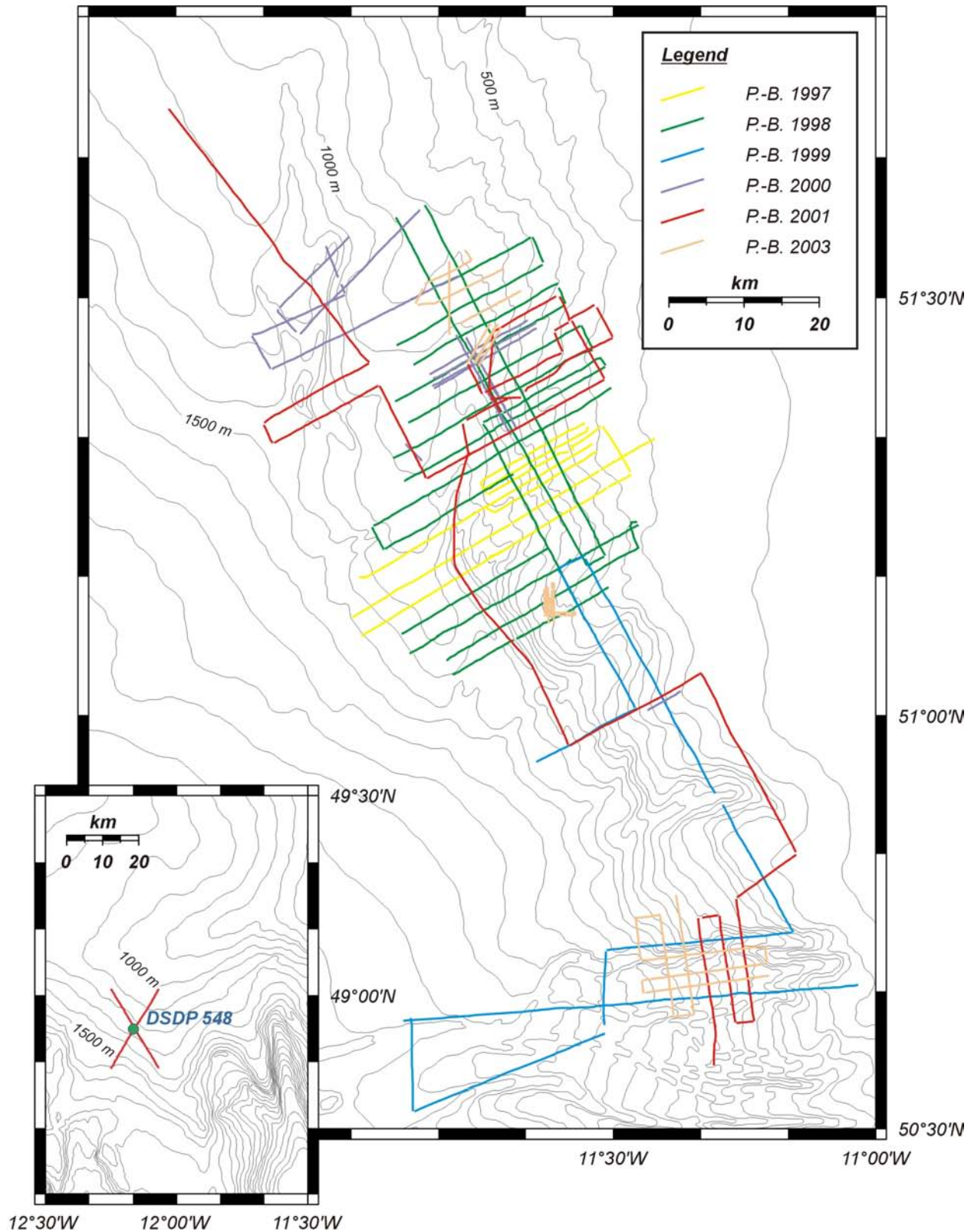


**Figure 3.1:** Overview map of the very high-resolution single-channel seismic reflection profiles acquired by the RCMG during the Porcupine-Belgica campaigns from 1997 to 2003 with R/V Belgica. Only the profiles used for this research project are displayed on this map.

### 3.1.2 Bathymetric data

General bathymetric data with a 100 m contour interval was available through the 1997 edition of the IOC/IHO *General Bathymetric Chart of the Ocean* (GEBCO).

Within the framework of the GEOMOUND project, detailed multibeam bathymetric information was acquired during the ANTXVII/4 cruise of R/V Polarstern (May-June 2000) over a 15 to 20 km wide strip on the eastern slope of the Porcupine Seabight (Fig. 3.2). These data were collected by means of a 15.5 kHz *Hydrosweep DS-2* multibeam echosounder and were processed at the Alfred-Wegener-Institut für Polar- und Meeresforschung (AWI), Bremerhaven. The accuracy of this system is expected to be about 1% of the water depth. Also the footprint size is dependent of the water depth, ranging from 4% near the center beam and 7% at the outer beam, or respectively 30 and 52.5 m at an average water depth of 750 m in the studied area (Beyer *et al.*, 2003).

### 3.1.3 Side-scan sonar data

Since 1997, several campaigns with side-scan sonar equipment were carried out in the PSB. Although their primary objective was to map and visualise the coral banks, the side-scan sonar imagery and the simultaneously recorded subbottom profiler records were also used to study the recent sedimentary processes (ECOMOUND). In this study, the data of two campaigns will be used as support data because most of these data have already been discussed by other authors (Fig. 3.2).

During the TTR7 campaign on board of R/V Prof. Logachev in July of 1997, four strips of high-resolution *OREtech* side-scan sonar imagery were acquired within the Belgica Mound Province. Two adjacent strips were recorded in a south-north direction and the two other ones in an east-west direction (Fig. 3.2). This system operates at 30 kHz and is able to insonify a swath of 2000 m (1000 m on either side). For this purpose, the vehicle was towed at about 130 m above the sea floor. In conjunction with the side-scan sonar, the *OREtech* system also contains a 6 kHz acoustic subbottom profiler yielding a penetration of about 10 m. The paper data were already discussed by Van Rooij (1998) and De Mol (2002) while a textural analysis of the digitally processed data was performed by Huvenne *et al.* (2002).

A more detailed and extensive side-scan sonar coverage was performed during the M2002 campaign on board of R/V Pelagia in June-July 2002 (de Haas *et al.*, 2002). The imagery was obtained by the 30 KHz side-scan sonar of the TOBI of the Southampton Oceanography Centre (SOC). Here, a total swath width of 6000 m (3000 on either side) could be obtained while the instrument was towed at about 300 to 400 m above the seabed. The 3.5 kHz subbottom profiler record on board R/V Pelagia was acquired simultaneously with the side-scan sonar imagery. Both the TOBI data processing with the SOC *PRISM* software system (Le Bas & Hühnerbach, 1999), as well as the description of the features encountered in the BMP, is explained in Huvenne (2003).

Within the framework of this research project, the previous two datasets will be interpreted and integrated with the other geophysical and sedimentological data, with a special focus on sedimentary processes around the coral banks.

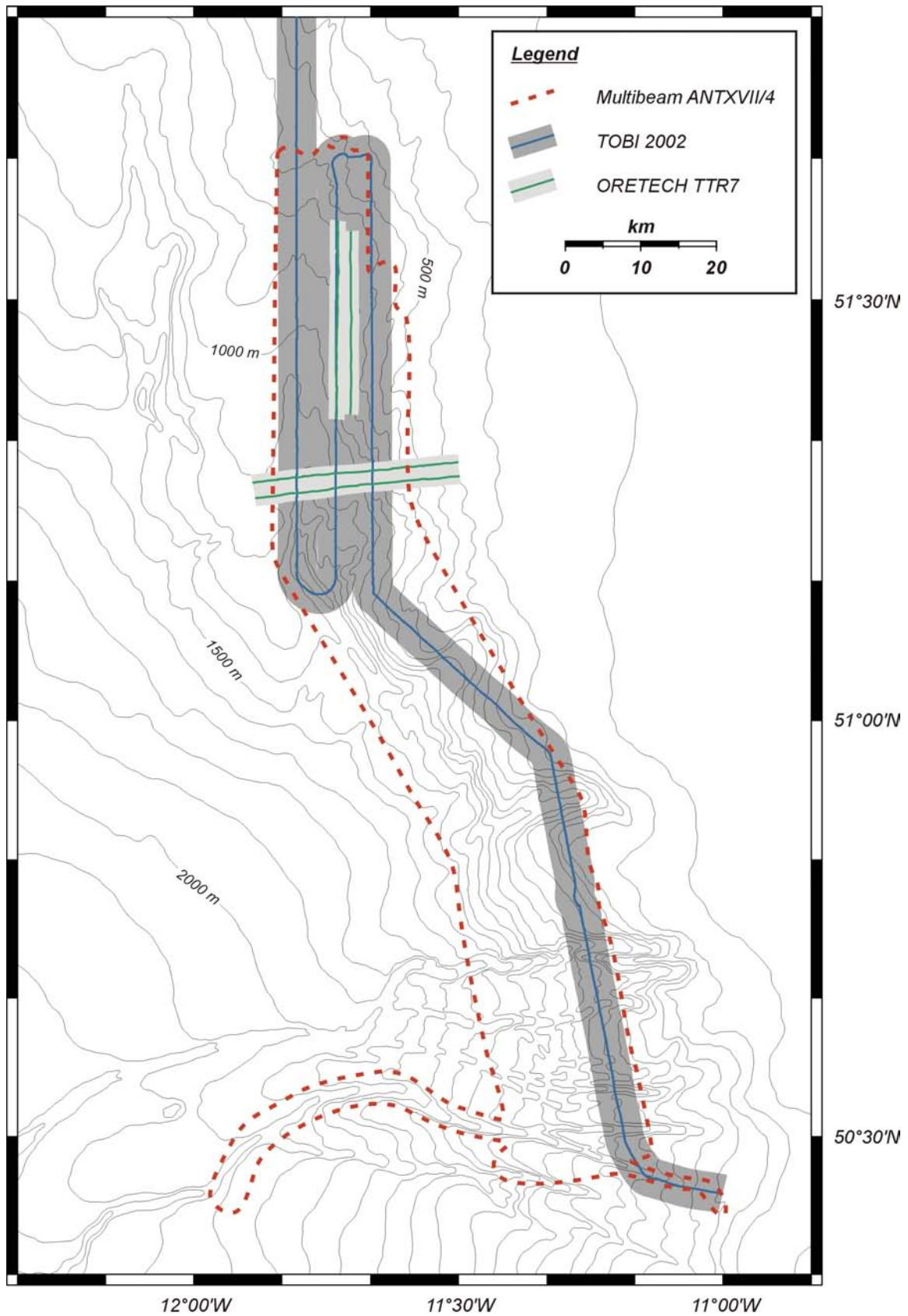


**Figure 3.2:** Overview map of the available bathymetric and side-scan sonar data in the study area. The outline of the ANTVXII/4 multibeam data is indicated in red dashed lines. The tracks and swath of the TTR7 and TOBI 2002 side-scan sonar and subbottom profiler data are also indicated.

Additional very-high resolution side-scan sonar information was made available through a cooperation with Dr. Andrew Wheeler and Max Kozachenko from the University College Cork, Ireland. A large area of the BMP was surveyed with a dual frequency *GeoAcoustic* (100 and 410 kHz) side-scan sonar in conjunction with a 3.5 kHz sub-bottom profiler on board of RRS Discovery in July and August 2000 (Wheeler *et al.*, 2000; Wheeler *et al.*, in press-a; Wheeler *et al.*, in press-b; Kozachenko, in prep.). The side-scan sonar swath width was 600 m at 100 kHz and 200 m at 410 kHz. The acquired digital side-scan sonar data also was processed at the SOC using the *PRISM* software. A part of this data was incorporated in a joint publication, submitted for the GEOMOUND-ECOMOUND book “Modern Carbonate Mound Systems: A window to Earth History” (Van Rooij *et al.*, submitted).

### 3.2. Sedimentological data

Core data provide an insight in both the nature of the present and past key sedimentary processes within the study area, and their temporal variability. In this section, an overview is presented of the available data, the framework in which they were acquired and the kind of analyses applied. This will be followed by a brief discussion of the background and methodology of the performed analyses.

#### 3.2.1 Overview of available core data

Within the framework of this research project, a number of sedimentary archives have been studied. These cores were acquired during campaigns framing into one or more of the earlier mentioned projects. The locations and specifications of the core, as well as an overview of the performed analysis are illustrated in table 3.2 and figure 3.3.

<b>Core</b>	<b>Type</b>	<b>Depth m</b>	<b>Length cm</b>	<b>Latitude</b>	<b>Longitude</b>	<b>P</b>	<b>L</b>	<b>X<sub>1</sub></b>	<b>X<sub>2</sub></b>	<b>M</b>	<b>I</b>	<b>T</b>	<b>G</b>
ENAM-9901	PC	948	635	51°25.750'N	11°45.970'W	x							x
ENAM-9905	PC	1025	633	51°26.380'N	11°46.940'W	x							x
MD99-2327	CC	651	2625	51°23.770'N	11°39.240'W	x	x	x	x	x	x	x	x
BBC00-0606	BC	651	21	51°23.770'N	11°39.240'W					x	x	x	x
MD01-2449	CC	435	2484	51°01.683'N	11°24.816'W	x	x		x			x	x
MD01-2450	CC	944	1197	51°22.521'N	11°43.812'W	x	x						
MD01-2452	CC	617	1843	52°19.396'N	12°41.477'W	x	x						
MD01-2453	CC	359	1763	53°04.441'N	12°31.584'W	x	x						
MD01-2457	CC	360	1769	53°04.599'N	12°31.300'W	x	x						
MD01-2464	CC	1014	1829	50°43.890'N	11°15.237'W	x	x		x			x	x
BBC03-1302a	BC	1168	13	51°23.572'N	11°48.859'W								
BBC03-1302b	BC	1175	13	51°23.567'N	11°48.843'W								
BBC03-1304a	BC	649	13	51°23.403'N	11°39.936'W								
BBC03-1304b	BC	646	13	51°23.454'N	11°39.901'W								

**Table 3.2:** Overview (chronological) of the available sedimentological data for this research project. Three types of coring equipment were used; standard piston core (PC), the R/V Marion Dufresne Calypso core (CC) and the boxcore (BC). All data has been visually described and is archived by photographic means. Extra analysis performed on these data are marked; physical properties core logging (P), luminosity (L), CORTEX XRF (X<sub>1</sub>), SCOPIX digital radiography (X<sub>2</sub>), mineralogy and lithology (M), biostratigraphy and isotopes (I), thin sections and smear slides (T) and grain size analysis (G).

Cores ENAM-9901 and ENAM-9905 were acquired during the Royal NIOZ ENAM-99 campaign on board of R/V Pelagia in August 1999 and were kindly made available by Dr. Tjeerd Van Weering and Dr. Henk de Haas. The cores were taken respectively on the eastern (upslope) and western (downslope, gully) flank of a mound in the BMP. Together with other cores from this campaign, they were firstly analysed and discussed by Lekens (2000) and later reinterpreted for this thesis.

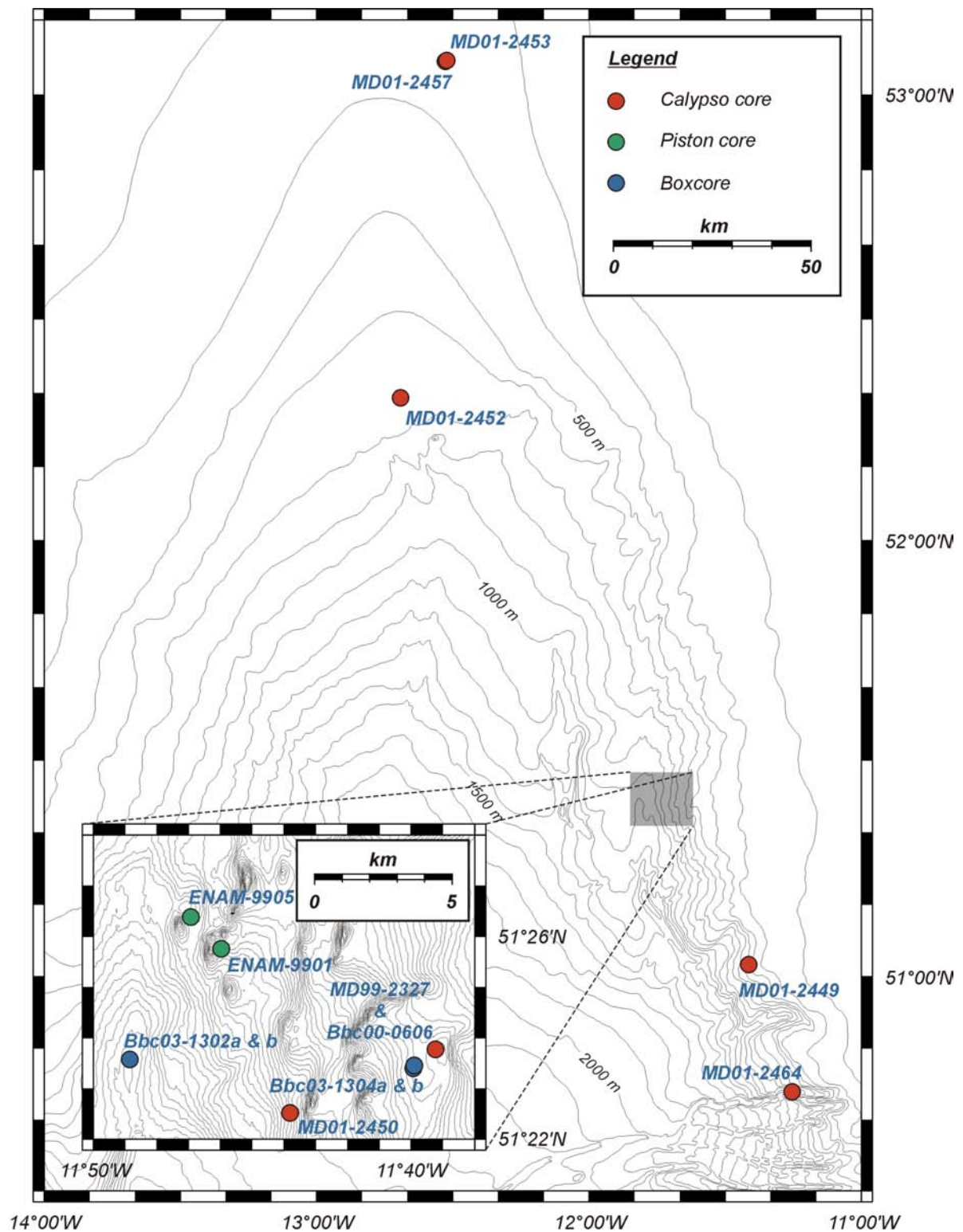


**Figure 3.3:** Overview map of the available core material on the eastern Porcupine Seabight. Due to the high concentration of cores within the Belgica mound province, an inset map with multibeam bathymetry is provided as inset.

Within the framework of the large INTERPOLE/IMAGES V campaign of R/V Marion Dufresne in August 1999 (MD114), Calypso (giant piston) core MD99-2327 was taken from the upper slope of the BMP during the 4<sup>th</sup> leg. This core was stored at the LSCE, Gif-sur-Yvette (France) and was made accessible within a cooperation with Prof. Dr. Laurent Labeyrie and Dr. Dominique Blamart. The analyses of this core constitute the backbone of the sedimentological part discussed in this thesis. A large part of the analyses were carried at the LSCE. Supporting analyses were performed by Dr. Andrew Wheeler and Max Kozachenko (University College Cork, Ireland) and by Dr. Thomas Richter (Royal NIOZ, the Netherlands). A full dataset of this core was submitted to the IMAGES data manager (<http://images.pclab.ifg.uni-kiel.de/frameDB.html>) and can also be retrieved from the PANGAEA database (<http://www.pangaea.de>).

During the Porcupine-Belgica 2000 campaign on board R/V Belgica, boxcore BBC00-0606 was taken on the same location as MD99-2327 in order to obtain the recent seabed surface sediment, which usually is missing when the Calypso core technique is applied (Skinner & McCave, 2003). The boxcore was subsampled into several subcores, which were split into 1 cm thick slices. These are stored at the RCMG and the Marine Biology Section of Ghent University for analyses of hyperbenthic fauna, within the framework of the Ph.D. project of Veronique Vanquickenberghe.

The GEOMOUND project enabled the acquisition of 16 gravity and Calypso cores on board of R/V Marion Dufresne during the MD123 Géosciences campaign in September 2001. These cores were targeted on several on- and off-mound sites within the PSB (BMP, HMP, MMP) and the Rockall Trough (Logachev and Pelagia mound provinces). In this study, 6 of these off-mound cores will be discussed, of which 2 in detail; MD01-2449 on the upper south flank of the Aragorn channel and MD01-2464 in the upper slope part of the Bilbo channel. The other cores were taken at the southern (downslope) side of a mound (MD01-2450), in the sedimentary series overlying a buried Magellan mound (MD01-2452) and two cores within the Connemara (gas) field (MD01-2453 and MD01-2457). Some of these cores were already analysed on their magnetic properties (Foubert, 2002) and will receive further attention within the course of the Ph.D. project of Anneleen Foubert. Core MD01-2452 also was the topic of a brief, but detailed paleoenvironmental study by Cornilly (2003).

Boxcores BBC03-1302(a&b) and BBC03-1304(a&b) were respectively taken on the floor of the Arwen channel and on top of a mounded morphology during the Porcupine-Belgica 2003 campaign on board of R/V Belgica. These cores were also subsampled and split into 1 cm thick slices. They are stored at the Marine Biology Section of Ghent University for meiofaunal analyses within the framework of the PhD project of Maarten Raes.

### 3.2.2 Multi-sensor core logger data

The *Geotek* multi-sensor core logger (MSCL) has become a very popular tool in climate and ocean sciences since its introduction in 1992 (Ortiz & Rack, 1999; Gunn & Best, 1998; Chi & Mienert, 1996). The strength of this tool is the ability to provide a fast, qualitative, fully automated and non-destructive dataset of gamma density, compressional (P) wave velocity, and magnetic susceptibility (Fig. 3.4). All cores acquired during the MD114 and MD123 campaigns were logged on board R/V

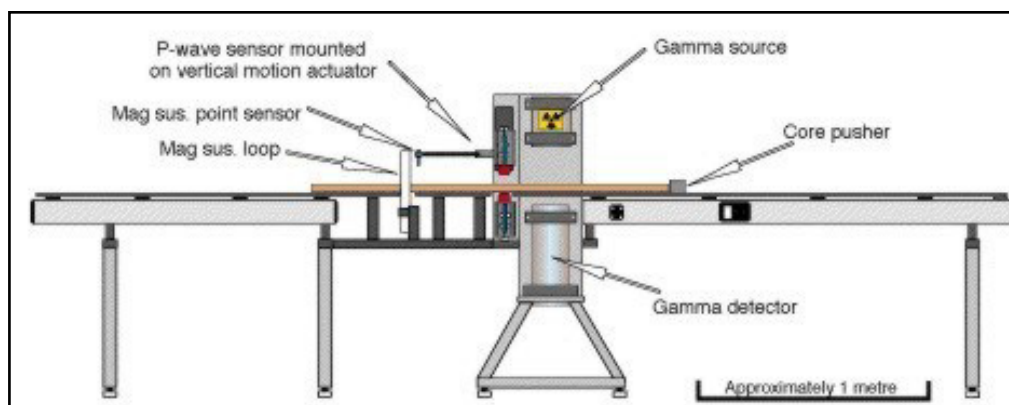


**Figure 3.4:** A typical Geotek multi-sensor core logger split/whole-core configuration as used during the MD114 and MD123 campaigns on board R/V Marion Dufresne (after <http://www.geotek.co.uk>)

Marion Dufresne at a downcore resolution of 2 cm. As a standard procedure, the cores were logged after being cut in sections of 1.5 m length and after the sediment temperature had reached the ambient value.

The MSCL consists of a conveyor system where core sections are pushed along the three main sensors (Schultheiss, 1997; Unterseh, 1997; Gunn & Best, 1998 and after <http://www.geotek.co.uk>):

1. The bulk or **gamma density** ( $\text{g.cm}^{-3}$ ) is measured by means of a  $^{137}\text{Cs}$  gamma source in a lead shield with a 5 mm collimator. The attenuated gamma radiation is measured by a Sodium Iodide scintillation detector. This source and detector are mounted diametrically across the core. The bulk density of the core is calculated by the Geotek MSCL software by comparing the attenuation of gamma rays through the whole core with the attenuation of gamma rays through a calibration section containing different-sized aluminium blocks with known density, filled up with demineralised water.
2. The **P-wave velocity** ( $\text{m.s}^{-1}$ ) and the core diameter, which is also needed for the gamma density calculations, are measured simultaneously by rectilinear displacement transducers. The compressional wave velocity is measured through a 500 kHz piezo-electric ceramic transducer, which is spring-loaded against the sample. However, the results obtained by using this method on whole-core sections should be taken with caution because they can be heavily biased by a bad transducer-core liner contact, voids, water pockets...
3. The **magnetic susceptibility** (MS) is measured by a Bartington MS2B loop sensor (150 mm diameter) or a point sensor for split cores. Both sensors create a low-frequency (0.46 kHz) magnetic field and measure the magnetisation of the material lying within its range. The output readings are generally in the SI scale, giving units in multiples of  $10^{-5}$ .

The data was processed and filtered with an Excel macro function, designed by Dr. Bernard Dennielou (IFREMER, France). Artefacts due to voids or section breaks were manually deleted. The raw and processed data were stored on CD-Rom and archived at the LSCE (Gif-sur-Yvette, France) or in one of the GEOMOUND partner institutes. The GEOMOUND MSCL dataset is also submitted to the PANGAEA database. Unfortunately, only a paper copy was available of the MD99-

2327 MSCL data. The ENAM-99 cores were only measured with a hand-held *Bartington Mark* sensor.

### 3.2.3 Visual sediment properties

All core material has been described visually, with major attention to sedimentary structures, contacts, fossils and colour changes. However, most of the cores in the North Atlantic Ocean are very homogeneous and thus only further analyses can yield more information. The surface of all split cores was photographed and archived as such. Cores taken on board R/V Marion Dufresne were photographed digitally at 50 cm intervals and reconstructed using *Adobe Photoshop*. For this purpose, a special frame has been constructed to assure a correct and homogenous lightning. These conditions are not only important to acquire a precise archived copy of the sediment surface, but do also matter for reflectance reconstructions (Van Rooij, 1999). According to Cortijo *et al.* (1995) and Bauch & Helmke (1999) the colour variations of a sediment core are dependent of three principal components of the sediment: biogenic carbonate, detrital material and volcanic ash. The colour variations due to the carbonate content are highly correlated with climatic variations. This proxy can yield the same variability as recorded in  $\delta^{18}\text{O}$  variations and can be obtained very fast.

The reflectance of a (fresh) sediment core surface can be obtained from the RGB (Red-Green-Blue) color composition of the digital photographs. In this case, the green channel (values from 0 to 256) is representative for the grey-scale (Cortijo *et al.*, 1995). However, this method is susceptible to many possible contaminating effects if no extreme care is taken to ensure the proper lightning.

Therefore, the reflectance of the MD cores was measured with a handheld *Minolta CM-2002 spectrophotometer* with a sample interval of 5 cm. The spectrophotometer was put on the sediment surface and performs its analyses within an 8 mm diameter optical sensor. The spectral reflectance is measured in a frequency band between 400 to 700 nm. In this case, the grey-level value is the luminosity  $L^*$  of the  $L^*a^*b^*$  colour space. Values for  $L^*$  vary from 0 (black) to 100 (white), while the chromatic coordinates  $a^*$  and  $b^*$  respectively represent a shift from red (+60) to green (-60) and from yellow (+60) to blue (-60) (Chapman & Shackleton, 1998; Bauch & Helmke, 1999). The advantage of this system is that the lightning conditions of each sample are identical and thus reproducible. A small disadvantage is that the actual value is calculated as an average over the 8 diameter opening. Very high-frequency colour changes in the sediment will thus be averaged.

### 3.2.4 CORTEX XRF

Since its introduction in 1998, the use of a non-destructive, semi-quantitative X-ray fluorescence (XRF) corescanner has become very popular in paleoceanography studies (Jansen *et al.*, 1998; Arz *et al.*, 1999; Behling *et al.*, 2000; Richter *et al.*, 2001). For this study, core MD99-2327 was scanned with the Royal NIOZ CORTEX scanner (courtesy of Dr. Thomas Richter) with a sample interval of 2 cm. The CORTEX scanner is equipped with an X-ray tube with a Mo target, while the fluorescent radiation is measured with an energy dispersive *Kevec* Si(Li) detector with a 10  $\mu\text{m}$  Be window. The X-ray detector is connected to a multi-channel analyser with a 20 eV spectral resolution. The X-ray tube and detector are oriented in such a way that the detector makes an angle of 45° with the surface of the sample

(Jansen *et al.*, 1998). In this way, major (Al, Ca, Fe, Ti, K and Si) and minor (Mn and Sr) element compositions can be obtained, expressed in counts per second (cps). Ideally, samples for XRF analysis should be dry, homogeneous and have a smooth surface. For XRF logging of the surface of split sediment cores, at least the first two conditions are not satisfied. Effects of sample inhomogeneity are more significant in coarse-grained sediments, and generally more pronounced for elements with lower atomic weight due to their lower response depth to the incident X-ray beam (Jansen *et al.*, 1998). Particularly, the relatively soft Si radiation can be strongly absorbed by ripples on the surface of the core; hence the Si record is less reliable than those of the other elements. Therefore, two intervals of core MD99-2327 (1812-1786 cm and 1651-1510 cm) were not analysed, because it was not possible to create the required smooth sediment surface. Results are presented as percentages of the total element counts. This normalizing procedure reduces noise levels and largely avoids artefacts related to variations in grain-size distribution and surface roughness.

### 3.2.5 SCOPIX radiography

Radiographies of sediment cores are widely used to distinguish the degree and type of bioturbation, observe sedimentary structures and investigate the composition of different beds. Especially in fine-grained clastic environments, radiographies can yield more insight in the nature of the (past) governing sedimentary processes (Leslie, 1993; Piper & Deptuck, 1997; Massé *et al.*, 1998; Yokokawa, 2001; Zaragosi *et al.*, 2001; Auffret *et al.*, 2002).

Digital X-ray images of cores MD99-2327, MD01-2449 and MD01-2464 were obtained from 1 cm thick core slabs with the SCOPIX system (Université Bordeaux I, France). SCOPIX uses a classical X-ray equipment (46 kV, 14mA radiation source) coupled with new radiology instrumentation, connected to a computer for data acquisition and processing (Migeon *et al.*, 1999). The images were obtained with a CCD camera and have each a length of 10 cm and are composed of 464 pixels in the length dimension. These images, with a pixel resolution of 0.21 mm, are plotted in intensity greyscale logs (0 to 256 values). For each core section, the 10 cm long images are linked in order to reconstitute the entire core slab (Lofi & Weber, 2001).

The X-ray attenuation of sediment cores is predominantly determined by the density of the substance. Theoretically, sand is considered to be opaque to X-rays and should have low values (close to 0). On the other hand, mud is transparent to X-rays, so it should have high values (near 255). Sometimes this rule is not followed, because of porosity changes (Migeon *et al.*, 1999; Lofi & Weber, 2001).

### 3.2.6 Sediment properties

An important, but time-consuming aspect of the study of sedimentary processes and paleoceanography concerns the analysis of the sediment properties. This encompasses a wide range of techniques including the study of thin sections and smear slides, the calculation of the bulk density, the separation of the Ice-Rafted Debris (IRD) fraction, the quantification and determination of the composing mineralogy and lithology, as well as the determination of planktonic foraminiferal assemblages. The latter can be further used to compose a stable isotope stratigraphy, which can be applied for relative datations, supported by absolute  $^{14}\text{C}$  datations. The following sections will discuss the rationale and methodology. These techniques were only applied on cores MD99-2327 and BBC00-0606.

### 3.2.6.1 Physical properties

A first part of the analysis consists in the calculation of the porosity **P** and the dry bulk density  $\rho_d$  (g.cm<sup>-3</sup>) of the sediment. The dry bulk density can be used to compare and verify the results of the Geotek MSCL. For this purpose, core MD992327 was sampled every 10 cm (20-30 g), while core BBC00-0606 was split in slabs of 1cm (25-30 g). These wet subsamples were firstly weighed, dried at 60°C and than weighed again (dry) in order to obtain the water content **W**: this is calculated from the difference in total sample weight before and after drying. The dry bulk density was obtained with equations 3.1 and 3.2, assuming a grain density  $\rho_g$  of 2.65 g.cm<sup>-3</sup> and an interstitial water density  $\rho_w$  of 1.024 g.cm<sup>-3</sup> (Auffret *et al.*, 2002; Dennielou, 1997; Van Rooij, 1999):

$$P = 1 / (((\rho_w / \rho_g) \cdot ((1-W) / W)) + 1) \quad (\text{eq. 3.1})$$

$$\rho_d = \rho_g \cdot (1-P) \quad (\text{eq. 3.2})$$

### 3.2.6.2 Coarse sand fraction **F<sub>150</sub>**

In order to obtain the coarse sand fraction with a grainsize superior to 150  $\mu\text{m}$  (**F<sub>150</sub>**), which is generally accepted as being representative for IRD (Grousset *et al.*, 1993; Bond & Lotti, 1995; Robinson *et al.*, 1995; Elliot *et al.*, 1998; Auffret *et al.*, 2002), 5 g of the dry sediment sample was sieved with demineralised water (3 g for the sandy part of core MD99-2327). Together with the lithic content, also the biogenic content (benthic and planktonic foraminifers, pteropods, shell debris...) is included in this fraction, which was dried again at 60 °C and weighed. The weight percentage of the fraction > 150  $\mu\text{m}$  (Wt %) is calculated with equation 3.3:

$$F_{150} = (W_{F150} \cdot 100) / W_d \quad (\text{eq. 3.3})$$

Here, **W<sub>F150</sub>** represents the weight of the fraction > 150  $\mu\text{m}$  (g) and **W<sub>d</sub>** is the weight of the dried sediment (g). **F<sub>150</sub>** was further split to approximately 500 to 1000 grains on which a quantitative and qualitative analysis of the lithic grains and the biogenic content was performed using a conventional binocular microscope. Among the lithic grains, several specific components were recorded: quartz, feldspars, calcite, mica, dark minerals, volcanic material and rock fragments. For the biogenic content, counts were made for planktonic and benthic foraminifera, shell fragments and worm tubes. More detailed information about the determination and use of the foraminifers is discussed in the section below. The obtained results were recalculated and presented as number of grains per 10 g of dry sediment.

### 3.2.6.3 Biostratigraphy and isotopic analysis

A full biostratigraphic analysis using planktonic foraminifera was limited to cores MD99-2327 and BBC00-0606. The classification and determination was performed using the key to genera as defined by Bé (1977), supported by additional information from Hemleben *et al.* (1989) and Boersma (1998). Sieving with a mesh of 150  $\mu\text{m}$  is generally accepted to obtain adult foraminifer species which are useful for stratigraphic and isotopic analyses. These calcareous-walled Globigerinacea dwell within the oceans photic zone and are very susceptible to changes in

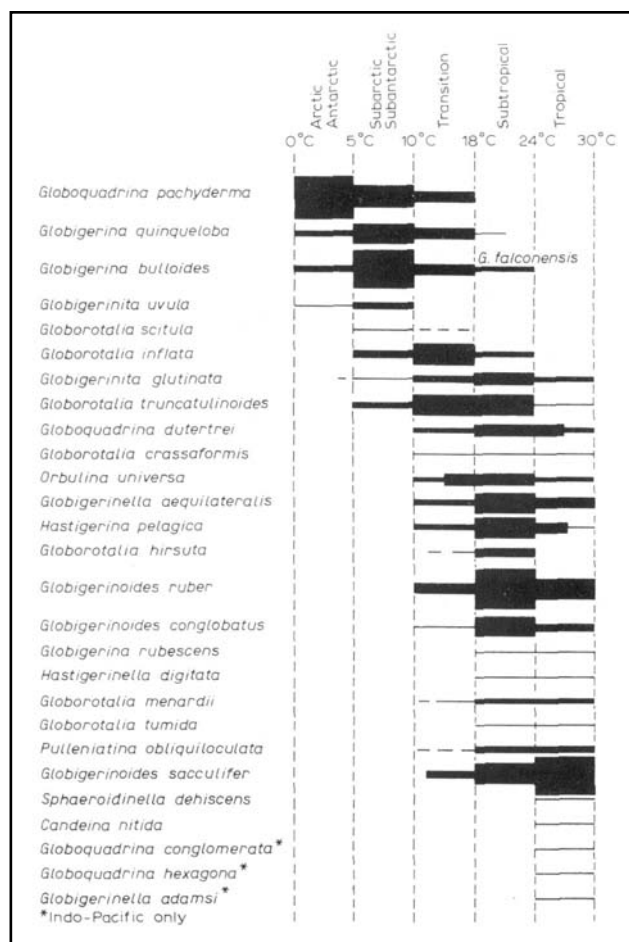


**Figure 3.5:** Planktonic foraminiferal species assemblages and ranges in the five major faunal provinces. Varying thickness represents relative abundance within each zone (Boersma, 1998).

paleotemperature. Bé (1977) distinguished five faunal zones with each a specific species composition: (ant)arctic, sub(ant)arctic, transition, subtropical and tropical (Fig. 3.5). Paleoclimatologic changes throughout the Quaternary, as recorded in ice cores, induce relocations of these faunal zones, which on their turn will be reflected in the assemblage of the planktonic foraminifers in cores. This allows to make bioclimatic subdivisions which are highly comparable with the Marine Isotope Stages (MIS) as defined by Imbrie *et al.* (1984) and Martinson *et al.* (1987) (Bé, 1977; Pujol & Duprat, 1984; Hemleben *et al.*, 1989; Boersma, 1998).

In this study, a total of 12 species and varieties were used in order to obtain a biostratigraphic or bioclimatic framework (from arctic to tropical zones): *Neogloboquadrina pachyderma* (s.), *Globigerina bulloides*, *Neogloboquadrina pachyderma* (d.), *Globigerina quinqueloba*, *Globorotalia inflata*, *Globigerinoides ruber*, *Globorotalia truncatulinoides*, *Globorotalia hirsuta*, *Globigerinella aequilateralis*, *Globigerinita glutinata*, *Orbulina universa* and *Neogloboquadrina dutertrei*.

Specifically, the most important species is the left-coiling variety of *N. pachyderma*. The percentage of left-coiling *N. pachyderma* (s.) relative to the total abundance of planktonic foraminifera (NPS) is generally considered as a proxy for surface water temperature changes. Of equal importance is the ratio of the percentage of the left-coiling variety relative to the entire abundance of both left- and right-coiling *N. pachyderma* (SDS).

In order to obtain a stable oxygen and carbon isotope stratigraphy of core MD99-2327, between 10 and 20 tests of *N. pachyderma* (s.) were picked from the size fraction between 150 and 250  $\mu\text{m}$  and were ultrasonically cleaned for stable isotope measurements ( $\delta^{18}\text{O}$  and  $\delta^{13}\text{C}$ ) at the LSCE (Gif-sur-Yvette, France). The analyses were performed on a *VG Optima* mass spectrometer equipped with a “Kiel device” for automatic acidification of individual samples. The isotopic values are reported as per mil deviation with respect to the international V-PDB standard. The uncertainties on the isotope measurements are 0.08 and 0.05 ‰ respectively for oxygen and carbon. The obtained results were compared with the orbital-tuned record proposed by Martinson *et al.* (1987) in order to obtain a chronostratigraphic framework.

Additionally, accelerator mass spectrometry  $^{14}\text{C}$  dates were obtained on two monospecific samples of *N. pachyderma* (s.) of core MD99-2327 (Table 3.3). These analyses were also performed at the LSCE and have been corrected for a mean reservoir age of 400 years (Bard, 1998).

<b>Laboratory reference</b>	<b>Material</b>	<b>Depth</b>	<b><math>^{14}\text{C}</math> age</b>	<b>Error (<math>1\sigma</math>)</b>
102 508 (LSCE, France)	<i>N. pachyderma</i> s.	90 cm	15.19 ka BP	130 a
102 509 (LSCE, France)	<i>N. pachyderma</i> s.	440 cm	17.38 ka BP	140 a

**Table 3.3:** AMS  $^{14}\text{C}$  ages of core MD99-2327, corrected for the reservoir effect of the ocean.

No detailed (isotope) stratigraphy was made for the benthic foraminiferal community, because their abundance within  $F_{150}$  is generally low, except for two species. *Uvigerina mediteranea* is like *Uvigerina bradyana* (or also *perigrina*) an outer shelf to slope species living in temperate environments, which is superabundant within PSB. It is considered as a key species of the upper bathyal realm (200-1000 m). *Planulina ariminensis* however, is recognised as a more cosmopolitan species (Coles *et al.*, 1996). It prefers an elevated position above the sediment/water interface (on a sponge or stone) for a better chance to catch food from slightly streaming water (Lutze & Thiel, 1989).

These two species make part of the opportunistic epibenthic group, described by Schönfeld (1997) in the Gulf of Cadiz. They are reported to occupy a special ecological niche where the hydrodynamic regime of the *Mediterranean Outflow Water* (MOW) has a strong impact on the benthic foraminiferal community. These epibenthic species settle at higher positions under stronger near-bottom currents to have a maximum food supply (Schönfeld & Zahn, 2000; Schönfeld, 2002). As such, they might provide a proxy for the variability of bottom currents in the sedimentary record of the PSB.

Other, additional analyses on calcareous nannoplankton were performed by Mertens (2002) and Cornilly (2003) respectively on cores MD99-2327 and MD01-2452.

#### **3.2.6.4 Sedimentation and accumulation rates**

After the establishment of a chronological framework, linear sedimentation rates **LSR** ( $\text{cm.k}^{-1}$ ) can be calculated between intervals (equation 3.4). Here,  **$\Delta d$**  is the depth interval (cm) between two dated levels, while  **$\Delta a$**  is the age difference (ka).

Subsequently, the bulk sediment accumulation rates **ARb** ( $\text{g}\cdot\text{cm}^{-2}\cdot\text{ka}^{-1}$ ) can be calculated with the LSR and  $\rho_d$  using equation 3.5.

$$\text{LSR} = \Delta d / \Delta a \quad (\text{eq. 3.4})$$

$$\text{ARb} = \text{LSR} \cdot \rho_d \quad (\text{eq. 3.5})$$

### 3.2.6.5 Thin sections

In this study, a limited number of smear slides and thin sections were used in order to study respectively the composition of the sediment and the nature of some rock samples. They were analyzed under a polarized light petrographic microscope.

During campaign MD123 smear slides were obtained at irregular intervals of cores MD01-2449 (10, 35, 110, 185, 230, 265, 390, 530, 680, 830 and 925 cm) and MD01-2464 (90, 250, 390, 540, 700, 820, 990, 1140, 1310, 1460, 1610, 1720, 1900 and 2050 cm).

The thin sections were made from rock samples observed in core MD99-2327 at 810 and 1320 cm. Other rocks were retrieved from boxcore samples of the Porcupine-Belgica 2000 campaign. These thin sections were prepared by the thin section workshop of the research group of Mineralogy and Petrology at Ghent University.

### 3.2.7 Grainsize analysis

Grainsize analyses were performed to obtain as detailed as possible information about the size composition of the sediment, which could yield more insight into the responsible sedimentary processes. As a standard procedure, statistical parameters as mean and median size, skewness and sorting were calculated. More specifically, special attention was paid to the silt-sized fraction between 10 and 63  $\mu\text{m}$ . This is considered as an indicator of relative bottom-current strength, since they sort coarse silt during events of resuspension and ensuing deposition. Well-sorted sediments behave in a non-cohesive manner down to about 10  $\mu\text{m}$ . Below this size, particles start to become cohesive partly because clay minerals enter the compositional spectrum and *van der Waals* forces become significant in particle adhesion. Stronger currents yield a coarser mean size of the non-cohesive silt fraction, acting through both selective deposition and winnowing (McCave *et al.*, 1995a; McCave *et al.*, 1995b).

Essentially three datasets of grainsize analysis were made available for this study. The principle all three instruments use to obtain the grainsize distribution is based on the optical diffraction of a laser beam on sediment particles in suspension. This kind of technique allows a fast and reproducible analysis which necessitates only a small amount of sample material.

The following sections will provide more insight about the different methodologies used for these analyses.

### **3.2.7.1 Coulter LS230**

Cores ENAM-9901 and ENAM-9905 were subsampled at an interval of 10 cm. The samples were weighed and freeze-dried at  $-40^{\circ}\text{C}$  in order to obtain the water content of each sample. Because in Lekens (2000) only the siliciclastic characteristics of the samples were studied, the carbonate content and organic matter of the sample was removed by adding 35 ml  $0.5\text{ mol.l}^{-1}$  HCl and 10 ml 30M  $\text{H}_2\text{O}_2$ . Subsequently, the samples were heated at  $80^{\circ}\text{C}$  during 2 hours in order to remove the excess  $\text{H}_2\text{O}_2$  and the present organic matter. Finally, 120 ml demineralised water was added to the samples which was left to settle for 48 hours. After extraction of the upper 100 ml, the grainsize distribution between  $0.04\text{ }\mu\text{m}$  and  $2000\text{ }\mu\text{m}$  was measured with the *Coulter LS230* of the Royal NIOZ (The Netherlands). The results were processed with *Excel* spreadsheets.

### **3.2.7.2 Malvern MasterSizer 2000**

The grainsize analysis of cores MD99-2327 and BBC00-0606 were performed on samples from the same intervals as used for the sediment properties. These samples were provided to Max Kozachenko of the University College Cork (Ireland). Prior to analysis, each subsample was dispersed in a 10% sodium polyphosphate solution made with distilled water and shaken for 24 hours in order to achieve a perfect dispersion of all particles within the sample. All subsamples were sieved and only the fraction  $< 2000\text{ }\mu\text{m}$  was used. The particle size analysis was measured for 5 to 10 times with a *Malvern Laser Particle Sizer MasterSizer 2000* counter (within a window of  $0.02\text{ }\mu\text{m}$  to  $2000\text{ }\mu\text{m}$ ). The grainsize distributions were statistically analysed with an *Excel* spreadsheet.

### **3.2.7.3 Coulter LS130**

Cores MD99-2327, BBC00-0606, MD01-2449 and MD01-2464 were sampled based on features recognized on the SCOPIX radiographies, the CORTEX XRF and the Geotek MSCL. A standard sampling interval of 5 cm was chosen, but at some distinct horizons, the sampling interval was increased up to 1 or even 0.5 cm. They were analysed with the *Coulter LS130* of the Marine Biology Section at Ghent University. The LS130 only allows calculating the size distribution between  $0.1$  to  $800\text{ }\mu\text{m}$ . In contrast with a previous analysis, the organic carbon and the carbonate content were not removed. The samples were put into suspension with demineralised water and placed in an ultrasonic bath during 1 minute in order to disaggregate the cohesive silt. The output data was processed with the "*Granulométrie v3.01*" programme, developed at IFREMER DRO/GM (France). Further calculations were made using an *Excel* spreadsheet.



## References

- Arz, H. W., Pätzold, J. & Wefer, G. (1999) Climatic changes during the last deglaciation recorded in sediment cores from the northeastern Brazilian Continental Margin. *Geo-Marine Letters*, **19**, 209-218.
- Auffret, G. A., Zaragosi, S., Dennielou, B., Cortijo, E., Van Rooij, D., Grousset, F. E., Pujol, C., Eynaud, F. & Siegert, M. (2002) Terrigenous fluxes at the Celtic margin during the last glacial cycle. *Marine Geology*, **188**, 79-108.
- Bard, E. (1998) Geochemical and geophysical implications of the radiocarbon calibration. *Geochimica et Cosmochimica Acta*, **62**, 2025-2038.
- Bauch, H. A. & Helmke, J. P. (1999) Glacial-interglacial records of the reflectance of sediments from the Norwegian-Greenland Iceland Sea (Nordic seas). *International Journal of Earth Sciences*, **88**, 325-336.
- Bé, A. W. H. (1977) An Ecological, Zoogeographic and Taxonomic Review of Recent Planktonic Foraminifera. In: *Oceanic Micropaleontology* (Ed. by A. T. S. Ramsay), Academic Press, London, **1**, 1-100.
- Behling, H., Arz, H. W., Pätzold, J. & Wefer, G. (2000) Late Quaternary vegetational and climate dynamics in northeastern Brazil, inferences from marine core GeoB 3104-1. *Quaternary Science Reviews*, **19**, 981-994.
- Beyer, A., Schenke, H. W., Klenke, M. & Niederjasper, F. (2003) High resolution bathymetry of the eastern slope of the Porcupine Seabight. *Marine Geology*, **198**, 27-54.
- Boersma, A. (1998) Foraminifera. In: *Introduction marine micropaleontology* (Ed. by B. U. Haq and A. Boersma), Elsevier Science Pte. Ltd., Singapore, 19-77.
- Bond, G. & Lotti, R. (1995) Iceberg Discharges into the North Atlantic on Millennial Time Scales During the Last Glaciation. *Science*, **267**, 1005-1010.
- Chapman, M. & Shackleton, N. J. (1998) What level of resolution is attainable in a deep-sea core? Results of a spectrophotometer study. *Paleoceanography*, **13**(4), 311-315.
- Chi, J. & Mienert, J. (1996) Linking physical property records of Quaternary sediments to Heinrich events. *Marine Geology*, **131**, 57-73.
- Coles, G. P., Ainsworth, N. R., Whatley, R. C. & Jones, R. W. (1996) Foraminifera and ostracoda from Quaternary carbonate mounds associated with gas seepage in the Porcupine Basin, offshore Western Ireland. *Revista Espanola de Micropaleontologia*, **28**(2), 113-151.
- Cornilly, W. (2003) Paleoenvironmental study of Heinrich Layers in the Porcupine Seabight; A case study of the Magellan Mound Province. M.Sc. thesis, Marelac. *Ghent University*, Gent, 39 pp.
- Cortijo, E., Reynaud, J.-Y., Labeyrie, L. D., Paillard, D., Lehman, B., Cremer, M. & Grousset, F. E. (1995) Etude de la variabilité climatique à haute résolution dans des sédiments de l'Atlantique Nord. *Comptes Rendus de l'Académie des Sciences Paris, Série II a*, **321**, 231-238.
- de Haas, H., Huvenne, V. A. I., Wheeler, A. J. & Unnithan, V. (2002) A TOBI Side Scan Sonar Survey of Cold Water Coral Carbonate Mounds in the Rockall Trough and Porcupine Sea Bight. Royal NIOZ, Texel.
- De Mol, B. (2002) Development of coral banks in Porcupine Seabight (SW Ireland): A multidisciplinary approach. Ph.D. thesis, Department of Geology and Soil Science. *Ghent University*, Gent, 363 pp.
- Dennielou, B. (1997) Dynamique sédimentaire sur le plateau des Açores pour les derniers 400 ka: distribution, lithologie, flux et processus. Implications paléocéanographiques. Ph.D. thesis, Université de Bretagne Occidentale. *Université de Bretagne Occidentale*, Brest, 341 pp.
- Elliot, M., Labeyrie, L. D., Bond, G., Cortijo, E., Turon, J.-L., Tisnerat, N. & Duplessy, J. C. (1998) Millennial-scale iceberg discharges in the Irminger Basin during the last glacial period:

- Relationship with the Heinrich events and environmental settings. *Paleoceanography*, **13**(5), 433-446.
- Faugères, J.-C., Stow, D. A. V., Imbert, P. & Viana, A. R. (1999) Seismic features diagnostic of contourite drifts. *Marine Geology*, **162**, 1-38.
- Foubert, A. (2002) Een paleomagnetische studie met zeer hoge resolutie op Calypso-kernen in Porcupine Seabight, ten zuidwesten van Ierland. M.Sc. thesis, Department of Geology and Soil Science. *Ghent University*, Gent, 151 pp.
- Grousset, F. E., Labeyrie, L. D., Sinko, J. A., Cremer, M., Bond, G., Duprat, J., Cortijo, E. & Huon, S. (1993) Pattern of ice-rafted detritus in the glacial North Atlantic. *Paleoceanography*, **8**(2), 175-192.
- Gunn, D. E. & Best, A. I. (1998) A new automated nondestructive system for high resolution multi-sensor core logging of open sediment cores. *Geo-Marine Letters*, **18**, 70-77.
- Hemleben, C., Spindler, M. & Anderson, O. R. (1989) *Modern Planktonic Foraminifera*. Springer-Verlag, New-York.
- Huvenne, V., Blondel, P. & Henriët, J.-P. (2002) Textural analyses of sidescan sonar imagery from two mound provinces in the Porcupine Seabight. *Marine Geology*, **189**, 323-341.
- Huvenne, V. A. I. (2003) Spatial geophysical analysis of the Magellan carbonate build-ups and the interaction with sedimentary processes: key to a genetic interpretation? Ph.D. thesis, Department of Geology and Soil Science. *Ghent University*, Gent, 285 pp.
- Imbrie, J., Hays, J. D., Martinson, D. G., McIntyre, A., Mix, A. C., Morley, J. J., Pisias, N. G., Prell, W. L. & Shackleton, N. J. (1984) The orbital theory of Pleistocene climate: support from a revised chronology of the marine  $\delta^{18}\text{O}$  record. In: *Milankovitch and Climate* (Ed. by A. Berger, J. Imbrie, J. D. Hays, G. Kukla and B. Saltzman), D. Reidel Publishing Company, Hingham, **126**, 269-305.
- Jansen, J. H. F., Van der Gaast, S. J., Koster, B. & Vaars, A. J. (1998) CORTEX, a shipboard XRF-scanner for element analyses in split sediment cores. *Marine Geology*, **151**, 143-153.
- Kozachenko, M. (in prep.) Present and Past Environments of the Belgica Mounds (deep-water coral carbonate mounds), Eastern Porcupine Seabight, NE Atlantic. Ph.D. thesis, Department of Geology and Environmental Research Institute. *University College Cork*, Cork.
- Le Bas, T. & Hühnerbach, V. (1999) *P.R.I.S.M. Processing of Remotely-sensed Imagery for seafloor Mapping Operators Manual Version 3.1*. Southampton Oceanographic Centre, UK.
- Lekens, W. (2000) Een studie van de driftsedimentatie in het Porcupine Bekken. M.Sc. thesis, Department of Geology and Soil Science. *Ghent University*, Gent, 93 pp.
- Leslie, A. (1993) Shallow Plio-Pleistocene contourites on the Hebrides Slope, northwest U.K. continental margin. *Sedimentary Geology*, **82**, 61-78.
- Lofi, J. & Weber, O. (2001) SCOPIX - digital processing of X-ray images for the enhancements of sedimentary structures in undisturbed core slabs. *Geo-Marine Letters*, **20**, 182-186.
- Lutze, G. F. & Thiel, H. (1989) Epibenthic foraminifera from elevated microhabitats: *C. wuellerstorfi* & *P. ariminensis*. *Journal of Foraminiferal Research*, **19**(2), 153-158.
- Martinson, D. G., Pisias, N. G., Hays, J. D., Imbrie, J., Moore, T. C. & Shackleton, N. J. (1987) Age dating and the Orbital Theory of the Ice Ages: Development of a High-Resolution 0 to 300,000-Year Chronostratigraphy. *Quaternary Research*, **27**, 1-29.
- Massé, L., Faugères, J.-C. & Hrovatin, V. (1998) The interplay between turbidity and contour current processes on the Columbia Channel fan drift, Southern Brazil Basin. *Sedimentary Geology*, **115**, 111-132.
- McCave, I. N., Manighetti, B. & Beveridge, N. A. S. (1995a) Circulation in the glacial North Atlantic inferred from grain-size measurements. *Nature*, **374**, 149-152.
- McCave, I. N., Manighetti, B. & Robinson, S. G. (1995b) Sortable silt and fine sediment size/composition slicing: Parameters for palaeocurrent speed and palaeoceanography. *Paleoceanography*, **10**(3), 593-610.

- Mertens, K. (2002) Ruimtelijke en temporele patronen in paleoproductiviteit van kalkschalig nannoplankton en diatomeeën langs NE-Atlantische continentale randen. M.Sc. thesis, Department of Biology. *Ghent University*, Gent, 186 pp.
- Migeon, S., Weber, O., Faugères, J.-C. & Saint-Paul, J. (1999) SCOPIX: A new X-ray imaging system for core analysis. *Geo-Marine Letters*, **18**, 251-255.
- Ortiz, J. D. & Rack, F. R. (1999) Non-invasive sediment monitoring methods: current and future tools for high-resolution climate studies. In: *Reconstructing Ocean History: A Window into the Future* (Ed. by F. Abrantes and A. C. Mix), Kluwer Academic/Plenum Publishers, New York, 343-380.
- Piper, D. J. W. & Deptuck, M. (1997) Fine-grained turbidites of the Amazon fan: facies characterization and interpretation (Ed. by R. D. Flood, D. J. W. Piper, A. Klaus and L. C. Peterson), Ocean Drilling Program, College Station, Proc. ODP, Sci. Results, **155**, 79-107.
- Pujol, C. & Duprat, J. (1984) Quaternary and Pliocene planktonic foraminifers of the northeastern Atlantic (Goban Spur), Deep Sea Drilling Project leg 80. In: *Initial Reports of the Deep Sea Drilling Project* (Ed. by P. C. de Graciansky, C. W. Poag, R. Cunningham, P. Loubere, D. G. Masson, J. M. Mazzullo, L. Montadert, C. Müller, K. Otsuka, L. A. Reynolds, J. Sigal, S. W. Snyder, S. P. Vaos and D. Waples), U.S. Government Printing Office, Washington, **80**, 683-707.
- Rebesco, M. & Stow, D. A. V. (2001) Seismic expression of contourites and related deposits: A preface. *Marine Geophysical Researches*, **22**(5-6), 303-308.
- Richter, T. O., Lassen, S., van Weering, T. C. E. & de Haas, H. (2001) Magnetic susceptibility patterns and provenance of ice-rafted material at Feni Drift, Rockall Trough: implications for the history of the British-Irish ice sheet. *Marine Geology*, **173**, 37-54.
- Robinson, S. G., Maslin, M. A. & McCave, I. N. (1995) Magnetic susceptibility variations in Upper Pleistocene deep-sea sediments of the NE Atlantic: Implications for ice rafting and paleocirculation at the last glacial maximum. *Paleoceanography*, **10**(2), 221-250.
- Schönfeld, J. (1997) The impact of the Mediterranean Outflow Water (MOW) on the benthic foraminiferal assemblages and surface sediments at the southern Portuguese continental margin. *Marine Micropaleontology*, **29**, 211-236.
- Schönfeld, J. (2002) A new benthic foraminiferal proxy for near-bottom current velocities in the Gulf of Cadiz, northeastern Atlantic Ocean. *Deep-Sea Research I*, **49**, 1853-1875.
- Schönfeld, J. & Zahn, R. (2000) Late Glacial to Holocene history of the Mediterranean Outflow. Evidence from benthic foraminiferal assemblages and stable isotopes at the Portuguese margin. *Palaeogeography, Palaeoclimatology, Palaeoecology*, **159**, 85-111.
- Schultheiss, P. J. (1997) Multi Sensor Core Logging: Operating Protocols and Calibration Issues. In: *Core Logging Workshop* (Ed. by G. A. Auffret), pp. 36-37. IFREMER, Plouzané, France.
- Skinner, L. C. & McCave, I. N. (2003) Analysis and modelling of gravity- and piston coring based on soil mechanics. *Marine Geology*, **199**, 181-204.
- Stow, D. A. V., Faugères, J.-C., Howe, J. A., Pudsey, C. J. & Viana, A. R. (2002) Bottom currents, contourites and deep-sea sediment drifts: current state-of-the-art. In: *Deep-Water Contourite Systems: Modern Drifts and Ancient Series, Seismic and Sedimentary Characteristics* (Ed. by D. A. V. Stow, C. J. Pudsey, J. A. Howe, J.-C. Faugères and A. R. Viana), Geological Society, London, *Memoirs*, **22**, 7-20.
- Unterseh, S. (1997) Calibration method. In: *Core Logging Workshop* (Ed. by G. A. Auffret), pp. 57-60. IFREMER, Plouzané, France.
- Van Rooij, D. (1998) Sequentie-stratigrafie met hoog-resolutie-seismiek aan de rand van de Keltische Zee en het Porcupine Bekken, ten zuidwesten van Ierland. M.Sc. thesis, Department of Geology and Soil Science. *Ghent University*, Gent, 103 pp.
- Van Rooij, D. (1999) Lithologie des délestages glaciaires (niveaux de Heinrich) de l'Eperon de Goban (Atlantique Nord-Est). D.E.A. thesis, Université de Bretagne Occidentale. *Université de Bretagne Occidentale*, Brest, 57 pp.

- Van Rooij, D., Blamart, D., Kozachenko, M., Wheeler, A. J., Richter, T. O. & Henriët, J.-P. (submitted) Quaternary drift sediment dynamics in the Belgica mounds province, Porcupine Seabight: a multidisciplinary approach. In: *Modern Carbonate Mound Systems: A window to Earth History* (Ed. by J.-P. Henriët and C. Dullo), Springer-Verlag, Heidelberg.
- Wessel, P. & Smith, W. H. F. (1991) Free Software helps Map and Display Data. *EOS Transactions AGU*, **72**(441), 445-446.
- Wheeler, A. J., Bett, B. J., Billet, D. S. M. & Masson, D. G. (2000) Very high resolution side-scan mapping of deep-water coral mounds: surface morphology and processes affecting growth. *EOS Transactions*, **81**(48).
- Wheeler, A. J., Beyer, A., Freiwald, A., de Haas, H., Huvenne, V. A. I., Kozachenko, M. & Olu-Le Roy, K. (in press-a) Morphology and Environment of Deep-water Coral Mounds on the NW European Margin. In: *Modern Carbonate Mound Systems: A window to Earth History* (Ed. by J.-P. Henriët and C. Dullo), Springer-Verlag, Heidelberg.
- Wheeler, A. J., Kozachenko, M., de Haas, H., Huvenne, V. A. I., Masson, D. G. & Olu-Le Roy, K. (in press-b) Hydrodynamically Influenced Small Deepwater Reefs (Moirá Mounds) in the Porcupine Seabight, NE Atlantic. In: *Modern Carbonate Mound Systems: A window to Earth History* (Ed. by J.-P. Henriët and C. Dullo), Springer-Verlag, Heidelberg.
- Yokokawa, M. (2001) Sedimentary Structures of Contourites and Turbidites Observed by X-Radiographic Prints: Samples from Blake-Bahama Outer Ridge and Sohm Abyssal Plain (Ed. by L. D. Keigwin, D. Rio, G. D. Acton and E. Arnold), Ocean Drilling Program, College Station, Proc. ODP, Sci. Results, **172**, 1-37.
- Zaragosi, S., Eynaud, F., Pujol, C., Auffret, G. A., Turon, J.-L. & Garlan, T. (2001) Initiation of the European deglaciation as recorded in the northwestern Bay of Biscay slope environments (Meriadzek Terrace and Trevelyan Escarpment): a multi-proxy approach. *Earth and Planetary Science Letters*, **188**, 493-507.

## Chapter IV: The offshore record of BIIS variability

The area under study is located relatively close to the Irish mainland, on which, during glacial episodes, a relatively large ice sheet was concentrated. The growth and decay of such ice sheet will have influenced the paleoceanography of the nearby sedimentary basins. The best known examples of such an influence are the Heinrich Events, caused by the destabilization of pan-Atlantic ice sheets. The characteristics of the sedimentary response on these events make it possible to give relative ages of deep sea cores in the NE Atlantic domain (Bond *et al.*, 1992; Broecker *et al.*, 1992; Chi & Mienert, 1996; Grousset *et al.*, 1993; Knutz *et al.*, 2001; Richter *et al.*, 2001). However, recent discoveries suggest that the destabilization history of the British-Irish Ice Sheet (BIIS) had its own influence on ice-rafting events along the NW European margin (Auffret *et al.*, 2002; Grousset *et al.*, 2000; Scourse *et al.*, 2000). According to Knutz *et al.* (2001), the BIIS was probably the most sensitive and earliest amplifier of climatic change in the North Atlantic region, because of its extreme maritime position at the southern limit of the last glaciation of NW Europe. Information on the processes by which the BIIS disintegrated during the last ice age, and the rate of ice-sheet decay resulting from those processes, have yet to be identified (Siegert & Dowdeswell, 2002). At present, all available information is largely based on on-land research (Bowen *et al.*, 2002) and from work in surrounding regions as the Celtic and Armorican margin and Goban Spur (Hall & McCave, 1998b; Grousset *et al.*, 2000; Scourse *et al.*, 2000; Zaragosi *et al.*, 2001; Auffret *et al.*, 2002; Knutz *et al.*, 2002b). However, the most obvious place to study the variability of BIIS, the eastern slope of the Porcupine Seabight, has not been studied as yet.

A better understanding of the nature and timing of the local, European events and their interaction with the global Heinrich events can be very useful on a local and global scale. Locally, they can provide a (chrono)stratigraphic framework for the relative dating of shallow cores. A stronger stratigraphic framework of these cores could help understanding the development and decay of the coral banks that are found along this margin. On a global or pan-Atlantic scale, they can yield a better insight in the influence of the (millennial) destabilization of smaller ice caps on the large Laurentide Ice Sheet (LIS) and its influence on the deep-water circulation and the climate system (Elliot *et al.*, 1998; Snoeckx *et al.*, 1999).

Therefore, this chapter will first of all give a brief overview of the known causes, processes and characteristics of the Heinrich Events. Through the study of a set of a SE-NW transect of cores along the Porcupine Seabight, this study will try to make a contribution in better constraining the characteristics, timing and intensity of the variability of the BIIS during the last glacial cycle. Special attention will be made in the differentiation of these "Irish" events from the pan-Atlantic Heinrich Events and in which way they have influenced each other.

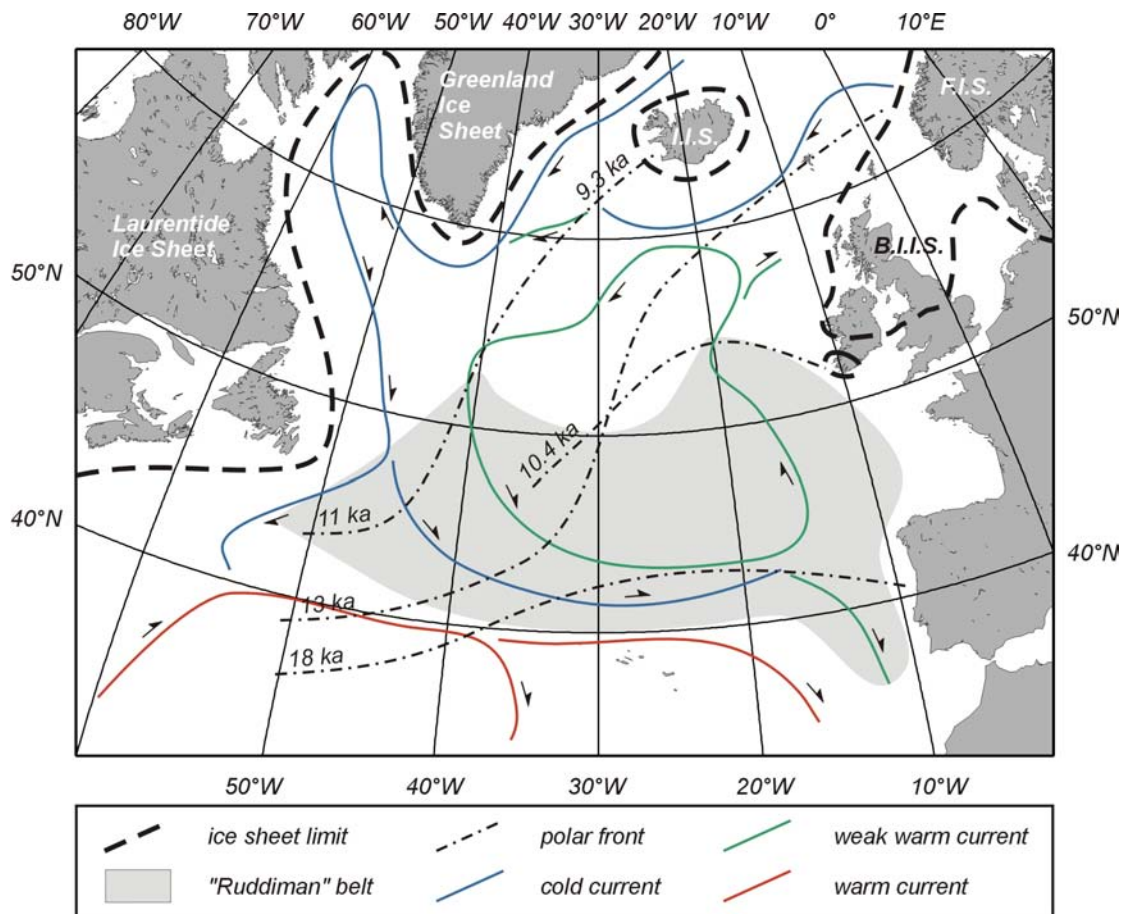


**Figure 4.1:** Reconstruction of the North Atlantic Ocean during the last glaciation with the location of the North Atlantic surface currents and Polar Front between the Last Glacial Maximum and the Early Holocene. The grey-shaded area corresponds to the Ruddiman belt. The limits of the major pan-Atlantic ice sheets are also indicated. I.I.S.; Icelandic Ice Sheet, B.I.I.S.; British-Irish Ice Sheet, F.I.S.; Fennoscandian Ice Sheet. Modified after Ruddiman (1977), Bond et al. (1992), Chapman & Maslin (1999), Grousset et al. (2001), Siebert (2001) and Auffret et al. (2002).

## 4.1 Current state-of-the-art of Heinrich Events

### 4.1.1 An introduction to Heinrich Events *sensu strictu*

When Harmut Heinrich published in 1988 his paper “Origin and Consequences of cyclic Ice Rafting in the Northeast Atlantic Ocean during the past 130000 years”, he was the first to link orbital cyclicity to the existence of ice rafted debris (IRD) in the Northeast Atlantic Ocean. Before, several authors (Pastouret *et al.*, 1975; Ruddiman, 1977; Smythe *et al.*, 1985; Caralp *et al.*, 1984) had already observed sand-enriched levels in the Quaternary sediments of the North Atlantic Ocean, without making the paleoclimatologic link with the Milankovitch cycles (Heinrich, 1988). A very important paper in this period before 1988 is the one of Ruddiman (1977) who has published a map with the limits of a region of IRD presence (Fig. 4.1). This region, located between 40° and 65°N is called the “Ruddiman belt”. It was in Broecker *et al.* (1992), that Heinrich’s name was attributed to these levels enriched in IRD (Heinrich Layers; HL) and to the events responsible for their deposition (Heinrich Events; HE).

Basically, 6 Heinrich layers have been recognized in the last glacial cycle sediments of the North Atlantic Ocean (Figs. 4.1, 4.2 and table 4.1). They have a centimeter to decimeter-scaled thickness with a relatively sharp base. A classic HL is composed of detrital grains within the sand fraction: angular quartz, hematite-coated grains, dolomite, detrital carbonate, micas, feldspars, rock fragments and volcanic glass. It is considered that all lithic grains larger than 150  $\mu\text{m}$  are IRD. While the abundance of detrital sand fraction is relatively large, there is an important decrease in the abundance of planktonic foraminifers, which is translated in a very high IRD to foraminifer ratio. However, within this low abundance of planktonic foraminifers, the percentage of the polar species *N. pachyderma s.* increases (up to 80%). The geophysical properties of the HL usually show an elevated density and a stronger magnetic susceptibility compared to the ambient sediment. Also the percentage of carbonate is higher due to the presence of detrital carbonate. During the deposition of the HL, the paleotemperature and paleosalinity of the glacial ocean show a significant cooling and decreasing salinity. This is observed through a lighter  $\delta^{18}\text{O}$  composition and a sudden decrease of 4 to 8°C of the mean sea surface temperature, jointly with a 1.5 to 3.0 ‰ surface salinity reduction (Heinrich, 1988; Bond *et al.*, 1992; Broecker *et al.*, 1992; Grousset *et al.*, 1993; Thouveny *et al.*, 1994; Robinson *et al.*, 1995; Chi & Mienert, 1996; Cortijo *et al.*, 1995; Vidal *et al.*, 1997; Chapman *et al.*, 2000; Grousset *et al.*, 2001).

	<b>Bond <i>et al.</i> (1992)</b>	<b>Grousset <i>et al.</i> (1993)</b>	<b>Chapman <i>et al.</i> (2000)</b>	<b>Elliot <i>et al.</i> (2001)</b>	<b>Auffret <i>et al.</i> (2002)</b>
HE 1	14.3	15.4	14.2	15.1-13.4	14.2
HE 2	21.0	20.0	21.4	22.1-20.4	21.0
HE 3	28.0	27.0	26.7	27.4-26.1	26.6
HE 4	41.0	38.0	34.8	34.9-33.9	34.2
HE 5	52.0	52.0	47.2		45.5
HE 6	69.0	67.0			62.0

**Table 4.1:** The ages of Heinrich Layers according to different authors. All ages are in  $^{14}\text{C}$  ka BP.

The IRD present in the Heinrich Layers were transported and deposited from an armada of floating icebergs which followed a cyclonic circulation with a periodicity between 7 and 11 ka (Table 4.1). Such a fleet of icebergs had a significant influence on the thermohaline ocean circulation. While an iceberg loses its IRD, it also loses very cold fresh meltwater, explaining the low temperatures and salinities (Cortijo *et al.*, 1997), as well as the polar species in the micro and nannofossil populations. Meanwhile, the warm tropical waters cannot reach the Northern Atlantic (due to a southward shift of the polar front), which strongly reduces or even switches off the thermohaline circulation (Bond *et al.*, 1992; Chapman & Shackleton, 1998; Vidal *et al.*, 1997; Seidov & Maslin, 1999; Crucifix & Berger, 2002).

Since their discovery in 1988, the age and timing of the 6 Heinrich Events can very well be estimated. According to Dowdeswell *et al.* (1995), one single event could last for 250 to 1250 years. Several authors have found more than the 6 classic HE in their cores. For example, Andrews *et al.* (1995) and Thouveny *et al.* (1994) have located a HL0 in the Younger Dryas (10 to 11 ka BP). Some authors described

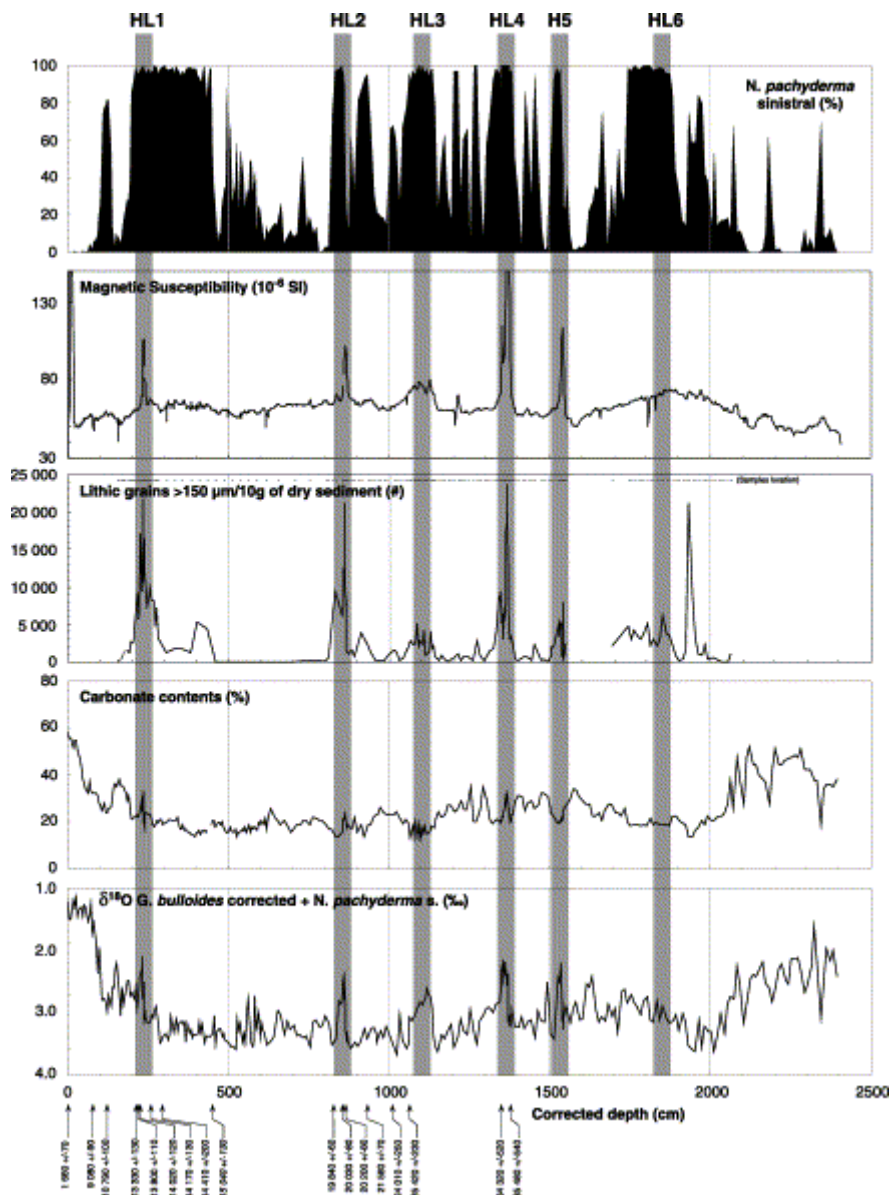


**Figure 4.2:** Characteristics of the Heinrich Layers, demonstrated by data from core MD95-2002, Meriadzek Terrace, Celtic Margin (Auffret *et al.* 2002).

up to HL13 at 201 ka in MIS 7 (van Kreveld *et al.*, 1996; Chapman & Shackleton, 1998; Rasmussen *et al.*, 2003).

#### 4.1.2 Provenance of the HE

One of the many questions about the Heinrich Events concerns their causal mechanism. Originally, Heinrich (1988) proposed a semi-precessional Milankovitch cyclicity, which seemed to be very well constrained by the  $\delta^{18}\text{O}$  and  $\delta^{13}\text{C}$  values observed in the GRIP core in Greenland (Bond *et al.*, 1993). Bond & Lotti (1995) even observed millennial-scaled maxima corresponding to small IRD levels. One such cycle starts with a slow cooling, followed by a sudden warming and displaying a periodicity of about 1500 a (Dansgaard *et al.*, 1993). These fluctuations on a millennial scale are the Dansgaard-Oeschger (D-O) events, seen as irregular “sawtooth” ice volume increases and climatic cooling in the  $\delta^{18}\text{O}$  record (Fig. 4.3).

Progressively colder D-O cycles are bundled into some major so-called Bond cycles, each ending with a cold phase, the Heinrich events (Bond et al., 1993; Bond & Lotti, 1995; Dansgaard et al., 1993). Such a Bond cycle has an average duration of about 10 ka (Dansgaard et al., 1993). These orbitally influenced cycles should have had an influence on the ice sheets in the northern hemisphere, but glaciologists were not able to prove that insolation only could cause such an event (McCabe & Clark, 1998; Oerlemans, 1993). MacAyeal (1993b), MacAyeal (1993a) and Alley & MacAyeal (1994) developed a model which only accounted for the stability of an ice sheet and the thermal flux. They demonstrated that the thermodynamics, height and the position of the ice sheet could very well cause the HE. They proposed long periods (7700 a) of ice sheet growth, followed by very short periods (750 a) of destabilization. They did not exclude insolation, which could only have had a small influence compared to the internal oscillatory dynamics of the Laurentide and Greenland Ice Sheets.

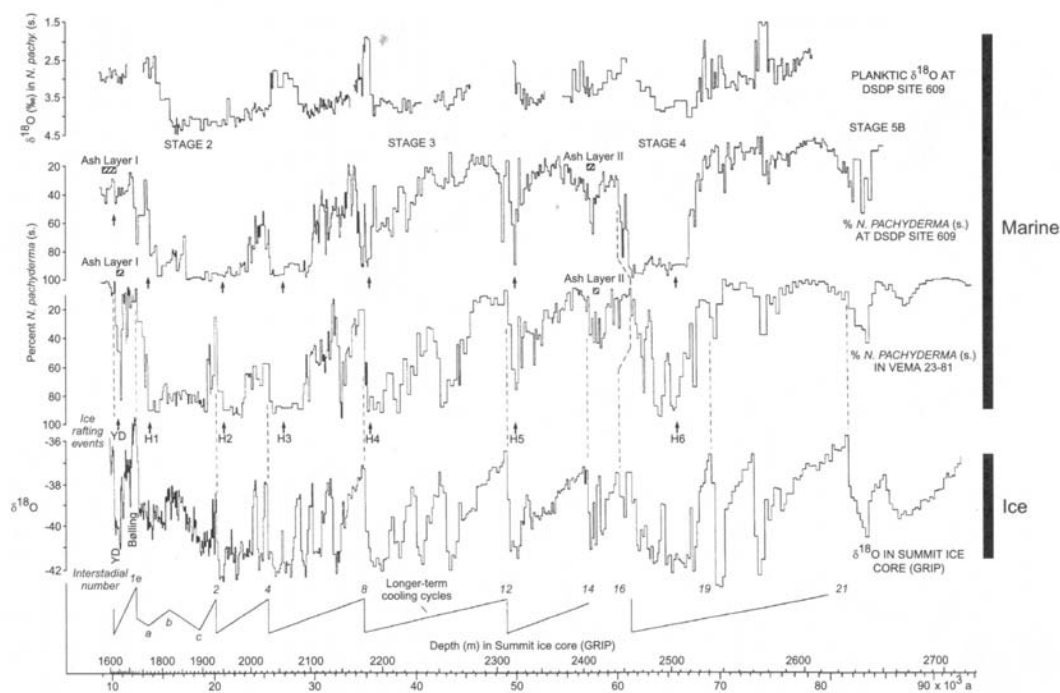


**Figure 4.3:** Comparison of  $\delta^{18}\text{O}$  and percentages of *N. pachyderma s.* in two ocean sediment cores from the North Atlantic, with the  $\delta^{18}\text{O}$  record from the GRIP ice core (Summit, Greenland). Dashed lines indicate common features used to match the records, but the timescale shown is based on radiocarbon dates for the past 35.5 ka and estimated ages of Heinrich events (shown as H1 to H6) derived in other studies. The ice-core record was then forced to fit the assumed sediment chronology. The lower schematic diagram shows how clusters of millennium-length cycles of  $\delta^{18}\text{O}$  in the ice-core record (D-O cycles) seem to form long-term cooling cycles (Bond cycles), which terminate abruptly at irregular intervals Bond et al. (1993).

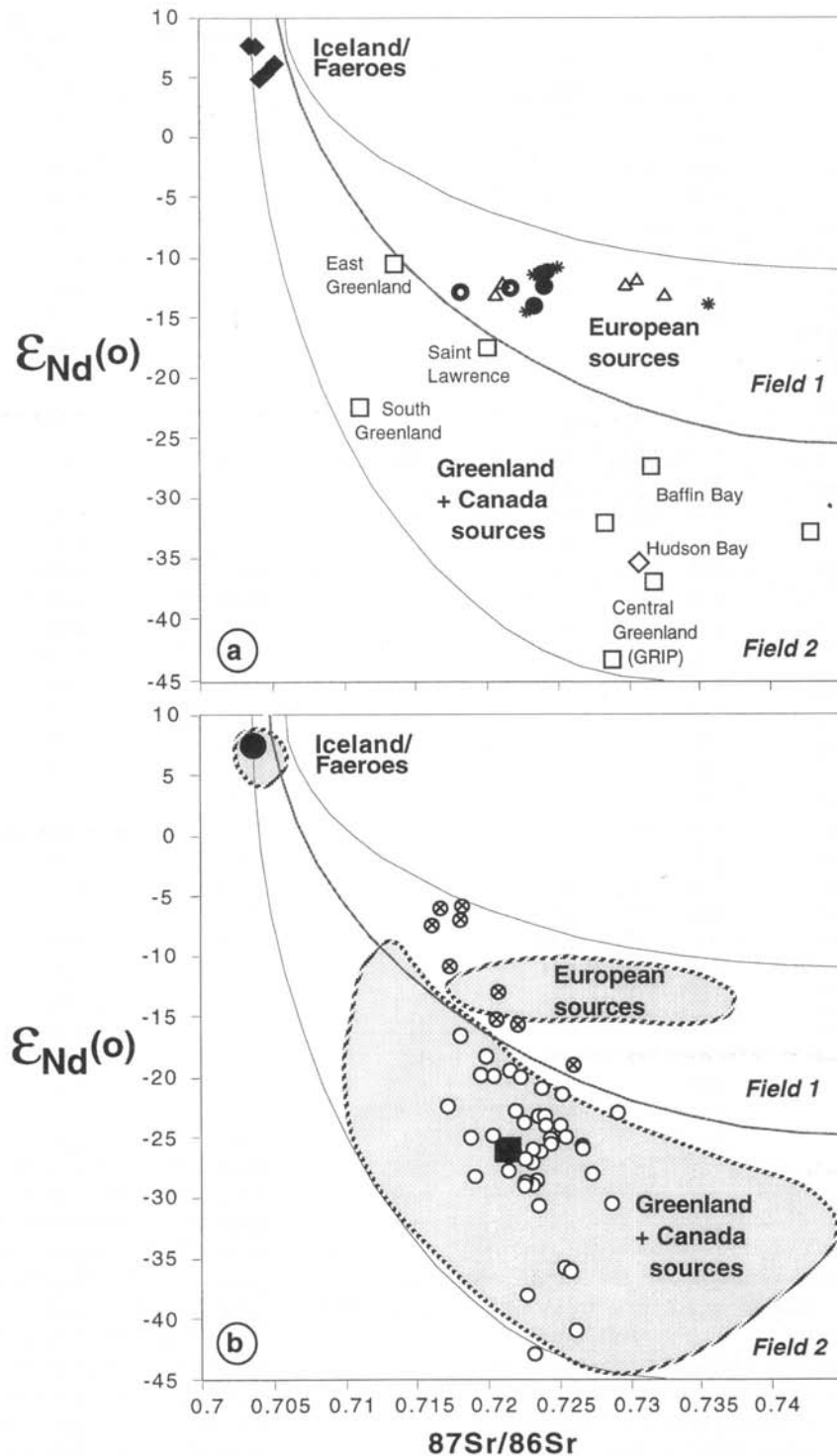


**Figure 4.4:**  $^{87}\text{Sr}/^{86}\text{Sr}$  ratios versus  $^{143}\text{Nd}/^{144}\text{Nd}$  ratios, expressed as  $\epsilon_{\text{Nd}}(o)$ . The error bars are smaller than the symbols. (a) The Potential Source Area (PSA) samples are reported as large solid diamonds (volcanic provinces), open triangles (British Isles sources), stars (Scandinavian sources), closed circles (other European sources) and open squares (North American sources) and their envelopes were contoured by hand, roughly following mixing hyperbolae. (b) Samples for main HL IRD (open circles) and precursor IRD (crossed circles) are represented along with the envelopes of the main source provinces (stippled areas). Volcanic glasses and quartz grains picked from within the European precursor of H1 are also plotted (solid circle and solid square, respectively) (Grousset et al., 2001).

The Heinrich Events are not only recorded in the Atlantic Ocean. In France, a study of pollen and magnetic susceptibility of lakes in the Massif Central allowed the identification of HE and D-O events (Thouveny *et al.*, 1994). Also studies of vegetation in lake Tulane (Florida, USA) allowed to correlate the abundance of the pollen of *Pinus* with HE1 to HE5 (Grimm *et al.*, 1993). Porter & Zhisheng (1995) have correlated the HE with the loess sequences in China.

Another major question concerns the geographic origin of the IRD. Initially, the IRD found in HL were thought to originate from the Laurentide Ice Sheet (LIS) in Canada and the Greenland Ice Sheet (GIS) (Andrews & Tedesco, 1992; Bond *et al.*, 1992; Gwiazda *et al.*, 1996b). These ice sheets were located during the glacial periods on Canada (the Archean Churchill province), around the Labrador Sea, Hudson Strait... (Fig. 4.1). This entire area is composed of large Paleozoic and Precambrian provinces with carbonates and dolomites (Andrews & Tedesco, 1992). Along the margins of these regions, so-called Detrital Carbonate (DC) events can be correlated with Heinrich Events (Andrews *et al.*, 1995). Later on, more clues for sources in Iceland and Scandinavia have appeared (Grousset *et al.*, 1993; Bond & Lotti, 1995; Gwiazda *et al.*, 1996b; Revel *et al.*, 1996). According to Elliot *et al.* (1998), the Icelandic and Scandinavian ice sheets were more sensible to destabilization due to their high latitude and their position in the North Atlantic Ocean. Therefore, they proposed two superimposed systems. First of all, there is an IRD release of "Nordic" icebergs every 1.2 to 3.8 ka. The second system contains the icebergs derived from LIS and GIS with a frequency between 5 to 10 ka. This combination of superimposed systems is directly linked to the Dansgaard-Oeschger events, recorded in the GRIP ice core.

A relatively reliable method to estimate the provenance of IRD is the Sr/Nd ratio (Grousset *et al.*, 1988; Grousset *et al.*, 1993; Gwiazda *et al.*, 1996a; Revel *et al.*, 1996; Hemming *et al.*, 1998). With this method, it has been demonstrated that the IRD of the "typical" HL (HL1, 2, 4 and 5) have a LIS, GIS, Scandinavian and Icelandic origin (Fig. 4.4). The IRD of the two "atypical" (HL3 and 6) rather seem to have an Icelandic and Scandinavian origin. Moreover, these HL do not show a very pronounced anomaly in the magnetic susceptibility and density (Snoeckx *et al.*, 1999). Recently, Sr/Nd analyses on a core on Meriadzek Terrace (Celtic Margin) have revealed a special European signature in the IRD fraction (Grousset *et al.*, 2000). This will be treated in the following paragraph.

### 4.1.3 HE along the NW European Margin

The first hints of the participation of the British-Irish Ice Sheet in the ice-rafting story were given through the common observation of reworked Cretaceous and Paleogene nannoplankton and detrital material in cores along the NW European margin (Müller, 1984; Rahman, 1995). Scourse *et al.* (2000) reported an association of chalk particles and European-sourced micas during the Last Glacial Maximum (LGM) and McCabe *et al.* (1998) showed a participation of the BIIS in the Heinrich Events through terrestrial data.

According to Grousset *et al.* (2001), the European Ice Sheets (EIS) showed more rapid cycles (1-2 ka) between typical HL, suggesting a high-frequency oscillation. On Goban Spur, layers defined on IRD counts are unusually thick in comparison with HL observed further west, indicating an enhanced flux from terrigenous material transferred across-shelf (Van Rooij, 1999; Scourse *et al.*, 2000;

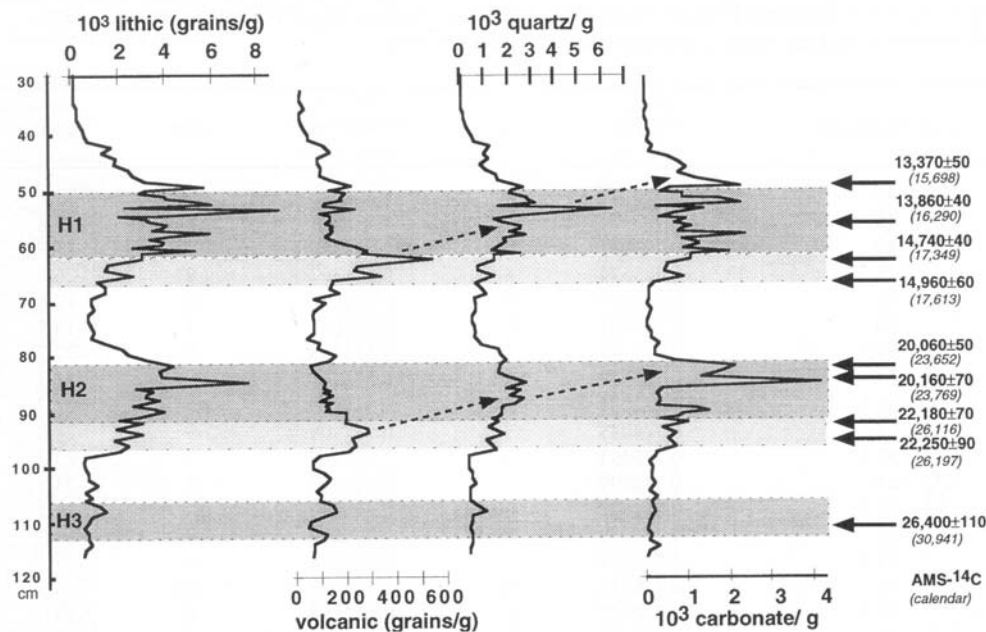


**Figure 4.5:** Abundances of lithic grains, detrital carbonate, volcanic glass and quartz grains in coarse sediments ( $> 150 \mu\text{m}$ ) from core SU90-09. Location of Heinrich Layers H1, H2 and H3 is shown by stippled areas (light grey band for the European precursors and dark grey band for the Laurentide-derived steps). Arrows emphasize the sequential deposition of (1) volcanic glass, (2) quartz and (3) detrital carbonate (Grousset *et al.*, 2001)

Auffret *et al.*, 2002). This resulted in a new view of HL along the European margin, where the internal structure of at least HL1 and 2 seems to include three consecutive steps (Fig. 4.5) (Scourse *et al.*, 2000; Grousset *et al.*, 2001; Auffret *et al.*, 2002). First of all, volcanic grains (ashes and basalts) were deposited at about 22.2 (HL2) and 14.9 ka (HL1), each lasting 1-2 centuries. This is a complex mixture of non-LIS IRD only (European and Icelandic material). Such a precursor event cannot be detected by magnetic susceptibility measurements, because these IRD contain less magnetic material. During this first step, European icebergs might have followed the same kind of counter clockwise trajectories as the one suggested for atypical events H3 and H6. During a second phase, quartz grains and crust-derived minerals were deposited, being the paroxysmal step of LIS. This second step may occur 1 to 1.5 ka after the precursor event, followed by the input of detrital carbonate from Canadian provinces (Labrador & Baffin Bay). The arrival of these Canadian icebergs during HE1 and HE2 are during short periods of about 300 a, coeval with cooler air temperatures in Greenland. A third step is a second European surge, following the Canadian IRD deposition. This means that IRD deposition during a HE is not a continuous event, but reflects a time-transgressive, multi-sourced release of icebergs.

As a consequence of BIIS destabilization, Scourse *et al.* (2000) suggest that the destabilization of LIS might be linked to stimuli originating from the European side of the Atlantic. It could cause a small sea level rise, which would be enough to promote buoyancy, destabilize the LIS margin and stimulate calving and possibly also surging. The increase in sea-level resulting from HE discharge of the LIS would be instantaneous and not subject to response lag. This main, massive HE causes

convective shutdown by meltwater introduction, while during the European precursor events the thermo-haline convection remained active.

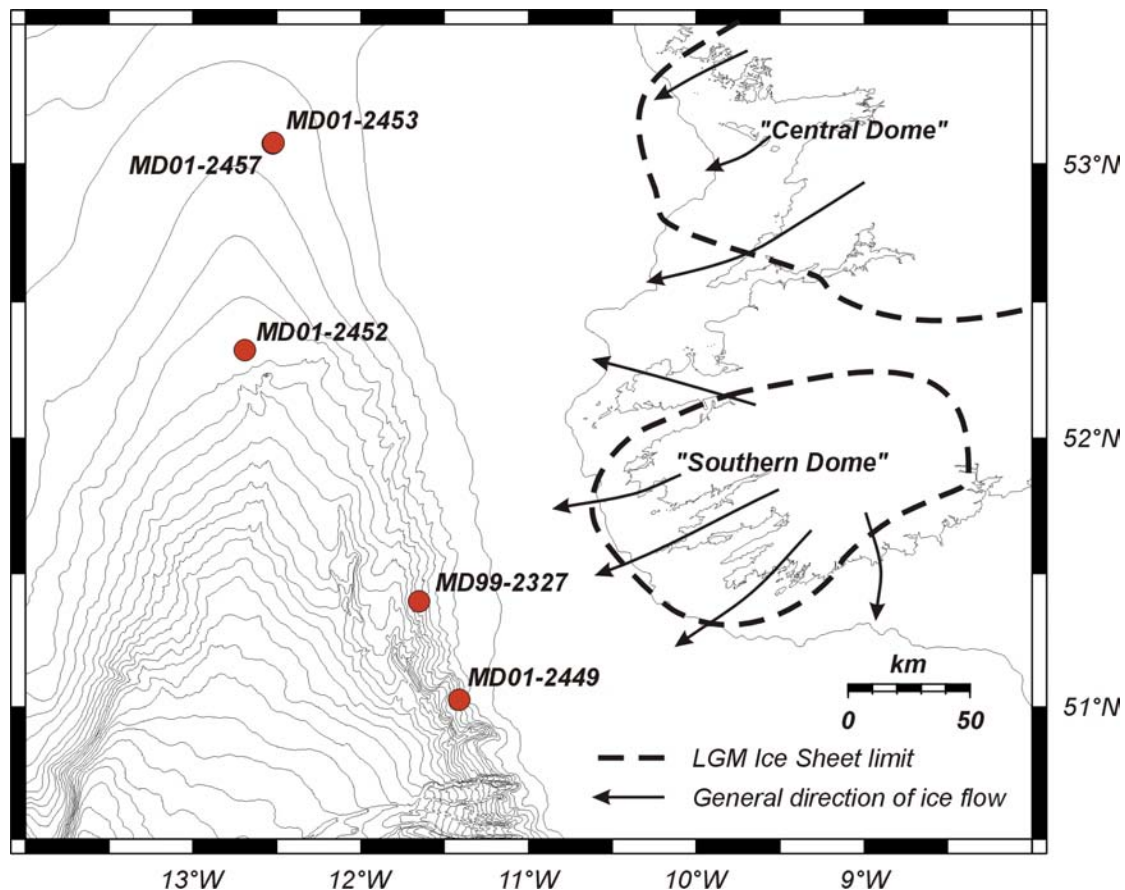


**Figure 4.6:** Location of the studied cores in the Porcupine Seabight, with respect to the position of the Irish components of the British-Irish Ice Sheet during the Last Glacial Maximum (LGM). Modified after Bowen et al. (2002) and Holland (2001).

#### 4.2 The IRD record in the Belgica mound province

The study area is very proximal to the Irish mainland, and thus also to the British-Irish Ice Sheet (BIIS) during glacial times (Fig. 4.6). Therefore, the ice-rafting history will be dominated by BIIS-sourced IRD and fluctuations, rather than a Laurentide one. It is evident that the determination of a correct glacial time frame for this part of the Porcupine Seabight requires an adjusted vision on IRD deposition compared to the normal North Atlantic paleoceanography. Here, our stratigraphy will be based on the occurrence of local ice-rafting events (IRE), rather than Heinrich Events (HE), which might be related. The likely millennial-scaled variability of these IRE necessitates the combination of several other proxies than just the one of IRD, whereas in other North Atlantic sites, the IRD abundance would be sufficient.

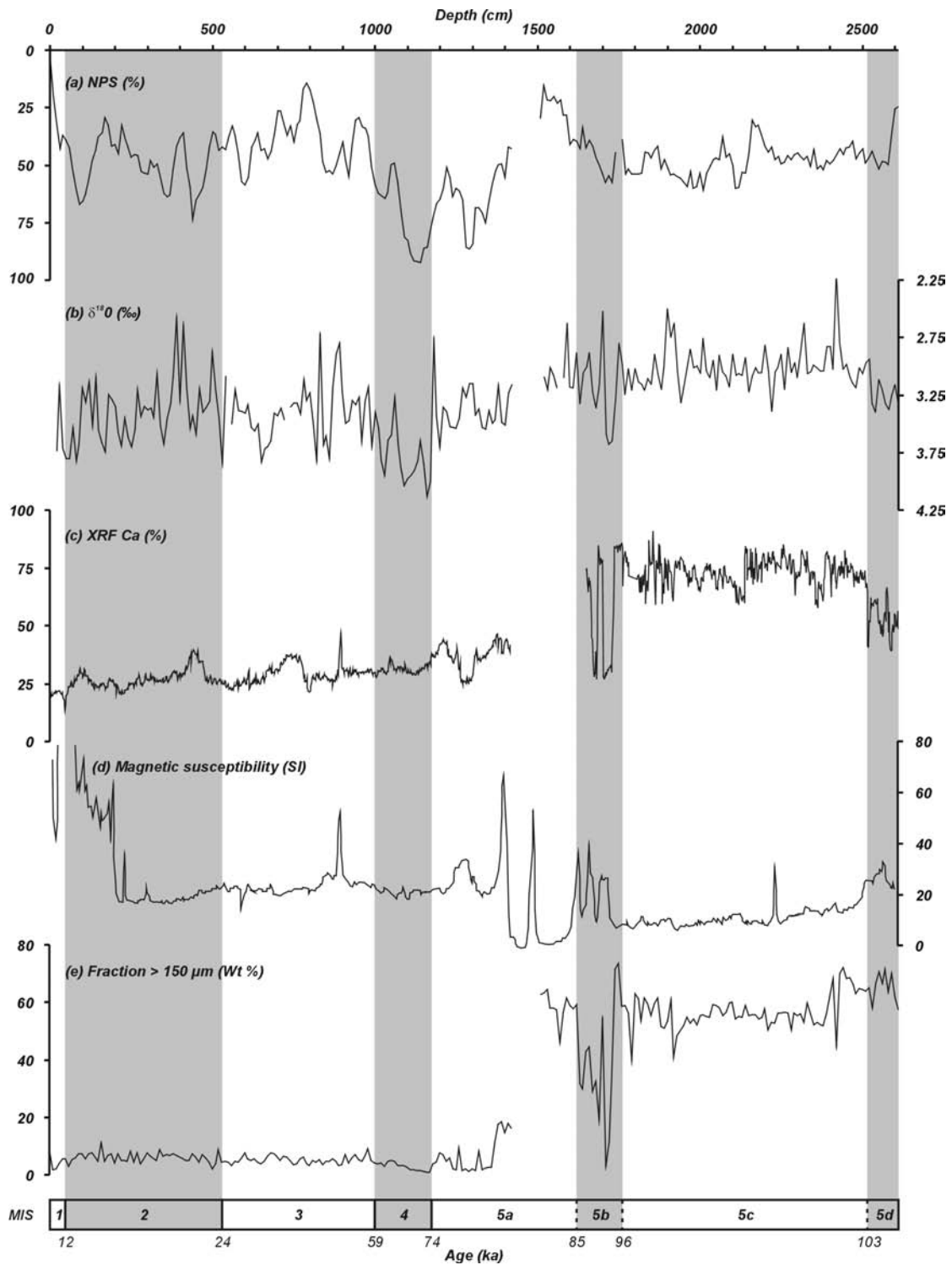


**Figure 4.7:** Lithological content and chronostratigraphy of core MD99-2327 with: (a) relative abundance of the polar planktonic foraminifer *N. pachyderma* s. (*NPS*), (b)  $\delta^{18}\text{O}$  stable isotopes (‰ vs. *PDB*), (c) *CORTEX* XRF Ca values (% of the total counts of Si, K, Ca, Ti, Mn, Fe and Sr), (d) magnetic susceptibility (SI) and (e) the fraction > 150  $\mu\text{m}$  (Wt %). The grey-shaded areas indicate colder (even) isotope stages.

The best sedimentary archive available for this purpose is provided by core MD99-2327. This core was subject of a wide range of analysis which might yield a better insight in the paleoceanographic evolution of the region. Moreover, the chronostratigraphy of this core is the best constrained one available for this study. This tentative age model is based on the main climatic events proposed by Martinson *et al.* (1987), as observed in one of the measured parameters (Fig. 4.7). The subdivision of the glacial section (Fig. 4.8), on the other hand, has been constructed on the occurrence of the subsequent IRE.

The XRF Ca, magnetic susceptibility and the fraction  $> 150 \mu\text{m}$  ( $F_{150}$ ) clearly show a break in characteristics of the core at about 14 m (Fig. 4.7). From 0 to 1400 cm, the core is featured as homogeneous, olive grey silty clay with sulphide strikes at some intervals. At the base of this section (1233 to 1425 cm), alternating layers of olive grey silty clay and muddy fine sand occur. The sediments are generally very poorly sorted, although sorting increases towards its base. X-ray imagery reveals extensive bioturbation (mottling, *planolites*, *chondrites*, *mycelia*) throughout, varying from faint structures to very heavy burrowing. This section is thought to represent the last glacial period comprising marine isotope stages 2, 3 and 4. A very clear indication of the cold MIS4 is observed between 1000 and 1170 cm, with rather high values of NPS and  $\delta^{18}\text{O}$  (Fig. 4.7) and by a rather low amount in  $F_{150}$  (Fig. 4.8). This might be evidence of the build-up of an ice cap on the British-Irish isles.

The section from 1500 to 2625 cm is a very poorly to poorly sorted olive grey foraminiferal fine to medium sand. Within these sediments occasional shell fragments, lithic grains and dark minerals are observed. Here, the values of XRF Ca and  $F_{150}$  are substantially higher and the magnetic susceptibility is lower. Moreover, the  $\delta^{18}\text{O}$  values are lower and suggest, together with the NPS values an interglacial environment, correlated with marine isotope stage 5 (MIS5). Subtle changes in these records, as well as in  $F_{150}$  and XRF Ca allow a further, tentative subdivision of this interglacial period (Fig. 4.7). The exceptionally high amount of  $F_{150}$  can not be interpreted in terms of ice-rafting events, but in terms of hydrodynamic activity, which will be discussed in chapter 6. The foraminiferal assemblage and their spectacularly high abundance suggest the interval between 1170 and 1620 cm (centred on 1540 cm) represents isotope stage 5a. Relatively low abundances of planktonic foraminifera and XRF Ca in between 1620 and 1760 cm could be illustrating MIS5b, containing the 2 layers of finer-grained sediment with high silt percentages. Event 5.33 is suggested to be recognized at 2525 cm and is considered as the limit between substage 5c and 5d. From this point downcore,  $\delta^{18}\text{O}$  values become heavier, indicating a colder climate. Also, the abundance of planktonic foraminifera decreases again. As in the presumed stage 5b, XRF data show low values of Ca. The interval between 2525 cm and the bottom of the core is thus believed to be the end of substage 5d. The sedimentary unit between 1760 and 2525 cm, interpreted as substage 5c, is characterized with slightly higher abundance of planktonic foraminifers compared with the 5b and 5d. In the XRF record, this unit is well delimited by high values of Ca.

These data very well constrain the glacial part of the core between 0 and 1200 cm (Fig. 4.8). This will allow to study the main characteristics of the IRE for the study area through the multi-tool analysis of this core. First of all, the different IRE will be identified and described, followed by a general comparison of these IRE with the HE.

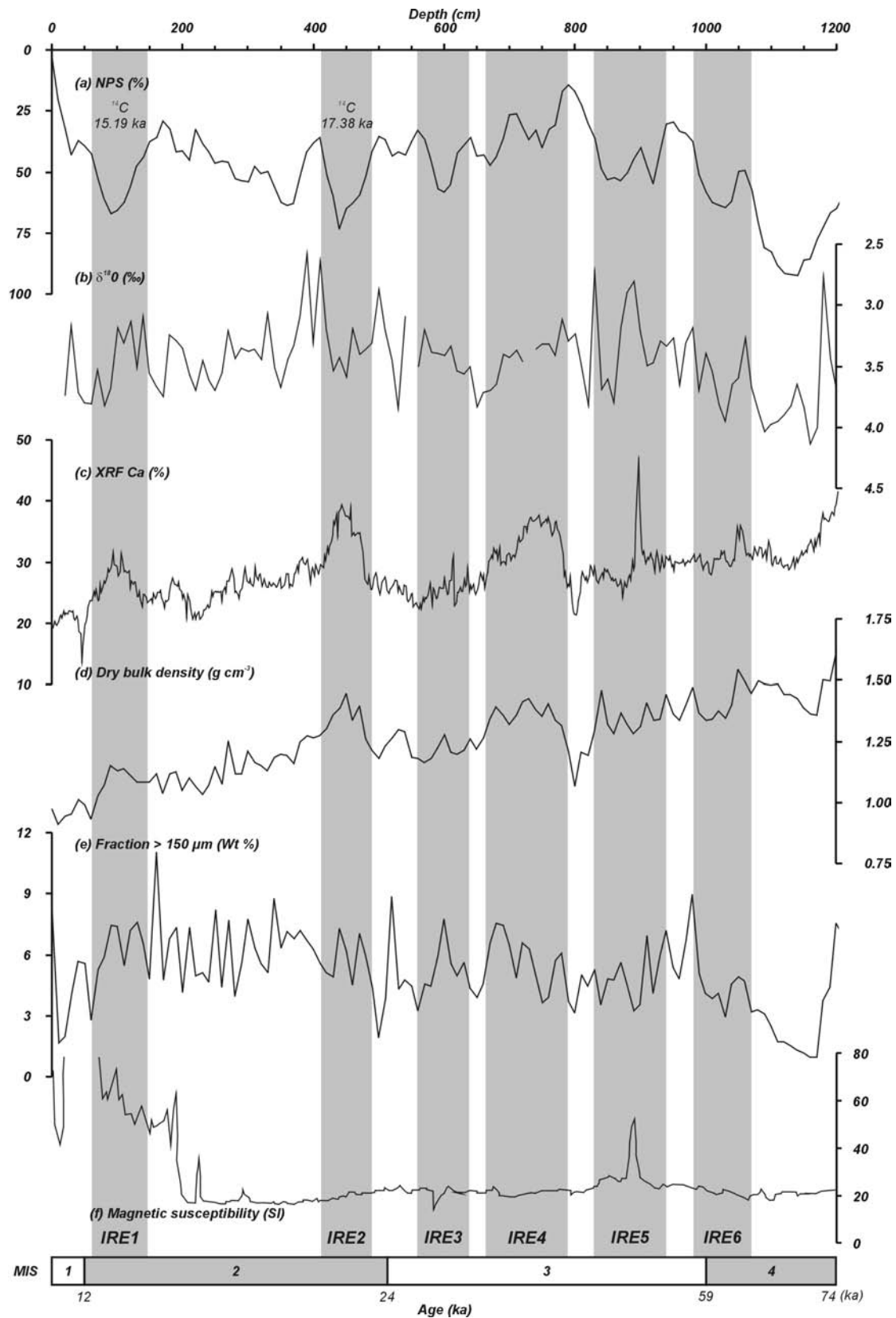


**Figure 4.8:** Detail of the lithological content and chronostratigraphy of the glacial part of core MD99-2327, with special attention to the occurrence of the IRE (grey areas), with (a) relative abundance of *N. pachyderma s.* (NPS), (b)  $\delta^{18}\text{O}$  stable isotopes (‰ vs. PDB), (c) CORTEX XRF Ca values (% of the total counts of Si, K, Ca, Ti, Mn, Fe and Sr), (d) magnetic susceptibility (SI) and (e) the fraction  $> 150\ \mu\text{m}$  (Wt %).

## 4.2.1 Ice-rafting events in MD99-2327

### 4.2.1.1 IRE1 (70-140 cm)

Figure 4.8 clearly shows a progressive cooling pattern followed by a fast warming-up in the NPS and  $\delta^{18}\text{O}$  record with culmination on 90 cm. Grainsize analysis indicates two levels of elevated IRD at 95 cm (IRE1a) and 135 cm (IRE1b) (Figs. 4.9, 4.10). Coeval, there is a rise in Ca, density (Fig. 4.8) and luminosity (Fig. 4.11). X-ray imagery also shows a higher density with several dropstones in a heavily burrowed environment (Fig. 12a). An AMS  $^{14}\text{C}$  datation on 90 cm yields an age of  $15.19 \pm 0.13$  ka BP, which is consistent with the age of HE1 ( $15 \pm 0.7$  ka) of Elliot *et al.* (1998), the theory of precursor events of Grousset *et al.* (2001) and land data of McCabe *et al.* (1998).

### 4.2.1.2 IRE2 (420-480 cm)

As in the previous IRE, NPS shows a clear, gradual cooling record with an abrupt culmination about 440 cm (Fig. 4.8). The abundance of planktonic foraminifera before and after this event is elevated, but during the culmination, the amount of planktonic foraminifera drastically drops, while the luminosity increases (Fig. 4.11). The XRF Ca record shows a “plateau” of elevated values from 430 to 470 cm (Fig. 4.8). Dry bulk density values also show an inversed V-shaped pattern with two small peaks (IRE2a and IRE2b), which can be linked with IRD maxima (Figs. 4.8, 4.9 and 4.10). These two peaks are also visible on SCOPIX as dark bands with abundant dropstones and remarkably less bioturbation (Fig. 4.12b). Right after IRE2, a decrease in  $\delta^{18}\text{O}$  and NPS values mark a warm period (Fig. 4.8). This response correlates very well with an environmental change with higher abundances of warmer species like *N. pachyderma d.*, *G. glutinata*, *G. bulloides* and *G. inflata* (Fig 4.13). The culmination of IRE2 has been dated at  $17.38 \pm 0.14$  ka BP, which is rather a young age compared to the generally accepted age of HE2 (20-21 ka) (Table 4.1). On the other hand, the timing of IRE2 fits perfectly with the BIIS Drumlin readvance at about 17 ka (Bowen *et al.*, 2002; Richter *et al.*, 2001) and the major meltwater discharge and ice sheet disintegration reported at 17.5 ka (McCabe *et al.*, 1998; Knutz *et al.*, 2002a). This also explains the relatively warm period following right after IRE2.

### 4.2.1.3 IRE3 (560-640 cm)

NPS, SDS and *T. quinqueloba* clearly show a colder assemblage, but this time, there is only a minor increase of Ca particles (Figs. 4.8 and 4.13). The IRD record shows a marked increase with one large pulse at 600 cm (IRE3b), preceded (IRE3c, 640 cm) and followed (IRE3a, 570 cm) by a smaller one (Figs. 4.9 and 4.10). Density only shows a subtle peak, but SCOPIX imagery clearly shows the onset of IRD at 619 cm with a following higher density and frequent IRD (Fig. 4.12c). Despite the clear environmental change observed in the foraminiferal assemblage,  $\delta^{18}\text{O}$  and XRF Ca do not help discriminating this event. IRE3 could thus be correlated with the atypical HE3 with an estimated age of 26.6 ka, according to Auffret *et al.* (2002).

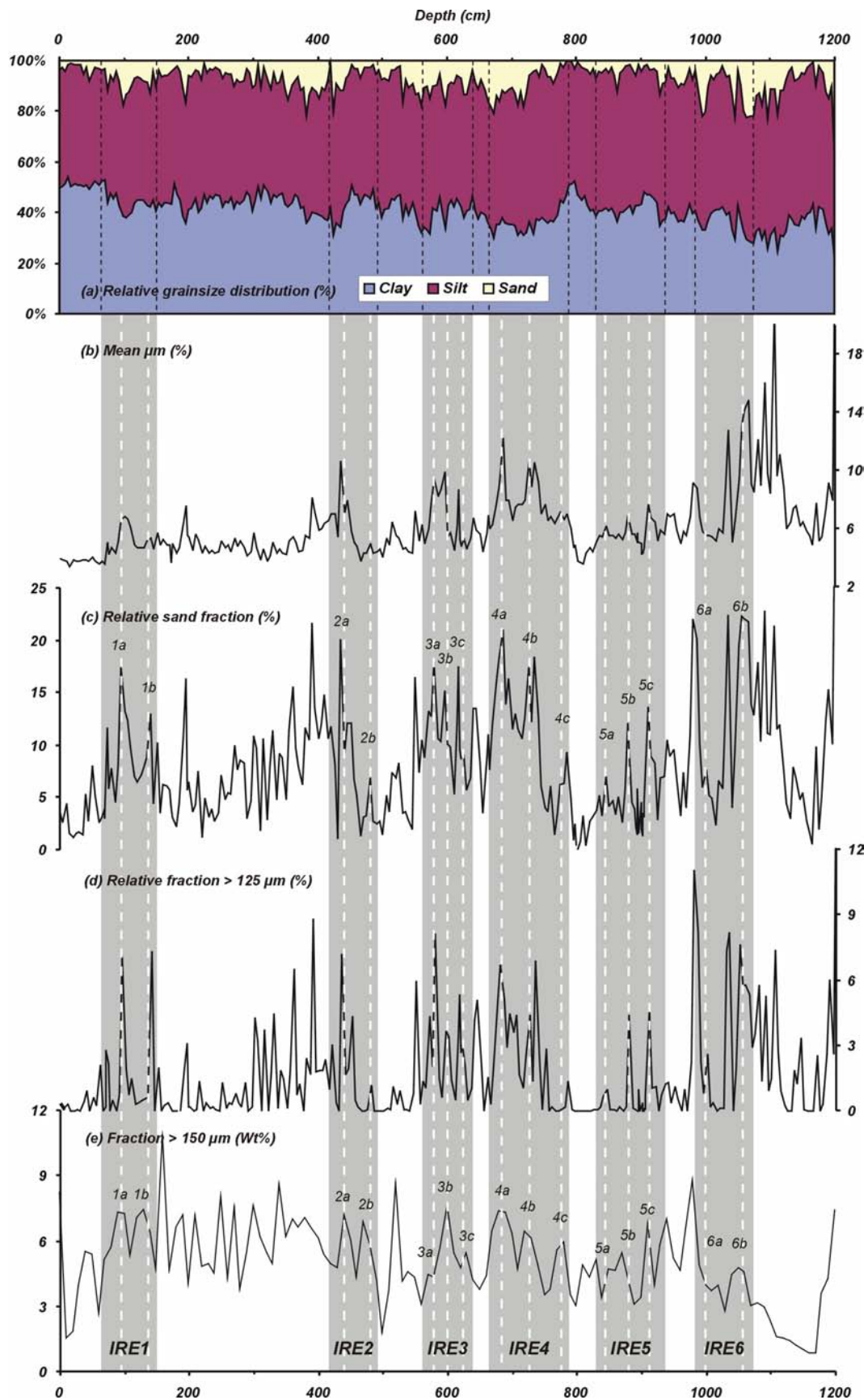


**Figure 4.9:** Grainsize characteristics and coarse fraction of core MD99-2327 with (a) relative grainsize distribution (%), (b) mean grainsize ( $\mu\text{m}$ ), (c) relative sand fraction (%), (d) relative fraction  $> 125 \mu\text{m}$  (%), (e) the fraction  $> 150 \mu\text{m}$  (Wt%). The 6 IRE are indicated (grey area) as well as their different peak phases (white dashed line).

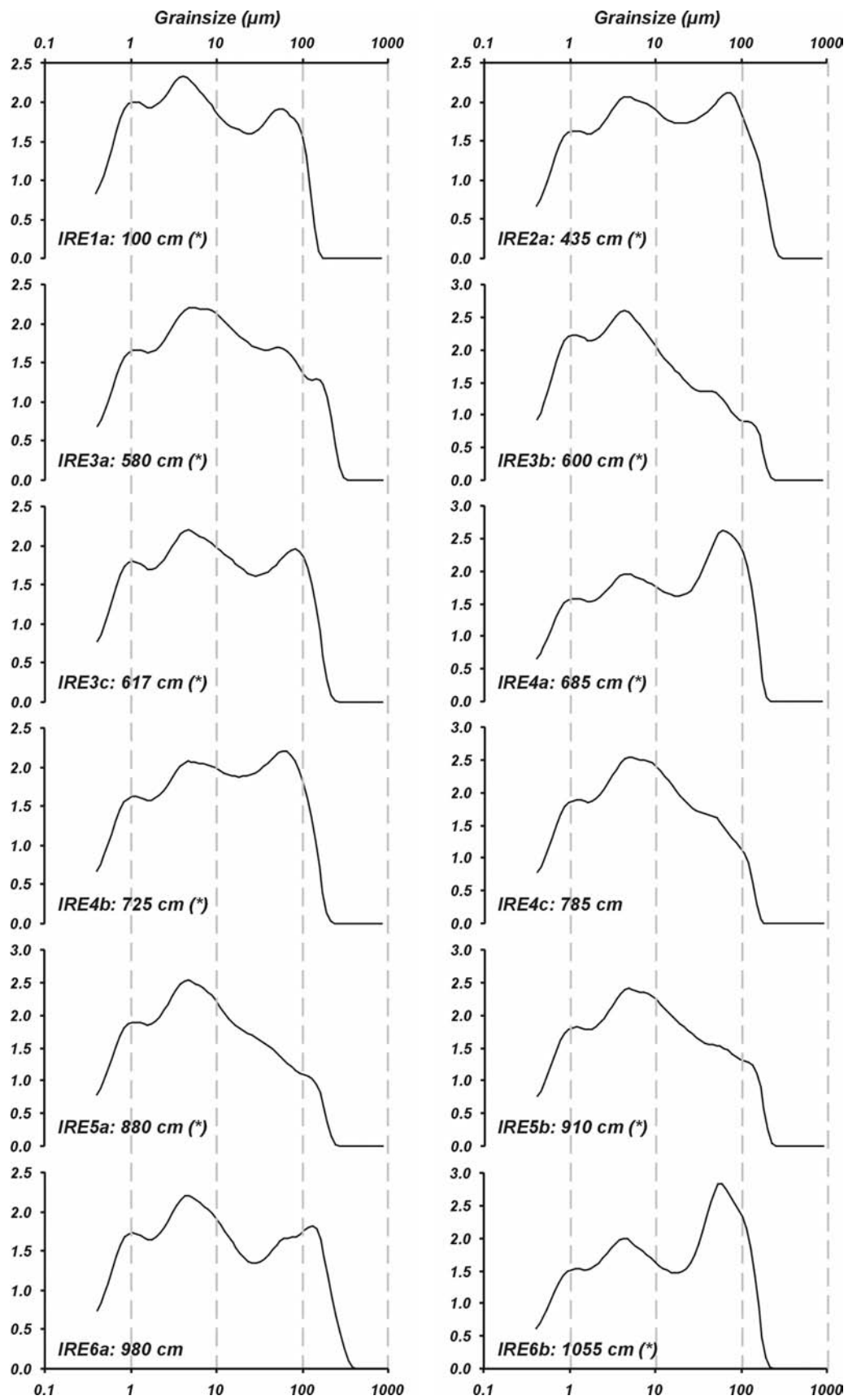


**Figure 4.10:** Grainsize distribution curves (%) of several IRE intervals observed in core MD99-2327. Samples marked with (\*) are located in the X-ray sections in figure 4.12.

#### 4.2.1.4 IRE4 (650-800 cm)

The main pulse of IRE4 is found on the Ca XRF and NPS record in between 700 and 800 cm, with a culmination at 730 cm in the luminosity record (Figs. 4.8 and 4.11). The bulk density, however, suggests locating the end of IRE4 at 650 cm. There is a broad increase of density in this depth range, featuring 3 single peak events, which can be correlated with IRD maxima and higher densities on the X-ray imagery (Figs. 4.8, 4.12d and 4.12e). These three peaks are also picked up in the grainsize signal as IRE4a, 4b and 4c (Figs. 4.9 and 4.10). Especially IRE4a, with a large coarse fraction, is very pronounced and visible in all records. NPS and *T. quinqueloba* do show colder assemblages over a very short time, but this is not fully confirmed by  $\delta^{18}\text{O}$  (Figs. 4.8 and 4.13). The proposed equivalent age of IRE4 is 34.2 ka (Auffret *et al.*, 2002).

#### 4.2.1.5 IRE5 (830-930 cm)

This IRE displays a very broad NPS maximum, with only one large Ca and luminosity peak (Figs. 4.8 and 4.11). This last one is not only very clearly observed on SCOPIX imagery (Fig. 4.12f), but also on the magnetic susceptibility record (Fig. 4.8). The dry density record does not show a very consistent pattern, although the SCOPIX images clearly show very coarse IRD in a finer, but denser matrix. Immediately after this event, 30 cm of very fine layering could bring evidence of a rapid accumulation from turbid plumes due to freshwater input (Auffret *et al.*, 2002). The grainsize characteristics also indicate this IRE is composed of three peak events (IRE5a, 5b and 5c), which however do not contain a very pronounced coarse fraction compared with the other events (Figs. 4.9 and 4.10). The  $\delta^{18}\text{O}$  record does show a significant cooling during this episode. The main peak of IRE5 is correlated with HE5, dated at 45.5 ka (Auffret *et al.*, 2002).

#### 4.2.1.6 IRE6 (980-1070 cm)

Several records as  $\delta^{18}\text{O}$  and NPS show a significant cooling in this depth range (Fig. 4.8). Although the Ca level does not seem to be that high, elevated values of luminosity are observed (4.11). The density and IRD maxima are offset with several centimeters downcore (earlier in time) with respect to the peak of cold events. SCOPIX data shows faint, dark banded patterns with sparse IRD (Fig. 4.12g). A tentative age for IRE6 is 62.00 ka (Auffret *et al.*, 2002), although the determination of this IRE should be treated with caution.

### 4.2.2 IRE characteristics versus HL characteristics

As already mentioned, the recognition of typical HL in the NE Atlantic ocean are based on several classic criteria; high values of magnetic susceptibility, a high amount of IRD (with detrital carbonate and red-stained quartz), a darker sediment colour, low abundance of planktonic fauna and flora, a high percentage of NPS, meltwater pulses within  $\delta^{18}\text{O}$  isotopes and a high density (Bond *et al.*, 1992; Broecker *et al.*, 1992; Chi & Mienert, 1996; Cortijo *et al.*, 1997; Grousset *et al.*, 1993; Robinson *et al.*, 1995). The characteristics of the IRE on the eastern slope of the Porcupine Seabight, however, are somewhat different compared with these well-known HL. In order to better understand and recognize these IRE in other cores (without an extensive data set), this section will discuss the nature and origin of the Irish IRD.

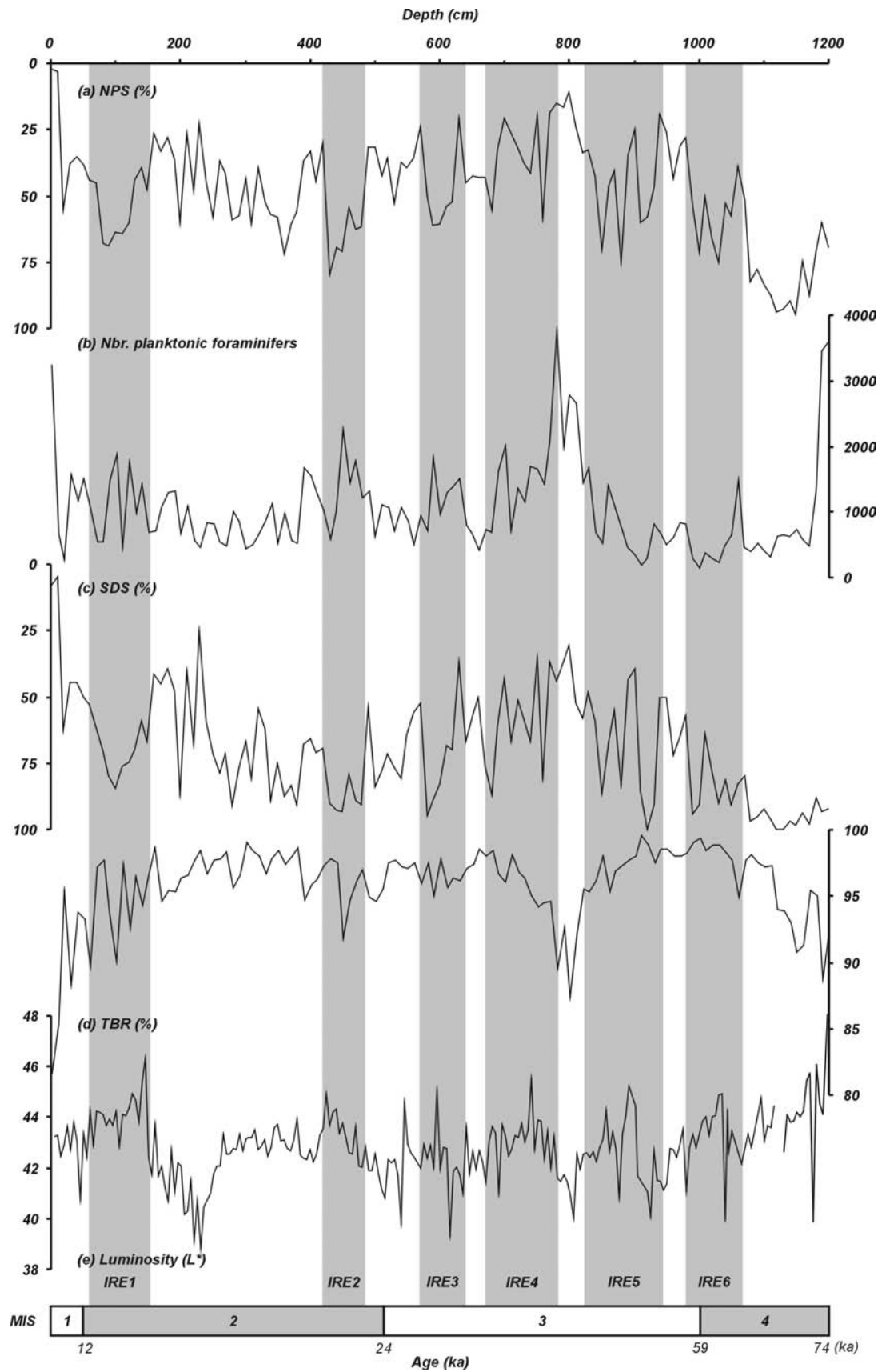


**Figure 4.11:** Paleoenvironmental proxies based on the content of planktonic foraminifers in core MD99-2327, with: (a) relative abundance of *N. pachyderma* s. (*NPS*), (b) abundance of planktonic foraminifera per 10 g of sediment, (c) ratio of left-coiling to right-coiling *N. pachyderma* (*SDS*), (d) the ratio of terrigenous fraction > 150  $\mu\text{m}$  to biogenic (abundance planktonic foraminifera) influence (*TBR*) and (e) luminosity ( $L^*$ ).

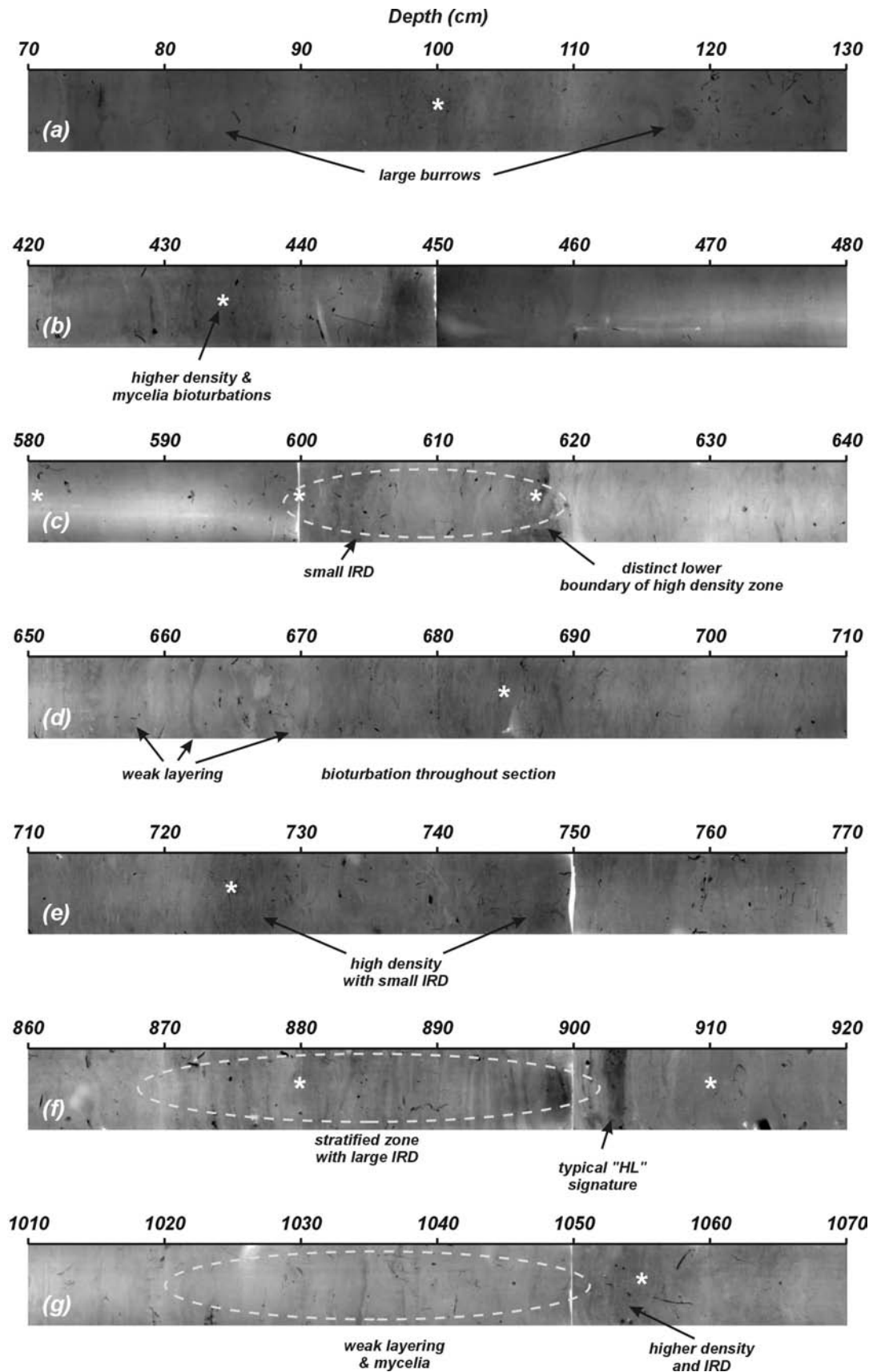


**Figure 4.12:** SCOPIX X-ray visualizations of the 6 IRE intervals; (a) IRE1, (b) IRE2, (c) IRE3, (d) IRE4a, (e) IRE4b and 4c, (f) IRE5 and (g) IRE6. The positions of grain size distribution curves in figure 4.10 are indicated with "\*".

#### 4.2.2.1 Magnetic susceptibility

The most-used and fastest method to detect HL in the NE Atlantic is the use of magnetic susceptibility (MS). It is well-known that only Laurentide material carries a strong magnetic signal, explaining why HL3 and 6, which were attributed a more Icelandic-Fennoscandic origin, do not show up as good in the MS record (Grousset *et al.*, 1993; Robinson *et al.*, 1995; Snoeckx *et al.*, 1999; Thouveny *et al.*, 1994). It can be expected that the relationship between IRD and MS does not seem straightforward at locations dominantly affected by discharges of other ice sheets (Richter *et al.*, 2001). Therefore, the closer to the BIIS, the more the MS signal is expected to be attenuated, due to the growing influence of IRD derived from Irish Palaeozoic carbonate rocks and chalk fragments (Richter *et al.*, 2001; Scourse *et al.*, 2000). The MS record of core MD99-2327 is comparable with a core in the Feni drift, described in Richter *et al.* (2001). However, the susceptibility signal in our core is fairly weak and only two events are recognized in the glacial part of the core; a high plateau is present from 0 to 200 cm (Holocene and parts of IRE1) and a sharp peak is observed at 900 cm (IRE5). The latter also stands out in the X-ray imagery (Fig. 4.12f). This already indicates a weakened influence of Laurentide-sourced IRD along the slopes of the Irish margin, except for maybe IRE5, which might contain more magnetic susceptible LIS material.

#### 4.2.2.2 Ice-Rafted Debris

In contrast with many other NE Atlantic studies using the IRD record, in this study the fraction > 150  $\mu\text{m}$  only (Fig. 4.8) does not allow to easily identify singular HL or equivalent IREs. In core MD99-2327, the amount of ice-rafted grains is fairly elevated (between 5 and 10%) and highly fluctuating. However, once compared with other parameters, single IRE can be recognized. Most of these show a 2 or 3-fold structure in density or grain size (Figs. 4.8 and 4.9). Textural analyses indicate quartz is the dominant grain type (between 80 and 97 %). Other lithic grain types are (igneous?) rock fragments and discrete feldspars. Detrital carbonates were observed, although their presence was rather rare. Their presence could also be suggested by peaks in XRF Ca (Fig. 4.8). Also the number of observed red-stained quartz, which is a marker for LIS-sourced IRD (Bond & Lotti, 1995), was very limited. This was also observed by Knutz *et al.* (2001) in a core on the Barra Fan, West of Scotland. On the other hand, chalk fragments indicative of an Irish or Celtic shelf source (Scourse *et al.*, 2000) were observed at some intervals, but their occurrence was certainly not focused.

Additionally, a few thin sections were studied from rocks or large IRD found in core MD99-2327, boxcore BBC00-0606 (same site) and rock dredges (Fig. 4.14). They display a wide range of rock types. Two of these samples (Fig. 4.14a and 14d) represent sedimentary rocks, probably sandstones with badly rounded quartz grains and some opaque minerals. The sample featured in figure 4.14b shows elongated feldspar phenocrysts in a very fine-grained matrix, suggesting basaltic material. The thin section represented in figure 4.14b shows fine chlorite and muscovite filaments, cross-cut by large quartz-rich veins. This texture suggests a metamorphic rock, which probably is granitic.

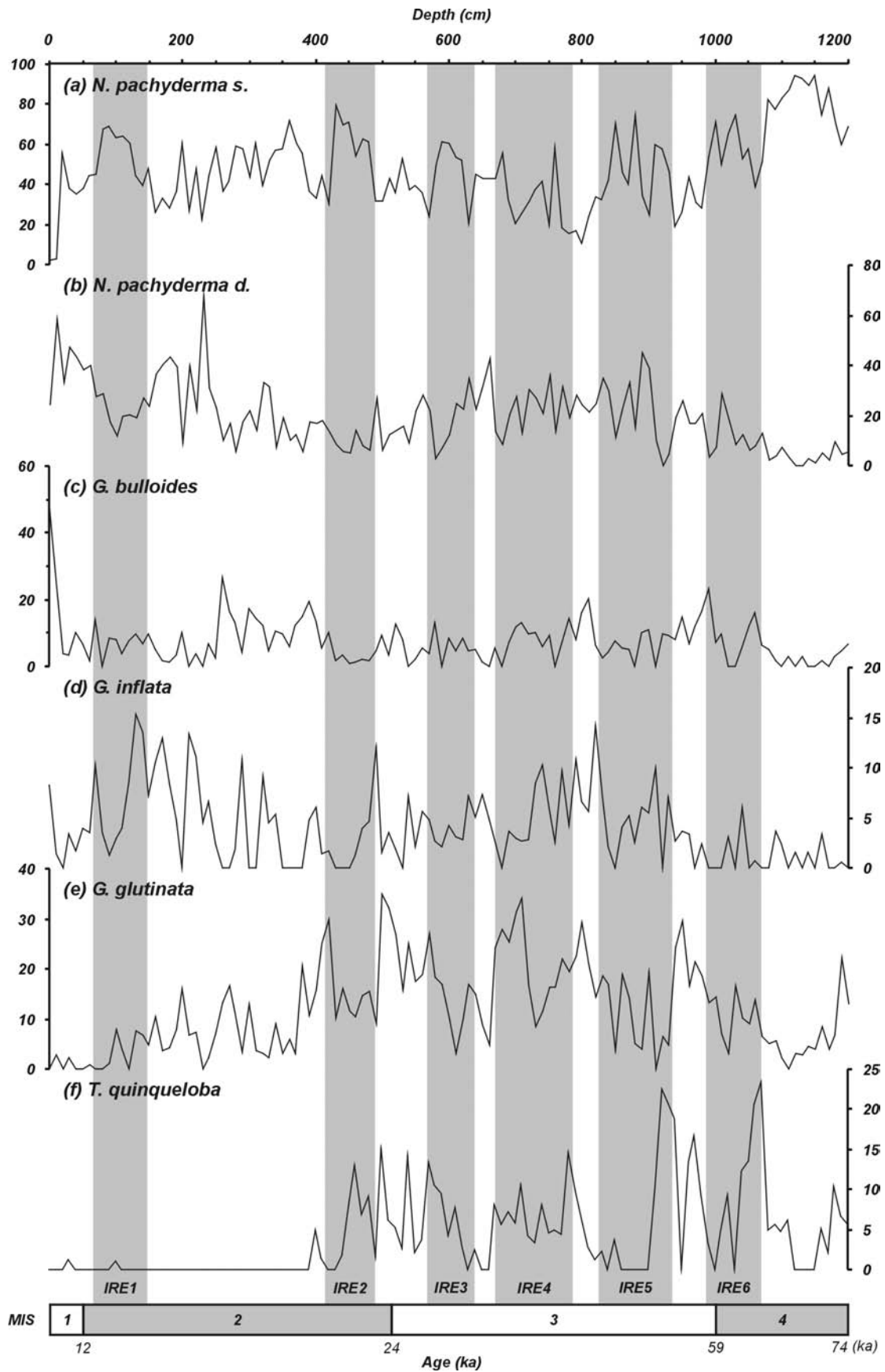


**Figure 4.13:** Downcore variation in planktonic foraminiferal faunal composition in core MD99-23247. The 6 IRE are indicated by the grey-shaded areas.

Knowing the positions of the main ice spreading centers on the Irish mainland during the LGM (Fig. 4.6), it can be predicted which type of rocks can be found in the BIIS-sourced IRD. The “Southern Dome” was spread over the bedrocks of Munster (Limerick, Kerry & Cork) (Holland, 2001) and most probably will have incorporated Devonian and Carboniferous (Silesian) rocks. According to Holland (2001) these are predominantly fluvial sandstones from the Munster basin. Also from the Dingle peninsula, Silurian sandstones and siltstones could be eroded. The western part of the “Central Dome” mostly affected the bedrock of Mayo, Clare and Galway. In the central part of the country, predominantly Carboniferous carbonate rocks can be found (Holland, 2001). However, more variety is found towards the coast. According to Knight (2000) the Connemara region is typically glacially eroded with Precambrian metamorphosed clastic rocks, migmatites and other intrusives. South of Galway, Caledonian igneous material can be found. This very well explains why the majority of the detrital material consists of quartz fragments. In cores located North of Ireland, Knutz *et al.* (2001) also recognized a minimal input of Carboniferous limestones of Ireland, possibly due to a southward drift of icebergs released from western Ireland. However XRF Ca does suggest the presence of detrital carbonate, only rare fragments were observed, suggesting a minimum of central Irish material was incorporated in the moving ice sheets. Except for the igneous rocks present in the County of Galway, the overall composition of the BIIS-sourced IRD will not yield significant increases in magnetic susceptibility. Hence, the MS peak observed during IRE5 (Fig. 4.8), most probably is due to LIS-sourced IRD.

#### 4.2.2.3 Calcium values & color

A higher Ca content in IRE can be related to a higher amount of terrigenous, detrital carbonate, coming either from the Laurentide ice sheet (Bond *et al.*, 1992; Bond & Lotti, 1995; Broecker *et al.*, 1992) and/or from extensive outcrops of Palaeozoic carbonates in Ireland (Richter *et al.*, 2001), or from Mesozoic chalk outcrops in the Irish Sea (Scourse *et al.*, 2000). In this regional study, an inverse relationship with NPS percentages and XRF Ca measurements can be observed (Fig. 4.8). The elevated XRF Ca values in the inferred interglacial part of the core reflect enhanced biogenic carbonate productivity coinciding with higher surface water temperatures (Fig. 4.7). Above 1200 cm, however, this relationship starts to break down. At 1220 cm, the planktonic foraminiferal abundances drastically drop and never again reach comparable levels in the overlying sediments. The earlier discussed sharp peak at 900 cm does not have a counterpart in the planktonic foraminifers’ record, and the coinciding minimum of NPS is a local one within a broader interval of high NPS percentages. The two uppermost Ca maxima (450 and 100 cm) coincide with maxima of NPS indicating surface water cooling (Fig. 4.8). All this suggests elevated Ca values in this part of the core would imply a higher amount of light-coloured grains of carbonate. As a consequence, a higher amount of quartz, detrital carbonate and chalk grains might show up as a lighter facies within the luminosity record. Since the HL in the Ruddiman belt are characterised by darker sediment colours (Grousset *et al.*, 1993; Grousset *et al.*, 2000), the atypical XRF Ca and luminosity records are supporting the idea of dominantly locally-derived IRD. Only the equivalents of HL3 and 6 (with a more Icelandic-Fennoscandic origin and thus with less carbonate content) are not expected to show up as nicely in the Ca record.

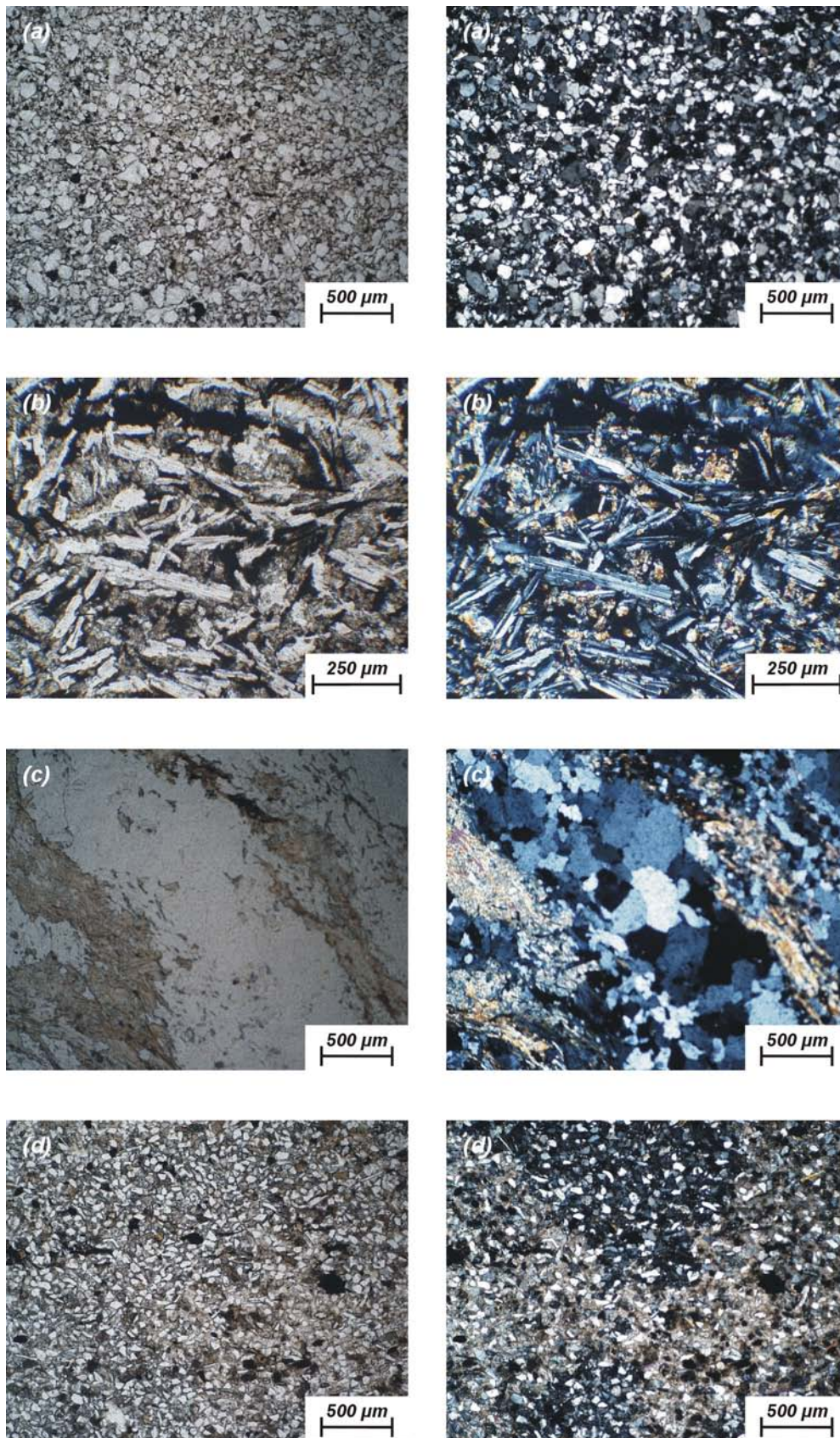


**Figure 4.14:** Thin section slides of IRD in plain polarized light (left) and with crossed polars (right): (a) sandstone with badly rounded quartz; (b) basalt with large, elongate feldspar phenocrysts; (c) inferred metamorphic rock with chlorite and muscovite, cross-cut by quartz veins and (d) angular quartz sandstone.

#### 4.2.2.4 Foraminifers and $\delta^{18}\text{O}$ stable isotopes

Regardless the presence of a proximal ice sheet, the reaction of planktonic foraminifers will remain the same during ice-rafter events. Due to an extensive sea ice cover, temperatures will decrease, together with the abundance of the entire planktonic faunal assemblage, whereas the percentage of mainly *N. pachyderma* s., but also other subpolar species will increase. (Bond *et al.*, 1992; Cortijo *et al.*, 1997; Elliot *et al.*, 1998; Grousset *et al.*, 2001). Like Chapman's *et al.* (2000) data, the present data only show a good positive response of *N. pachyderma* s. and *T. quinqueloba*, while *N. pachyderma* d. clearly shows a negative response (Fig. 4.13). Other important species in the faunal assemblage as *G. bulloides*, *G. inflata* and *G. glutinata* do not display conclusive changes to identify an IRE. On the other hand, they do assist in discriminating warm from cold long-term periods. MIS2 is characterized by higher abundances of *G. inflata*, while MIS3 is characterized by higher values of *G. glutinata*.

Due to the frequently observed meltwater events and the frequent ice volume changes, the  $\delta^{18}\text{O}$  isotope values should not be used unambiguously. The large scatter in the oxygen (and carbon) isotope records could mean that (some of the) forams were reworked, which suggests treating this data with caution.

#### 4.2.2.5 Density

It was previously demonstrated that there is a frequent positive relationship between the amount of IRD in marine sediments and the dry bulk density (Auffret *et al.*, 1996; Chi & Mienert, 1996; Moros *et al.*, 1997; Moros *et al.*, 2002). This can be attributed to lower porosities in poorly sorted IRD deposits (Moros *et al.*, 1997; Moros *et al.*, 2002), and possibly to higher grain densities and diagenetic calcite precipitation (Auffret *et al.*, 1996; Kassens & Sarnthein, 1989). Bond *et al.* (1992) and Grousset *et al.* (2001) also recognized this correlation. It was confirmed by X-ray imagery, where they can be observed as dark, fairly homogenous levels, owing to increased IRD and water content decrease (Fig. 4.12f). In the studied core (Fig. 4.8), almost all increases in dry bulk density were correlated with higher percentages of NPS and therefore they were the main tool to detect the HL-equivalent IRE. Some events, like IRE4, even clearly display 3 distinct pulses in the density record, which is also observed in the NPS, IRD and grain size record (Figs. 4.8 and 4.9).

### 4.3 A SE to NW transect in PSB

In order to document and understand the variability of IRE in the Porcupine Seabight, a SE to NW transect of long cores was studied. These data were compared with the observations made in core MD99-2327, which made it possible to confirm the validity of the characteristics of IRD deposition in this area.

#### 4.3.1 Kings Channels (MD01-2449)

Core MD01-2449 was taken on an upslope (435 m) area, south of the Aragorn channel (Fig. 4.15). Due to its location, it is not situated in a region of high current speed, compared to MD99-2327 (which is located 50 km NW). This rules out the possibility that the detrital or the biogenic components would have been subject to major reworking through bottom currents. This core should thus provide a continuous record of sedimentary input from dominantly BIIS-sourced material.

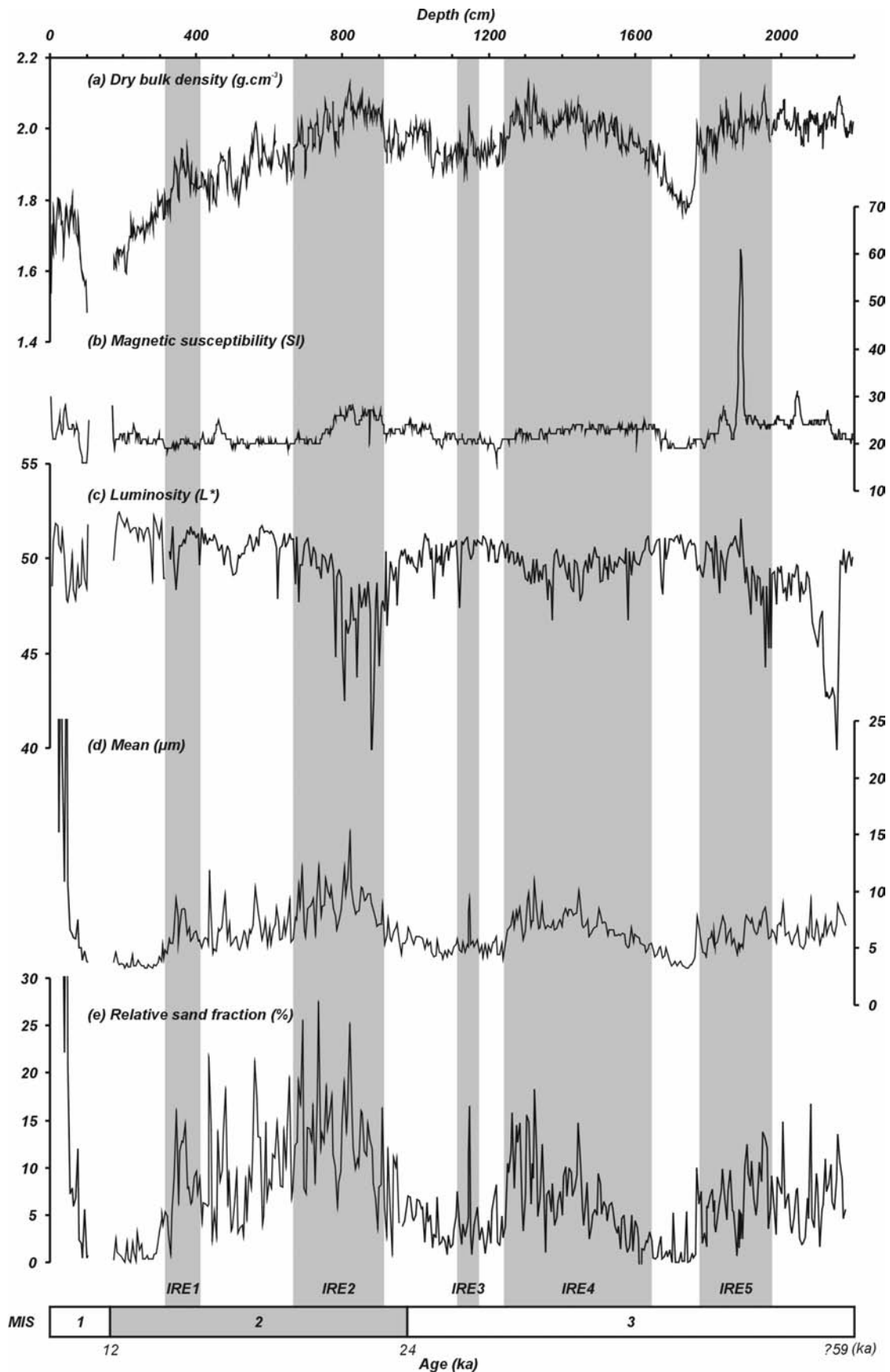


**Figure 4.15:** Detail of lithological characteristics and physical properties of core MD01-2449 with (a) dry bulk density ( $\text{g}\cdot\text{cm}^{-3}$ ), (b) magnetic susceptibility (SI), (c) luminosity ( $L^*$ ), (d) mean grainsize ( $\mu\text{m}$ ) and (e) the relative sand fraction (%). The 6 IRE are indicated by the grey-shaded areas.

This 2484 cm long core has a top part (0 to 26 cm) which consists of olive clayey very fine quartz-foram sands. This grades downcore into olive grey to grey silty clays. Nannofossils and fine sand pockets were commonly observed in varying quantities. Two coarser-grained intervals were also observed; between 600 and 900 cm and between 1200 and 1400 cm. These two intervals are also characterized by elevated plateaus of dry bulk density (Figs 4.15 and 4.16). A complete flow-in occurs below 2215 cm (Fig. 4.18g). As a consequence, only the first 22 m of this core will be used.

The variations in mainly dry bulk density, mean grainsize, but also magnetic susceptibility enable to identify several IRE (Fig. 4.15) and to compare the record of this core with MD99-2327 (Fig. 4.16). Since no paleoenvironmental study of this core has been made, it only relies on this comparison for the construction of a tentative stratigraphy. Both cores have a similar amount of sand content (up to 20%), mean grainsize and magnetic susceptibility (Fig. 4.16).

#### **4.3.1.1 IRE1 (315-410 cm)**

IRE1 is the first significant rise in density and in mean grainsize. Compared with MD99-2327, there is no significant increase in magnetic susceptibility. On the other hand, also two main peaks in ice-rafted sand can be observed. Grainsize characteristics of this event (Fig. 4.17) show a large coarse silt fraction (up to 3 %). On the X-ray imagery (Fig. 4.18a), IRE1 clearly shows up as a high density interval with frequent small IRD, but also with frequent bioturbation.

Two significant density peaks (488 and 566 cm), which also stand out in grainsize, can be correlated with density rises in core MD99-2327. The 488 cm event also has a signature in magnetic susceptibility.

#### **4.3.1.2 IRE2 (662-911 cm)**

The nature of the increase in density and the mean grainsize signature between 662 and 911 cm are very similar to IRE2 in core MD99-2327 (Fig. 4.16). The two consecutive mean peaks at 755 and 820 cm have similar counterparts in core MD99-2327. However, in this case the second peak and the density plateau around 800 and 900 cm are accompanied by a subtle rise in magnetic susceptibility and the luminosity shows significantly darker shades (Fig. 4.15). In figure 4.18b, the X-ray facies of this zone displays a high density and a high degree of bioturbation. In contrast with other IRE, no significant IRD are observed, although the grainsize distribution curve in figure 4.17 shows a very pronounced coarse silt fraction. In a way, this could suggest a relatively larger influence of finer-grained LIS-sourced material, which has a higher magnetic susceptibility. This relatively larger amount of 'darker' IRD could be responsible for lower luminosity values.

At about 1000 cm, prior to IRE2, a small density plateau with concurrent subtle increases in MS and mean grainsize can be correlated with similar features in core MD99-2327 at 525 cm.

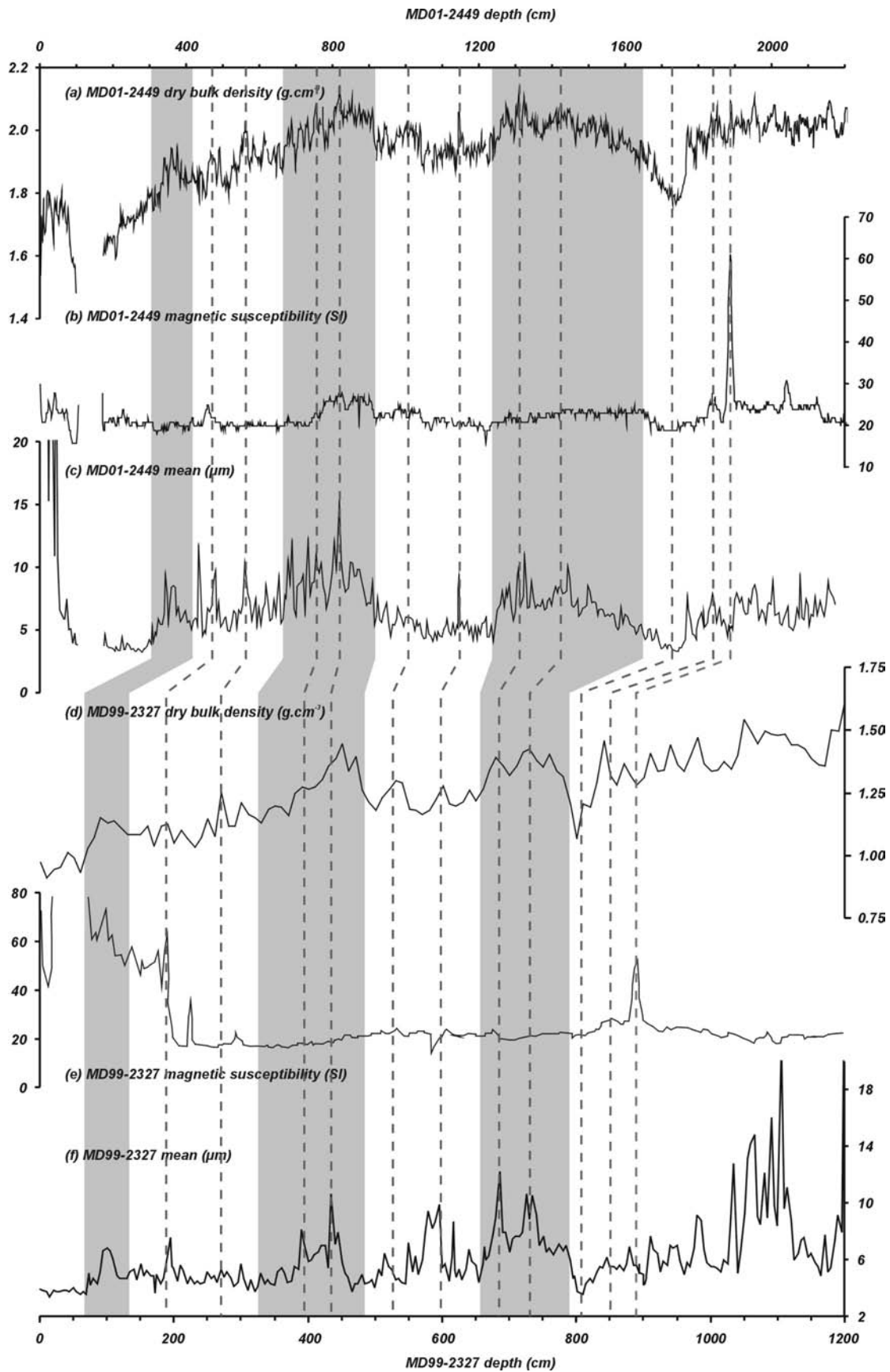


**Figure 4.16:** Correlation of core MD01-2449 with MD99-2327, based on respectively (a, d) dry bulk density ( $\text{g.cm}^{-3}$ ), (b, e) magnetic susceptibility (SI) and (c, f) mean grainsize ( $\mu\text{m}$ ). Specific correlation areas and points are indicated by respectively grey-shaded areas or dashed lines.

#### **4.3.1.3 IRE3 (1115-1185 cm)**

As in MD99-2327, IRE3 is a very small event located in a saddle-like position between two zones of elevated density. Nevertheless, there is a pronounced density increase, which is also observed in the mean grainsize record (Fig. 4.16). Radiographs show a subtle increase in higher density and more IRD around the culmination of this event (Fig. 4.18c). Again, darker shades in the luminosity record suggest a more significant non-BIIS influence (Fig. 4.15). In this case, this could very well mean a contribution of IIS or FIS-sourced material.

#### **4.3.1.4 IRE4 (1245-1645 cm)**

The most pronounced IRE in both cores, IRE4, is located in a zone with elevated density, immediately deposited after a zone with a very low density (Fig. 4.16). As in the mean grainsize record, the density suggests up to two peak events (1325 and 1435 cm), although a primary, smaller one can also be identified at 1500 cm. Again, in both cores, this event does not cause an anomaly in the MS record. However, over the entire zone, the luminosity seems to indicate darker values (Fig. 4.15). In the radiographies, this event is characterized by a very dark facies with extensive bioturbation and frequent IRD particles (Fig. 4.18d). Selected grainsize analysis in the first two peaks (Fig. 4.17) indeed show a very high silt content, especially in the sample about 1450 cm.

One of the more diagnostic points of comparison between the two cores is the density minimum located downcore of IRE4, roughly between 1680 and 1780 cm in MD01-2449 (Fig. 4.16). It is accompanied by a lower magnetic susceptibility signal and also a significantly lower mean grainsize (about 3  $\mu\text{m}$ ). The grainsize distribution shows a predominantly clayey to very fine silty-clayey composition (Fig. 4.17). On X-ray imagery, relatively large burrows are observed (Fig. 4.18e).

#### **4.3.1.5 IRE5 (1787-1977 cm)**

Finally, the most diagnostic feature that ties the stratigraphy of the two cores is located between 1787 and 1977 cm. From top to bottom, the MS is characterized by a small excursion at about 1847 cm, followed by a local minimum at 1871 cm after which the largest MS anomaly occurs (Fig. 4.16). Moreover, on the X-ray images, this main peak is characterized by an almost classic signature of a typical HL: an almost abrupt onset of higher density with large IRD fragments (Figs. 4.18f and 4.12f). After the deposition of this main "IRD surge", a zone up to 30 cm occurs with very fine bands of IRD. Even at 80 cm above the main event, large IRD particles are observed, which do not give a signal in the magnetic susceptibility record (Fig. 4.18 e). Both cores show almost the same configuration during IRE5. The dry bulk densities of this event are not very pronounced and luminosity shows a lighter shade (Fig. 4.15). The grainsize distribution curves over this event do not show a very coarse-grained IRD signature, with sometimes a more dominating silty-clayey composition (Fig. 4.17). The characteristics of this event and also its appearance in two cores, strengthens the idea that classic HL-IRD (LIS, IIS and FIS source) did reach the "near-coast" area of Ireland. On the other hand, the IRD seen in the X-ray images, which does not possess a pronounced MS signature, could very well have a European or even BIIS source. However, the latter could be questioned, since non-BIIS icebergs reached the shelf edge, suggesting an ice-free sea, possibly without a large BIIS ice sheet.

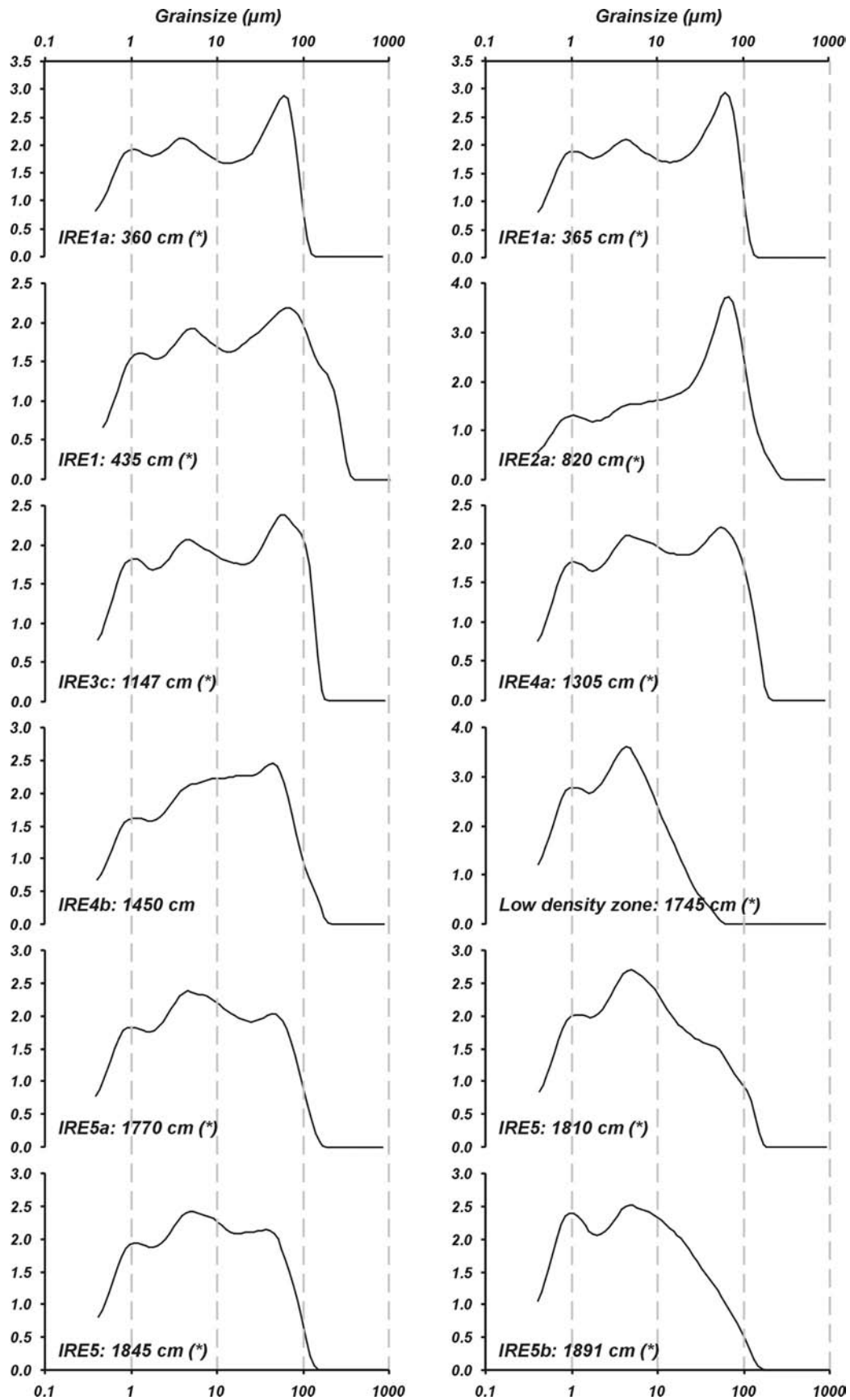


**Figure 4.17:** Grainsize distribution curves (%) of several IRE intervals observed in core MD01-2449. Samples marked with (\*) are located on the X-ray sections in figure 4.18.

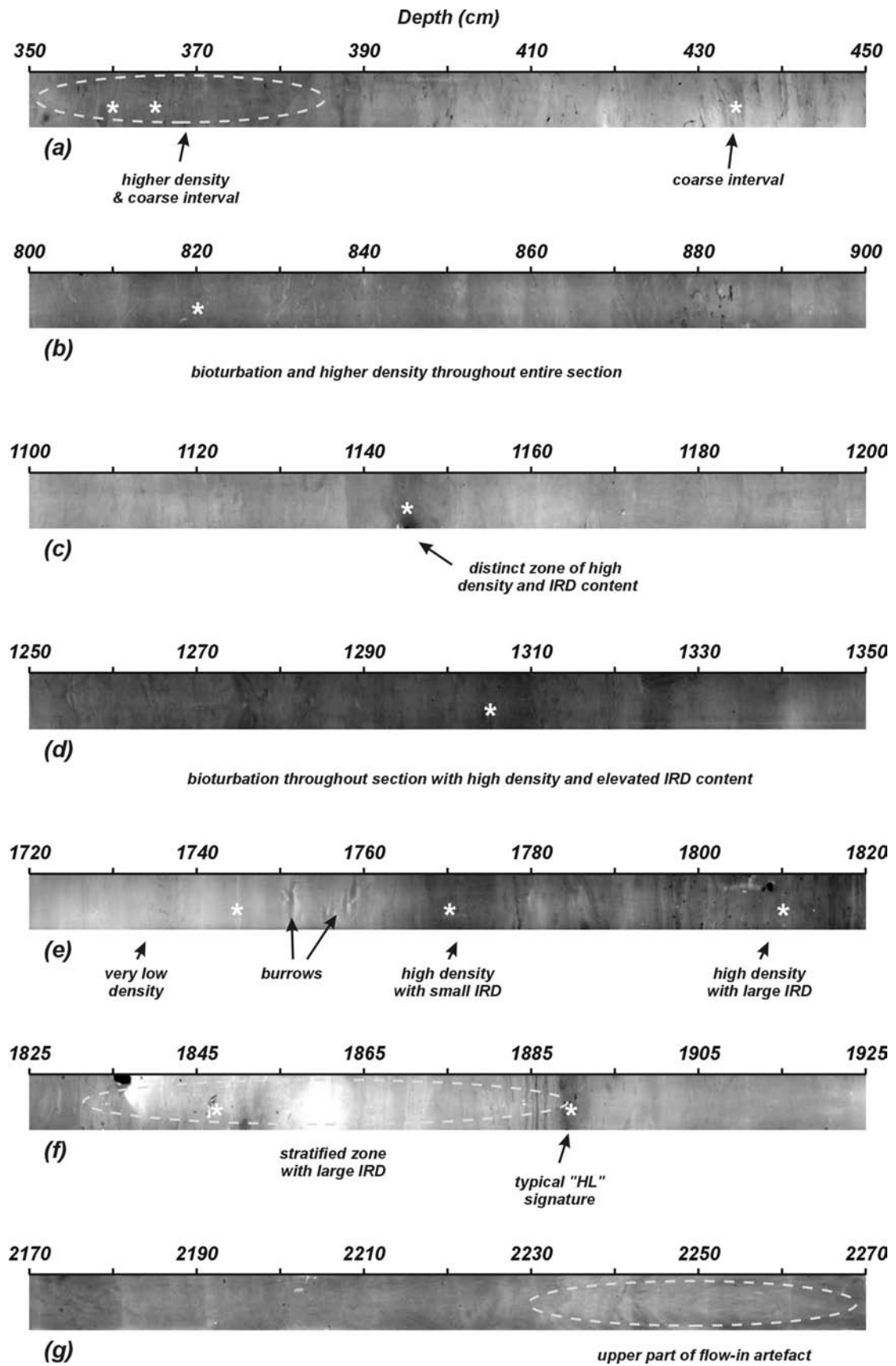


**Figure 4.18:** SCOPIX X-ray visualizations of specific intervals observed in core MD01-2449; (a) IRE1, (b) IRE2, (c) IRE3, (d) IRE4, (e) density minimum after IRE5, (f) IRE5 and (g) flow-in. The positions of grainsize distribution curves in figure 4.17 are indicated with (\*).

### 4.3.2 Magellan mound province (MD01-2452)

Core MD01-2452 was taken in a water depth of 617 m at a position 100 km NW of core MD99-2327 (Fig. 4.6). The initial purpose for this core was to sample the top a buried Magellan mound (Van Rooij *et al.*, 2001), but with its 1830 cm it did not reach its goal. However, the sedimentary environment of this core site does not seem to be influenced by significant bottom current or turbidity action (Huvenne, 2003; Cornilly, 2003). This core offers thus an ideal opportunity to study the paleoceanography of the Magellan mound province. Within this framework, Cornilly (2003) made a paleoenvironmental study of this core site and improved the age model that earlier was proposed by Foubert (2002). However, in these earlier studies, only certain aspects of ice-rafting events were studied and the results were not interpreted in a large framework, comparing other cores from the basin. On the other hand, more detailed information concerning the sedimentary environment and the time frame of this core is discussed by Foubert (2002), Cornilly (2003) and Huvenne (2003).

#### 4.3.2.1 Core description and time frame

The physical properties of this core, displayed in figure 4.19, already show a completely different setting compared to the previously discussed cores. Core MD01-2452 consists of dark grayish brown silty clays with rare to abundant nannofossils. However, the first meter contains (pockets of) fine, soupy foraminiferal sands, indicative of the interglacial MIS1. Centimeter-scaled layers of fine to medium sand occur from 812 to 870 cm and light brownish grey sandy intervals between 1038 and 1140 cm. This level is characterized by a significantly lower magnetic susceptibility and a pronounced lighter luminosity (Fig. 4.19). The paleoenvironmental analysis suggests this is a warm period, comparable with MIS5a observed in core MD99-2327 (Cornilly, 2003). This also suggests that the zone from 0 to 1038 comprises MIS1 to 4. From 1355 cm downcore, the dry bulk density starts decreasing and the susceptibility increases. Together with a change to a colder faunal composition (Cornilly, 2003), this zone is correlated with the glacial MIS6. From 1610 to 1810 cm, faint mm-scaled silt laminae are present within silty clay, which could be fine ice-rafting events.

#### 4.3.2.2 Last glacial ice-rafting events

In this core, the last glacial period is situated between 0 and 1038 cm. In contrast with cores MD99-2327 and MD01-2449, several peaks in magnetic susceptibility are present. Although no extensive quantitative and qualitative study of the planktonic foraminifer assemblage and the composition of the present IRD has been performed, the MS signal strongly suggests the presence of HL with most probably a LIS-sourced material. Therefore, it is considered to be correct to identify these “ice-rafting events” as Heinrich Layers.

All classic North-Atlantic Heinrich Layers have been identified in this core, from Younger Dryas (or HLO) to HL6. The magnetic susceptibility of HLO, 1, 3 and 6 is not very much pronounced, compared to the “typical” HL as HL2, 4 and 5. Most of the HL have a counterpart in the dry bulk density record, although those of HL1 and HL3 are not very elevated. Only HL3 and HL5 seem to have multiple components. As in core MD01-2449, HL5 is characterized by a relatively darker luminosity. HLO, 2, 3 and 6 seem to be significantly lighter.

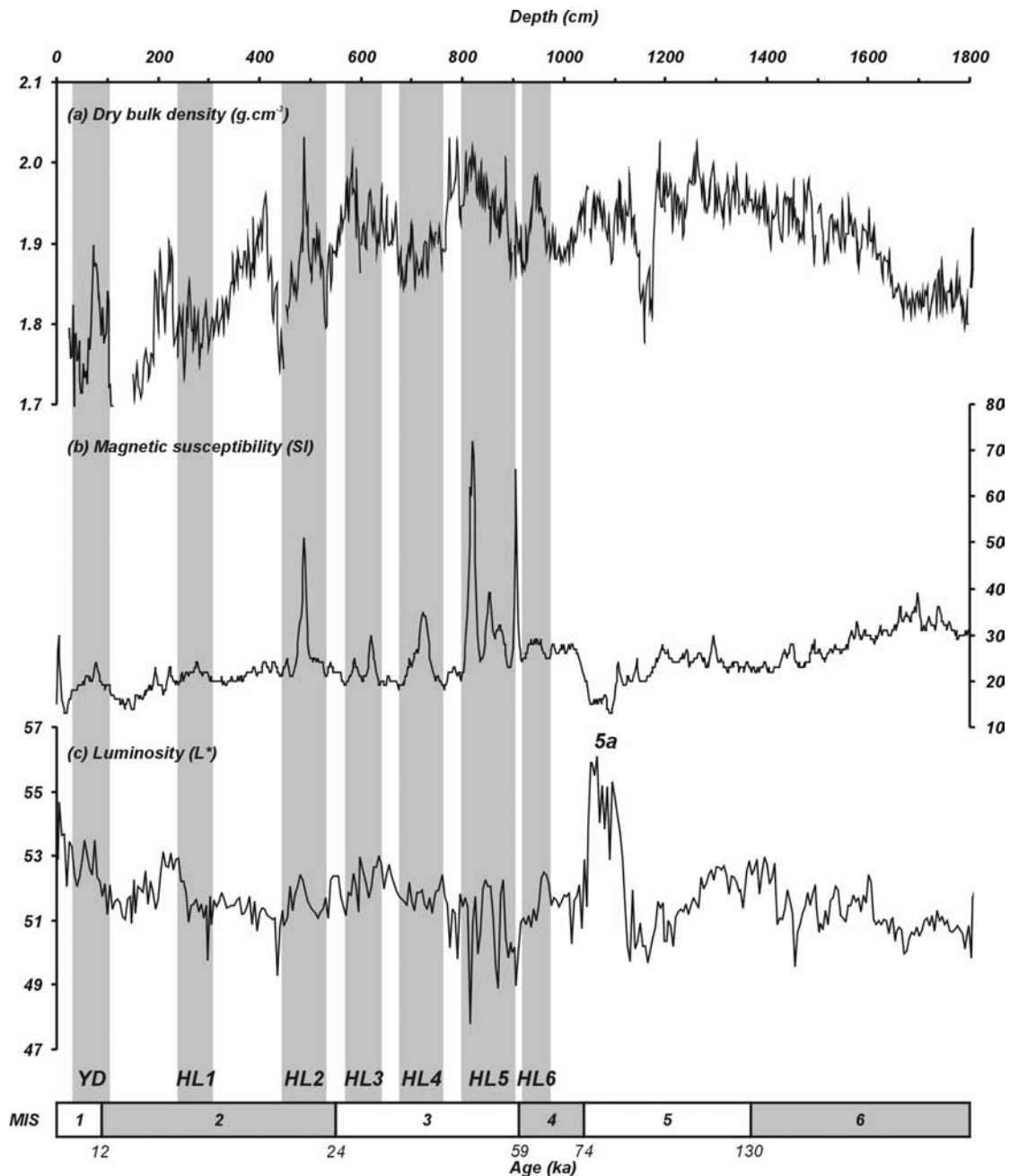


**Figure 4.19:** Physical properties of core MD01-2452 with (a) dry bulk density ( $\text{g.cm}^{-3}$ ), (b) magnetic susceptibility (SI) and (c) luminosity ( $L^*$ ). Heinrich-(like) events are indicated in grey-shaded areas.

### 4.3.3 Connemara (MD01-2453 & MD01-2457)

Both cores are located in a water depth of about 360 m at 130 km NW of MD99-2327. Their principle objective was to sample presumed fluid escape structures observed on sparker lines above the Connemara gas field. However, both cores were not able to penetrate beneath a presumed consolidated level at 1763-1769 cm below the sea floor (Van Rooij *et al.*, 2001). On the other hand, this yielded two nearby located cores with a similar length, which is ideal for paleoceanographic purposes. In this way, coring disturbances, logging artifacts and other possible errors can be filtered out through a comparison of both data sets.

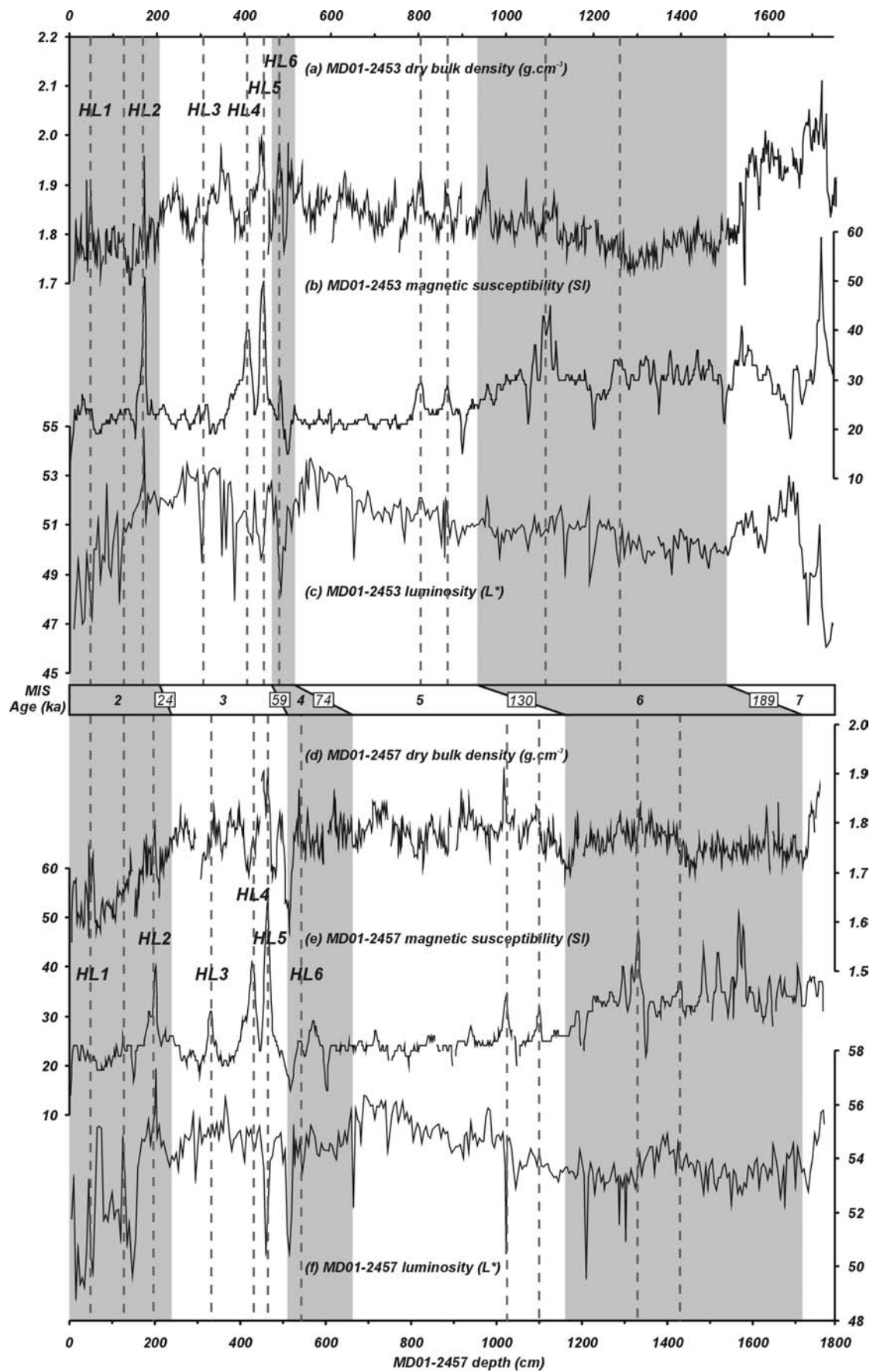


**Figure 4.20:** Correlation of core MD01-2453 with MD01-2457, based on respectively (a, d) dry bulk density ( $\text{g.cm}^{-3}$ ), (b, e) magnetic susceptibility (SI) and (c, f) luminosity ( $L^*$ ). The grey-shaded areas indicate colder (even) isotope stages.

#### **4.3.3.1 Core description and time frame**

Although both cores have a similar length, there is a significant stretching or compression of about 2 m in respectively core MD01-2457 or MD01-2453 (Fig. 4.20). Because it is a common feature that Calypso corers tend to stretch sediment, rather than compress it (which is more likely to happen with gravity corers) (Skinner & McCave, 2003), it is assumed that core MD01-2453 more likely approaches the true length of the sedimentary record. Hence, all description will refer to this core and MD01-2357 will be used to assist removing possible artifacts.

The cores consist of grey to olive grey to dark grayish brown silty clays with sulphide specks, frequent to abundant nannofossil and occasional fine sand. Sandy intervals are present from 4 to 5 m and at the base of the core. As in core MD01-2452, the first sandy interval is concurrent with a more elevated density and magnetic susceptibility, representing ice-rafted sands. A lighter sediment color between 524 and 660 cm and a relatively “flat” MS signal from 524 to 942 cm suggest the interglacial MIS5. An increasing and fluctuating magnetic susceptibility, together with a relatively darker sediment color indicates another cold period, which is MIS6. From 1500 cm to the bottom of the core, the bulk density and the luminosity drastically increases, suggesting the interglacial MIS7.

#### **4.3.3.2 Last glacial ice-rafting events**

The last glacial period in the Connemara region only makes out a limited part of the sedimentary record and the ice-rafting events are located relatively close to each other. The signature of the Heinrich Layers is comparable with those observed in core MD01-2452. All HL have a pronounced peak in magnetic susceptibility, except for HL1 and HL6. Only HL4 does not display a pronounced peak in dry bulk density. On the other hand, all HL but HL2 has a darker shade. The morphology of the MS and luminosity peaks of HL2 are very similar. This suggests that together with magnetic susceptible material, also light-colored IRD as detrital carbonate could be present, which is very diagnostic for LIS-sourced IRD.

#### **4.3.4 Sedimentation rates within PSB**

The identification and correlation of last-glacial ice-rafting events along the eastern to northern margin of the Porcupine Seabight, enables to compare the linear sedimentation rates (LSR) of these different sites (Fig. 4.21). It immediately strikes that the sedimentation rates gradually decrease from SE to NW. Core MD01-2449 shows an average glacial LSR of 37 cm.ka<sup>-1</sup>, which is not surprising due to its high upslope position and its presence near the Gollum channel system. Together with MD99-2327, which has an average LSR of 15 cm.ka<sup>-1</sup>, they have a most pronounced rise in LSR between IRE1 and IRE2. This could be due to their proximity of the BIIS and the beginning destabilization of the BIIS. Such a sharp increase in sedimentation rates remains present in all cores, although it is attenuated more to the north. Core MD01-2452 has a comparable sedimentation rate with MD99-2327, although it decreases gently during MIS3 and 4. The lowest sedimentation rates are found in the Connemara cores, which display a very similar pattern from MIS2 to the start of MIS3, where the probable artificial stretching of MD01-2457 becomes clear.

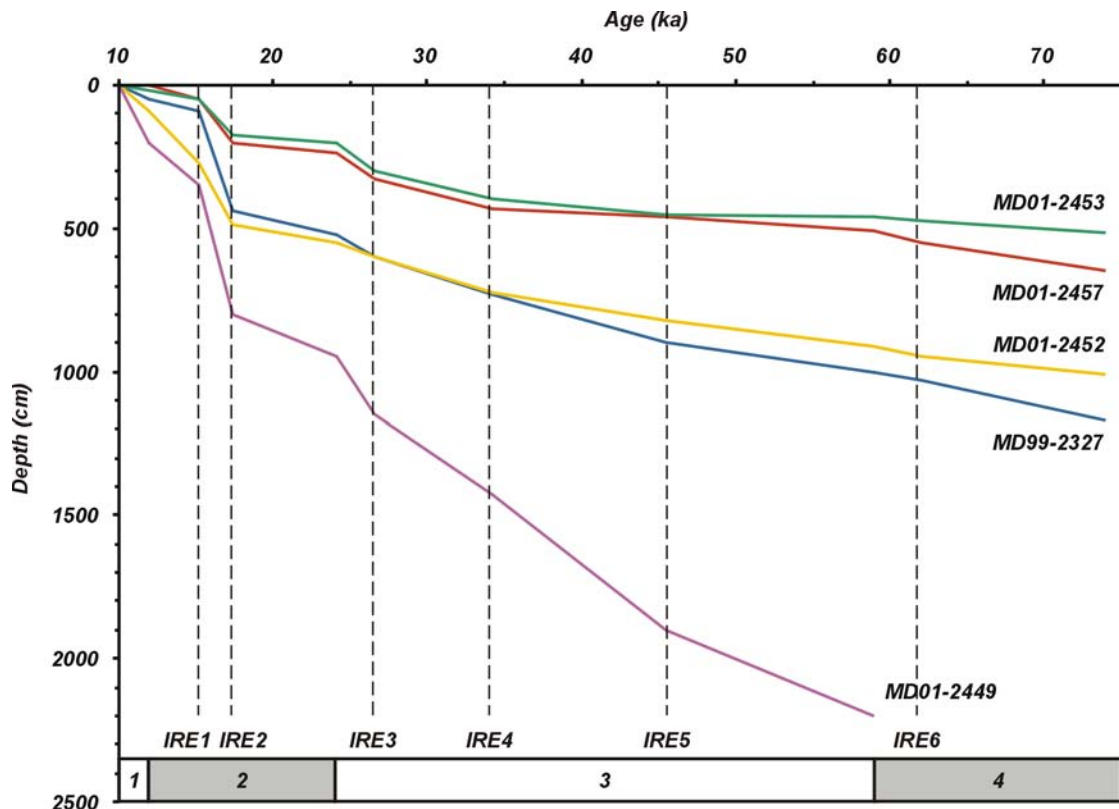


**Figure 4.21:** Linear sedimentation rates (LSR) of the five studied cores in the Porcupine Seabight. Note the enhanced sedimentation rates during the LGM, as well as the decrease in LSR from cores located in the SE towards the cores in the NW.

## 4.4 Discussion

### 4.4.1 Patterns of IRD distribution in PSB

The five cores studied in the SE to NW transect show a distinct difference in IRD distribution pattern. The sedimentary history of cores MD99-2327 and MD01-2449 shows a very atypical situation with a large and very essential BIIS signature. These regional IRE do not share exactly the same characteristics with the typical North Atlantic HL. Of course, IRE may have many common features with HE, which partly helped recognizing them: the high percentage of *N. pachyderma* s., an elevated high dry bulk density and the X-ray signature. However, the recognition and interpretation of the IRE is not obvious for several reasons and some new BIIS-specific markers have been used.

Especially the lack of anomalies in the magnetic susceptibility made it very difficult to trace these events. This can partly be explained due to the mineralogical and geochemical composition of the IRD (Figs. 4.8 and 4.14). The influence of detrital carbonate is clearly higher, because during Ca maxima, the biogenic component becomes rather low. This relative increase in Ca could be important enough to induce colour changes at the level of the IRE (Fig. 4.11). The structure of IRE1, 2, 3 and 4 remind of the several IRD pulses that were observed in typical NE

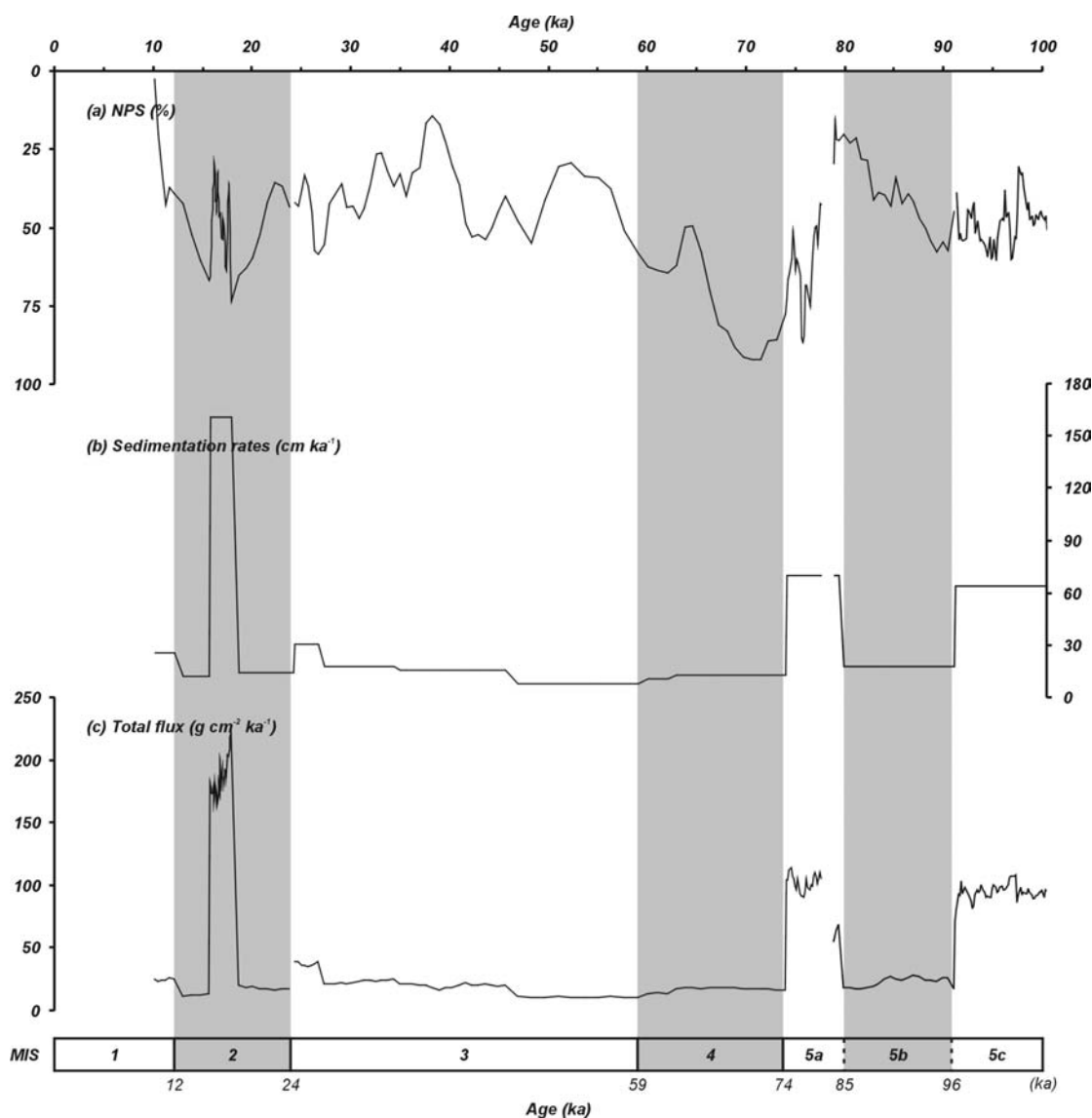


**Figure 4.22:** The (a) relative abundance of *N. pachyderma s.* (NPS) within core MD99-2327 is compared with (b) the linear sedimentation rates (cm.ka<sup>-1</sup>) and (c) total fluxes (g.cm<sup>-2</sup>.ka<sup>-1</sup>) over the last 100 ka BP. The grey-shaded areas indicate colder (even) isotope stages.

Atlantic Heinrich Layers by Auffret *et al.* (2002), Grousset *et al.* (2000) and Grousset *et al.* (2001). These HE contained a central Laurentide-sourced peak preceded and followed by a European-sourced event. This 3-fold structure is only recognized in IRE3, 4 and possibly 5, suggesting the middle peak could very well contain LIS material, due to a high magnetic susceptibility (Fig. 4.8). IRE1 and 2, however, only have a double pulsation, which might imply that during the last 25 ka no Laurentide material reached this site and only the precursor and after-event were recorded. In summary, the IRD characteristics of these cores suggest that, except for IRE5, they all originate from the Irish mainland.

The last glacial ice-rafting events observed in the other three cores, located at the northern edge of the basin are very similar to the HL as described in the Ruddiman belt. However, since neither grainsize analysis nor a lithological study was performed on these last cores, their interpretation should be treated with

caution. Nevertheless, already the magnetic susceptibility variation strongly suggests the influence of LIS-sourced IRD.

This fractionation could be explained through the local surface current system during the LGM. Hall & McCave (1998a) suggested a general SW surface current drift along the Celtic shelf edge. This was confirmed by Knutz *et al.* (2001) and Grousset *et al.* (2001) who suggested a southward drift of icebergs released from western Ireland. Together with this present data, it can be suggested that BIIS icebergs were almost immediately subject to this southward drift and, by consequence, their products were only deposited along the eastern slope of the Seabight. Most probably, only a minimum of BIIS-sourced IRD reached the sites in the northern part of the Porcupine Seabight. On the other hand, these other three cores do show typical HL deposition. Shallow seismic data have demonstrated the presence of presumably BIIS iceberg ploughmarks in the Connemara region (Games, 2001; Mathys, 2001). In view of the physical properties of the IRD in this area, it seems plausible that these possibly grounded icebergs could also have had a LIS, FIS or IIS source. A similar situation has been observed near Goban Spur, where Scourse *et al.* (2000) observed a greater LIS IRD flux than a BIIS one. They suggested probable grounding, collision and in situ melting of large LIS icebergs along the margin. Together with the presumed southward drift of the BIIS-icebergs, this might possibly explain why certainly during MIS2 almost no LIS-sourced IRD is found along the eastern slope; or they become grounded near Connemara, or they are picked up by the southward drift. Therefore, only on this side of the slope is suitable to monitor BIIS variability.

#### 4.4.2 Implications for BIIS variability

After recognition and interpretation of the IRE, a tentative age model of the cores MD99-2327 and MD01-2449 was constructed, which allowed the calculation of sedimentation rates and sedimentary fluxes (Fig. 4.22). This allows discussing the variability of the BIIS in the Porcupine Seabight and compare our data with the well-studied Celtic margin (Auffret *et al.*, 2002).

The inferred MIS4 contains a relative minimum of IRD (Figs. 4.7, 4.8 and 4.9) with moderate to low fluxes (Fig. 4.22). Therefore a BIIS in a constructional stage with a period of decreasing sea level is supposed (Auffret *et al.*, 2002; Labeyrie *et al.*, 1987). The high variability record of IRD starts at about 62 ka, with the deposition of IRE6. All subsequent influx of terrigenous particles (IRD) can be attributed to a probably millennial-scaled destabilisation of the BIIS (Fig. 4.9). During MIS3, all IRE (3-6) are succeeding very closely and even grade smoothly the one into the other (4.16). This suggests that at the same time no other major sediment-supplying processes must have been active but ice-rafting, hemipelagic rain-out and limited lateral supply of bottom-current transported sediment. The slight increase of the sedimentation rates and IRD fluxes at about 45 ka (Fig. 4.22), illustrates a further expansion of European ice sheets and subsequent supply of detrital material (Auffret *et al.*, 2002). A small peak observed in the total flux values could be related with a pre-LGM deglaciation about 25 to 37 ka which was observed by Bowen *et al.* (2002).

However, with the start of MIS2, the sedimentation rates start to increase drastically (Figs. 4.9, 4.15 and 4.22). This episode of sedimentation reflects an even higher variability of the BIIS with more IRD discharges than from IRE1 and 2 only. This could very well be a record of a millennial-scaled disintegration of the BIIS.

Grousset *et al.* (2001) already mentioned rapid 1-2 ka cycles by European ice sheets in order to feed the precursor and after-events for the Heinrich Layers. Knutz *et al.* (2001) considers the high frequency of BIIS-sourced IRD peaks to contribute to the millennial-scaled pattern of iceberg discharges in the NE Atlantic. Moreover, McCabe & Clark (1998) also recognized significant BIIS oscillations during this last deglacial cycle. This also underlines again that BIIS was a long-lived feature that acted as a mobile and sensitive ice sheet (Bowen *et al.*, 2002). The Irish inland ice began a rapid advance after 30 ka with a maximum extent between 24 and 20 ka (Richter *et al.*, 2001). According to Bowen *et al.* (2002) the final retreat for the BIIS from the shelf occurred at 25 ka. The cold pulses of IRE1 and 2 also are the most pronounced in the NPS record and probably reflect very local ice-rafting events without LIS influence, whereas the previous IRE still could be under influence of the other ice sheets. Especially the, on the first sight, anomalous dates for these two events compared with Auffret *et al.* (2002) make believe these events have a much more local significance and thus more connected to the BIIS history. For this reason it is hard to compare the oxygen isotope values with GRIP data because in this study local events with a rather low global significance and spreading are dominant. However, several sources report two major shelf edge advances and BIIS collapses from 26 to 18 ka and at 15 ka (Dowling & Coxon, 2001; Knutz *et al.*, 2002a), fitting with the ages of respectively IRE2 and IRE1. Bowen *et al.* (2002) and McCabe & Clark (1998) even attributed a significant deglaciation of southern BIIS at about 17.4 ka. This could very well explain the  $\delta^{18}\text{O}$  meltwater peaks after IRE2. Moreover, Siegert & Dowdeswell (2002) estimated the main iceberg production along the western Irish margin between 15 and 22 ka with a maximum of  $20 \text{ km}^3 \cdot \text{a}^{-1}$  at 16 ka. Over 10 ka, approximately  $40000 \text{ km}^3$  of icebergs were released into the ocean. From 10 to 25 ka, Ireland had a relatively high meltwater production with peaks at about 15 ka. The rate of melting increased from  $1 \text{ km}^3 \cdot \text{a}^{-1}$  at 20 ka to  $15 \text{ km}^3 \cdot \text{a}^{-1}$  at 14 ka, when the ice sheet was modelled at less than 50 m thick. Melt values for northern margin were significantly lower, since the dominant source of meltwater was at the southern margin of the ice sheet. These modelling data also very well explain the timing and high IRD content of the two studied cores and emphasize the importance of this area.

A comparable pattern of sedimentary fluxes has been recognized in cores located to the south on Goban Spur and the Celtic margin described by Auffret *et al.* (2002). The total terrigenous flux is slightly higher compared to core MD95-2002 on Meriadzek Terrace and significantly higher compared to core NKS12 on Goban Spur. This means that the net sedimentary evolution during the last glacial period along the Irish-Celtic margin has been relatively similar, but still features several important differences. Our study area occupies the most proximal location to the source area while the ones of Auffret *et al.* (2002) are more distant. The Meriadzek Terrace core records more likely variations in supply through the channel river coming from a large NW-European drainage area, while cores MD01-2449 and MD99-2327 record direct variations of the British-Irish Ice Sheet.

## 4.5 Summary

The study of a SE to NW transect of five long cores has demonstrated the role of the BIIS variability in the Porcupine Basin. The two cores located on the eastern slope of the Porcupine Seabight almost exclusively contain BIIS-sourced material. Six ice-rafting events (IRE) were described and can be compared with the North Atlantic Heinrich Events. These regional events carry a very strong BIIS signature with mainly sands originating from Devonian and Carboniferous sandstones. Only a limited influence of Laurentide icebergs was found. Most of these IRE have been deposited during a two- or three-phased pulsation, suggesting a millennial-scaled variability of the BIIS. It also gives more evidence of BIIS-sourced ice-rafting events prior to and after HL on the European margins as described by Scourse *et al.* (2000), Grousset *et al.* (2001) and Auffret *et al.* (2002). The abundance of the IRD record shows a massive disintegration of the BIIS from 25 ka with distinct ice-rafting pulses about 17.4 and 15 ka BP. A comparison with cores on the Celtic margin and in the northern part of the Porcupine Seabight shows a decreasing importance of the BIIS-derived IRD and an increase of LIS-derived IRD when moving towards more distal position from the Irish mainland.

The three other cores located in the northern part of the Porcupine Seabight, on the other hand, do show the presence of LIS-sourced IRD. This might confirm that BIIS-sourced icebergs released along the western side of Ireland probably were transported by a southward surface current along the Irish and Celtic shelf edges (Hall & McCave, 1998a). Therefore, the position of cores MD99-2327 and MD01-2449 is ideal to study BIIS variability. They contain only a minimum of non-BIIS material due to probable grounding about the Connemara region and Goban Spur (Scourse *et al.*, 2000).

## References

- Alley, R. B. & MacAyeal, D. R. (1994) Ice-rafted debris associated with binge/purge oscillations of the Laurentide Ice Sheet. *Paleoceanography*, **9**(4), 503-511.
- Andrews, J. T., Jennings, A., Kerwin, M., Kirby, M., Manley, W., Miller, G. H., Bond, G. & MacLean, B. (1995) A Heinrich-like event, H-0 (DC-0): Source(s) for detrital carbonate in the North Atlantic during the Younger Dryas chronozone. *Paleoceanography*, **10**(5), 943-952.
- Andrews, J. T. & Tedesco, K. (1992) Detrital carbonate-rich sediments, northwestern Labrador Sea: Implications for ice-sheet dynamics and iceberg rafting (Heinrich) events in the North Atlantic. *Geology*, **20**, 1087-1090.
- Auffret, G. A., Pujol, C., Baltzer, A., Bourillet, J. F., Müller, C. & Tisot, J. P. (1996) Quaternary sedimentary regime on the Berthois Spur (Bay of Biscay). *Geo-Marine Letters*, **16**, 76-84.
- Auffret, G. A., Zaragosi, S., Dennielou, B., Cortijo, E., Van Rooij, D., Grousset, F. E., Pujol, C., Eynaud, F. & Siegert, M. (2002) Terrigenous fluxes at the Celtic margin during the last glacial cycle. *Marine Geology*, **188**, 79-108.
- Bond, G., Broecker, W. S., Johnsen, S., McManus, J., Labeyrie, L. D., Jouzel, J. & Bonani, G. (1993) Correlations between climate records from North Atlantic sediments and Greenland ice. *Nature*, **365**, 143-147.
- Bond, G., Heinrich, H., Broecker, W. S., Labeyrie, L. D., McManus, J., Andrews, J. T., Huon, S., Jantschik, R., Clasen, S., Simet, C., Tedesco, K., Klas, M., Bonani, G. & Ivy, S. (1992) Evidence for massive discharges of icebergs into the North Atlantic ocean during the last glacial period. *Nature*, **360**, 245-249.
- Bond, G. & Lotti, R. (1995) Iceberg Discharges into the North Atlantic on Millennial Time Scales During the Last Glaciation. *Science*, **267**, 1005-1010.
- Bowen, D. Q., Phillips, F. M., McCabe, A. M., Knutz, P. C. & Sykes, G. A. (2002) New data for the Last Glacial Maximum in Great Britain and Ireland. *Quaternary Science Reviews*, **21**, 89-101.
- Broecker, W. S., Bond, G., Klas, M., Clark, E. & McManus, J. (1992) Origin of the Northern Atlantic's Heinrich Events. *Climate Dynamics*, **6**, 265-273.
- Caralp, M. H., Pujol, C., Duprat, J. & Labracherie, M. (1984) Quaternary paleoceanography of the northeastern Atlantic: microfaunal and stable isotope evidence at sites 548 and 549. In: *Initial Reports of the Deep Sea Drilling Project* (Ed. by P. C. de Graciansky, C. W. Poag, R. Cunningham, P. Loubere, D. G. Masson, J. M. Mazzullo, L. Montadert, C. Müller, K. Otsuka, L. A. Reynolds, J. Sigal, S. W. Snyder, S. P. Vaos and D. Waples), U.S. Government Printing Office, Washington, **80**, 817-820.
- Chapman, M. & Maslin, M.A. (1999) Low-latitude forcing of meridional temperature and salinity gradients in the subpolar North Atlantic and the growth of glacial ice sheet. *Geology*, **27**, 875-878.
- Chapman, M. & Shackleton, N. J. (1998) Millennial-scale fluctuations in North Atlantic heat flux during the last 150,000 years. *Earth and Planetary Science Letters*, **159**, 57-70.
- Chapman, M., Shackleton, N. J. & Duplessy, J. C. (2000) Sea surface temperature variability during the last glacial-interglacial cycle: assessing the magnitude and pattern of climate change in the North Atlantic. *Palaeogeography, Palaeoclimatology, Palaeoecology*, **157**, 1-25.
- Chi, J. & Mienert, J. (1996) Linking physical property records of Quaternary sediments to Heinrich events. *Marine Geology*, **131**, 57-73.
- Cornilly, W. (2003) Paleoenvironmental study of Heinrich Layers in the Porcupine Seabight; A case study of the Magellan Mound Province. M.Sc. thesis, Marelac. *Ghent University*, Gent, 39 pp.
- Cortijo, E., Labeyrie, L. D., Vidal, L., Vautravers, M., Chapman, M., Duplessy, J. C., Elliot, M., Arnold, M., Turon, J.-L. & Auffret, G. A. (1997) Changes in sea surface hydrology associated with Heinrich event 4 in the North Atlantic Ocean between 40° and 60°N. *Earth and Planetary Science Letters*, **146**, 29-45.

- Cortijo, E., Reynaud, J.-Y., Labeyrie, L. D., Paillard, D., Lehman, B., Cremer, M. & Grousset, F. E. (1995) Etude de la variabilité climatique à haute résolution dans des sédiments de l'Atlantique Nord. *Comptes Rendus de l'Académie des Sciences Paris, Série II a*, **321**, 231-238.
- Crucifix, M. & Berger, A. (2002) Simulation of ocean-ice sheet interactions during the last deglaciation. *Paleoceanography*, **17**(4), 1054, doi:10.1029/2001PA000702.
- Dansgaard, W., Johnsen, S., Clausen, H. B., Dahl-Jensen, D., Gunderstrup, N. S., Hammer, C. U., Hvidberg, C. S., Steffensen, J. P., Sveinbjörnsdottir, A. E., Jouzel, J. & Bond, G. (1993) Evidence for general instability of past climate from a 250-kyr ice-core record. *Nature*, **364**, 218-220.
- Dowdeswell, J. A., Maslin, M. A., Andrews, J. T. & McCave, I. N. (1995) Iceberg production, debris rafting, and the extent and thickness of Heinrich layers (H-1, H-2) in North Atlantic sediments. *Geology*, **23**(4), 301-304.
- Dowling, L. A. & Coxon, P. (2001) Current understanding of Pleistocene temperate stages in Ireland. *Quaternary Science Reviews*, **20**, 1631-1642.
- Elliot, M., Labeyrie, L., Dokken, T. & Manthé, S. (2001) Coherent patterns of ice-rafted debris deposits in the Nordic regions during the last glacial (10-60 ka). *Earth and Planetary Science Letters*, **194**, 151-163.
- Elliot, M., Labeyrie, L. D., Bond, G., Cortijo, E., Turon, J.-L., Tisnerat, N. & Duplessy, J. C. (1998) Millennial-scale iceberg discharges in the Irminger Basin during the last glacial period: Relationship with the Heinrich events and environmental settings. *Paleoceanography*, **13**(5), 433-446.
- Foubert, A. (2002) Een paleomagnetische studie met zeer hoge resolutie op Calypso-kernen in Porcupine Seabight, ten zuidwesten van Ierland. M.Sc. thesis, Department of Geology and Soil Science. *Ghent University, Gent*, 151 pp.
- Games, K. P. (2001) Evidence of shallow gas above the Connemara oil accumulation, Block 26/28, Porcupine Basin. In: *The Petroleum Exploration of Ireland's Offshore Basins* (Ed. by P. M. Shannon, P. Haughton and D. Corcoran), Geological Society, London, Special Publication, **188**, 361-373.
- Grimm, E. C., Jacobson, G. L., Watts, W. A., Hansen, B. C. S. & Maasch, K. A. (1993) A 50,000-Year Record of Climate Oscillations from Florida and Its Temporal Correlation with the Heinrich Events. *Science*, **261**, 198-200.
- Grousset, F. E., Biscaye, P. E., Zindler, A., Prospero, J. & Chester, R. (1988) Neodymium isotopes as tracers in marine sediments and aerosols: North Atlantic. *Earth and Planetary Science Letters*, **87**, 367-378.
- Grousset, F. E., Cortijo, E., Huon, S., Hervé, L., Richter, T. O., Burdloff, D., Duprat, J. & Weber, O. (2001) Zooming in in Heinrich layers. *Paleoceanography*, **16**(3), 240-259.
- Grousset, F. E., Labeyrie, L. D., Sinko, J. A., Cremer, M., Bond, G., Duprat, J., Cortijo, E. & Huon, S. (1993) Pattern of ice-rafted detritus in the glacial North Atlantic. *Paleoceanography*, **8**(2), 175-192.
- Grousset, F. E., Pujol, C., Auffret, G. A. & Boelaert, A. (1999) Did the North Atlantic Heinrich Events begin first in Europe? In: *European Union of Geosciences* (Ed. by N. Koç). EUG, Strasbourg.
- Grousset, F. E., Pujol, C., Labeyrie, L. D., Auffret, G. A. & Boelaert, A. (2000) Were the North Atlantic Heinrich events triggered by the behavior of the European ice sheets? *Geology*, **28**(2), 123-126.
- Gwiazda, R. H., Hemming, S. R. & Broecker, W. S. (1996a) Provenance of icebergs during Heinrich event 3 and the contrast to their sources during other Heinrich episodes. *Paleoceanography*, **11**(4), 371-378.
- Gwiazda, R. H., Hemming, S. R. & Broecker, W. S. (1996b) Tracking the sources of icebergs with lead isotopes: The provenance of ice-rafted debris in Heinrich layer 2. *Paleoceanography*, **11**(1), 77-93.

- Hall, I. R. & McCave, I. N. (1998a) Glacial-interglacial variation in organic carbon burial on the slope of the N.W. European Continental Margin. *Progress in Oceanography*, **42**, 37-60.
- Hall, I. R. & McCave, I. N. (1998b) Late Glacial to Recent accumulation fluxes of sediments at the shelf edge and slope of NW Europe, 48-50°N. In: *Geological Processes on Continental Margins: Sedimentation, Mass-Wasting and Stability* (Ed. by M. S. Stoker, C. D. R. Evans and A. Cramp), Geological Society, London, Special Publication, **129**, 339-350.
- Heinrich, H. (1988) Origin and Consequences of Cyclic Ice Rafting in the Northeast Atlantic Ocean during the Past 130,000 Years. *Quaternary Research*, **29**, 142-152.
- Hemming, S. R., Broecker, W. S., Sharp, W. D., Bond, G., Gwiazda, R. H., McManus, J., Klas, M. & Hadjas, I. (1998) Provenance of Heinrich layers in core V28-82, northeastern Atlantic:  $^{40}\text{Ar}/^{39}\text{Ar}$  ages of ice-rafted hornblende, Pb isotopes in feldspar grains, and Nd-Sr-Pb isotopes in the fine sediment fraction. *Earth and Planetary Science Letters*, **164**, 317-333.
- Holland, C. H. (2001) *The Geology of Ireland*. Dunedin Academic Press Ltd., Edinburgh, 531 pp.
- Huvenne, V. A. I. (2003) Spatial geophysical analysis of the Magellan carbonate build-ups and the interaction with sedimentary processes: key to a genetic interpretation? Ph.D. thesis, Department of Geology and Soil Science. *Ghent University*, Gent, 285 pp.
- Kassens, H. & Sarnthein, M. (1989) A link between paleoceanography, early diagenetic cementation, and shear strength maxima in late Quaternary deep-sea sediment? *Paleoceanography*, **12**, 253-269.
- Knight, J. (2000) Geology, glaciation and the development of landscape 'character' in Ireland. *Geology Today*, **16**(4), 148-153.
- Knutz, P. C., Austin, W. E. N. & Jones, E. J. W. (2001) Millennial-scaled depositional cycles related to British Ice Sheet variability and North Atlantic paleocirculation since 45 kyr B.P., Barra Fan, U.K. margin. *Paleoceanography*, **16**(1), 53-64.
- Knutz, P. C., Hall, I. R., Zahn, R., Rasmussen, T., Kuijpers, A., Moros, M. & Shackleton, N. J. (2002a) Multidecadal ocean variability and NW European ice sheet surges during the last deglaciation. *Geochemistry Geophysics Geosystems*, **3**(12), 1077, doi:10.1029/2002GC000351.
- Knutz, P. C., Jones, E. J. W., Austin, W. E. N. & van Weering, T. C. E. (2002b) Glacimarine slope sedimentation, contourite drifts and bottom current pathways on the Barra Fan, UK North Atlantic margin. *Marine Geology*, **188**, 129-146.
- Labeyrie, L. D., Duplessy, J. C. & Blanc, P. L. (1987) Variations in mode of formation and temperature of oceanic deep waters over the past 125,000 years. *Nature*, **327**, 477-482.
- MacAyeal, D. R. (1993a) Binge/purge oscillations of the Laurentide Ice Sheet as a cause of the North Atlantic's Heinrich Events. *Paleoceanography*, **8**(6), 775-784.
- MacAyeal, D. R. (1993b) A low-order model of the Heinrich Event cycle. *Paleoceanography*, **8**(6), 767-773.
- Martinson, D. G., Pisias, N. G., Hays, J. D., Imbrie, J., Moore, T. C. & Shackleton, N. J. (1987) Age dating and the Orbital Theory of the Ice Ages: Development of a High-Resolution 0 to 300,000-Year Chronostratigraphy. *Quaternary Research*, **27**, 1-29.
- Mathys, M. (2001) Hoge-resolutie geofysische studie van gasmigratie in oppervlakkige mariene sedimenten ter hoogte van olie- en gasreservoirs, Porcupine Bekken (SW Ierland). M.Sc. thesis, Department of Geology and Soil Science. *Ghent University*, Gent, 157 pp.
- McCabe, A. M. & Clark, P. U. (1998) Ice-sheet variability around the North Atlantic Ocean during the last deglaciation. *Nature*, **392**, 373-377.
- McCabe, A. M., Knight, J. & McCarron, S. (1998) Evidence for Heinrich event 1 in the British Isles. *Journal of Quaternary Science*, **13**(6), 549-568.
- Moros, M., Endler, R., Lackschewitz, K. S., Wallrabe-Adams, H.-J., Mienert, J. & Lemke, W. (1997) Physical properties of Reykjanes Ridge sediments and their linkage to high-resolution Greenland Ice Sheet Project 2 ice core data. *Paleoceanography*, **12**, 687-695.

- Moros, M., Kuijpers, A., Snowball, I., Lassen, S., Bäckström, D., Gingele, F. & McManus, J. (2002) Were glacial iceberg surges in the North Atlantic triggered by climatic warming? *Marine Geology*, **192**, 393-417.
- Müller, C. (1984) Biostratigraphic and paleoenvironmental interpretation of the Goban Spur region based on a study of calcareous nannoplankton. In: *Initial Reports of the Deep Sea Drilling Project* (Ed. by P. C. de Graciansky, C. W. Poag, R. Cunningham, P. Loubere, D. G. Masson, J. M. Mazzullo, L. Montadert, C. Müller, K. Otsuka, L. A. Reynolds, J. Sigal, S. W. Snyder, S. P. Vaos and D. Waples), U.S. Government Printing Office, Washington, **80**, 573-597.
- Oerlemans, J. (1993) Evaluating the role of climate cooling in iceberg production and the Heinrich events. *Nature*, **364**, 783-785.
- Pastouret, L., Auffret, G. A., Hoffert, M., Melguen, M., Needham, H. D. & Latouche, C. (1975) Sédimentation sur la Ride de Terre-Neuve. *Canadian Journal of Earth Sciences*, **12**, 1019-1035.
- Porter, S. C. & Zhisheng, A. (1995) Correlation between climate events in the North Atlantic and China during the last glaciation. *Nature*, **375**, 305-308.
- Rahman, A. (1995) Reworked nannofossils in the North Atlantic Ocean and subpolar basins: Implications for Heinrich events and ocean circulation. *Geology*, **23**(6), 487-490.
- Rasmussen, T., Oppo, D., Thomsen, E. & Lehman, S. J. (2003) Deep sea records from the southeast Labrador Sea: Ocean circulation changes and ice-rafting events during the last 160,000 years. *Paleoceanography*, **18**(1), 1018, doi: 10.1029/2001PA000736.
- Revel, M., Sinko, J. A. & Grousset, F. E. (1996) Sr and Nd isotopes as tracers of North Atlantic lithic particles: Plaeoclimatic implications. *Paleoceanography*, **11**(1), 95-113.
- Richter, T. O., Lassen, S., van Weering, T. C. E. & de Haas, H. (2001) Magnetic susceptibility patterns and provenance of ice-rafted material at Feni Drift, Rockall Trough: implications for the history of the British-Irish ice sheet. *Marine Geology*, **173**, 37-54.
- Robinson, S. G., Maslin, M. A. & McCave, I. N. (1995) Magnetic susceptibility variations in Upper Pleistocene deep-sea sediments of the NE Atlantic: Implications for ice rafting and paleocirculation at the last glacial maximum. *Paleoceanography*, **10**(2), 221-250.
- Ruddiman, W. F. (1977) Late Quaternary deposition of ice-rafted sand in the subpolar North Atlantic (lat 40° to 65°N). *Geological Society of America Bulletin*, **88**, 1813-1827.
- Scourse, J. D., Hall, I. R., McCave, I. N., Young, J. R. & Sugdon, C. (2000) The origin of Heinrich layers: evidence from H2 for European precursor events. *Earth and Planetary Science Letters*, **182**, 187-195.
- Seidov, D. & Maslin, M. A. (1999) North Atlantic deep water circulation collapse during Heinrich events. *Geology*, **27**(1), 23-26.
- Siegert, M. (2001) *Ice Sheets and Late Quaternary Environmental Change*. Wiley, Chichester, 231 pp.
- Siegert, M. & Dowdeswell, J. A. (2002) Late Weichselian iceberg, surface-melt and sediment production from the Eurasian Ice Sheet: results from numerical ice-sheet modelling. *Marine Geology*, **188**, 109-127.
- Skinner, L. C. & McCave, I. N. (2003) Analysis and modelling of gravity- and piston coring based on soil mechanics. *Marine Geology*, **199**, 181-204.
- Smythe, F. W., Ruddiman, W. F. & Lumsden, D. N. (1985) Ice-rafted evidence of long-term North Atlantic circulation. *Marine Geology*, **64**, 131-141.
- Snoeckx, H., Grousset, F. E., Revel, M. & Boelaert, A. (1999) European contribution of ice-rafted sand to Heinrich layers H3 and H4. *Marine Geology*, **158**, 197-208.
- Thouveny, N., de Beaulieu, J.-L., Bonifay, E., Creer, K. M., Guiot, J., Icole, M., Johnsen, S., Jouzel, J., Reille, M., Williams, T. & Williamson, D. (1994) Climate variations in Europe over the past 140 kyr deduced from rock magnetism. *Nature*, **371**, 503-506.

- van Krevelend, S. A., Knappertsbusch, M., Ottens, J., Ganssen, G. M. & van Hinte, J. E. (1996) Biogenic carbonate and ice-rafted debris (Heinrich layer) accumulation in deep-sea sediments from a Northeast Atlantic piston core. *Marine Geology*, **131**, 21-46.
- Van Rooij, D. (1999) Lithologie des délestages glaciaires (niveaux de Heinrich) de l'Eperon de Goban (Atlantique Nord-Est). D.E.A. thesis, Université de Bretagne Occidentale. *Université de Bretagne Occidentale*, Brest, 57 pp.
- Van Rooij, D., Blamart, D. & Unnithan, V. (2001) Cruise Report MD123-Géosciences: Leg 2, part GEOMOUND. RCMG, Gent.
- Vidal, L., Labeyrie, L. D., Cortijo, E., Arnold, M., Duplessy, J. C., Michel, E., Becqué, S. & van Weering, T. C. E. (1997) Evidence for changes in the North Atlantic Deep Water linked to meltwater surges during the Heinrich events. *Earth and Planetary Science Letters*, **146**, 13-27.
- Zaragosi, S., Eynaud, F., Pujol, C., Auffret, G. A., Turon, J.-L. & Garlan, T. (2001) Initiation of the European deglaciation as recorded in the northwestern Bay of Biscay slope environments (Meriadzek Terrace and Trevelyan Escarpment): a multi-proxy approach. *Earth and Planetary Science Letters*, **188**, 493-507.



## Chapter V: A stratigraphic framework for the eastern Porcupine Seabight

### 5.1 Rationale

Although this study can rely on a large dataset of high-quality seismic data, there is no sufficient age control of the Neogene to Quaternary series within the Porcupine Basin. Only few boreholes are present, but they are unfortunately located on the upper shelf slope along the northern margin and only offer data for the Mesozoic and Paleozoic series (McDonnell & Shannon, 2001). It has already been reported that the coral banks in the Porcupine Seabight are related with several unconformities (De Mol *et al.*, 2002; Huvenne *et al.*, 2003), of which the timing and nature could yield vital information on the insight of the initial coral settling and mound development. A better age control of the observed unconformities can also enable the comparison of the local responsible hydrodynamic environments with the governing (pale)oceanographic events on a larger (world-wide) scale.

A first approach towards the definition of a Neogene stratigraphic framework for the entire Porcupine Basin was undertaken by McDonnell & Shannon (2001), describing four major Tertiary correlation surfaces, recognized in the Rockall and Porcupine Basins, in accordance with the Neogene chronostratigraphy defined by Stoker *et al.* (2001) for the Rockall Trough and the Faroe-Shetland Channel. These correlation surfaces are a Paleocene regional unconformity (C40), a latest Eocene to Early Oligocene unconformity surface (C30), an early Middle Miocene marker (C20) and an Early Pliocene unconformity (C10). However, McDonnell & Shannon (2001) recognize that due to the lack of significant Neogene age constraints in the Porcupine Basin, a detailed inter-basin correlation is extremely speculative. Only the C20 event is considered to have chronostratigraphic significance in both basins.

Moreover, it is observed by McDonnell (2001) that the closer to the margin, the majority of unconformities are converging or onlapping on each other, making it extremely difficult to distinguish unconformities on higher resolution profiles. Especially the age and nature of the Early Pliocene C10 reflector, which is located at the mound base, provides the highest controversy and has already been debated by De Mol *et al.* (2002), Van Rooij *et al.* (2003) and Huvenne *et al.* (2003). Huvenne *et al.* (2003) for example, reported a near base Quaternary age for the Magellan mound base reflector, which was based on nearby surveys and wells.

According to Pearson & Jenkins (1986), local circulation can have a significant effect on Cenozoic stratigraphic sequences. It can be suspected that the particular location of the Porcupine Seabight along the NW European margin, as well as its proximity to the Irish mainland, might have influenced local circulation patterns and deep-marine erosion events. The most nearby available source for the recognition of such events is located on Goban Spur. In 1981, a transect of four IPOD-DSDP holes were drilled, with exactly the intention “to document the age and nature of significant post-rift chronostratigraphic boundaries and prominent seismic unconformities and assess their relationships to basin subsidence, global sea-level changes and tectonism” and “to analyse the effects of changing paleoceanographic

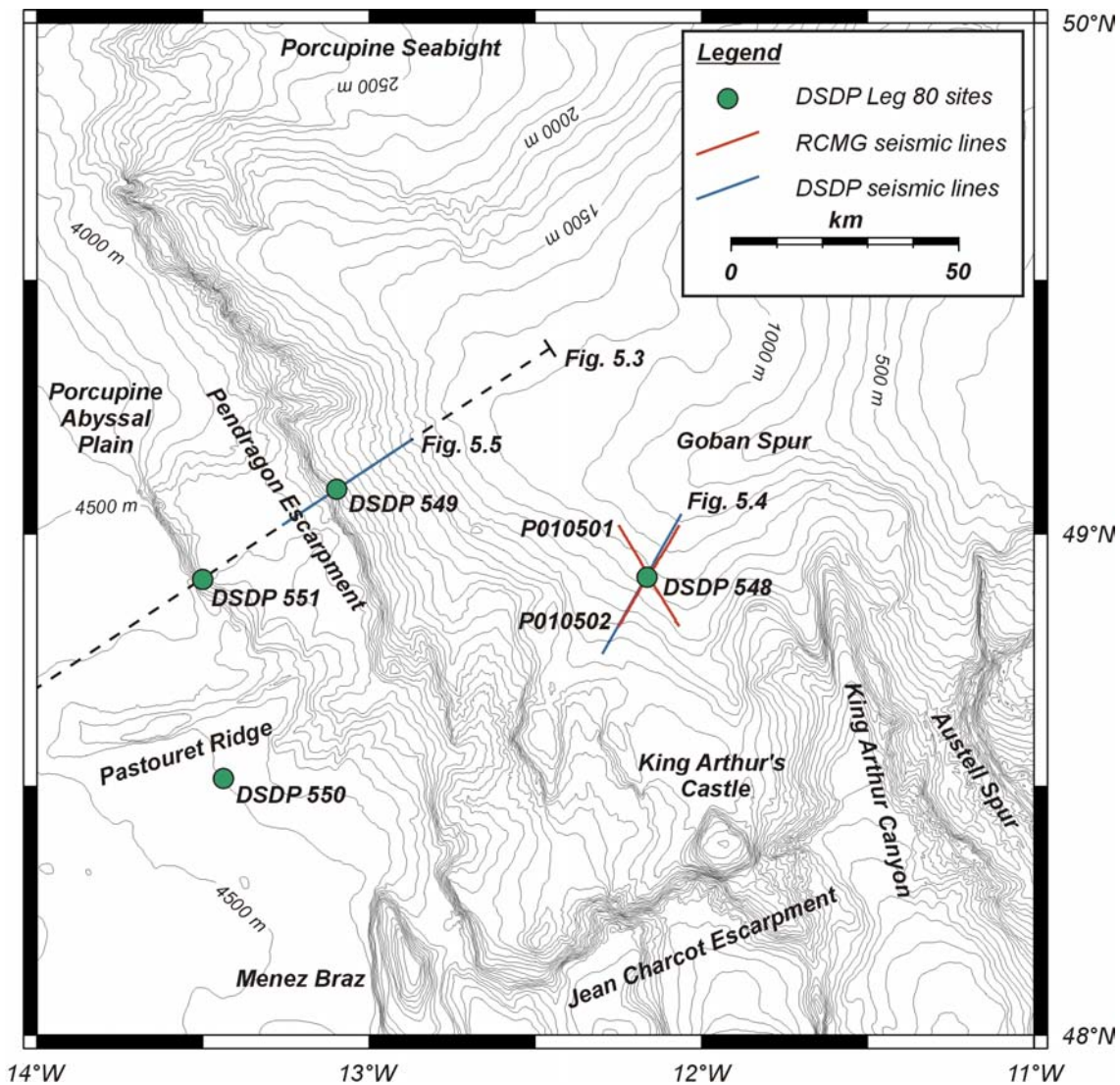


**Figure 5.1:** Morphological elements of the Goban Spur margin with the location of the DSDP Leg 80 sites and the RCMG very high-resolution seismic profiles, after de Graciansky & Poag (1984).

conditions, paleodepths, paleoclimates, rates of subsidence...” (de Graciansky *et al.*, 1985). de Graciansky *et al.* (1984a) and Masson *et al.* (1984) recognized four Cenozoic unconformities in Site 548, which could be precisely correlated with four of the largest Tertiary sea-level drops postulated by Vail & Hardenbol (1979).

In order to obtain a best possible insight in the Late Cenozoic stratigraphic framework of the Porcupine Seabight, DSDP site 548 was used as a “calibration” and was investigated with two perpendicular, very high-resolution single-channel seismic profiles (sparker), crossing on site 548 (Fig. 5.1). The observed unconformities on the seismic profiles were correlated with lithologic units and hiatuses observed in site 548. On its turn, the Goban Spur stratigraphy will be discussed and compared with the present, larger-scale chronostratigraphic knowledge of this part of the margin. The obtained stratigraphy will be used as a tool to provide a tentative age to unconformities observed in the seismic profiles, which will be discussed in the following chapter.

## 5.2 Brief geological overview of Goban Spur

Goban Spur is a marginal submarine plateau, situated 250 km SW of Ireland. It separates the northwest trending Celtic margin from the north-trending Porcupine Basin. The Goban Spur bathymetry gently descends southwest down to 2500 m, where it is sharply truncated by the Pendragon Escarpment (Fig. 5.1). 35 km west of Pendragon, there is a second, smaller and unnamed escarpment at a water depth of about 4400 m. It forms the eastern boundary of the Porcupine Abyssal Plain. The northern and southern flanks of Goban Spur are asymmetrical. The southern flank is characterized by the presence of submarine canyons and the long and steep Jean Charcot fault-scarp, deeply incised by the Whittard and King Arthur canyons. Its northern flank is a smooth gentle slope leading down into the PSB (Naylor & Shannon, 1982; de Graciansky & Poag, 1984; Masson *et al.*, 1984).

The hydrography of Goban Spur is relatively complex. Four main water masses can be distinguished. Below the seasonal variable thermocline the ENAW is observed at about 300 m. It is characterized by an elevated temperature and

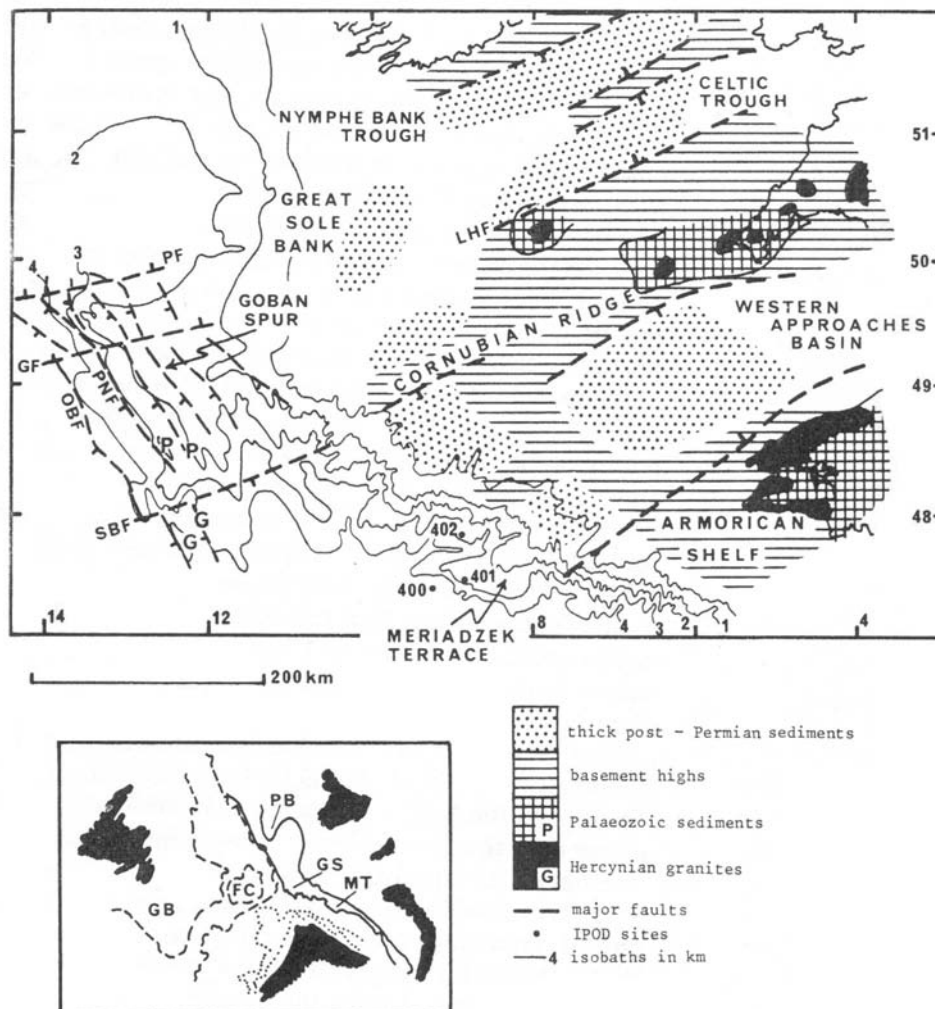


**Figure 5.2:** Regional tectonic setting of Goban Spur (bathymetry in kilometres). LHF, Lundy/Haig Frasn Fault; PF, Porcupine Fault; GF, Goban Fault; PNF, Pendragon Fault; OBF, Outer Boundary Fault; SBF, Southern Boundary Fault. The inserted map shows a pre-drift reconstruction. GB, Grand Banks; FC, Flemish Cap; PB, Porcupine Bank; GS, Goban Spur; MT, Meriadzek Terrace (Dingle & Scrutton, 1979).

salinity. The temperature gradually decreases at about 800 m, reaching together with the salinity more elevated values than the overlying water masses, which indicates the presence of MOW. From 1200 to 3500 m, NADW is observed including about 5% of the silica rich Antarctic Bottom Water. Below, a core of LDW is found (Caralp, 1984; van Weering *et al.*, 1998).

Most authors consider Goban Spur as a classic example of a sediment starved passive continental margin (Dingle & Scrutton, 1979; Hall & McCave, 1998; Masson *et al.*, 1984; Naylor & Shannon, 1982). The relatively thin sedimentary cover is a consequence of the presence of Variscan granites which have kept this part of the margin afloat. This has exposed this region to heavy submarine erosion and therefore there is a high probability it contains a record of most of the Cenozoic erosion events. According to Evans (1990) and Naylor & Shannon (1982) it appears to be the southwestward extension of the Cornubian Massive, separating the Celtic Sea Basin from the Western Approaches Basin on the adjacent European shelf (Fig. 5.2).

The general structure of the Goban Spur basement is composed of a series of horsts, grabens and tilted fault blocks formed during the Mesozoic rifting (Figs. 5.2 and 5.3). These are metamorphic Paleozoic sediments with granitic intrusions (Dingle & Scrutton, 1979). During the start of the North Atlantic rifting in the Upper Jurassic, Goban Spur was located at the NW extremity of the Biscay system, which was a part of a triple junction together with the North and South Atlantic systems (Fig. 5.2). Subsequent rifting separated Goban Spur from Flemish Cap and Orphan Knoll (Dingle & Scrutton, 1979; Masson & Miles, 1986; Naylor & Shannon, 1982). The basement structure is controlled by three main fault orientations. A probable Variscan ENE-WSW orientation can be observed in the two most important faults. The Porcupine Fault north of Goban Spur is considered as the boundary with the Porcupine Basin, while the abyssal plain and the continental platform of the Celtic Sea are separated from Goban Spur by the Southern Boundary Fault. The most important fault orientation, however, is a NW-SE one. Most of the horsts and grabens are aligned along this direction, as well the Pendragon Fault as the Outer Boundary Fault. The latter can be considered as the ocean-continent transition. The third, NE-SW orientation is believed to be the eldest direction, being the reactivation of a Caledonian structure during the Triassic, however it is rarely observed. After rifting these faults are not believed having been active (Dingle & Scrutton, 1979; Shannon, 1991).

In analogy to the Porcupine Basin, the post-rift evolution of Goban Spur has been mainly subject to thermal subsidence. Masson *et al.* (1984) subdivided the Mesozoic-Cenozoic sedimentary cover, which is completely controlled by the basement structures, into three seismostratigraphic sequences. The upper two sequences are draped over the basement and the lower sedimentary unit topography and are characterized by parallel or subparallel reflecting horizons. They have not been affected by any major tectonic events. In contrast, the lower syn-rift sequence (Upper Hauterivian to Upper Barremian) occurs in discrete wedge-shaped fault-bounded basins. It is characterized by a series of moderate to strong, divergent reflecting horizons. Syn-depositional faulting is common, which might result in an almost chaotic appearance. Two types of mound-like buildups are interpreted as reefs and volcanic bodies. This sequence is separated from the overlying one by a discontinuity. The second, central sequence shows an extremely variable seismic

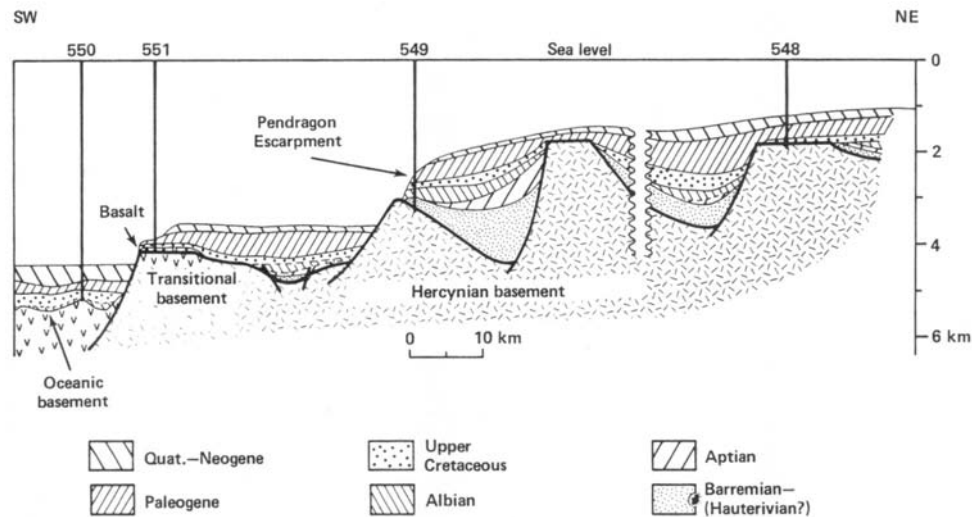


**Figure 5.3:** Schematic geologic section across Goban Spur showing the sites drilled during DSDP Leg 80. This section is approximately coincident with multichannel seismic line CM10 (Figs. 5.1 and 5.5). Sites 548 and 550 are projected northwestward to the line of section, whereas sites 549 and 551 are on the line (de Graciansky & Poag, 1984).

facies and thickness (from 0 to 1000 m). These are Lower Albian to Lower Eocene sediments, containing several discontinuities and condensed sections. The style of deposition clearly separates sequence 2 from the underlying sequence 3. The youngest sequence contains sediments from a Middle Eocene to recent age. The thickness of this sequence is rather uniform, except on the tips of the tilted fault blocks, where the sedimentary cover is less thick. Masson *et al.* (1984) describe weak layering in the upper part and discontinuous to chaotic reflections in its lower part. Most of the time, it overlies the central sequence unconformably with channels, truncations and downlapping reflectors, suggesting a period of erosion.

The most recent sediments on Goban Spur have been studied intensively by Hall & McCave (1998), van Weering *et al.* (1998), Van Rooij (1999) and Auffret *et al.* (2002). Most of the Quaternary sedimentation is a hemipelagic one with a clear influence of Heinrich Layers. A study of a SE-NW transect of 12 cores within water depths between 1000 and 4500 m clearly demonstrated a decrease in sedimentation rates towards the Pendragon Escarpment and a strong morphological control on the thickness and nature of the deposits (Van Rooij, 1999). Cores located near the margins of escarpments and in deeper parts of the basin contained turbidites and were readily influenced by bottom currents. A lithological study of the Heinrich events identified in these cores also strongly suggests the contribution of European IRD, constituting a multiple-layered Heinrich Layer. This signal was confirmed by Auffret *et al.* (2002) who recognized similar signals along the entire Celtic margin.

### 5.3 DSDP leg 80

The Goban Spur transect was performed in 1981 during DSDP Leg 80 with D/V *Glomar Challenger*. The primary objective of this leg was to obtain a complete record of the depositional and structural history of a sediment-starved continental margin in the northeast Atlantic. The most complete Cenozoic sedimentary record was observed in sites 548 and 549 (de Graciansky & Poag, 1984). Already the seismic profiles along the sites (Figs. 5.3, 5.4 and 5.5) explain why site 548 is more favourable for a calibration site for our study, compared to site 549. First of all, because of its shallow location, it is more comparable to the Porcupine Basin environment. Moreover, site 549 is already considered to be too deep to be affected by Quaternary climatic fluctuations. Site 548 also seems to contain the most complete and thickest Cenozoic section, while site 549, which is located at the tip of a tilted fault block, seems to have a more condensed Neogene to Quaternary section. Therefore, only the stratigraphy of site 548 will be discussed more extensively.

#### 5.3.1. Site 548

The chief objectives of this site were to determine the nature, age and subsidence history of the basement and the nature, age and paleoenvironments of the post-rift sediments. It was drilled near the seaward edge of a tilted block of Hercynian basement at about 1256 m of water depth. At the maximum penetration depth of 551.5 m below the sea floor, Middle to Late Devonian rocks have been recovered. A total of 8 units were described (de Graciansky *et al.*, 1984a).

The site profile, featured in figure 5.4, clearly shows three distinctive sequences. The youngest sequence has a thickness of approximately 300 ms TWT and has an inferred Neogene to Quaternary age. It is underlain by a relatively thinner sequence of Paleogene age, unconformably overlying the basement. Basinward of the drill site, the upper boundary of the Paleogene sequence is characterised by a set of two sigmoidal features, which seem to have a slight morphologic effect on the overlying strata. An erosive event, described by de Graciansky *et al.* (1985) as a channel, seems to be lying at their base.

##### 5.3.1.1 Unit 1

This youngest unit is found from 0 to 72 m and has been given an early Middle Pleistocene to Holocene age. The recovered sediments are bathyal oozes with evidence of a rapid input of terrigenous detritus. Müller (1984) observed common reworked Cretaceous and Paleogene nannoplankton and detrital material within glacial deposits. Moreover, a pronounced alternation between layers rich and poor in nannoplankton is observed within the Upper Pleistocene, although a similar but weaker signal is present throughout the entire Pleistocene section and even within the Upper Pliocene. Caralp (1984) on the other hand, recognized within the upper part of the Quaternary the presence of quartz sands which are not associated with displaced microfauna. They contain very few benthic foraminifers but many polar planktonic foraminifers, suggesting an ice-rafted origin. This alternation of glacial and interglacial sediments and fossil assemblages provides an excellent record of Quaternary paleoclimates. Two subunits can be distinguished, based on carbonate content, sedimentary structures and gamma ray intensity data.

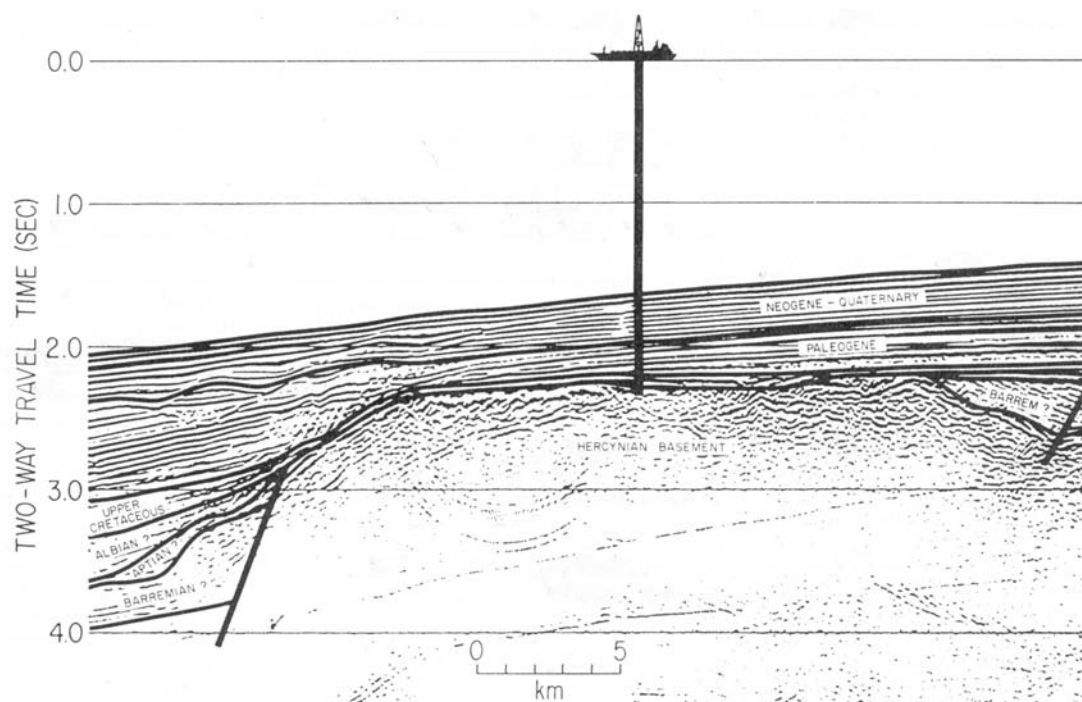


**Figure 5.4:** Geologic interpretation of seismic profile OC202 crossing site 548, located on figure 5.1. Note the sigmoidal reflector configuration near the Neogene lower boundary (de Graciansky *et al.*, 1985).

Subunit 1a (0 to 59.9 m) contains muds with rare nannofossils, foraminifers and low carbonate values. These sediments are intensively bioturbated and occasionally have a large IRD content. Gradual alternations between marly oozes and calcareous muds reflect sea level fluctuations due to glacial advances and retreats. Occasionally, graded muds were observed and interpreted as turbidite deposits.

An abrupt erosional contact separates subunit 1a from subunit 1b (59.9 to 72 m). It contains a marked increase in calcium carbonate and a decrease in terrigenous debris (de Graciansky *et al.*, 1984a).

### 5.3.1.2 Unit 2

This relatively thin unit is predominantly composed of bathyal clays and oozes of Late Pliocene to Early Pleistocene age between 72 to 108.5 m. It is a complex interbedded sequence of nannofossil and foraminiferal-nannofossil oozes. Compared with Unit 1, it is generally coarser and contains more graded layers (de Graciansky *et al.*, 1984a).

### 5.3.1.3 Unit 3

Between 108.5 and 304.75 m, the Late Miocene to Late Pliocene is represented by light greenish grey nannofossil oozes. From the Upper Miocene through the Lower Pliocene, turbiditic silty muds are observed. At about 210 m a pronounced peak in gamma ray, calliper, resistivity, density, neutron and sonic velocity logs mark the boundary between the Pliocene and the Miocene. This unit lies unconformably above unit 4, separated by a 6 Ma hiatus (de Graciansky *et al.*, 1984a).

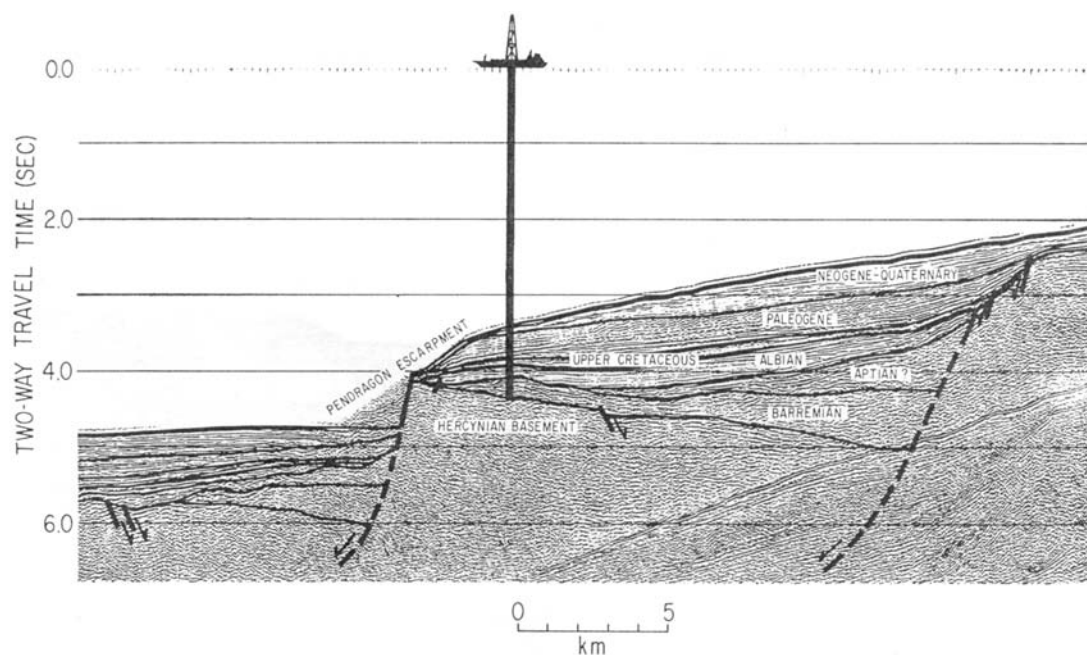


**Figure 5.5:** Geologic interpretation of seismic profile CM10 crossing site 549, located on figure 5.1. The Neogene-Quaternary sequence is seriously reduced in this location (de Graciansky *et al.*, 1985).

#### 5.3.1.4 Unit 4

The Middle Eocene through early Middle Miocene sediments of unit 4 are found in water depths from 304.75 to 412.6 m. It contains outer sub-littoral to upper bathyal light greenish grey foraminifer and nannofossil chalks with glauconite. In the lowest third of this unit, observed cherts imply a diagenetic alteration. A significant Middle Oligocene 4 Ma hiatus separates this unit into two subunits 4a and 4b. This unconformity is correlated with the dramatic erosional event observed within the seismic profiles of figure 5.4, cutting a deep channel into Lower Oligocene and Upper Eocene strata. Another unconformity from about 1.5 Ma separates Unit 4 from the Lower Eocene Unit 5 (de Graciansky *et al.*, 1984a; de Graciansky *et al.*, 1985).

#### 5.3.1.5 Unit 5

The Lower Eocene sediments (412.6 to 469.9 m) are characterised by a brownish and greenish grey marly nannofossil chalk. At the base of this unit, a Lower Paleocene 10 Ma hiatus is observed. These sediments have an outer littoral to upper bathyal nature (de Graciansky *et al.*, 1984a).

#### 5.3.1.6 Units 6, 7 and 8

These three units represent sediments of Paleozoic to Mesozoic age. Unit 6 (469.9 to 530 m) is composed of outer sub-littoral to upper bathyal white foraminifer to nannofossil chalk from Late Campanian through Danian age. The base of this unit is an unconformity of unknown duration. Unit 7 (530 to 535.5 m) is a sideritic, pyritic hardground formed in a marine sedimentary environment. The lowest unit is present from 535.5 to 551.5 m and contains light metamorphic feldspathic quartzitic sandstones of Middle Devonian age (de Graciansky *et al.*, 1984a).

### 5.3.2 Site 549

Site 549 is located at 2515 m water depth above the seaward tip of a tilted basement high on the crest of Pendragon Escarpment. 1005.5 m of sediment was recovered with a thin unit (27 m) of Pleistocene to Holocene sediments. A large hiatus of 3 Ma lies at the base of this unit, with lowest Pleistocene and Pliocene sediments lacking. The alternation between cooler and warmer paleoclimates is clearly visible as major changes in fossil assemblages, depositional style and sediment source. Also in this site Caralp (1984) identified several ice-rafted quartz sand levels with few benthic foraminifers and only polar planktonic forams. The other Cenozoic units are a very condensed Miocene unit, deposited on an Upper Paleocene to Lower Eocene unit with brown and grey nannofossil chalks. The main unconformities are Early Eocene, Middle Oligocene (4-5 Ma), uppermost Oligocene to Early Miocene (5 Ma), Middle to Late Miocene (5 Ma) and the entire Pliocene and Early Pleistocene (3.5 Ma) (de Graciansky & Poag, 1984; de Graciansky *et al.*, 1984b).

### 5.3.3 Sites 550 and 551

Site 550 is located 10 km southwest of the seaward edge of Goban Spur at 4432 m water depth. It predominantly yielded volcanic material. The upper, Cenozoic section contained argillaceous foraminiferal and nannofossil chalks deposited in an abyssal environment. The principal unconformities are of Late Paleocene, Middle Eocene to Oligocene, Early to Middle Miocene and Middle to Late Miocene age (de Graciansky & Poag, 1984).

Finally, site 551 is located at the seaward site of Goban Spur at 3909 m water depth. It is located over a raised basement block in order to identify the composition and age of the basement. The recovery of the post-Eocene sediments was not sufficient (de Graciansky *et al.*, 1984c).

## 5.4 Seismic stratigraphic control of DSDP site 548

In order to make a most effective comparison between the units described by de Graciansky *et al.* (1984a) in site 548 and the high-resolution seismic stratigraphy in the Porcupine Basin, two crossing sparker profiles have been acquired with each an approximate length of 25 km and centred on the drill site. Line P010502 also coincides with DSDP line OC202 (Fig. 5.4). Due to an acoustic penetration of minimal 400 ms TWT, it was possible to distinguish 5 major units. Although de Graciansky *et al.* (1984a) reported only one real unconformity within this depth range in the cores and on the available seismic line, this study clearly revealed the presence of several unconformities.

### 5.4.1 The sea floor

In general, the sea floor is relatively flat and shows a gentle dip of 1.5° towards the south. The sea floor on profile P010501 has a very gentle slope of 0.5° with smooth depressions. The first, upslope part of profile P010502 approaches a slope of 1° that increases from about shotpoint 1700 to a slope of 1.5°. On this steeper part, a set of 3 consequently following clinoforms with variable wavelengths (from 1 to 2 km) and amplitudes between 30 to 40 ms TWT (25 to 30 m) have been observed.

### 5.4.2 Unit G1

This unit can be subdivided into 2 subunits. Unit **G1a** is observed everywhere and features in both profiles a rhythmic succession of continuous, high to medium amplitude reflections. They drape conformably various basal morphological features (e.g. the channels in figure 5.6) and reflect a steady hemipelagic sedimentation environment. Within the clinoform features observed in profile P010502, there is no evidence of any particular form of up- or downslope migration (Figs. 5.7 and 5.8). The average thickness of this youngest unit is about 60 ms TWT (approximately 54 m, calculated at a sound velocity of 1800 m.s<sup>-1</sup>).

The lower boundary of unit G1a is characterized by a set of three parallel, medium amplitude reflections. On several locations, this boundary cuts into underlying units, appearing on P010501 as channel-like structures with a very flat floor. In these depressions, unit **G1b** is observed as a low amplitude infill unit with sometimes acoustically transparent to chaotic structures, which bear resemblance with post-depositional fluid escape features. At the base of these depressions and especially at their sides, high-amplitude reflections (HAR) are present, overlapping on the flanks, creating small moats. This might invoke the presence of a bottom current intervening during the infill stage of this channel-like feature (Rebesco & Stow, 2001).

Towards the northwest, smaller depressions are observed with flank slopes of about 30° (Figs. 5.6 and 5.9). They are approximately 162 and 310 m wide and respectively 30 and 50 ms TWT deep. In a NW-SE profile, the southernmost incision seems to be 2.3 km wide and 50 ms TWT deep with flank slopes of about 6°. On the other, NE-SW oriented profile, the northern slope of the depression is much steeper (30°) and has much similarities with a headwall scar of a large slide. On figure 5.9, this depression can be seen as a U-shaped cut into the slope with its opening

towards the southwest. The morphology of this large depression, its flat floor and the fluid escape features suggest this could be evidence of a large paleo-slide on this part of the slope. According to Gardner *et al.* (1999), Locat & Lee (2002) and Huvenne *et al.* (2002), many slides are generated due to overpressure in the sedimentary package through rapid sedimentation, which might explain the presence of fluid escape features. Also temperature changes and a higher sediment supply due to glaciations could contribute in slope failure of upper slope areas. The smaller, more northern located incision features could also be smaller slide scars, possibly related with the larger slide.

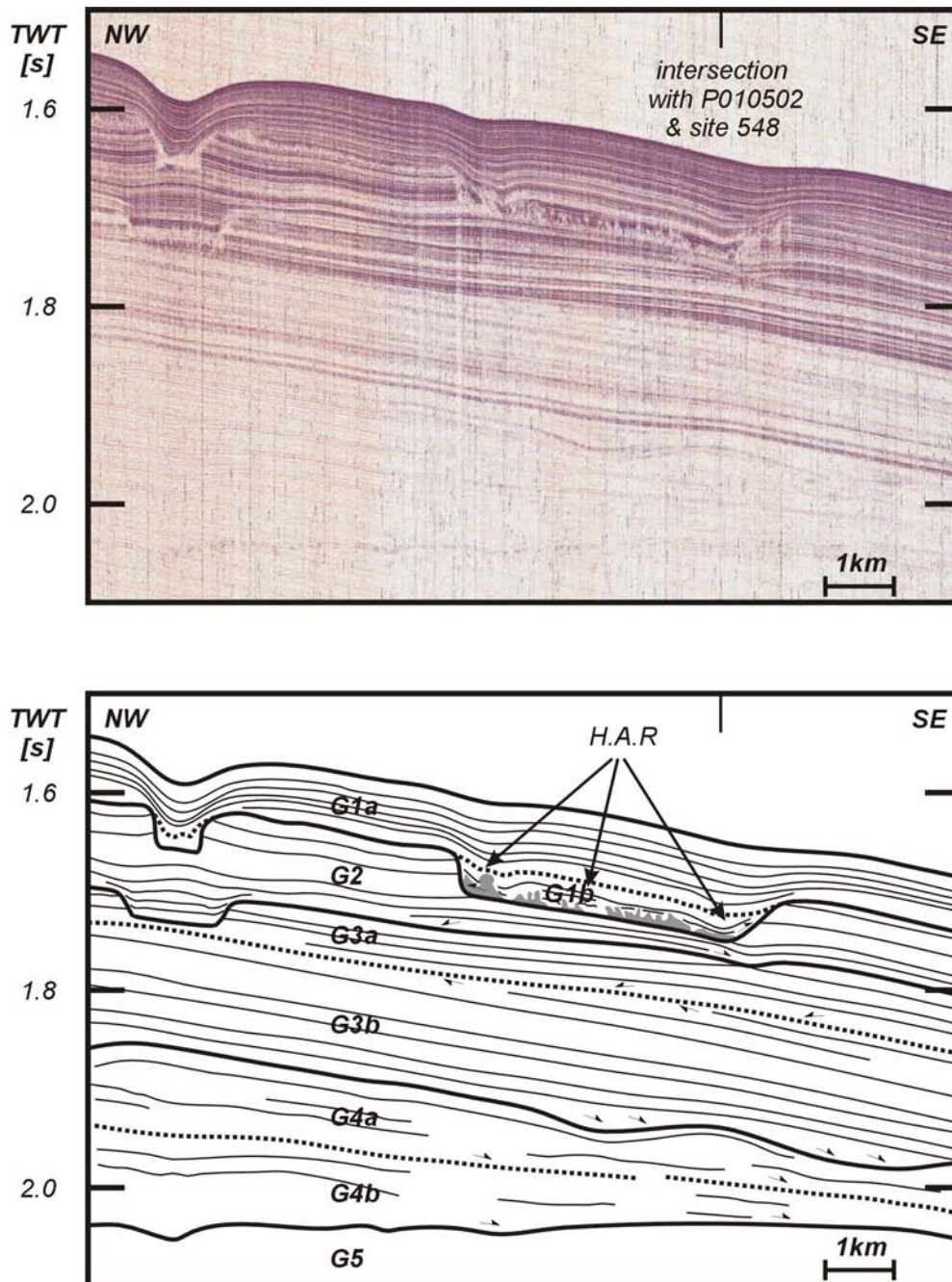


**Figure 5.6:** Interpretation of the NW-SE oriented profile P010501, located on figures 5.1 and 5.9. The grey shaded areas within the G1b depression represent an irregular acoustic transparent seismic facies.

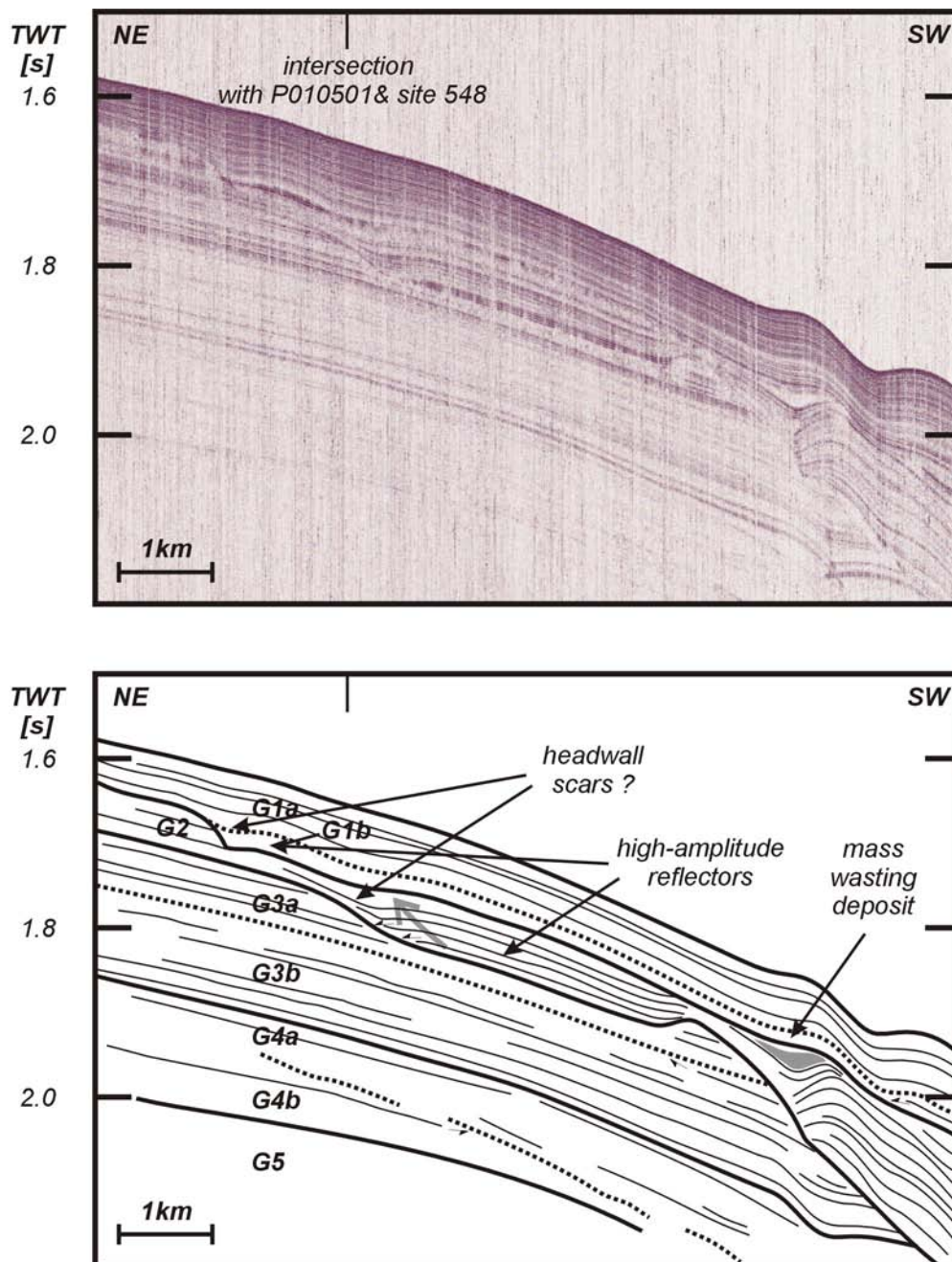


**Figure 5.7:** Interpretation of the NE-SW oriented profile P010502, located on figures 5.1 and 5.9. Note the apparent upslope migration of some reflectors within unit G2.

### 5.4.3. Unit G2

The erosive lower boundary of unit **G2** has a very irregular morphology with a wide range of reflection terminations; onlap, downlap and conformable deposition. Dependent of its location on the relatively flat upper part of the slope or the oceanward steeper side, this unit also has different reflector configurations.

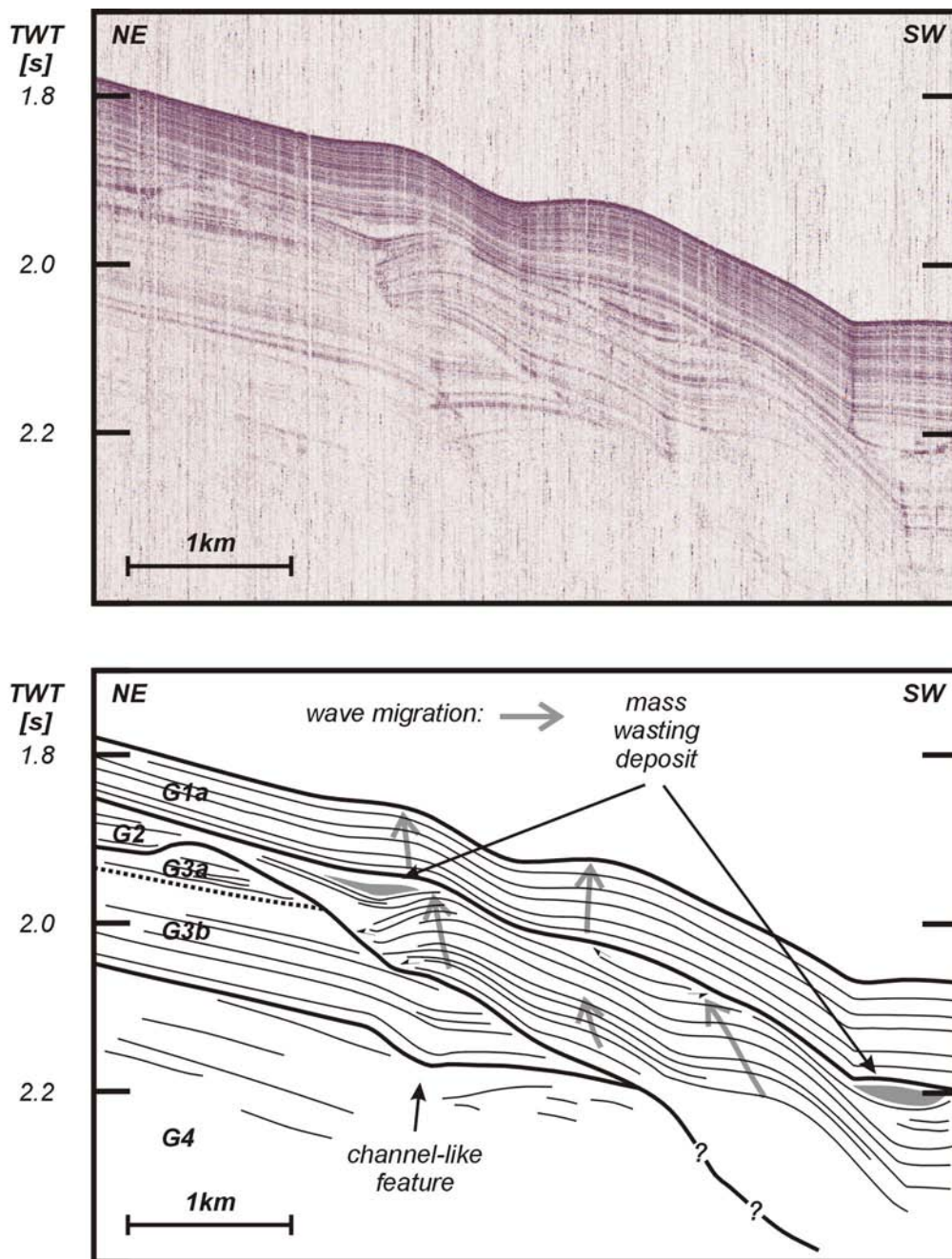


**Figure 5.8:** Detailed view on the clinoform features observed on profile P010502, as well as in DSDP profile OC202 (Fig. 5.4). While the clinoforms in the uppermost unit seem to be draping and aggradating, those in unit G2 clearly seem to prograde upslope. Their troughs seem to be filled with ponded turbidites.

On the upper slope part, again two channel-like features can be observed (Figs. 5.6 and 5.9). On profile P010501, the depression is 30 to 35 ms TWT (about 27 m) deep, 752 m wide and its flanks have a dip of about 6.5°. It is located directly underneath a slide scar of the overlying unit. The depression on profile P010502, on the other hand, is slightly dipping, 1.9 km wide and has a depth of 25 ms TWT ( $\pm$  23 m). The slopes of the depression flanks are varying between 3° (N) and 6° (S). In analogy with the overlying depressions, it could be suggested these might be a slide scars as well.

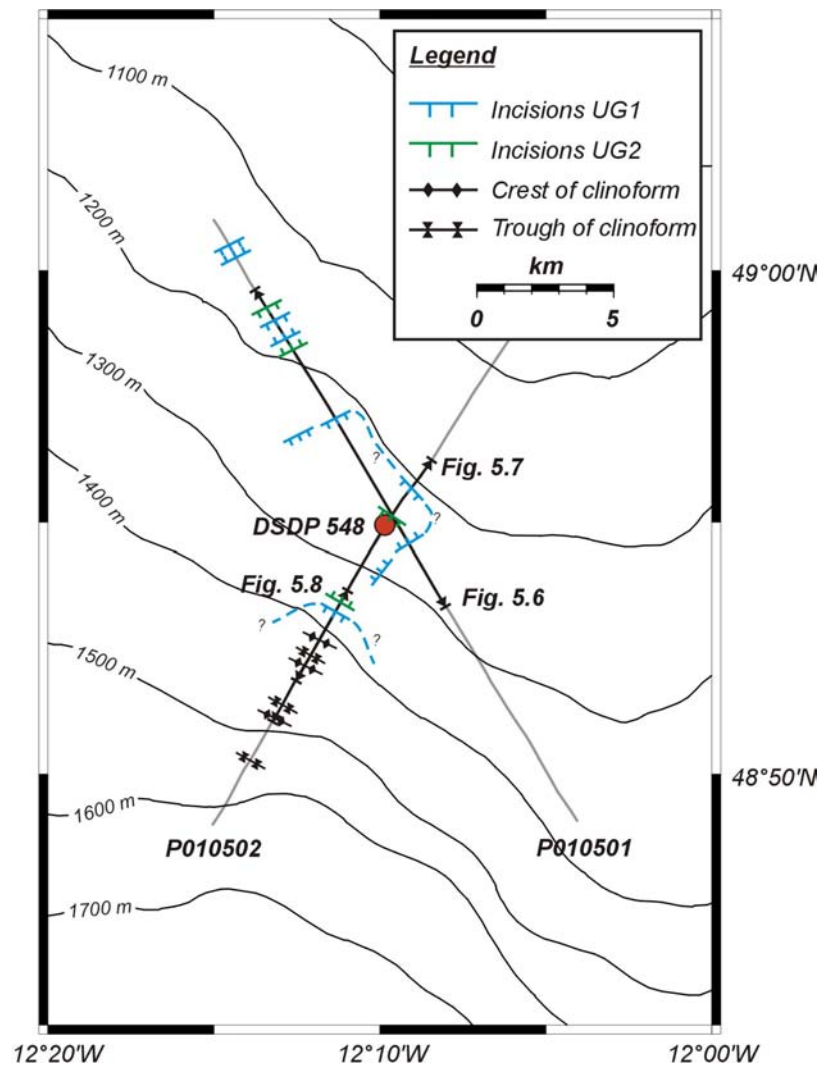


**Figure 5.9:** Detailed location map of lines P010501 and P010502 with indication of the most important seabed features and location of the incisions cut in the lower boundaries of units G1 and G2.

In general the upper slope reflector configuration is a parallel one with high-frequency reflectors displaying high to medium amplitudes. Above the depression on figure 5.6, there seems to be a relief inversion. This might again be attributed to bottom currents at the channel edges and a major sediment supply, creating a mounded drift (Rebesco & Stow, 2001; Stow *et al.*, 2002). On profile P010502 the reflectors inside the depression seem to onlap on the lower boundary and form an upslope prograding sediment body.

Towards the steeper part of the slope, the lower boundary of unit G2 cuts deeply in to units G3 to G4 and possibly deeper (Fig. 5.8). Here, the reflector configuration of unit G2 is characterised as a set of continuous, sigmoidal, medium to low amplitude reflectors. This sediment body is onlapping on the lower boundary and clearly progrades upslope as wavy clinoforms. Two clinoform troughs are filled with an acoustically nearly transparent deposit, topped by nearly horizontally reflectors. It is suggested these might be mass wasting deposits. The upper part of this unit clearly has been eroded by the early G1 unconformity.

Although these features are observed on only one seismic profile, already some of their characteristics might give some clues towards their origin. The average slope of the unconformity on which this sediment body is deposited, amounts to approximately 5°. According to Faugères *et al.* (2002), this slope seems not to be steep enough to create a large-scale gravity deformation process. Moreover, the reflector configuration clearly shows a general apparent upslope migration and over the entire package, no offset between reflectors are found. The reflector progradation with a relatively higher sedimentation rate on the NE flank fits with the sediment wave model proposed by Wynn & Stow (2002) with enhanced bottom current velocities on downstream flanks, leading to an upstream (upslope) progradation.

Several authors suggest this part of the margin is swept by a northward flowing bottom current (Pingree & Le Cann, 1989; New *et al.*, 2001). The only two clues that might suggest these are bottom current sediment waves are the irregularity of the waves and the downslope thickening of the sequence (Fig. 5.8). Turbidite sediment waves are more regular, their dimensions progressively decrease downslope, as well as their thickness (Wynn & Stow, 2002). Therefore, we suggest upon these few observation these sediment waves are formed under a bottom current environment rather than turbidite or gravity deformation processes. Only a broader network of seismic profiles or multibeam bathymetry could yield more insight in the involved processes.

#### 5.4.4 Unit G3

Unit G3 is relatively thick (max. 200 ms TWT,  $\pm$  180 m) with a sometime gently undulating lower boundary. In some places, the lower strata of unit G3 onlap on this lower boundary. In a NE-SW transect, however, it is very difficult to distinguish and is presumed to be conformable. Near its southern limit, a modest channel feature is observed (Fig. 5.8).

The upper 50 ms (45 m) of this unit are well stratified with frequent and continuous high-amplitude reflectors. Below, the amplitude of the reflectors becomes very low, as well as their frequency. Based upon this change of seismic facies, this unit is subdivided in respectively subunit **G3a** (high amplitudes) and subunit **G3b** (low amplitudes). There also seems to be a subtle unconformity separating both subunits, cutting gently in the underlying strata. The overlying G3a lower strata sometimes onlap on this boundary.

#### 5.4.5 Units G4 and G5

Due to the attenuation of the seismic signal, the lowermost unit **G4** is characterised by relatively low amplitude reflections, with sometimes a poor continuity. The general reflector configuration is gently undulating. Based on some more prominent reflections, this unit was subdivided in to two subunits.

On a NW-SE transect, the lower boundary of subunit **G4a** is erosive and sometimes truncates subunit **G4b** (Fig. 5.7). The overall reflector configuration of this unit seems to be subparallel. The lower boundary of G4b is an unconformity with relatively higher amplitudes, upon which the strata of unit *G4b* onlap. This, however, is the deepest observed reflector, which might suggest an important change in lithology between unit G4 and the underlying unit **G5**.

## 5.5 A Cenozoic stratigraphic framework

Generally, the nature, origin and timing of unconformities result from a blend of tectonics, climate and paleoceanographic circulation. The middle to late Cenozoic evolution of the margin off western Ireland was influenced by a number of important tectonic and climatic events, which influenced the gradual development of the deep-water circulation system (Stow, 1982). Major disturbances or changes in the relative intensity of the bottom water circulation may have given rise to non-deposition or erosion, leading to the creation of the most important unconformities (Pearson & Jenkins, 1986). According to de Graciansky & Poag (1984), most of the encountered unconformities in site 548 might also be correlated with eustatic sea-level falls recorded at other widespread locations in the North Atlantic basin. According to Dingle & Scrutton (1979) and Masson *et al.* (1984) the observed discontinuities in the Goban Spur transect can be observed along the entire margin, which was confirmed by the very good correlation of the DSDP sites 548-551 on Goban Spur and DSDP sites 400-402 on Meriadzek Terrace (Celtic Margin).

However, the very high-resolution seismic stratigraphy of site 548 on Goban Spur shows more Cenozoic discontinuities than initially was reported by de Graciansky *et al.* (1984b), although the units can be perfectly correlated (Fig. 5.10). This section will discuss the timing, cause and margin-wide relevance of the encountered unconformities throughout the Cenozoic. Here, a new regional chronostratigraphic nomenclature is proposed, partly based upon those of Stoker *et al.* (2002) and McDonnell & Shannon (2001). The five major regional discontinuities (RD) will be named RD1 to RD5, respectively the youngest and the oldest.

### 5.5.1 RD5: Lower Paleocene

The base of unit G5 was not observed on the RCMG seismic profiles. The DSDP core data suggest it correlates with the important Early Paleocene to Late Paleocene C40 "Top chalk" reflector of McDonnell & Shannon (2001). This intra-Paleocene unconformity is considered as an oceanic disturbance, tentatively correlated with the separation between Rockall Bank and Greenland. The opening of the Norwegian Greenland Sea allowed the incursion of cold bottom waters into the North Atlantic (de Graciansky *et al.*, 1985). During the Late Paleocene to Early Eocene, a marked uplift of the Irish landmass supplied abundant terrigenous debris to Goban Spur (de Graciansky & Poag, 1984).

### 5.5.2 RD4: Middle Eocene

The lowest observed higher amplitude reflector, which constitutes the lower boundary of unit G4, is equivalent with a Middle Eocene hiatus, observed by de Graciansky & Poag (1984) in DSDP core 548. Coeval discontinuities were reported by Pearson & Jenkins (1986) in the Rockall Trough. However, on a basin-wide scale, more attention is paid to a Late Eocene hiatus (Stow, 1982; McDonnell & Shannon, 2001), which was unfortunately not observed in the Goban Spur transect. This Late Eocene to Early Oligocene C30 discontinuity is thought to be related with the onset of global cooling. The AABW, which was formed at high southern latitudes, started flowing into the North Atlantic (Stow, 1982).

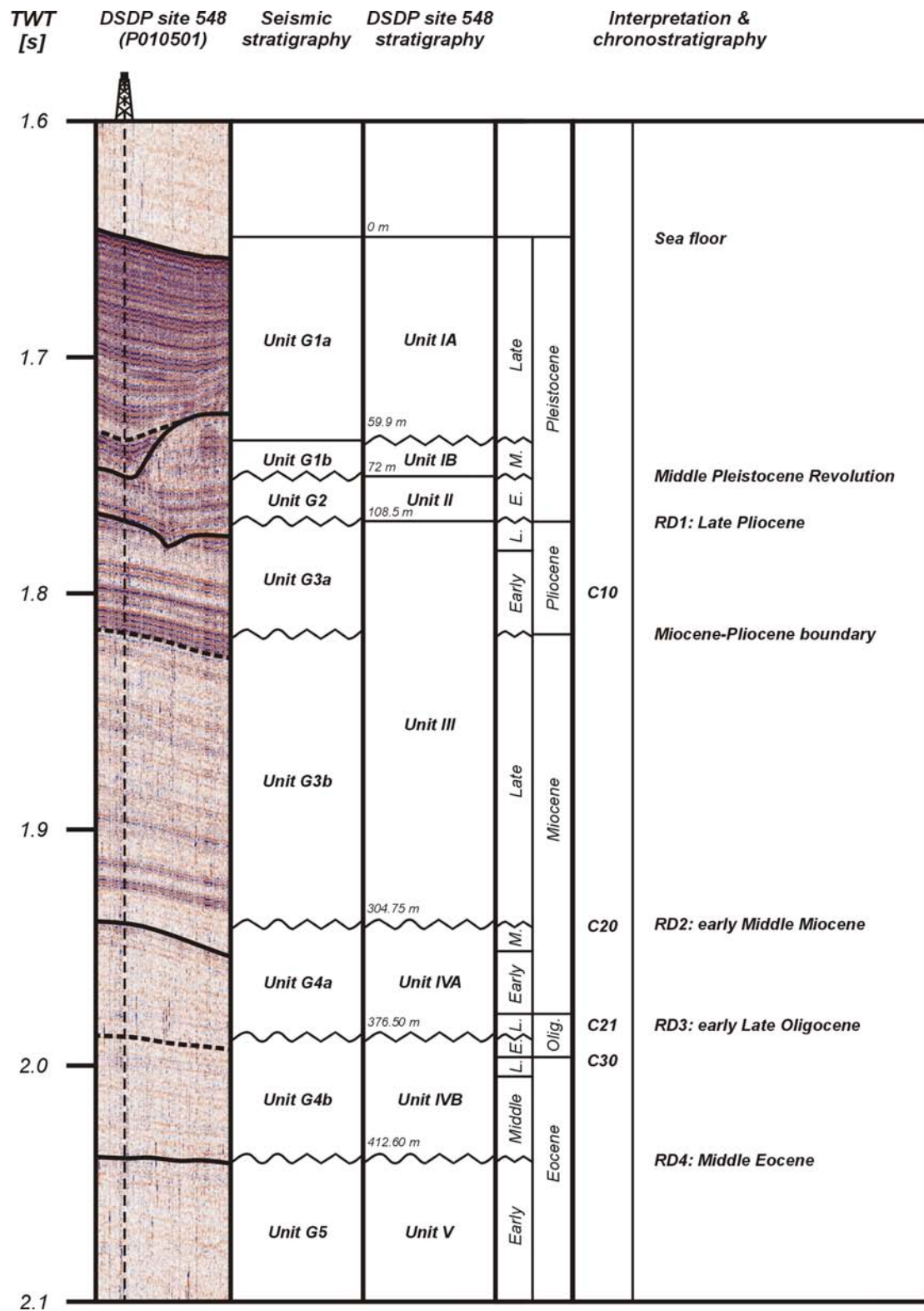


**Figure 5.10:** Correlation of DSDP site 548 with the seismic stratigraphic interpretation of P010501 (Fig. 5.6) and an overview of the major unconformities, after de Graciansky & Poag (1984), Stoker et al. (2001) and McDonnell & Shannon (2001).

Together with the development of the deep cold LSW and possibly NSW overflow, the important NE Atlantic deep-water circulation pattern was initiated (de Graciansky & Poag, 1984; Stoker *et al.*, 2002). Within the Rockall Trough, this event created a basin-wide erosional event and marked the establishment of regional contour-hugging bottom currents (McDonnell & Shannon, 2001; Stoker *et al.*, 2001).

Like the C30 event, a more vigorous deep-water circulation could indeed explain the presence of the high-amplitude reflector and the onlap upon the lower boundary of G4 in terms of sediment drift deposition. According to de Graciansky & Poag (1984) the Eocene was an active time in the North Atlantic history with regard to the number of climatic and tectonic events. One of these events did significantly affect Goban Spur during the Middle Eocene. The few available data suggest this regional RD4 discontinuity was caused by global events which affected the entire water column.

### 5.5.3 RD3: early Late Oligocene

The boundary between subunits G4a and G4b, as observed on seismic profiles, is correlated with a deep erosive event observed by de Graciansky *et al.* (1985) in DSDP core 548 (Fig. 5.10). According to the stratigraphy of de Graciansky *et al.* (1984a) this is an early Late Oligocene discontinuity. Micropaleontological data indicate that the surface and bottom environments changed at site 548 just before the hiatus. This unconformity has been recognized over the entire North Atlantic on as well abyssal as on shelf sites (de Graciansky *et al.*, 1985), representing a hiatus of approximately 4 Ma, which can be directly related to a major sea level fall (Pearson & Jenkins, 1986; Poag *et al.*, 1984). Although the cause of this sea-level fall is not fully documented, it is thought to be caused by the general build-up of the continental ice caps (Pearson & Jenkins, 1986). Within Oligocene times, the circum-antarctic flow is initiated and fostered the intensification of the Antarctic glaciation (Stow, 1982). This RD3 discontinuity correlates with C21 of McDonnell & Shannon (2001). Although it only vaguely visible on figure 5.7, this event was responsible for the creation of several deeply incised channels (de Graciansky *et al.*, 1985).

### 5.5.4 RD2: early Middle Miocene

Seismic unit G3 can be correlated with core unit III, which was attributed a Late Miocene to Late Pliocene age by de Graciansky *et al.* (1984a). The lower boundary represents a very important early Middle Miocene erosive event coupled to a hiatus of about 6 Ma (de Graciansky *et al.*, 1984a; Pearson & Jenkins, 1986). This particular unconformity between the early Middle Miocene and the Late Miocene was also observed in the other DSDP holes on Goban Spur and Rockall Trough, where it was identified by Stoker *et al.* (2001) as the C20 reflector. According to McDonnell & Shannon (2001), this is the only known unconformity which has a chronostratigraphic significance in as well the Rockall as the Porcupine Basin. The regional discontinuity related to this event will be referred to as RD2.

Several causes have been identified that may have been responsible for this global climatic and oceanographic disturbance. Benthic foraminiferal evidence suggests that the environmental conditions shifted prior to the early Middle Miocene event. de Graciansky & Poag (1984) related this to the rapid expansion of the

Antarctic ice cap, causing a reorganisation of deep-sea benthic foraminiferal communities and a marked eustatic sea-level drop as demonstrated by Vail & Hardenbol (1979). Additionally, during the early Middle Miocene the MOW and the NSW started to flow within the Atlantic domain, establishing the North Atlantic Deep Water formation and its vigorous bottom currents (Stow, 1982; de Graciansky *et al.*, 1984a; Schnitker, 1986). The initiation of a fully established pattern of deep-water exchange is most likely a Miocene phenomenon (Stoker *et al.*, 2002). This major change in the North Atlantic paleoceanography enabled the first occurrences of sediment drifts formed by geostrophic contour currents (Schnitker, 1986; Stow, 1982; Stow *et al.*, 2002).

The marked difference in physical characteristics between subunits G3a and G3b could represent the transition from the Miocene to the Pliocene, which was initially observed by de Graciansky *et al.* (1984a) in DSDP core 548. The subtle erosive discontinuity could be related with the temporarily diminution of NADW formation during the latest Miocene Messinian salinity crisis. Due to the isolation of the Mediterranean basin, there was not enough saline outflow to assist the production of NADW (Schnitker, 1986). According to Llave *et al.* (2001) and Vail & Hardenbol (1979) this episode was also characterized by a prominent sea-level fall between 5.2-5.5 Ma.

### 5.5.5 Quaternary events

The inferred age of units G2 and G1 is correlated with a Late Pliocene to Pleistocene interval in core DSDP 548, defined by de Graciansky *et al.*, 1984a. This interval is characterised by major and frequent sea-level falls (Haq *et al.*, 1987). These short-term, but marked sea-level falls are frequently associated with worldwide major unconformities. Already from the Oligocene, sea-level falls may be in large part due to the increasing influence of glaciation. After the Messinian sea-level fall, there was an Early Pliocene sea level rise at 4.2 Ma. The Early Pliocene (5-3.5 Ma) global climatic system was controlled by high-amplitude precessional fluctuations of about 20 ka, modulated by low-frequency eccentricity cycles of about 400 ka. This changed drastically towards the Late Pliocene (3.5-1.8 Ma) with a dominance of 41 ka obliquity cycles and the onset of growth and decay of large continental ice sheets. The cause of this Northern Hemisphere amplified ice growth is uncertain, but several mechanisms have been proposed, in both external and internal to the climate system: plateau uplift, variations in the Earth's orbit and closing of major gateways (Kleiven *et al.*, 2002). This global cooling had a major impact on the climatic, sea-level and hydrodynamic conditions (Hernandez-Molina *et al.*, 2002). The discontinuities observed in units G2 and G1 can be explained in the framework of this climatically very complex period. The Pliocene to Pleistocene time scale is illustrated in figure 5.11.

#### 5.5.5.1 RD1b: Late Pliocene

In the Goban Spur transect, the hiatus at the base of unit G2 is correlated with the Late Pliocene lower boundary of core unit II, as defined by de Graciansky *et al.* (1984a). Along other DSDP and ODP sites in the Norwegian Sea, Rockall Trough and even in the Gibraltar region, a Late Pliocene hiatus at 2.5 to 2 Ma is observed (Pearson & Jenkins, 1986; Stein *et al.*, 1986). This regional discontinuity was created when modern oceanographic conditions were established in the NE Atlantic

TIME (Ma)	CHRONOS	POLARITY	EPOCH	AGE	PLANKTONIC FORAMINIFERA		CALCAREOUS NANNOPLANKTON					
					Berggren (1973, 1977a, this work)		Martini (1971)	Bukry (1973, 1975)				
					ATLANTIC	INDO-PACIFIC						
1	C1n	[Black]	PLEISTOCENE	LATE	PT1	b	N23 <i>Gt. truncatulinoides</i> PRZ	NN21	CN15			
				MIDDLE				a		NN20	b	
	EARLY	CALABRIAN	a	<i>Gd. fistulosus</i> - <i>Gt. tosaensis</i> ISZ	NN19	CN14	a					
							2	C2n	[Black]	LATE	PIACENZIAN	GELASIAN
	C2r	[Black]	1	PL5	<i>D. altispira</i> - <i>Gt. miocenica</i> IZ	<i>D. altispira</i> - <i>Gt. pseudomiocenica</i> IZ						
							2	PL4	<i>D. altispira</i> - <i>Gt. pseudomiocenica</i> IZ	NN16	b	
	3	C2An	[Black]	LATE	PIACENZIAN	GELASIAN	PL3					<i>Gt. margaritae</i> - <i>Sph. seminulina</i> IZ
	4							C2Ar	[Black]	EARLY	ZANCLEAN	
	5	C3n	[Black]	MIOCENE	LATE	MESS.	PL1					b
								1	a	<i>Gt. tumida</i> - <i>Gt. cibaoensis</i> ISZ	NN11b	
2	C3r	[Black]	LATE	MESS.	M14	<i>Gt. linguaensis</i> - <i>Gt. tumida</i> IZ	NN11b	CN9				d
3									C3An.1n	[Black]	LATE	MESS.
4	C3r	[Black]	LATE	MESS.	M14	<i>Gt. linguaensis</i> - <i>Gt. tumida</i> IZ	NN11b	CN9				
5									C3r	[Black]	LATE	MESS.
	C3r	[Black]	LATE	MESS.	M14	<i>Gt. linguaensis</i> - <i>Gt. tumida</i> IZ	NN11b	CN9				
									C3r	[Black]	LATE	MESS.
	C3r	[Black]	LATE	MESS.	M14	<i>Gt. linguaensis</i> - <i>Gt. tumida</i> IZ	NN11b	CN9				
									C3r	[Black]	LATE	MESS.
	C3r	[Black]	LATE	MESS.	M14	<i>Gt. linguaensis</i> - <i>Gt. tumida</i> IZ	NN11b	CN9				

Figure 5.11: Detail of the Pliocene-Pleistocene time scale (Berggren et al., 1995)

with the reintroduction of MOW (Pearson & Jenkins, 1986; Schnitker, 1986). The glacial-interglacial cycles started to have a pronounced effect on the production of the North Atlantic Deep Water, the Antarctic Bottom Water and the Norwegian Sea Outflow Water. These changes resulted in the variability of the thermohaline circulation and thus affected the construction and evolution of the well-known sediment drifts along the margins of the North Atlantic (Stow, 1982; Faugères *et al.*, 1993). This discontinuity could also be related with the 2.4 Ma sea level fall between MIS100/101 ka (Llave *et al.*, 2001). This so-called "Upper Pleistocene Revolution" (UPR) is coeval with global cooling and with an important change in climatic cyclicity (Hernandez-Molina *et al.*, 2002).

However, according to Stoker *et al.* (2002) and McDonnell & Shannon (2001) this same event has an Early Pliocene age in the Rockall and Porcupine Basin. They do consider the age of this C10 event as problematic due to the lack of significant Neogene age constraints in the Porcupine Basin. Moreover, the C10 age was proposed on an inter-basin correlation, which was considered by the same authors as extremely speculative. In the Rockall Trough, the C10 event marks the instigation of shelf-margin progradation. It is observed as an angular unconformity representing submarine erosion by deep-water currents. According to Stoker *et al.* (2002) there is an increasing evidence for uplift and seaward tilting of NW Britain, Ireland and the Faroes during the late Neogene. A consequence of this late Cenozoic uplift, in combination with a climatic cooling, may have been the triggering of glaciation with elevated plateaus becoming sites for snowfields that ultimately develop in ice-sheets (Stoker *et al.*, 2002).

Although we do recognize the importance of the Late Neogene uplift for the nucleation of the British-Irish Ice sheet, there still is no proven evidence of an Early Pliocene erosional event in Goban Spur, nor in the Porcupine Basin. As proposed by (Pearson & Jenkins, 1986), the proximity of the Irish mainland and the specific local morphology and circulation must have had a significant effect on the local Cenozoic stratigraphic sequences. Another possible explanation is provided by Schnitker (1986), suggesting that the present-day circulation pattern started nearly 4 Ma ago on abyssal sites, while at intermediate depth this was only introduced at about 2.5 Ma. As already was mentioned earlier, due to the different locations and water depths of the Rockall and Goban sites, a delay of oceanographic effects might have been recorded.

As a consequence, the regional discontinuity RD1 at the lower boundary of unit G2 is attributed a Late Pliocene age with an erosion event along the shelf edges. Especially the seaward side of Goban Spur seemed to be seriously affected, with the creation of an extensive erosion surface.

#### **5.5.5.2 The Middle Pleistocene Revolution**

DSDP core data attributes an early Middle Pleistocene to the base of their unit Ib (de Graciansky *et al.*, 1984a). This suggests that the slides observed at the base of unit G1 were apparently created during this period. The cause of these events, can probably also be related to climatic changes in the Quaternary.

Stein *et al.* (1986) observed a coeval hiatus occurring at a distinct shift in the benthic oxygen isotope composition during a period of expansion of major polar ice sheets. After 900/920 ka (MIS 22/23) the glacial-interglacial variations became dominated by a 100 ka cyclicity. This Mid-Pleistocene Revolution (MPR) invoked longer glacial-interglacial cycles, and thus the beginning of a glacial Pleistocene. The MPR is also correlated with a major sea-level fall caused by this new cooling pulse (Llave *et al.*, 2001; Hernandez-Molina *et al.*, 2002).

According to Locat & Lee (2002) such a sea-level fall might be responsible for sediment failure on upper slope environments. Another contributing factor might be higher sedimentation rates since the start of the Quaternary. After the sliding, the depression was filled with draping hemipelagic deposits. However, the amplitude changes in this youngest section might be an expression of Quaternary climate

fluctuations, as observed in sediment drifts in the Gulf of Cadiz by Hernandez-Molina *et al.* (2002).

## 5.6 Summary

Earlier studies (McDonnell & Shannon, 2001) related all the discontinuities within the Paleogene-Neogene Connaught Megasequence of the Porcupine Basin with the stratigraphy proposed by Stoker *et al.* (2001) for the adjacent Rockall Trough basin. This study, however, gives evidence based on a correlation between very high-resolution seismic lines and DSDP data that the Paleogene to Neogene stratigraphy of Rockall Trough is not necessarily fully applicable along the entire NW European margin. Therefore the stratigraphic framework proposed by Stoker *et al.* (2001) and applied by McDonnell & Shannon (2001) for the Porcupine Basin is modified in to a new, regional chronostratigraphy based on the observations made on DSDP site 548 on Goban Spur. This allowed the definition of several very important erosive events or regional discontinuities:

- During the **Quaternary**, two important paleoclimatological and erosive events are described; the **Middle Pleistocene Revolution** and a **Late Pliocene RD1** event. Both events are related to reorganizations of the global climatic system at the beginning of the Quaternary and are responsible for erosion and possibly sliding. Vigorous bottom currents between both events are thought to be responsible for the development of a sediment wave field
- **RD2** is an **early Middle Miocene** margin-wide unconformity related with the rapid expansion of the Antarctic ice cap and the establishment of the present-day ocean circulation with onset of the intensive bottom currents. A subtle discontinuity was found at the transition between Miocene and Pliocene strata, probably related to the Messinian sea-level fall
- **RD3** refers to an **early Late Oligocene** deep erosion event related with the initiation of the Antarctic glaciation
- **RD4** is a poorly documented **Middle Eocene** hiatus which might have been caused by a combination of tectonic and climatic events, such as the onset of the Antarctic Bottom Water regime
- **RD5** is related to the opening of the Norwegian Greenland Sea and the incursion of cold bottom waters into the North Atlantic domain within the **Lower Paleocene**

## References

- Auffret, G. A., Zaragosi, S., Dennielou, B., Cortijo, E., Van Rooij, D., Grousset, F. E., Pujol, C., Eynaud, F. & Siegert, M. (2002) Terrigenous fluxes at the Celtic margin during the last glacial cycle. *Marine Geology*, **188**, 79-108.
- Berggren, W. A., Kent, D.V., Swisher III, C. C. & Aubry, M.-P. (1995). A revised cenozoic geochronology and chronostratigraphy. In: *Geochronology, Time Scales and Global Stratigraphic Correlation* (Ed. by W. A. Berggren, D. V. Kent, M.-P. Aubry and J. Hardenbol). SEPM Special Publication, **54**.
- Caralp, M. H. (1984) Quaternary calcareous benthic foraminifers, leg 80. In: *Initial Reports of the Deep Sea Drilling Project* (Ed. by P. C. de Graciansky, C. W. Poag, R. Cunningham, P. Loubere, D. G. Masson, J. M. Mazzullo, L. Montadert, C. Müller, K. Otsuka, L. A. Reynolds, J. Sigal, S. W. Snyder, S. P. Vaos and D. Waples), U.S. Government Printing Office, Washington, **80**, 725-747.
- de Graciansky, P. C. & Poag, C. W. (1984) Geologic history of Goban Spur, northwest Europe continental margin. In: *Initial Reports of the Deep Sea Drilling Project* (Ed. by P. C. de Graciansky, C. W. Poag, R. Cunningham, P. Loubere, D. G. Masson, J. M. Mazzullo, L. Montadert, C. Müller, K. Otsuka, L. A. Reynolds, J. Sigal, S. W. Snyder, S. P. Vaos and D. Waples), U.S. Government Printing Office, Washington, **80**, 1187-1216.
- de Graciansky, P. C., Poag, C. W., Cunningham, R., Loubere, P., Masson, D. G., Mazzullo, J. M., Montadert, L., Müller, C., Otsuka, K., Reynolds, L. A., Sigal, J., Snyder, S. W., Townsend, H. A., Vaos, S. P. & Waples, D. (1985) The Goban Spur transect: Geologic evolution of a sediment-starved passive continental margin. *Geological Society of America Bulletin*, **96**, 58-76.
- de Graciansky, P. C., Poag, C. W., Cunningham, R., Loubere, P., Masson, D. G., Mazzullo, J. M., Montadert, L., Müller, C., Otsuka, K., Reynolds, L. A., Sigal, J., Snyder, S. W., Vaos, S. P. & Waples, D. (1984a) Site 548. In: *Initial Reports of the Deep Sea Drilling Project* (Ed. by P. C. de Graciansky, C. W. Poag, R. Cunningham, P. Loubere, D. G. Masson, J. M. Mazzullo, L. Montadert, C. Müller, K. Otsuka, L. A. Reynolds, J. Sigal, S. W. Snyder, S. P. Vaos and D. Waples), U.S. Government Printing Office, Washington, **80**, 33-122.
- de Graciansky, P. C., Poag, C. W., Cunningham, R., Loubere, P., Masson, D. G., Mazzullo, J. M., Montadert, L., Müller, C., Otsuka, K., Reynolds, L. A., Sigal, J., Snyder, S. W., Vaos, S. P. & Waples, D. (1984b) Site 549. In: *Initial Reports of the Deep Sea Drilling Project* (Ed. by P. C. de Graciansky, C. W. Poag, R. Cunningham, P. Loubere, D. G. Masson, J. M. Mazzullo, L. Montadert, C. Müller, K. Otsuka, L. A. Reynolds, J. Sigal, S. W. Snyder, S. P. Vaos and D. Waples), U.S. Government Printing Office, Washington, **80**, 123-176.
- de Graciansky, P. C., Poag, C. W., Cunningham, R., Loubere, P., Masson, D. G., Mazzullo, J. M., Montadert, L., Müller, C., Otsuka, K., Reynolds, L. A., Sigal, J., Snyder, S. W., Vaos, S. P. & Waples, D. (1984c) Site 551. In: *Initial Reports of the Deep Sea Drilling Project* (Ed. by P. C. de Graciansky, C. W. Poag, R. Cunningham, P. Loubere, D. G. Masson, J. M. Mazzullo, L. Montadert, C. Müller, K. Otsuka, L. A. Reynolds, J. Sigal, S. W. Snyder, S. P. Vaos and D. Waples), U.S. Government Printing Office, Washington, **80**, 357-369.
- De Mol, B., Van Rensbergen, P., Pillen, S., Van Herreweghe, K., Van Rooij, D., McDonnell, A., Huvenne, V., Ivanov, M., Swennen, R. & Henriët, J.-P. (2002) Large deep-water coral banks in the Porcupine Basin, southwest of Ireland. *Marine Geology*, **188**, 193-231.
- Dingle, R. V. & Scrutton, R. A. (1979) Sedimentary succession and tectonic history of a marginal plateau (Goban Spur, Southwest of Ireland). *Marine Geology*, **33**, 45-69.
- Evans, C. D. R. (1990) *The geology of the western English Channel and its western approaches*. HMSO for the British Geological Survey, London, 93 pp.
- Faugères, J.-C., Gonthier, E., Mulder, T., Kenyon, N. H., Cirac, P., Gribouillard, R., Berné, S. & Lesuavé, R. (2002) Multi-process generated sediment waves on the Landes Plateau (Bay of Biscay, North Atlantic). *Marine Geology*, **182**, 279-302.

- Faugères, J.-C., Mézerais, M. L. & Stow, D. A. V. (1993) Contourite drift types and their distribution in the North and South Atlantic Ocean basins. *Sedimentary Geology*, **82**, 189-203.
- Gardner, J. V., Prior, D. B. & Field, M. E. (1999) Humboldt slide - a large shear-dominated retrogressive slope failure. *Marine Geology*, **154**, 323-338.
- Hall, I. R. & McCave, I. N. (1998) Glacial-interglacial variation in organic carbon burial on the slope of the N.W. European Continental Margin. *Progress in Oceanography*, **42**, 37-60.
- Haq, B. U., Hardenbol, J. & Vail, P. R. (1987) Chronology of Fluctuating Sea Levels Since the Triassic. *Science*, **235**, 1156-1166.
- Hernandez-Molina, F. J., Somoza, L., Vazquez, J. T., Lobo, F., Fernandez-Puga, M. C., Llave, E. & Diaz-del Rio, V. (2002) Quaternary stratigraphic stacking patterns on the continental shelves of the southern Iberian Peninsula: their relationship with global climate and palaeoceanographic changes. *Quaternary International*, **92**, 5-23.
- Huvenne, V. A. I., Croker, P. F. & Henriët, J.-P. (2002) A refreshing 3-dimensional view of an ancient sediment collapse and slope failure. *Terra Nova*, **14**, 33-40.
- Huvenne, V. A. I., De Mol, B. & Henriët, J.-P. (2003) A 3D seismic study of the morphology and spatial distribution of buried coral banks in the Porcupine Basin, SW of Ireland. *Marine Geology*, **198**, 5-25.
- Kleiven, H. F., Jansen, E., Fronval, T. & Smith, T. M. (2002) Intensification of Northern Hemisphere glaciations in the circum Atlantic region (3.5-2.4 Ma) - ice-rafted detritus evidence. *Palaeogeography, Palaeoclimatology, Palaeoecology*, **184**, 213-223.
- Llave, E., Hernandez-Molina, F. J., Somoza, L., Diaz-del Rio, V., Stow, D. A. V., Maestro, A. & Alveirinho Dias, J. M. (2001) Seismic stacking pattern of the Faro-Albufeira contourite system (Gulf of Cadiz): a Quaternary record of paleoceanographic and tectonic influences. *Marine Geophysical Researches*, **22**, 487-508.
- Locat, J. & Lee, H. J. (2002) Submarine landslides: advances and challenges. *Canadian Geotechnical Journal*, **39**, 193-212.
- Masson, D. G. & Miles, P. R. (1986) Development and Hydrocarbon Potential of Mesozoic Sedimentary Basins Around Margins of North Atlantic. *The American Association of Petroleum Geologists Bulletin*, **70**(6), 721-729.
- Masson, D. G., Montadert, L. & Scrutton, R. A. (1984) Regional geology of the Goban Spur continental margin (Ed. by P. C. de Graciansky, C. W. Poag et al.), U.S. Government Printing Office, Washington, Initial Reports of the Deep Sea Drilling Project, **80**, 1115-1139.
- McDonnell, A. (2001) Comparative Tertiary basin development in the Porcupine and Rockall Basins. Ph.D. thesis, Department of Geology. *University College Dublin*, Dublin, 201 pp.
- McDonnell, A. & Shannon, P. M. (2001) Comparative Tertiary stratigraphic evolution of the Porcupine and Rockall basins. In: *The Petroleum Exploration of Ireland's Offshore Basins* (Ed. by P. M. Shannon, P. Houghton and D. Corcoran), Geological Society, London, Special Publication, **188**, 323-344.
- Müller, C. (1984) Biostratigraphic and paleoenvironmental interpretation of the Goban Spur region based on a study of calcareous nannoplankton. In: *Initial Reports of the Deep Sea Drilling Project* (Ed. by P. C. de Graciansky, C. W. Poag, R. Cunningham, P. Loubere, D. G. Masson, J. M. Mazzullo, L. Montadert, C. Müller, K. Otsuka, L. A. Reynolds, J. Sigal, S. W. Snyder, S. P. Vaos and D. Waples), U.S. Government Printing Office, Washington, **80**, 573-597.
- Naylor, D. & Shannon, P. M. (1982) *The Geology of Offshore Ireland and West Britain*. Graham & Trotman Ltd., London, 161 pp.
- New, A. L., Barnard, S., Herrmann, P. & Molines, J.-M. (2001) On the origin and pathway of the saline inflow to the Nordic Seas: insights from models. *Progress in Oceanography*, **48**, 255-287.
- Pearson, I. & Jenkins, D. G. (1986) Unconformities in the Cenozoic of the North-East Atlantic. In: *North Atlantic Palaeoceanography* (Ed. by C. P. Summerhayes and N. J. Shackleton), Geological Society, London, Special Publication, **21**, 79-86.

- Pingree, R. D. & Le Cann, B. (1989) Celtic and Armorican slope and shelf residual currents. *Progress in Oceanography*, **23**, 303-338.
- Poag, C. W., Reynolds, L. A., Mazzullo, J. M. & Keigwin, L. D. (1984) Foraminiferal, lithic, and isotopic changes across four major unconformities at deep sea drilling project site 548, Goban Spur. In: *Initial Reports of the Deep Sea Drilling Project* (Ed. by P. C. de Graciansky, C. W. Poag, R. Cunningham, P. Loubere, D. G. Masson, J. M. Mazzullo, L. Montadert, C. Müller, K. Otsuka, L. A. Reynolds, J. Sigal, S. W. Snyder, S. P. Vaos and D. Waples), U.S. Government Printing Office, Washington, **80**, 539-555.
- Rebesco, M. & Stow, D. A. V. (2001) Seismic expression of contourites and related deposits: A preface. *Marine Geophysical Researches*, **22**(5-6), 303-308.
- Schnitker, D. (1986) North-east Atlantic Neogene benthic foraminiferal faunas: tracers of deep-water palaeoceanography. In: *North Atlantic Palaeoceanography* (Ed. by C. P. Summerhayes and N. J. Shackleton), Geological Society, London, Special Publication, **21**, 191-203.
- Shannon, P. M. (1991) The development of Irish offshore sedimentary basins. *Journal of the Geological Society of London*, **148**, 181-189.
- Stein, R., Sarnthein, M. & Suendermann, J. (1986) Late Neogene submarine erosion events along the north-east Atlantic continental margin. In: *North Atlantic Palaeoceanography* (Ed. by C. P. Summerhayes and N. J. Shackleton), Geological Society, London, Special Publication, **21**, 103-118.
- Stoker, M. S., Nielsen, T., van Weering, T. C. E. & Kuijpers, A. (2002) Towards an understanding of the Neogene tectonostratigraphic framework of the NE Atlantic margin between Ireland and the Faroe Islands. *Marine Geology*, **188**, 233-248.
- Stoker, M. S., van Weering, T. C. E. & Svaerdborg, T. (2001) A mid- to late Cenozoic tectonostratigraphic framework for the Rockall Trough. In: *Petroleum Exploration of Ireland's offshore basins* (Ed. by P. M. Shannon, P. Haughton and D. Corcoran), Geological Society, London, Special Publication, **188**, 411-438.
- Stow, D. A. V. (1982) Bottom currents and contourites in the North Atlantic. *Bull. Inst. Géol. Bassin d'Aquitaine*, **31**, 151-166.
- Stow, D. A. V., Faugères, J.-C., Howe, J. A., Pudsey, C. J. & Viana, A. R. (2002) Bottom currents, contourites and deep-sea sediment drifts: current state-of-the-art. In: *Deep-Water Contourite Systems: Modern Drifts and Ancient Series, Seismic and Sedimentary Characteristics* (Ed. by D. A. V. Stow, C. J. Pudsey, J. A. Howe, J.-C. Faugères and A. R. Viana), Geological Society, London, Memoirs, **22**, 7-20.
- Vail, P. R. & Hardenbol, J. (1979) Sea-level changes during the Tertiary. *Oceanus*, **22**, 71-79.
- Van Rooij, D. (1999) Lithologie des délestages glaciaires (niveaux de Heinrich) de l'Eperon de Goban (Atlantique Nord-Est). D.E.A. thesis, Université de Bretagne Occidentale. *Université de Bretagne Occidentale*, Brest, 57 pp.
- Van Rooij, D., De Mol, B., Huvenne, V., Ivanov, M. K. & Henriët, J.-P. (2003) Seismic evidence of current-controlled sedimentation in the Belgica mound province, upper Porcupine slope, southwest of Ireland. *Marine Geology*, **195**(1-4), 31-53.
- van Weering, T. C. E., Hall, I. R., de Stigter, H. C., McCave, I. N. & Thomsen, L. (1998) Recent sediments, sediment accumulation and carbon burial at Goban Spur, N.W. European Continental Margin (47-50°N). *Progress in Oceanography*, **42**, 5-35.
- Wynn, R. B. & Stow, D. A. V. (2002) Classification and characterisation of deep-water sediment waves. *Marine Geology*, **192**, 7-22.



## Chapter VI: Seismic stratigraphy of the Belgica mound province and Quaternary sedimentary processes

The available network of high-resolution seismic profiles allows discussing the regional seismic stratigraphic framework of the Belgica mound province, located on the upper eastern slope of the Porcupine Seabight, between 51°00'N - 51°40'N and 11°20'W - 12°10'W, in water depths between 200 m and 1500 m (Fig. 6.1). Within this area, 4 major seismic units (U4 to U1) were distinguished, separated by three regional discontinuities (RD1 to RD3), as illustrated by profiles P000665, P980521, P980519 and P010521 (Fig. 6.2, 6.3, 6.4 and 6.5). This chapter will discuss these units in terms of changes in seismic facies, thickness, local occurrence and bounding unconformities. The timing and cause of the discontinuities will be related to the regional stratigraphy as proposed in chapter 5.

The main outline of this chapter has already been published in Van Rooij, D., De Mol, B., Huvenne, V., Ivanov, M.K. & Henriët, J.-P. (2003) Seismic evidence of current-controlled sedimentation in the Belgica mound province, upper Porcupine slope, southwest of Ireland. *Marine Geology*, **195**, 31-53. In this chapter, the data and conclusions presented in the Marine Geology paper are complemented with some new data and extracts of a second, submitted paper: Van Rooij, D., Blamart, D., Kozachenko, M., Wheeler, A. J., Richter, T. O. & Henriët, J.-P. (submitted) Quaternary drift sediment dynamics in the Belgica mounds province, Porcupine Seabight: a multidisciplinary approach. In: *Modern Carbonate Mound Systems: A window to Earth History* (Ed. by J.-P. Henriët and C. Dullo), Springer-Verlag, Heidelberg.

Before presenting and discussing the seismic stratigraphy of the area, the major morphological and seabed characteristics are presented.

### 6.1 Some morphological aspects

The morphology of this relatively gentle slope shows two features: seabed mounds and alongslope channels (Figs. 6.1 and 6.6). The seafloor characteristics of the study area based on side-scan observations has already been largely discussed by Huvenne (2003) (Fig. 6.7).

The multibeam bathymetry reveals that this part of the eastern slope is dominated by seabed mounds at water depths between 700 and 1100 m (Fig. 6.6). Most of the mounds appear to be more or less north - south elongated, with an approximate length of 1 km and a relief up to 300 m above the surrounding sea floor. Video truthing (Olu-Le Roy *et al.*, 2000; Wheeler *et al.*, submitted-a) shows that most of the mounds have been colonised by deep-water coral associations, mainly based on species such as *Lophelia pertusa* and *Madrepora oculata*. However, recent footage only shows few mounds with living coral (Henriët, pers. comm.). Numerous bedforms indicative of strong bottom currents and active sediment transport around these mounds were observed on the side-scan sonar records (Figs. 6.7 and 6.8). These include sediment waves, gravel ridges, barchan dunes and seabed striations (Fig. 6.8a). Figure 6.8b even shows that these seabed striations are

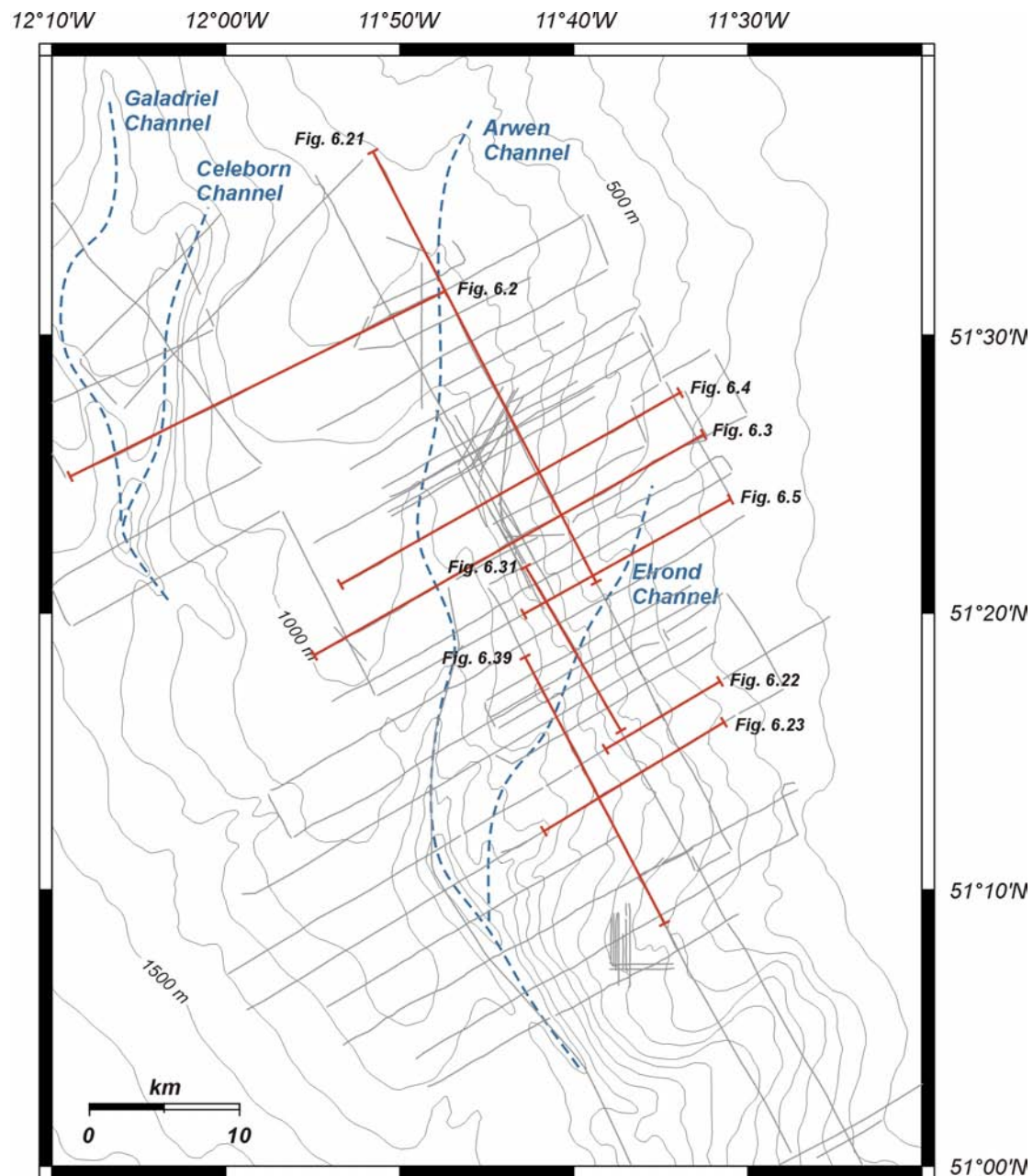


**Figure 6.1:** General setting of study area, with indication of all used profiles (GEBCO bathymetry, contour intervals are drawn every 100 m).

associated with active seabed erosion. Side-scan sonar can thus add to hydrographic observations and models concerning sediment mobility, but it is important to note these bedforms provide a record of the peak events and may not reflect the current regime (Akhmetzhanov *et al.*, 2001; Wheeler *et al.*, submitted-a). Sediment wave trains and bedforms indicative of corridors of higher benthic current strength seem to work their way around and between mounds, implying that the presence of these mounds causes benthic currents to accelerate around them. Away from these fast flowing confined currents, the seabed is typified by more dispersed sediment wave fields and rippled sands implying moderate to strong benthic currents and along-slope active sedimentation (Wheeler *et al.*, submitted-a; Huvenne, 2003; Huvenne *et al.*, submitted-b).

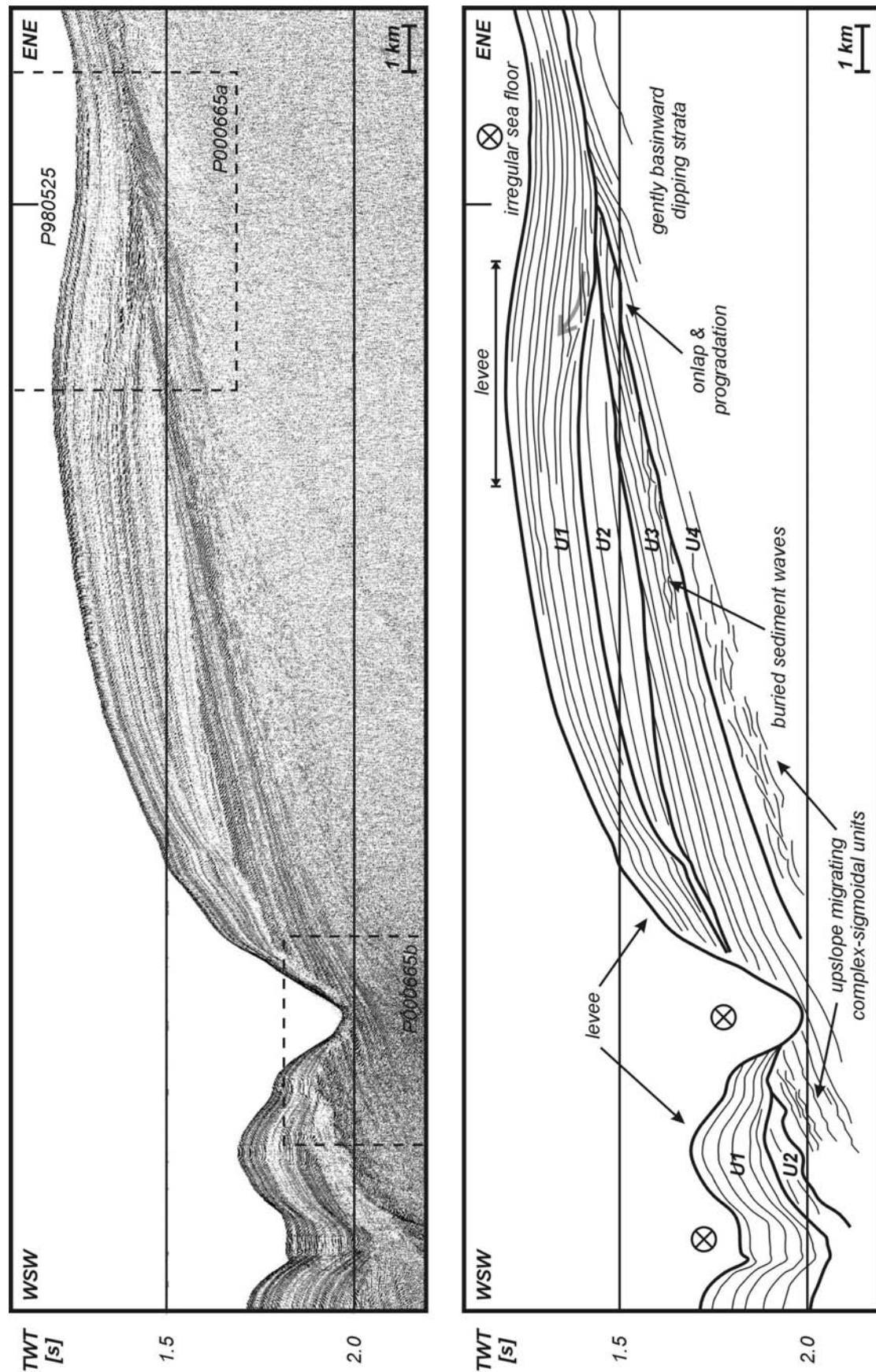


**Figure 6.2:** P000665: Overview profile on the northern edge of the study area, illustrating the typical seismic facies and discontinuities. The grey arrow indicates a shift in depocentre along the Arwen channel.

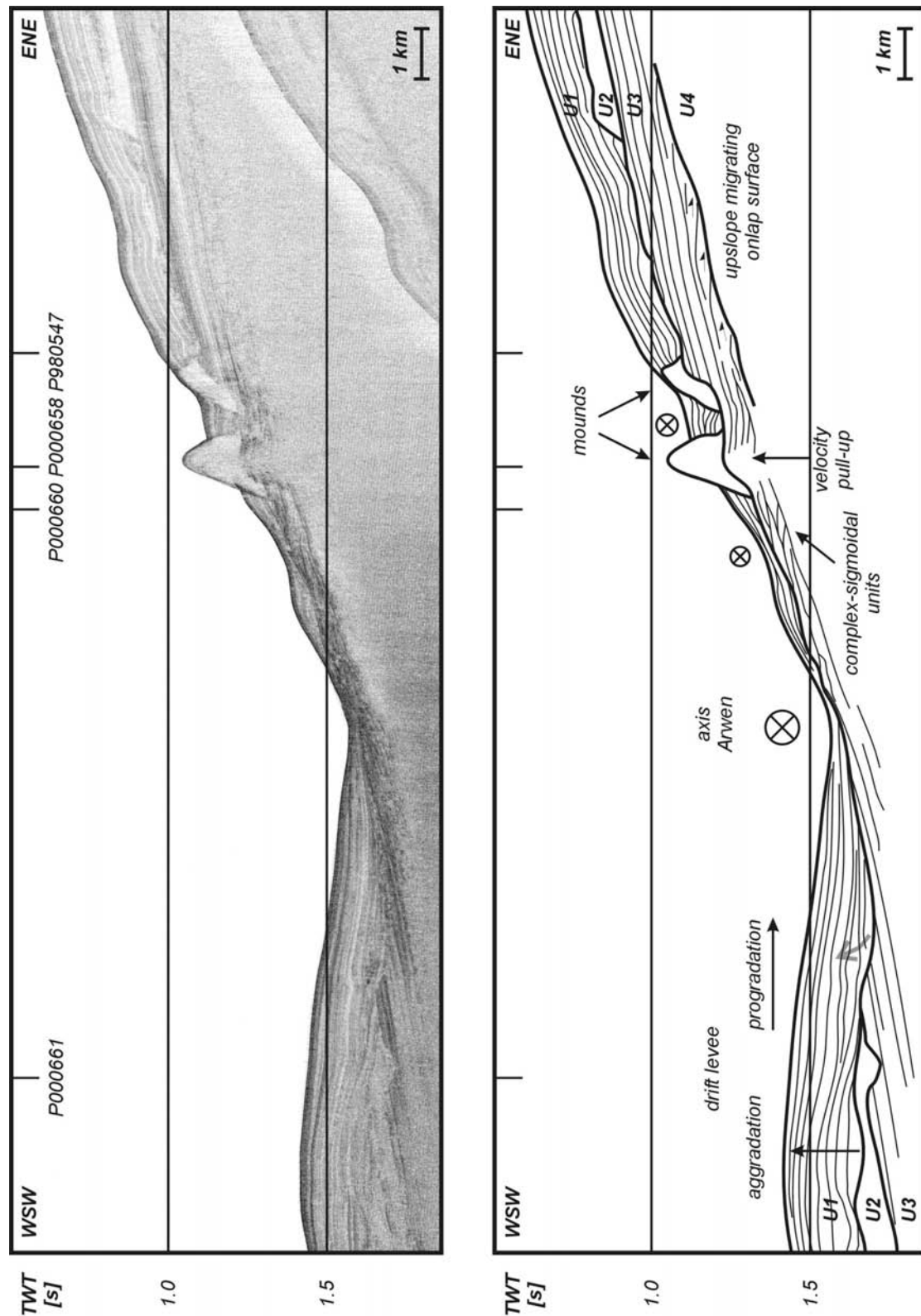


**Figure 6.3:** P980521: Overview profile featuring two mounds and sediment drift properties. Note the several erosional steps along the lower boundary of unit U1 and the incision into unit U3 at the WSW flank of the channel.

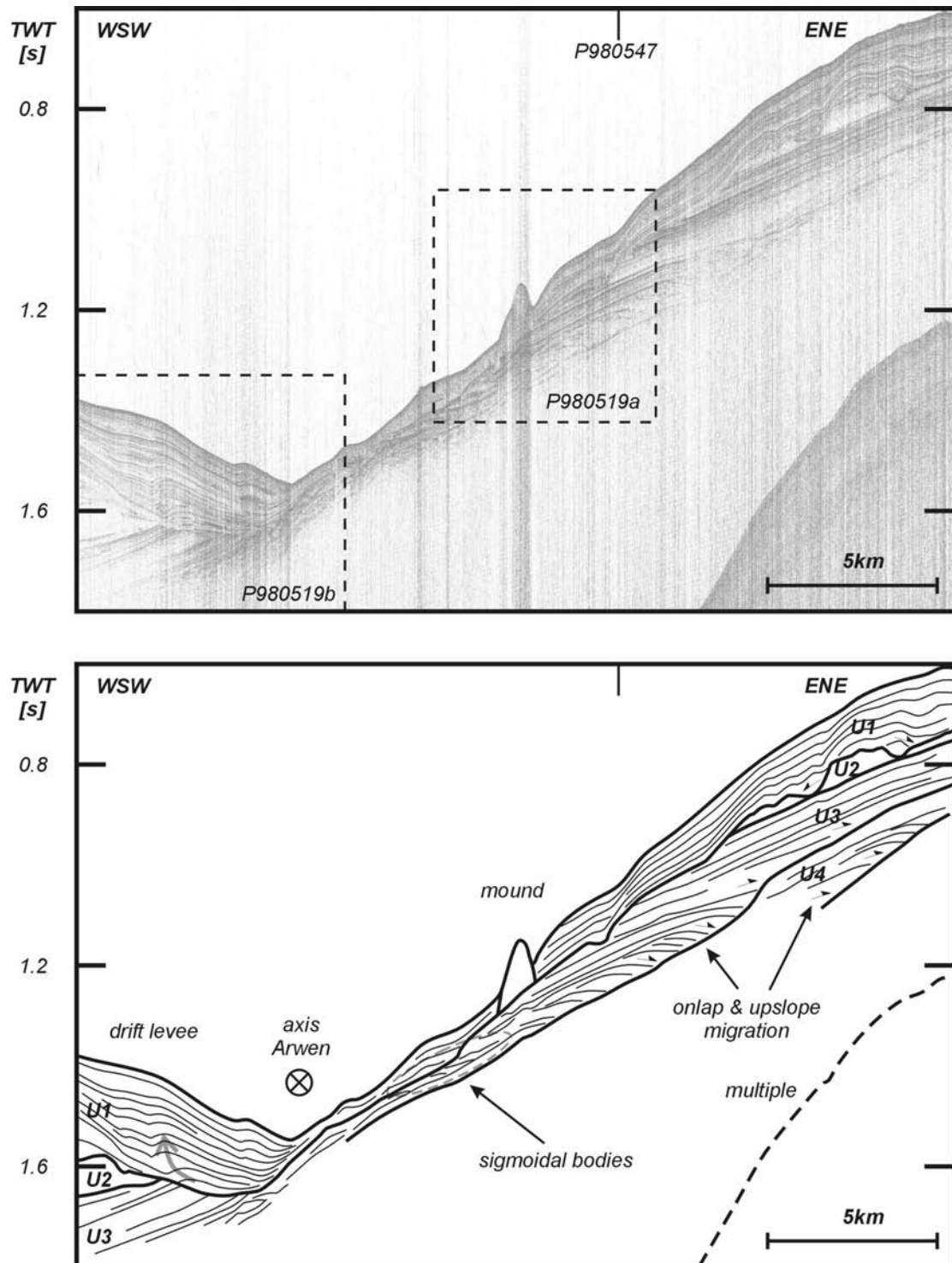


**Figure 6.4:** P980519: Overview profile, featuring a single mound on an eroded surface above sigmoidal deposits and the onlap of units U3 and U4 on their lower boundaries. The grey arrow indicates the retrogradation of the channel levee unit.

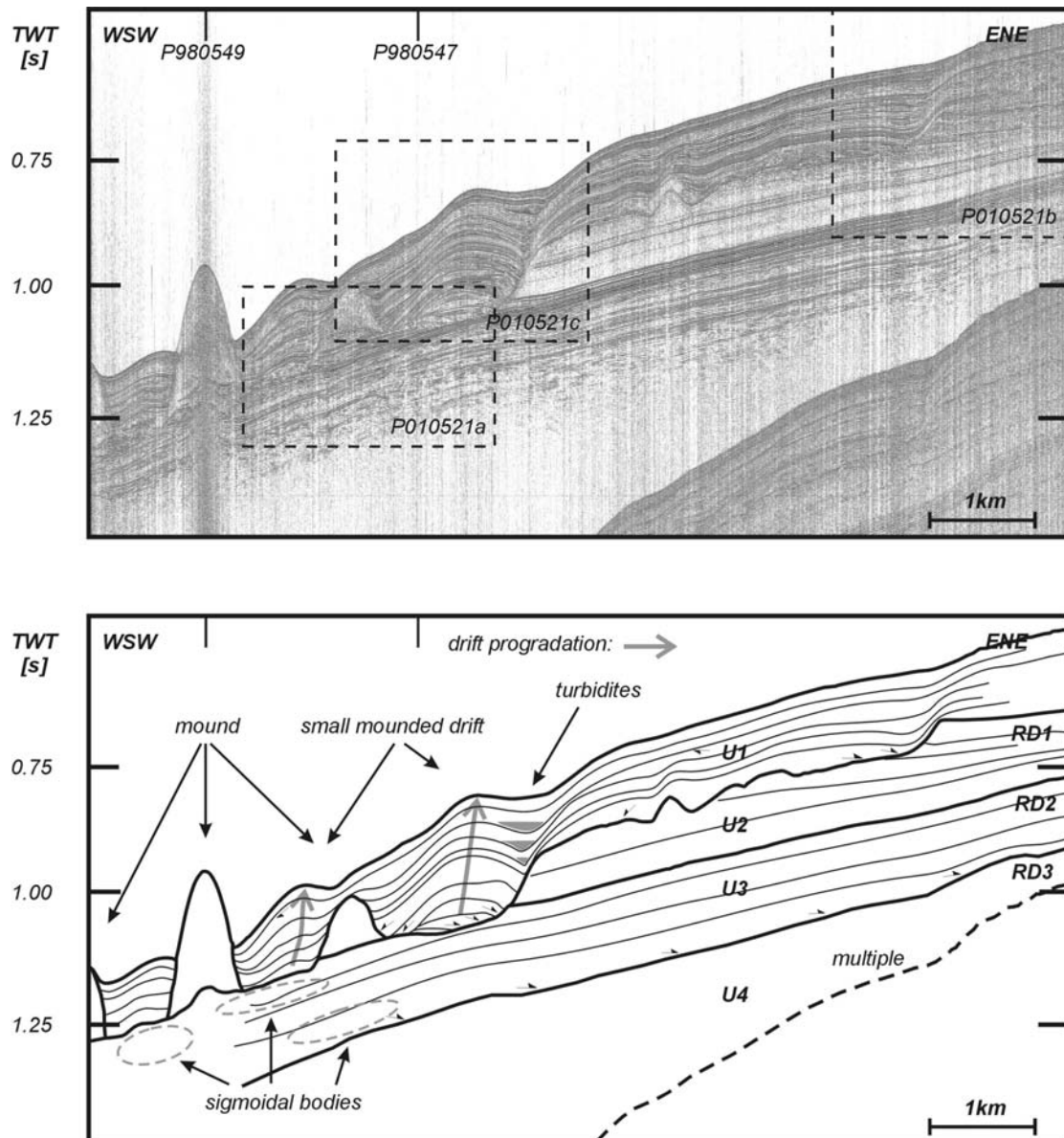


**Figure 6.5:** P010521: Overview profile along the eastern upper slope of the Porcupine Seabight, with a surface and buried mound and a heavily eroded unit U2. The grey arrows indicate drift progradation. Note the gradual change in acoustic facies along the ENE side of unit U2.

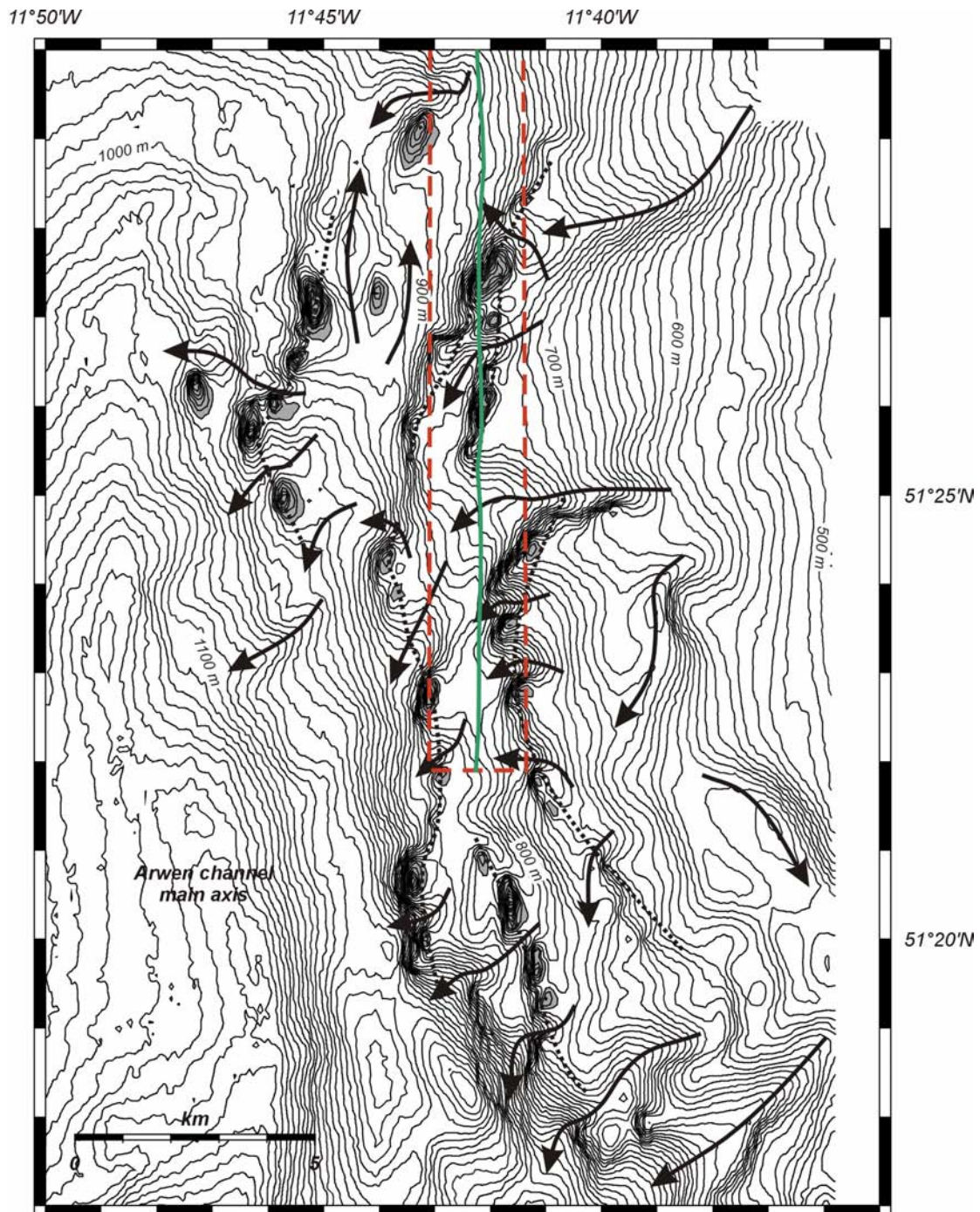


**Figure 6.6:** Multibeam bathymetry map illustrating the diversity of morphologies in the Belgica mound province. The contour interval is set at 10 m and all inferred outcropping mounds are indicated in grey. The dotted lines accentuate the apparent alignment of the mounds. The black arrows indicate the possible pathway of the currents running down the gullies close to the mounds. The position (green line) and coverage (red dashed area) of the side-scan sonar strip of figure 6.8 is also indicated.

Additionally, the mounds seem to be aligned in four along-slope trending ridges with steep west flanks (N 25-40° and N 160-170°). These are the ridges previously interpreted by Kenyon (1987) as slump folds. At the eastern side of the mound ridges the slope is generally shallower, suggesting an accumulation of sediments. These ridges are interrupted by downslope-running gullies flanking the northern or southern flanks of the mounds with an approximate N 225° orientation. However, sometimes a south-north orientation can be inferred. These gullies are relatively short (1 to 2 km) and they do not seem to coalesce directly with the Arwen channel, which seems to be the western limit of the Belgica mound province.

Together with the Celeborn-Galadriel channels, the Arwen channel is a major, partially alongslope directed channel recognized in the surveyed area (Figs. 6.1 and 6.6). The characteristics of these channels have already been described in chapter 1. According to Huvenne (2003), side-scan sonar observations in the Arwen channel infer the presence of local coarse channel floor deposits, suggesting recent activity with local accelerations of current velocity.

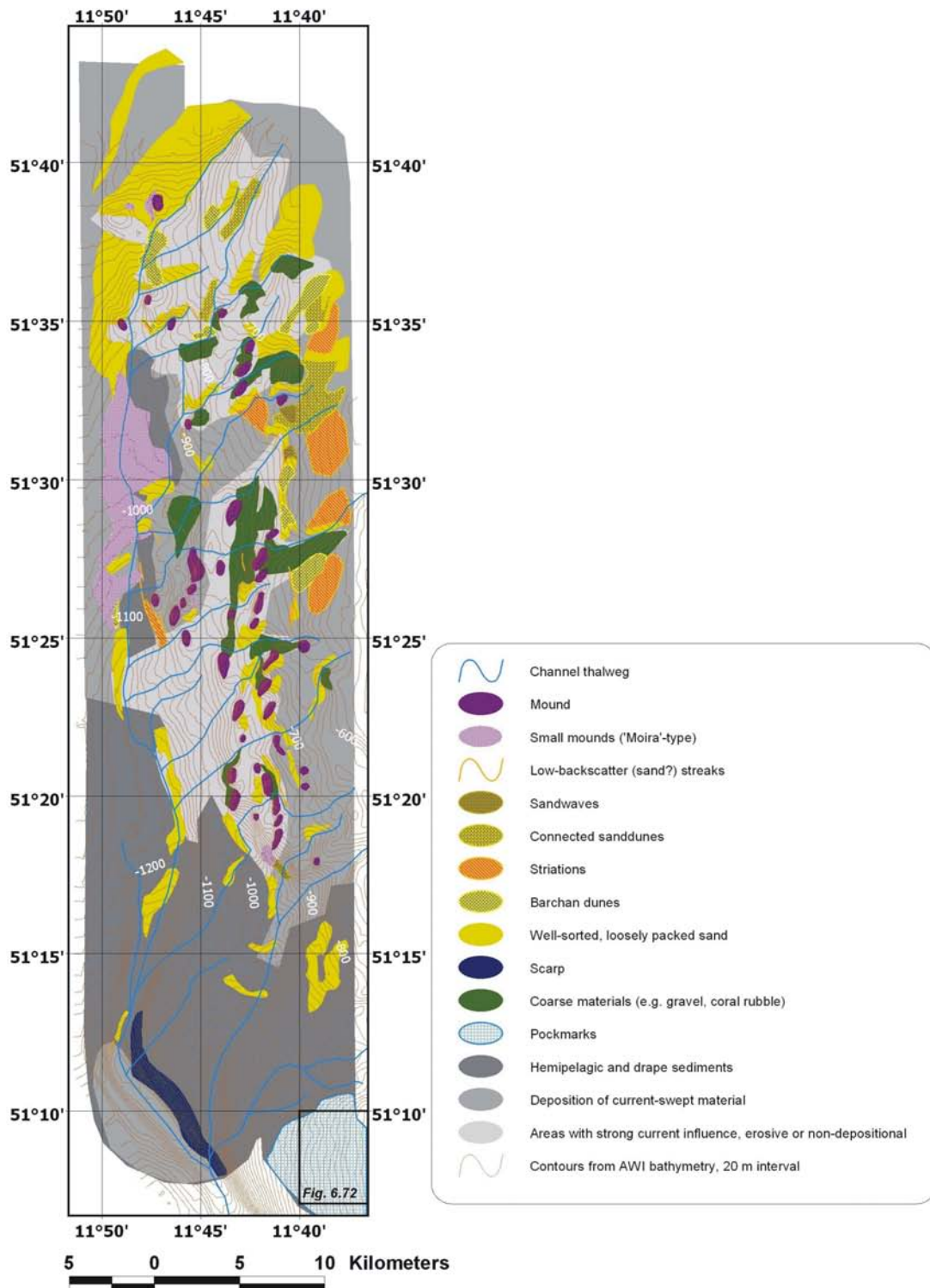


**Figure 6.7:** Interpretation and legend of the TOBI side-scan sonar and AWI bathymetry data sets in the Belgica mound province (Huvenne et al., submitted-b).

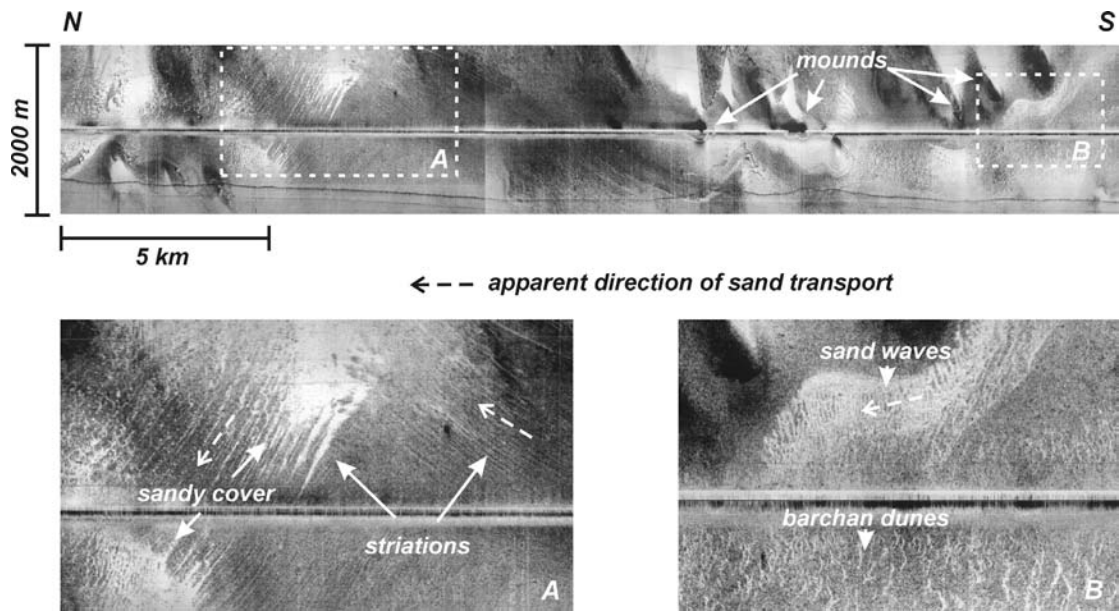


**Figure 6.8a:** Side-scan sonar profile (located on figure 6.6), illustrating the diverse seabed features surrounding the Belgica mounds.

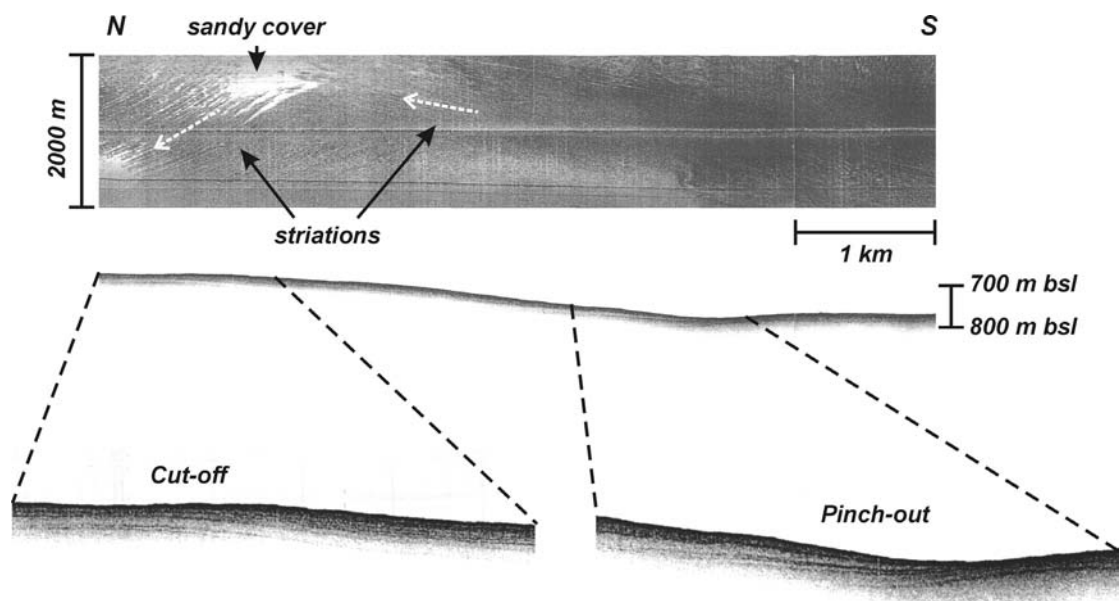


**Figure 6.8b:** Detail of figure 6.8a with echosounder profile illustrating the lensoid geometry of a sand sheet.

## 6.2 Units U4 and U3; markers of sediment drift development

### 6.2.1 Unit U4

This unit has been recognized on only a few profiles. By consequence, it is rather difficult to comment on the distribution and the characteristics of this unit. Only profiles located at the northwestern or northeastern extremity of our dataset show the presence of this unit (Fig. 6.9). Predominantly profiles P000665 (Fig. 6.2) and P980519 (Fig. 6.4) indicate this is a separate unit, after which a correlation was possible with other profiles.

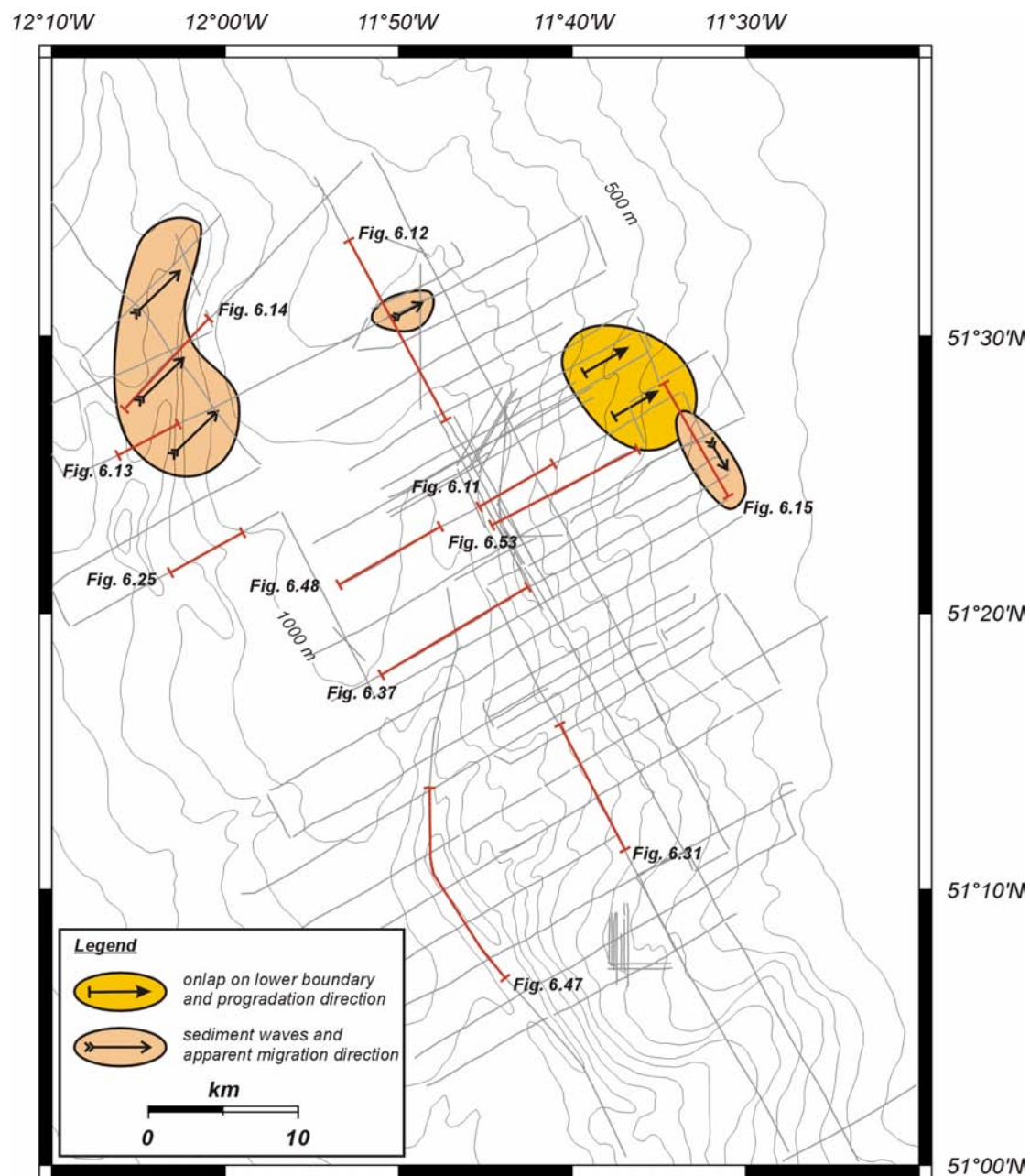


**Figure 6.9:** Facies distribution of unit U4, with positions of significant profiles. Zones of occurrence of sediment waves and onlap on the lower (RD4) boundary are indicated, together with inferred migration directions. All available profiles are presented by grey lines.

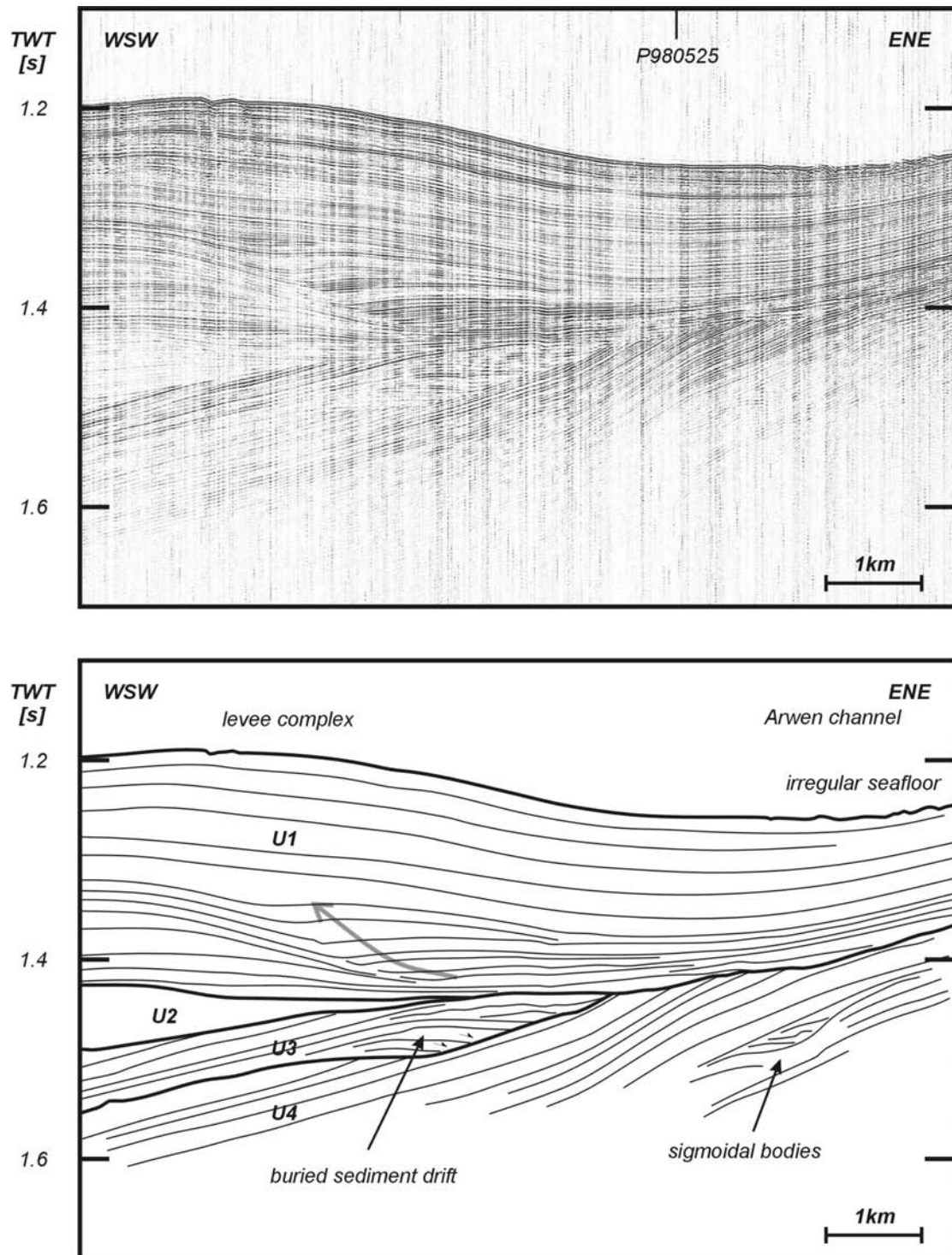


**Figure 6.10:** P000665a: Detailed profile of the special configuration of units U3 and U4. Note the onlap of the buried sediment drift within unit U3 and the irregular channel floor.

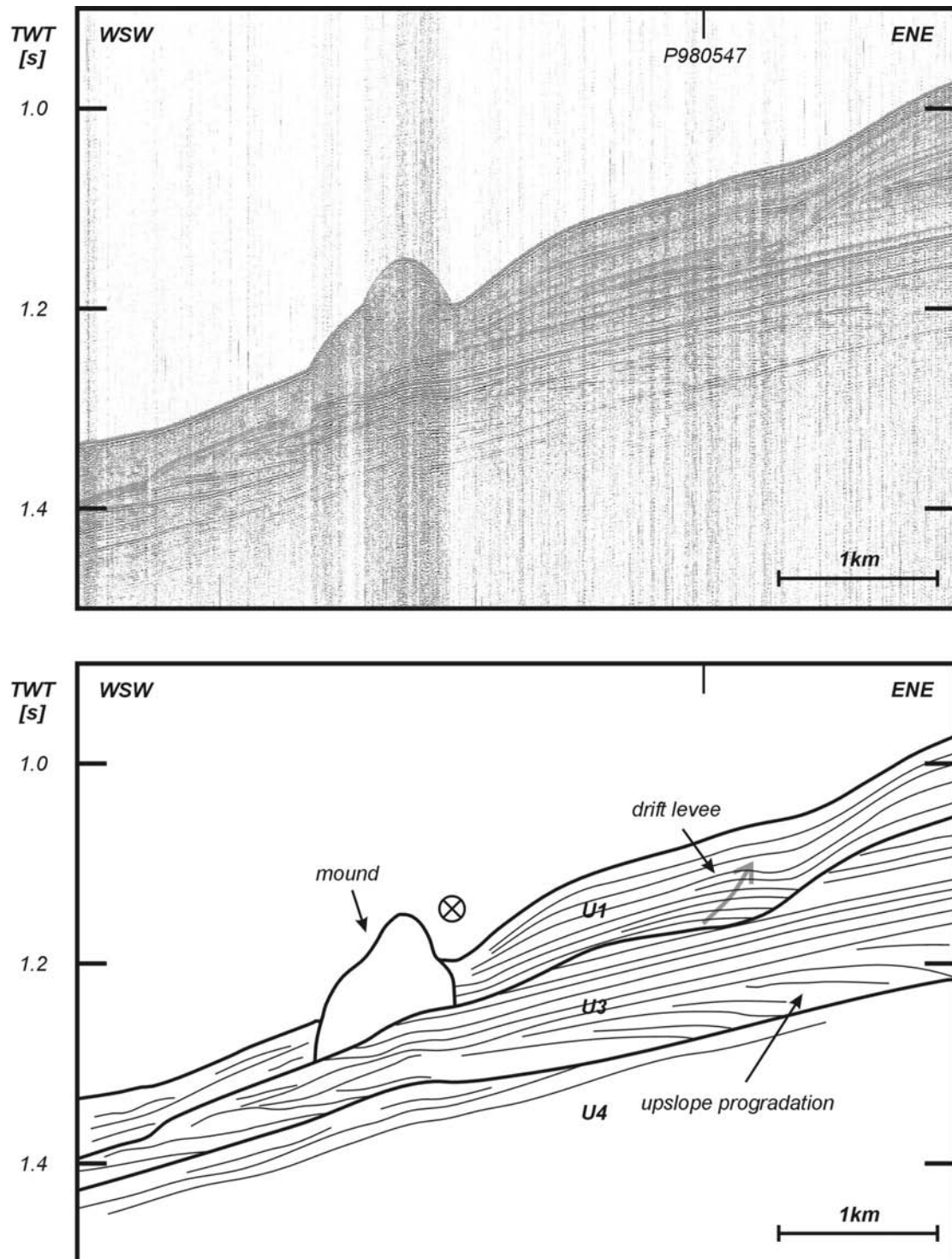


**Figure 6.11:** P980519a: Detailed profile focussing on the onlap and upslope progradation on the lower boundary of unit U3. Note the absence of unit U2. The grey arrow indicates the progradation of the small drift body installed downslope of a scarp in the upper boundary of unit U3.

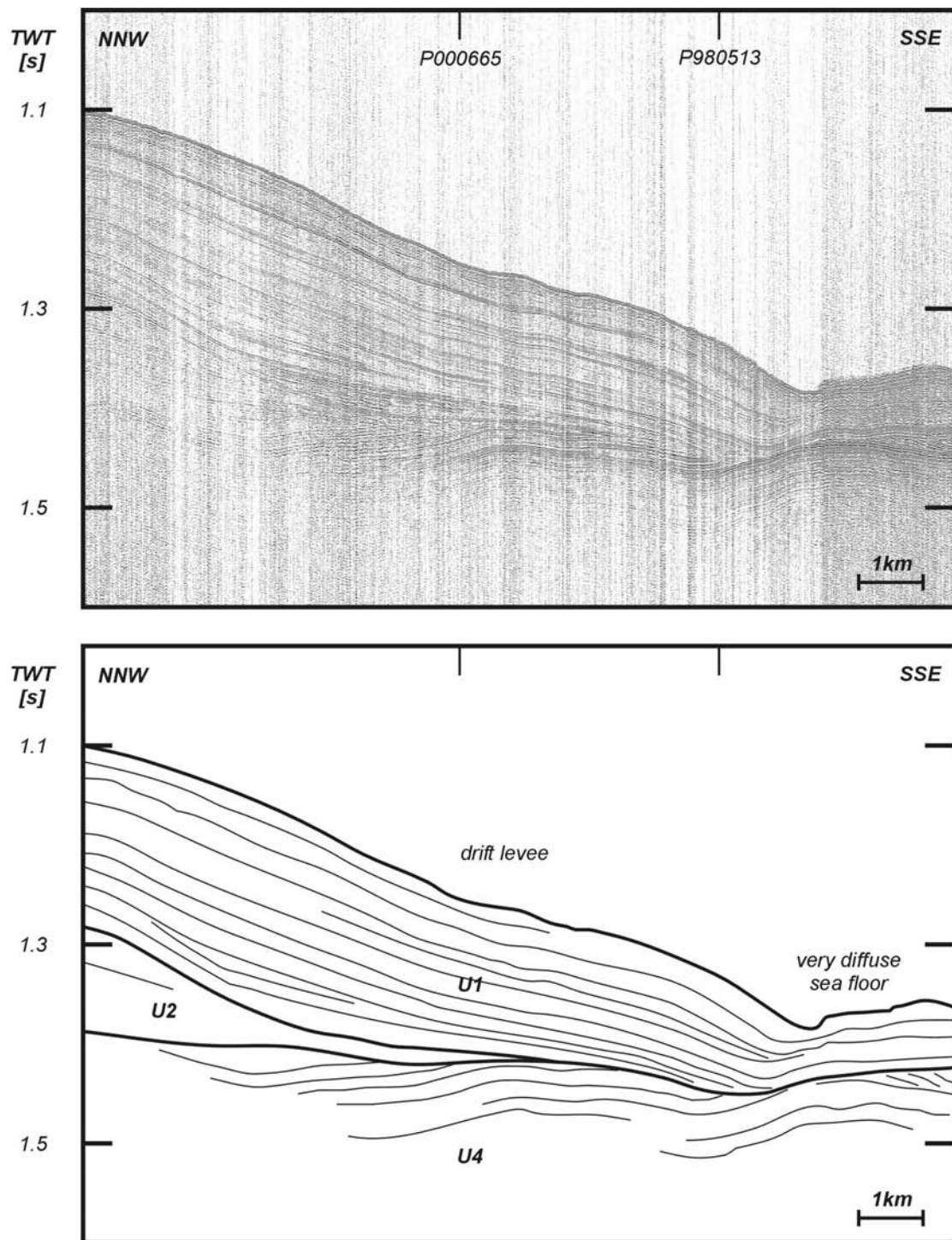


**Figure 6.12:** P980525: NNW-SSE profile across a broader part of the Arwen channel. The channel axis is characterized by a very diffuse seafloor. Note the undulating reflectors of unit U4, cut off by the lower boundary of units U2 and U1.

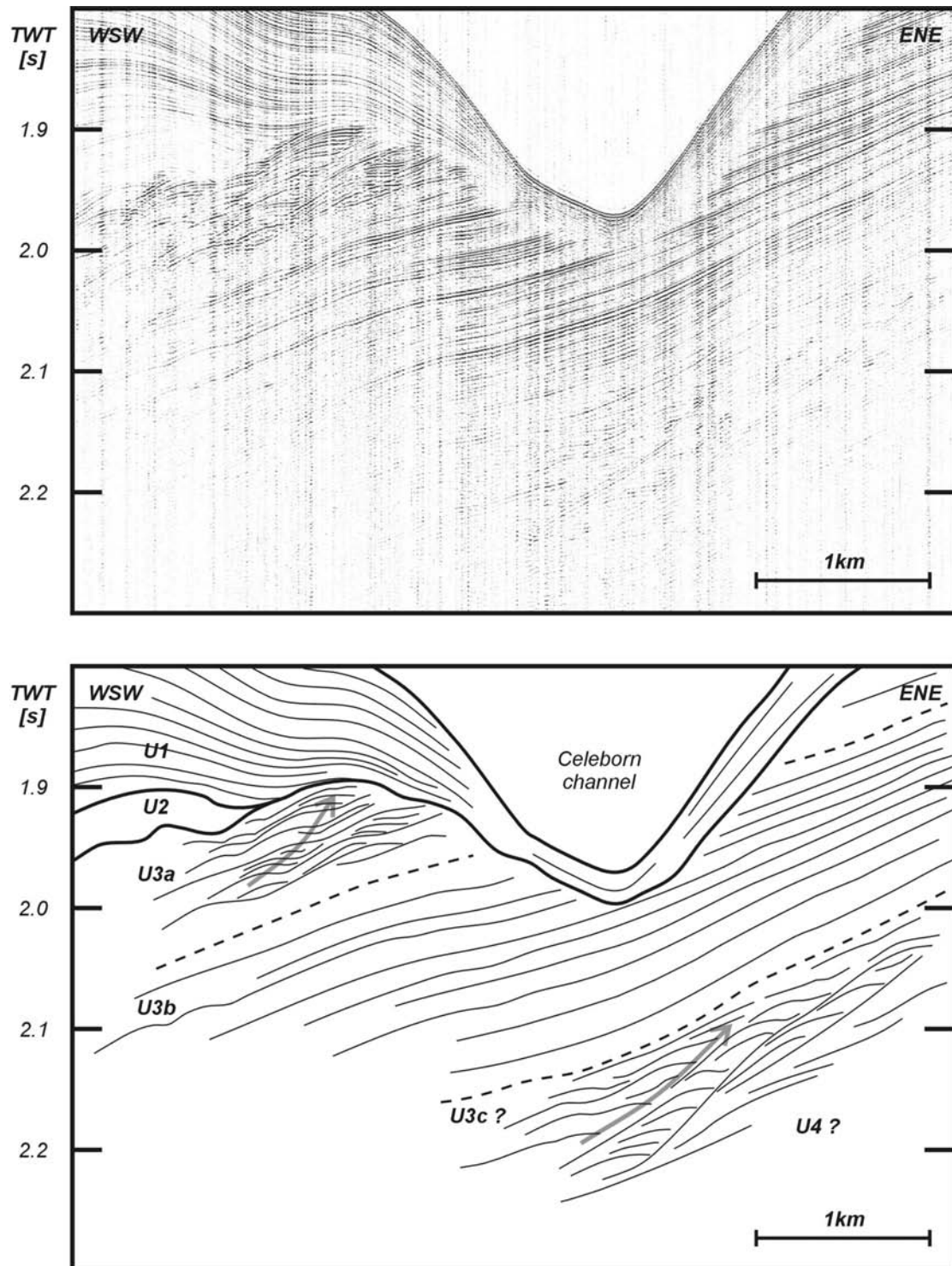


**Figure 6.13:** P000665b: Detail of profile P000665 (Fig. 6.2), underneath the Celeborn channel. The grey arrows indicate the upslope migration direction of the sets of sigmoidal units.

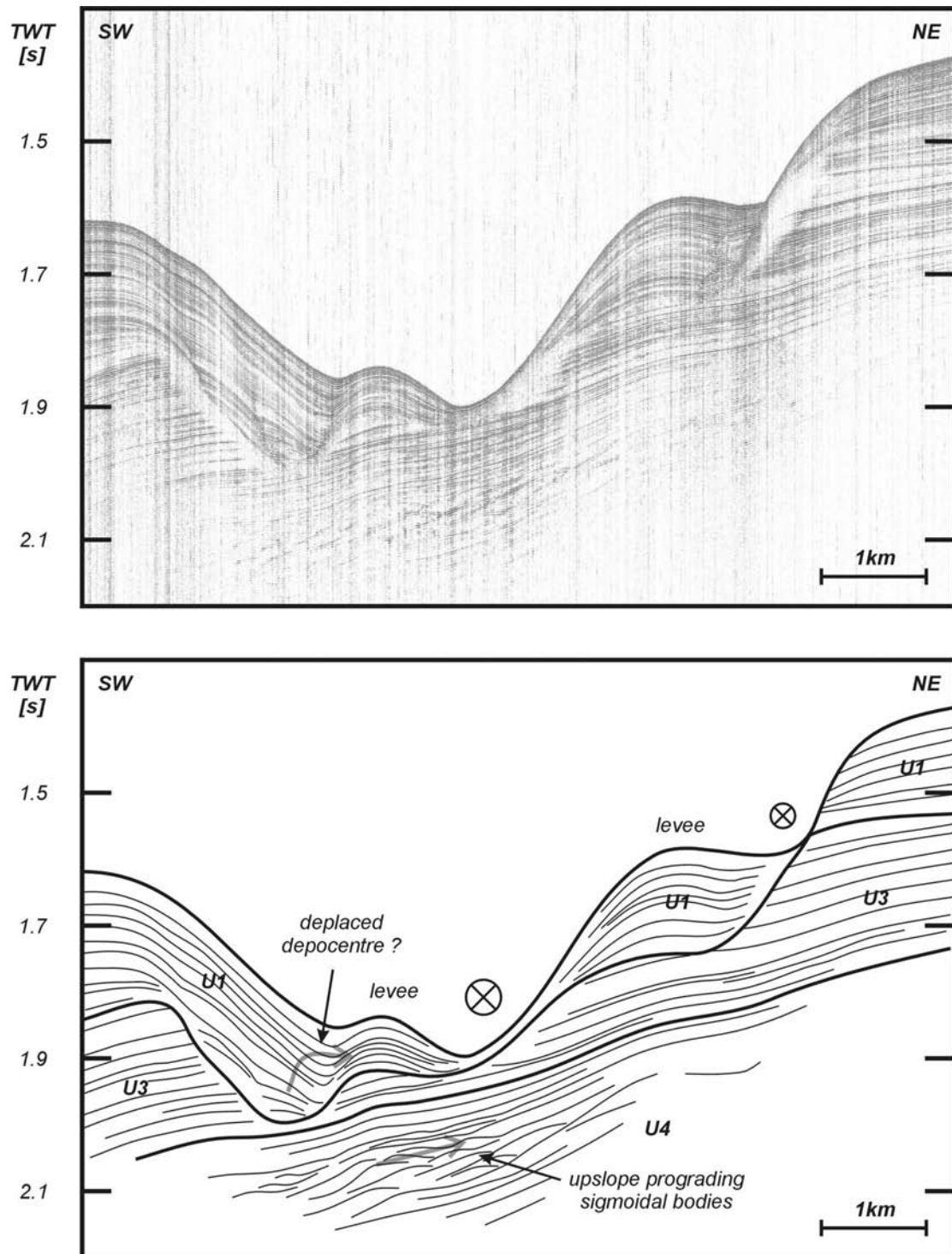


**Figure 6.14:** P000662: Profile across a wider and shallower part of the Celeborn channel. The channel is heavily eroded into unit U3, which overlies upslope migrating sigmoidal deposits of unit U4. From the SW, the U1 sediment prograde into the channel and form a small levee. Another levee-like structure is observed on the northeastern flank of the channel.

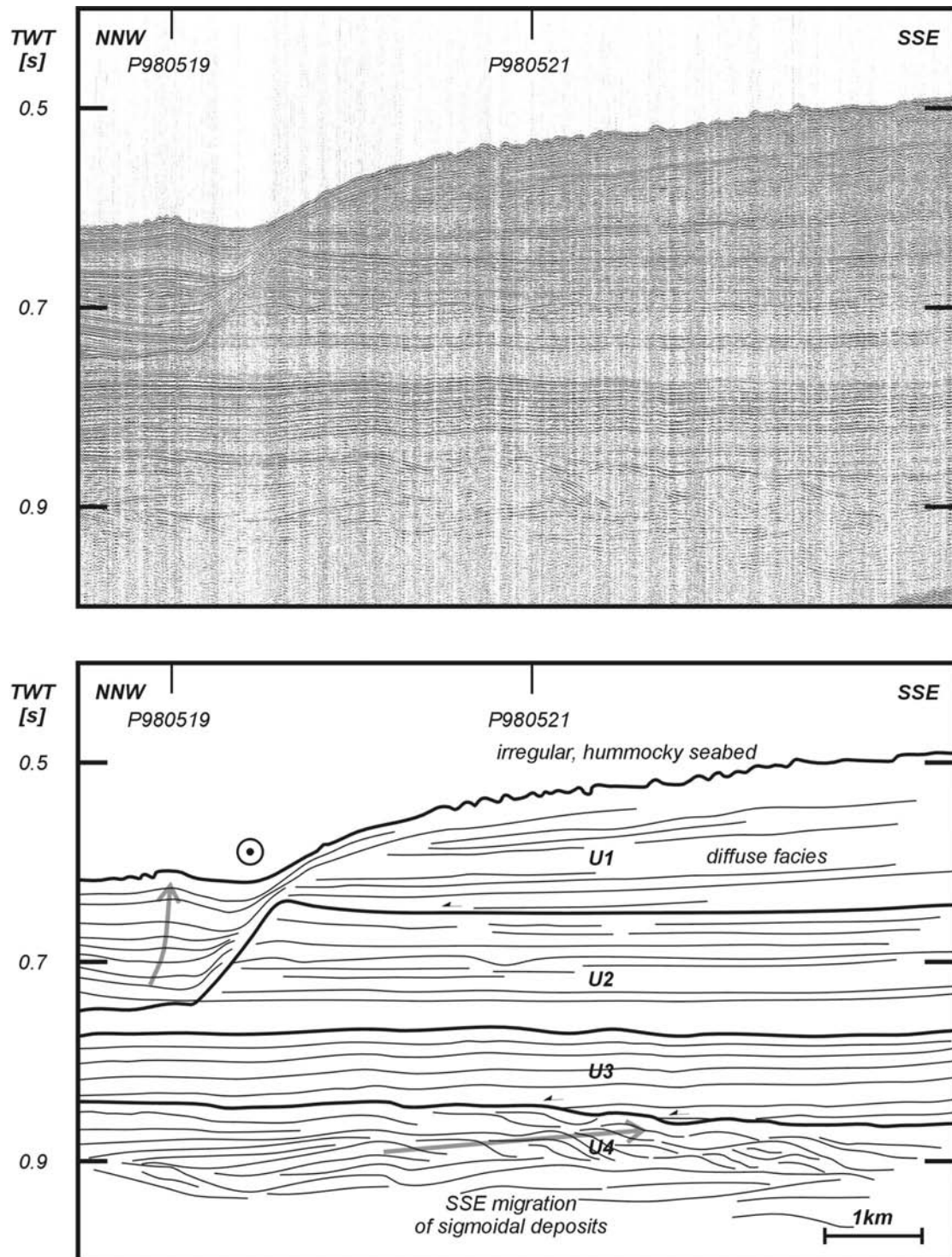


**Figure 6.15:** P010520: Detail of a profile located on the upper slope of the study area. Unit U4 is characterized by SE prograding sigmoidal deposits, while unit U3 features a relatively thin package of parallel reflectors, onlapping on the upper boundary of U4. Note the gradual change in acoustic facies from bottom to top of unit U2. Unit U1 shows an irregular, hummocky seabed and a diffuse facies.

### **6.2.1.1 Seismic characteristics and distribution**

In general, unit U4 is characterized by gently dipping parallel strata, with a basinward angle from 1.5 to 2° on WSW to ENE oriented profiles (Figs. 6.10 and 6.11). On one of the northernmost profiles, P980225 (Fig. 6.12), the reflector configuration seems to be gently undulating. The reflectors have rather low amplitudes and are not very continuous, which is most probably due to the detection limit of the seismic acquisition system.

However, on some particular locations, there is evidence of a more dynamic sedimentary environment. First of all, on the northeastern profiles, the lower boundary of this unit is visible (Fig. 6.7). As on figure 6.4, the lower part of this unit is onlapping on this lower boundary in a roughly NE direction. Secondly, underneath the Celeborn channel, presumably roughly NE prograding complex sigmoidal deposits are observed (Figs. 6.13 and 6.14), intercalated between subparallel reflectors. In the NE, however, only profile P010520 (Fig. 6.15) shows a very clear SSE progradation of sigmoidal units. The orientations of sigmoid progradation are, due to the few profiles, rather tentative.

More information is available of the upper boundary of unit U4. On most of the profiles (Figs. 6.12 and 6.10) it is observed as an unconformity.

### **6.2.1.2 A Late Paleogene sediment drift initiation**

The few observed characteristics of unit U4 suggest similarities with the large North Atlantic elongated sediment drifts (Stow *et al.*, 2002; Faugères *et al.*, 1999). They are all deposited on an erosive discontinuity and show an upslope progradation. Most of these sediment drifts are also associated with sediment wave fields with active upslope migration (Masson *et al.*, 2002; Howe, 1996). The presumed NE progradation of unit U4 suggests a north to northwest flowing current. Although it is difficult to propose a reliable progradation direction of the sigmoidal deposits, the ones observed on profile P010520 (Fig. 6.15) could be sediment waves, reinforcing the idea of a NE flowing current. Most of these fine-grained sediment waves have thicker beds on the upcurrent face, leading to an upcurrent and upslope wave migration (Flood & Shor, 1988; Howe, 1996; Wynn & Stow, 2002). This means that a similar sediment wave field located under the Celeborn channel was created under a flow oblique to the earlier suggested one. The complex nature of the sigmoidal deposits however suggests the real progradation direction might be different than a NE oriented one. On the other hand, the relationship between the orientation of sediment waves and the current flow direction is not really straightforward and might allow an oblique migration upslope and upcurrent (Wynn & Stow, 2002). It has also been recognized that in areas where bottom currents show frequent variations in flow directions, sediment waves can be produced, aligned at an oblique angle to the flow. If the responsible bottom currents were created under similar processes as in the present day, such a variable flow direction variability might have been present, creating a small field of oblique sediment waves.

According to McDonnell & Shannon (2001) and Stoker *et al.* (2002) the initiation of contour-hugging bottom currents and the establishment of sediment drifts in the North Atlantic basins and also the Porcupine Basin, most probably is an Intra-Eocene event. Therefore, the lower boundary of unit U4 is correlated with the Middle Eocene RD4 discontinuity. Throughout the Late Eocene and the Early

Oligocene, an elongated drift could be developed by an alongslope current on the eastern slope of the Porcupine Seabight. By the early Late Oligocene, a general sea-level fall, attributed to the construction of the ice caps (Pearson & Jenkins, 1986; Poag *et al.*, 1984) caused the RD3 erosive discontinuity that topped the Paleogene strata of U4.

## 6.2.2 Unit U3

### 6.2.2.1 Seismic characteristics and distribution

Unit U3 can be seen as the most diverse unit in this study area, due to the different reflector configurations that can be encountered. Generally, the reflectors have a moderate to high amplitude, with a moderate to low frequency. The reflector configuration of this unit is characterized by several levels of sigmoidal deposits intercalated between gently dipping subparallel deposits. Ideally, three different subunits can be distinguished, as illustrated in profile P010521a (Fig. 6.16). Unfortunately, due to the very irregular character of the erosive upper boundary, it is difficult to distinguish these subunits on all profiles.

**U3c** is the oldest subunit and is characterized by onlap on the lower (RD3) boundary (Figs. 6.10, 6.11, 6.16 and 6.3). Moreover, the onlap shows a roughly NE upslope progradation, limited to a NW-SE elongated zone at the northeastern edge of the data set. This zone is approximately 10 km wide and 40 km long (Fig. 6.17). On profile P010521a (Fig. 6.16), this zone of onlap is overlain by a set of upslope migrating sigmoidal deposits, which can be composed of different sets of stacked sigmoids (Figs. 6.18 and 6.19). Some profiles, like P000660 (Fig. 6.19) and P030509 (Fig. 6.20) show higher amplitude reflections (HAR) associated to these convex reflectors. Recent analysis suggests these HAR can be attributed to the presence of hydrocarbons (Henriet, pers. comm.).

The high energetic facies of subunit U3c is overlain by **U3b**, characterized by subparallel to continuous reflections (Figs. 6.11, 6.15, 6.21 and 6.19). In contrast to the other subunits, this facies is observed over the entire study area and is not limited to a certain zone. These mostly continuous strata are gently basinward-dipping with an angle between 1.75° and 2.5°.

The most characteristic facies, however, is presented by subunit **U3a**, which is located at the upper boundary with sigmoidal to chaotic reflector configuration. This configuration consists of small lenticular bodies enclosed between wavy reflectors, and changes upslope towards a subparallel reflector configuration, as illustrated in figures 6.22 and 6.23. These profiles, located in the southeastern part of the Belgica mound province, also show a kind of paleo-slope break, which separates a slope section with an apparent sub-horizontal stratification (0.75°) from a slope of approximately 2°.

The main part of these sigmoidal sediment bodies are located in a confined zone in the centre of the BMP (Fig. 6.17). This zone again has a roughly NNW to SSE orientation, is about maximum 10 km wide and 30 km long. The sigmoidal deposits are observed at a constant depth between 1.2 to 1.5 s TWT (Figs. 6.24, 6.22, 6.23, 6.5, 6.19 and 6.21). Moreover, it is located directly south to southwest of the earlier identified zone of onlap on the RD3 discontinuity. It should be noted that similar features were observed in profiles over the Celeborn channel (Figs. 6.25 and 6.10).

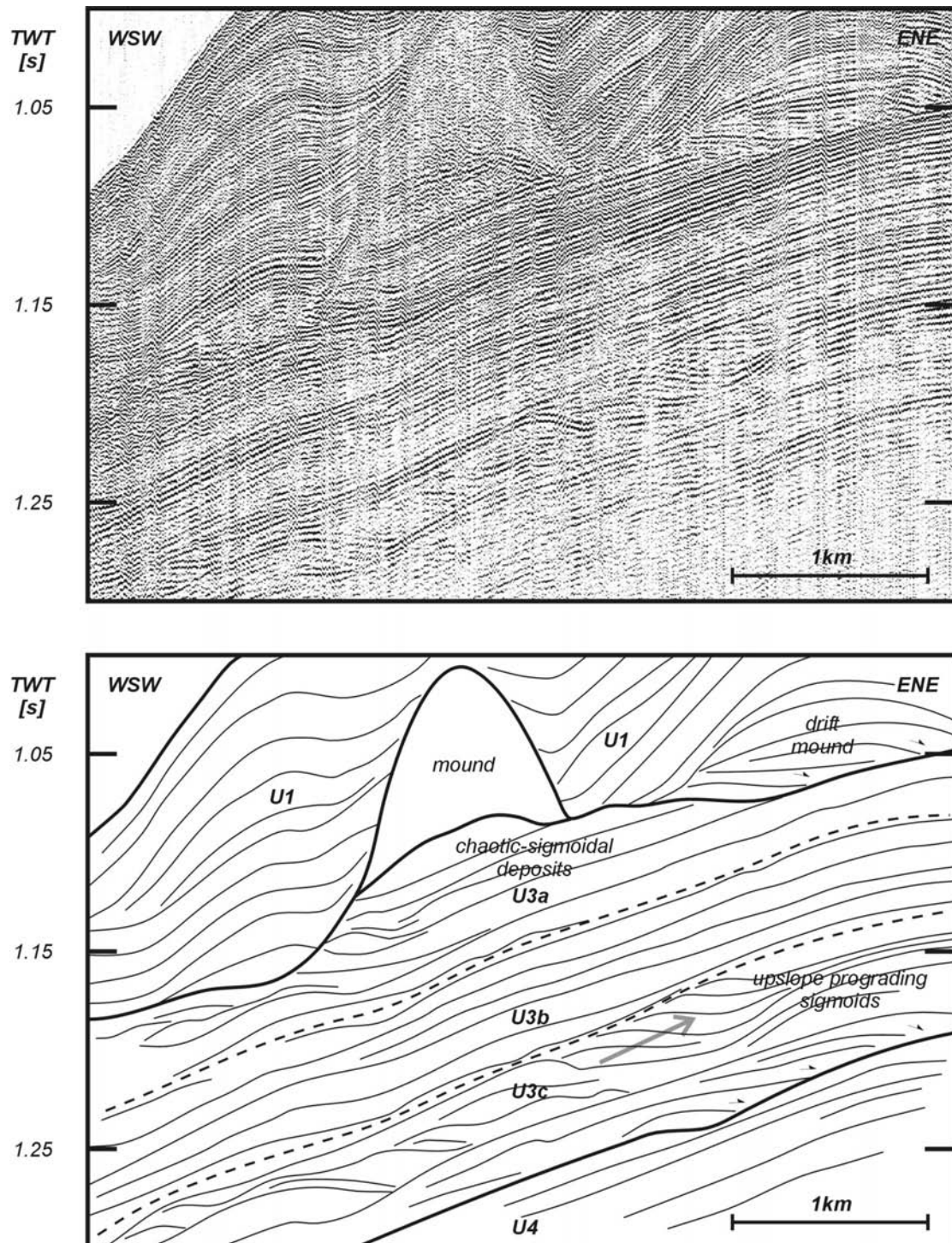


**Figure 6.16:** P010521a: Detail of profile P010521 (Fig. 6.5) with special attention on the subunits within U3. The grey arrow indicates the progradation direction of the sigmoidal units.

However, the sigmoidal units are located deeper and unfortunately no seismic profile is present to “genetically” link these sigmoidal deposits to those in the central part of the BMP.

Because these features were observed on a large number of profiles, the progradation direction might be estimated more accurately compared to the sigmoidal deposits observed in unit U4. On WSW-ENE profiles these bodies seem to migrate upslope to the ENE (Figs. 6.5 and 6.25), while on NNW-SSE profiles they

seem to migrate SSE-ward, though being more irregularly stacked (Figs. 6.24 and 6.21). Combined, this might suggest a probable E to ESE migration direction of these sigmoidal units. A small set of profiles, located south of BMP, also shows a clear E progradation of sigmoidal deposits in a same depth range (Fig. 6.26).

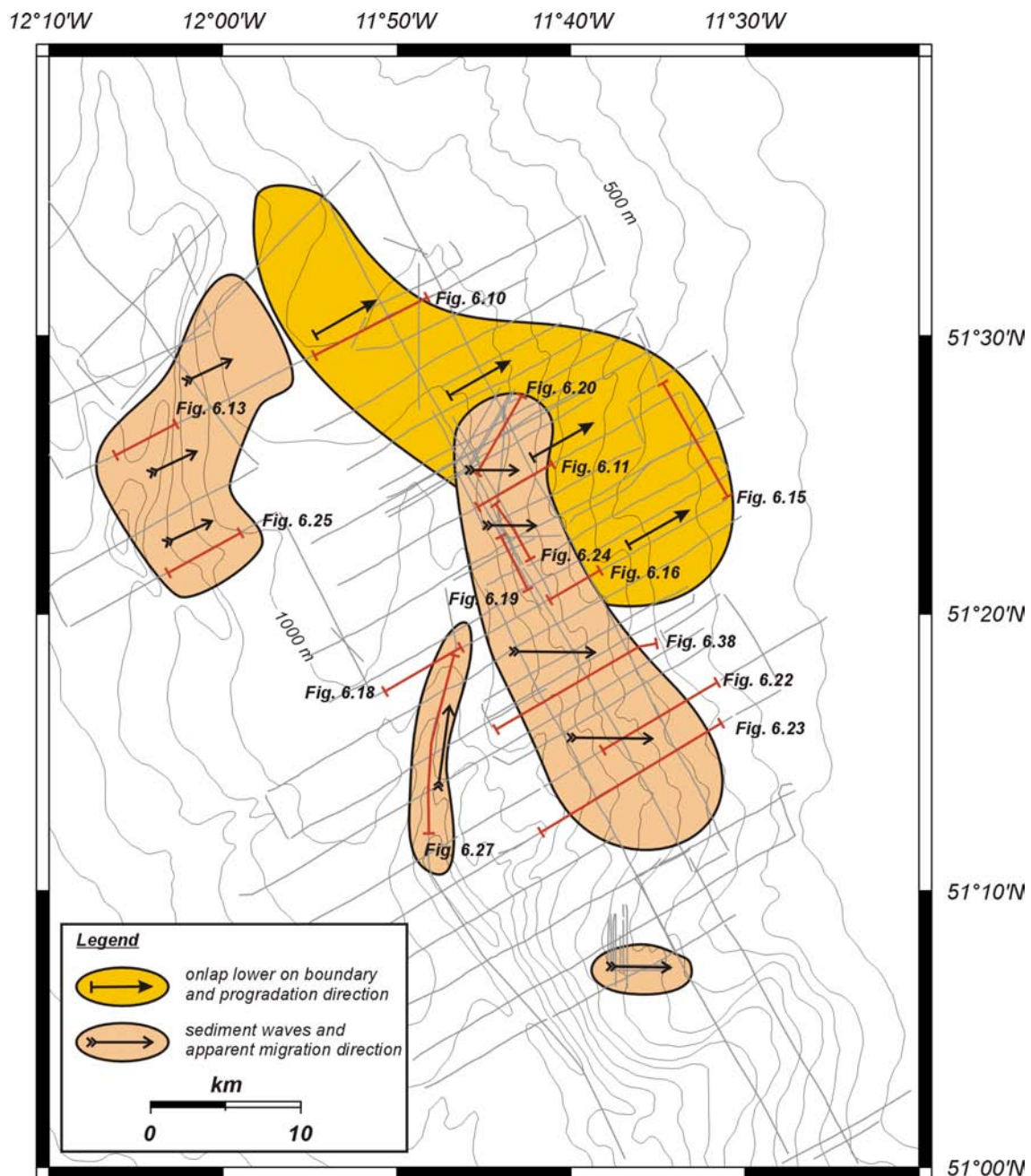


**Figure 6.17:** Facies distribution of unit U3, with positions of significant profiles. Zones of occurrence of sediment waves and onlap on the lower (RD3) boundary are indicated, together with inferred migration directions. All available profiles are presented by grey lines.

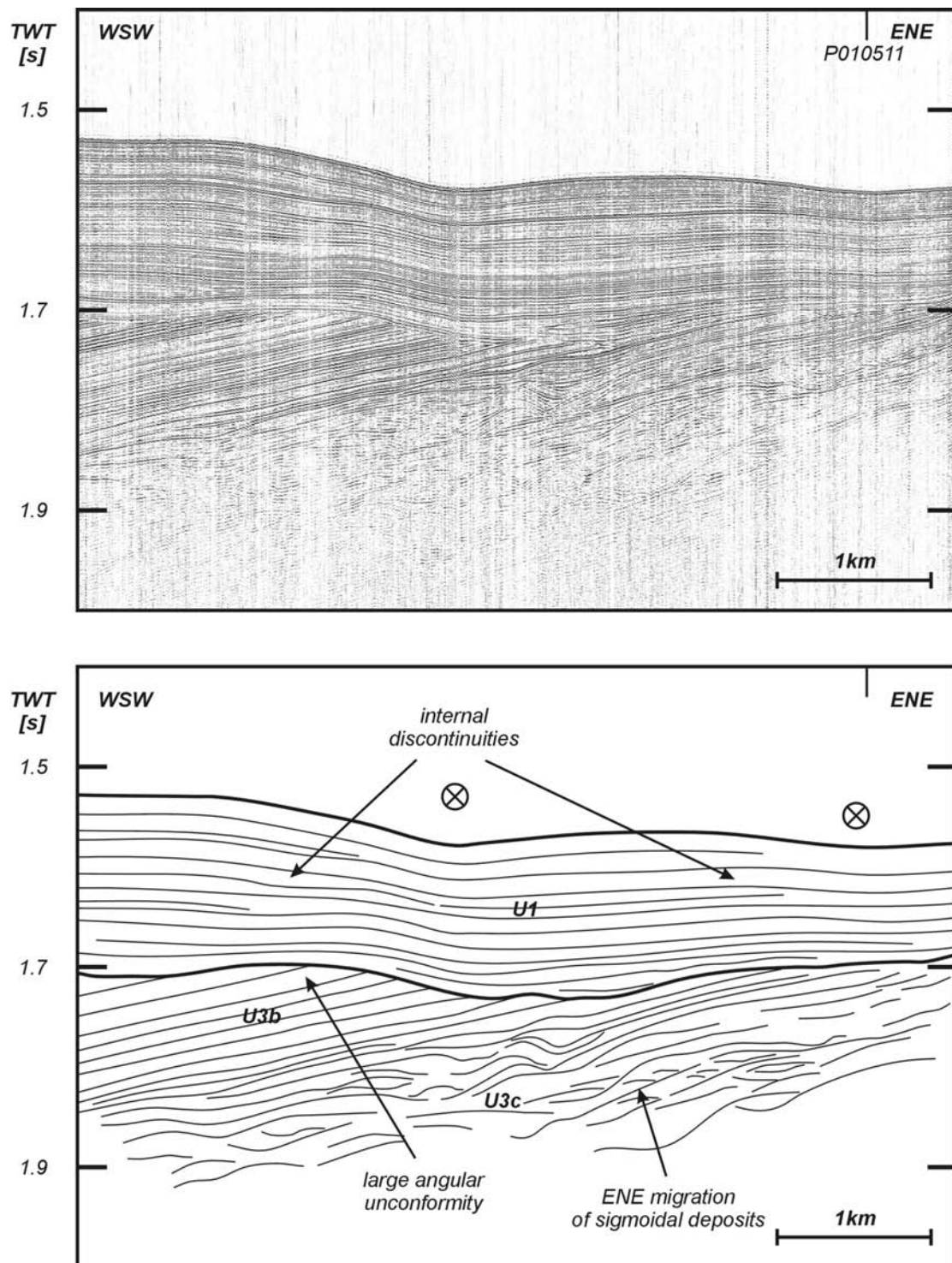


**Figure 6.18:** P010529: Detailed profile of ENE prograding sigmoidal deposits within unit U3, underneath the main axis of the Arwen channel. Due to different current flow axis, several discontinuities are observed within unit U1.

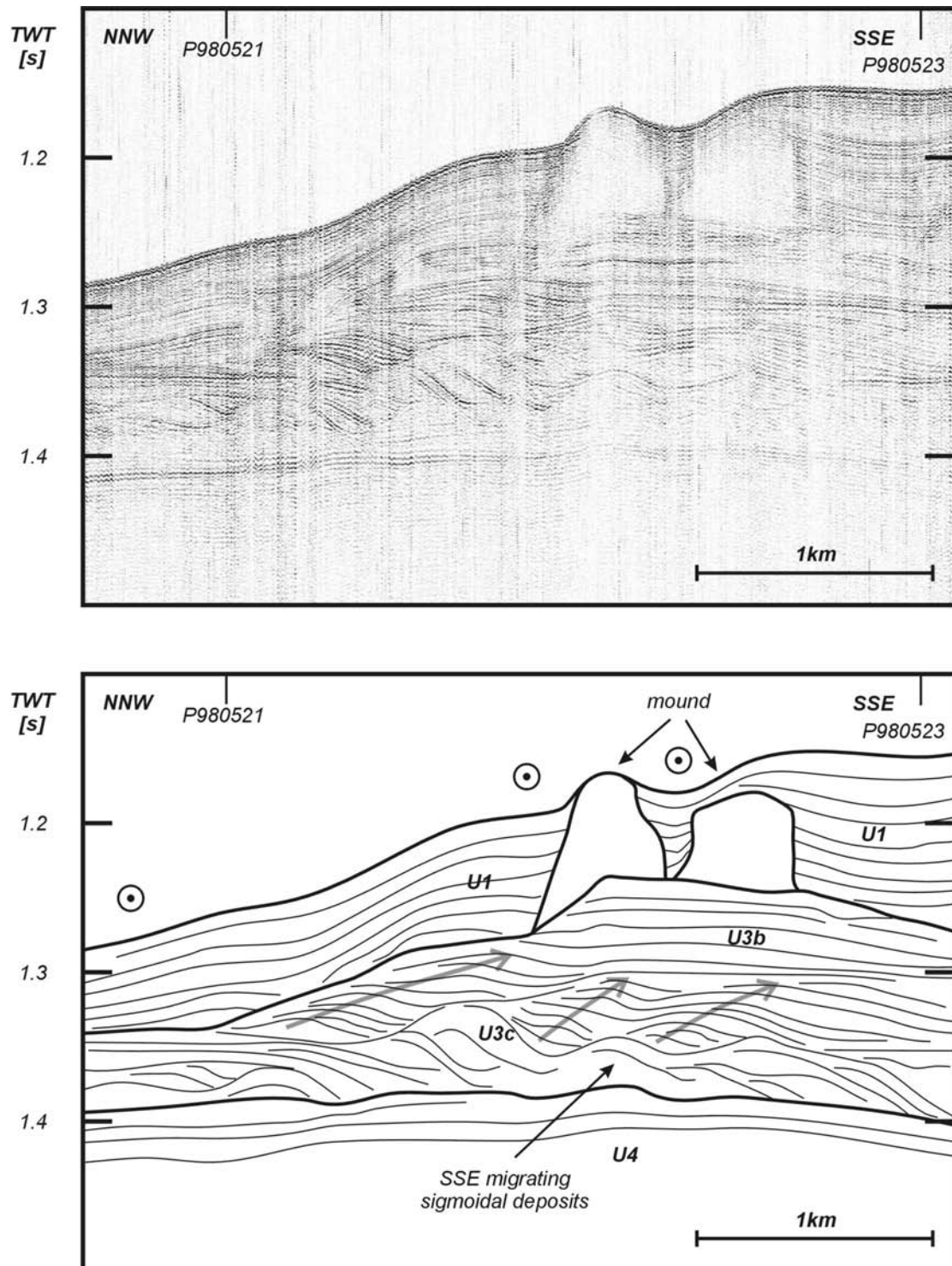


**Figure 6.19:** P000660: Detailed profile indicating the clear SSE progradation as observed on alongslope profiles. Note the subtle upper discontinuity of unit U4. Two mounds have been installed on a probable scarp eroded into unit U3.

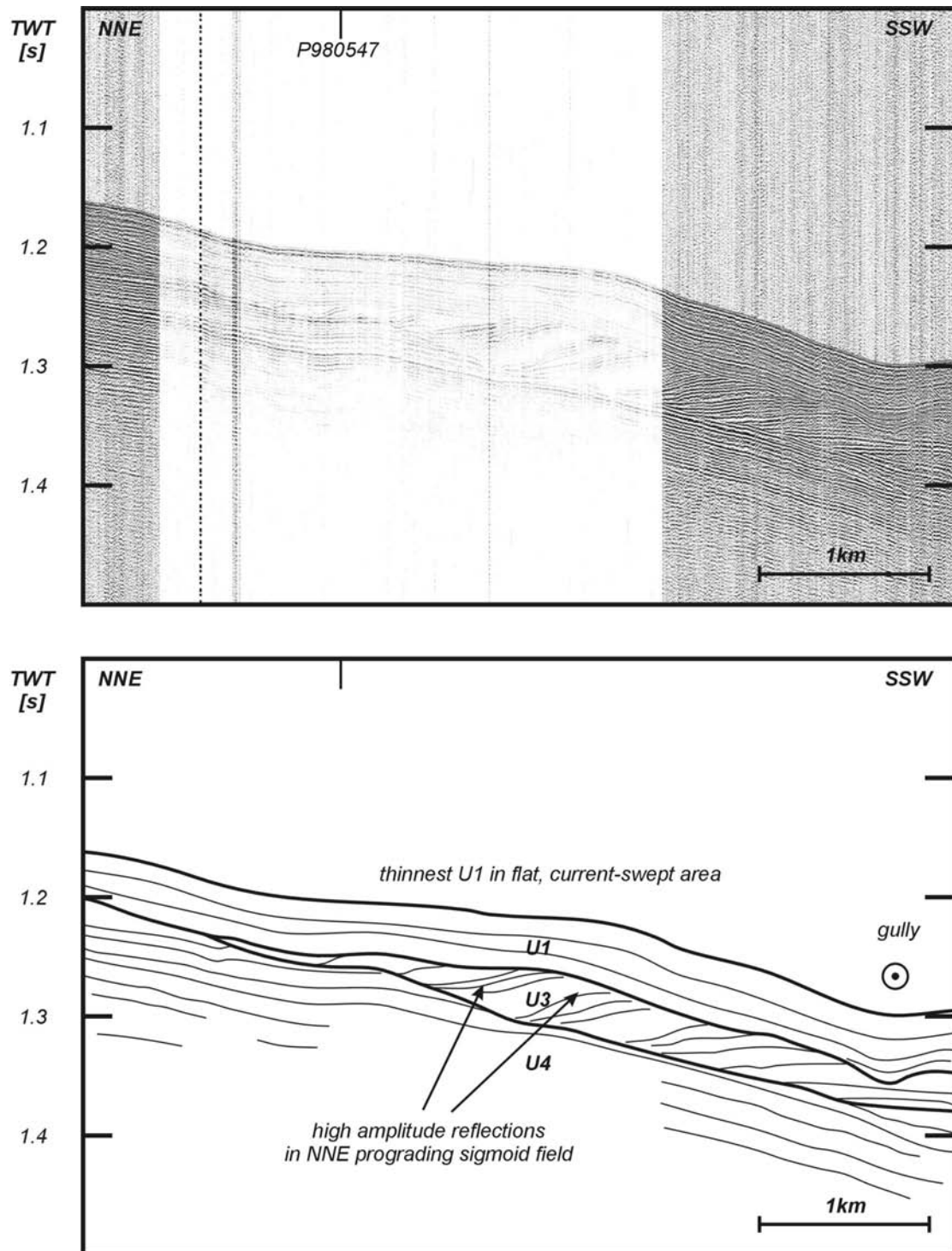


**Figure 6.20:** P030509: Profile located in a flat area in between to mound ridges. Unit U1 is extremely thin due to an intensified current action. Note the NNE progradation of the reflectors in unit U3.

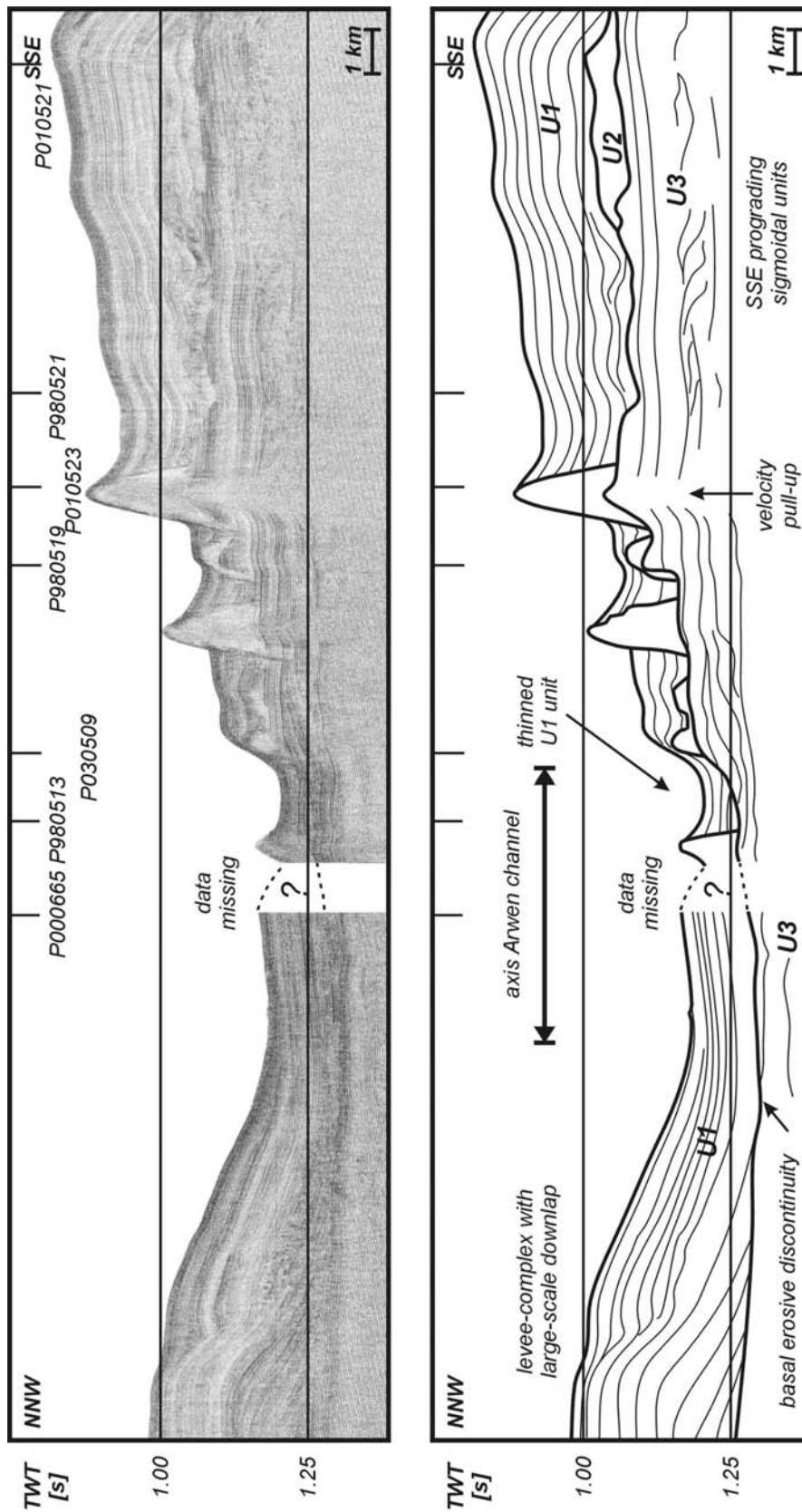


**Figure 6.21:** P980547: Alongslope overview profile, illustrating the variability of especially units U2 and U3. Note the elevated position of unit U3 underneath the surfacing mound.

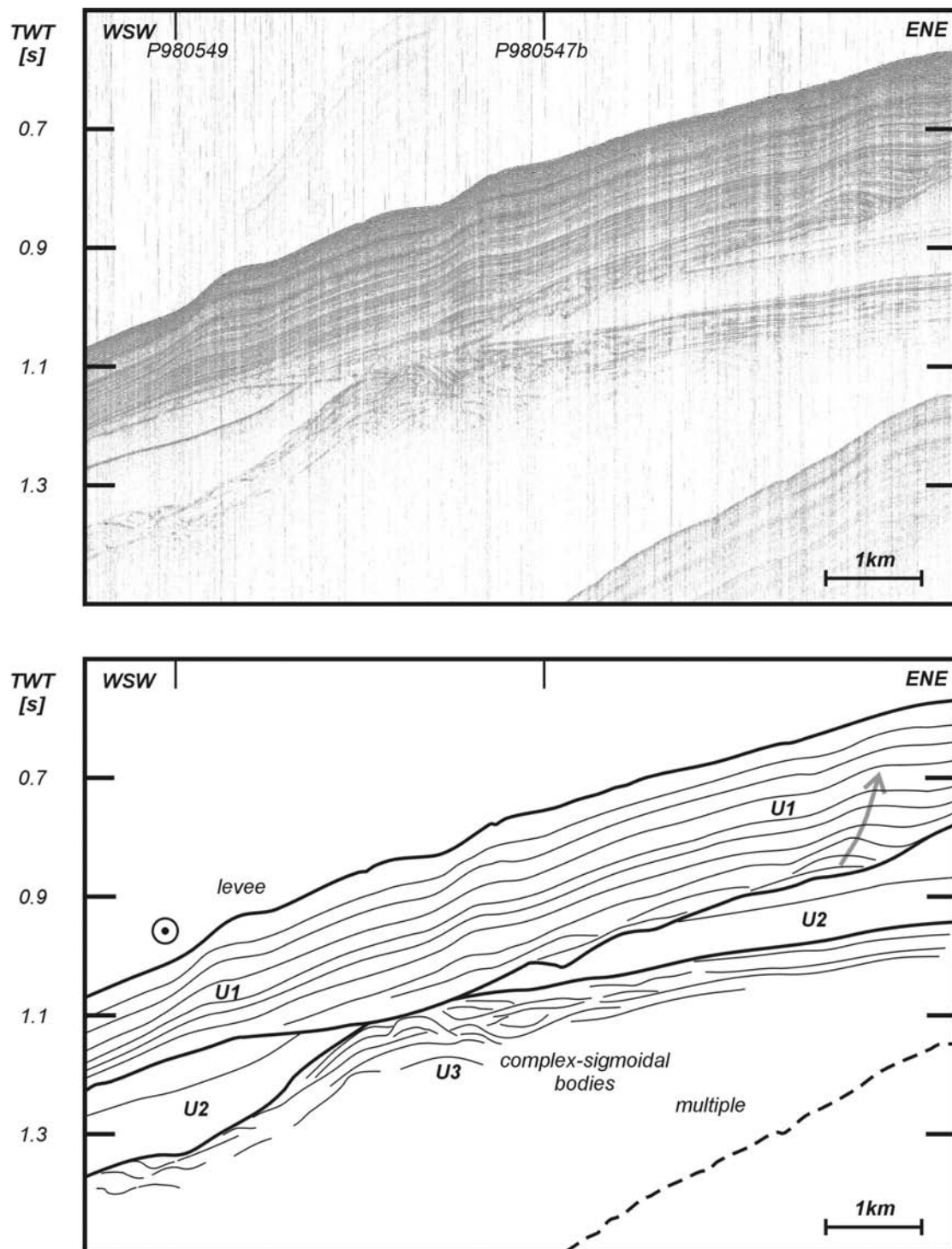


**Figure 6.22:** P970531a: Overview profile illustrating the complex sigmoidal deposits in unit U3, as well as the heavily eroded upper part of unit U2. Also note the gently wavy reflector configuration of unit U1. The grey arrow indicates an upslope progradation.

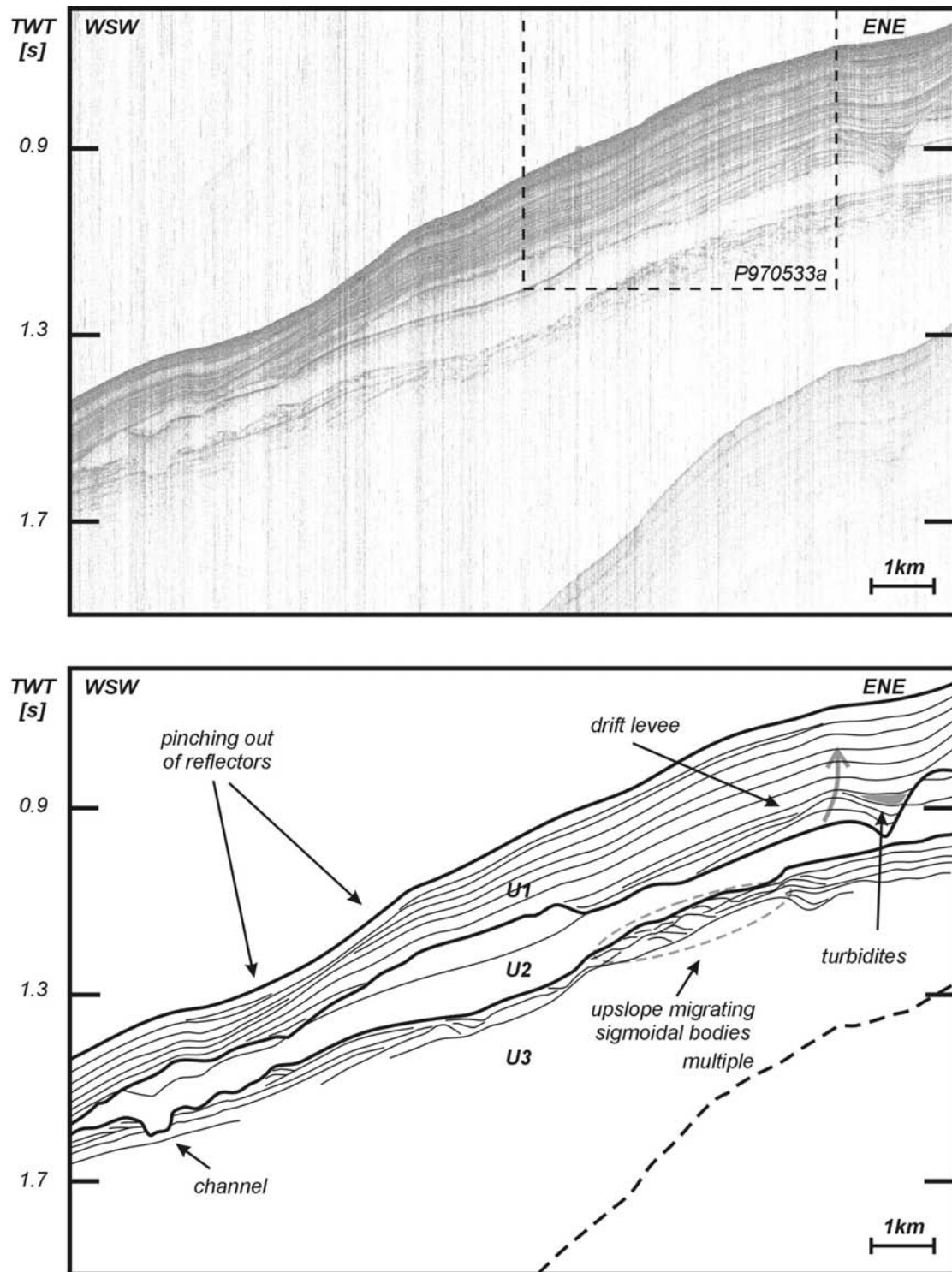


**Figure 6.23:** P970533: Overview profile illustrating the variability of units U1 and U2. Note the channel-like incision into unit U3, created during the RD2 erosion event. The grey arrow indicates the progradation of a small drift levee.

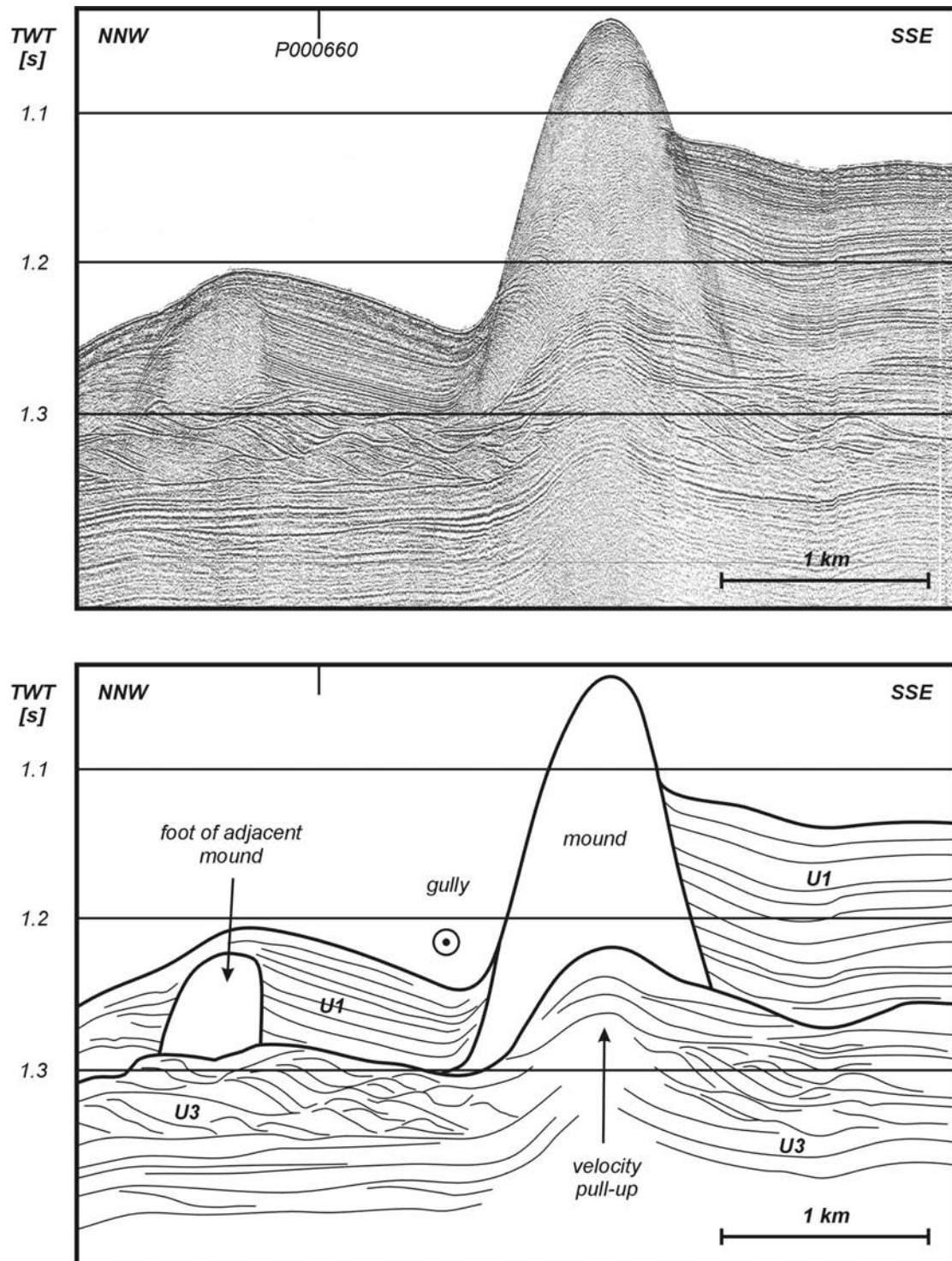


**Figure 6.24:** P000658: Detailed profile along a giant single mound, overlying a wide variety of SSE prograding sigmoidal units within unit U3. Note the asymmetry in thickness between the SSE and NNW side of the mound, due to the current action along the NNW flank of the mound.

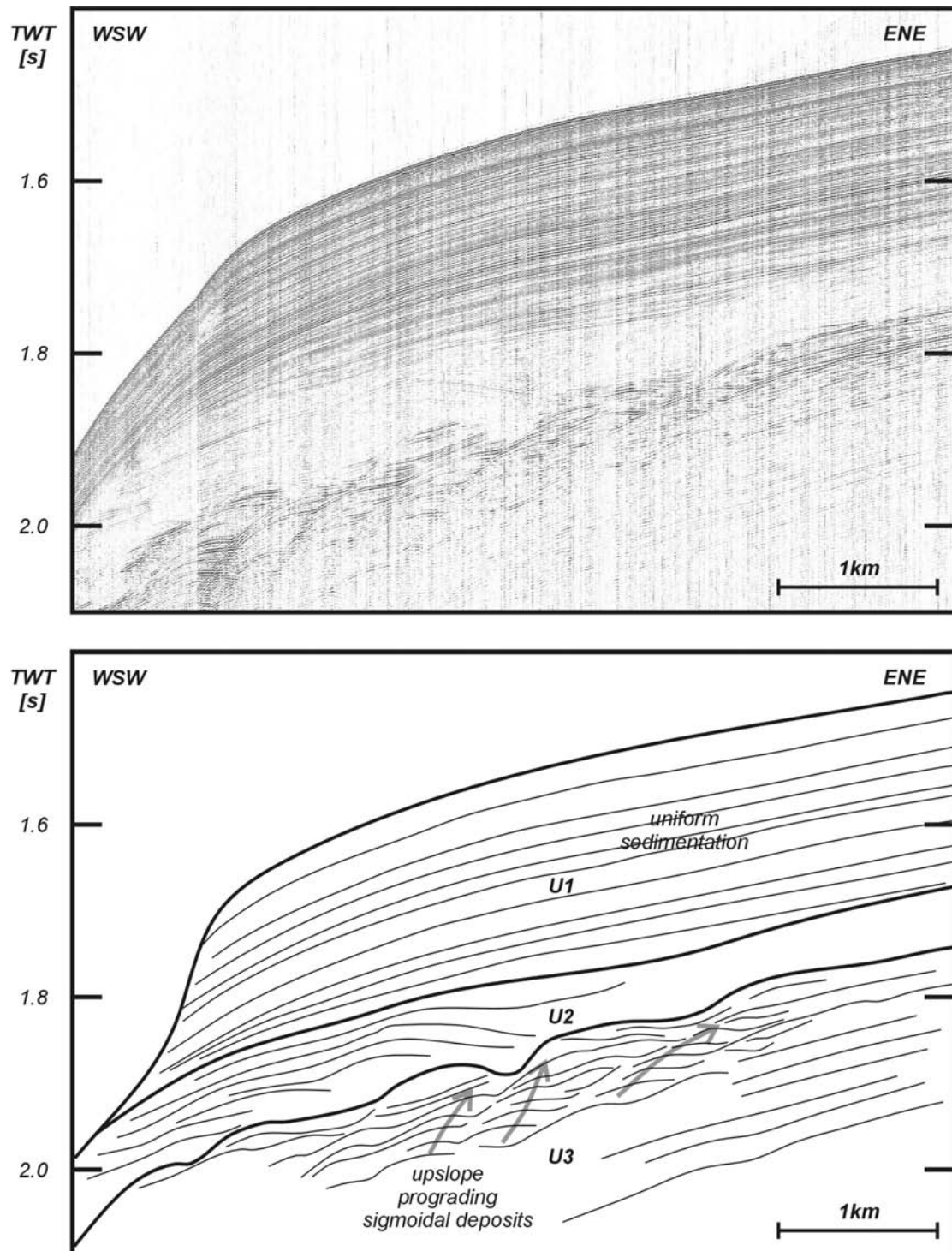


**Figure 6.25:** P010531a: Profile illustrating the eastern flank of the Celeborn channel. The lowermost unit U3 is characterized by upslope migrating sigmoidal deposits (grey arrows). Its upper boundary is the undulating RD2 discontinuity. Unit U1 shows a very uniform, hemipelagic sedimentation.

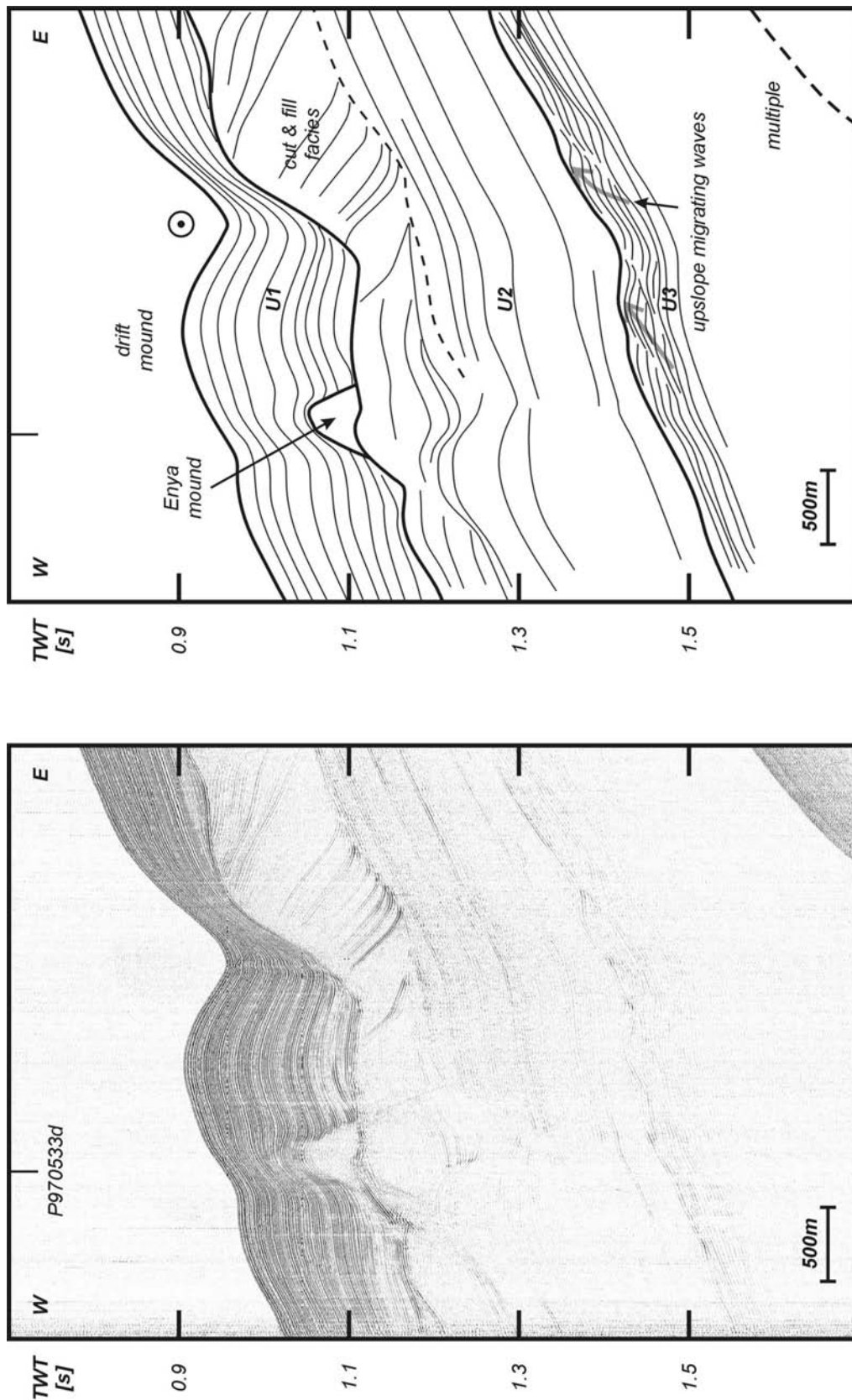


**Figure 6.26:** P030531: Profile across the Enya mounds, illustrating a very thick unit U2 with several high-amplitude reflectors. Again, the upper part of unit U2 is characterized by cut and fill facies. Underneath unit U2, also clearly upslope migrating sediment waves are observed. A small Enya mound is observed, associated with a mounded U1 unit.

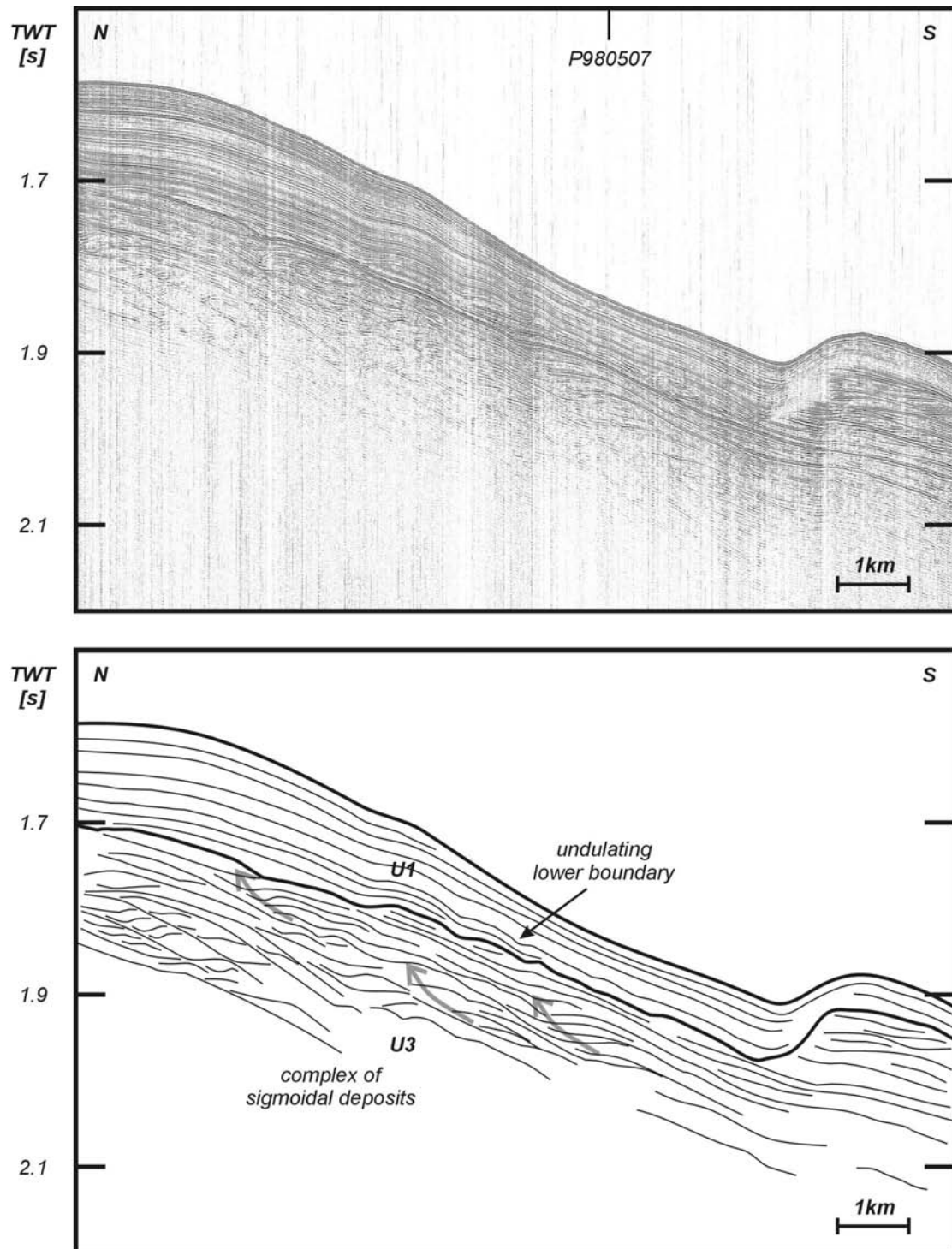


**Figure 6.27:** P010511c: Continued profile along the axis of the Arwen channel. Unit U3 shows northwards prograding sigmoidal units. This unit is cut off by a undulating unconformity.

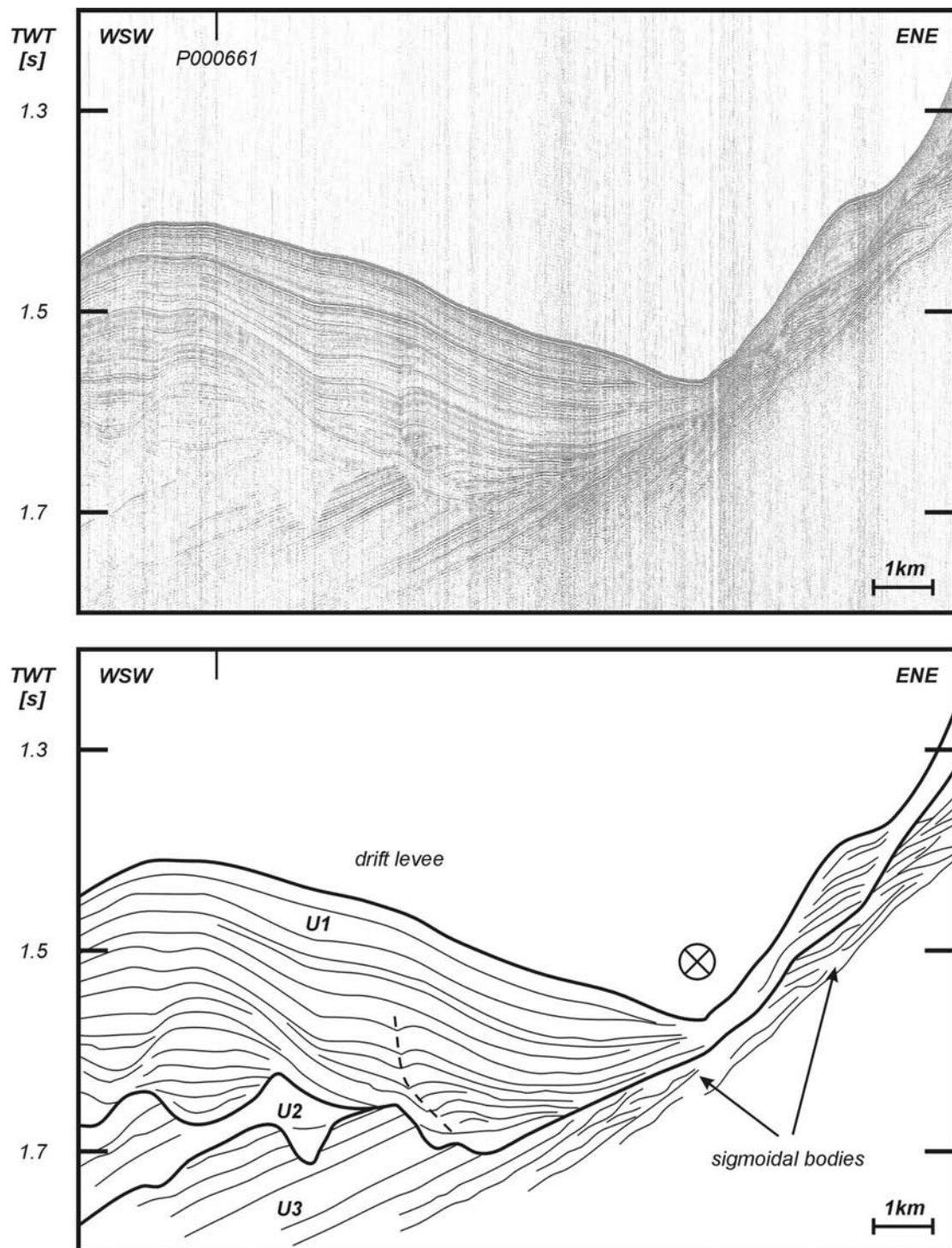


**Figure 6.28:** P980521: Detail of the sediment drift levee and its associated moat channel. Note the incision along the lower boundary of unit U2. The lower part of unit U1 is characterized by a complex reflector configuration. The narrowest zone of the channel indicates the main pathway of a northward directed current.

However, one exception should be noted. Profile P010511c (Fig. 6.27), which makes a transect along the main axis of the Arwen channel, also encountered sigmoidal deposits which seem to migrate in a northward direction. However, because they were only observed on one profile, it is very difficult to interpret these features.

#### **6.2.2.2 RD2 discontinuity**

The upper boundary of this unit is an erosional unconformity which sometimes incises deeply into U3 (Figs. 6.23 and 6.28). However, it seems to have been active in a limited zone since several upper slope profiles show an apparent conformable transition into the overlying unit U2 (Figs. 6.3, 6.5 and 6.15). Unfortunately, this RD2 erosive event is not very well documented because it is masked in several locations by a younger and more extensive erosional unconformity (Figs. 6.2, 6.21 and 6.28).

This RD2 discontinuity is inferred to be an early Middle Miocene erosion event (see Chapter 4). It was recognized in DSDP cores on Goban Spur and Rockall Trough, representing hiatuses of about 6 Ma (de Graciansky & Poag, 1984; Pearson & Jenkins, 1986). According to de Graciansky & Poag (1984) it is related to vigorous bottom currents due to the introduction of Norwegian Sea Water (NSW) in the North Atlantic Ocean.

#### **6.2.2.3 Early Neogene sediment wave fields**

Most of the U3 strata reflect a hemipelagic sedimentary environment. In a water depth of about 600 m (upper slope), the parallel reflectors dip about 2° to the SW. Stratigraphically equivalent reflectors on industrial seismic profiles have been interpreted as Early to Middle-Miocene in age (A. McDonnell, pers. comm.). However, on the upper part of the slope below a paleo-slope break, between 1.2 to 1.5 s TWT, probably E to ESE migrating sigmoids appear (Fig. 6.17), suggesting a local more dynamic environment. The origin of the break in the palaeo-slope might be related to the presence of underlying basement features (e.g. rift blocks). This zone of sigmoidal deposits is located S to SW of a zone characterized by NE prograding onlap. According to the definition of Faugères *et al.* (1999), Rebesco & Stow (2001) and Stow *et al.* (2002), and similar to the interpretation of unit U4, this could be a buried elongated drift. Especially the onlap on the lower boundary shares characteristics with the mounded elongated Lofoten drift, described by Laberg *et al.* (2002). Although the geometry and migration direction of these irregularly stacked lenticular bodies was tentatively inferred from a set of perpendicularly crossing profiles (Fig. 6.17), they can be compared to upslope migrating sediment waves created by contour currents, which are a common feature associated with sediment drifts (Howe, 1996; Masson *et al.*, 2002). Ediger *et al.* (2002), for example, described a similar set of sediment waves in the Mediterranean Cilician basin, migrating upslope in an opposite direction to the present water circulation pattern (Fig. 6.29). As a general model of wave-forming process, Wynn & Stow, (2002) follow the lee wave model, to explain to migration of fine-grained bottom current waves. Bottom current flow velocities on downstream flanks are higher than those on the upstream flanks, leading to enhanced deposition on the upstream flank and upstream wave migration (Flood & Shor, 1988; Wynn & Stow, 2002). This implies the presence of a presumably N to NW flowing bottom-current on this part of the slope during the

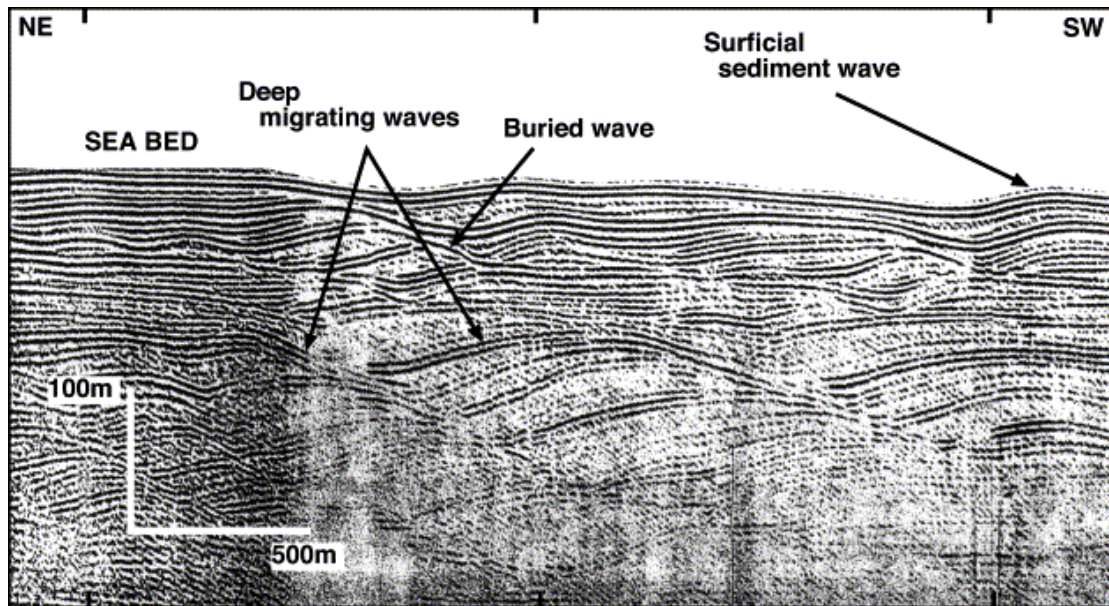


**Figure 6.29:** Upslope migrating sediment waves under a westward flowing bottom current in the Cilician basin, Northeastern Mediterranean (Ediger et al., 2002).

Early Miocene. The zone of onlap probably traces the main pathway of this bottom current, while the rather large sediment wave field was constructed during a later phase of drift construction. Unfortunately, most of these features are cut by a younger unconformity, preventing a full understanding of the entire development of these deposits.

## 6.3 Unit U2 and the Belgica mounds

### 6.3.1 Seismic characteristics and distribution

Unit U2 is characterized by a nearly transparent seismic facies of limited lateral extent (Fig 6.30), deposited on the RD2 erosional unconformity (Figs. 6.23, 6.26 and 6.3). Within this unit, only a few sets of continuous, relatively high-amplitude reflectors are observed (Figs. 6.22, 6.31 and 6.32).

However, the eastern upper slope part of the unit mostly bears more continuous reflectors with relatively higher amplitudes and frequencies. The reflectors of this part of U2 are relatively flat to nearly horizontal and sometimes seem to continue conformably into the overlying unit (Fig. 6.15). The change towards this better stratified unit seems to be accompanied with a gentle angular unconformity (Fig. 6.33). This area is only limited in extent and at its western side, it is abruptly terminated by a scarp in the upper boundary. From that part, the upper boundary gently slopes down and is rather undulating (Figs. 6.5 and 6.15).

This unit shows an irregular distribution and is present in two large zones, separated by an erosional channel (Fig. 6.30). Generally it disappears towards the NNW (Fig. 6.21) and towards the SW, whereas it extends beyond the data coverage in the northeastern (Figs. 6.2 and 6.3) and southeastern part of the study area where it reaches its maximum thickness of over 200 ms TWT (Figs. 6.31 and 6.34). Here, the upper part of U2 has been incised creating an undulating boundary (Fig. 6.31). Moreover, several zones have been identified where the thickness of U2 dramatically drops from approximately 100 ms TWT to 0 ms TWT over about 350 m, creating relatively steep flanks of about 15° (Figs. 6.30, 6.23 and 6.5). Downslope from this point, nearly the complete unit is eroded although some profiles in the southern part of the area still show some remnants of this transparent layer (Figs. 6.22, 6.4 and 6.21). Several profiles show the presence of unit U2 at the western side of the erosional channel, still bearing the same dip as on the eastern side (Figs. 6.3 and 6.4). The boundary between units U2 and U3 can easily be correlated from one side of the channel to the opposite one. Also this part of the transparent layer has been eroded. Profile P000661 (Fig. 6.35) illustrates the incision of a small channel (Fig. 6.30). All this implies that the sediments of unit U2 were deposited over the entire slope and eroded later on.

At the southeastern extremity of this unit, some profiles display a very special facies at the top of this unit. Profiles P99009a (Fig. 6.36), P030524 (Fig. 6.34) and P030525 (Fig. 6.32) show a southward dipping erosional unconformity cut into U2. This has been filled with a very complex facies, resembling a cut-and-fill geometry. The W-E oriented profile P030531 (Fig. 6.26) shows a gradual upslope eastward fill. This suggests a small erosional event, caused by a very focussed current, followed by a later stage of a very high-energetic river-like fill-up. It has been eroded afterwards by the same erosional event that created the upper boundary of the rest of unit U2.

Although no lithological information is known about this acoustically transparent unit, its distribution and the seismic facies hint that it might contain very homogenous sediments. The sets of internal reflectors with high amplitude could hint a possible post-depositional diagenesis or periods of non-deposition. The transparent character seems to disappear towards the youngest depositions of the

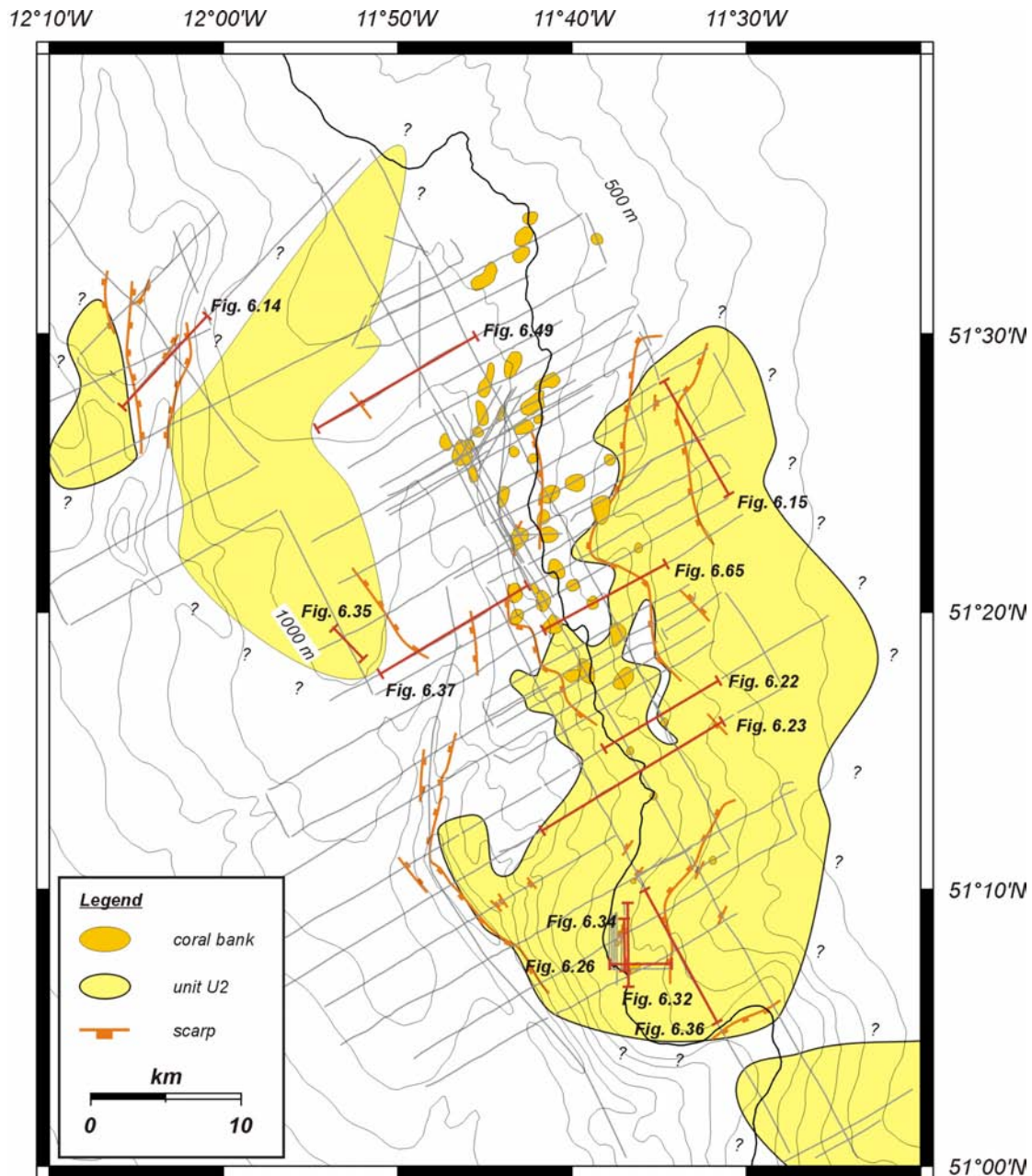


**Figure 6.30:** Distribution of unit U2, the mounds and the steep scarp, created by the RD1 erosion event, as observed on the seismic profiles. The positions of significant seismic profiles are indicated. All available profiles are presented by grey lines.

unit at its eastern limit. Recent observations of RCMG very high-resolution seismic lines across DSDP Hole 548 on Goban Spur, suggest this change could be related to the transition from Miocene to Pliocene. According to McDonnell & Shannon (2001), this period should have been characterized by deep-marine sedimentation with the development of a large slope-parallel drift. However, a lack of information about the geometry and extent of this unit, due to extensive erosion, does not enable to confirm this.

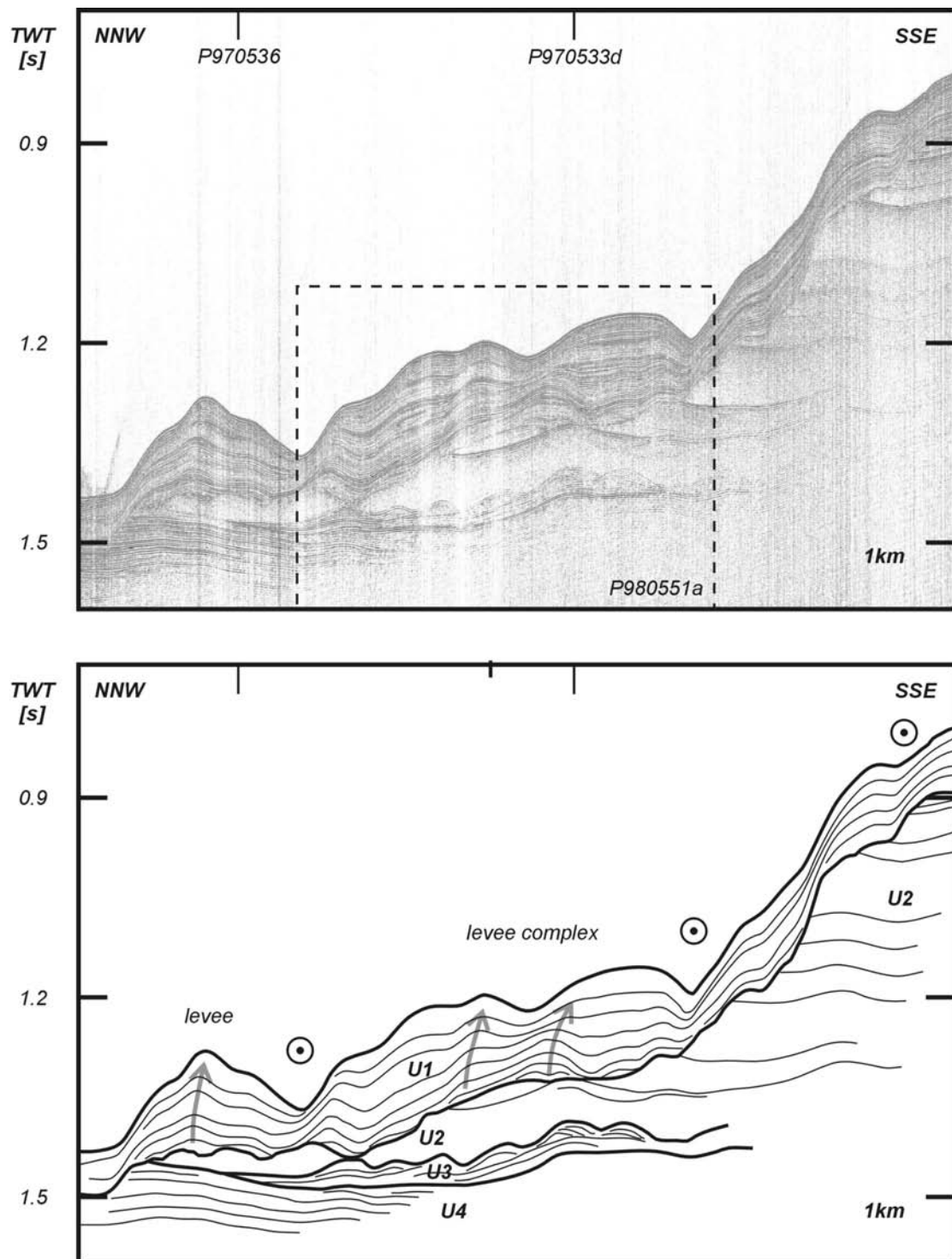


**Figure 6.31:** P980551: Alongslope overview profile featuring the large variability in thickness of unit U2. The grey arrows indicate the progradation of the levees within unit U1. Although unit U3 is relatively thin, there still is a clear SSE progradation.

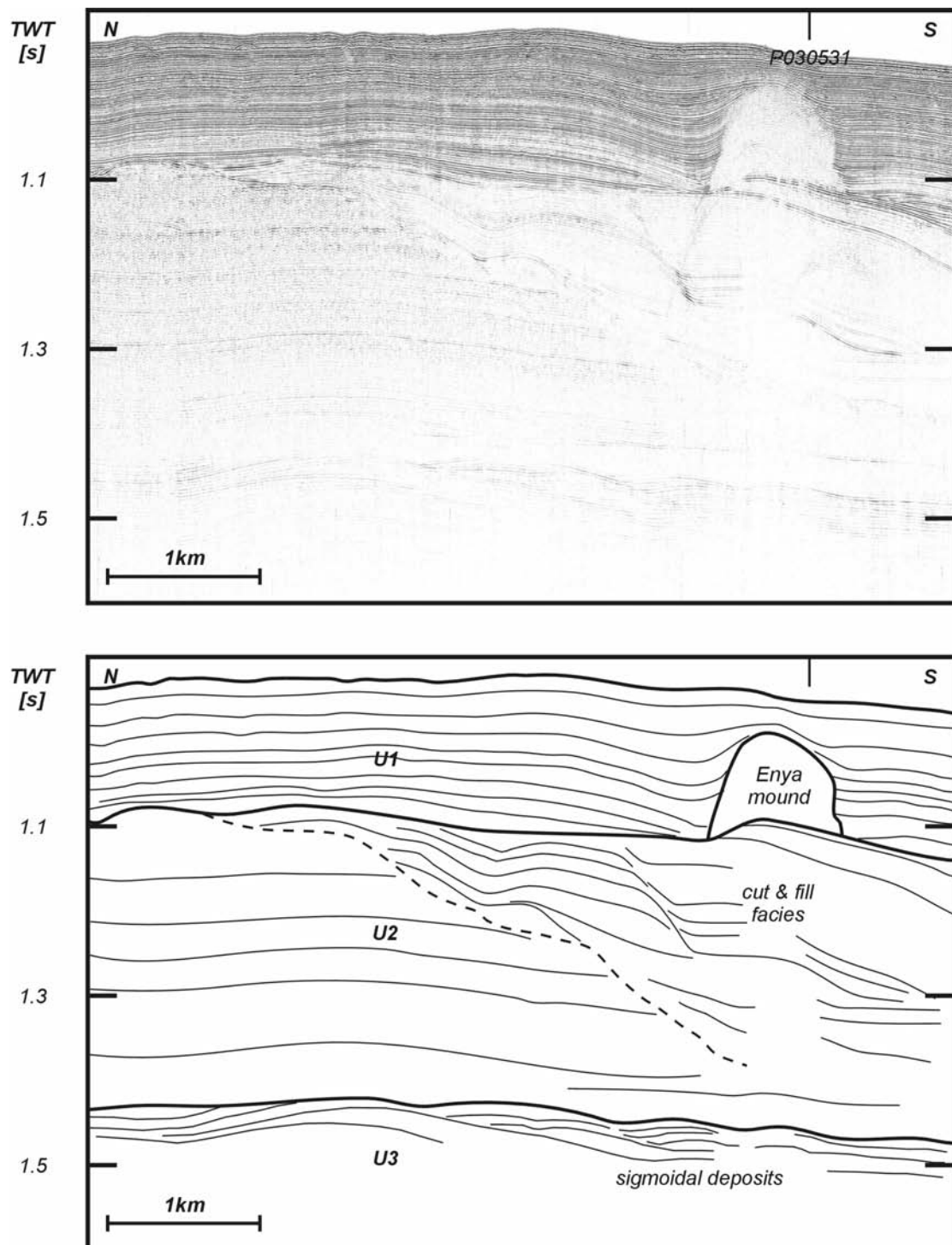


**Figure 6.32:** P030525: N-S oriented profile across the Enya mounds, showing sigmoidal deposits in unit U3 and a thick unit U2. The southern part of unit U2 is characterized by an incision, filled up with a cut and fill facies. On top of this deposit, a small Enya mound is observed.

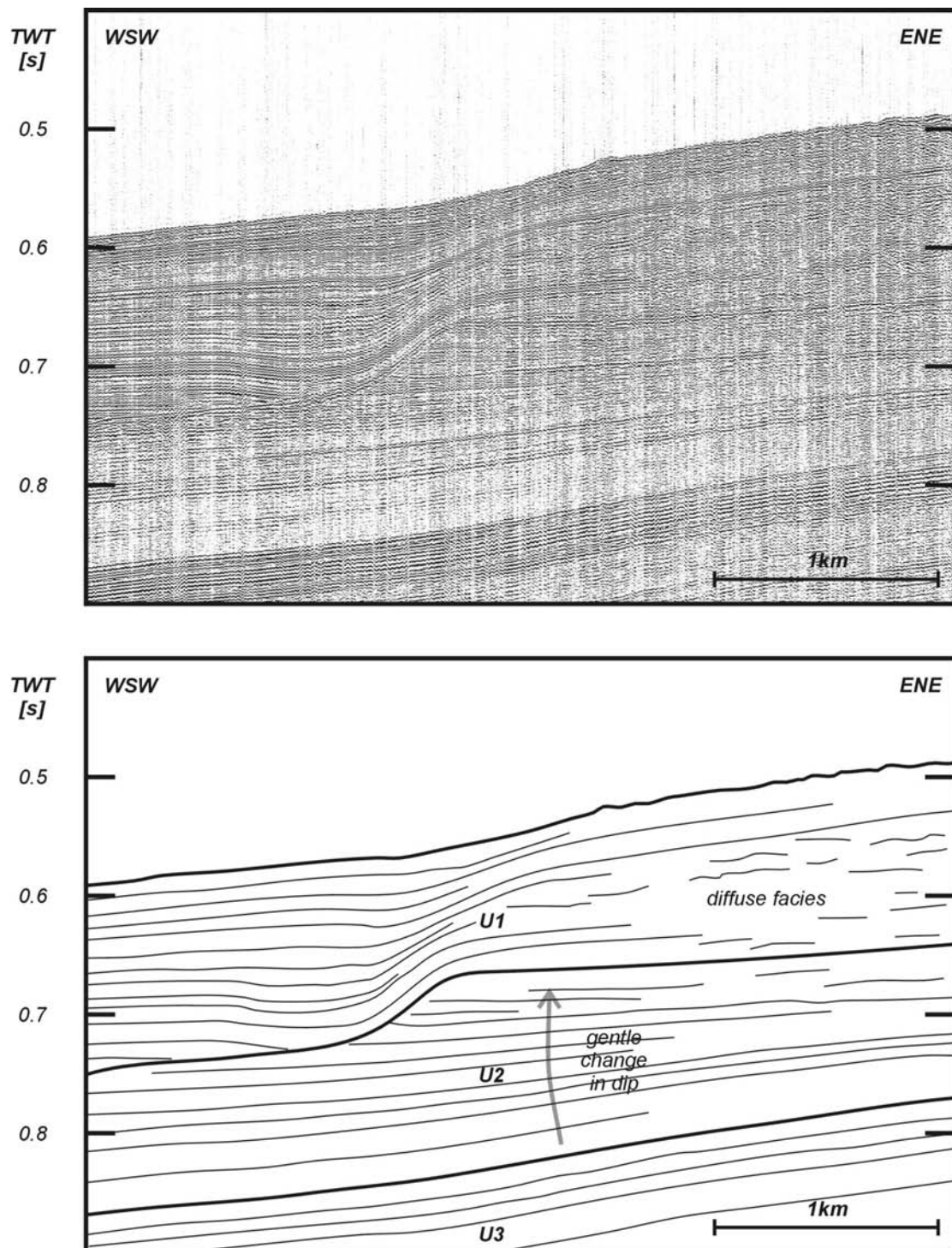


**Figure 6.33:** P010521b: Detail of the upper slope part of profile P010521 (Fig. 6.5), illustrating the change in seismic facies and dip within unit U2. Note the hummocky seafloor and the diffuse facies of unit U1.

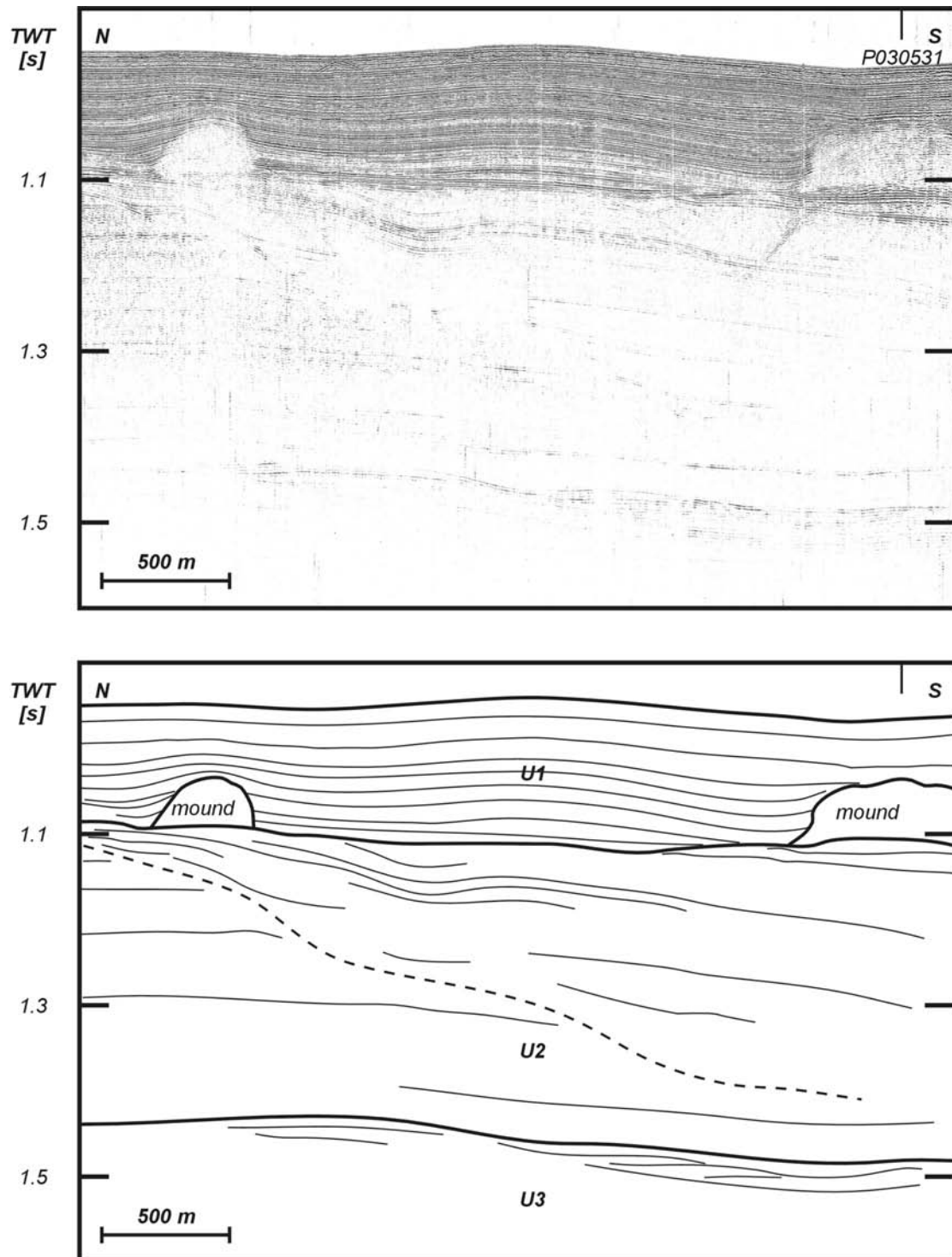


**Figure 6.34:** P030524: N-S oriented profile across the Enya mounds, showing a thick unit U2. The southern part of unit U2 is characterized by an incision, filled up with a cut and fill facies. On top of this deposit, two small Enya mounds are observed.

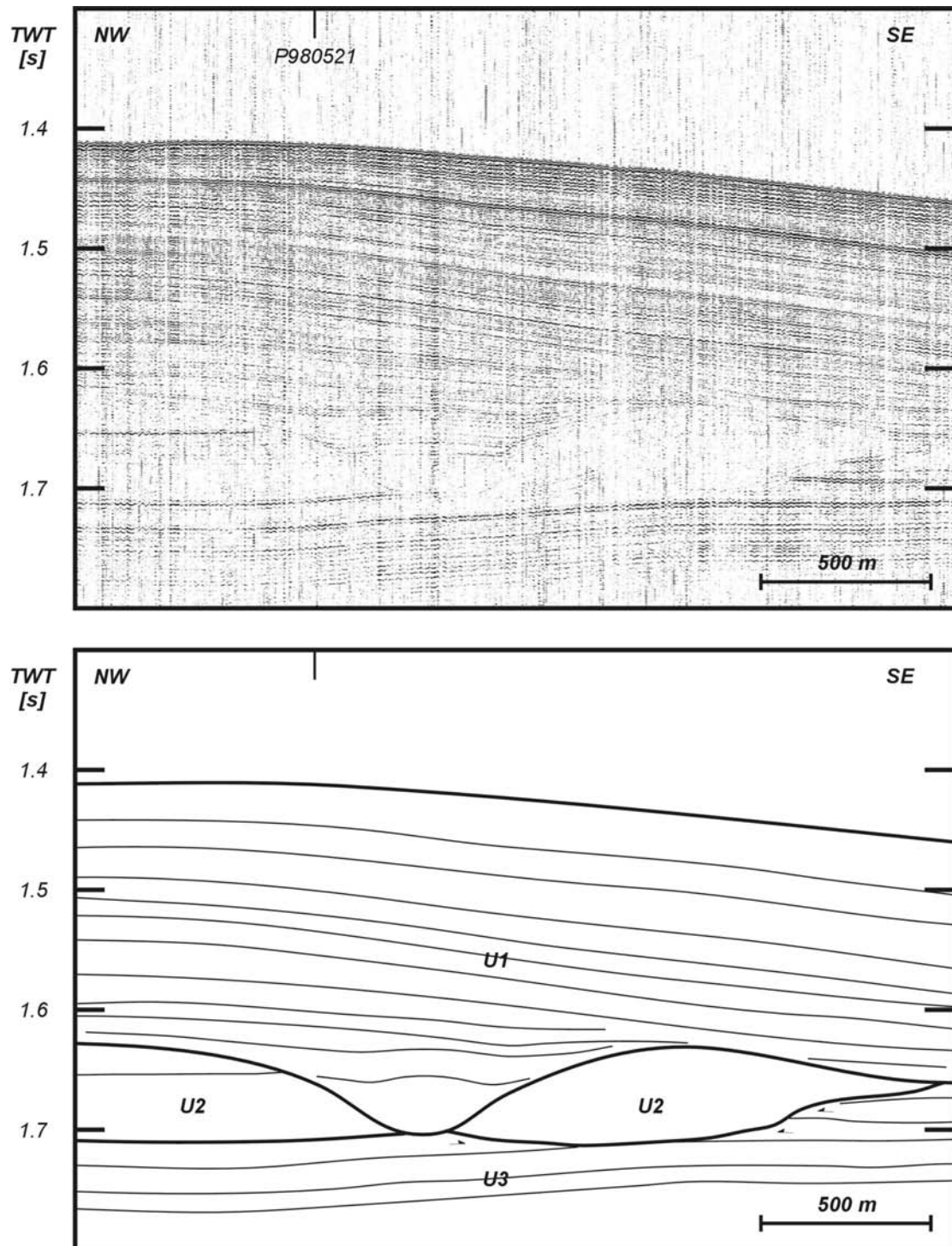


**Figure 6.35:** P000661: Profile on the western levee of the Arwen channel. Unit U3 has been eroded and filled up with the transparent unit U2. Subsequently, this unit has been incised by the RD1 discontinuity, creating a small channel.

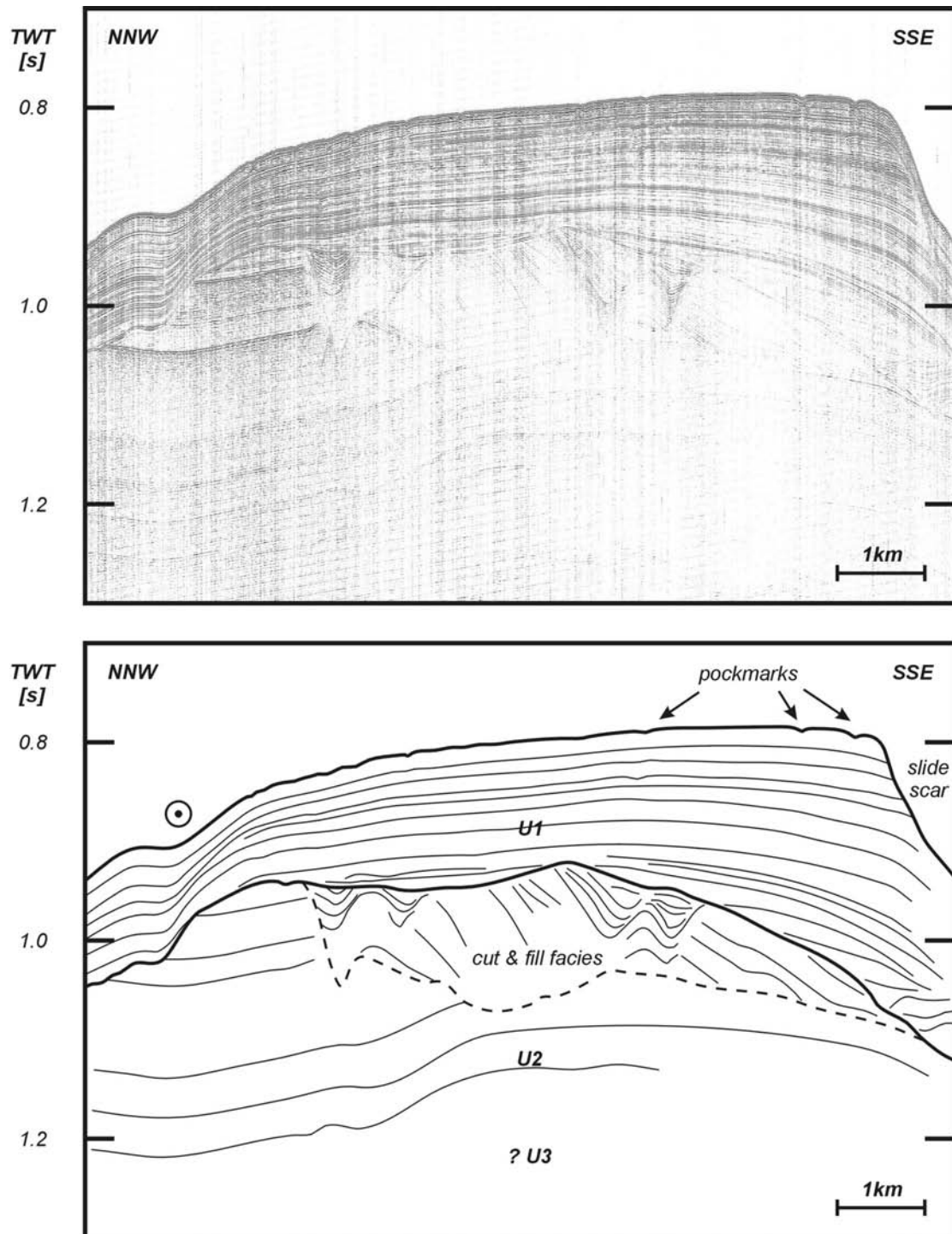


**Figure 6.36:** P99009a: Profile at the southern extremity of the study area. Unit U2 is relatively thick and shows several high-amplitude reflections. The upper part of this unit is characterized by a cut and fill deposits. The top strata of the thick, overlying unit U1 show small depression, interpreted as pockmarks.

### 6.3.2 RD1 discontinuity

After the deposition of unit U2, a major change in oceanographic conditions was responsible for a large-scale erosive event along the entire slope of the Porcupine Seabight. This RD1 discontinuity removed a large part of unit U2, leaving a very irregular terrace-like paleotopography (Figs. 6.3 and 6.4). Together with the complex incision along the southern limit of the study area, it suggests this erosion event could have known several phases, cutting each time deeper into the underlying sediment. These deep incisions into unit U2 as well as some U3 strata, created large roughly south-north oriented ridges with steep flanks (Figs. 6.11 and 6.37), which are still evident in the present-day topography (Figs. 6.6 and 6.30). This erosion event also created the basis of the Arwen, Celeborn and Galadriel channels, cutting sometimes very deep into Late Paleogene deposits (Figs. 6.3, 6.14 and 6.23). Hence, this extensive erosional surface largely coincides with the upper boundary of U3, thus forming a composite erosion surface (Figs. 6.2, 6.3 and 6.4).

As discussed in the previous chapter, a regional Late Pliocene hiatus, found in the Rockall-Goban Spur transect could be the possible cause for this regional RD1 discontinuity. It is interpreted in terms of the reintroduction of MOW in the NE Atlantic and the effect of glacial-interglacial events on deep-water circulation (Stow, 1982; Pearson & Jenkins, 1986).

### 6.3.3 Belgica mounds

The position, morphology and distribution of the Belgica mounds has been extensively studied and discussed by De Mol (2002). However, within the stratigraphic framework of this study, their most important characteristics will be briefly summarized. Also some new elements will be presented.

On the seismic profiles, the Belgica mounds are characterized as almost acoustically transparent elevated structures with a parabolic outline. Within the mounds no clear internal reflections are observed. The real shape of the mounds however is masked by diffraction hyperbolae. The best approach of the mound shape is deduced from the reflection termination of the surrounding sediments at the mound and the apex of the hyperbolae (Figs. 6.24 and 6.4).

In general the mounds display a broad base, which roots on the composite erosion surface (Figs. 6.38 and 6.39). In a SSE-NNW direction the mounds have a broader footprint than in the NE-SW direction. Some apparently single mounds merge at their base and form a composite mound. This results in ellipsoidal to conical structures with several summits, lined up in a general SSE-NNW direction (Fig. 6.30). The base of the mounds is not always easy to delineate, especially on the southernmost profiles, where they root on unit U2. Here, the remains of strongly eroded U2 strata occupy an elevated position in the paleobathymetry. This is expressed in a change of gradient from nearly horizontal to a slope of approximately 2° (Fig. 6.38). To the north, the mounds tend to step off the eroded P2 unit (Fig. 6.21 and 6.39). In this case, the mounds are resting on a scarp of U3 sediment. The base of the mound and underlying reflectors are distorted by velocity pull-up (Figs. 6.38, 6.24, 6.21 and 6.39). This acoustic artefact is particularly evident where the mounds are exposed (and the lateral acoustic velocity contrast is high).

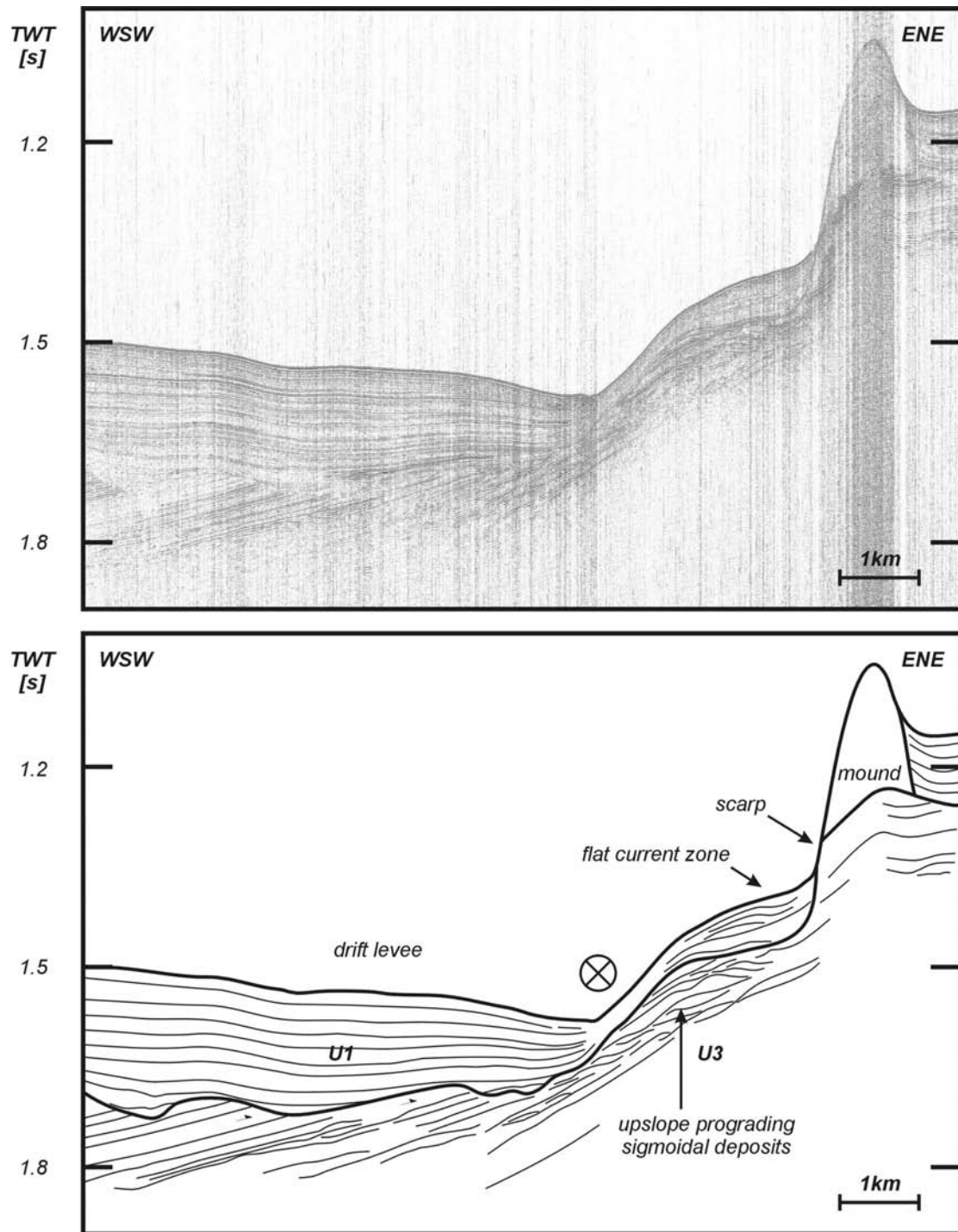


**Figure 6.37:** P980523: Profile across the Arwen channel and a single mound, rooted on a scarp in unit U3. Note the upslope prograding sigmoidal deposits in this unit. The U1 drift levee is deposited as an angular, undulating unconformity.

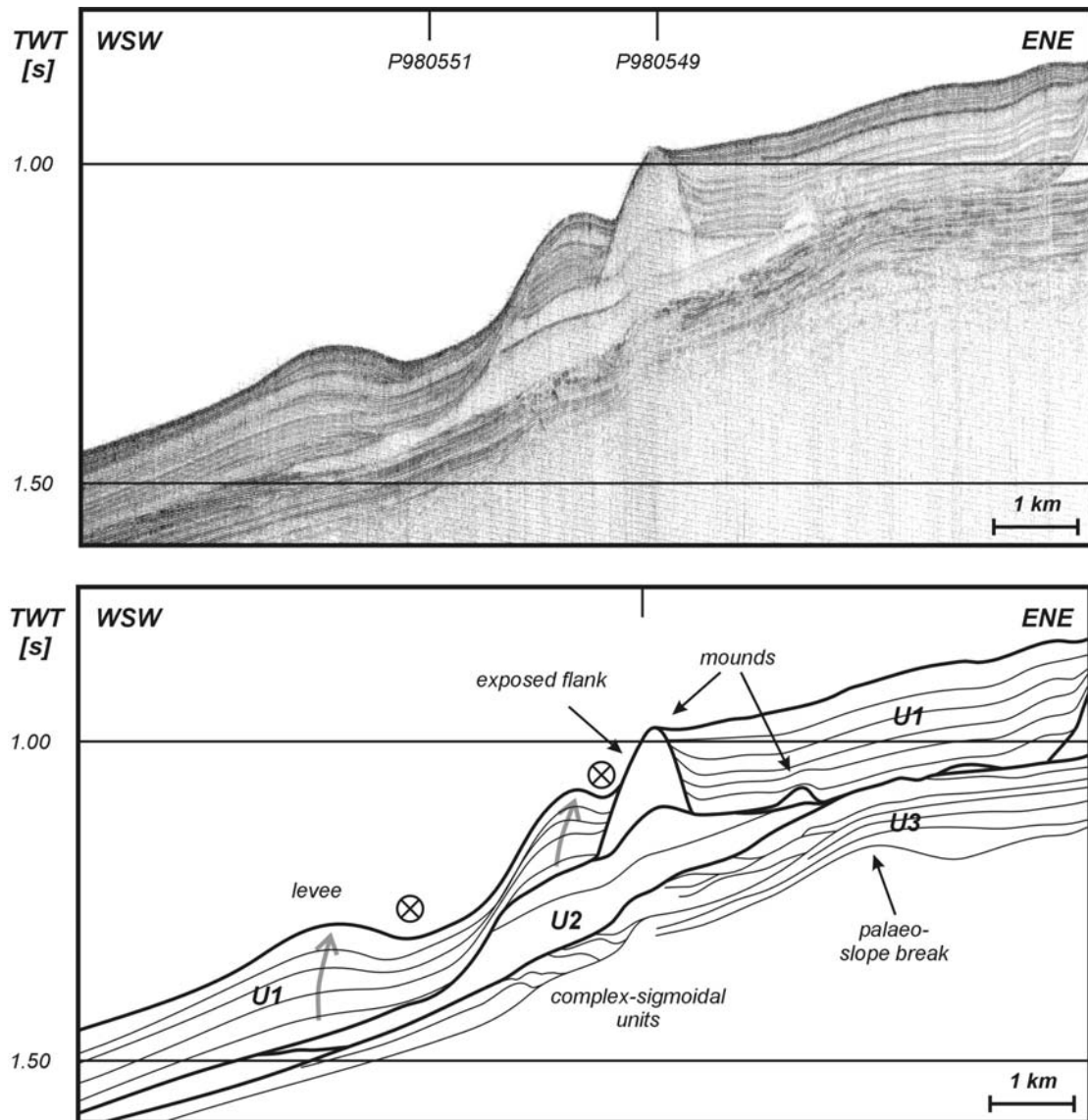


**Figure 6.38:** P970536: Profile across a typical Belgica mound, rooted on a remnant of the unit U2. Note the change in dip and the palaeo slope-break in unit U3. Also note the asymmetry of unit U1 at both sides of the mound. The upslope migration of the levee-like units are indicated by the grey arrows.

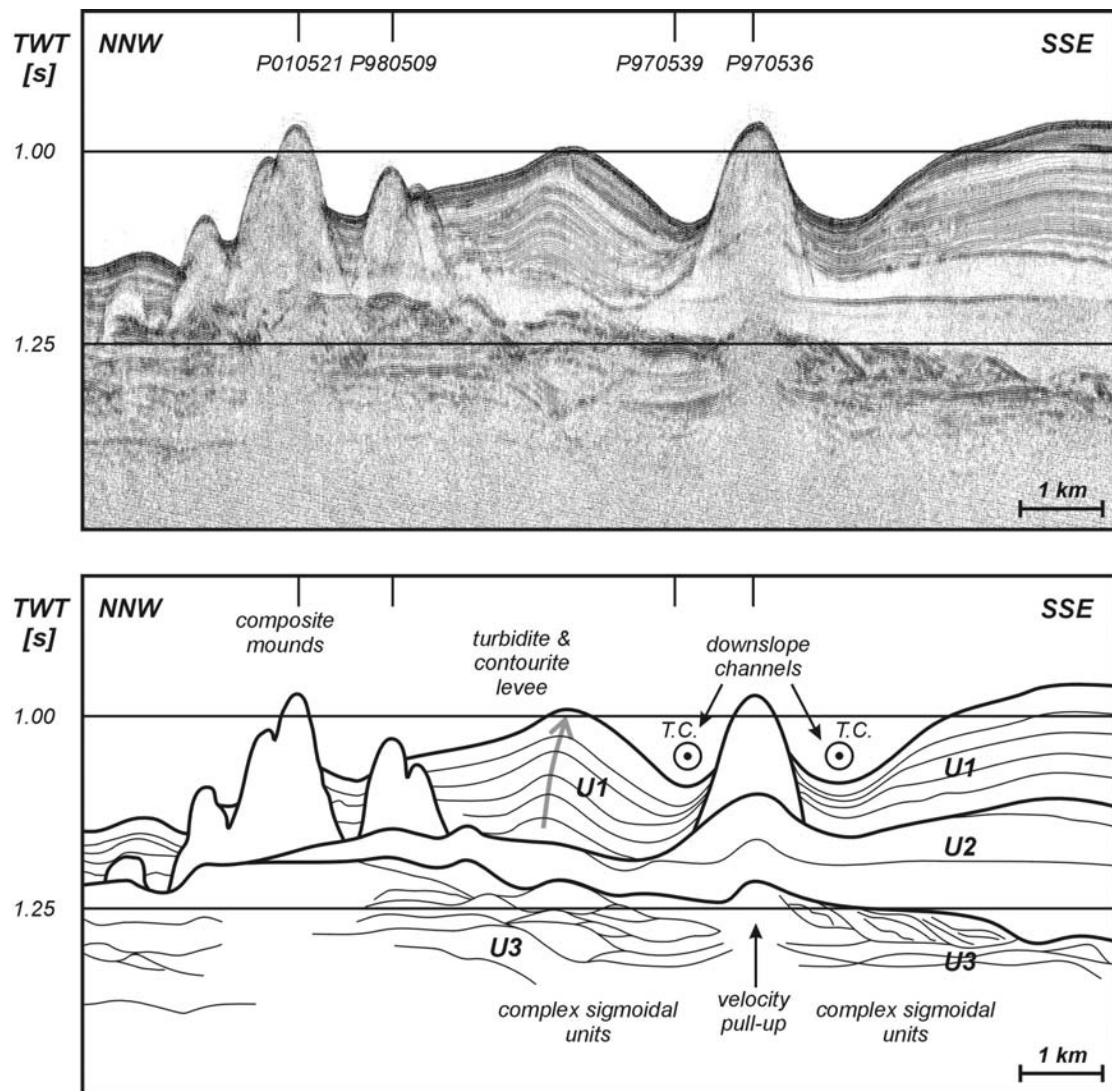


**Figure 6.39:** P980549: Alongslope overview profile through a composite mounds and a single mound, rooted on the acoustically transparent unit U2. Note the SSE progradation of the sigmoidal units in U3 and the asymmetry between the levees at the NNW and SSE side of the single mound. The grey arrow indicates the progradation of the levee unit. T.C. : turbidite current.

The size of the mounds tends to decrease from north to south, where they generally are buried under a thin sedimentary cover (4 - 12 m). Their height can range from 35 up to 175 ms TWT in the northern part. The basal width of the mounds varies from 300 m up to 1800 m. Hence, the average slope of a mound ranges between 10 and 15°.

This study can add three new buried mounds, discovered during the Porcupine-Belgica 2003 campaign (Van Rooij *et al.*, 2003). They are located at the extreme southern edge of the study area (Fig. 6.30). These mound, called the Enya mounds, are all rooted on a very thick unit U2, at the edge of the cut-and-fill facies (Figs. 6.34, 6.32 and 6.26). One mound is up to 100 ms TWT high and approximately 800 m wide, buried under 50 ms TWT of sediment. The other two, smaller mounds are both about 75 ms TWT high and 400 m wide, buried under approximately 100 ms TWT of sediment.

### 6.3.4 Influence of the Late Pliocene environment on mound growth

Our observations do not add much to those of De Mol (2002) who interprets the mounds in the Porcupine Basin as coral banks. However, it is interesting to briefly address the possible Late Pliocene environmental controls on the development of the mounds. Their location on this part of the margin and their size will be of importance during the later development of the sediments surrounding these mounds. Freiwald *et al.* (1999) and De Mol (2002) already pointed out that the builders of these coral banks, most often *Lophelia pertusa* and *Madrepora oculata*, prefer to settle on a hard substratum on an elevated position. They need strong bottom currents to get sufficient nutrients, but also to keep them free from sediment burial. So the mere presence of the mounds may already be an indicator of (strong) bottom currents after the Late Pliocene erosion.

The multibeam map (Fig. 6.6) shows the Belgica mounds occur in a very narrow bathymetric interval between 700 and 1000 m below sea level, lined up as alongslope oriented ridges. Most of the observations confirm the mounds started to grow on a scarp or a topographic irregularity in unit U3 or U2, depending on the extent of the RD1 erosion event. Moreover, the sigmoidal units observed in unit U3 and interpreted as sediment waves are located within the same slope section, exactly underneath the mounds (Fig. 6.39, 6.24 and 6.19). Recent models, combined with the few current meter data and the side-scan sonar imagery indicate the Belgica mound province nowadays is located in an area affected by enhanced currents (Pingree & Le Cann, 1989; Pingree & Le Cann, 1990; Rice *et al.*, 1991; New *et al.*, 2001; Akhmetzhanov *et al.*, 2001; White, submitted). So it appears this slope section might have been under the influence of enhanced bottom currents already since the beginning of the Neogene. Moreover, the U2 scarps and other presumed hard substratum (e.g. the top of the sigmoidal bodies) were suitable targets to be colonised by framework-building corals under a vigorous bottom current flow and could have largely assisted the initiation of carbonate mound growth (De Mol *et al.*, 2002).

## 6.4 Quaternary sedimentary processes

The Late Pliocene erosive RD1 discontinuity was created when modern oceanographic conditions were established in the North Atlantic (Pearson & Jenkins, 1986; Schnitker, 1986) and glacial-interglacial cycles started to have a pronounced effect on the production of the North Atlantic Deep Water (NADW), the Antarctic Bottom Water (AABW) and the Norwegian Sea Outflow Water (NSW). These changes resulted in the variability of the thermohaline circulation and thus affected the construction and evolution of the well-known sediment drifts along the margins of the North Atlantic (Stow, 1982; Faugères *et al.*, 1993). The Belgica mound province, however, is located in a relatively small embayment of this North Atlantic margin, out of reach of the bottom current activity caused by deep-water circulation. Nevertheless, a complex oceanographic regime is responsible for the enhanced currents observed in recent times in a narrow zone of the slope (Rice *et al.*, 1991). Moreover, during and after the RD1 erosion event, already a few topographic features were created under the influence of intensified bottom currents: (1) the irregular paleotopography with steep flanks, cut into both units U2 and U3, and (2) the Belgica mounds. In this section we will discuss the significance of both features and of bottom currents on the deposition of the most recent unit U1.

### 6.4.1 General features, facies and distribution

In contrast with previous units, the large-scale reflection configuration and the geometries of this last unit are very diverse. This most recent unit covers the entire study area. In general, the seismic facies is characterized by high-frequency, continuous, parallel reflectors with variable amplitudes. Over the entire study area, some major changes in geometry can be observed, possibly resulting from the interaction between the surrounding topography and the current regime. This section will describe the most general features as observed in the central area of the Belgica mound province. The following sections will respectively discuss the alongslope channels, the depositional features around mounds and the construction of a small mounded sediment drift.

In the central area surrounding the mounds and east of them, the thickness of U1 is gradually decreasing from 250 ms TWT in the south to 50 ms TWT in the north. The most upslope part of this unit, deposited on the flat upper surface of U2 can be characterized by diffuse reflections (Figs. 6.42, 6.25 and 6.40). The sea floor shows undulating features, up to 15 ms TWT (approximately 10 m) high. In a SSE-NNW transect, the geometry is wavy with gentle undulations and condensed sections (Figs. 6.21 and 6.39). On NE-SW oriented profiles, however, the thickness remains relatively constant with a sheeted geometry, consisting of mainly parallel reflectors (Figs. 6.38, 6.4 and 6.3). On the upper part of the slope this unit is deposited on the undulating upper boundary of U2 (Figs. 6.4 and 6.23). The slope of the seafloor and underlying strata dips about 2° to the SW. The U1-reflectors are downlapping or onlapping on this boundary, although they sometimes seem to be deposited conformably. A first visible change in geometry can be encountered between the 650 and 800 ms TWT isobath where the thickness of unit U2 drops drastically, creating steep flanks in the palaeobathymetry (Fig. 6.5). The thickness of U1 decreases towards this scarp. Here, the seafloor slope can locally increase up to 6°. Further downslope, the thickness and average slope of Unit U1 are the same as before, but more irregularities are met when approaching the mounds.

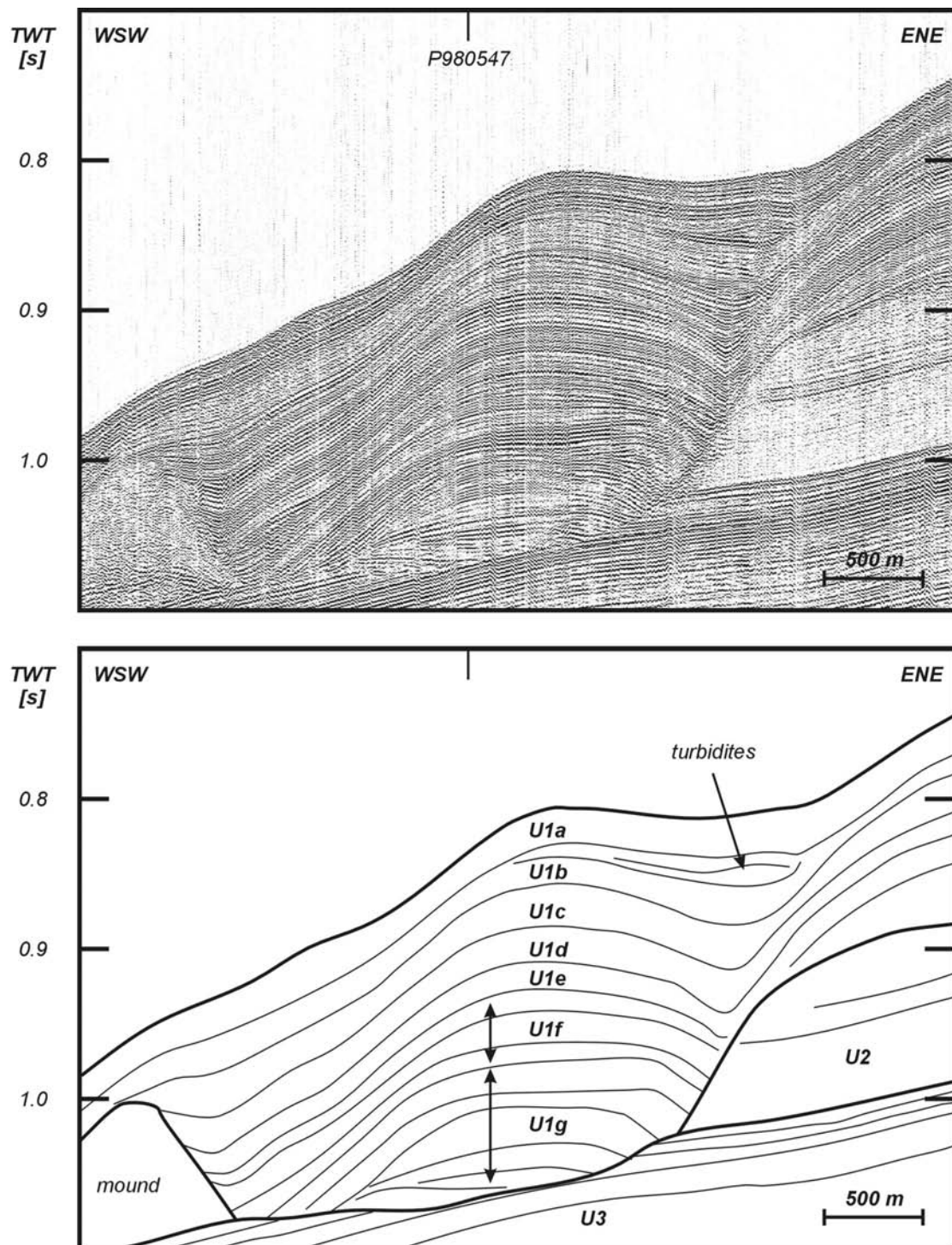


**Figure 6.40:** P010521c: Detailed part of profile P010521 (Fig. 6.5), illustrating the seven different sections as observed in the small mounded drift at the centre of the Belgica mound province. The moat channel at the ENE side of the mounded unit U1 can contain flat reflectors, suggesting the presence of turbidite deposits.

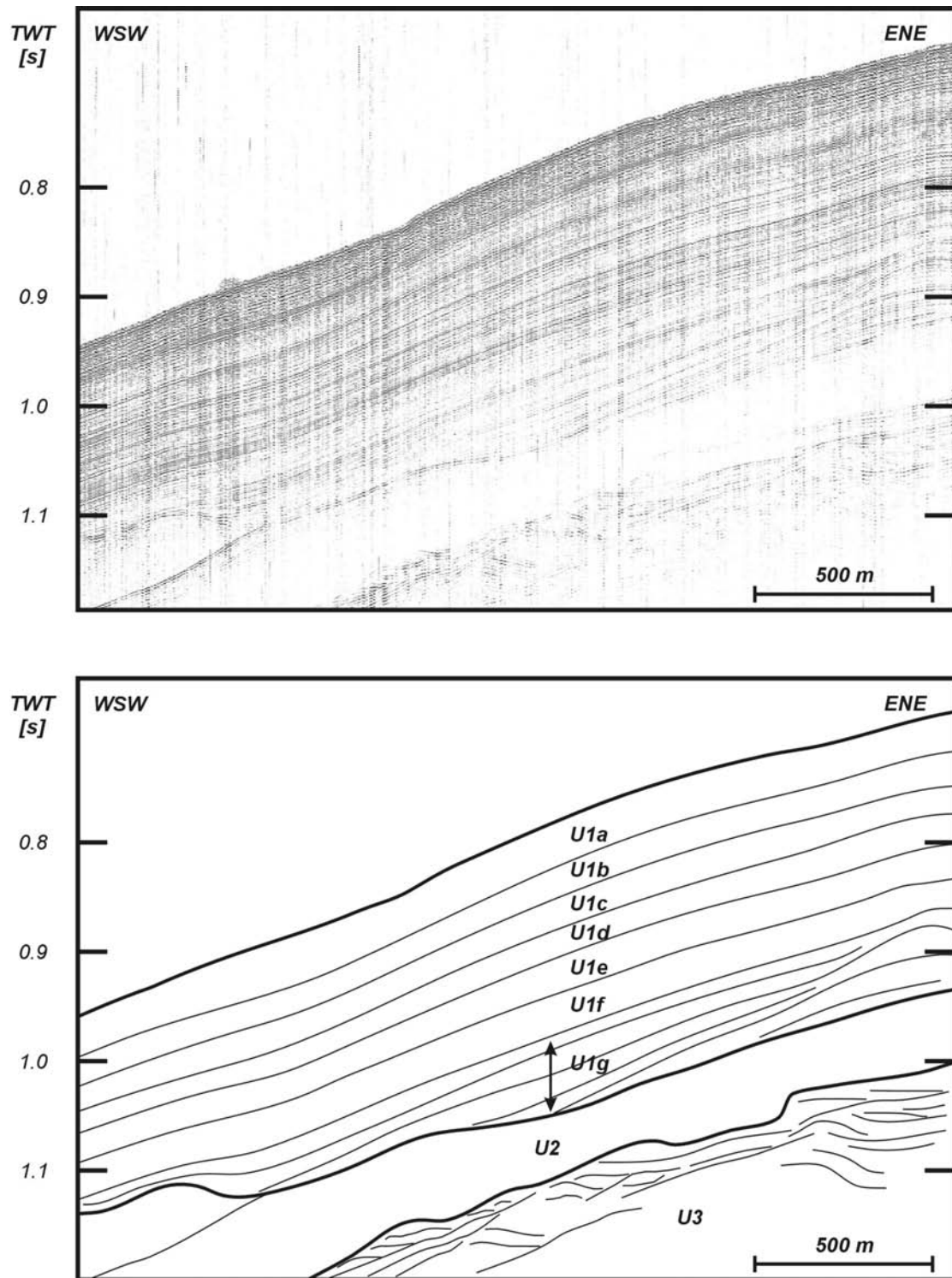


**Figure 6.41:** P970533a: Detailed section of profile P970533 (Fig. 6.23), illustrating the different 7 sections characteristic of the central part of the Belgica mound province, based upon changes in seismic facies. They overly a thinned unit U2 and a complex unit U3.

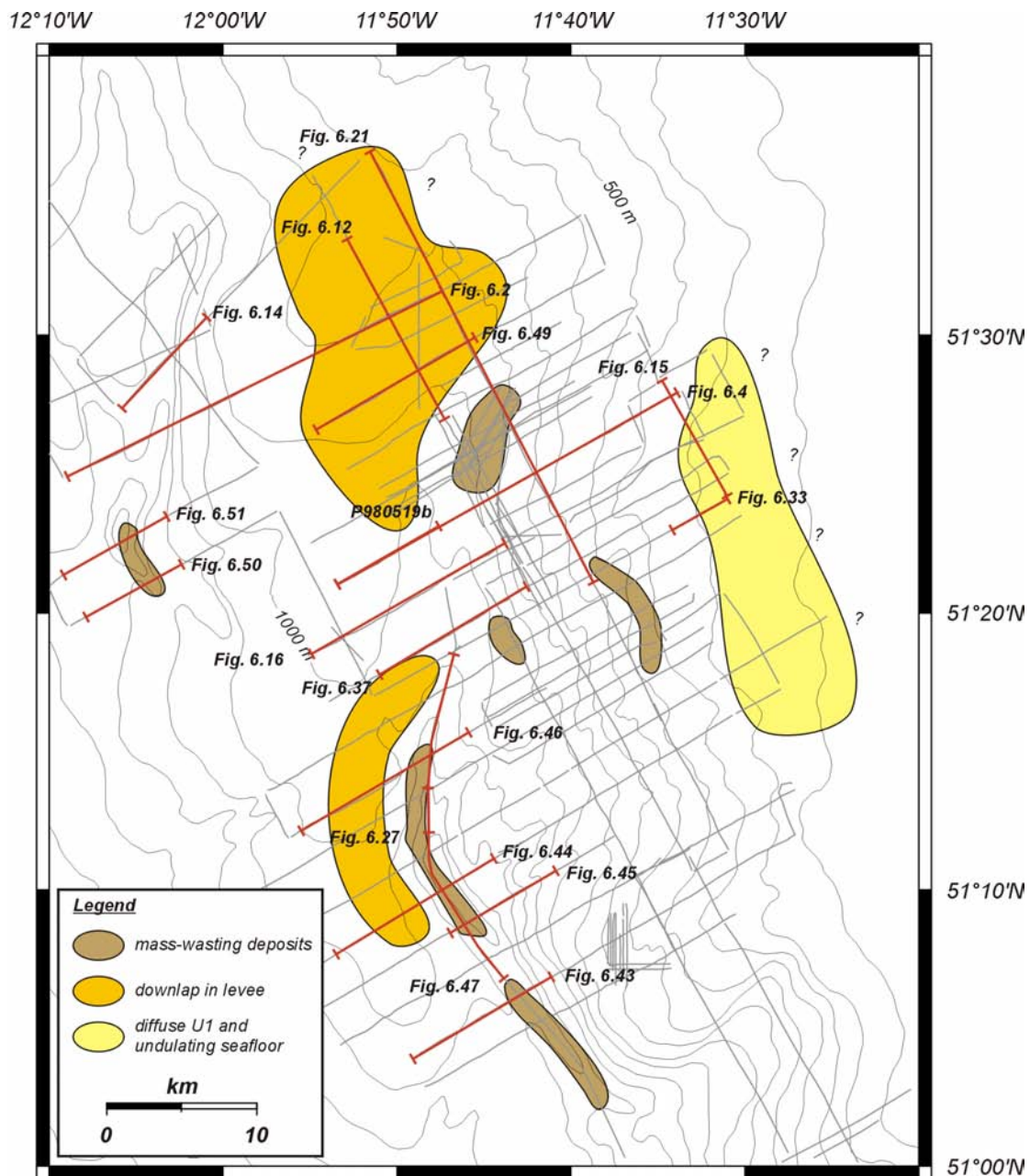


**Figure 6.42:** Positions of profiles illustrating the general characteristics of unit U1 and detailed profiles illustrating the alongslope channels. Special attention is paid to the location of downlap in drift levees, mass-wasting deposits and the diffuse zone within unit U1.

Within this central part, unit U1 can be subdivided up to several sections, based on seismic reflection patterns. These vertical changes of the reflection pattern seem to be best pronounced only within the zone limited by the mounds on the western side and the sediments east of them (Figs. 6.40 and 6.41). From the seafloor towards the lower boundary of U1, 7 sections, respectively U1a to U1g, can be recognized. Section **U1a** is the youngest one and is characterized by a high amplitude reflection. **U1b** features a zone of low amplitudes. Its lower boundary is constituted of 2 to 3 high amplitude reflections. The upper part of section **U1c** is characterized by high amplitudes. Towards its lower boundary, the intensity of these amplitudes weakens. Similar to section U1c, **U1d** starts with higher amplitudes. It is

a changing set of high to low amplitude reflectors. Section **U1e** is a small set of high amplitude reflectors. Section **U1f** comprises a set of low amplitude reflections. The lowest section, **U1g** is not frequently observed, except at the base of large depressions and is associated with frequent discontinuities.

## 6.4.2 Alongslope channels

Two large sets of roughly south-north oriented channels have been observed in the study area (Figs. 6.1 and 6.42). The most pronounced and best documented channel is the Arwen channel, which is known to form the western limit of the Belgica mound province. The Celeborn-Galadriel channels are located a few kilometres to the west.

### 6.4.2.1 Arwen channel

The development and the sedimentary processes associated to this channel will be described and discussed through a transect of WSW to ENE oriented profiles from the southern to the northern edge of the channel. In general, a very thick U1 unit (200 - 250 ms TWT) has been deposited on the RD1 angular unconformity west and north of this channel (Figs. 6.3, 6.21, 6.39 and 6.2). However, the geometry of this levee-like unit and the channel wall geometry show significant changes along this transect, suggesting the action of a south-north directed bottom current.

In the southern part of the study area, the main axis of the Arwen channel can be up to 500 ms TWT (approximately 375 m) deep with steep flanks (up to 15°), keeping the eastern flank free of sedimentation (Figs. 6.43, 6.44 and 6.45). On the other hand, from the less steep western flank (9°) of the channel, wedges of unit U1 start prograding into the channel. The decrease in thickness of this main aggradating unit towards the channel happens rather abruptly (Figs. 6.44 and 6.46). Several features observed in this levee unit suggest the presence of synsedimentary faults, which are responsible for a depression in the overlying strata and the seafloor. In this deepest part of the channel, an infill of flat, interbedded, acoustically transparent lens-shaped bodies is observed, with a thickness up to 120 ms TWT. These probable mass-wasting deposits, slumped from the steep channel walls, are also observed on a N-S oriented profile along the channel axis (Figs. 6.42 and 6.47). The presence of these mass-wasting deposits in the deepest and steepest part of the channel, associated with possible faulting, suggests that its evolution might have been tectonically influenced. This might also explain the strange geometry of this part of the channel. However, no mechanism or cause can be proposed.

More to the north, this decrease in thickness is more subtle (Figs. 6.37, 6.3, 6.48, 6.49 and 6.12). Here, the aggradation of the main sediment body seems to be characterized by a slightly prograding trend. In tracing the onlap of U1-strata upon the basal erosive discontinuity, a subtle upslope migration of the channel axis is observed. Also, the channel becomes less deep and seems to be less easy to define than in the south; there are no clear flanks to the channel. Unit U1 is about 250 ms TWT thick to the SW of the channel, but it is reduced to a very thin cover in the channel axis due to both pinch out (onlap) of the lower reflectors and erosion of the upper ones. The earliest deposits of unit U1, observed on profiles P980521 (Fig. 6.3) and P980519b (Fig. 6.48), contain several discontinuities and undulating reflectors. This suggests that at the start of the levee sedimentation, possibly a vigorous and

variable current was present. Towards younger deposits, and on the other profiles, there is a subparallel progradation, clearly indicating one south-north oriented current focus.

Profile P970547 (Fig. 6.21) adds more complexity to this levee-like build-up. Initially, there is a southward progradation with downlapping reflectors ( $2^\circ$  angle) on the erosion surface. This is followed by a subsequent reversed (northward prograding) trend. The channel also seems to be much less erosive here compared to its southern part. On profile P000665 (Fig. 6.2) only subtle variations in reflector configuration suggest the presence of the Arwen channel. Only the uppermost reflectors are cut by the seafloor, indicating the presence of relatively strong currents only in recent times. The observation of small diffraction hyperbolae on the supposed channel floor suggests a coarse seabed morphology (Figs. 6.10, 6.49 and 6.12). This is confirmed by boxcores and benthic sledges carried out during the Porcupine-Belgica 2000 and 2003 surveys, which yielded the presence of a gravel lag on this location (Fig. 6.52). Also the TOBI side-scan sonar imagery, interpreted by Huvenne *et al.* (submitted-b) has documented deep scouring features in this part of the channel, strengthening the idea of a focused current along this channel (Fig. 6.7).

#### **6.4.2.2 Celeborn-Galadriel channels**

A similar trend as the Arwen channel is observed in the development of the Galadriel-Celeborn channel system, although the available seismic profiles do not allow a full south to north transect. Both channels deeply incise the Paleogene deposits. From south to north, the channels become shallower. Profile P010531b (Fig. 6.50) shows a very deep channel floor (400 ms TWT), flanked by two steep channel walls. The channel floor is flat, suggesting the presence of mass-wasting deposits. Again, the configuration of the reflectors on the western side, suggest possible faulting and even uplift of this side of channel flank. More to the north, the eastern side of the Celeborn channels shows undulating, levee-like structures (Figs. 6.14, 6.2 and 6.51). At their western side, the U1 deposits gently prograde into the channel centre and even show levee features (Figs. 6.14 and 6.51). Here, the sediments in the channel axis can still contain mass-wasting deposits, but are mostly characterized by intra-channel levees.

The spur separating the Arwen from the Celeborn channel, has a typical U1 seismic facies and is shaped into a mounded morphology by the presence of the two slope channels.

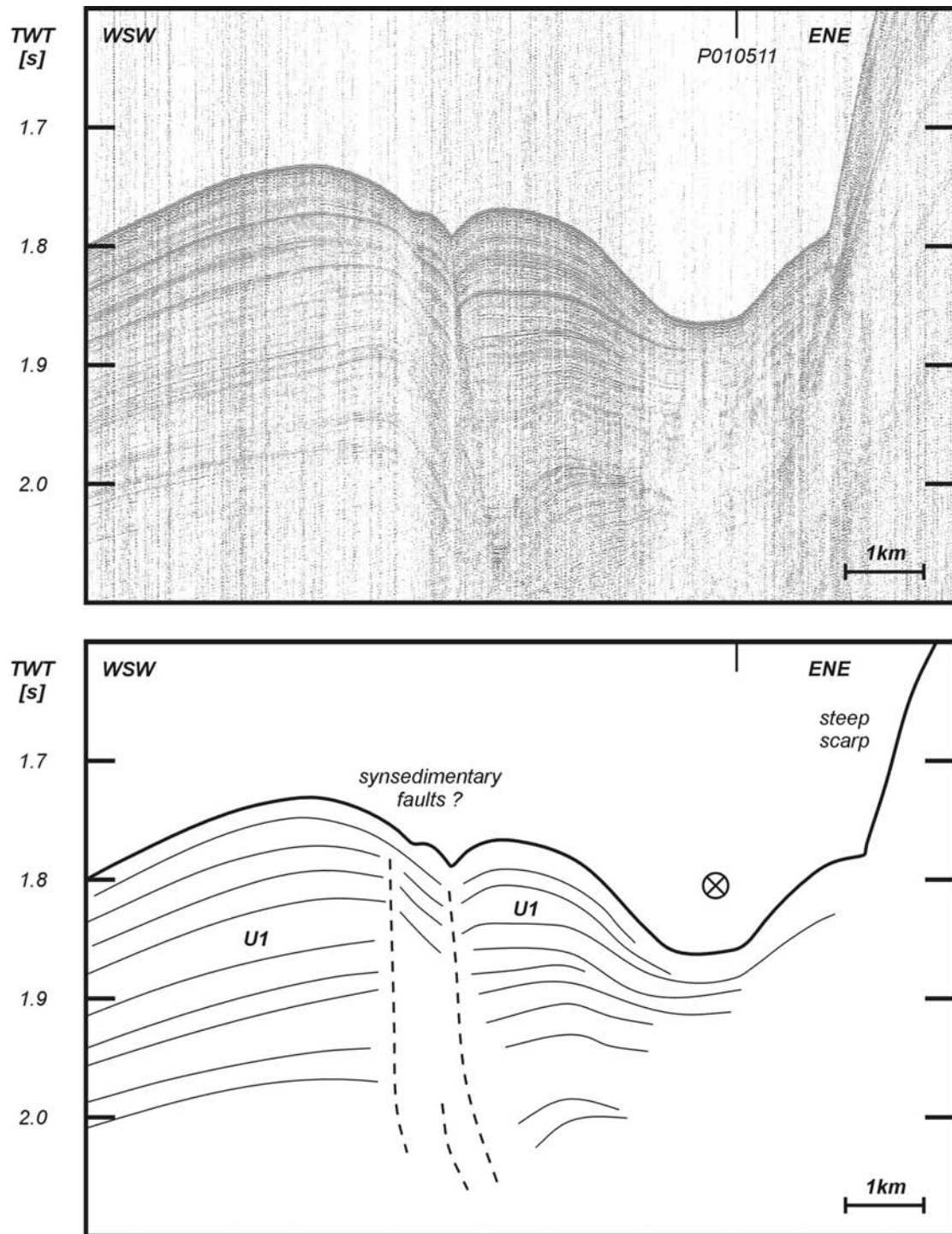


**Figure 6.43:** P980503: Profile across the Arwen channel and its levee unit. The channel axis is relatively broad and flat. The levee unit is characterized by probably synsedimentary faults.

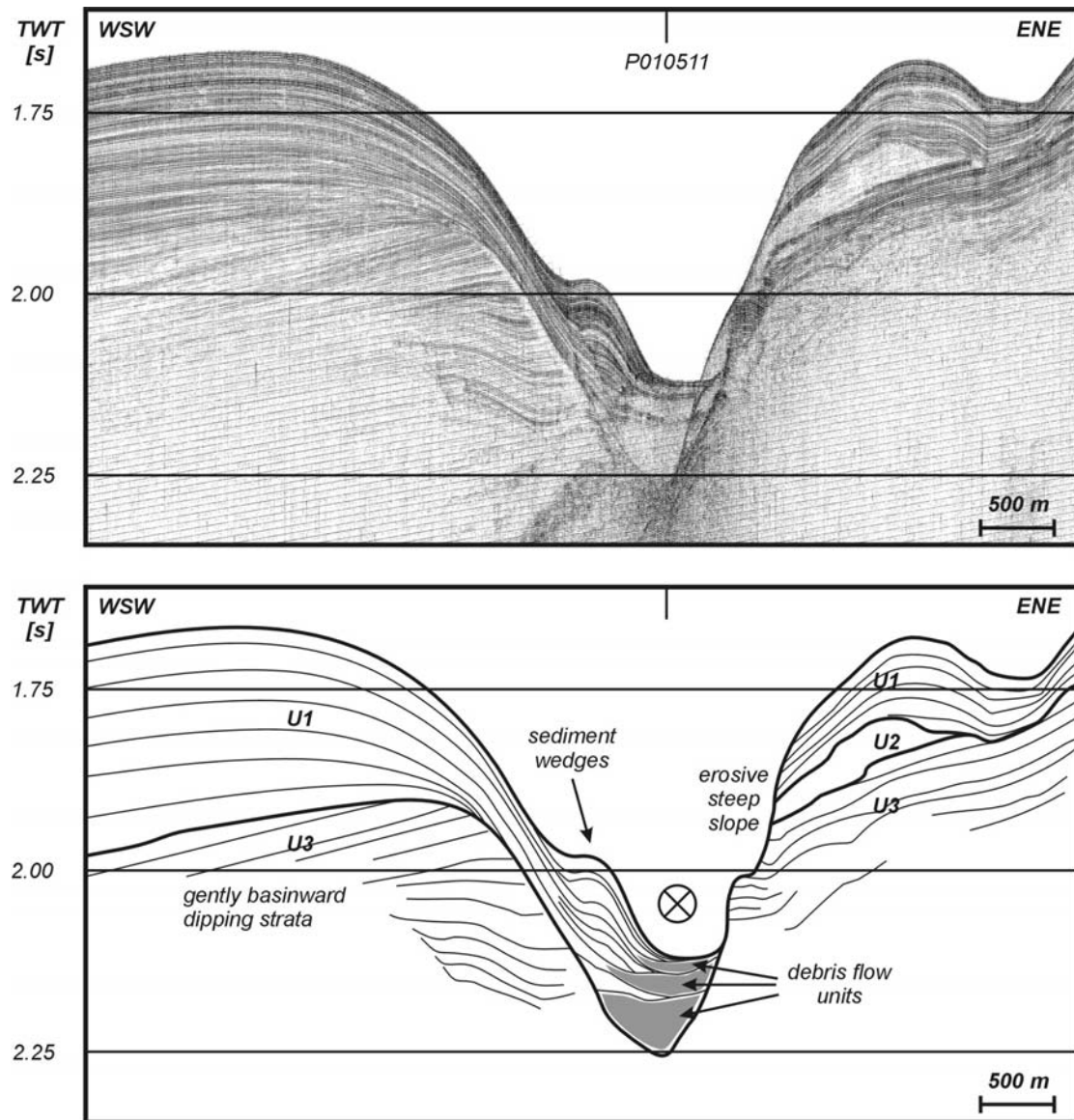


**Figure 6.44:** P970533: Profile across the deepest part of the Arwen channel, which cuts very deeply into unit U3. Only a small outlier of unit U2 is present on the eastern flank. Unit U1 is very thick in the WSW, gently decreasing in thickness towards the channel. Debris flow units are intercalated between prograding units into the channel.

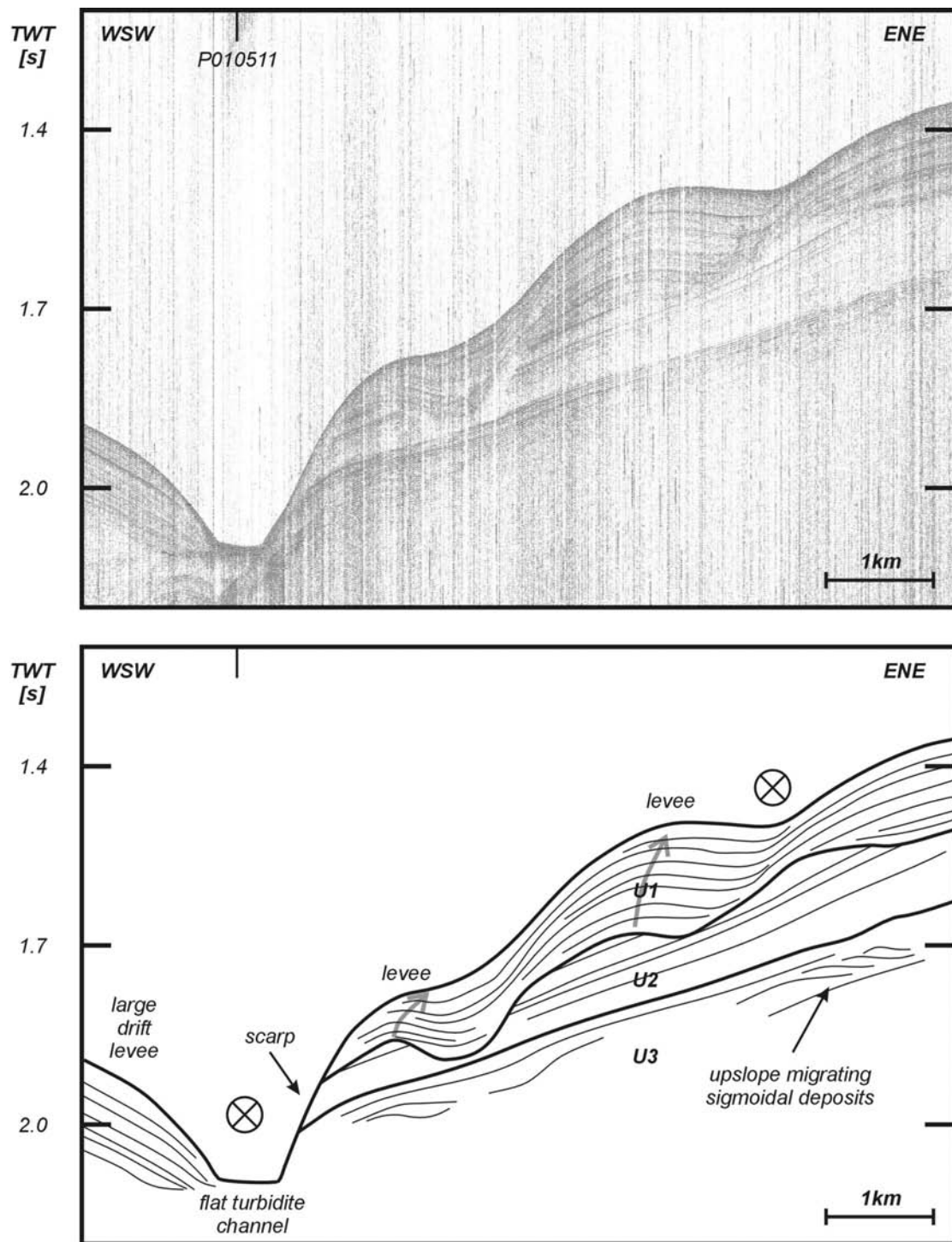


**Figure 6.45:** P980506: Profile across the Arwen channel and its eastern flank. Unit U2 is heavily incised and shows converging high-amplitude reflectors. The channel floor is relatively flat. Note the ENE prograding sediment levees along the ENE flank, associated with the downslope running Elrond channel.

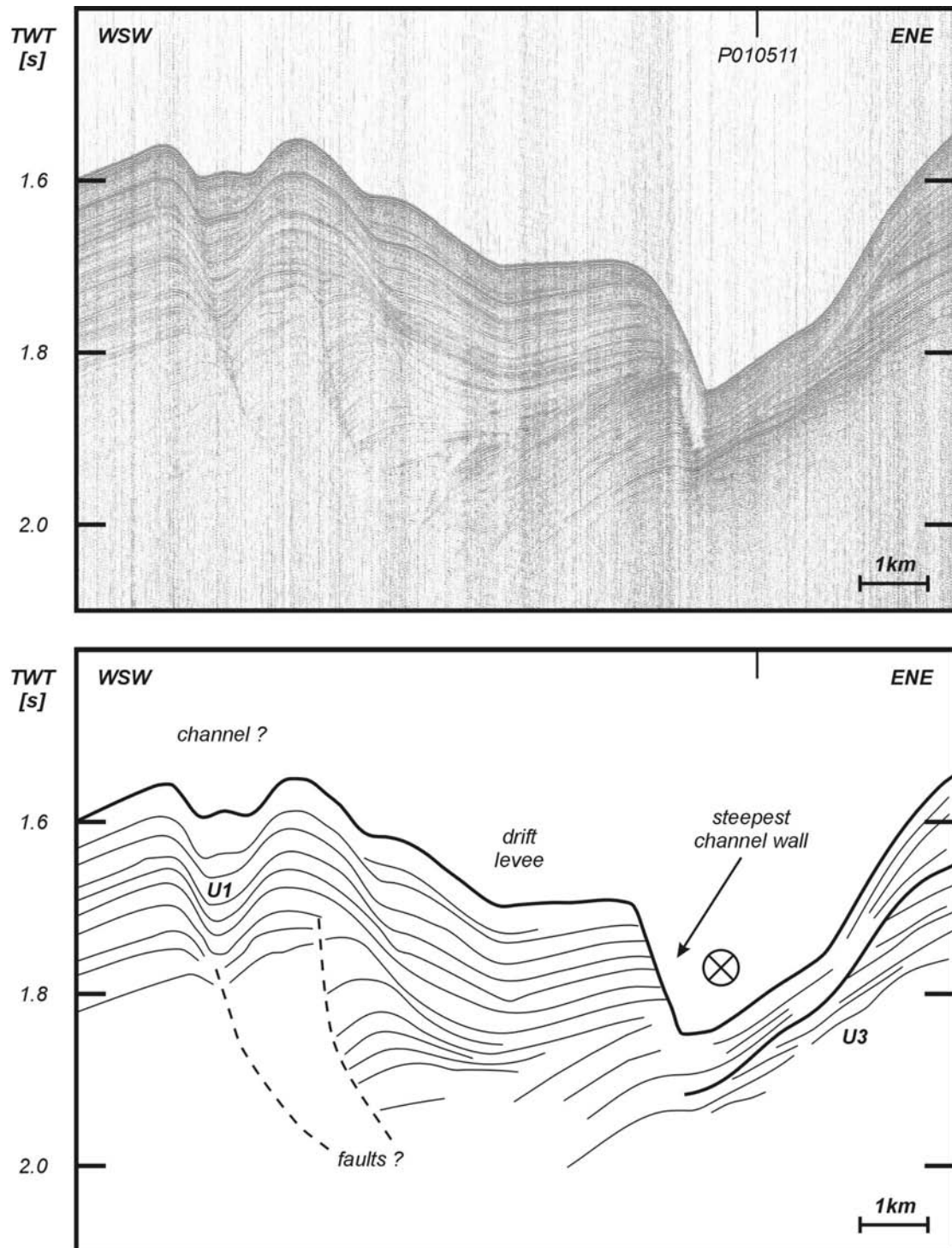


**Figure 6.46:** P980507: Profile across the Arwen channel and its western flank. Note the very steep western wall and the presumed syndimentary faults in the western levee. The channel-like feature at the seafloor seems to be related with these faults.

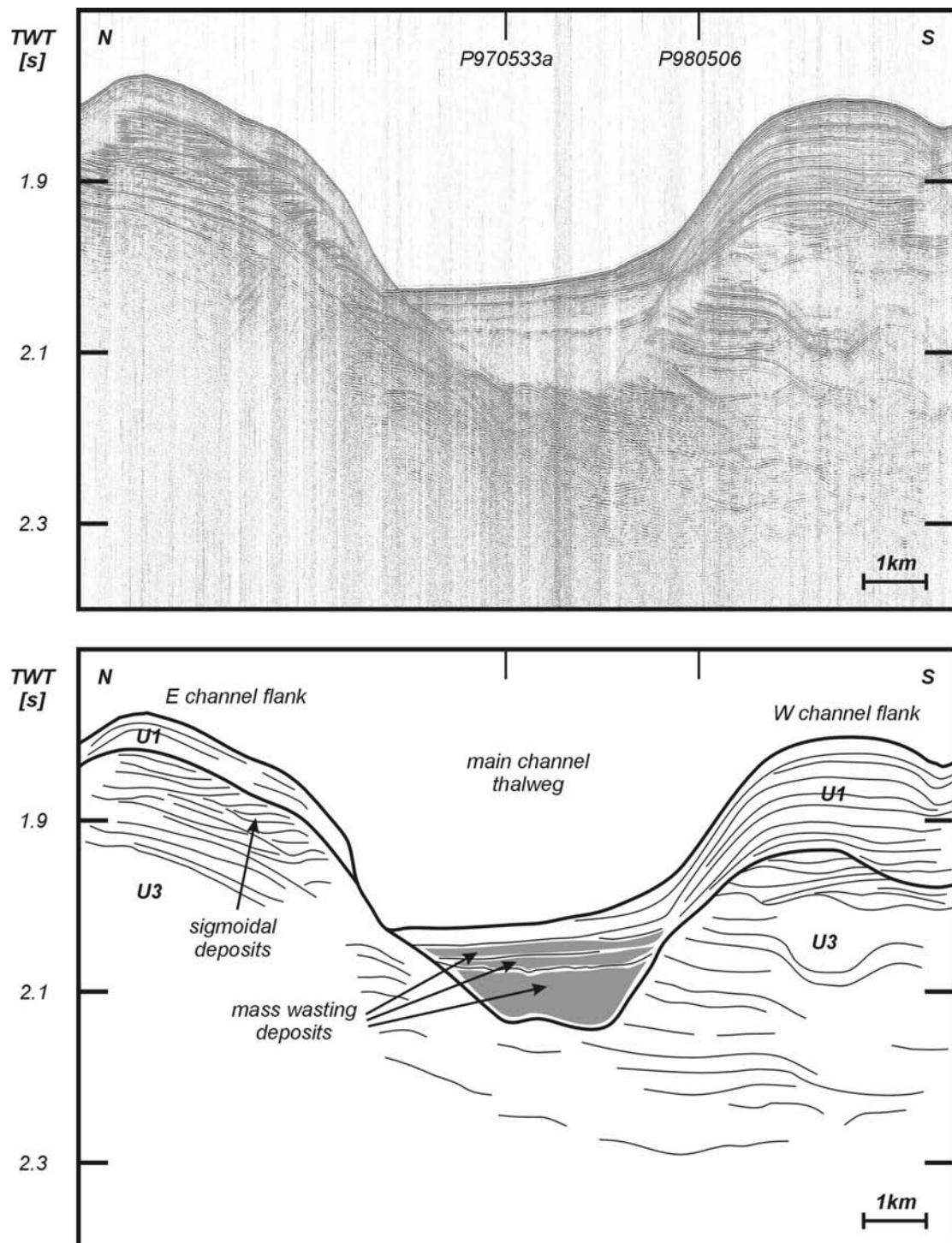


**Figure 6.47:** P010511b: Profile along the main axis of the Arwen channel. Note the major mass wasting deposits within the main channel thalweg. In the north, unit U3 is characterized by sigmoidal deposits.

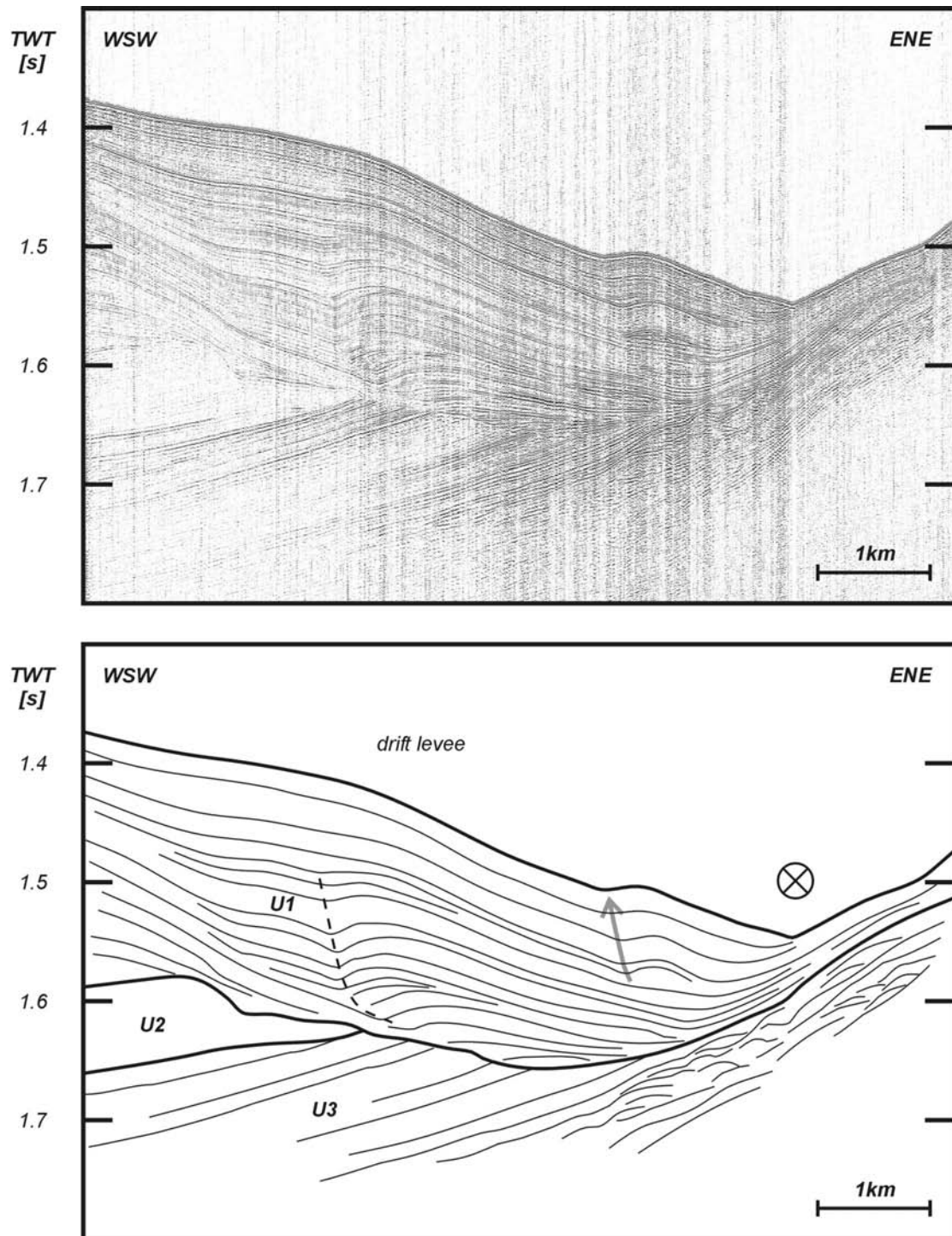


**Figure 6.48:** P980519b: Detail of profile P980519 (Fig. 6.4) across the Arwen channel and its drift levee. Unit U3 is characterized by upslope complex sigmoidal deposits. Like profile P980521 (Fig. 6.3), the lower deposits of unit U1 are characterized by a complex reflector configuration with a WSW progradation.

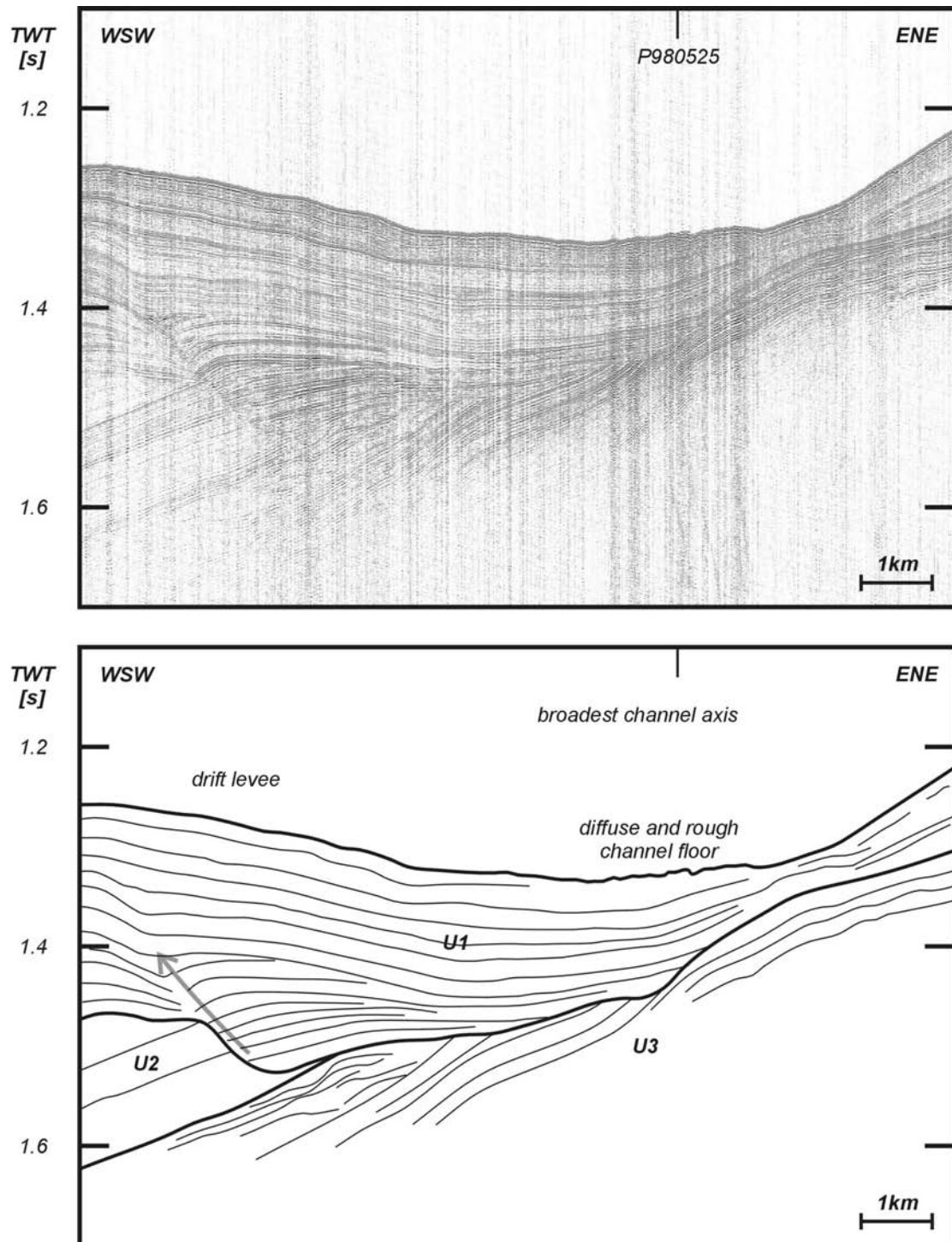


**Figure 6.49:** P980513: Profile across a broad Arwen channel with a rough and diffuse seafloor. Note the very deeply buried and incised unit U2.

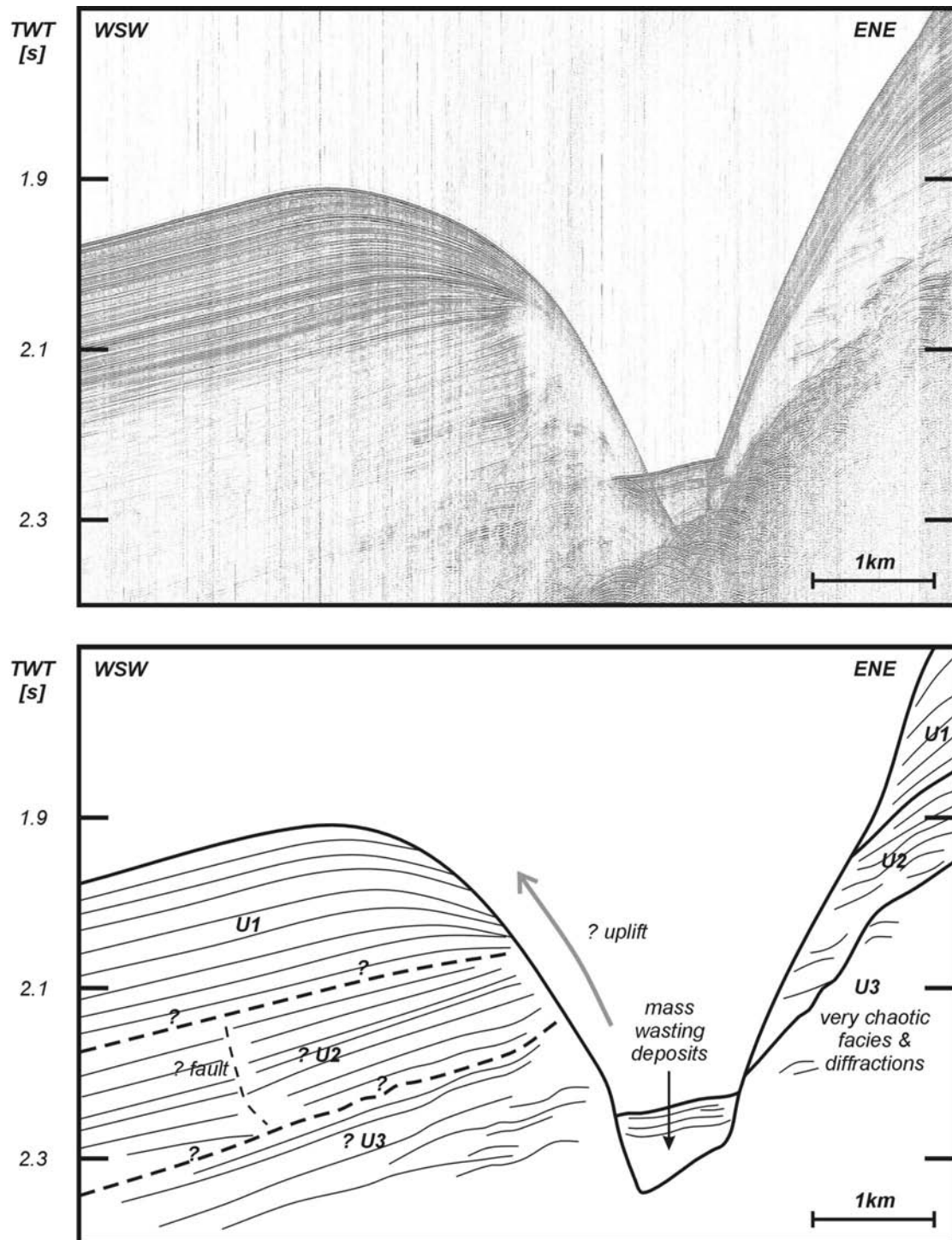


**Figure 6.50:** P010531b: Profile across the southern part of the Celeborn channel. Both channel walls are very steep. The reflector configuration of the presumed unit U2 at the western flank of the channel suggests the presence of a fault. The entire unit seems to be tilted basinward.

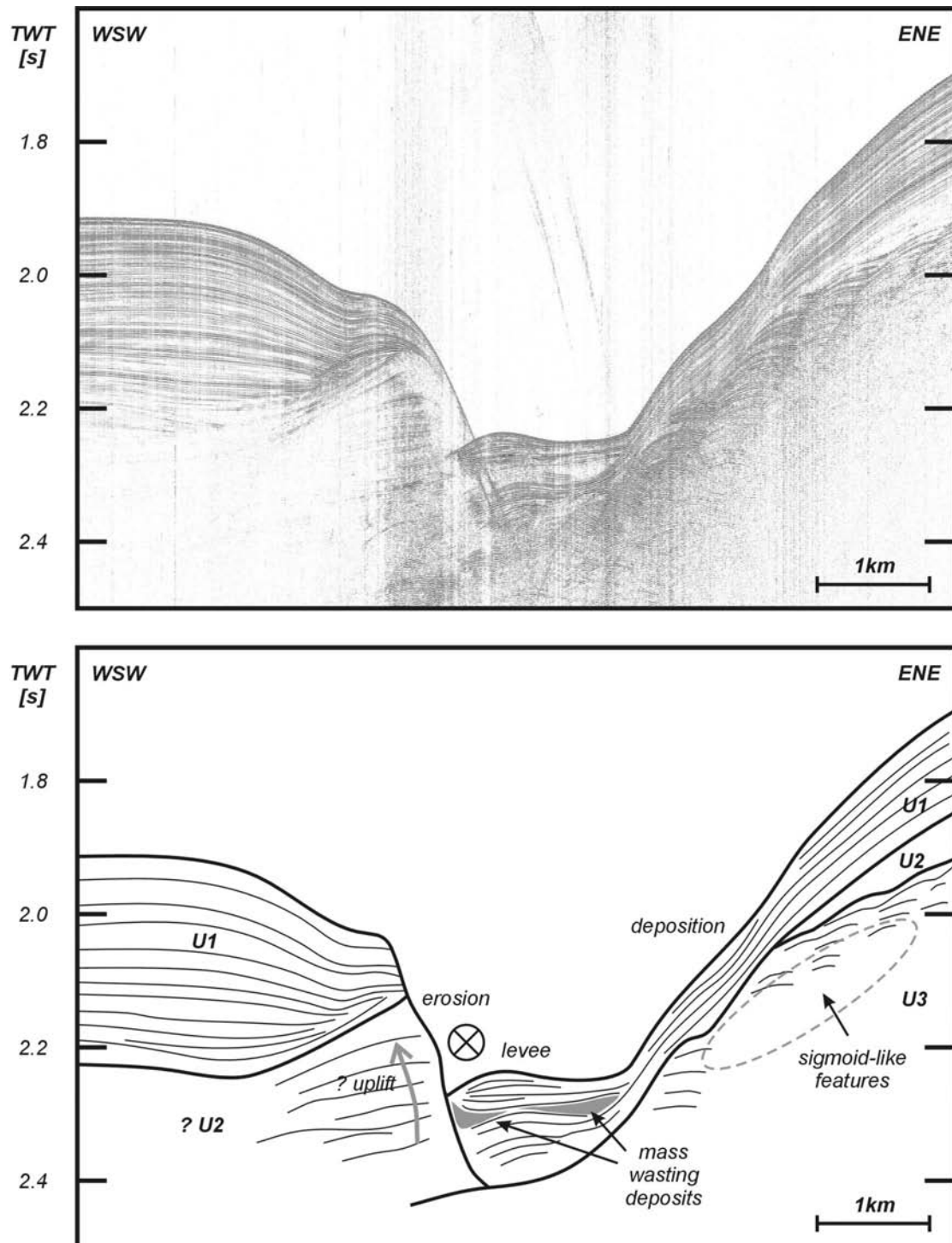


**Figure 6.51:** P010533: Profile across the Celeborn channel. Note the presence of the mass-wasting deposits intercalated with an intra-channel levee. The current seems to be focussed along the western channel flank. The lower reflections of unit U1 onlap upon their lower boundary, which also seems to be lifted up.

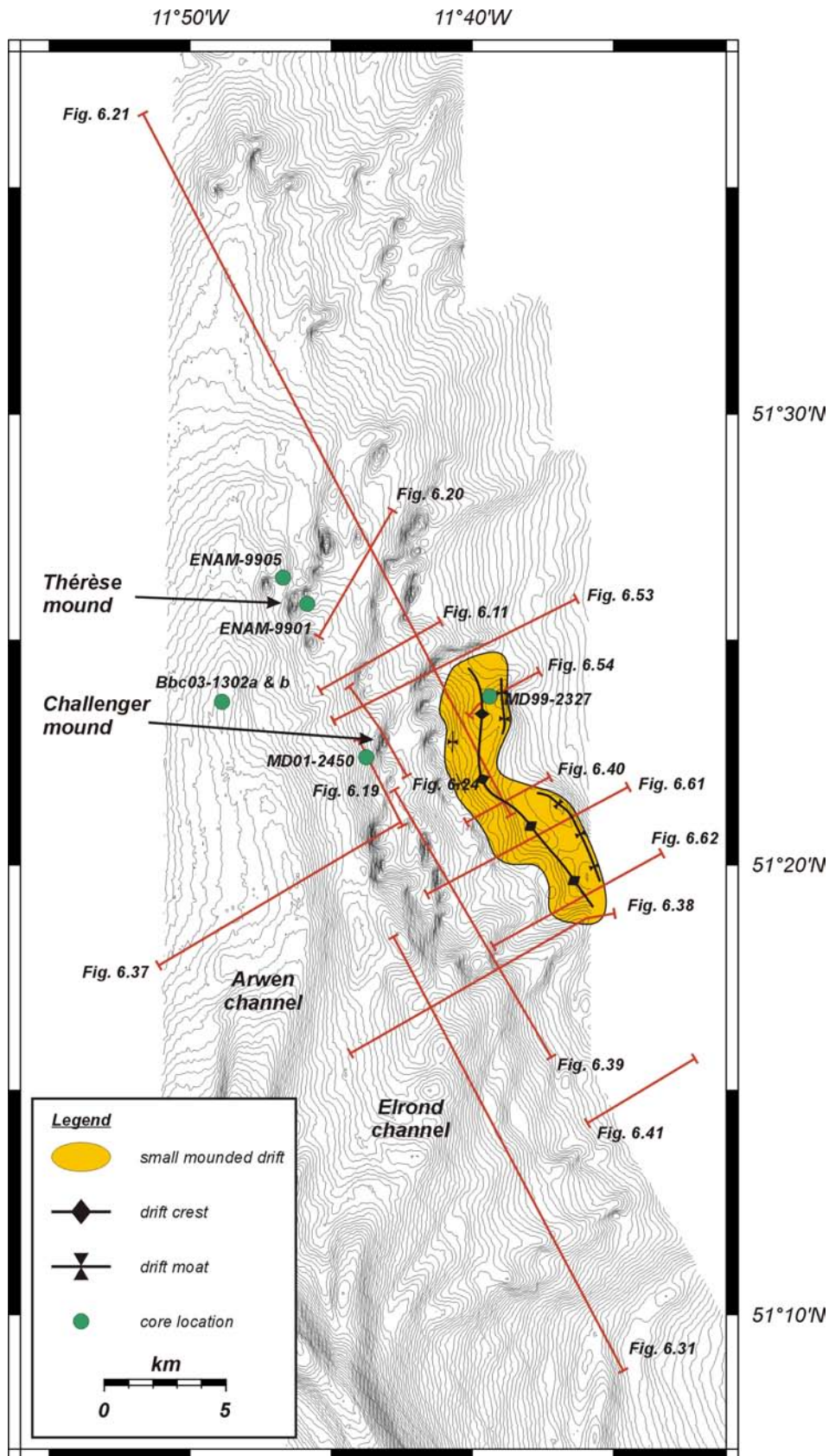


**Figure 6.52:** Positions of cores and significant profiles on a multibeam background, illustrating the location, morphology and characteristics of the small mounded drift in the Belgica mound province.

### 6.4.2.3 Discussion

These alongslope channels were created during a Late Pliocene erosion event, after which the current seems to keep flowing. At their southern extremities, the channels are deeper and less covered with sediments, implying a vigorous current preventing deposition. To the north, the channels broaden, become less deep and more sedimentation occurs. The current is thus less vigorous, but still a channel is present. Eventually, the entire channel deflects gently to the north and shallows. The contour current is thus plastered against the eastern slope of the Porcupine Seabight, flowing towards the north and is eventually forced to climb upslope where it will lose intensity and disappear. Nevertheless, the possible contribution of downslope flows can not be excluded. As a consequence, a thick levee (approximately 200 to 300 ms TWT) is built up by strata that progressively terminate approaching the channel axis with an onlap (Fig. 6.3) and downlap configuration (Fig. 6.21). The geometry of such contour parallel, upslope-prograding levee shares many similarities with drift levees and associated moat channels, typical for most of the separated, elongated-mounded drifts (Fulthorpe & Carter, 1991; Faugères et al., 1999; Stow et al., 2002). The Faro drift, for example, features upslope prograding trends and various seismic facies underline the depositional patterns: e.g. a shift from aggradation with continuous semi-parallel reflections to less continuous, oblique to sigmoidal reflections (progradation) towards the moat channel. Faugères et al. (1999) consider variations in geometry to be dependent of the interaction with the morphology, but also of the intensity of the current system, as this is the case with the Arwen and Galadriel-Celeborn channels and their associated levees.

### 6.4.3 Depositional features around mounds

The geometry and reflector terminations of the U1 strata around the mounds can yield more information concerning the mound settlement and growth. Secondly, they can assess the influence of the mounds on the deposition of unit U1. Therefore, a few mounds have been selected to study the nature of reflector termination and behaviour of the earlier defined seismic sections. Also, a few cores have been studied within the vicinity of these mounds to create a better insight in the recent sedimentary environment.

#### 6.4.3.1 Geophysical evidence

The mound shown on profiles P970536 and P980549 appears as a single mound rooted on U2 (Figs. 6.38 and 6.39). Northeast of the mound, all reflectors within U1 are parallel and onlap against the mound. SW of the mound, the section is reduced in thickness and shows an upslope migrating wavy geometry with reflectors overlapping on the mound. The uppermost reflectors even feature small moats with a width of about 100 m, suggesting the action of currents. In a NNE-SSW profile (Fig. 6.39), the geometry of U1 is dominated by the presence of moat structures with a width of about 1 km on both sides of the mound. These structures seem to have been present since the deposition of the lowermost U1 reflectors and probably are a transverse section through the downslope running gullies flanking this mound as observed in figure 6.52. Both gullies coalesce into the Elrond channel (Fig. 6.52). Yet, there is a striking difference between the sediment bodies at both sides of the mound. On the NNW side, the geometry is mounded and seems to prograde gently towards the gully. Some of the lowermost reflectors do not even

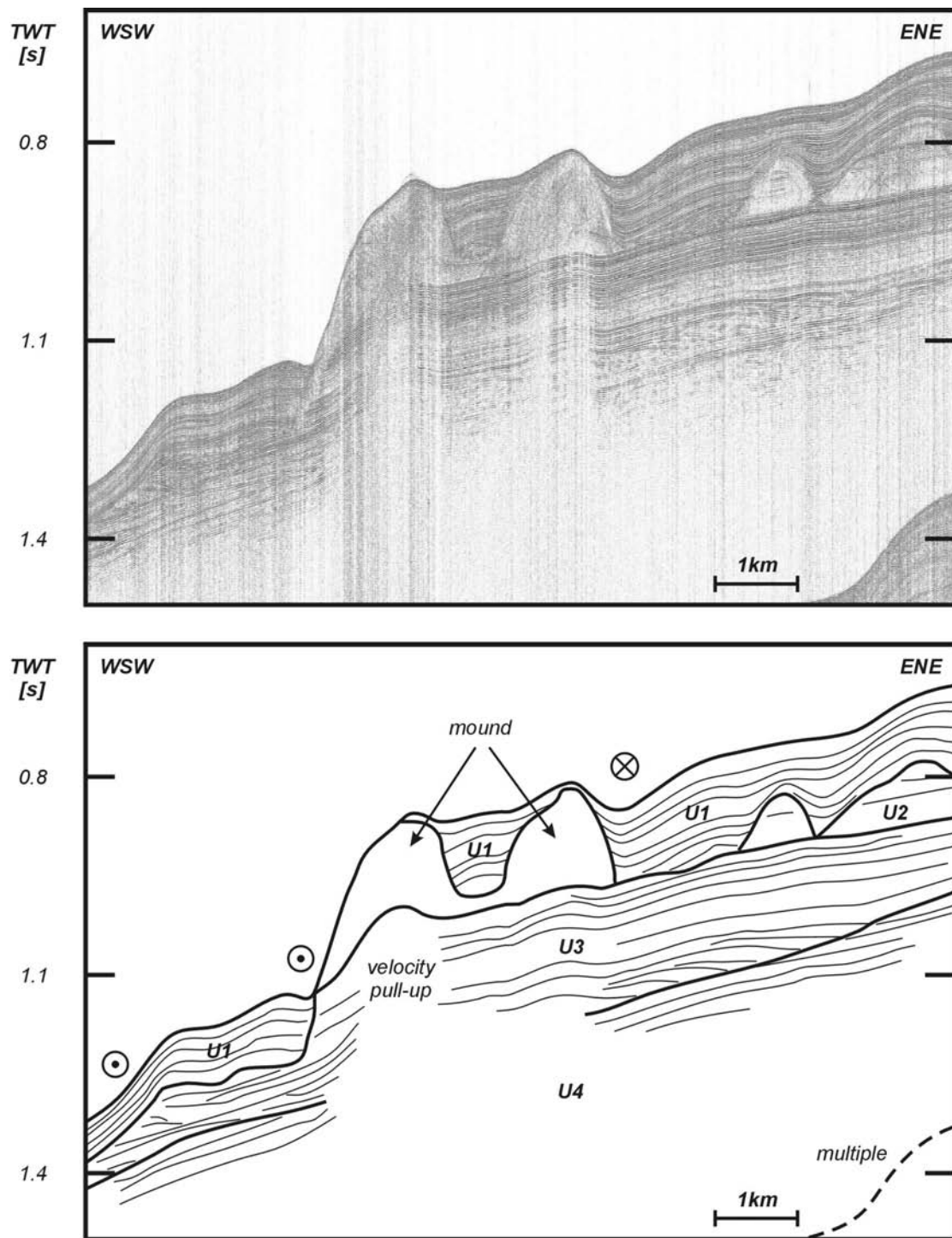


**Figure 6.53:** P010523: Profile along the northern edge of the small mounded drift. The lower strata of unit U3 are onlapping upon their lower boundary. Note the steep incision of this unit, upon which two mounds are rooted. The downslope side is influenced by currents coming from a nearby downslope running gully.

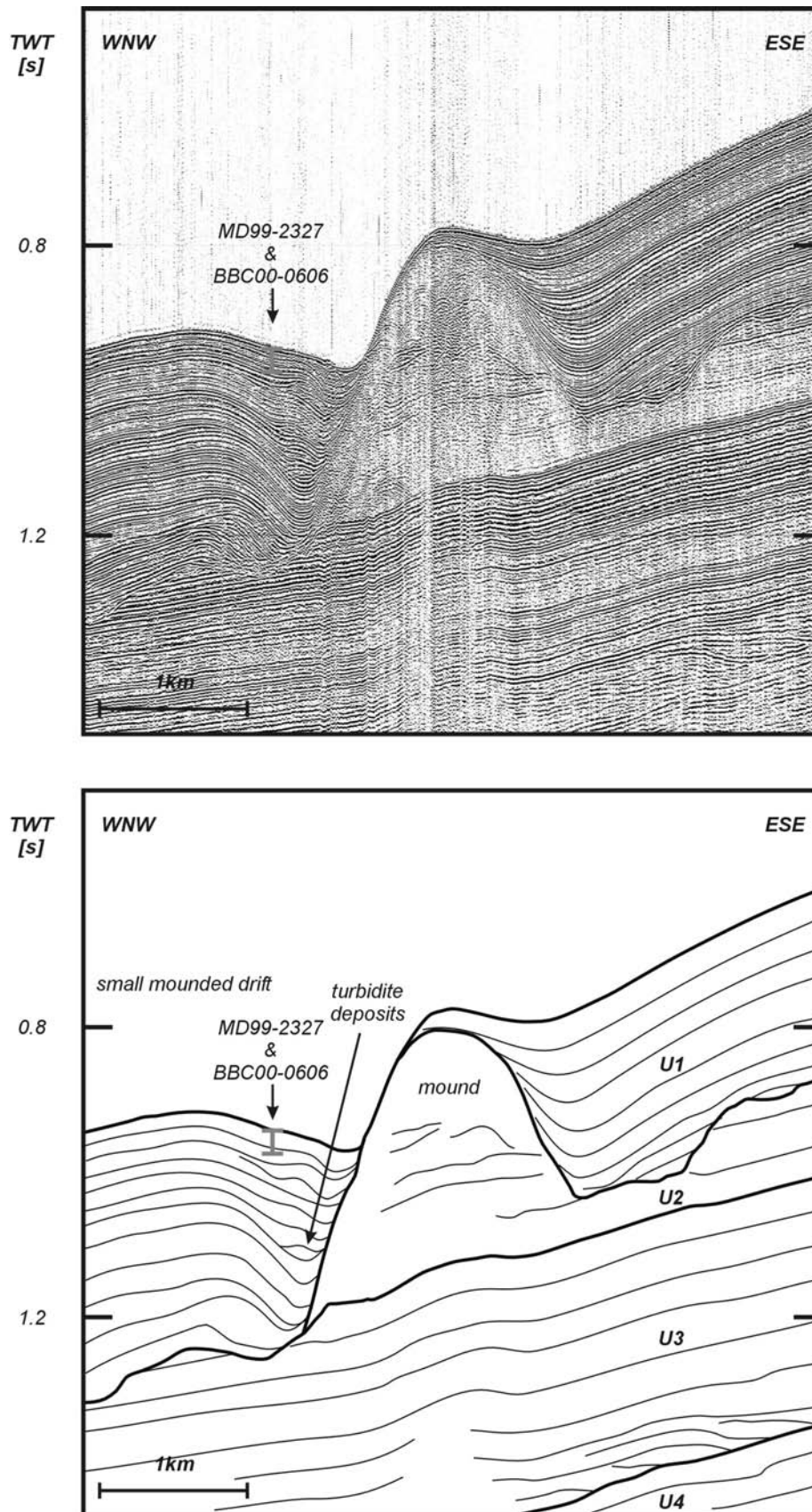


**Figure 6.54:** P010507: Detailed seismic profile across the core site of MD99-2327 and Bbc00-0606 on the eastern flank of a small mounded drift at the foot of a large mound. At the eastern side of this mound, the unit U1 strata are ponded against this mound.

seem to reach the foot of the mound. SSE of the mound, the geometry is more sheeted, suggesting a more aggradational style, though a slight southward progradation is evident.

Moreover, the influence of the Arwen channel on the geometry of the sedimentary deposits surrounding the mounds should also not be underestimated. In general, the upslope side of the mounds, a thick unit U1 is always present, ponded against the mounds. On the downslope side, generally the side faced to the Arwen channel, the flank of the mound mostly remains exposed (Figs. 6.3, 6.24, 6.21, 6.53, 6.54 and 6.38). In this part of the study area, the channel broadens and shallows, whereas in the south it is deeper and narrower (Figs. 6.42 and 6.52). Here, the northward focussed current of the channel can meet and interact with the mounds and the steep topography created by the RD1 discontinuity. Therefore, at this eastern side of the channel, the geometry, thickness and reflection termination of unit U1 is quite variable. These generally wavy and undulating sediment bodies are relatively thin and have been deposited on a palaeo-slope which is steeper in the south (approximately 4°) than in the north (2°). The total thickness can be locally reduced to 50 ms TWT, with a wavy reflector configuration. Profile P030509 (Fig. 6.20) is located in such a flat area in between two mound ridges with a maximum U1 thickness of 30 ms TWT. On profile P970536 (Fig. 6.38), this part of the slope can be interpreted as characterized by gently upslope migrating sediment waves, since according to the definition of Wynn & Stow (2002), sediment waves are large-scale undulating, depositional bedforms that are generally observed beneath a current (turbidite or contourite) flowing at, or close to, the seafloor. A few kilometres to the north, the amplitude of these sediment waves seems more reduced (Figs. 6.3 and 6.4). Further to the south, similar features are encountered, but can rather be interpreted as levees (Figs. 6.31 and 6.45), since they seem to be related to the irregularly downslope running NNE-SSW Elrond channel. Moreover, it was demonstrated earlier (Fig. 6.6) that this entire part of the slope was also characterized by downslope running gullies. Side-scan sonar imagery indicates well-sorted sands associated to these downslope running gullies, influenced by alongslope running contour currents (Huvenne, 2003). These authors also suggested this wide area was influenced by a strong dynamic environment, influenced by the irregular topography. The presence of a coarse seafloor, observed on the side-scan sonar record (Fig. 6.7), was attributed to local current intensifications between the mounds. This suggests that the wavy and undulating sediment bodies between the mounds and the main axis of the Arwen channel were created under a regime of mixed influence of as well downslope as alongslope (bottom) currents. Therefore, these deposits are considered to be sediment waves with a mixed turbiditic-contouritic origin.

#### **6.4.3.2 Core evidence**

Seismic and side-scan sonar imagery have already demonstrated the influence of bottom currents on the youngest deposits of the Belgica mound province. A study of three cores within the vicinity of two well-studied mounds was carried out to verify the presence of (turbiditic as contouritic) bottom current deposits, as well as to reveal possible fluctuations in intensity of these processes (Fig. 6.52). Cores ENAM-9901 (635 cm) and ENAM-9905 (633 cm) were taken respectively at the upslope NE side (948 m bsl) and at the downslope SW foot (1025 m bsl) of Thérèse mound. Both cores were analysed within the framework of the

M.Sc. thesis of Lekens (2000). Core MD01-2450 (1197 cm) was acquired at the foot of Challenger mound (Fig. 6.24) at a water depth of 944 m. A detailed paleomagnetic study of this core was performed by Foubert (2002).

The sediments of core ENAM-9901 (Fig. 6.55) are poorly sorted silty clays with a relatively high sand content (Lekens, 2000). As already was discussed in chapter 4, the relatively high content of ice-rafted sand does not allow to unambiguously identify IRE. However, in contrast with cores MD99-2327 and MD01-2449, subtle variations in magnetic susceptibility do suggest the presence of a limited amount of LIS or GIS-sourced IRD. Therefore, these peaks are correlated with HL1, 2 and 3. Although these cores are located a few kilometres west of MD99-2327, the only possible factor that might have contributed in the presence of more typical HL IRD, is the greater water depth. This might have reduced the risk of grounded BIIS icebergs, allowing non-BIIS icebergs to reach this location. On the other hand, the IRD peaks outside the HL intervals most probably have a BIIS source. The relative changes in the intensity of the paleo bottom current strength in this core can best be approached by variations in the mean grainsize of the silt fraction between 10 and 63  $\mu\text{m}$  (McCave *et al.*, 1995). This fraction is the most sensitive to erosion by bottom currents, where the mean grainsize of this fraction will increase with the currents vigour, since the fine material is winnowed away. This method allows to distinguish three episodes of enhanced currents, separated by episodes of weaker bottom current flow (A, B and C). Episodes B and C seem to be associated with respectively HL 1 and 2.

A different sedimentary environment is illustrated by core ENAM-9905 (Fig. 6.56) at the foot of Thérèse mound. Compared with ENAM-9901, this core has a higher content of sand, coral and shell debris (Lekens, 2000). HL 3 has not been observed, although another well-defined peak in the IRD fraction was observed, most probably linked to the Younger Dryas event (10-11 ka B.P.). However, the two major differences are observed at the top and bottom of the core, characterized by relatively thick sand layers. The lowermost layer is characterized by a sharp lower boundary and as well the decrease in sorting as the grainsize suggest this is a turbidite deposit. The sand observed at the core top also is characterized by a better sorting after episode A, indicating an increasing bottom current. This is in accordance with observations at the foot of Thérèse mound, where side-scan sonar imagery suggests sand waves (Foubert *et al.*, in press; Huvenne, 2003).

A similar situation can be met at the foot of Challenger mound, illustrated by core MD01-2450 (Fig. 6.57). This core consists of dark grey silty clays with common to abundant nannofossil and fine to medium cm-scaled sand layers. Sulphide specks are observed throughout this core and are found in laminations between 750 to 1050 cm. Therefore, only the first seven metres of this core are considered, although no grainsize analyses were performed. As in the previously discussed cores, Heinrich layers were observed, characterized by a higher density or magnetic susceptibility. The luminosity of HL2 is significantly higher than the other IRD events. The zone between 508 and 532 cm is characterized by a sharp lower boundary, higher magnetic susceptibility, a sharp density and a darker shade, which is also observed on the core photograph. Like core ENAM-9905, this is a turbidite deposit, illustrating the turbulent environment at the foot of a mound.

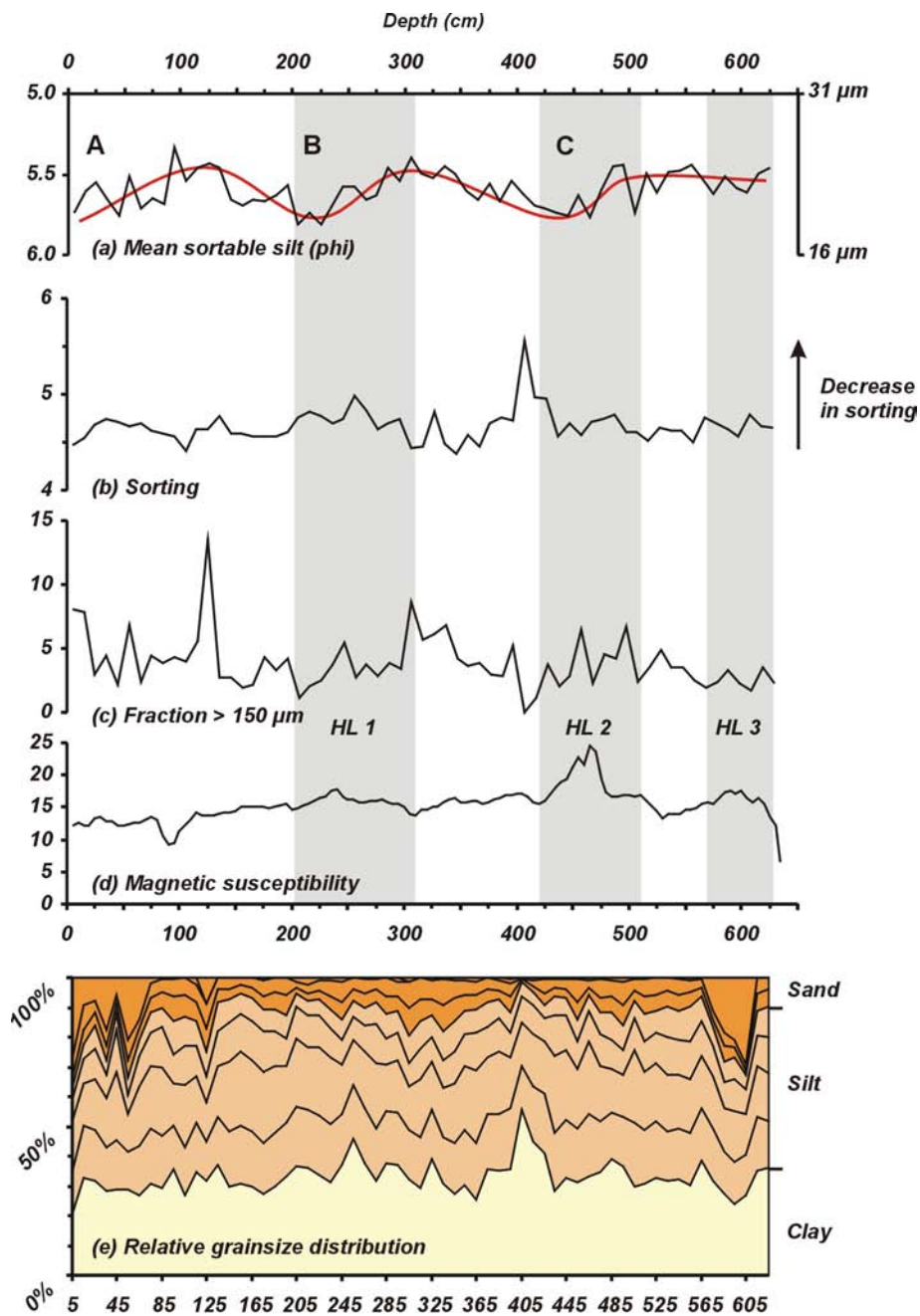


**Figure 6.55:** Physical properties and grainsize characteristics of core ENAM-9901 with (a) mean sortable silt, (b) sorting, (c) the fraction > 150  $\mu\text{m}$ , (d) magnetic susceptibility and (e) the relative grainsize distribution. A, B and C indicate episodes of lower bottom current activity and the red line illustrates the average trend in mean sortable silt.

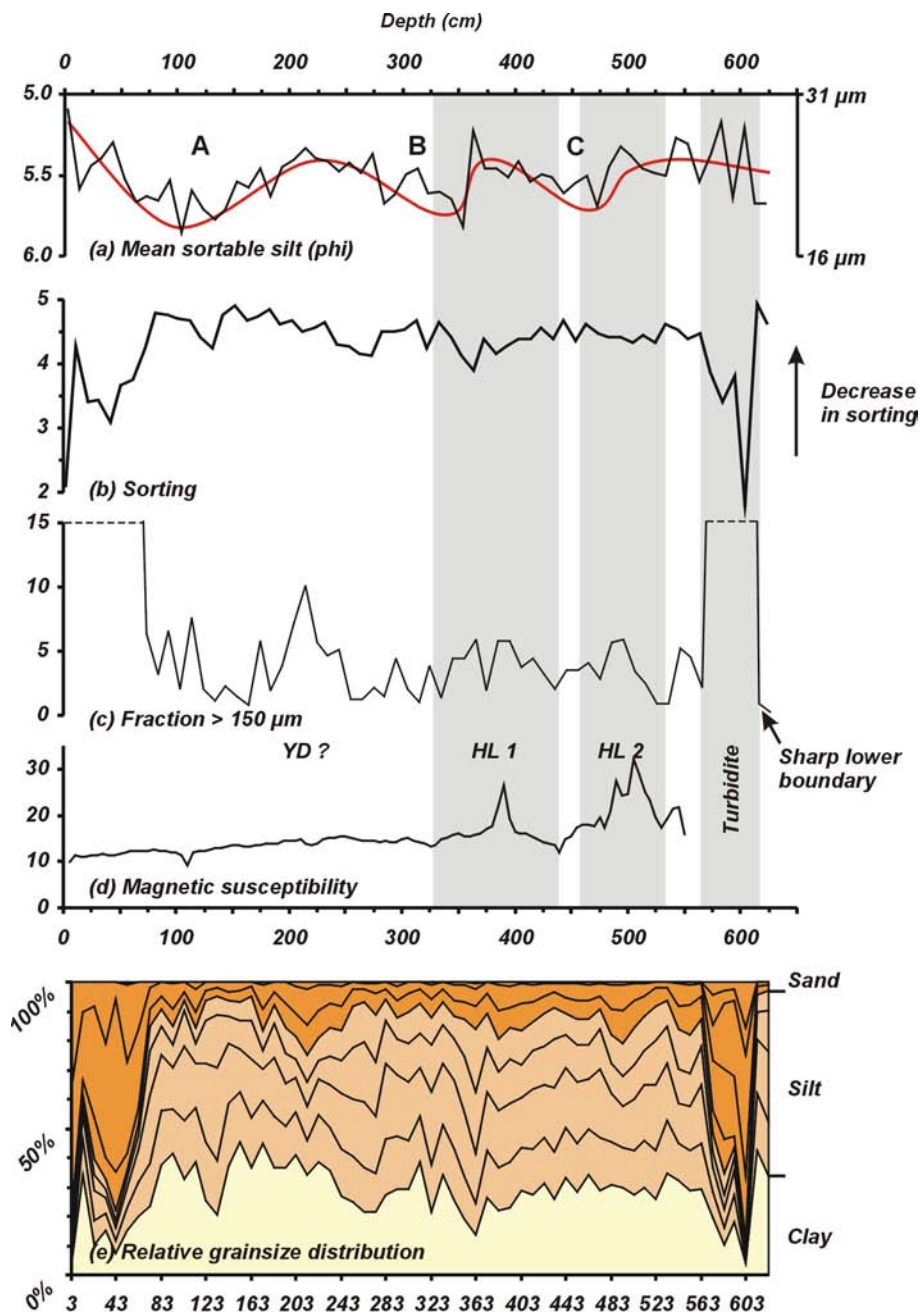


**Figure 6.56:** Physical properties and grainsize characteristics of core ENAM-9905 with (a) mean sortable silt, (b) sorting, (c) the fraction > 150  $\mu\text{m}$ , (d) magnetic susceptibility and (e) the relative grainsize distribution. A, B and C indicate episodes of lower bottom current activity and the red line illustrates the average trend in mean sortable silt.

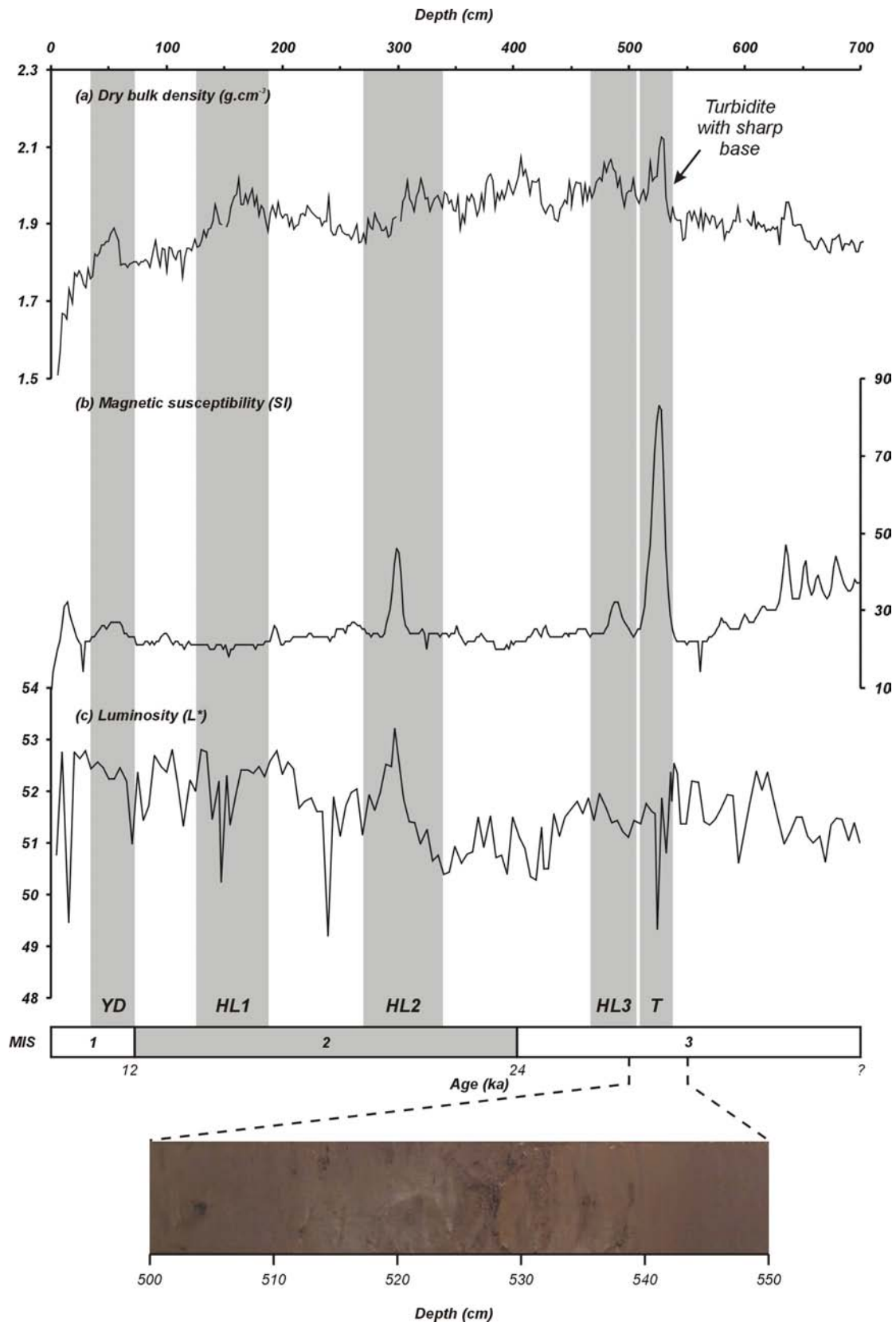


**Figure 6.57:** Physical properties of core MD01-2450 with (a) dry bulk density ( $\text{g.cm}^{-3}$ ), (b) magnetic susceptibility (SI) and (c) luminosity ( $L^*$ ). The inferred turbidite interval is illustrated with a core section photograph.

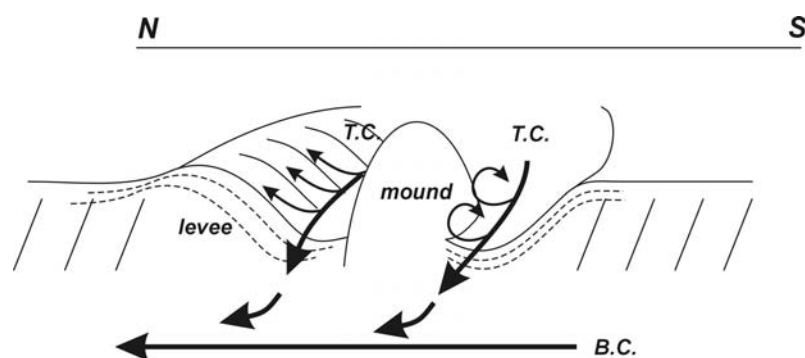


**Figure 6.58:** 3D sketch illustrating the possible function of the gullies flanking the mound. T.C.: Turbidity Current; B.C.: Bottom Current at the foot of one of the alongslope running ridges.

#### 6.4.3.2 Discussion

Between the channel and the mounds, the sedimentation is under the influence of bottom currents. Large-scale sediment waves with variable amplitude and levee-like deposits suggest the interaction of contour-parallel currents sweeping the foot of the (alignment of) mounds and the downslope running gullies. This also explains the reduction in thickness of unit U1 at this location. On the other side, it seems that respectively at the NE and SSE side of the mounds, unit U1 is ponded against them. Here, the mounds truly act as a barrier, piling up the sediments 'behind' them, suggesting: (1) currents are less vigorous upslope of the mounds, (2) sedimentation is due to downslope flowing turbidity currents efficiently stopped by the mounds, or (3) sedimentation is allowed in the eastern, lee-side of the mounds. The current flowing along the flank of the mound facing the channel is likely stronger, as illustrated by core ENAM-9905. According to Faugères *et al.*, (1993) and Faugères *et al.* (1999), steep slopes (in this case the flanks of the mounds) can cause an intensification of the current, which is responsible for the creation of subtle moats surrounding the obstacles. In this case such a depression is sometimes evident on the SW (steep) side of the mounds. Furthermore, as observed on the multibeam map, the mounds are flanked by gullies. Most of these gullies are rather local and only seem to influence the seabed morphology close to the mounds. A hint on the true nature of these gullies is given by the alongslope profile P980549. The NNW gully is flanked by a small, mounded and slightly prograding levee-like feature which could very well be a turbidite levee (Faugères *et al.*, 1999). This, however is not observed on the SSE side of the mound, where only aggradation is observed. We suggest that in general, these gullies are minor turbiditic channels (Fig. 6.58), responsible for small turbidite deposits at the foot of the mound. When inferring turbidite currents, the build-up of a levee on its right-hand side is expected to be due to the deflection by the Coriolis force in the northern hemisphere (Faugères *et al.*, 1999). Here, the presence of a mound at this side might be one of the restraining factors of the construction of a levee. However, we can not exclude any influence of a northward flowing bottom current in the creation of the gullies on the southern side of the mounds. As well, these bottom currents can explain the local character of these small turbidite channels. At the lowermost part of these gullies, the energy of the northward directed bottom currents might be stronger, taking up the downslope transported material and smoothen the seafloor at the foot of the alongslope running ridges. This can be observed as mobile sand sheets, observed in the top of core ENAM-9905 and side-scan sonar imagery.

#### 6.4.4 Small mounded drift

A very peculiar area, east of an alignment of mounds, draws our attention due to its topography and the geometry of unit U1 (Figs. 6.52 and 6.59). In between the individual mound clusters, the mounds are flanked by southwest oriented gullies. More to the west, yet another elongated mounded feature is observed with a relief of approximately 50 to 60 m above the sea floor, 12 km length and maximum 4 km width. A sub-bottom profiler record at the northern side of this sediment body only shows lightly mounded, subparallel strata (Fig. 6.60). At its eastern side, this sediment body is limited by a (north-south elongated) moat channel, which seems to be, on its turn, flanked by a buried coral bank (Figs. 6.59 and 6.60). Although this buried mound is relatively local (approximately 1.5 km diameter), this structure makes part of a north-south elongated wall or flank. Core site MD99-2327 is located on the flank of a moat channel at the foot of a mound, where intense currents can be expected. Figure 6.60 indeed reveals the presence of a seabed typified by rippled sands. Moreover, seismic profiles discussed earlier and located in this zone, display the typical seven sections, characterized by changing amplitudes (Fig. 6.40). In this area, the geometry and reflector terminations of the U1 strata around the mounds can give an indication of the relative chronology of mound growth.

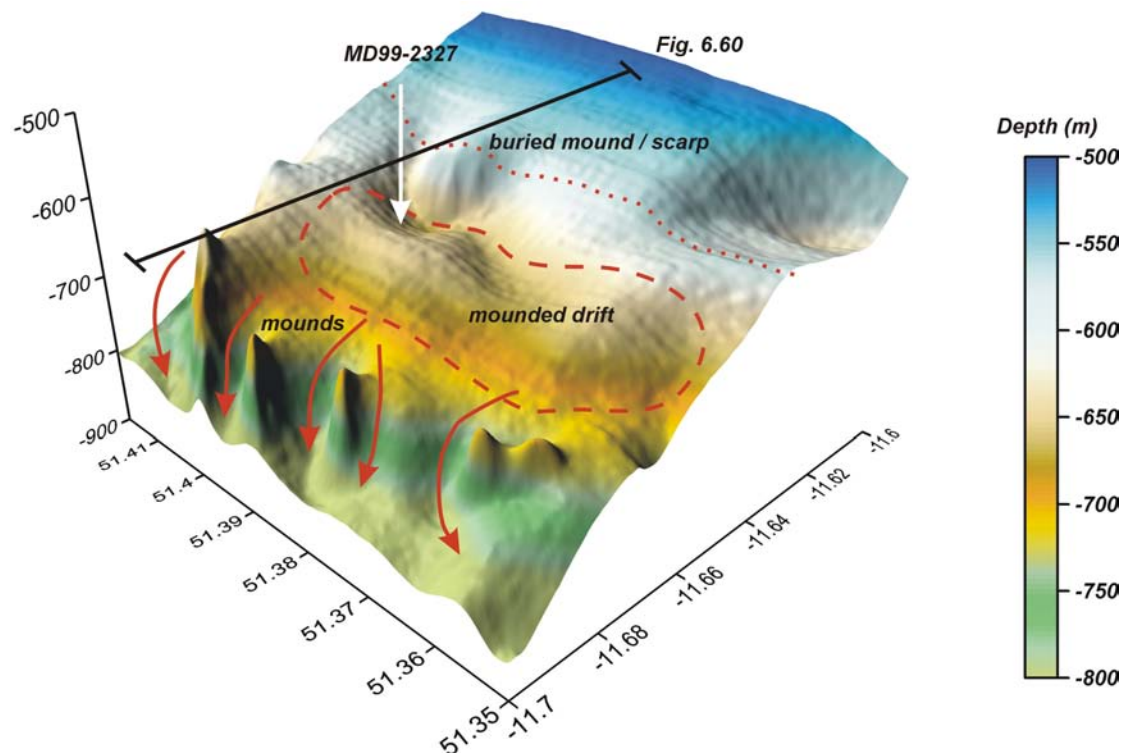


**Figure 6.59:** Surface 3D map of the northern part of the small mounded drift (red dashed lines) with position of core MD99-2327 and figure 6.60. The downslope running gullies flanking the mounds are indicated by the red arrows. The position of the U2 scarp is indicated with a red dotted line.

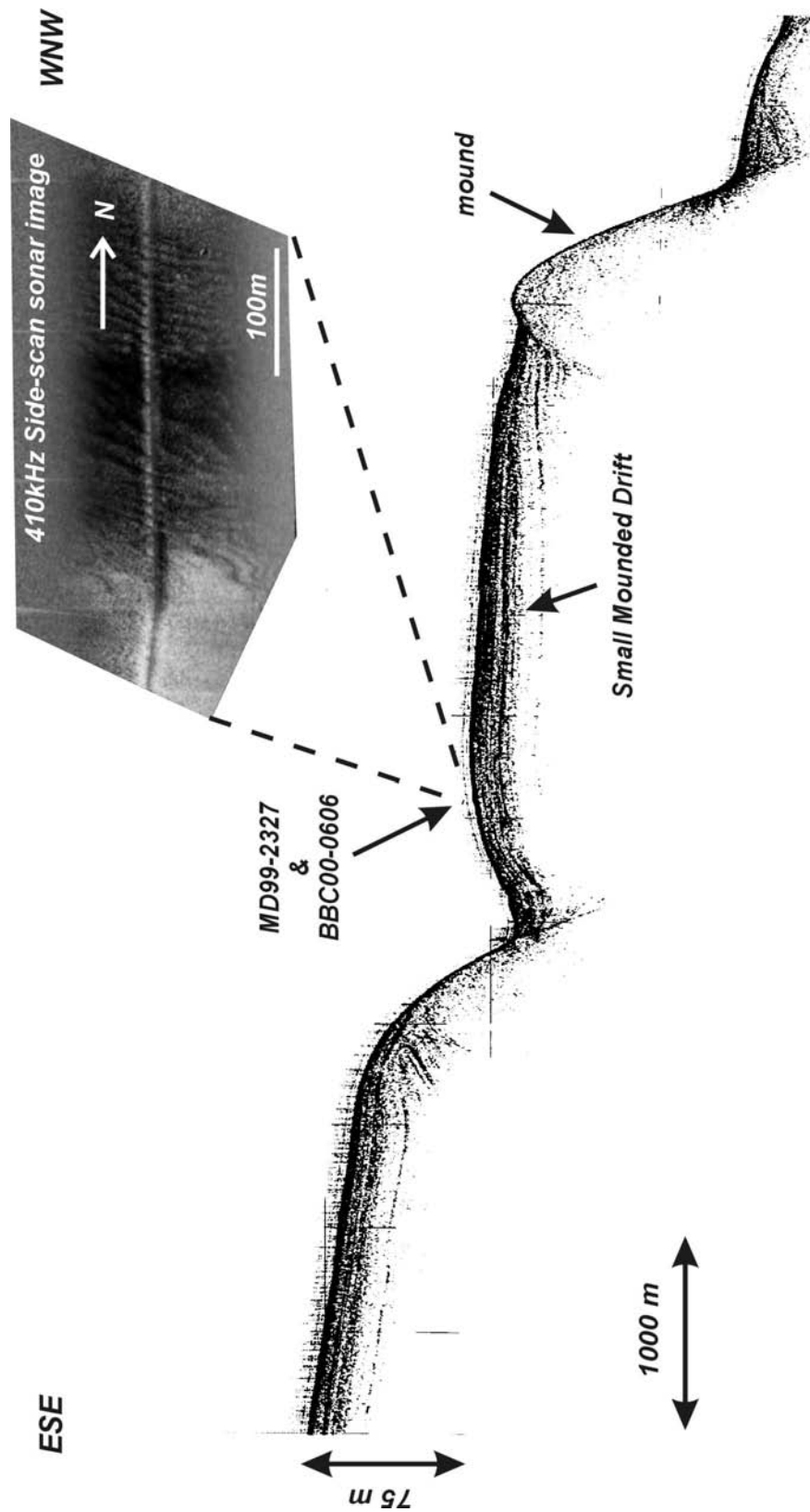


**Figure 6.60:** ESE-WNW oriented 3.5 kHz sub-bottom profiler line over the coring site MD99-2327 with inset of a 410 kHz side-scan sonar image with sand waves (RRS Discovery 248, courtesy of A. Wheeler, UCC, Ireland).

#### 6.4.4.1 Seismic and morphologic features

In between the mounds and the irregular paleotopography created by the RD1 erosion, one can observe unit U1 has a mounded feature with a moderate ENE progradation. In this area, the geometry of unit U1 seems to be controlled by the distance between the steep flanks of the mound and the U2 scarp. In a previous example (Fig. 6.38), the distance of this passage exceeds 5 km and a sheeted geometry is found. Only minor irregularities such as downlap features are found against the lower boundary. In this case (Figs. 6.40, 6.61, 6.62 and 6.38) however, the passage is relatively narrow (2 km or less) and the overall geometry has a mounded appearance with moats on both sides. The oldest deposits seem to downlap towards the WSW and the ENE. In this case, unit U1 is deposited within a narrow passage in between the steep flank of a mound, and a U2-scarp. In particular on the side of this scarp, large moat-like features (width up to 500 m) are observed. In some cases, they are filled with flat-topped acoustically transparent deposits (Figs. 6.61 and 6.40). The thickness of this mounded sediment body varies from 150 to 250 ms TWT. The crest of this mounded unit seems to be migrating to the ENE (Fig. 6.61). On the southwestern side of the mound, the thickness and reflector terminations are less pronounced, although subtle moats can be inferred.

The geometry and the reflector configuration of this sediment body suggests that (1) the mounds were already present before the deposition of unit U1 and, (2) mounds were large and steep enough to intensify currents at their foot and the U2 scarp since the start of the deposition of unit U1. In this way, the first deposits of U1 are only observed in the centre of this passage from where they progressively prograded through time towards the flanks, creating a mounded geometry with remarkable downlap on both sides. After the passage became filled the reflectors started to onlap, but currents (still active, though possibly reduced in strength) created moats on both sides. This change is also accompanied by discontinuities on other seismic profiles. In a way, this drift can be compared to mounded confined drifts as e.g. Louisville drift (Carter & McCave, 1994), the Sicily channel drift (Marani *et al.*, 1993) and the Sumba drift (Reed *et al.*, 1987) as defined by Faugères *et al.* (1999). Confined drifts appear similar to elongate drifts, but are deposited in passages between tectonic or volcanic highs and are confined by boundary channels on both sides. In the Belgica mound province however, the dimension of this small mounded drift is relatively small and it does not occur in a morphotectonically peculiar area such as the Louisville drift (Carter & McCave, 1994). In this case, the narrow passage is constructed by (1) an erosion event creating a scarp and (2) a coral bank. Nevertheless, confined drifts remain very rare and this example on one hand confirms their occurrence in peculiar areas, but on the other hand demonstrates that they do not need to be peculiar in a pure morphotectonical way.

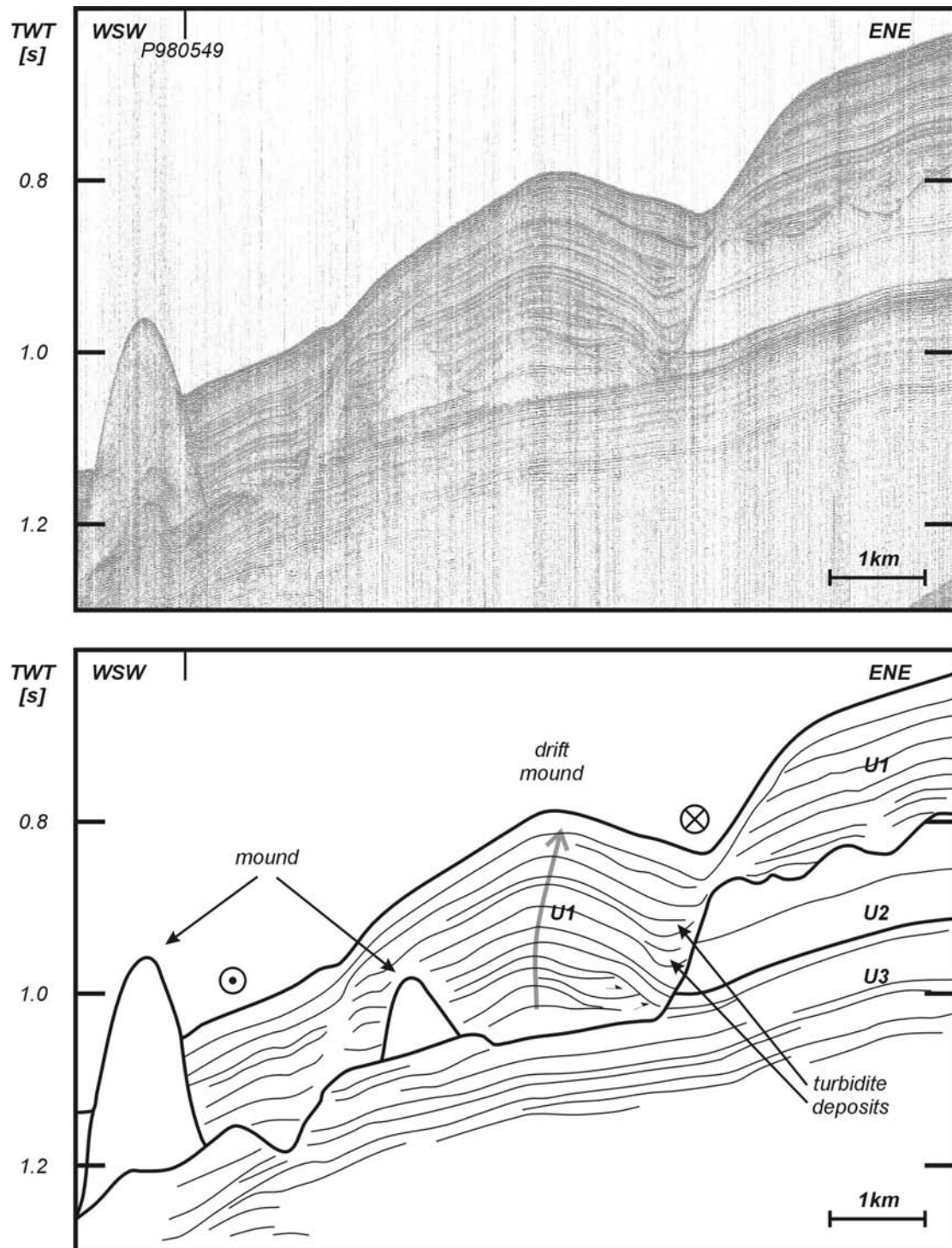


**Figure 6.61:** P980509: Profile across the small mounded drift in the central Belgica mound province. The mounded drift morphology is installed between the foot of a buried mound and a scarp in the flank of unit U2. The grey arrow indicates an upslope progradation of the crest of the drift mound. The moat indicating the pathway of a northward flowing current are filled up with turbidite deposits.

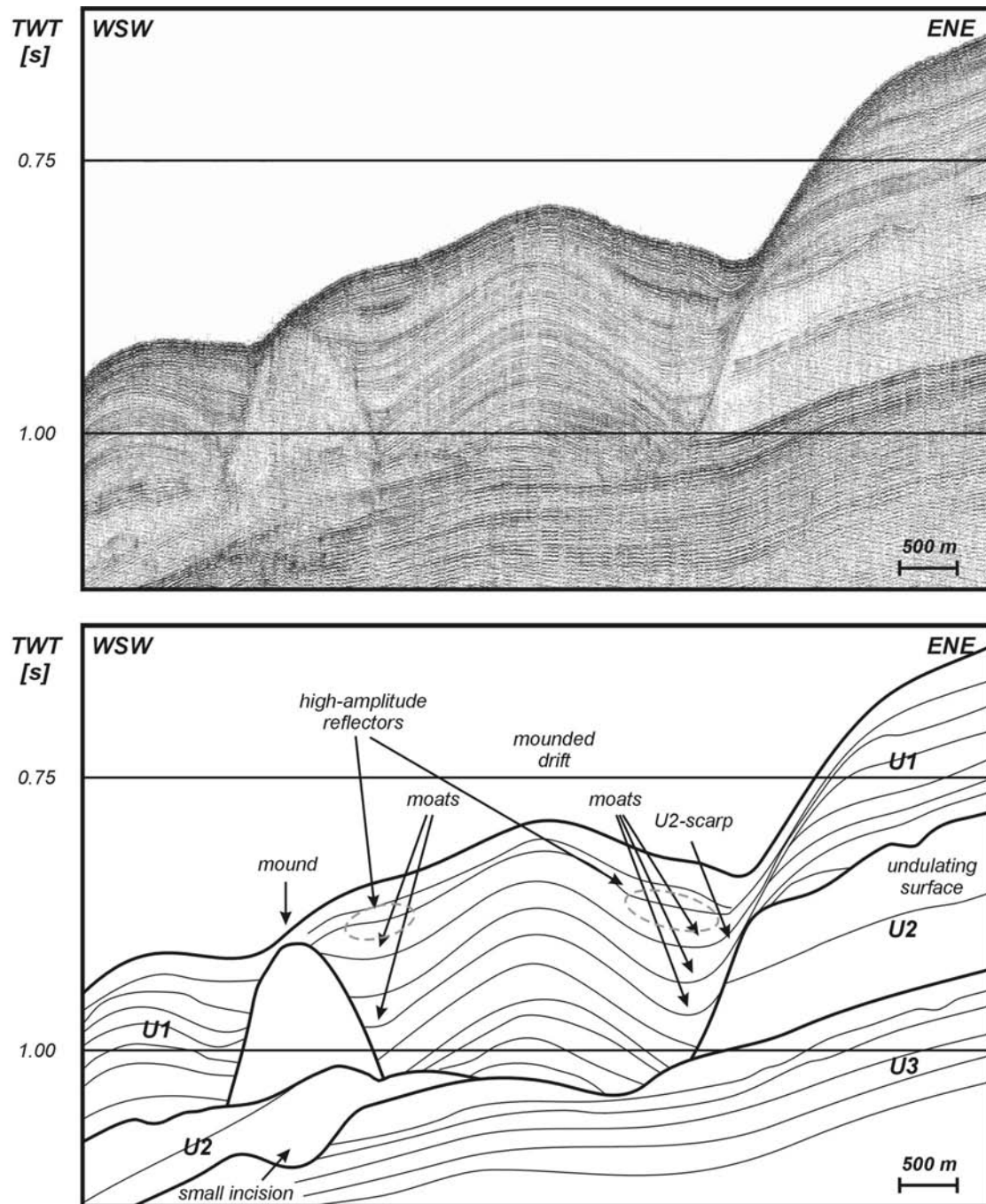


**Figure 6.62:** P970539: Profile across a typical drift mound of the Belgica mound province. On both sides, the moats show high-amplitude reflectors and also probable turbidite deposits. The drift mound is installed in between a large coral bank and the scarp in the U2 unit.

#### 6.4.4.2 Sedimentary characteristics

Core MD99-2327 is located on the eastern flank of this small mounded drift (Figs. 6.59 and 6.54) and can yield important information of its sedimentary characteristics. In chapter 4, this core was subdivided in one glacial and two interglacial intervals. The stratigraphy, physical properties and characteristic X-ray facies of this core are illustrated by figures 6.63, 6.64 and 6.65. In this section, the core data will be discussed in terms of changing hydrodynamic environments.

The most dominant feature of the glacial unit is the record of several episodes of ice-rafting processes, extensively discussed as the 6 IRE in chapter 4. The inferred IRD abundance is relatively high and fluctuating between 5 and 10% (Fig. 6.66). Particle size analysis shows, in general, that this unit is fine grained with a significantly high percentage of silt (averaging 65%), whereas clay tends to make up 8 to 24% of the sediments and the sand fraction is limited to an average of 18 %. However, towards the base of the unit, the sand fraction increases up to 54%. The total sample generally is very poorly sorted and has a near-symmetrical skewness (Fig. 6.67). A more detailed study of the grainsize variations in this core shows short-term variations in the sortable silt index, which can provide estimates in current strength variations (McCave *et al.*, 1995). Since the inferred MIS 4, five intervals of peak currents (28 to 33  $\mu\text{m}$ ) and five intervals of low currents (22 to 26  $\mu\text{m}$ ) are observed. Transitions from minimum to maximum values on the sortable silt curve can be interpreted as accelerations of the bottom current, and vice versa. These peak current events (PCE) obviously behave in a more long-term way compared with the variations in the fraction  $> 150 \mu\text{m}$  (Figs. 6.66 and 6.67e). Additionally, it does not seem that the 5 peak current intervals coincide with the 6 IRE peaks, as was also observed in the earlier discussed cores around Thérèse mound. Although caution should be taken not to completely disconnect changes in sortable silt (thus benthic current variability) and the IRD (ice-rafting events), because IRD also covers silt-sized particles, we suggest treating these two processes as independent ones. While all IRE are culminating during cold events, four of the five PCE are peaking during warm periods, prior to or after an IRE (Fig. 6.66). Only PCE1 seems to be centred on IRE1. Together with PCE2, this event is very close to coeval IRE. Probably, in this case, current-sorted silt and ice-rafted silt are interfering (Fig. 6.67d). As an additional observation, most of the PCEs are also accompanied by a sharp rise in the abundance of the benthic foraminifer *U. mediterranea* and other species as *P. ariminensis* (Fig. 6.66), which also seems to be occurring during warmer periods. Schönfeld (2002a) and Schönfeld & Zahn (2000) recognized these species among others in the epibenthic group of foraminifers, dwelling in an environment with elevated benthic currents within the core of MOW within the Gulf of Cadiz. Most probably a likewise comparable environmental association can be found on the slopes of the Porcupine Seabight. Due to the extensive bioturbation and burrowing, seen on X-ray imagery, primary sedimentary structures are very difficult to be observed. This bioturbation seems to be episodic and contains variations between mottling, isolated pockets and filaments (Fig. 6.64). All this probably reflects several sediment sources in a biologically and hydrodynamically active area: current-sorted mud, biogenic components and ice-rafted debris (Fig. 6.67).

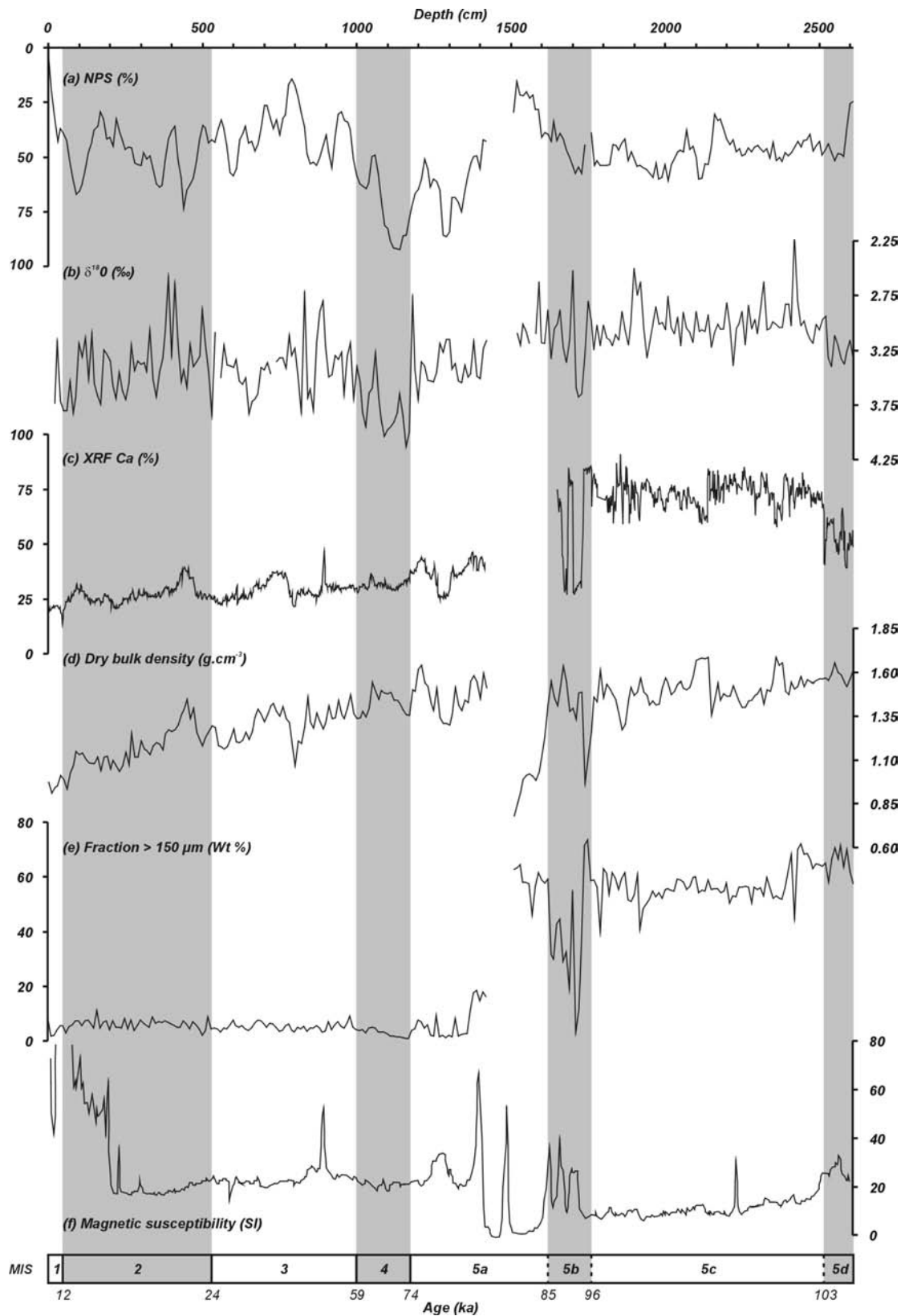


**Figure 6.63:** Lithological content and chronostratigraphy of core MD99-2327 with: (a) relative abundance the polar foraminifer *N. pachyderma* s. (%), (b)  $\delta^{18}O$  stable isotopes (‰ vs. PDB), (c) CORTEX XRF Ca values (% of the total counts of Si, K, Ca, Ti, Mn, Fe and Sr), (d) dry bulk density ( $g.cm^{-3}$ ), (e) fraction > 150  $\mu m$  (Wt %) and (f) the magnetic susceptibility (SI).

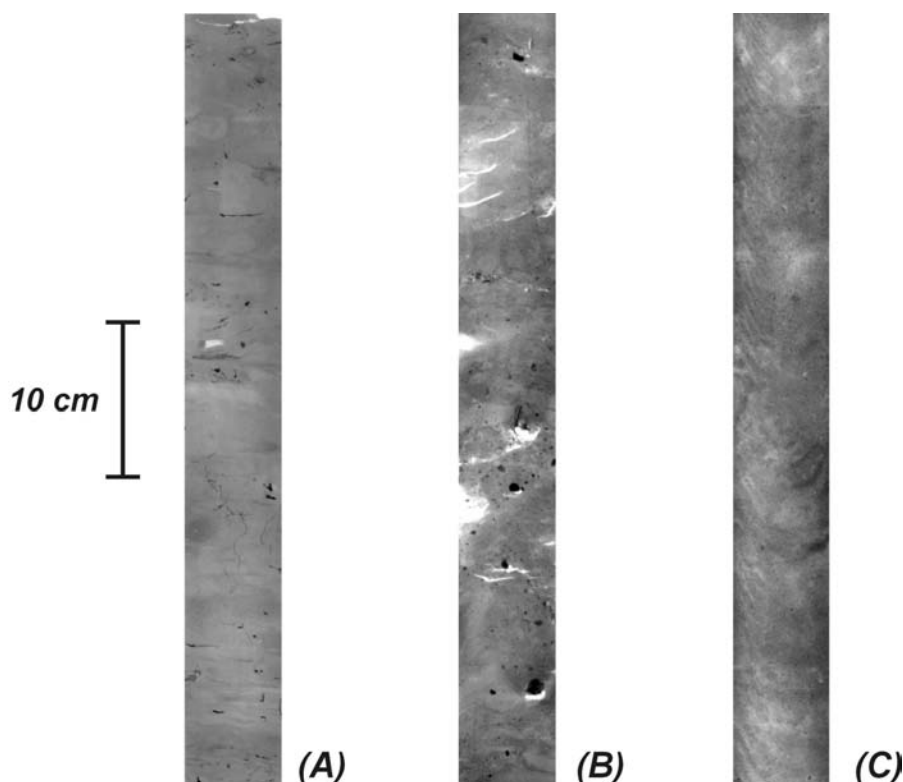


**Figure 6.64:** X-ray facies of core MD99-2327. (a) Silty clay with frequent bioturbation (burrow, Mycelia filaments), occasional dropstones and faint layering (150-200 cm). (b) Silty clay with muddy fin sand intercalations at the base of the glacial interval (1375-1425 cm). (c) Medium sand of the interglacial interval (1975-2025 cm).

Despite a considerable difference in thickness, both interglacial units (MIS1 and MIS5) have comparable lithologic and biogenic characteristics. Already the CORTEX data of MIS5 shows remarkable differences with MIS1; high levels of Ca, low levels of Fe and significant amounts of Si (Fig. 6.65). Considerable short-term scatter for all three elements is certainly due to grain-size variability rather than changes in chemical composition. The sand percentage of this part of the core runs up to 95% (with an average of 84%) and contains mostly quartz grains, detrital carbonate grains, a high percentage of (reworked) planktonic and benthic foraminifera. Thus, in this case, the high XRF Ca values do reflect a high biogenic productivity. This would also explain the large scatter in the oxygen and carbon isotope records meaning that (some of the) forams were reworked (Fig. 6.63). These sediments are more sorted compared to the overlying units (although they still are poorly sorted), suggesting a significant benthic current influence (Fig. 6.67). However, the sortable silt proxy cannot be applied in this part because of the very low silt content, which probably has been winnowed by strong currents. An alternative proxy for this benthic current strength can be suggested on the mean of the 63 to 150  $\mu\text{m}$  fraction, which encompasses the majority of the sediment, but excludes grains larger than 150  $\mu\text{m}$ , whose origin are more likely to be related to ice-rafting. Fluctuations in this sortable sand index correspond well with fluctuation in skewness of the total sample, which has, in this case, an overall fine skew (Fig. 6.67). An increase in the sortable sand index due to increasing currents corresponds with a coarsening in skewness as the finer components are winnowed. This trend

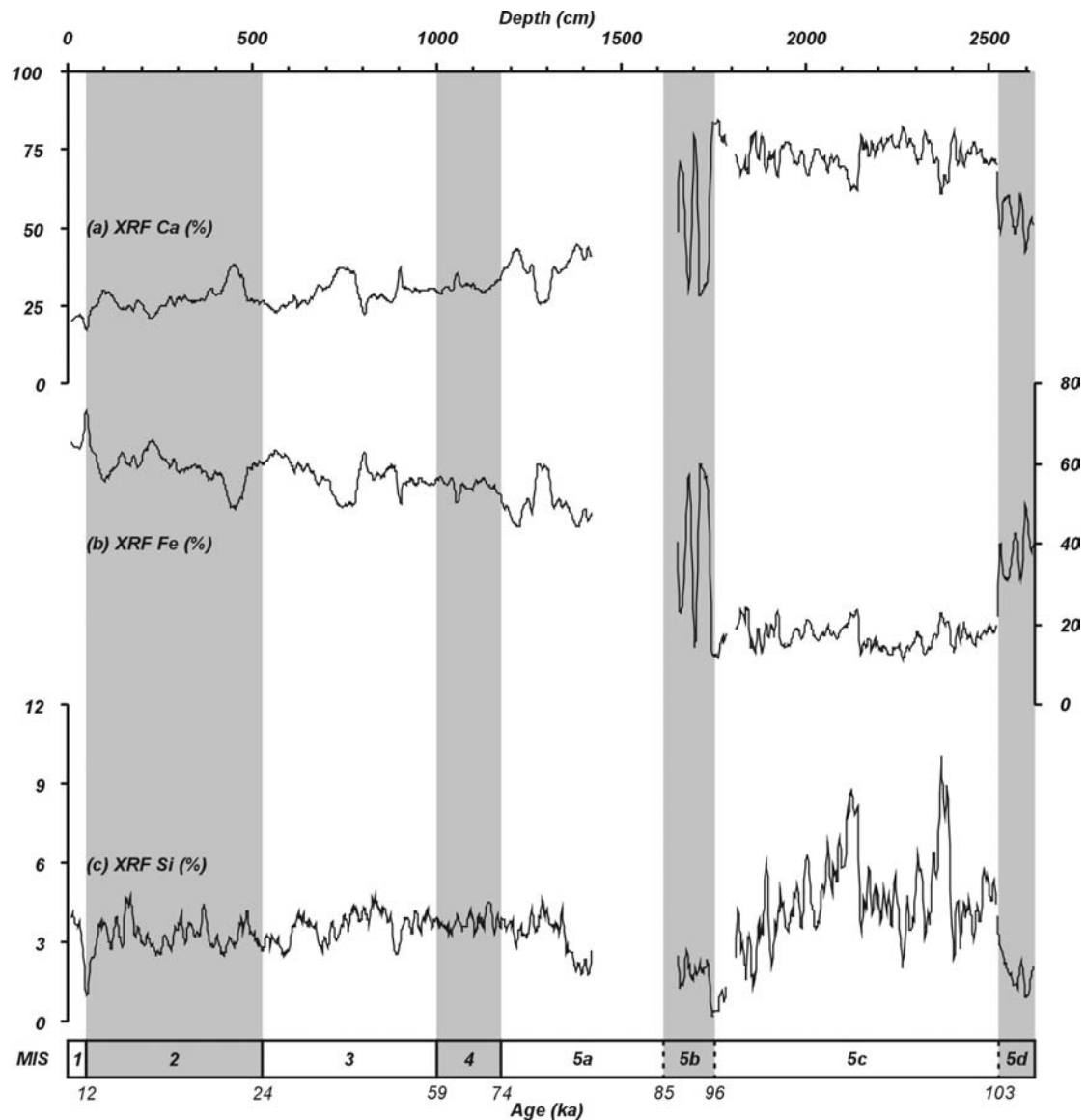


**Figure 6.65:** Five point moving average of the CORTEX XRF Ca (a), Fe (b) and Si (c) values in core MD99-2327. These values are displayed as the percentage of the total counts of Si, K, Ca, Ti, Mn, Fe and Sr.

also corresponds with an increase in the degree of sorting, although mostly a fine tail remains present (Fig. 6.67f). As such, several fluctuations in current strength can be observed during MIS5, with peak currents within the central part. As an exception on the general characteristics of this unit, the two finer-grained layers in MIS5a would be representing small intervals of more sluggish currents displaying almost glacial values.

#### 6.4.4.3 Late Quaternary variability of the hydrodynamic environment

Many observations on and around the area of the small mounded drift prove a very active hydrodynamic environment in present days. This is seen on ROV images (Wheeler *et al.*, submitted-b), side-scan sonar imagery (Huvenne *et al.*, 2002; Wheeler *et al.*, submitted-a) and current velocity models and observations (New *et al.*, 2001; White, submitted). The boxcore sample on the core site confirms this with the presence of a quartz-rich current-sorted foraminiferal sand.

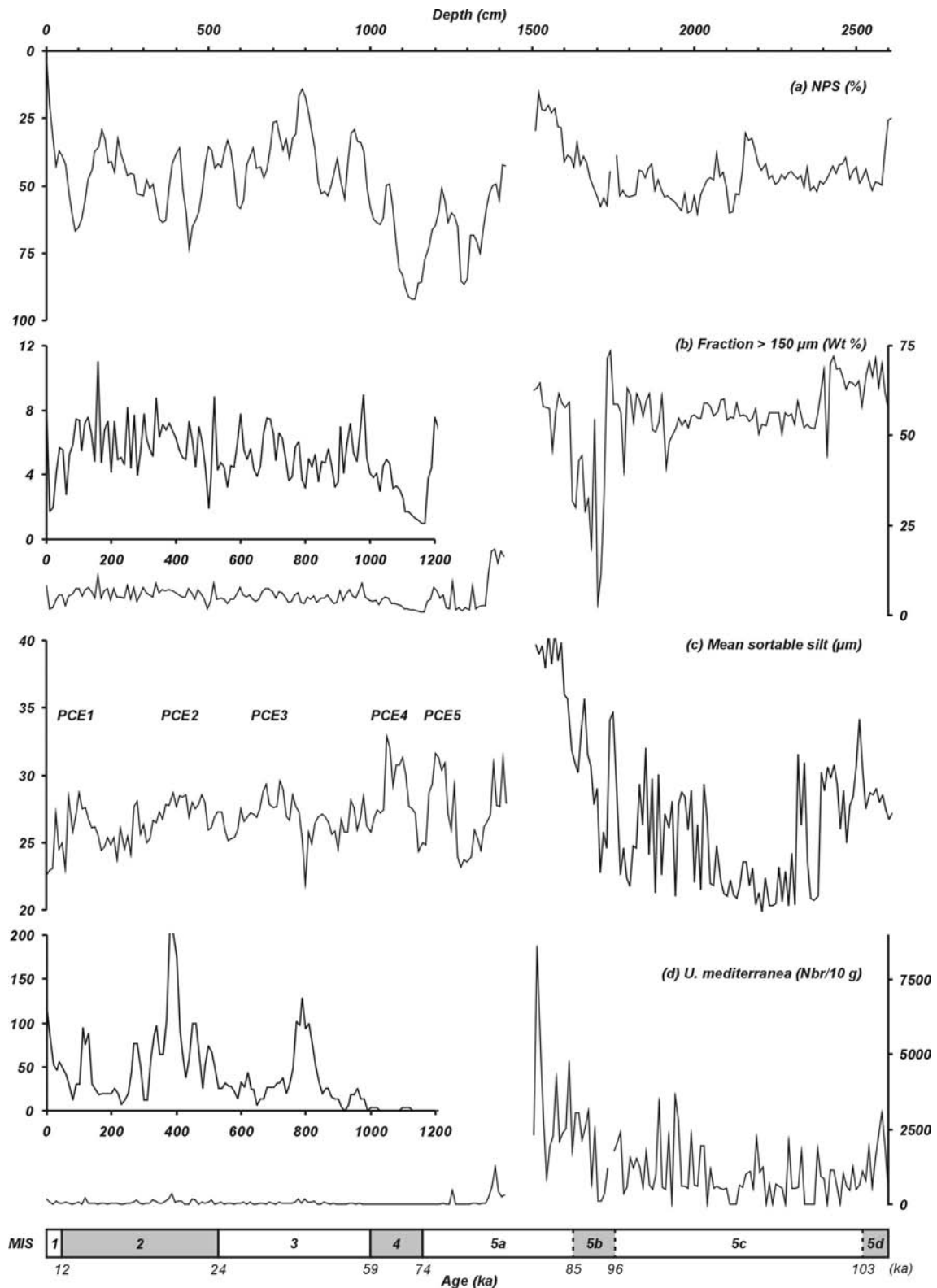


**Figure 6.66:** Sedimentary processes and paleoceanographic interpretation of core MD99-2327 with (a) relative abundance the polar foraminifera *N. pachyderma* s. (*NPS*), (b) fraction > 150 μm (*Wt %*), (c) mean sortable silt (μm) and (d) abundance of the benthic foraminifer *U. mediterranea* (*Nbr per 10 g*). Within part (b) and (d), a zoom of the glacial detail is presented.

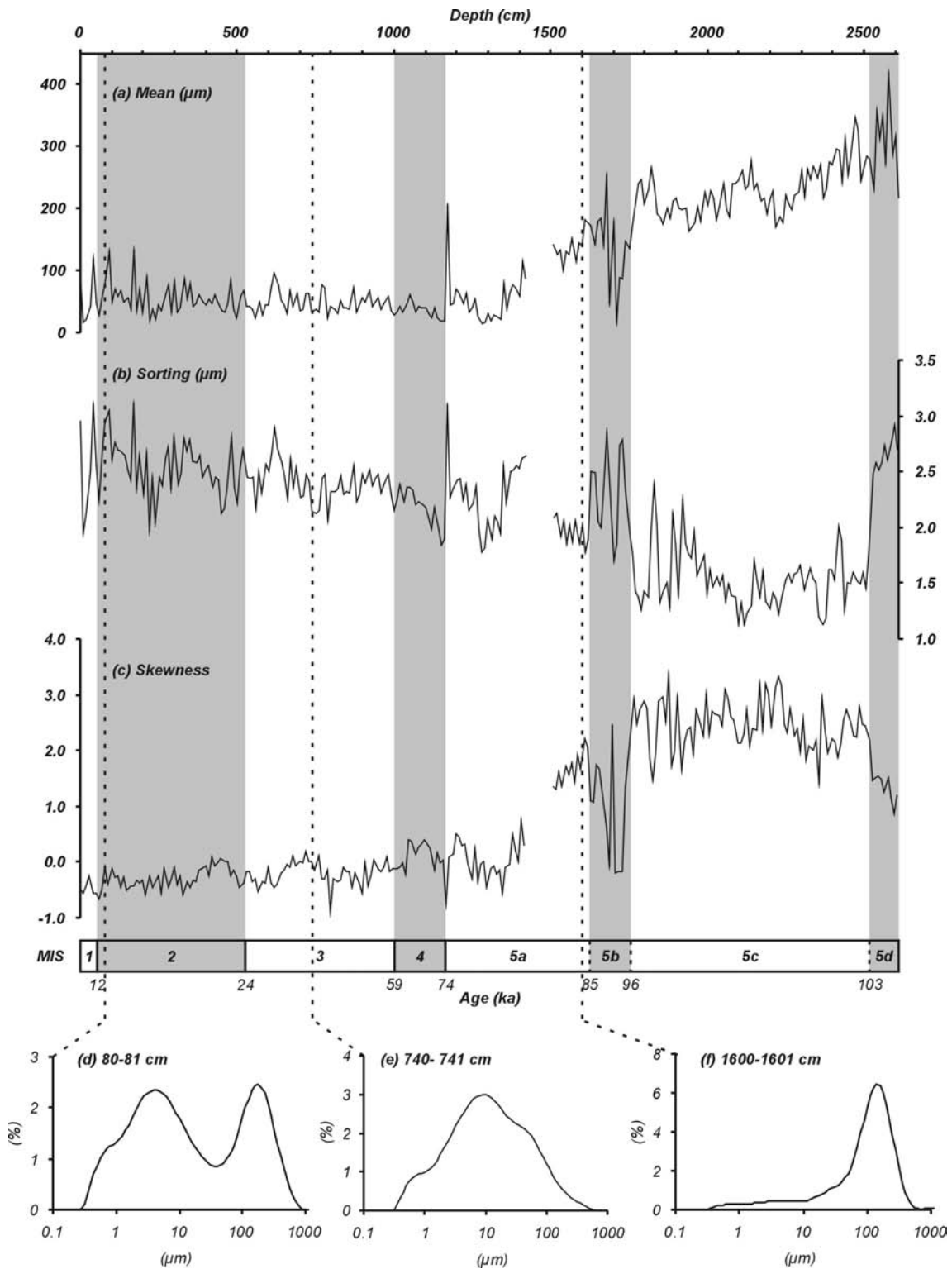


**Figure 6.67:** Sedimentary parameters of core MD99-2327; (a) mean ( $\mu\text{m}$ ), (b) sorting ( $\mu\text{m}$ ) and (c) skewness. Frequency distribution curves are inserted of (d) Ice-rafting event 1 (IRE1), illustrating the presence of ice-rafted debris on top of a current-sorted background sediment, (e) a peak current event (PCE3) in the muddy contourite and (f) the sandy contourite section with a coarse current-sorted mode and a subtle fine-grained tail.

Such a thin surface veneer was also observed on the Hebridean shelf within the Faroe-Shetland channel, but over a wider area, and was interpreted as a contourite sand sheet (Akhurst *et al.*, 2002; Armishaw *et al.*, 2000). This requires the presence of a relatively strong, semi-permanent benthic current at intermediate depths at a velocity of more than 30 cm.s<sup>-1</sup>. The measured and inferred bottom current velocities for the Belgica mound province are consistent with the requirements of Stow *et al.* (2002) for contourites which have an average current velocity of 10-20 cm.s<sup>-1</sup> and can be accelerated up to 100 cm.s<sup>-1</sup> or more near steep slopes or narrow passageways. The observed sedimentary structures on side-scan sonar imagery, nearby or away from a mound, indeed show such an association. The required sediment supply zone can be variable, with upstream erosion, pirating and winnowing of slope sands (Armishaw *et al.*, 2000). In this case, several sources are probable. First of all, the Gollum channel system, which is located upstream, could very well be a supply zone of sands during glacial times. These sands could be remobilized by enhanced currents during climatic optima. Due to the proximity of the glacial BIIS, the eastern slope of the Porcupine Seabight is a privileged site for the deposition of ice-rafted sands, which could also be remobilized during periods of enhanced bottom currents.

Many parameters point out the entire core consists of contourite sediments. The glacial unit meets many of the conditions of the muddy contourite facies as defined by Faugères *et al.* (1984), Rebesco & Stow (2001), Stow *et al.* (2002). However this is combined with a strong ice-rafting component. First of all, it is a mainly siliciclastic fine-grained muddy silt. Indications for a mean grain size are given by Stow & Piper (1984) suggesting 5-40 µm as a range for muddy contourites. Also a sand percentage of 10 to 15% is inferred, but in this case, caution is necessary because a significant part of the sand content is originating from ice-rafting. Only sporadically, primary structures can be found, but most of the time the core is structureless. The X-ray imagery confirms the extensive bioturbation with (sulphide) filaments, *planolites*, *mycelia* and *chondrites* burrows. The nature of the bioturbation, and especially those of the filaments, seems to be variable within the core.

The large scatter in the oxygen and carbon isotope records could mean that (some of the) forams were reworked, in particular in the sandy part. This problem was also recognized by Stow *et al.* (1986) suggesting that local reworking by bottom currents makes it difficult to provide a precise chronostratigraphy. All analyses indicate that the nature and characteristics of the interglacial units are very similar, suggesting they were deposited by the same sedimentary process. The conditions proposed by Armishaw *et al.* (2000) and also observed in the present-day sedimentary and hydrodynamic environment must thus also have been the same. Most of these sandy contourites were observed in a morphotectonic special environment where they are a mixture of a terrigenous and biogenic content with evidence of abrasion and fragmental bioclasts (Faugères & Stow, 1993; Stow *et al.*, 2002). A very thick bedded, structureless coarse-grained deposit such as this one is extremely rare in this kind of environment and can, according to Stow & Mayall (2000), be classified as a deep-water massive sand, which is a good deep-water reservoir facies. Mostly these are sandy debris flows, although these sands can originate from various processes. In this case, many parameters point out that the possibility that the sediments deposited during MIS5 are mass-wasting deposits is

rather small. Moreover, seismic profile P010507 through the coring site does not display features characteristic for a large debris flow or turbidite deposit. Also, the variability of the paleoceanographic proxies characterizing this unit, refers to climatologic variability, which would have been difficult to notice in mass-wasting deposits. The general characteristics of such a deep-water massive sand were defined by Stow & Johansson (2000) and meet with the characteristics of the MIS5 sediments. They are poorly to moderately sorted and have a high degree of reworking. Examples of sandy contourites as deep-water massive sands are rare and are found in morphologically and hydrodynamically special environments with fluctuating enhanced currents as near the Gulf of Cadiz (Habgood *et al.*, 2003) and the Sicilian gateway (Stow & Johansson, 2000). Moreover, the massive (4.4 m) contourite sand deposits described by Habgood *et al.* (2003), share a lot of similarities with the inferred contourite sands in core MD99-2327. In general, the until now reported size of a sandy contourite or a deep-water massive sand is rarely bigger than 1 m (Stow & Johansson, 2000). Within this morphologic and sedimentary context the presence of a 10 m thick sandy contourite is unique and requires further research.

Although no simple global response from climate on bottom current activity can be found, it is very likely that the switch between the sandy to a muddy contouritic environment is coupled to paleoclimatologic events. Faugères *et al.* (1993) already linked a glacial dampened bottom current regime due to the presence of sea ice, while climate instability means enhanced bottom current activity. Recent observations of Akhurst *et al.* (2002) describe the presence of sandy contourites on the Hebrides slope during interglacials and interstadials, relating them to enhanced current activity. They also recognize the presence of bottom current action during glacial times, but less intense. This probably also is the case in our study area, where the 2 finer-grained intercalations, deposited during MIS5a, could be interpreted as silty contourites due to more sluggish currents during the colder periods of MIS 5.

Since the presence of enhanced currents in the Belgica mound province is highly dependent on the interaction with the Mediterranean Outflow Water (MOW) (De Mol *et al.*, 2002; New *et al.*, 2001; White, submitted), it is plausible that glacial times seriously weaken the current regime to a muddy contourite sedimentation. The reduced outflow of MOW was then only restricted to the Gulf of Cadiz and did not penetrate any further in the Atlantic Ocean (Schönfeld & Zahn, 2000) so the conditions for enhanced currents were not met. The variability within the glacial contourite, however, is less clear. Most of the peak current events (PCE) are coeval with presumed warmer periods before or after an IRE. This event is also coupled to a higher abundance of some benthic foraminiferal species like *U. mediterranea* and *P. ariminensis*. Within the core, the abundance of these species reaches a maximum during a warm period in MIS5 and within MIS1. Schönfeld (2002b) and Schönfeld & Zahn (2000) classify these species under the epibenthic group, which is largely dependent of fast-flowing water within a core of MOW. During a climatic warmer period (interstadial), the sea-level could be more elevated, especially after a pan-Atlantic ice-rafting event. This could very well encourage an enhanced MOW production which also could reach further into the Atlantic Ocean and create weak pulses of enhanced currents within the Porcupine Seabight.

#### **6.4.4.4 A special case: the Enya mound drift**

Although higher in this chapter it was postulated that the centre of the Belgica mound province was ideal and unique to develop small mounded drifts in association with coral banks, a new discovery during the Porcupine-Belgica 2003 campaign revealed an exception to this case. The characteristics of unit U1 and the seabed in the Enya mound province (Fig. 6.68), do not only suggest an important role of environmental factors, but also from deeper, geological factors.

First of all, the seabed morphology shows a 4 km long, clearly south-north elongated moat channel with a width of approximately 500 m (Figs. 6.68 and 6.69). Directly west of this channel, an elongate mounded morphology is observed, which on the available seismic profiles seems to be located between mounds and a steep flank created by the upper boundary of unit U2 (Fig. 6.69). This steep flank can be traced over 6 km and more (Fig. 6.68). The W-E oriented seismic profiles indeed show a mounded reflector configuration (Fig. 6.69). Above the mound, the overlying sediment package shows a convergence of reflectors, suggesting the influence of currents. Also the S-N oriented profiles illustrate gently mounded reflectors in between two mounds (Figs. 6.70 and 6.71). Seen the earlier example from the Belgica small mounded drift, this confirms that the U1 sedimentation occurred after the proto-mounds were installed. Moreover, all these observations suggest the presence of a focused northward flowing current in this area since the installation of the local coral banks. This is confirmed by the predictions of enhanced tidal currents through internal waves (Rice et al., 1990), illustrated by figure 2.5.

Yet another remarkable feature in this area is observed and might add a possible clue for the creation of the Enya mounds. On seismic profiles, including P99009a (Fig. 6.36) and on the side-scan sonar imagery (Figs. 6.68 and 6.72), pockmarks are observed. According to Huvenne (2003), the average diameter of these pockmarks might be about 140 m, which is relatively large (Paull et al., 2002). Pockmarks are crater-like depressions, found in fine-grained, soft sediments. Generally, they are formed under the action of upward fluid flow through sediments. This fluid most commonly is gas or even pore water (Hovland & Judd, 1988; Jensen et al., 2002; Paull et al., 2002). The presence of these relatively large pockmarks in this specific zone calls for a focused fluid seepage. According to Paull et al. (2002) most of the pockmarks are found over large hydrocarbon provinces. Although in this part of the Porcupine Basin, the presence of hydrocarbons was not yet fully demonstrated, Croker & Shannon (1995) and Johnston et al. (2001) inferred the presence of possible reservoirs in Permo-Triassic sandstones. Hence, these pockmarks might be related to seepage of thermogenic gas from these possible reservoirs. On the other hand, it is at least remarkable that the mounds are rooted above the cut-and-fill facies earlier described in unit U2. In the Magellan mound province, Huvenne (2003) also described the presence of mounds above a similar facies. However, this was rather related to the expulsion of biogenic gas and pore water, associated to the inferred rapid high-energy deposits of the cut-and-fill facies. Both the role of thermogenic gas, pore-water and biogenic gas can not be excluded in this case. The steep southward dipping erosion surface underlying the Enya mounds (Figs. 6.70 and 6.71) might provide a sort of conduit surface for the migration of these fluids.

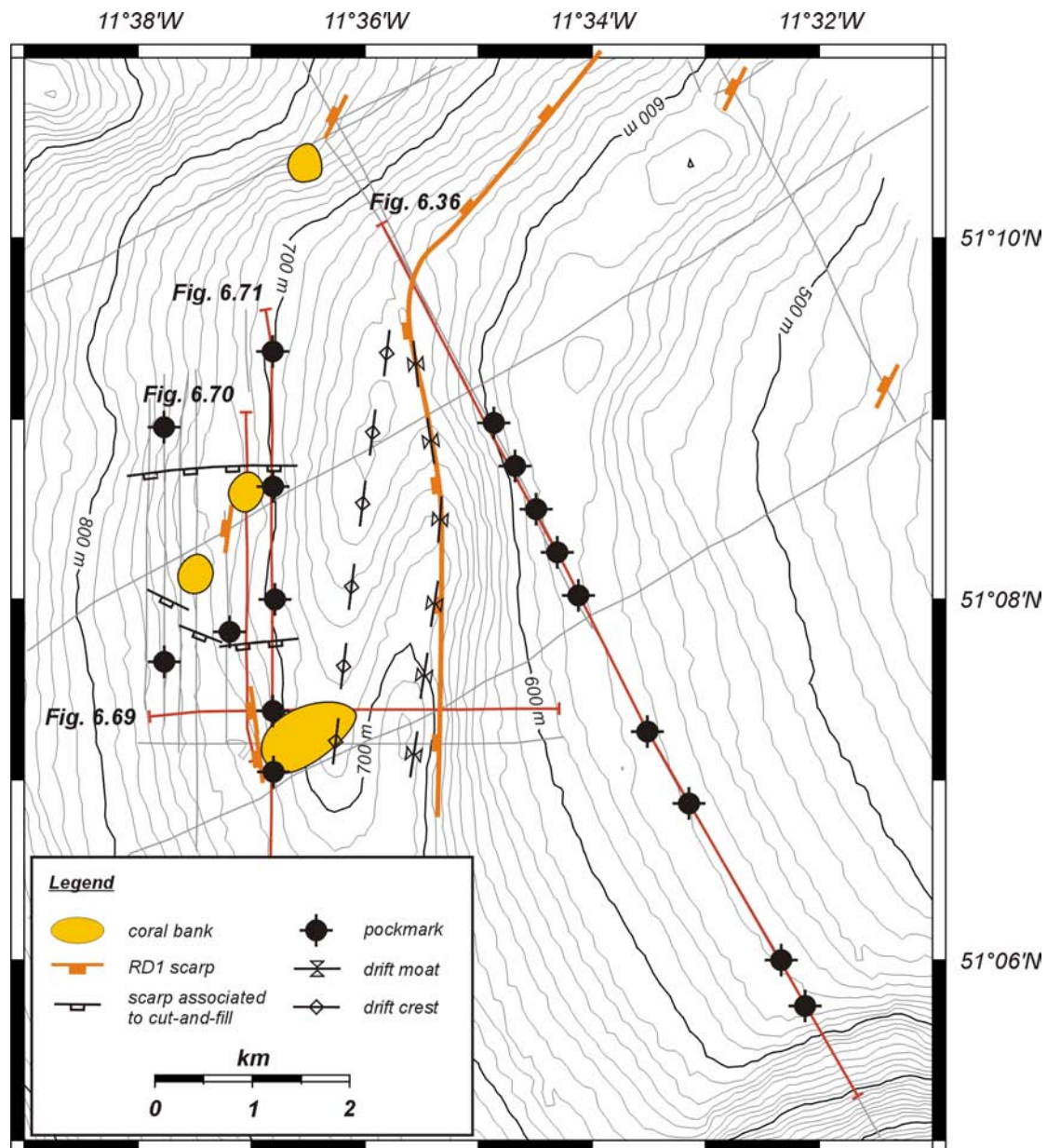


**Figure 6.68:** Special characteristics of the Enya drift system, with positions of the three Enya mounds, pockmarks, U2 scarp, the cut-and-fill scarp, drift mound crest and trough.

In any case, the presence of the Enya mounds is associated with a dynamic hydrologic environment, as well as fluid seepage. Although the role of fluid seepage always was inferred for the Porcupine mound provinces (Henriet *et al.*, 2001), their role in the construction of the Belgica coral banks could not be demonstrated as yet (De Mol, 2002). All the observations point out that the development of the Belgica mounds rather can be attributed to an environmental control (De Mol, 2002; Kenyon *et al.*, 2003; Huvenne, 2003). Therefore, the observations in the Enya mound area demonstrate a unique synergy between the environmental and fluid seepage control on mound growth.

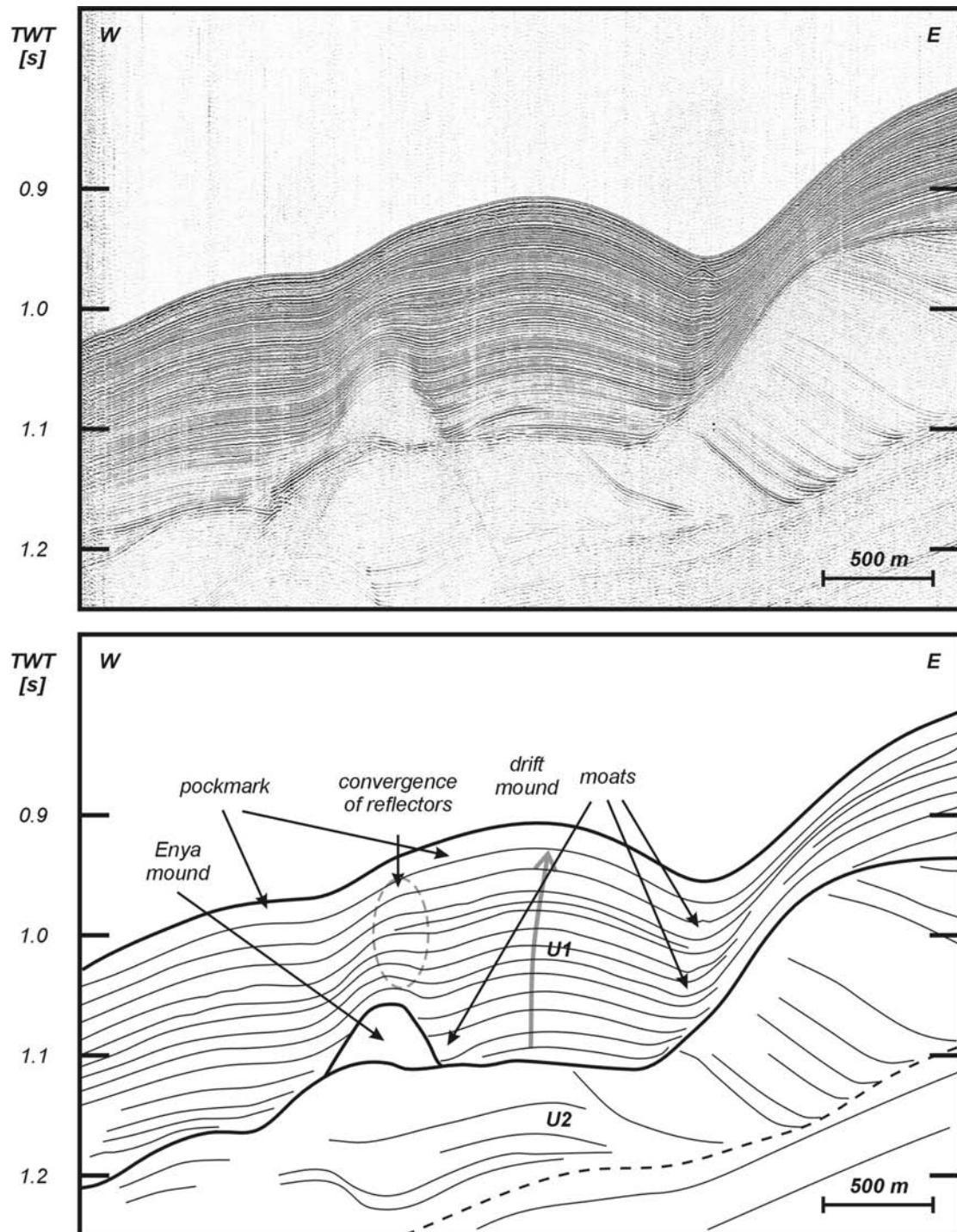


**Figure 6.69:** P030531: Detailed profile of unit U1 in the Enya mound province. The geometry of unit U1 is comparable with the one of a drift mound. Above the Enya mound, there is a convergence of reflectors and pockmarks are observed. This drift mound shows a gentle upslope progradation, indicated with a grey arrow.

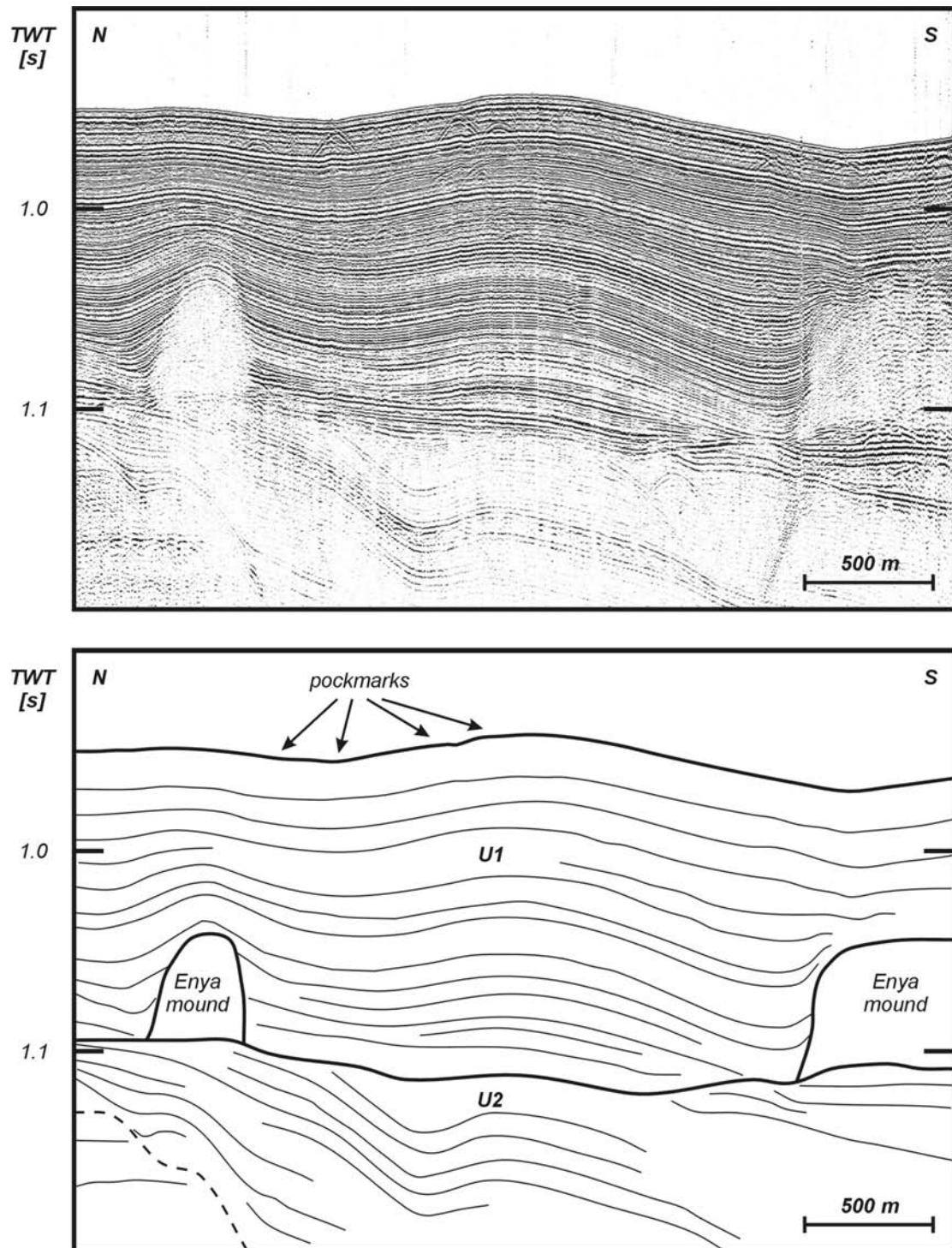


**Figure 6.70:** P030524: Detailed profile of unit U1 in the Enya mound province. The reflector configuration between the two mounds is mounded. The upper strata are characterized by several depression, which can be interpreted as pockmarks. Note the mounds are rooted above a very irregular U2 infill unit.

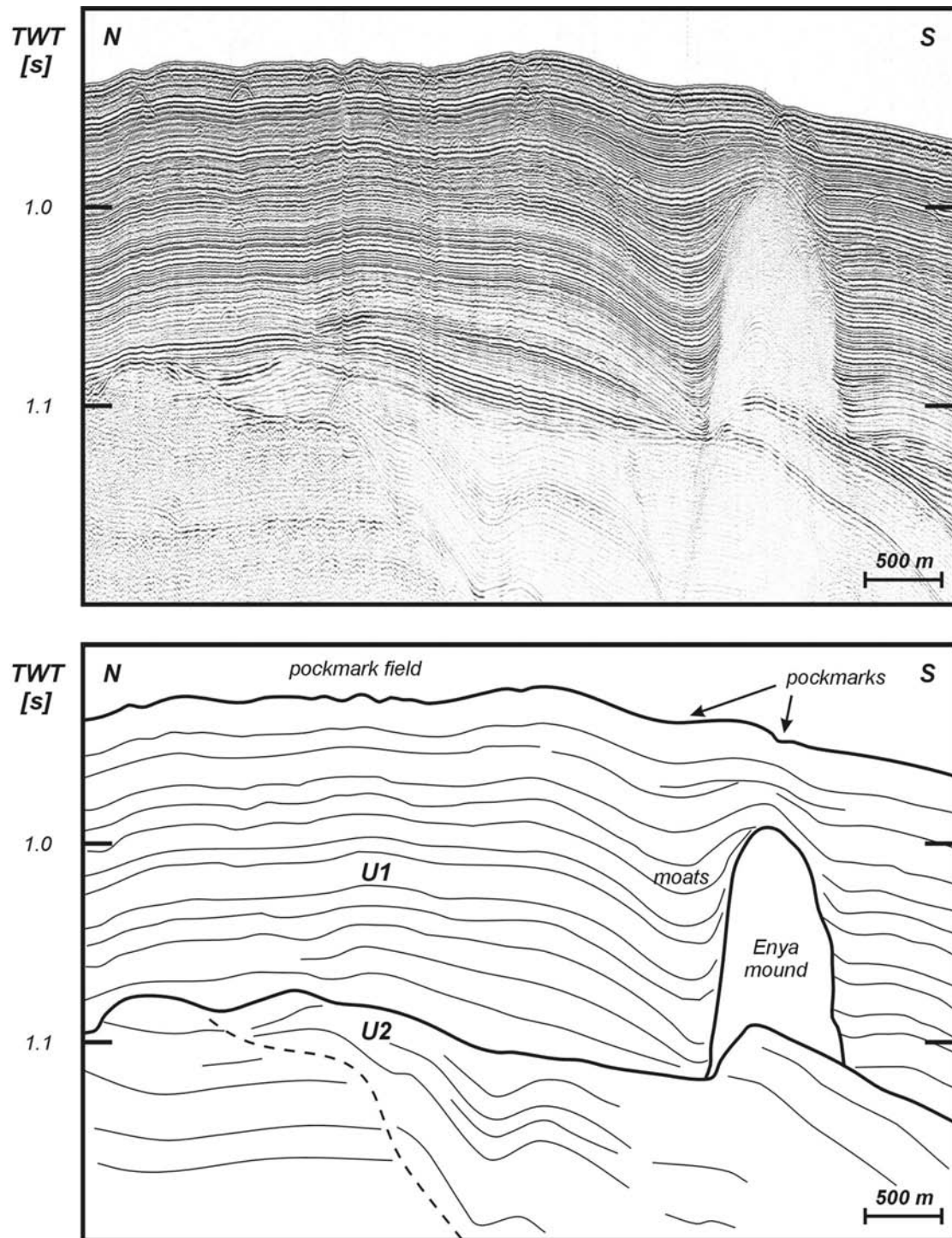


**Figure 6.71:** P030525: Detailed profile over the Enya mound province. The northern side of the Enya mound is flanked by very clear moats and the reflectors show a subtle mounded geometry. On this profile, the seabed is clearly undulating, suggesting the presence of large pockmarks.

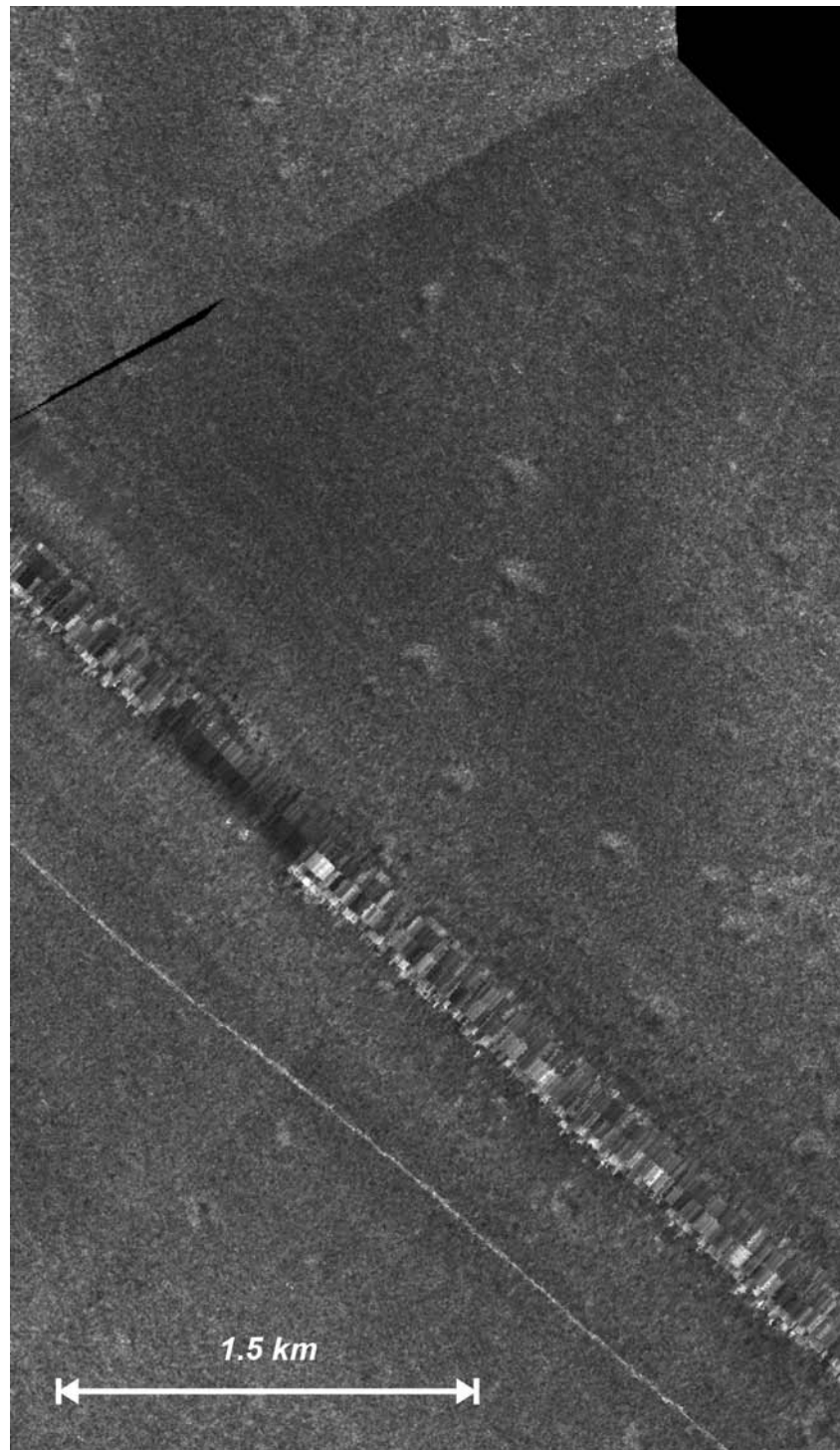


**Figure 6.72:** TOBI side-scan sonar detail of a set of depressions, in the south of the Belgica mound province. These features are interpreted as pockmarks with an average diameter of 140 m (Huvenne, 2003). The position of this figure is indicated on figure 6.7.

#### 6.4.4.5 Consequences for regional sedimentary history

The sedimentological study of this site confirms that the sediment body located in between the mounds and the steep flank of seismic unit U2 is a confined drift. Moreover, the sedimentary facies observed in the core suggest the entire unit is influenced by fluctuating current intensities and thus the entire unit can be called a contourite drift at mid-water range (Stow *et al.*, 2002). The sediment body features many similarities with well-known contourite drift systems such as a downcurrent elongation, sub-regional discontinuities and sub-parallel moderate to low amplitude reflectors with gradual change in seismic facies (Faugères *et al.*, 1999; Rebesco & Stow, 2001; Stow *et al.*, 2002). Compared with the dimensions of known contourite drifts, the confined drift in the Porcupine Seabight is one of the smaller ones (approximately 50 km<sup>2</sup>). The few other examples of this type of drift are known within small basins (Stow *et al.*, 2002), but still they are much larger. The best comparison can indeed be made with the Sumba drift (Sunda Arc, Indonesia); a smooth asymmetric mound with boundary channels and sandy contourites (15 km elongation) (Reed *et al.*, 1987). Due to lateral velocity gradients within the Sumba drift, muddy contourites were deposited on the central part and sandy contourites in boundary channels. However, the Sumba confined drift is 15 km wide, while our equivalent only is 4 km wide. It could thus very well be possible that lateral facies changes are less pronounced in our small mounded drift and such changes can only be observed in depth (or time). The nature of the bathymetric restrictions that are responsible for the acceleration of deep currents, however are of a completely different nature and lie at the base of the smaller dimension. Whereas within the Sumba drift and other confined drifts a more tectonically-controlled background is present, the interaction between water-mass mixing and bathymetric interaction is steered in this case by a combination of a turbulent sedimentary history with several erosion episodes and current-controlled biogenic build-ups. Within such a dynamic and irregular environment, it is expected that besides contourites also turbiditic and other mass-wasting deposits can be inferred.

Based upon our tentative age model, we tried to estimate the age of the onset of sedimentation of the small mounded drift. The thickness of this drift mound above the RD1 discontinuity on profile P010507 was estimated at 300 m (based on an estimated P-wave velocity of 1800 m.s<sup>-1</sup> within the sedimentary series). Combined with a total average sedimentation rate of 24.45 cm.ka<sup>-1</sup> (core MD99-2327), this yields an age of about 1.2 Ma. Due to various uncertainties on these data, we tend to suggest the onset of the drift mound sedimentation started somewhere in the middle Early Pleistocene, while the lower boundary of the seismic unit U1 is suggested to have a Late Pliocene age. This implies that since the RD1 erosion event, there was a significant period of non-sedimentation between the onset of mound growth in the Late Pliocene and the onset of drift sedimentation, as illustrated in figures 6.73a and 6.73b. This period of non-sedimentation gives enough time for the “start-up” phase of the mound growth, required by De Mol *et al.* (2002) for corals to settle on the hard substratum provided by the bottom-current swept and eroded U2 unit (Fig. 6.73c). From a paleoceanographic point of view, we could very well imagine the contouritic sedimentation was well under way during a major climatologic change within the Pleistocene. The Mid-Pleistocene revolution (MPR, ~940-640 ka) marks the road towards an increasing mean global ice volume and increasing amplitude of 100 ka climatologic cycles (Hernandez-Molina *et al.*, 2002; Raymo *et*

*al.*, 1997). This interval was also characterized by “weaker” North Atlantic Deep Water formation, relative to the early and late Pleistocene (Raymo *et al.*, 1997). On the other hand, since the MPR the pulsations between glacial and interglacial periods became more pronounced and could lie at the base of the start of the muddy-sandy contourite deposition in the Belgica mound area, as well as the acoustic amplitude variations within seismic unit U1.

Within the Belgica mound province, the presence of this small mounded drift is a common feature everywhere the paleotopography and the presence of the coral banks allows a similar setting. Side-scan sonar imagery of the entire Belgica mound province proves that in the similar depth-range and within the vicinity of the mounds, almost always enhanced currents are inferred, thus a likewise build-up of hydrodynamic variability through time can be expected. However, since the presence of the current enhancement is strictly bound to the water mass-topography interaction in this region on the slope, we must conclude that the presence of this confined contourite drift only is a very local feature, bound to several geological, climatological, biological and hydrodynamic variables. Therefore, except for the Enya mounds, we do not expect to find any important contourite drift deposit outside the occurrence of the central part of the Belgica mound province. In other mound sites in the Porcupine basin like the Hovland and Magellan mound province, the measured and predicted slope currents are much weaker than in the Belgica mound province (De Mol *et al.*, 2002; Huvenne *et al.*, 2002). The only indication of current-controlled deposition is observed nearby the mounds as moat structures, but these features are rather limited in impact (Huvenne *et al.*, submitted-a; Huvenne *et al.*, 2003). According to Rebesco & Stow (2001) and Stow *et al.* (2002) it is more likely to refer to the sediment around the Hovland and Magellan mound provinces as sediment drifts. Nearby the moats and the mounds, muddy contourite facies can be expected, which will grade into a hemipelagic facies away from the mounds.

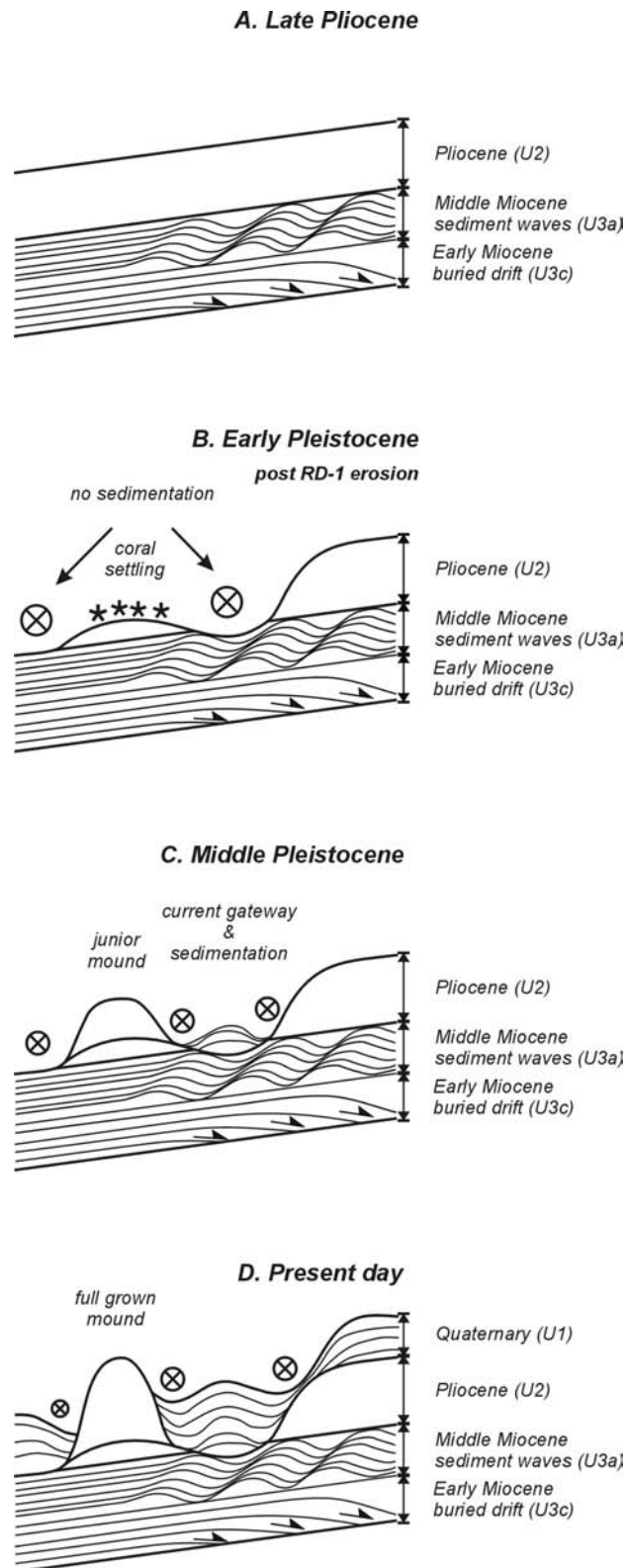


**Figure 6.73:** Reconstruction of the depositional evolution, in an idealised SW-NE section, of the small confined contourite drift in relationship with the growth of a coral bank. The crossed circles illustrate the presence of a northward flowing bottom current.

## 6.5 Summary

As well from a sedimentological as a paleoceanographic point of view, the Porcupine basin is "small but interesting". More specifically, the Belgica mound province, located on the eastern slope of the Porcupine Seabight can be considered as a unique environment within the North Atlantic domain. In this chapter it was demonstrated that since the Paleogene, strong northward flowing currents on this part of the margin were responsible for the deposition of classic elongated sediment drifts with sediment waves. Moreover, since the start of the Quaternary, the interplay of several environmental factors such as morphology, geology, oceanography and hydrodynamics have been responsible for the settling of deep-water coral banks and a variety of special deep-sea sedimentary processes. In this section, the stratigraphic evolution since the Paleogene will be summarized and illustrated by figure 6.74.

Figure 6.74a illustrates the Early to Middle Miocene environment on the eastern slope of the Porcupine Seabight. Probably since the Middle Eocene (RD4), two elongate mounded drifts were installed on this part of the slope, separated by an early Late Oligocene discontinuity (RD3). The supposed sediment drift of unit U4 was installed by an inferred NE flowing current during an episode where a relatively young system of deep-water bottom current circulation was responsible for the establishment of sediment drifts all over the North Atlantic basins. The overlying unit U3 generally shows a relatively calm environment on a slope of approximately 2°. However, a large zone of strata onlapping on the lower boundary of U3 is observed, sharing similarities with well-studied North Atlantic sediment drifts. Moreover, downslope of a break in the paleo-slope and in a narrow zone of constant depth, another large zone of probably eastward migrating sediment waves is observed, inferring a N to NW flowing bottom current on this part of the slope during the Early Miocene. In the lower Middle-Miocene, the introduction of the Norwegian Sea Water in the North Atlantic Ocean was responsible for a margin-wide erosion (RD2) of this sediment drift.

After this first erosion event, an acoustically transparent unit with yet unknown lithology was deposited over the entire slope (Fig. 6.74b). A change in seismic facies near the inferred top of this unit is believed to represent the Miocene-Pliocene boundary, similar to seismic sections on Goban Spur. Due to a major change in oceanographic conditions, the large-scale RD1 erosion event was responsible for the removal of a large part of unit U2 and has cut very deeply into unit U3 and U4 in the Late Pliocene (Fig. 6.74c). This episode also marks the start of glacial-interglacial cycles and their effects on the deep-water circulation. During this erosion event, the basis of the Arwen and Celeborn-Galadriel channels have been created by a strong south-north directed current. These channels remain the pathway of this current during the Quaternary, fostering the construction of a sediment drift body in this part of the slope. However, some evidence suggests that a possible tectonic control might have influenced the morphology and sedimentation of these channels.

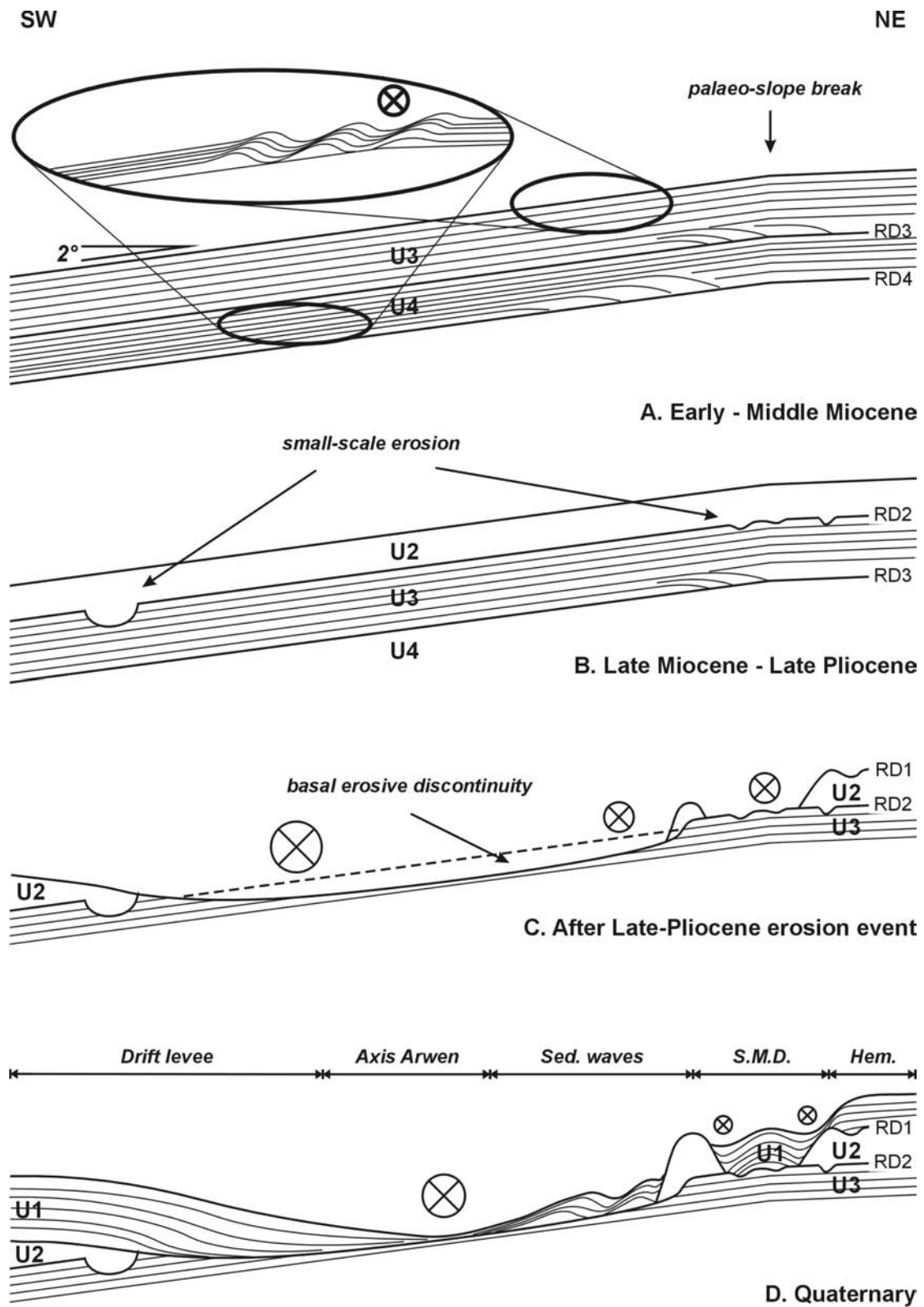


**Figure 6.74:** Reconstruction of the depositional history in an ideal NE-SW profile (S.M.D.= small mounded (confined) drift; Hem.= undisturbed hemipelagic sedimentary environment).

Subsequent to the RD1 event, corals began to settle on topographic irregularities in the palaeobathymetry (Fig. 6.74d). The coral banks were built spectacularly fast in a period when the adjacent areas experienced non-deposition. They are located in a zone within the influence of a complex system of enhanced currents, which is believed to be the main driving force of the controls in their development. However, in the southern part of the study area, three newly discovered Enya mounds are observed rooting on a cut-and-fill facies. Although there seems to be a substantial environmental control by currents, the presence of pockmarks suggests the influence of fluid seepage (of possibly thermogenic gas from deeper reservoirs).

The Quaternary unit (U1) deposited surrounding the mounds, has similarities with some of the well-known sediment drift types reviewed by Faugères et al. (1999) and Rebesco & Stow (2001). However, these so-called drift-types are only end-members of a continuous spectrum. The unique geographic and hydrodynamic setting of the study area is responsible for the creation of a contourite system, constituted out of two main sediment drift bodies (Fig. 6.74d). A first drift body is bound at its right-hand side by the Arwen channel and displays the typical aggradation-progradation of a drift levee towards the channel, located at the foot of the slope. Between the channel and the mounds, a very complex zone of sediment waves and levees suggests the combined action of the broad northward flowing current coming from the channel (locally enhanced by the presence of the steeper mound ridges) and the downslope running turbidite gullies. The sedimentary environment around these mounds is influenced by contour currents with variable strength and by turbidite deposits at the foot of the mounds.

Within the central part of the Belgica mound province, a small confined mounded contourite drift is described. The special setting of this sediment body, of which the morphology has been influenced by the presence of the coral banks and the underlying paleotopography, makes this drift probably one of the smallest known confined contourite drifts in a very unique setting. Core data and side-scan sonar imagery prove the presence of a sandy contourite sheet with sand waves over a large part of the confined contourite drift. This Holocene sandy contourite shares many characteristics with the interglacial part of the core, located between 1500 and 2625 cm. During this period, we can infer a similar environmental situation as the present one. This entire unit can be considered as a sandy contourite and also one of the largest known deep-water massive sands.

During the transition from isotope stage 5 to stage 4, the accumulating ice volumes of the pan-Atlantic ice sheets were responsible for a global sea-level drop and the distribution of the MOW in the Eastern Atlantic was seriously hampered. Since the presence of the MOW was vital to the vigorous hydrodynamic environment in the Belgica mound province, the activity of the glacial bottom currents was reduced. However, evidence of current reactivation, coupled with warmer periods and the increase of epibenthic foraminifers, suggests enough MOW sporadically entered the Porcupine Seabight in order to shortly enhance the bottom current production. This glacial part of the core is a typical muddy contourite with a significant glacio-marine contribution.

In combining the obtained sedimentological and chronostratigraphic results, an estimate for the age of the lower boundary of the contourite drift was made. This revealed an important time gap between the age of the basal unconformity RD1 and the onset of the contourite drift, estimated within the middle Early Pleistocene. Within such a time window, the environmental factors would have been ideal for the corals to settle and start the construction of the coral banks. Towards a later phase of the Pleistocene, when the frequency between glacial and interglacial periods began to shift towards a 100 ka frequency, a contouritic sedimentation regime was installed and created small confined contourite drifts closely related to almost full-grown coral banks.

Within this relatively small embayment in the NE Atlantic margin, the usual features diagnostic of sediment drifts are encountered. However, the key-elements allowing the construction of this contourite system are unique because of the interaction between a complex oceanographic regime with obstacles in the (paleo)bathymetry, located in a relatively narrow zone of the slope. Unfortunately, not yet all elements contributing to the construction and evolution of the Belgica mound province are known, which calls for further research and drilling.

## References

- Akhmetzhanov, A. M., Kenyon, N. H., Nielsen, T., Habgood, E., Ivanov, M. K., Henriët, J.-P. & Chachkine, P. (2001) Deep-sea bottom current depositional systems with active sand transport on the north-eastern Atlantic Margin. In: Geological Processes on Deep-Water European Margins (Ed. by M. K. Ivanov and S. Bouriak), IOC Workshop Report, 175, 14-15.
- Akhurst, M. C., Stow, D. A. V. & Stoker, M. S. (2002) Late Quaternary glacialic contourite, debris flow and turbidite process interaction in the Faroe-Shetland Channel, NW European Continental Margin. In: Deep-Water Contourite Systems: Modern Drifts and Ancient Series, Seismic and Sedimentary Characteristics (Ed. by D. A. V. Stow, C. J. Pudsey, J. A. Howe, J.-C. Faugères and A. R. Viana), Geological Society, London, Memoirs, 22, 73-84.
- Armishaw, J. E., Holmes, R. W. & Stow, D. A. V. (2000) The Barra Fan: A bottom-current reworked, glacially-fed submarine fans system. *Marine and Petroleum Geology*, 17, 219-238.
- Carter, L. & McCave, I. N. (1994) Late Quaternary sediment pathways through the deep ocean, east of New Zealand. *Paleoceanography*, 9(6), 1061-085.
- Crocker, P. F. & Shannon, P. M. (1995) The petroleum geology of Ireland's offshore basins: introduction. In: The Petroleum Geology of Ireland's Offshore Basins (Ed. by P. F. Crocker and P. M. Shannon), Geological Society, London, Special Publication, 93, 1-8.
- de Graciansky, P. C. & Poag, C. W. (1984) Geologic history of Goban Spur, northwest Europe continental margin. In: Initial Reports of the Deep Sea Drilling Project (Ed. by P. C. de Graciansky, C. W. Poag, R. Cunningham, P. Loubere, D. G. Masson, J. M. Mazzullo, L. Montadert, C. Müller, K. Otsuka, L. A. Reynolds, J. Sigal, S. W. Snyder, S. P. Vaos and D. Waples), U.S. Government Printing Office, Washington, 80, 1187-1216.
- De Mol, B. (2002) Development of coral banks in Porcupine Seabight (SW Ireland): A multidisciplinary approach. Ph.D. thesis, Department of Geology and Soil Science. Ghent University, Gent, 363 pp.
- De Mol, B., Van Rensbergen, P., Pillen, S., Van Herreweghe, K., Van Rooij, D., McDonnell, A., Huvenne, V., Ivanov, M., Swennen, R. & Henriët, J.-P. (2002) Large deep-water coral banks in the Porcupine Basin, southwest of Ireland. *Marine Geology*, 188, 193-231.
- Ediger, V., Velegrakis, A. F. & Evans, G. (2002) Upper slope sediment waves in the Cilician Basin, northeastern Mediterranean. *Marine Geology*, 192, 321-333.
- Faugères, J.-C., Gonthier, E. & Stow, D. A. V. (1984) Contourite drift molded by deep Mediterranean outflow. *Geology*, 12, 296-300.
- Faugères, J.-C., Mézerais, M. L. & Stow, D. A. V. (1993) Contourite drift types and their distribution in the North and South Atlantic Ocean basins. *Sedimentary Geology*, 82, 189-203.
- Faugères, J.-C. & Stow, D. A. V. (1993) Bottom-current-controlled sedimentation: a synthesis of the contourite problem. *Sedimentary Geology*, 82, 287-297.
- Faugères, J.-C., Stow, D. A. V., Imbert, P. & Viana, A. R. (1999) Seismic features diagnostic of contourite drifts. *Marine Geology*, 162, 1-38.
- Flood, R. D. & Shor, A. N. (1988) Mud waves in the Argentine Basin and their relationship to regional bottom circulation patterns. *Deep-Sea Research*, 35(6), 943-971.
- Foubert, A. (2002) Een paleomagnetische studie met zeer hoge resolutie op Calypso-kernen in Porcupine Seabight, ten zuidwesten van Ierland. M.Sc. thesis, Department of Geology and Soil Science. Ghent University, Gent, 151 pp.
- Foubert, A., Beck, T., Wheeler, A. J., Opderbecke, J., Grehan, A., Klages, M., Thiede, J., Henriët, J.-P. & the Polarstern ARK-XIX/3a shipboard party (in press) New view of the Belgica Mounds, Porcupine Seabight, NE Atlantic: Preliminary Results from the Polarstern ARK-XIX/3a ROV cruise. In: Deep-water Corals & Ecosystems (Ed. by A. Freiwald and J. M. Roberts), Springer-Verlag, Heidelberg.

- Freiwald, A., Wilson, J. B. & Henrich, R. (1999) Grounding Pleistocene icebergs shape recent deep-water coral reefs. *Sedimentary Geology*, 125, 1-8.
- Fulthorpe, C. S. & Carter, R. M. (1991) Continental-shelf progradation by sediment-drift accretion. *Geological Society of America Bulletin*, 103, 300-309.
- Galanes-Alvarez, H. (2001) A pseudo 3D very high resolution seismic study of the Thérèse mound, Porcupine Basin, offshore SW Ireland. M.Sc. thesis, School of Ocean Sciences. University of Wales, Bangor, 114 pp.
- Habgood, E., Kenyon, N. H., Masson, D. G., Akhmetzhanov, A. M., Weaver, P. P. E., Gardner, J. & Mulder, T. (2003) Deep-water sediment wave fields, bottom current sand channels and gravity flow channel-lobe systems: Gulf of Cadiz, NE Atlantic. *Sedimentology*, 50, 483-510.
- Henriet, J.-P., De Mol, B., Vanneste, M., Huvenne, V., Van Rooij, D. & the "Porcupine-Belgica" 97, a. s. p. (2001) Carbonate mounds and slope failures in the Porcupine Basin: a development model involving past fluid venting. In: *The Petroleum Exploration of Ireland's Offshore Basins* (Ed. by P. M. Shannon, P. Haughton and D. Corcoran), Geological Society, London, Special Publication, 188, 375-383.
- Hernandez-Molina, F. J., Somoza, L., Vazquez, J. T., Lobo, F., Fernandez-Puga, M. C., Llave, E. & Diaz-del Rio, V. (2002) Quaternary stratigraphic stacking patterns on the continental shelves of the southern Iberian Peninsula: their relationship with global climate and palaeoceanographic changes. *Quaternary International*, 92, 5-23.
- Hovland, M. & Judd, A. G. (1988) Seabed pockmarks and seepages, impact on geology, biology and the environment. Graham & Trotman Ltd., London, 293 pp.
- Howe, J. A. (1996) Turbidite and contourite sediment waves in the northern Rockall Trough, North Atlantic Ocean. *Sedimentology*, 43, 219-234.
- Huvenne, V., Blondel, P. & Henriet, J.-P. (2002) Textural analyses of sidescan sonar imagery from two mound provinces in the Porcupine Seabight. *Marine Geology*, 189, 323-341.
- Huvenne, V. A. I. (2003) Spatial geophysical analysis of the Magellan carbonate build-ups and the interaction with sedimentary processes: key to a genetic interpretation? Ph.D. thesis, Department of Geology and Soil Science. Ghent University, Gent, 285 pp.
- Huvenne, V. A. I., Bailey, W., Shannon, P. M., Naeth, J., di Primio, R., Henriet, J.-P., Horsfield, B., de Haas, H., Wheeler, A. J. & Olu-Le Roy, K. (submitted-a) The Magellan mound province in the Porcupine Basin. In: *Modern Carbonate Mound Systems: A window to Earth History* (Ed. by J.-P. Henriet and C. Dullo), Springer-Verlag, Heidelberg.
- Huvenne, V. A. I., Beyer, A., de Haas, H., Dekindt, K., Henriet, J.-P., Kozachenko, M., Olu-Le Roy, K., Wheeler, A. J. & the TOBI/Pelagia 197 and CARACOLE cruise participants (submitted-b) An intercomparison of the seabed appearance of coral bank provinces in the Porcupine Seabight, NE Atlantic: results from sidescan sonar and ROV seabed mapping. In: *Deep-water corals and ecosystems* (Ed. by A. Freiwald and J. M. Roberts), Springer-Verlag, Heidelberg.
- Huvenne, V. A. I., De Mol, B. & Henriet, J.-P. (2003) A 3D seismic study of the morphology and spatial distribution of buried coral banks in the Porcupine Basin, SW of Ireland. *Marine Geology*, 198, 5-25.
- Jensen, J. B., Kuijpers, A., Bennike, O., Laier, T. & Werner, F. (2002) New geological aspects for freshwater seepage and formation in Eckernförde Bay, western Baltic. *Continental Shelf Research*, 22, 2159-2173.
- Johnston, S., Doré, A. G. & Spencer, A. M. (2001) The Mesozoic evolution of the southern North Atlantic region and its relationship to basin development in the south Porcupine Basin, offshore Ireland. In: *The Petroleum Exploration of Ireland's Offshore Basins* (Ed. by P. M. Shannon, P. Haughton and D. Corcoran), Geological Society, London, Special Publication, 188, 237-263.
- Kenyon, N. H. (1987) Mass-wasting features on the continental slope of Northwest Europe. *Marine Geology*, 74, 57-77.

- Kenyon, N. H., Akhmetzhanov, A. M., Wheeler, A. J., van Weering, T. C. E., de Haas, H. & Ivanov, M. K. (2003) Giant carbonate mud mounds in the southern Rockall Trough. *Marine Geology*, 195, 5-30.
- Laberg, J. S., Vorren, T. O. & Knutsen, S.-M. (2002) The Lofoten Drift, Norwegian Sea. In: *Deep-Water Contourite Systems: Modern Drifts and Ancient Series, Seismic and Sedimentary Characteristics* (Ed. by D. A. V. Stow, C. J. Pudsey, J. A. Howe, J.-C. Faugères and A. R. Viana), Geological Society, London, Memoir, 22, 57-64.
- Lekens, W. (2000) Een studie van de driftsedimentatie in het Porcupine Bekken. M.Sc. thesis, Department of Geology and Soil Science. Ghent University, Gent, 93 pp.
- Marani, M., Argnani, A., Roveri, M. & Trincardi, F. (1993) Sediment drifts and erosional surfaces in the central Mediterranean: seismic evidence of bottom-current activity. *Sedimentary Geology*, 82, 207-220.
- Masson, D. G., Howe, J. A. & Stoker, M. S. (2002) Bottom-current sediment waves, sediment drifts and contourites in the northern Rockall Trough. *Marine Geology*, 192, 215-237.
- McCave, I. N., Manighetti, B. & Robinson, S. G. (1995) Sortable silt and fine sediment size/composition slicing: Parameters for palaeocurrent speed and palaeoceanography. *Paleoceanography*, 10(3), 593-610.
- McDonnell, A. & Shannon, P. M. (2001) Comparative Tertiary stratigraphic evolution of the Porcupine and Rockall basins. In: *The Petroleum Exploration of Ireland's Offshore Basins* (Ed. by P. M. Shannon, P. Haughton and D. Corcoran), Geological Society, London, Special Publication, 188, 323-344.
- New, A. L., Barnard, S., Herrmann, P. & Molines, J.-M. (2001) On the origin and pathway of the saline inflow to the Nordic Seas: insights from models. *Progress in Oceanography*, 48, 255-287.
- Olu-Le Roy, K., Caprais, J.-C., Crassous, P., Dejonghe, E., Eardly, D., Freiwald, A., Galeron, J., Grehan, A., Henriot, J.-P., Huvenne, V. A. I., Lorange, P., Noel, P., Opderbecke, J., Pitout, C., Sibuet, M., Unnithan, V., Vacelet, J., van Weering, T. C. E., Wheeler, A. J. & Zibrowius, H. (2000) CARACOLE Cruise Report. 30/07/2001 (Cobh) - 15/08/2001 (Foynes) N/O L'Atalante & ROV VICTOR, Vols. 1&2. IFREMER, Brest.
- Paull, C., Ussler III, W., Maher, N., Rehder, G., Lorenson, T. & Lee, H. (2002) Pockmarks off Big Sur, California. *Marine Geology*, 181, 323-335.
- Pearson, I. & Jenkins, D. G. (1986) Unconformities in the Cenozoic of the North-East Atlantic. In: *North Atlantic Palaeoceanography* (Ed. by C. P. Summerhayes and N. J. Shackleton), Geological Society, London, Special Publication, 21, 79-86.
- Pingree, R. D. & Le Cann, B. (1989) Celtic and Armorican slope and shelf residual currents. *Progress in Oceanography*, 23, 303-338.
- Pingree, R. D. & Le Cann, B. (1990) Structure, strength and seasonality of the slope currents in the Bay of Biscay region. *Journal of the Marine Biological Association of the United Kingdom*, 70, 857-885.
- Poag, C. W., Reynolds, L. A., Mazzullo, J. M. & Keigwin, L. D. (1984) Foraminiferal, lithic, and isotopic changes across four major unconformities at deep sea drilling project site 548, Goban Spur. In: *Initial Reports of the Deep Sea Drilling Project* (Ed. by P. C. de Graciansky, C. W. Poag, R. Cunningham, P. Loubere, D. G. Masson, J. M. Mazzullo, L. Montadert, C. Müller, K. Otsuka, L. A. Reynolds, J. Sigal, S. W. Snyder, S. P. Vaos and D. Waples), U.S. Government Printing Office, Washington, 80, 539-555.
- Raymo, M. E., Oppo, D. & Curry, W. B. (1997) The mid-Pleistocene climate transition: A deep sea carbon isotopic perspective. *Paleoceanography*, 12(4), 546-559.
- Rebesco, M. & Stow, D. A. V. (2001) Seismic expression of contourites and related deposits: A preface. *Marine Geophysical Researches*, 22(5-6), 303-308.

- Reed, D. L., Meyer, A. W., Silver, E. A. & Prasetyo, H. (1987) Contourite sedimentation in an intraoceanic forearc system: eastern Sunda Arc, Indonesia. *Marine Geology*, 76(3-4), 223-242.
- Rice, A. L., Billet, D. S. M., Thurston, M. H. & Lampitt, R. S. (1991) The Institute of Oceanographic Sciences Biology programme in the Porcupine Seabight: background and general introduction. *Journal of the Marine Biological Association of the United Kingdom*, 71, 281-310.
- Rice, A. L., Thurston, M. H. & New, A. L. (1990) Dense aggregations of a hexactinellid sponge, *Pheromena carpenteri*, in the Porcupine Seabight (northeast Atlantic Ocean), and possible causes. *Progress in Oceanography*, 24, 179-196.
- Schnitker, D. (1986) North-east Atlantic Neogene benthic foraminiferal faunas: tracers of deep-water palaeoceanography. In: *North Atlantic Palaeoceanography* (Ed. by C. P. Summerhayes and N. J. Shackleton), Geological Society, London, Special Publication, 21, 191-203.
- Schönfeld, J. (2002a) A new benthic foraminiferal proxy for near-bottom current velocities in the Gulf of Cadiz, northeastern Atlantic Ocean. *Deep-Sea Research I*, 49, 1853-1875.
- Schönfeld, J. (2002b) Recent benthic foraminiferal assemblages in deep high-energy environments from the Gulf of Cadiz (Spain). *Marine Micropaleontology*, 44, 141-162.
- Schönfeld, J. & Zahn, R. (2000) Late Glacial to Holocene history of the Mediterranean Outflow. Evidence from benthic foraminiferal assemblages and stable isotopes at the Portuguese margin. *Palaeogeography, Palaeoclimatology, Palaeoecology*, 159, 85-111.
- Stoker, M. S., Nielsen, T., van Weering, T. C. E. & Kuijpers, A. (2002) Towards an understanding of the Neogene tectonostratigraphic framework of the NE Atlantic margin between Ireland and the Faroe Islands. *Marine Geology*, 188, 233-248.
- Stow, D. A. V. (1982) Bottom currents and contourites in the North Atlantic. *Bull. Inst. Géol. Bassin d'Aquitaine*, 31, 151-166.
- Stow, D. A. V., Faugères, J.-C. & Gonthier, E. (1986) Facies distribution and textural variation in Faro Drift contourites: Velocity fluctuation and drift growth. *Marine Geology*, 72, 71-100.
- Stow, D. A. V., Faugères, J.-C., Howe, J. A., Pudsey, C. J. & Viana, A. R. (2002) Bottom currents, contourites and deep-sea sediment drifts: current state-of-the-art. In: *Deep-Water Contourite Systems: Modern Drifts and Ancient Series, Seismic and Sedimentary Characteristics* (Ed. by D. A. V. Stow, C. J. Pudsey, J. A. Howe, J.-C. Faugères and A. R. Viana), Geological Society, London, Memoirs, 22, 7-20.
- Stow, D. A. V. & Johansson, M. (2000) Deep-water massive sands: nature, origin and hydrocarbon implications. *Marine and Petroleum Geology*, 17, 145-174.
- Stow, D. A. V. & Mayall, M. (2000) Deep-water sedimentary systems: New models for the 21st century. *Marine and Petroleum Geology*, 17, 125-135.
- Stow, D. A. V. & Piper, D. J. W. (1984) Deep-water fine-grained sediments: facies models. In: *Fine Grained Sediments, Deep-Water Processes and Facies* (Ed. by D. A. V. Stow and D. J. W. Piper), Geological Society, London, Special Publication, 15, 611-646.
- Van Rooij, D., Raes, M., Tseu, G. & Henriët, J.-P. (2003) Cruise Report Belgica 03/13 Porcupine seabight, off Western Ireland. RCMG, Gent.
- Wheeler, A. J., Beyer, A., Freiwald, A., de Haas, H., Huvenne, V. A. I., Kozachenko, M. & Olu-Le Roy, K. (submitted-a) Morphology and Environment of Deep-water Coral Mounds on the NW European Margin. In: *Modern Carbonate Mound Systems: A window to Earth History* (Ed. by J.-P. Henriët and C. Dullo), Springer-Verlag, Heidelberg.
- Wheeler, A. J., Kozachenko, M., de Haas, H., Huvenne, V. A. I., Masson, D. G. & Olu-Le Roy, K. (submitted-b) Hydrodynamically Influenced Small Deepwater Reefs (Moirá Mounds) in the Porcupine Seabight, NE Atlantic. In: *Modern Carbonate Mound Systems: A window to Earth History* (Ed. by J.-P. Henriët and C. Dullo), Springer-Verlag, Heidelberg.

White, M. (submitted) The hydrographic setting for the carbonate mounds of the Porcupine Bank and Sea Bight. In: Modern Carbonate Mound Systems: A window to Earth History (Ed. by J.-P. Henriet and C. Dullo), Springer-Verlag, Heidelberg.

Wynn, R. B. & Stow, D. A. V. (2002) Classification and characterisation of deep-water sediment waves. *Marine Geology*, 192, 7-22.



## Chapter VII: Structure and development of the Gollum channel system

The most prominent feature in the Porcupine Basin, observed on the Gebco bathymetry is the east-west oriented tributary Gollum channel system (GCS, Fig. 7.1), initially described by Berthois & Brenot (1966) and further described by Kenyon *et al.* (1978). Wheeler *et al.* (2003) considered this channel as one of the few lengthy channels on the NE European Atlantic margin.

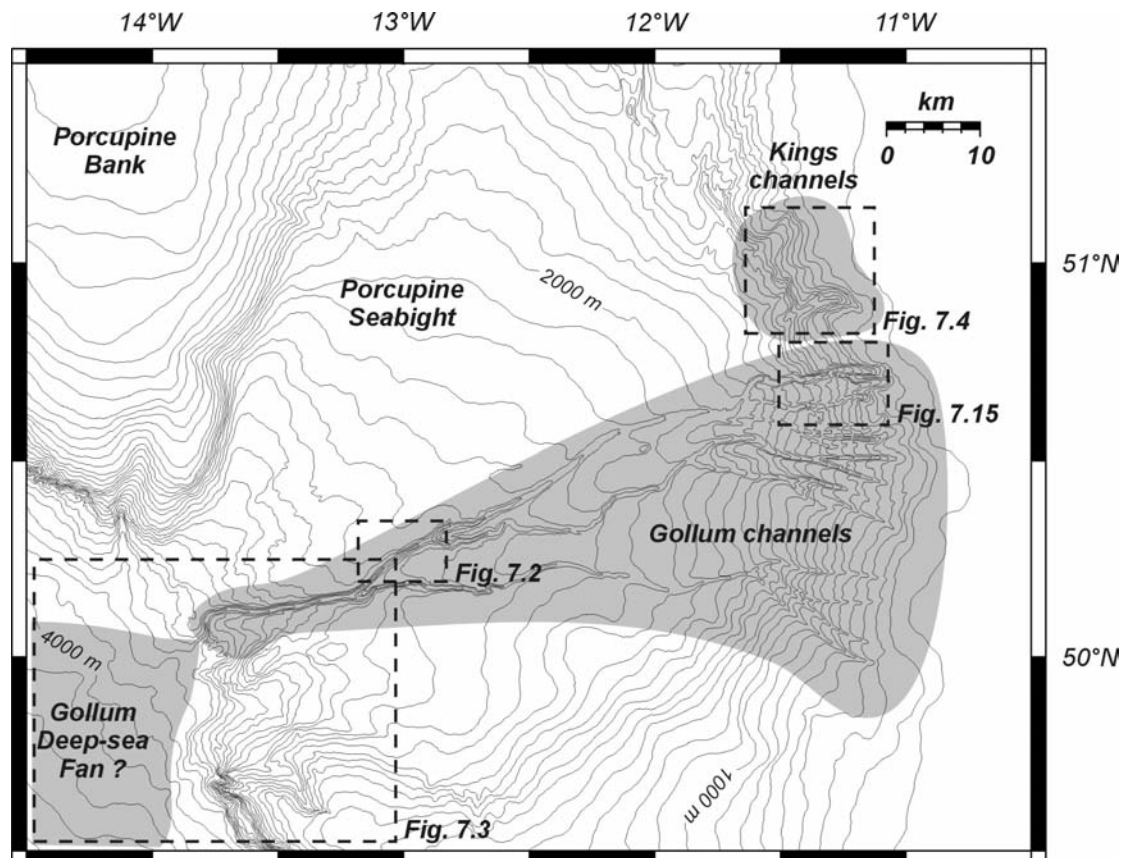


**Figure 7.1:** Overview map (GEBCO bathymetry, contour intervals are drawn every 100 m) and location of the Kings channel system (KCS) and the Gollum channel system (GCS) with indication of the inferred Gollum deep-sea fan.

In general, the upper part of GCS is built of about 10 branches that converge in basinward direction into one large Gollum channel, making its way towards the Porcupine Abyssal Plain. However, the channel heads are not very prominent in the bathymetry and furthermore no paleo-valleys have been observed along the continental margin. This suggests that this system is nowadays inactive, which has been partly confirmed by Rice *et al.* (1991) and Wheeler *et al.* (1998).

The upper branches of the GCS feed dendritically into narrow and low sinuosity channels with steep sides. Wheeler *et al.* (2003) described asymmetric upper channels, progressively filled in from the south due to the influence of northerly contouritic sand transport. Kenyon *et al.* (1998) and Wheeler *et al.* (2003)

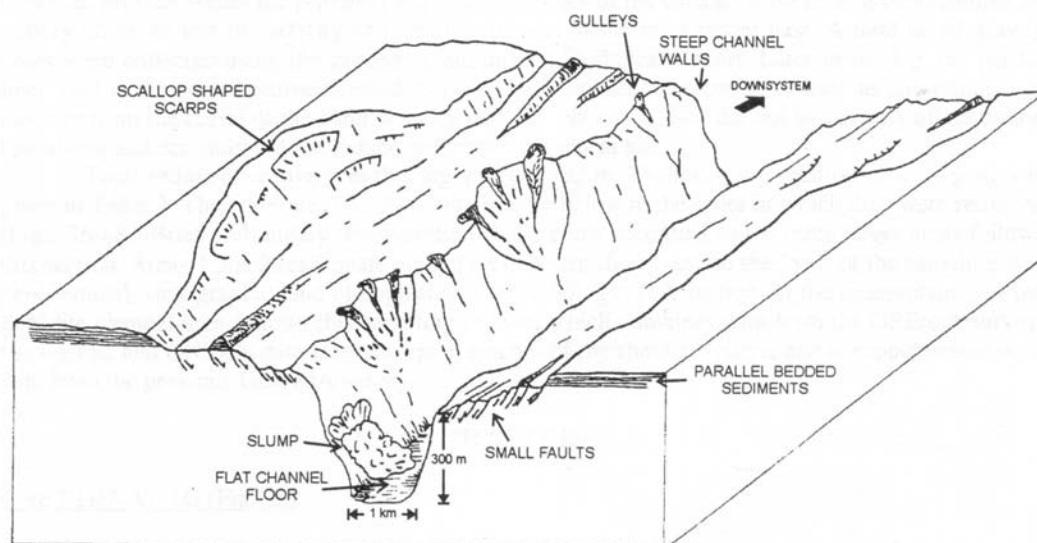


**Figure 7.2:** Schematic block diagram of the middle reaches of the Gollum Channel (Fig.7.1) based on interpretation of side-scan sonar imagery. The channel possesses a “steerhead geometry” with a steeply incised thalweg channel (300 m deep by 1000 m wide) with terraced margins (2 km wide) flanked by a laterally extensive levee/overbank system (Wheeler *et al.*, 2003).

described broad terraces flanking the central thalweg on the middle reach of the channel system (Fig. 7.2). Along the entire channel wall, frequent observations were made of slide and slump scars.

It is generally assumed that these channels funneled turbidity currents into the southern part of the PSB (Wheeler *et al.*, 2003; Weaver *et al.*, 2000; Kenyon *et al.*, 1998). Dating of turbidite deposits, suggested a principal activity during glacial stages and very limited to no activity during the last 10 ka (Wheeler *et al.*, 2003). According to submersible observations reported by Tudhope & Scoffin (1995), a large part of the channel floor shows firmly rippled moderately well-sorted fine sand. It is suggested they were deposited by reversing bottom currents. Moreover, these recent observations did not infer a significant turbidity current activity since the past few decades. This low turbidite current activity has also been inferred by Weaver *et al.* (2000). They attributed the absence of pronounced levees in the GCS to the lack of a significant turbiditic overspill. These supposed fine-grained turbiditic channels all feed into one single Gollum channel at about 3000 m, where sediment continues to be transported downslope to the Porcupine Abyssal Plain.

At the extremity of this system, Akhmetzhanov *et al.* (2003) identified a number of channels, associated with inferred turbidite and debris flow deposits (Fig. 7.3). 3.5 kHz profiles over the sides of these channels infer fine-grained overbank deposits. This probable deep-sea fan is less prominent due to the likely reworking by intense bottom currents, as observed at the foot of Goban Spur (Van Rooij, 1999).

The GCS is the only major downslope sediment supplying system located in the southern part of the Porcupine Seabight. However, compared to its counterparts on the Celtic and Armorican margins (Droz *et al.*, 1999; Zaragosi *et al.*, 2000), its structure and development are yet poorly studied. A variety of new data, collected during several campaigns from 1999 to 2002, can however contribute to the

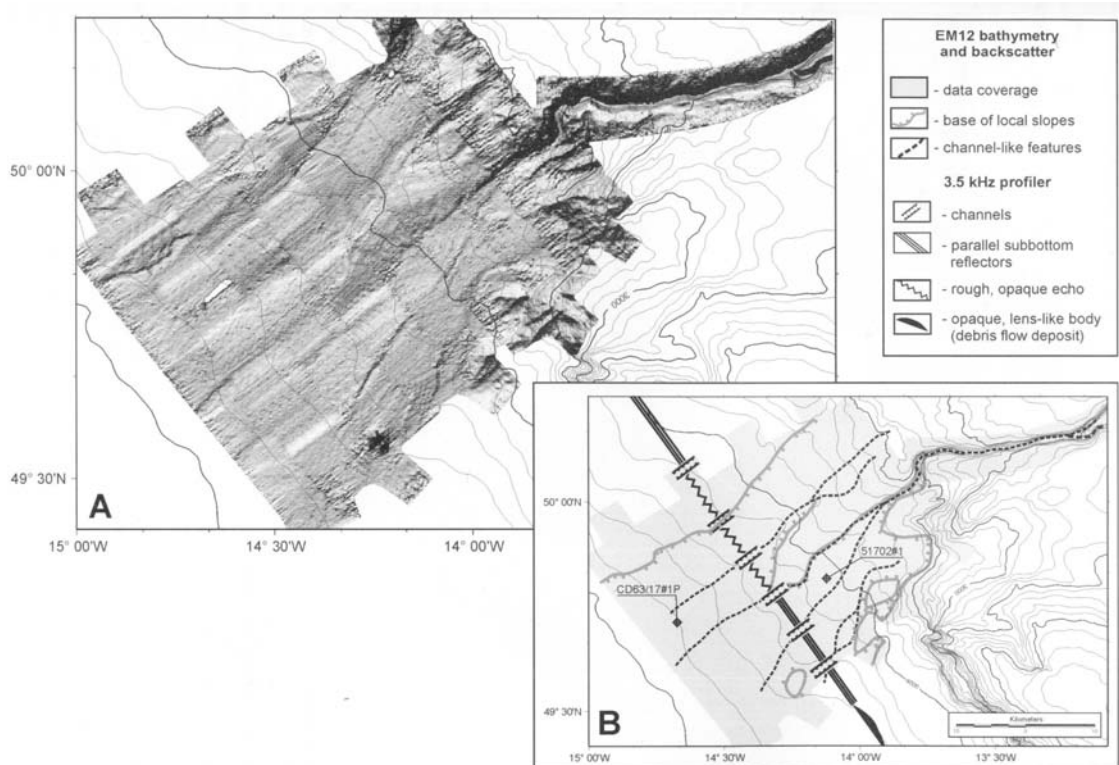


**Figure 7.3:** (A) Shaded bathymetry from EM12 swath data; (B) Interpretation of the swath bathymetry, 3.5 kHz profile and backscattering data, in terms of major sedimentary features (Akhmetzhanov et al., 2003).

knowledge about the structure, development and activity of this large channel system. Moreover, the new multibeam bathymetric data from Beyer *et al.* (2003) already allow to distinguish two different channel settings on this part of the slope (Fig. 7.1); the large Gollum channel system (GCS) and the smaller Kings channel system (KCS). These data called for a nomenclature of these newly documented channels, which was already presented in the first chapter.

In this section, the available seismic profiles will be used to provide more insight in the structure and development of these two channel systems. Moreover, a core (MD01-2464) taken within one of the branches of GCS will allow to yield more information about the sedimentary environment of these channels.

### 7.1 The Kings channels

The Kings channels are the first major gullies in an otherwise smooth sea floor, south of the Belgica mound province. None of the four channels in this system (Aragorn, Faramir, Boromir and Theoden) seems to be elongated towards the edge of the basin, as the main Gollum channels do (Fig. 7.1). They rather seem to end in a zone with dramatic incisions, slides and slumps (Fig. 7.4). In general, these channels have relatively smooth flanks with only few slide scars. In this section, four units will be discussed: Aragorn channel, the upper Theoden channel, the Faramir channel, leading to the Denethor (slump) area.

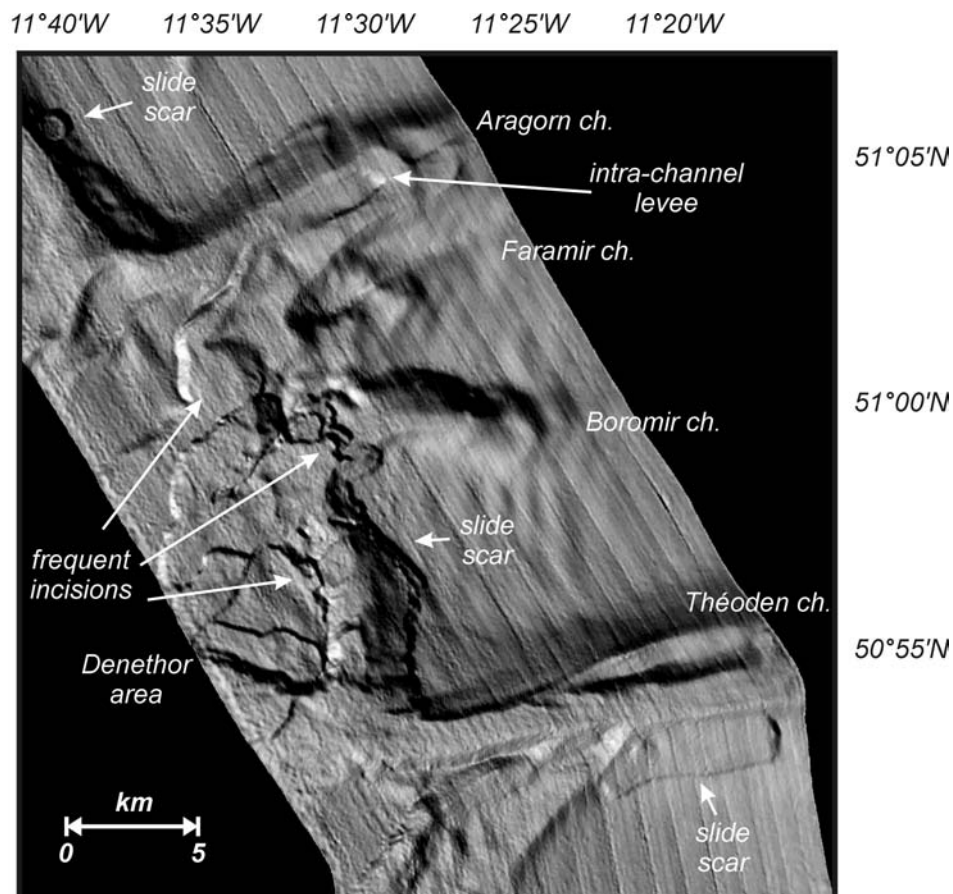


**Figure 7.4:** Shaded relief bathymetry map of the Kings channel system (KCS), highlighting the main morphological features.

### 7.1.1 Aragorn channel

The morphology and stratigraphy of this broad channel is illustrated by profiles P99009b (Fig. 7.6) and P99007b2 (Fig. 7.7), located on figure 7.5. Along these profiles, the channel is 3.6 to 5.2 km wide, while the thalweg is about 2.7 km wide. However, this channel does not seem to be limited to one downslope running pathway. A large elongate mounded sedimentary body of 3.7 km length and 1 km width separates the channel into two flow paths of 600 to 700 m width. The mean downslope angle of the channel floor is about 2.8°. Both the seismic profiles and the multibeam bathymetry show smooth channel flanks with an angle of 10 to 16° along the northern flank and 7 to 14° on the southern flank.

The channel is filled with about 200 ms TWT (175 m) of subparallel stratified deposits, with intercalated mass-wasting deposits, especially along the southern side of the channel floor. The large elongated body on the channel floor can be interpreted in terms of a turbidite levee, built on the right hand side of the downslope running flow. This might indicate that since the creation of this channel, the strength and focus of the downslope running current has significantly decreased. The northern channel flank shows few slump scars, suggesting that several mass-wasting deposits within the channel are due to slumping on this relatively steep channel wall.

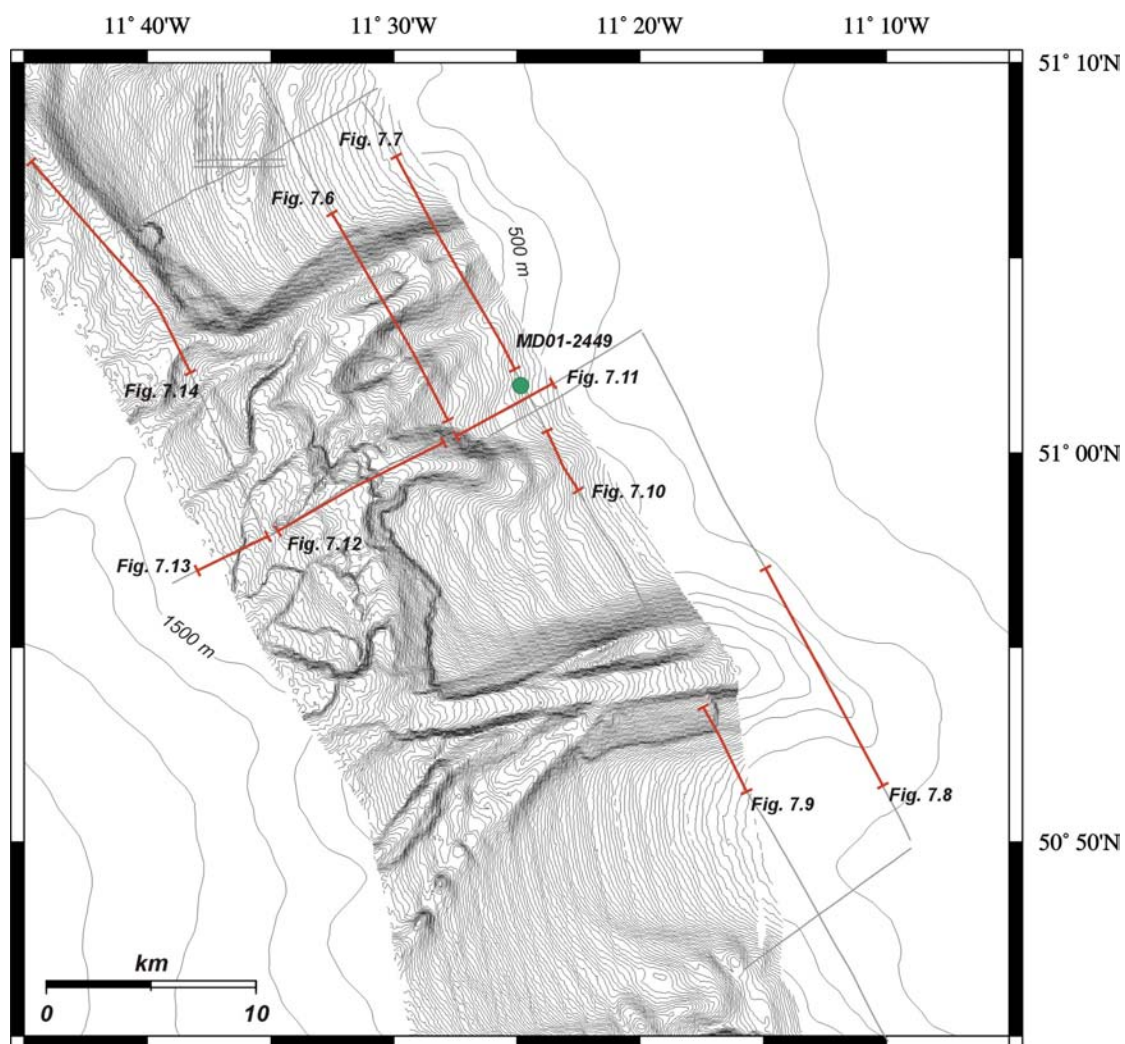


**Figure 7.5:** Location map of the seismic profiles and core used in the Kings channel area (all available profiles are indicated in grey). The bathymetry is a combination of AWI multibeam bathymetry (contour interval every 10 m) and GEBCO bathymetry (contour interval every 100 m).

Underneath the channel base, SSE migrating sigmoidal bodies are observed, suggesting the presence of unit U3. Moreover, the stratigraphy of the channel flanks and underlying unconformities might yield more information concerning the timing of the event responsible for the creation of this channel. Both profiles show a steep northern flank with an almost parallel stratified (hemipelagic) unit U1 on a steeply incised unit U2. Along the southern flank, unit U2 seems to be more eroded and especially profile P99007b2 suggests the flank deposits have been influenced by currents and can be considered as a large levee unit. This levee has been built between the Aragorn and the Faramir channel and has evolved together with the channel deposits (Fig. 7.7). The latter, smaller channel also seems to be located above a depression in the upper boundary of unit U2.

### 7.1.2 Theoden channel

The Theoden channel is the southernmost King channel and splits into the Eowyn and Eomer branch (see chapter 1). Upslope, this channel can be up to 6 km wide, narrowing to 1.5 km downslope. The width of the thalweg remains relatively

constant at about 1.2 km, under a gently downslope running channel floor with an average slope of 2°. At its narrowest part, the flanks of this channel are relatively steep with angles up to 18°. However, on profile P010509 (Fig. 7.8), both flanks have a slope of about 4°.

The southern flank of this channel is characterized by a very large slide scar with an affected area of about 13 km<sup>2</sup>. Here, the slope amounts to 8°. Seismic profile P99007 (Fig. 7.9) shows a cross-section through the slide scar, suggesting this might have been a relatively recent event. Moreover, within the Quaternary unit U1, yet another discontinuity has been observed, suggesting that during its deposition there has been a sequence of sliding or slumping events.

This is also on illustrated figure 7.8, where the inferred Quaternary U1 section is a complex stacking of irregular sediment bodies, separated by several discontinuities. In the main thalweg of this channel, a large mass-wasting deposit is observed, intercalated between the complex stratification. This entire U1 unit has been built in an irregular depression cut into U2 strata. Like the Aragorn channel, the base of the channel reaches the inferred sediment waves of unit U3.

### 7.1.3 Boromir channel & Denethor area

In between the large Aragorn and Theoden channels, the smaller Boromir channel leads to the much dissected Denethor area. The uppermost part of this channel is a very round depression, similar to a slump scar. This channel is about 2.4 to 2.6 km wide and has a slope of 3°. Both channel flanks are relatively steep, with values ranging from 11 to 17°. The width of the thalweg seems to remain relatively constant at 800 m, along the entire downslope course of the channel.

Profile P99007b1 (Fig. 7.10) shows a very subtle depression along the sea floor, which most probably is the uppermost part of the Boromir channel. However, the underlying sedimentary series show several discontinuities, above a synsedimentary fault along the presumed upper boundary of unit U2. NNW of this feature, all strata along this U2/U1 boundary gently bend down, while SSE of it, all strata are bent upwards. Since this feature is located upslope of the main Boromir channel, one could infer this channel has a tectonic origin. However, this feature has only been observed on one NNW-SSE profile and it calls for more research.

On the other hand, profile P010510a (Fig. 7.11), located NW of previous profile, also shows a depression in the upper boundary of unit U2. The U2 strata seem to be disturbed at a certain level, but at this moment, not enough data is available to link this feature to the presumed synsedimentary fault on the previous profile. Nevertheless, within this depression, an upslope prograding sediment body has been installed, which can be interpreted as a small infill sediment drift body.

This Boromir channel flows into the Denethor area, which has an estimated surface of about 120 km<sup>2</sup> on the multibeam bathymetry (Fig. 7.4). Only very few seismic profiles are available to understand the geology of this area. Along its eastern limit, between the Boromir and Theoden channel, a steep flank with a large slump scar is observed. The sea floor is cut by several large scarps, from 40 up to 100 m high, forming a terrace-like environment. Much of these features seem to be a prolongation of the Aragorn, Faramir, Boromir and Theoden channels, suggesting they might be levees or even erosional scars. Unfortunately, the few available profiles do not allow to distinguish a stratigraphy which can be correlated with the upper

slope. Moreover, profile P010510b (Fig. 7.12) rather suggests these features are slump scars, with mass-wasting deposits located at their feet. Also profile P99010b shows various mass-wasting deposits along the foot of a scarp, which however seems to be the western flank of a small gully (Fig. 7.5). Most probably, the key area which can yield more information about the true nature of this area is located SE of these profiles and directly downslope of the large slump scar.

Possibly, a similar situation as observed on profile P010511a (Fig. 7.14) can be met. The SE part of this profile is the relatively narrow downslope prolongation of the Aragorn area. At the NW side, a gully marks the start of the NW flowing Arwen channel. In between, a massive mounded deposit is observed, where continuous, high-amplitude reflectors outline the presence of a large quantity of mass-wasting deposits. Most probably, they originate from the very steep wall at their NE side, on which a nice, rounded slump scar is observed on figure 7.4.

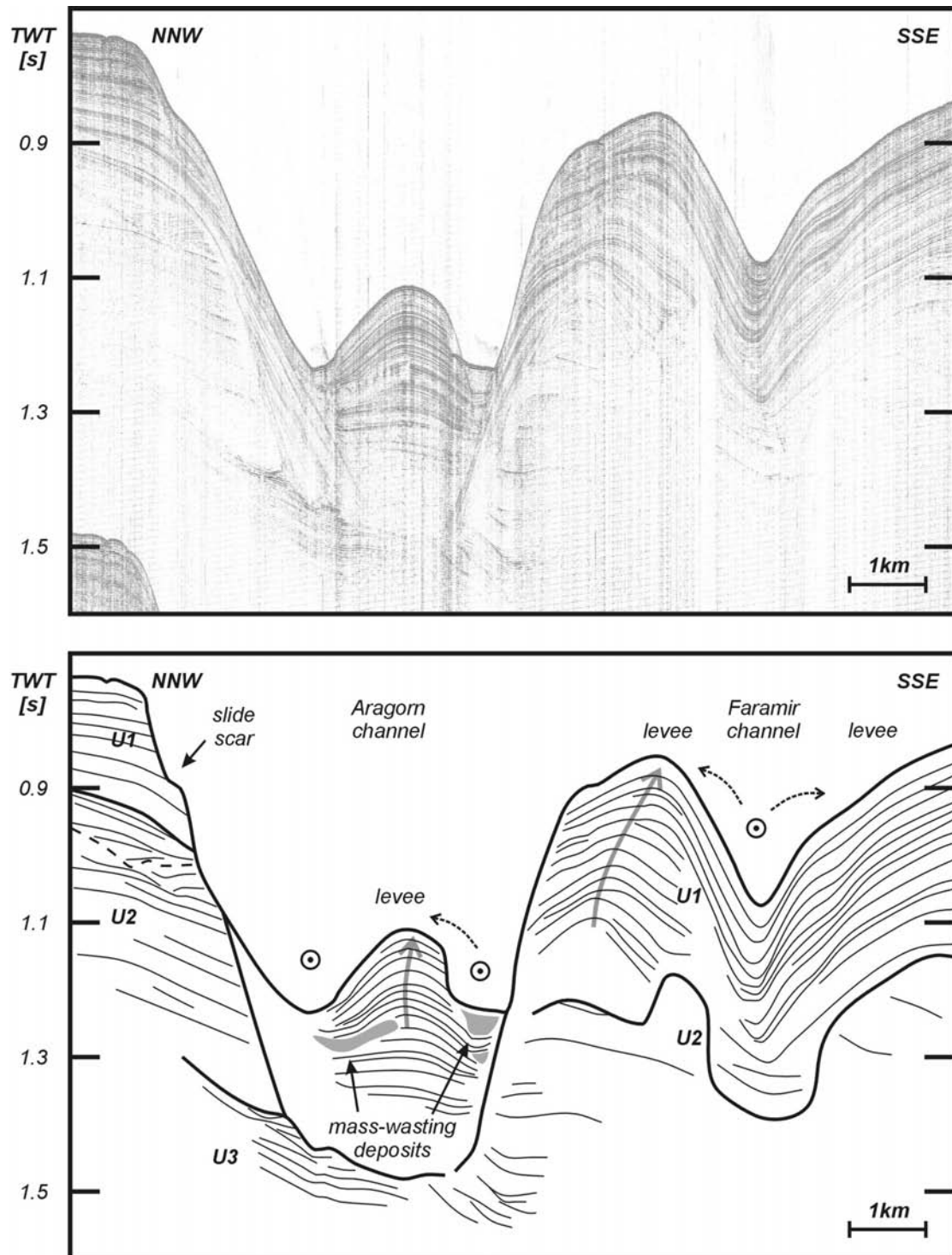


**Figure 7.6:** P99009b: Cross-section along the Aragorn and Faramir channel. Note the levee-like structure within the Aragorn channel, overlying various mass-wasting deposits. The channel floor seems to cut into unit U3, probably due to the RD1 erosion event. The Faramir channel is a constructional channel, built in a depression in the U2 upper boundary

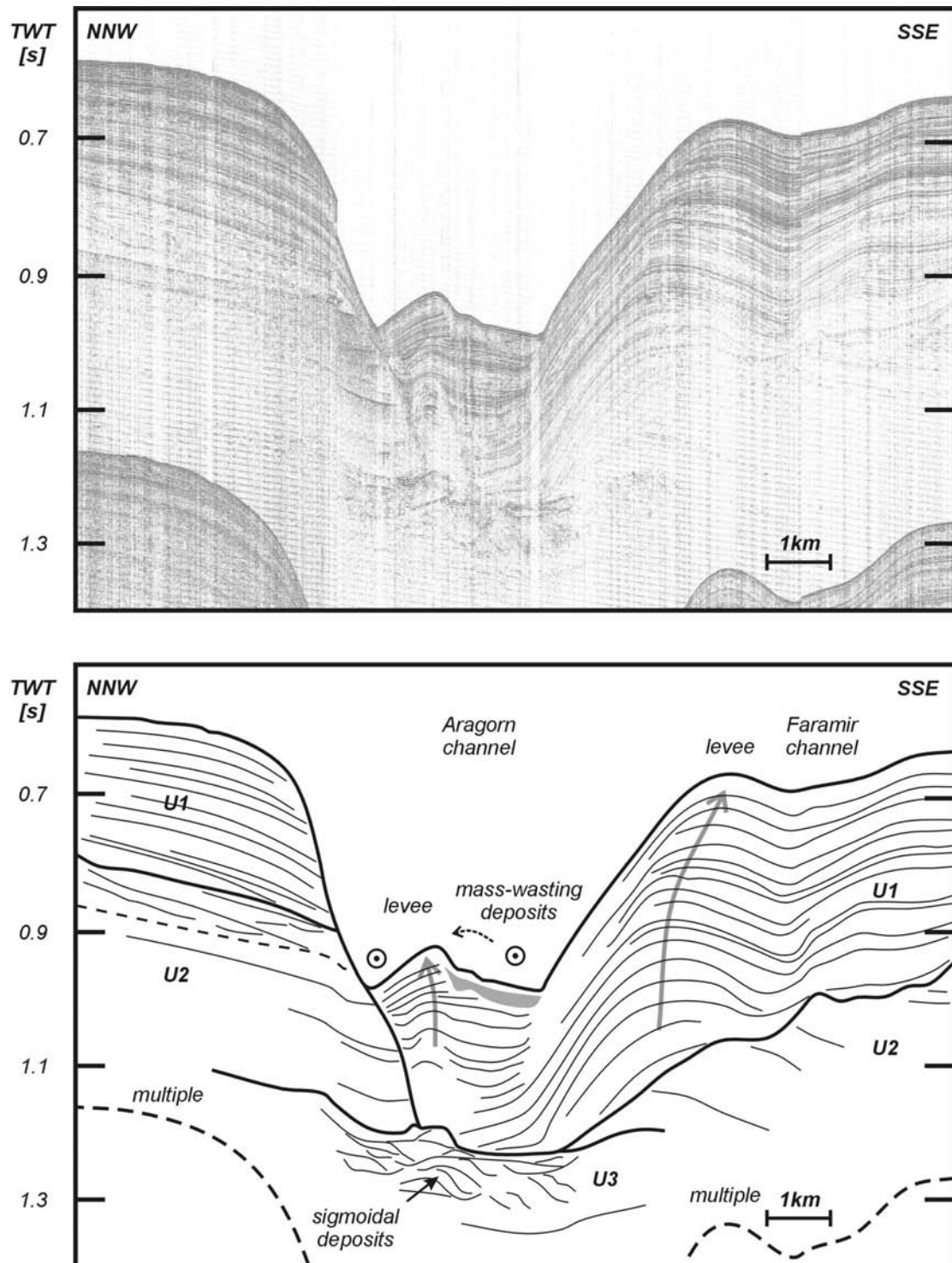


**Figure 7.7:** P99007b2: Alongslope profile across the upper reaches of the Aragorn and Faramir channels. Here, an intra-channel levee is also present. A large, pronounced levee is only built on the southern flank. The channel is cut into units U2 and U3.

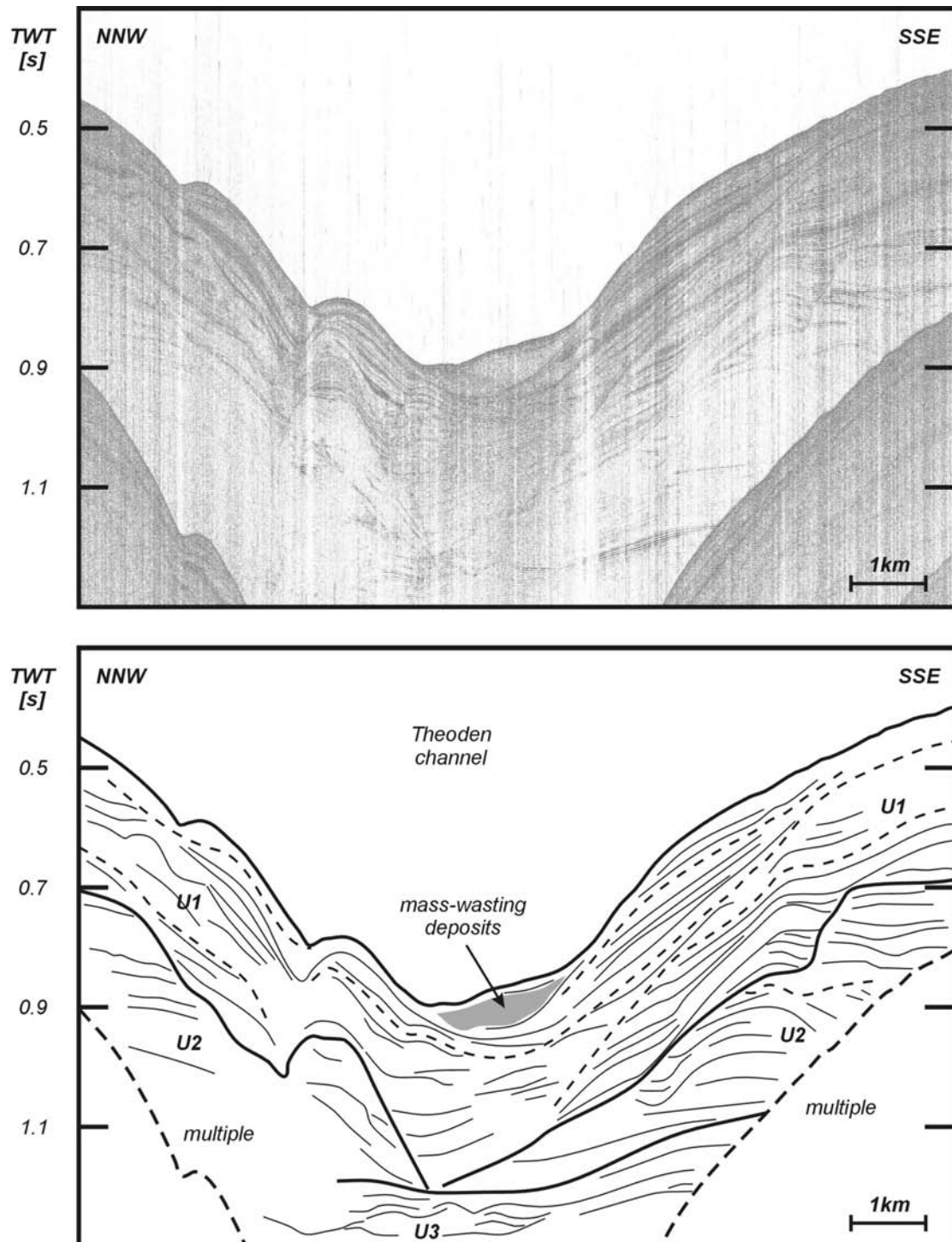


**Figure 7.8:** P010509: Cross-section across the upper reaches of the broad Theoden channel. The recentmost unit is characterized by a very complex reflector configuration, with multiple erosion surfaces and mass-wasting deposits. The channel has been installed in a depression mainly cut into unit U2.

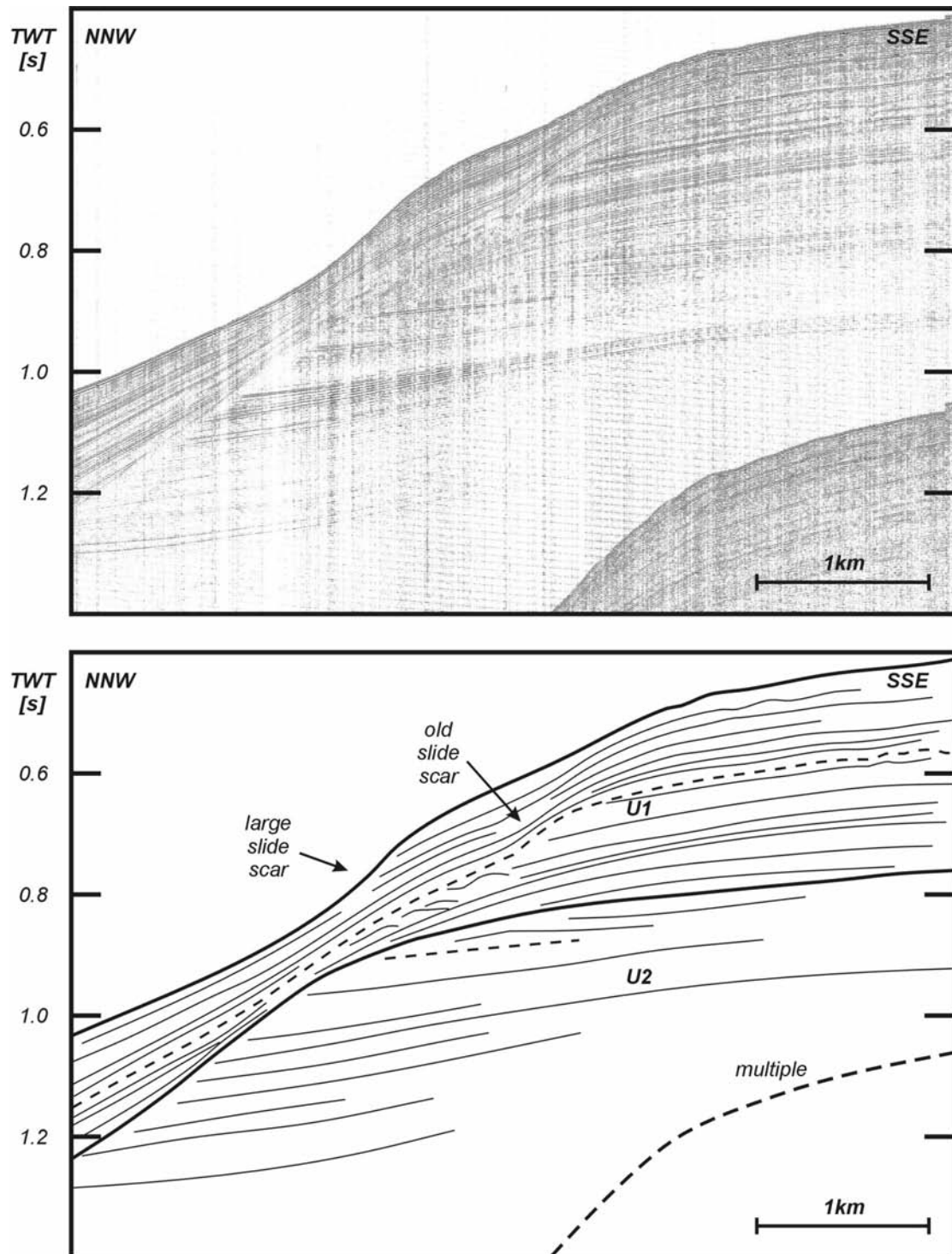


**Figure 7.9:** P99007: Profile across the upper southern flank of the Theoden channel, showing an incised unit U2. Within unit U1, an ancient and a recent slide scar are observed.

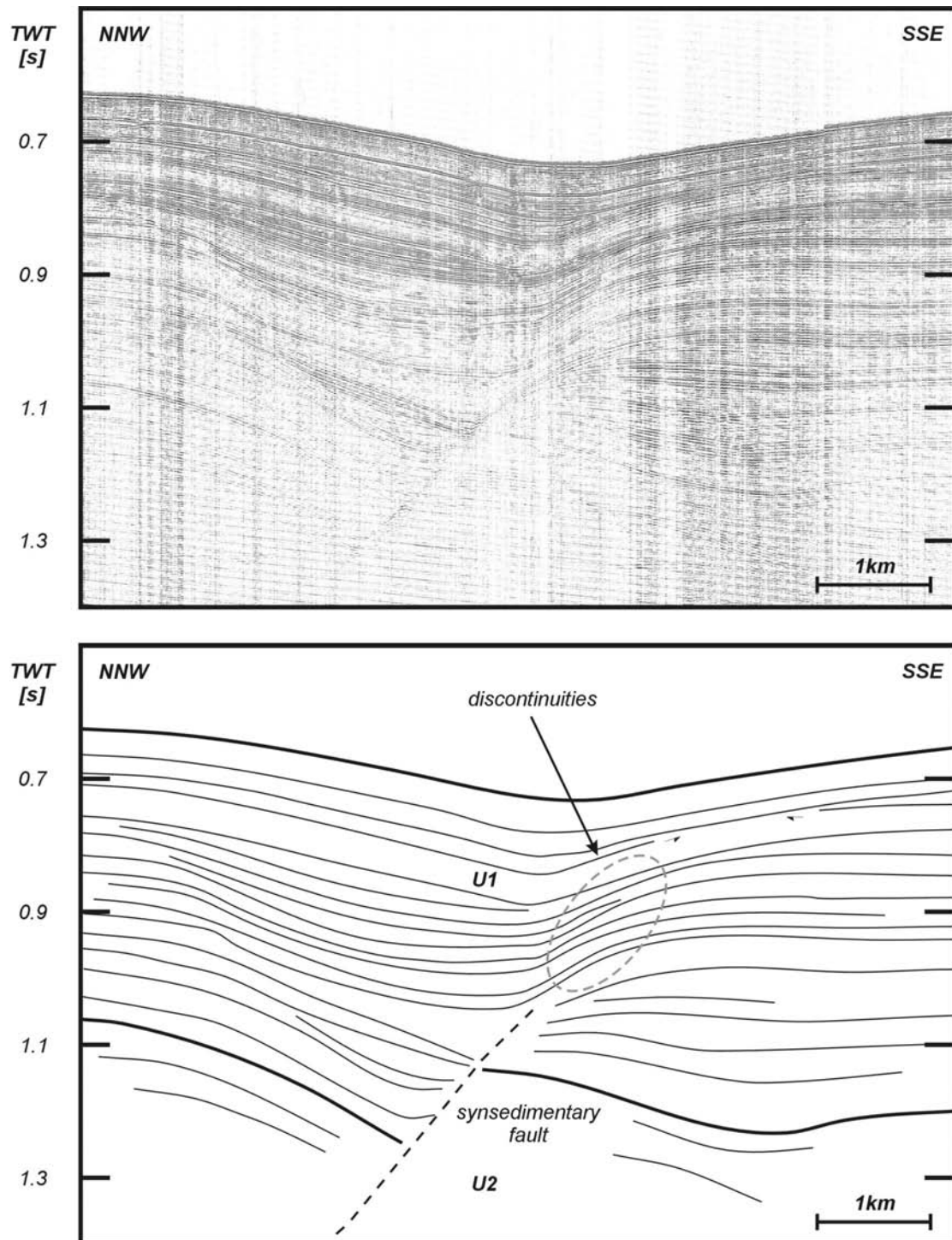


**Figure 7.10:** P99007b1: Profile east of the Boromir channel head. The geometry of unit U1 is influenced by the presence of a possible syn-sedimentary fault below its lower boundary. Within this part of U1, several internal discontinuities are observed.

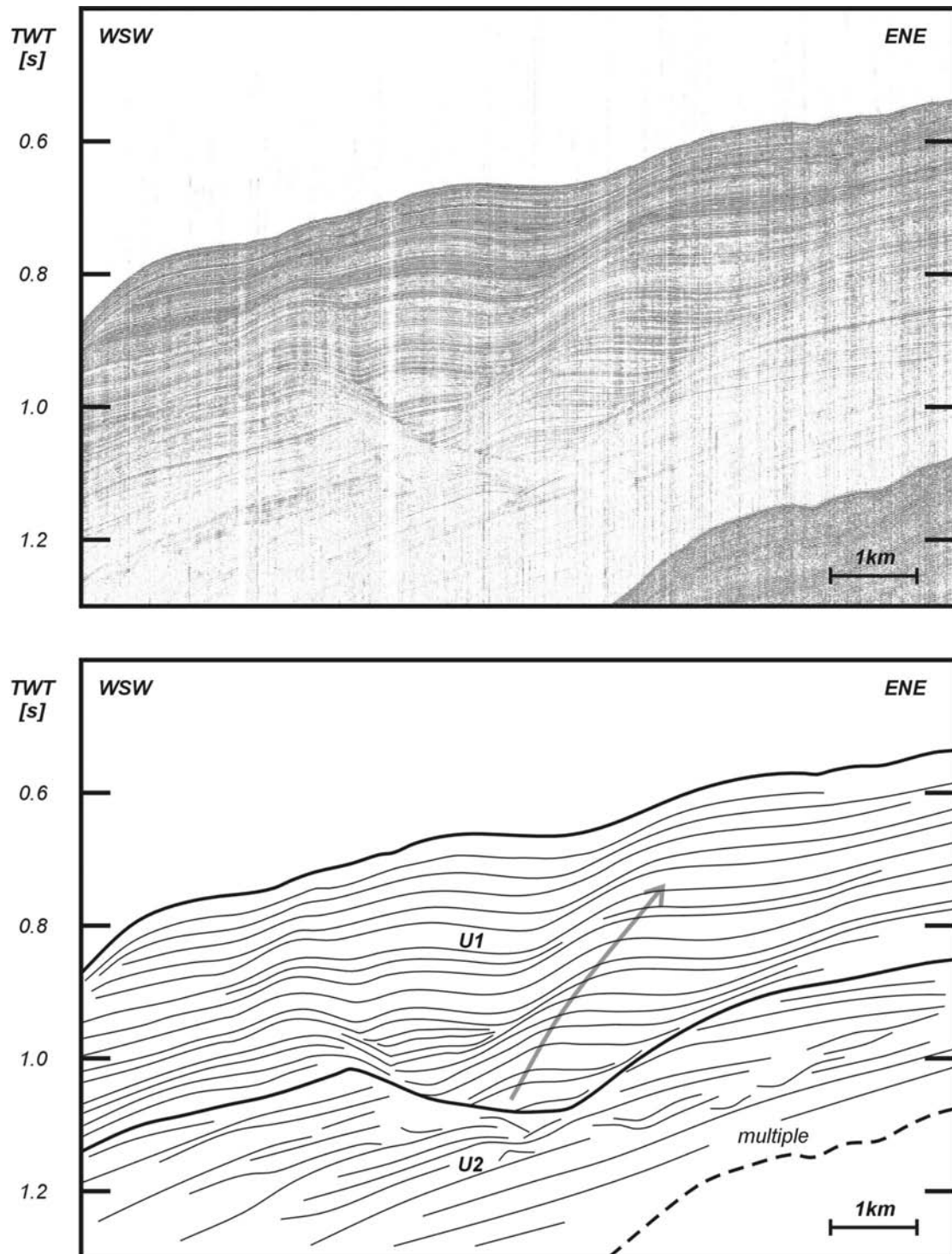


**Figure 7.11:** P010510a: Profile along the northwestern flank of the Boromir channel. An upslope prograding sediment body is installed in a depression, probably related with the erosive discontinuity lying at the base of the Boromir channel.

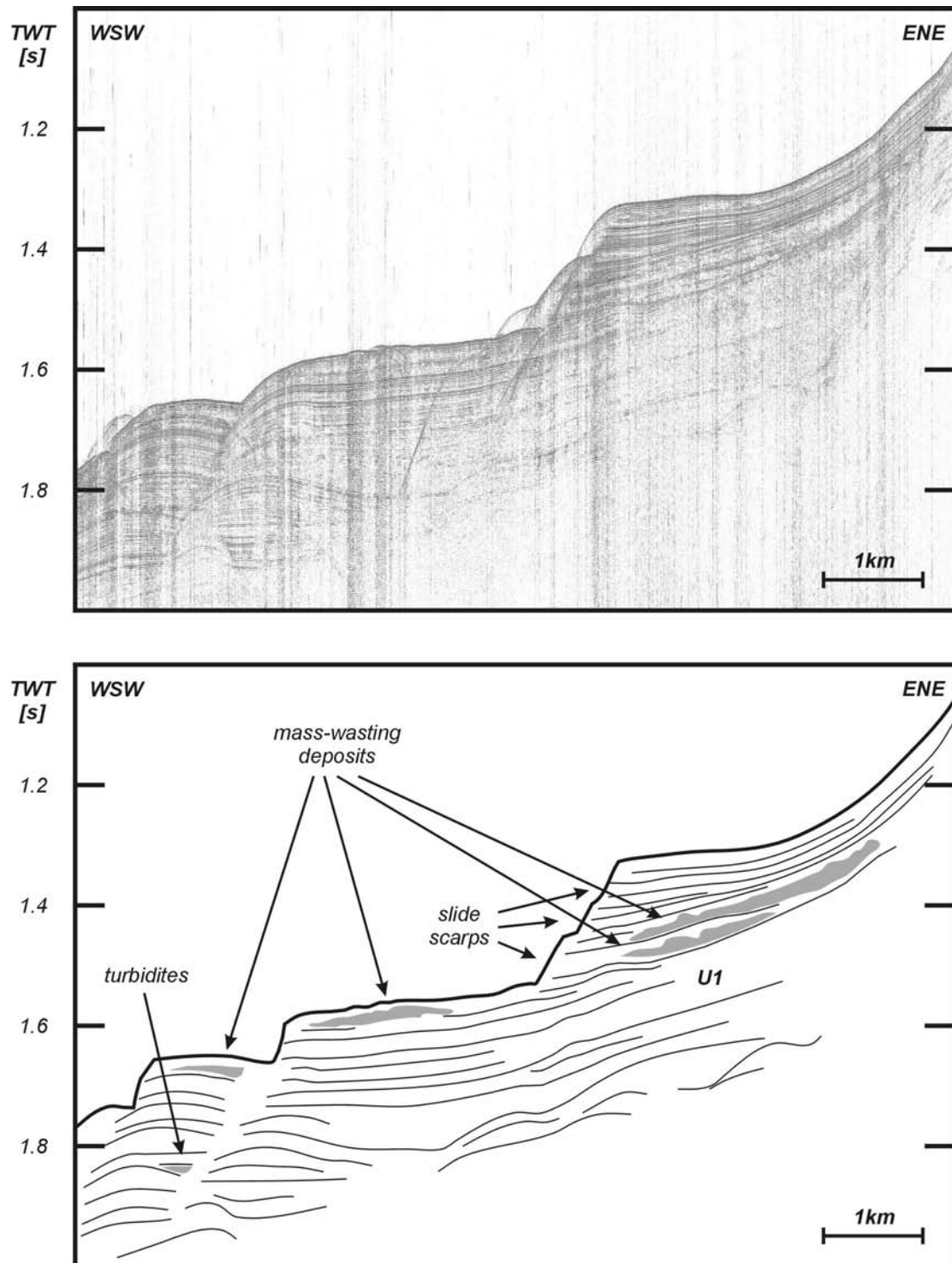


**Figure 7.12:** P010510b: Downslope running profile along the axis of the Boromir channel into the Denethor area. The seafloor morphology is characterized by steep slide scarps and mass-wasting deposits.

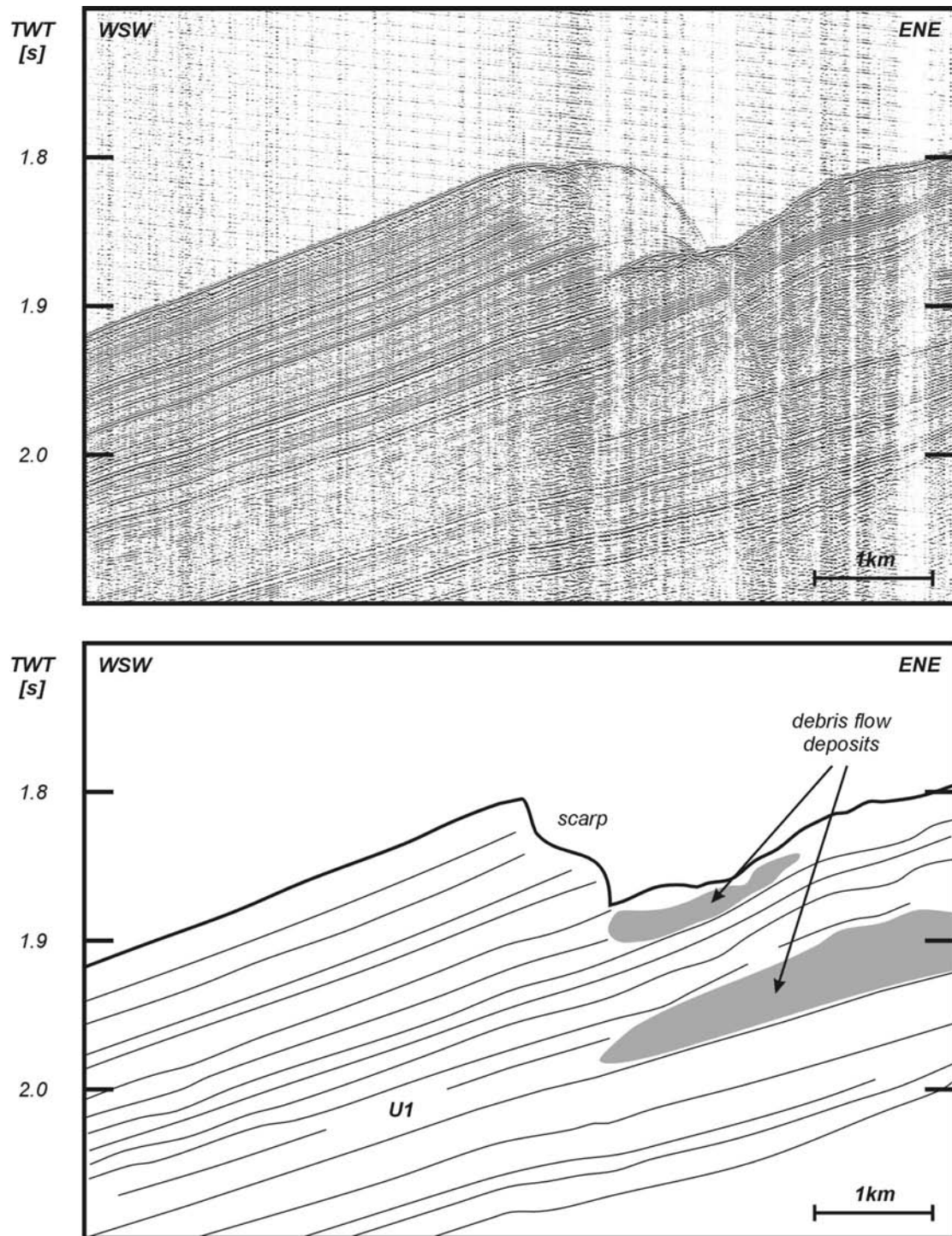


**Figure 7.13:** P99010b: Downslope section across the Denethor area with a scarp and several debris flow deposits.

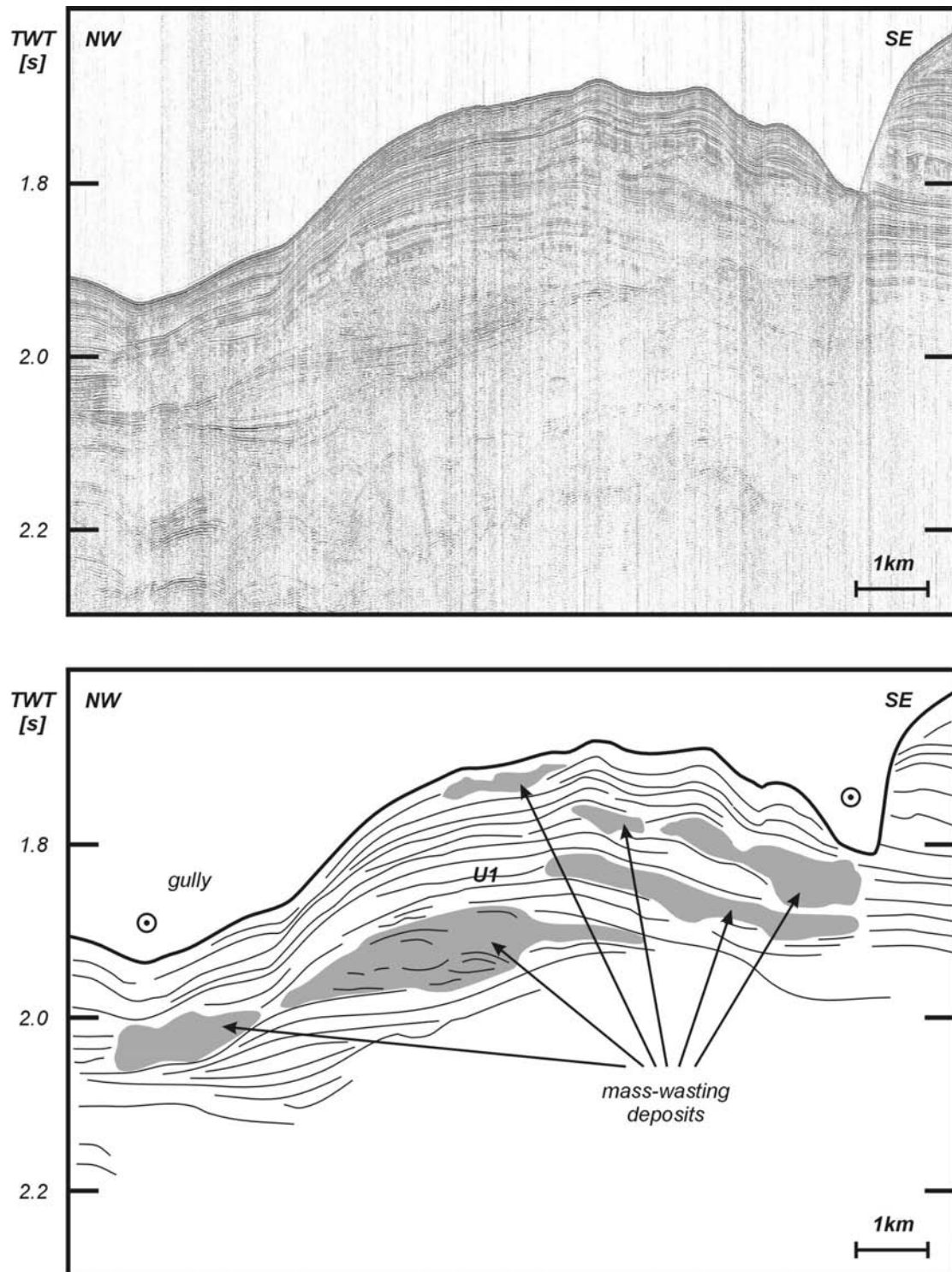


**Figure 7.14:** P010511a: Downslope section of the Aragorn channel, at the start of the Arwen channel and at the foot of a steep scarp. Unit U1 is characterized by the presence of several mass-wasting deposits, intersected by downslope running gullies.

#### 7.1.4 Clues for the development of KCS

The observations in the Kings channel area suggest that the erosion event responsible for the creation of these broad channels has happened prior to the deposition of unit U1 and after the deposition of unit U2. Consequently, it seems plausible that the Late Pliocene RD1 erosion event can be considered as a causal mechanism. Like on Goban Spur and the Belgica mound province, this erosion event is coupled to the onset of modern oceanographic conditions and the start of glacial-interglacial cycles. In this area, large downslope east-west depressions were cut into the Neogene strata. Some evidence shows the influence of possible syn-sedimentary faulting. The present-day course of these channels seems to strictly follow the pathway created during the Late Pliocene. However, throughout the Quaternary, the strength of these downslope running currents has been very variable. First of all, the upper Theoden channel shows several periods of incision or repositioning of the current focus. Secondly, the presence of a large intra-channel levee in the Aragorn channel clearly illustrates that towards recent times, only a small focused current can be inferred. These currents are predominantly downslope running turbidite currents, with the build-up of sediment levees on their right-hand side (Faugères *et al.*, 1999). Except for the northern flank of the Aragorn channel, the sedimentation on the other flanks has been significantly influenced by these downslope running currents. They have grown together with the channel deposits as associated levees. Outside the reach of these currents, on upper slope areas like the northern flank of the Aragorn channel or surrounding the Boromir channel, a largely intact U2 can still be inferred, with a fairly thick hemipelagic sedimentation. The generally smooth morphology and the observation of some bottom-current influenced features on the upper slope suggest a smoothening by a (relatively weak) northward flowing bottom current.

However, not only turbiditic processes are observed in this area. Along steeper slopes, slump or slide scars are numerous, with the presence of sometimes very voluminous mass-wasting deposits at the foot of these slopes. Although few data is available in the Denethor area, the Quaternary sedimentary environment seems to have been influenced by current incisions, sliding and slumping. Like on Goban Spur, this suggests a dramatic phase of slope instability within the Pleistocene. Most probably, a combination of a very hydrodynamic regime with turbidite currents, changing Pleistocene sea-levels, the inherited irregular paleotopography and a high sediment stress has led to frequent instabilities since the Pleistocene, which is not uncommon on upper slope environments (Locat & Lee, 2002). However, more seismic and core observations are needed to understand the Neogene development of this area.

## 7.2 The Gollum channels

South of the KCS, the upper channels of the Gollum channel system (GCS) form all together a low sinuosity tributary channel system in the southern part of the Porcupine Seabight (Fig. 7.1). In contrast with the Kings channels, these channels are smaller, steeper and merge into one big feeder channel. Both channels also show strange changes along their course, resembling the shape of a bayonet (Fig. 7.16). The available seismic profiles, together with the multibeam bathymetry data only allow discussing the architecture along a 55 km transect of the upper northern two Gollum channels; Bilbo and Frodo (Figs. 7.15 and 7.16). Additionally, core MD01-2464 can yield more information about the deposits found on the floor of the Bilbo channel and might shed more light on the sedimentary processes governing this channel environment.

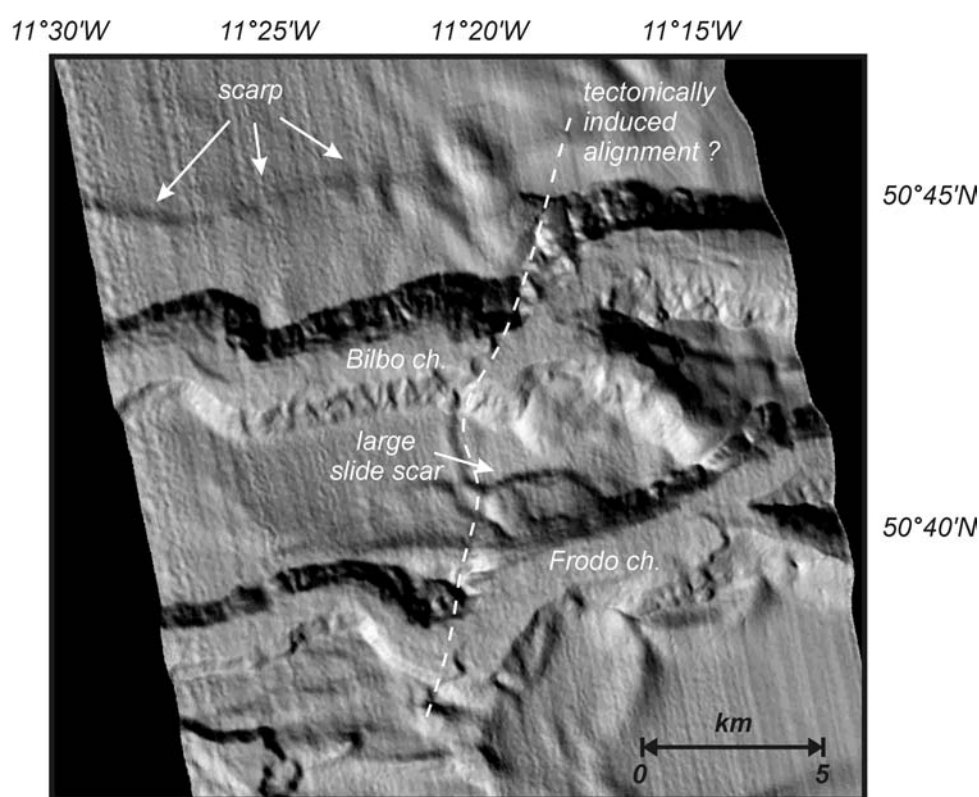


**Figure 7.15:** Shaded relief bathymetry map of the northern two Gollum channel heads; Bilbo and Frodo, highlighting the morphological features.

### 7.2.1 The Bilbo channel

The general morphology of this part of the GCS, as illustrated on figure 7.15, indeed shows a “steer’s head” profile, which is also visible on all seismic profiles of figure 7.16. The thalweg generally has a width varying between 1 and 1.5 km, flanked by steep slopes ranging from 14° to 22°. The main width of the channel seems to be fairly constant with values between 2.5 to 3 km. The channel depth however can vary along the described transect from about 350 m in the east (Fig. 7.17) to 75 m in the west (7.24). The decrease in channel depth seems to happen

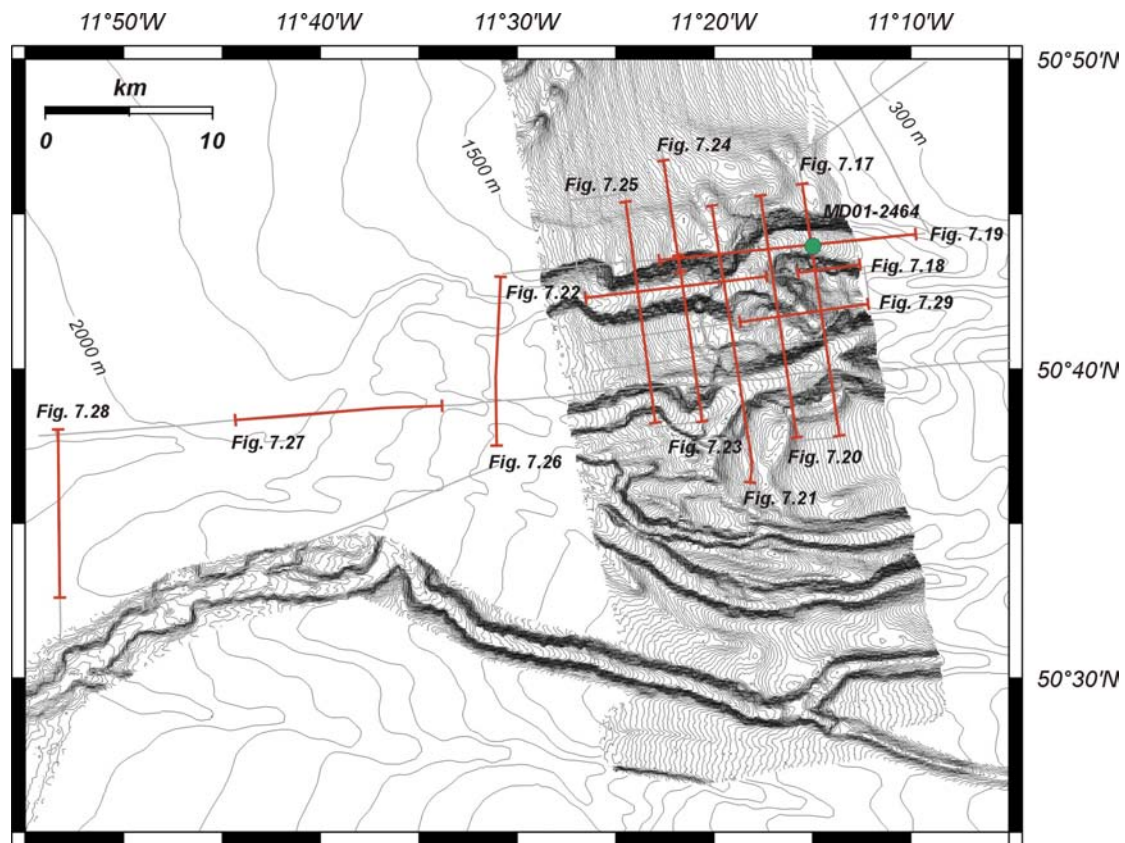


**Figure 7.16:** Location map of the used seismic profiles and core in the Gollum channel area (all available profiles are indicated in grey). The bathymetry is a combination of AWI multibeam bathymetry (contour interval every 10 m) and GEBCO bathymetry (contour interval every 100 m).

rather suddenly at about the 1600 m contour line (Fig. 7.16), where the seismic profile P99005a (Fig. 7.22) starts showing a channel depth of 160 m. All seismic lines east of this profile show depths between 300 and 400 m (Figs. 7.17, 7.19, 7.20, 7.21, 7.23 and 7.21). The channel floor gently slopes under an average angle of 2 to 3° (Figs. 7.19 and 7.22). However, this is interrupted by an important bayonet-shaped change along the course of the channel pathway (Fig. 7.15). The shaded relief map shows a clear NNE-SSW alignment of several features. First of all, the southward deflection of the Bilbo channel flank can also be traced along the Frodo channel. Moreover, it also corresponds to a 18 m scarp in the channel floor, illustrated on profile P030537a (Fig. 7.22). This alignment might be connected with a possibly reactivated Mesozoic fault, which has been observed by McCann *et al.*, (1995) along this part of the basin. However the available data do not allow to accurately demonstrate this. In order to find proof of such a fault, deeper seismic data should be investigated.

Profiles P010507 (Fig. 7.17) and P010503 (Fig. 7.21) show the channel has been cut into a presumed unit U2 substratum. A high amplitude reflector on profile P010507 at 1.6 ms TWT depth is thought to be the base of the channel floor, inferring a channel infill of about 200 ms TWT (approximately 180 m). Other profiles, such as P010505 (Fig. 7.20), show channel floor deposits with a maximum thickness up to 300 ms TWT ( $\pm$  250 m). On seismic profiles perpendicular to the channel axis, the seismic facies of these deposits are characterized by small, discontinuous reflectors with a high to moderate amplitude, located in a generally

acoustically transparent to chaotic facies (Figs. 7.17, 7.20, 7.23, 7.25). Seismic profiles located across the shallower channels in the west allow to distinguish distinct packages inferring large mass-wasting events (Figs. 7.26 and 7.28). Most of the time, the channel floor morphology is rather rough with chaotic packages along the foot of the flanks, suggesting slumped material (Figs. 7.20). Moreover, both the multibeam bathymetry and the seismic profiles show the presence of a small gully running through the entire channel floor (Figs. 7.20, 7.21 and 7.25). This small gully has also been observed on axial profiles, such as P99006 (Fig. 7.19) and P030537a (Fig. 7.22). As on other profiles, they illustrate a very irregular channel floor, with longer, continuous, downslope dipping reflectors. Profile P99006 (Fig. 7.19) illustrates channel floor deposits inside the bayonet-shaped structure, where the main axis of the channel is deflected to the south. 3 km before reaching the channel wall, the reflectors fade out into an acoustically transparent and chaotic facies, representing various turbidite and mass-wasting deposits caught in this perched environment.

These observations strongly suggest that the Bilbo channel floor mainly has been built by turbidite and mass-wasting deposits such as debris flows and slumps. Plenty of evidence of this kind of mass-wasting can be observed along the channel flanks with various slump scars, observed on multibeam bathymetry (Fig. 7.15) and seismic profiles (Figs. 7.19, 7.20, 7.21 and 7.23). Profile P030537b clearly cuts along a larger slide scar, visible on the multibeam bathymetry (Fig. 5.15), suggesting a slumped volume of about  $31.5 \cdot 10^6 \text{ m}^3$ .

Other evidence of possible mass movement can be observed along the northern flank of the Bilbo channel on figures 7.24 and 7.25. On the multibeam bathymetry, an area of about  $35 \text{ km}^2$  is limited by the channel wall on the southern side and by a 30 m high scarp in the seafloor on the other sides. Both profiles cut across this depression and especially profile P030533b shows several zones with reflector offset, resembling creep fault planes (Fig. 7.24). The uppermost fault planes are inferred to be about 25 to 50 m long and separate uniform, parallel reflectors. According to Stow (1994) and Mulder & Cochonat (1996), creep is affected by a slow strain and downslope movement along a (gentle) decollement zone due to load-induced stress with little internal deformation. In this case, the cause of this creep and also of the large depression can be found in the lower part of the unit. Here, a larger vertical disturbance marks a zone with reduced thickness of U1 sediments on the SE side, while the seismic reflection characteristics can be traced along this disturbance. This part is rooted on a diffuse, transparent zone, overlying a set of high-amplitude reflectors (Figs. 7.24 and 7.25). This might indicate a larger mass movement (creep?) during the “early” days of the U1 sediment deposition, and still affecting the later sedimentation on this part of the slope.

As discussed earlier in the text, the channel depth decreases from east to west. This also implies a possible influence of the channel flanks. The seismic profiles in the east (Figs. 7.17, 7.20 and 7.21) still show the channel floor is cut into unit U2. Here, the overlying Quaternary unit U1 shows a subparallel configuration and does not suggest the presence of a classic channel levee. However, on profiles located downslope, the channel flank is entirely constructed of U1 sediments. But, as on figure 7.23, the SSE flank remains characterized by a (sub)parallel reflector configuration, suggesting a continuous hemipelagic sedimentation. The next profile (Fig. 7.25) shows gently mounded reflectors along the base of the channel flanks,

which may be compared with typical channel levee structures. This first evidence of levee expression disappears towards the younger sediments, suggesting that the role of levee-creating turbiditic processes is gently overtaken by hemipelagic sedimentation. All other downslope profiles (Figs. 7.26, 7.27 and 7.28) do show the presence of distinct levees flanking the channel. Moreover, figures 7.1 and 7.16 show an important change in slope gradient from  $2.3^\circ$  to  $0.9^\circ$  at about the 1500 m contour line. Even east of the Bilbo channel on profile P99002, a field of sediment waves can be observed (Fig. 7.27) in an area where the Frodo and Bilbo channel join (Fig. 7.16). However, on only this one profile, it is difficult to estimate the migration angle and direction. Moreover, the relatively imprecise information provided by the GEBSCO-sourced bathymetry, compared with the multibeam data, does not allow an accurate location of both channels with respect to the seismic profile. On the deepest profile, P99003 (Fig. 7.28), the southern levee of the Bilbo channel again shows the presence of creep movement.

### 7.2.2 The Frodo channel

The Frodo channel generally shows the same information as the Bilbo channel, however fewer profiles are available. This channel seems to be less pronounced compared to the Bilbo channel. First of all, its thalweg is about 800 to 1300 m wide, flanked by steep slopes of 10 to  $20^\circ$ . Generally, it has an overall similar main width between 2 and 3 km. The channel depth varies from 280 m in the east to 200 and less in the west. The deepest part of the Frodo channel is about 330 m (Fig. 7.20). As the Bilbo channel, the channel floor slopes with an angle of about  $2^\circ$ . In the prolongation of the higher discussed alignment, the Frodo channel also shows a strange bend in the channel pathway.

The Frodo channel floor shows the presence of mass-wasting deposits with a maximum thickness of about 300 ms TWT ( $\pm 250$  m) on figures 7.17 and 7.20. However, on figures 7.21 and 7.25, only small mass-wasting deposits can be inferred, with a relatively smooth sea floor. Moreover, on figure 7.21 one reflector can be traced from the northern to the southern channel flank, implying that the Frodo channel has not cut too deeply into the substratum and suggesting a minor channel infill. The morphology of the surrounding channel walls, do suggest frequent slumping: large slump scars are evident (Figs. 7.15, 7.20 and 7.21). Similarly to the Bilbo channel, the multibeam bathymetry shows a depression on its northern flank, linked with another possible sliding event on figure 7.25. Thus in contrast with the nature of the channel floor deposits on the seismic profiles, the channel walls show enough evidence of mass-wasting. On the other hand, about 10 km downslope, figure 7.26 shows again a pronounced channel infill with mass-wasting deposits.

The Frodo channel also shows a minor levee expression along its upper reaches. Profiles P010507 (Fig. 7.17) and P010505 (Fig. 7.20) do show a levee along the southern flank, which is however originating from a smaller secondary channel, flowing parallel to the Frodo channel (Fig. 7.16). Only the profile in figure 7.26 shows the construction of a levee unit along the lower reaches of the channel.

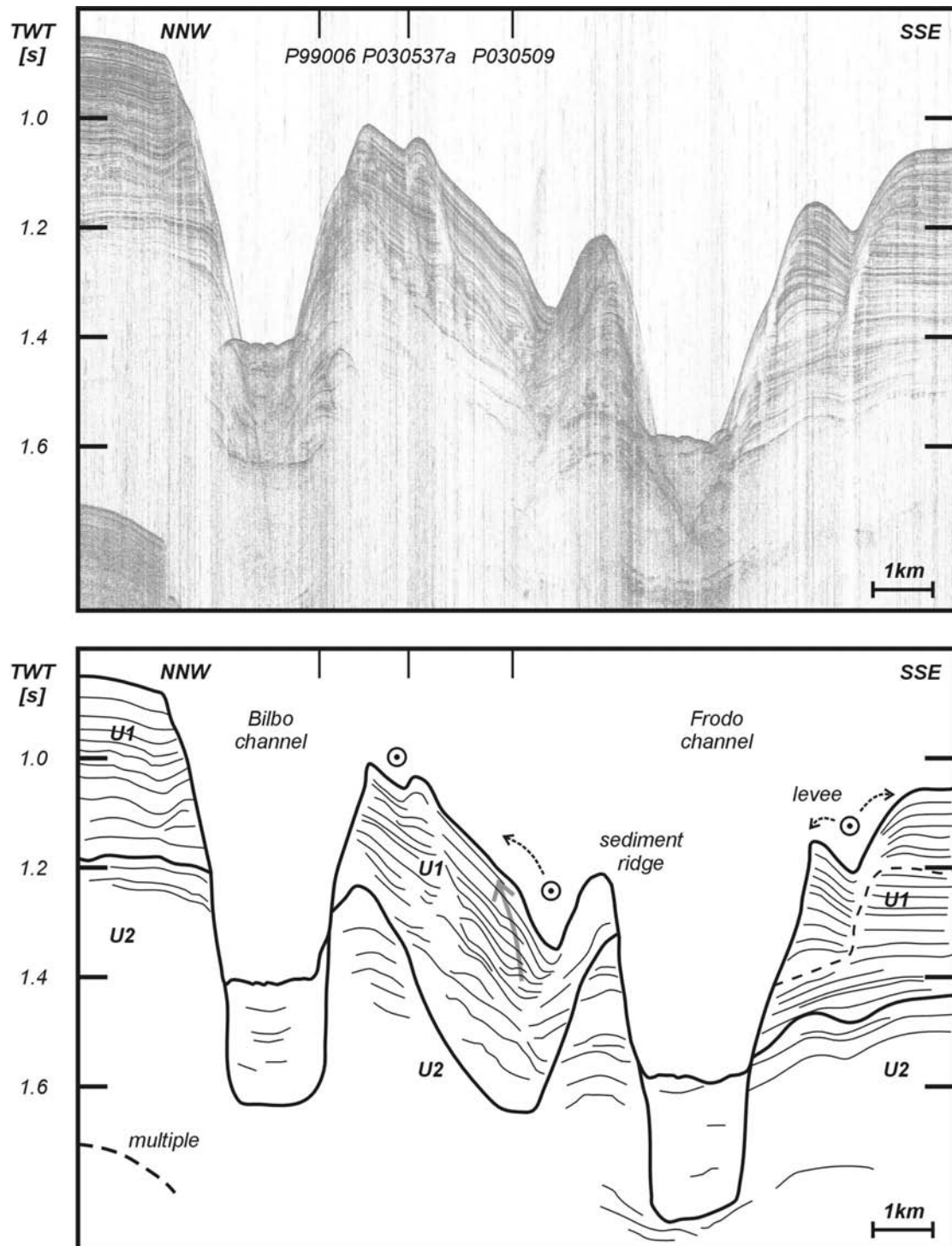


**Figure 7.17:** P010507: cross-section through the Bilbo and Frodo channels. Both have been incised into unit U2. The area in between the two channels also shows a small downslope running channel, building a large levee on its right-hand side.

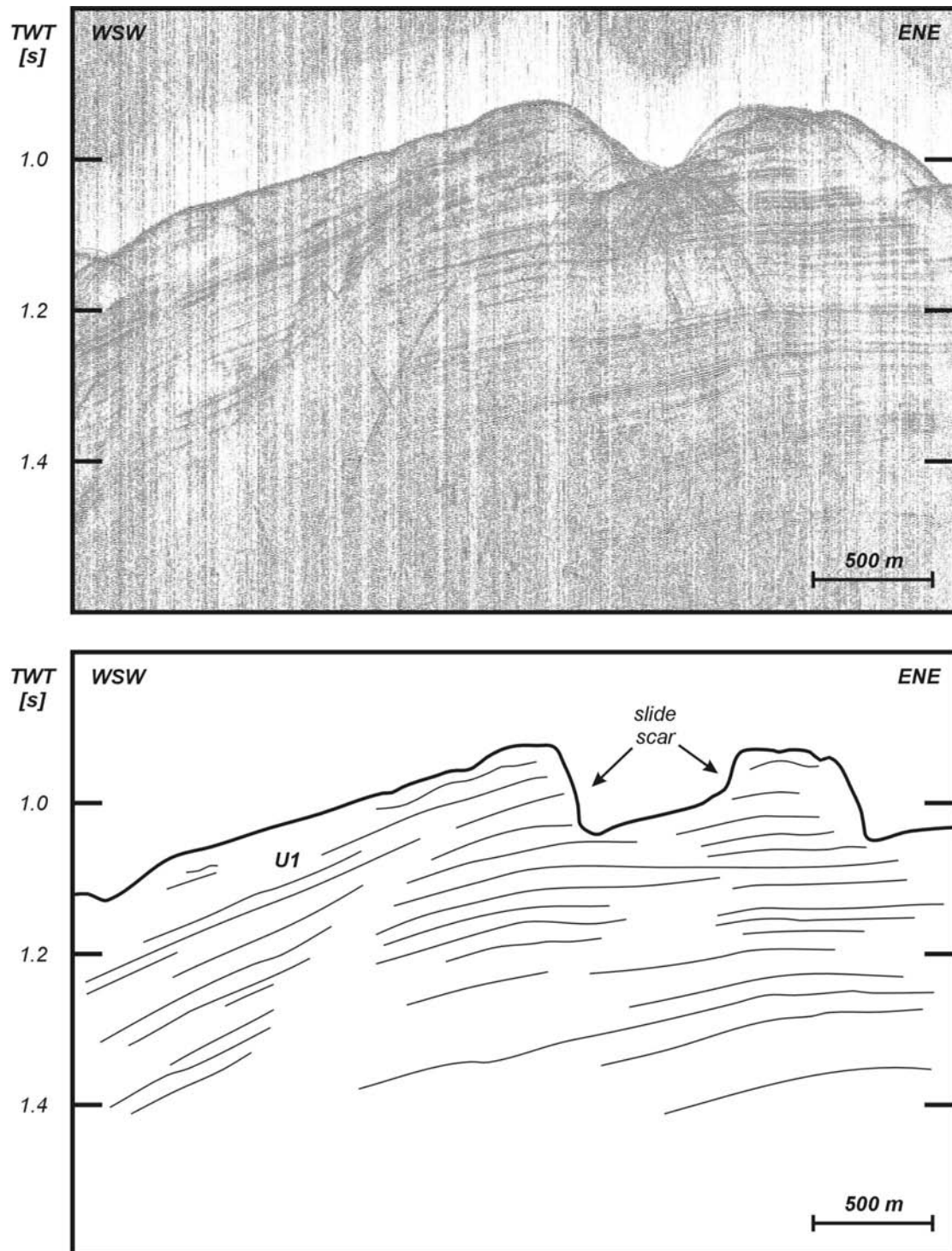


**Figure 7.18:** P030537b: profile along the southern flank of the Bilbo channels along its upper reaches. The morphology of a large slide scar can be inferred.

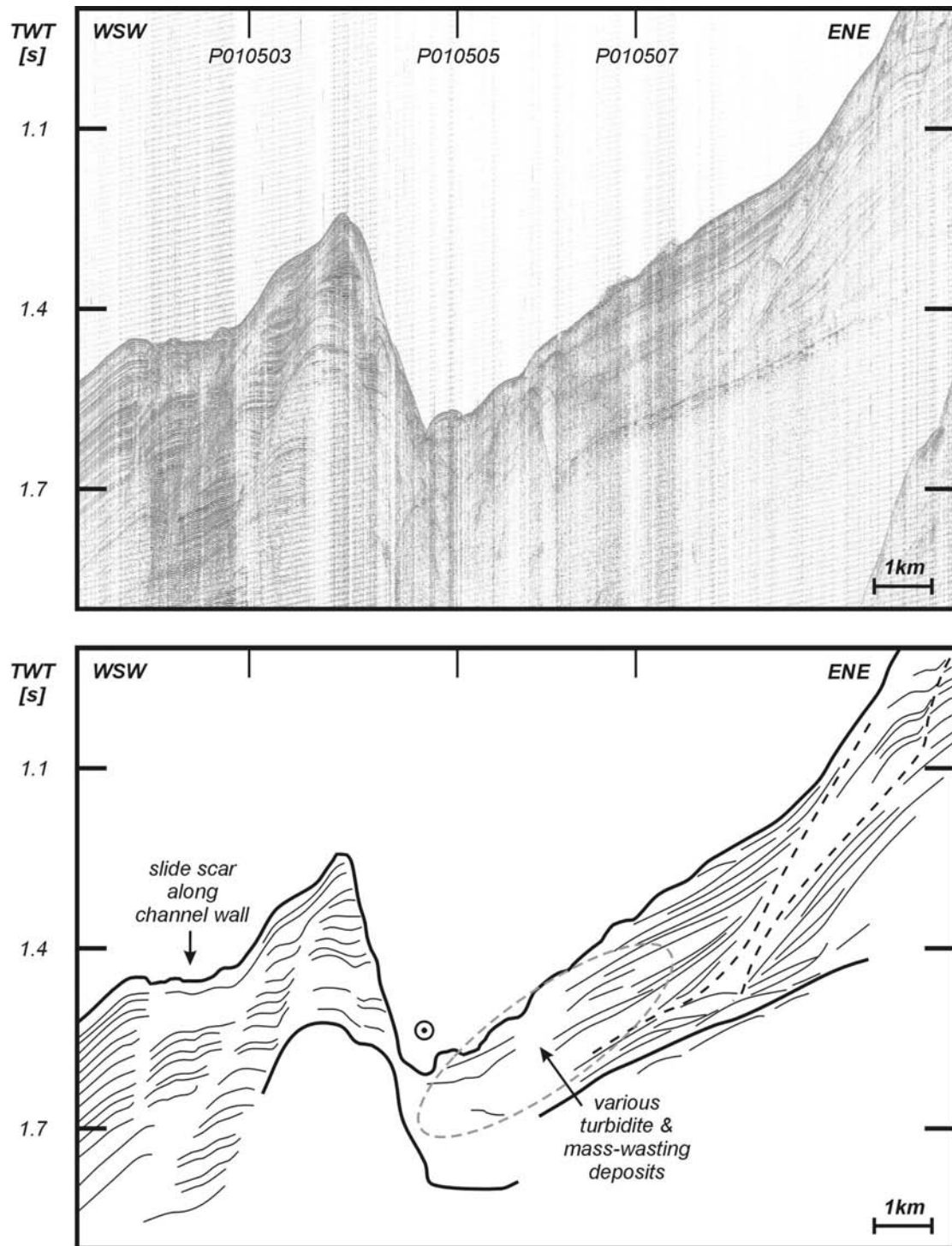


**Figure 7.19:** P99006: downslope profile along the main upper axis of the Bilbo channel. All channel floor strata abut against a jump in the channel flank. At the WSW side, a slide scar is observed.

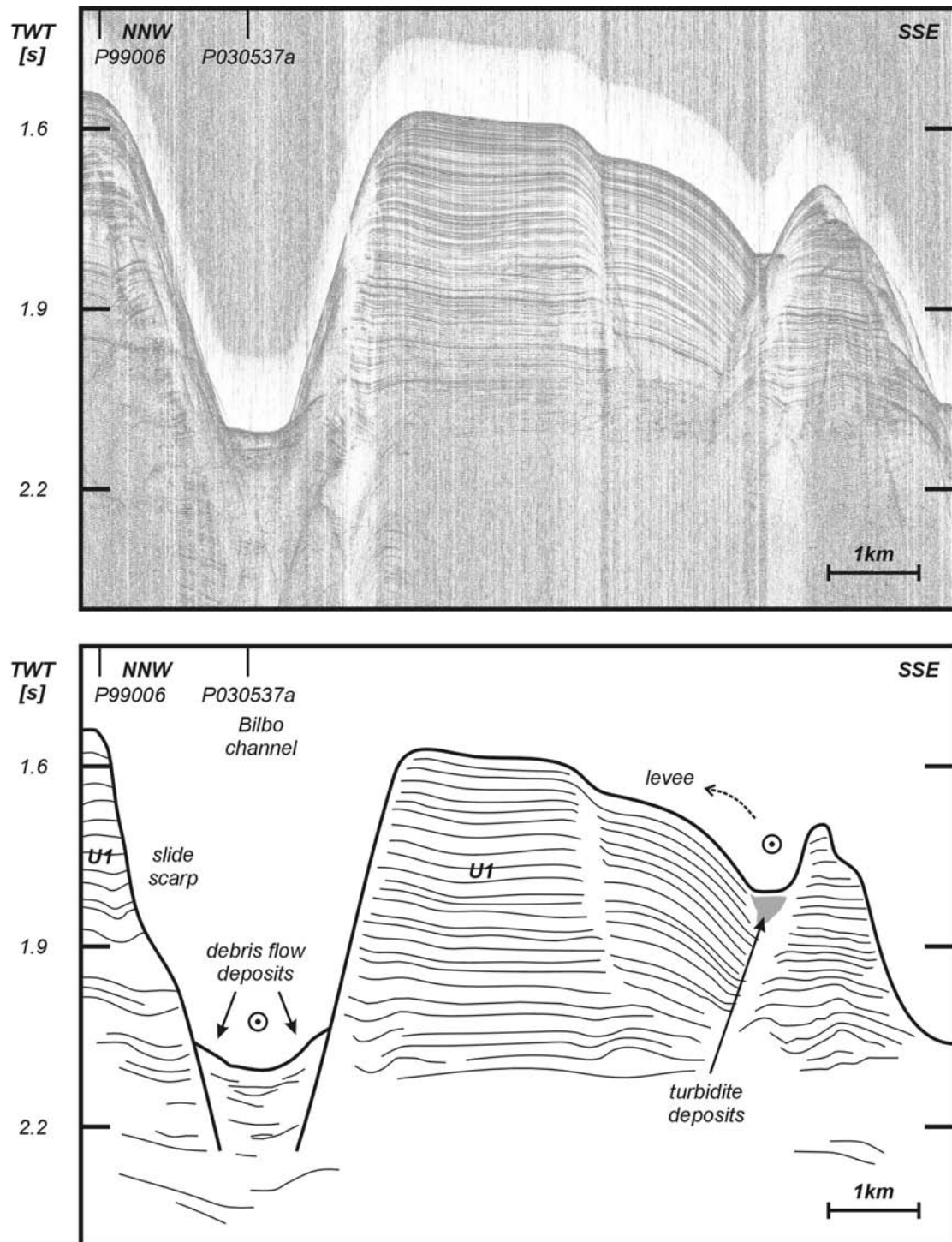


**Figure 7.20:** P010505: cross-section through the Bilbo and Frodo channels. The Bilbo channel seems to be larger, but on figure 7.16 shows this is a location where two channels converge.

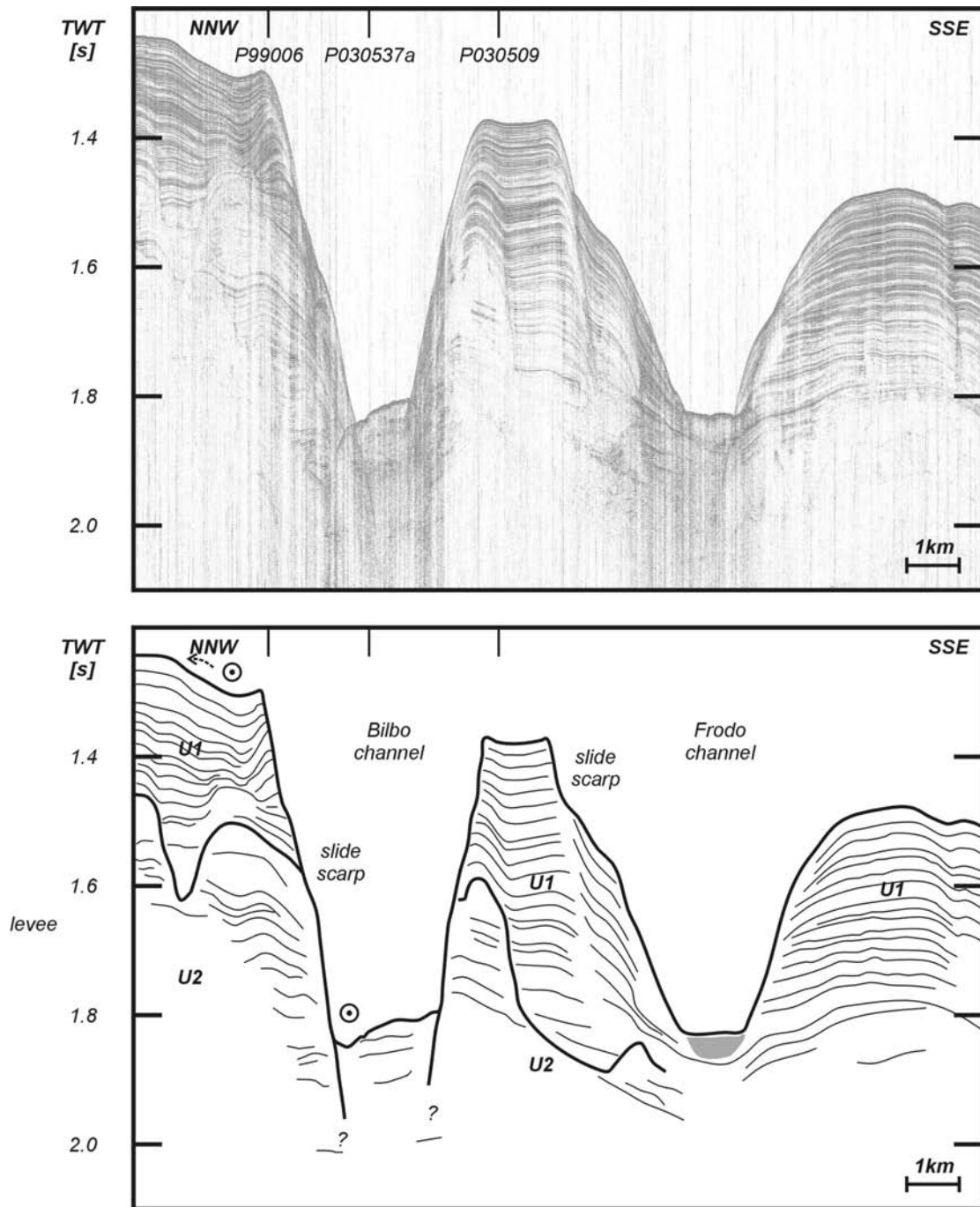


**Figure 7.21:** P010503: cross-section through the Bilbo and Frodo channels. The Frodo channel is flanked by two levee units.

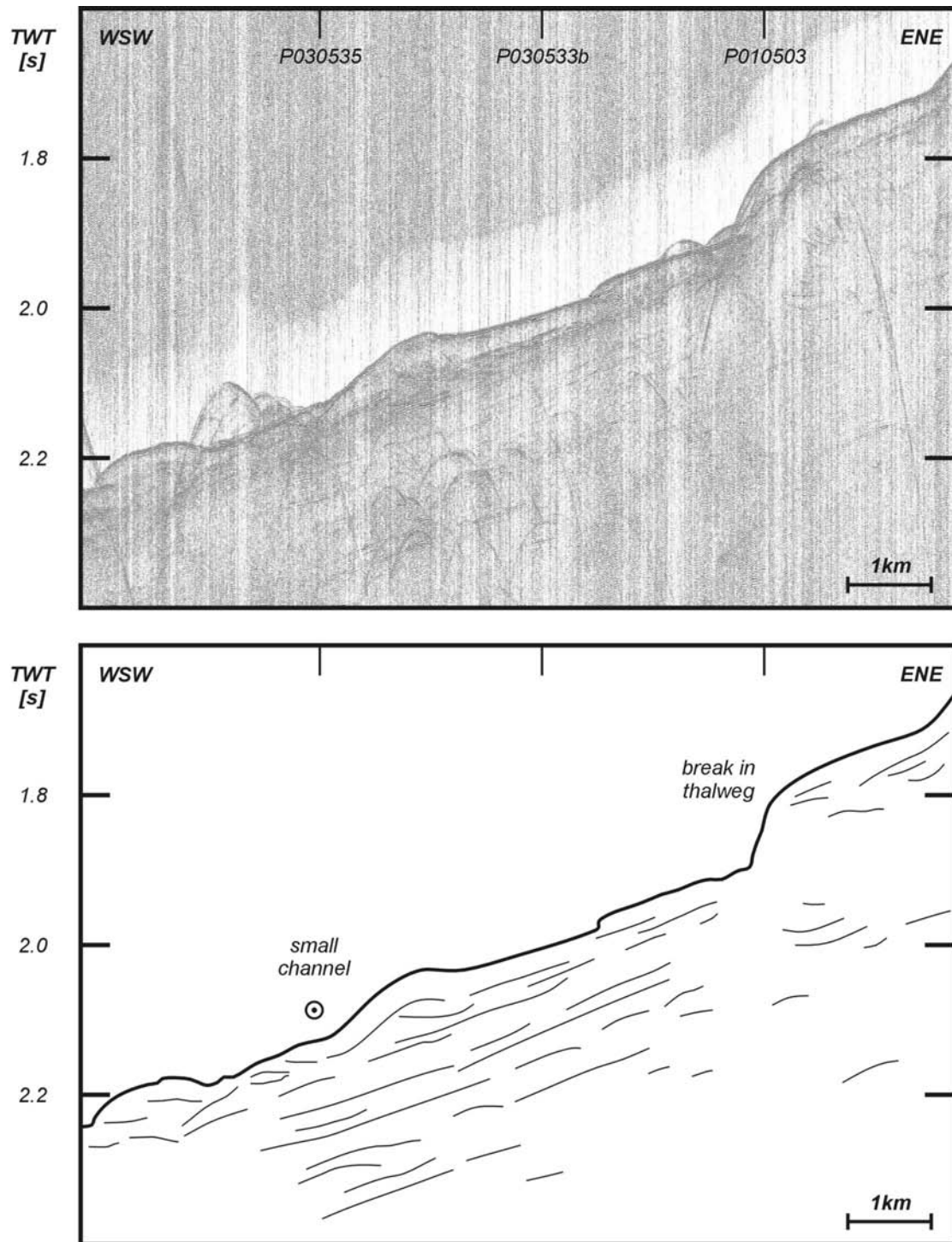


**Figure 7.22:** P030537a: downslope profile along the lower axis of the Bilbo channel, illustrating an important break in the thalweg.

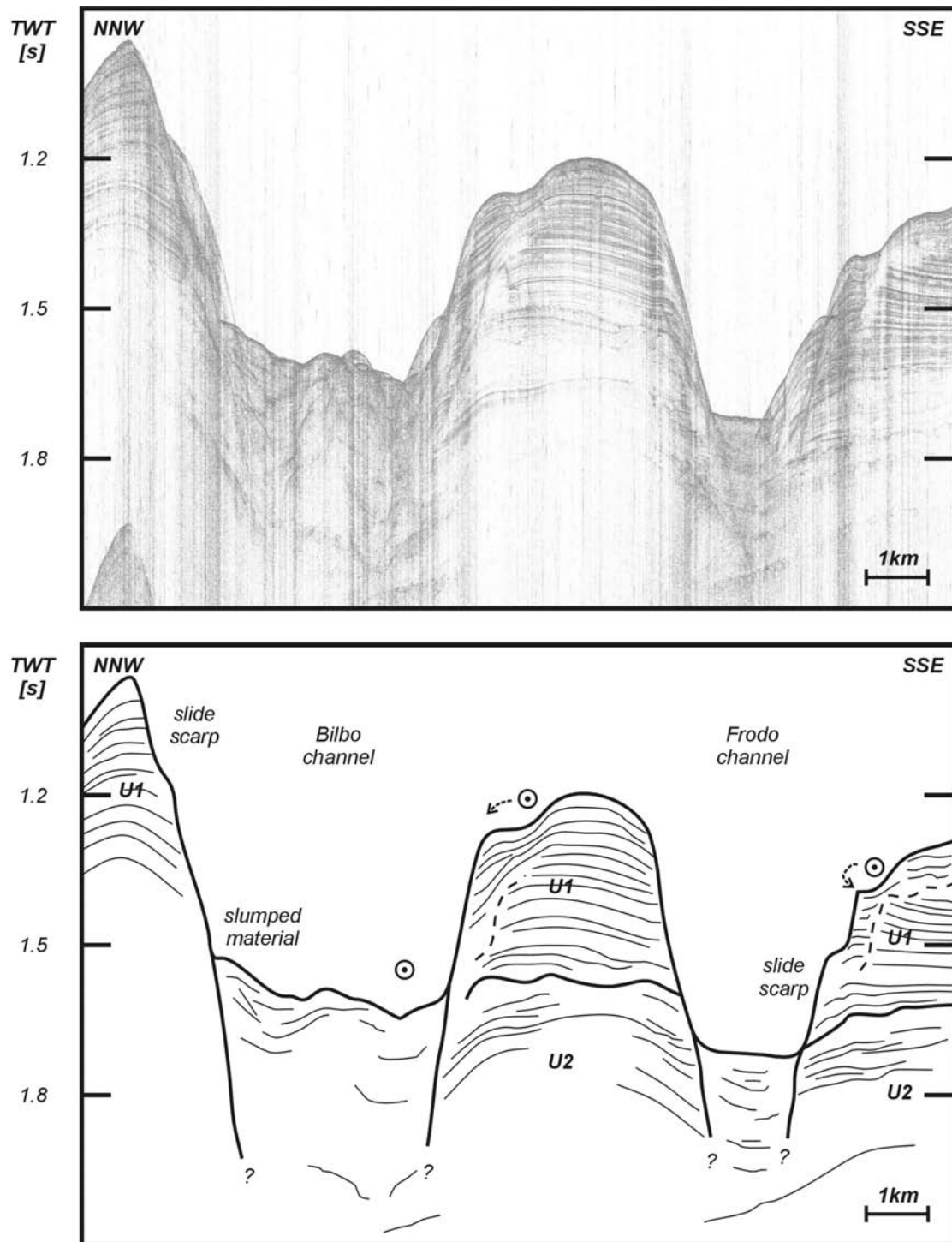


**Figure 7.23:** P030533b: cross-section through the Bilbo channel and the intra-channel area. A small channel is observed with a large levee on its right-hand side.

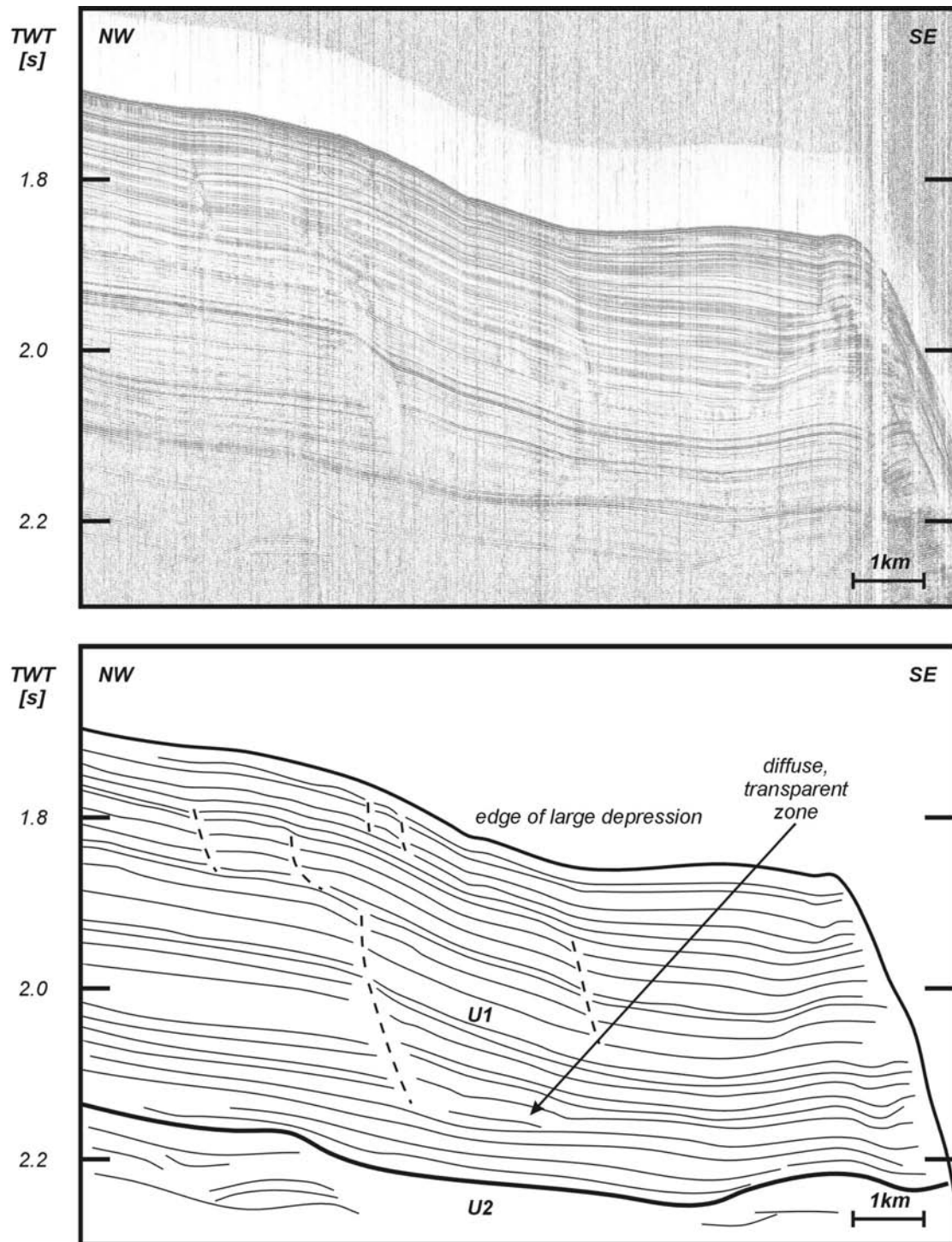


**Figure 7.24:** P030533: profile along the northern flank of the Bilbo channel, cross-cutting a large depression visible on figure 7.15. Several creep or sliding planes can be observed.

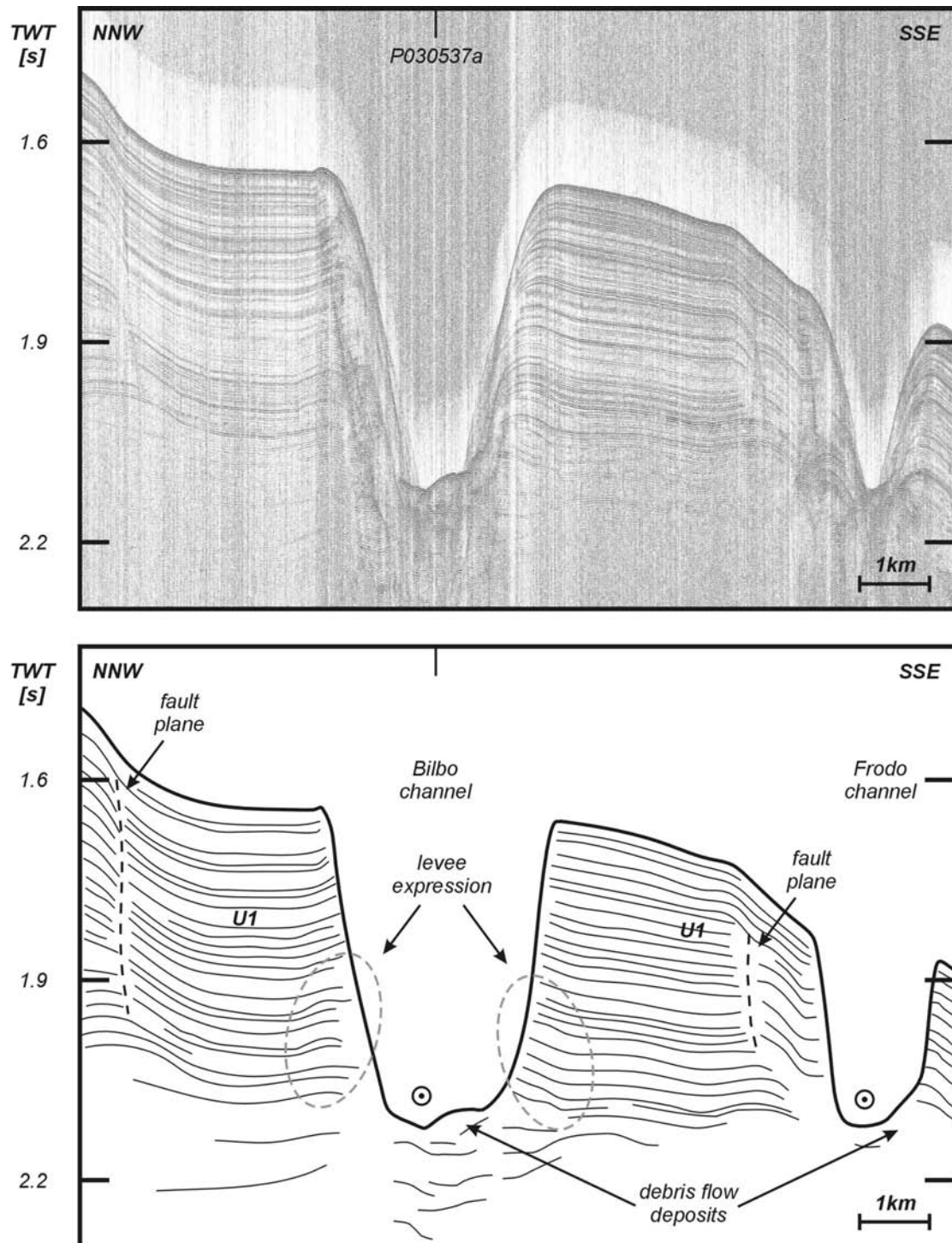


**Figure 7.25:** P030535: cross-section through the Bilbo and Frodo channels. Both channel flanks show possible fault planes. Along the lower parts of both the Bilbo channel flanks, a levee expression can be observed.

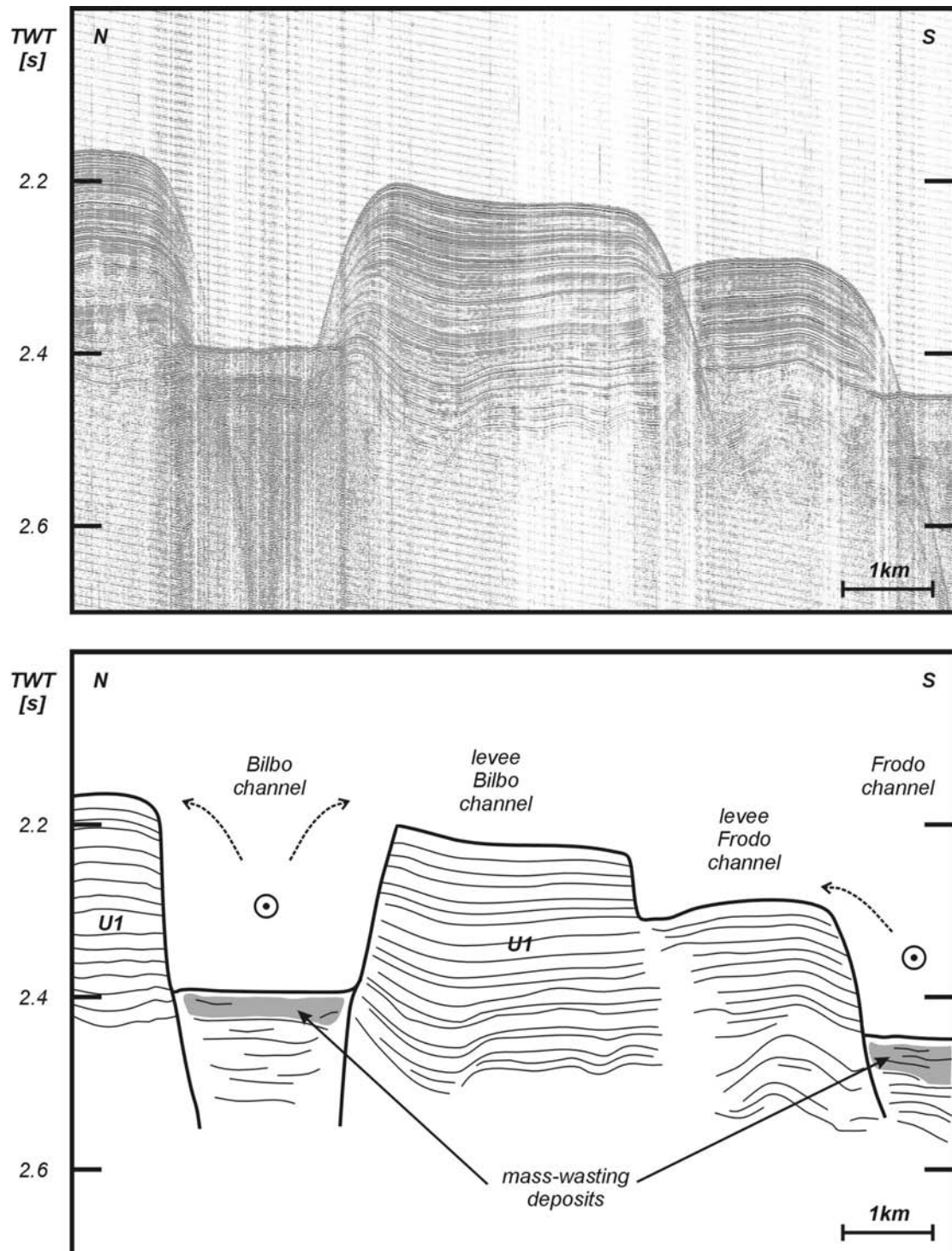


**Figure 7.26:** P99005a: cross-section through the Bilbo and Frodo channels, this time with a leveled expression of both channels. Both channel floors show clear mass-wasting deposits.

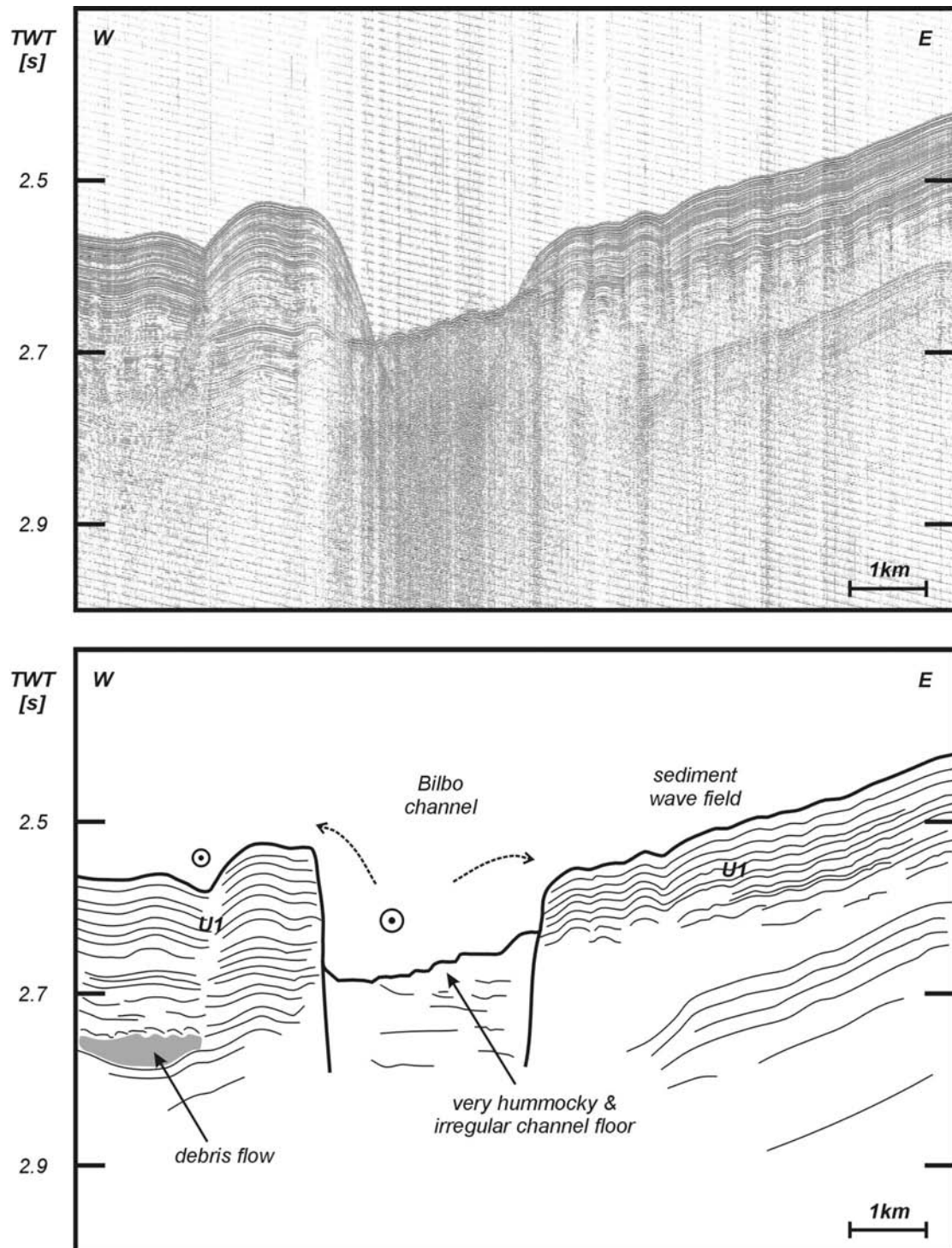


**Figure 7.27:** P99002: cross-section through the Bilbo channel with clear sediment levees. The eastern levee shows the presence of a sediment wave field.

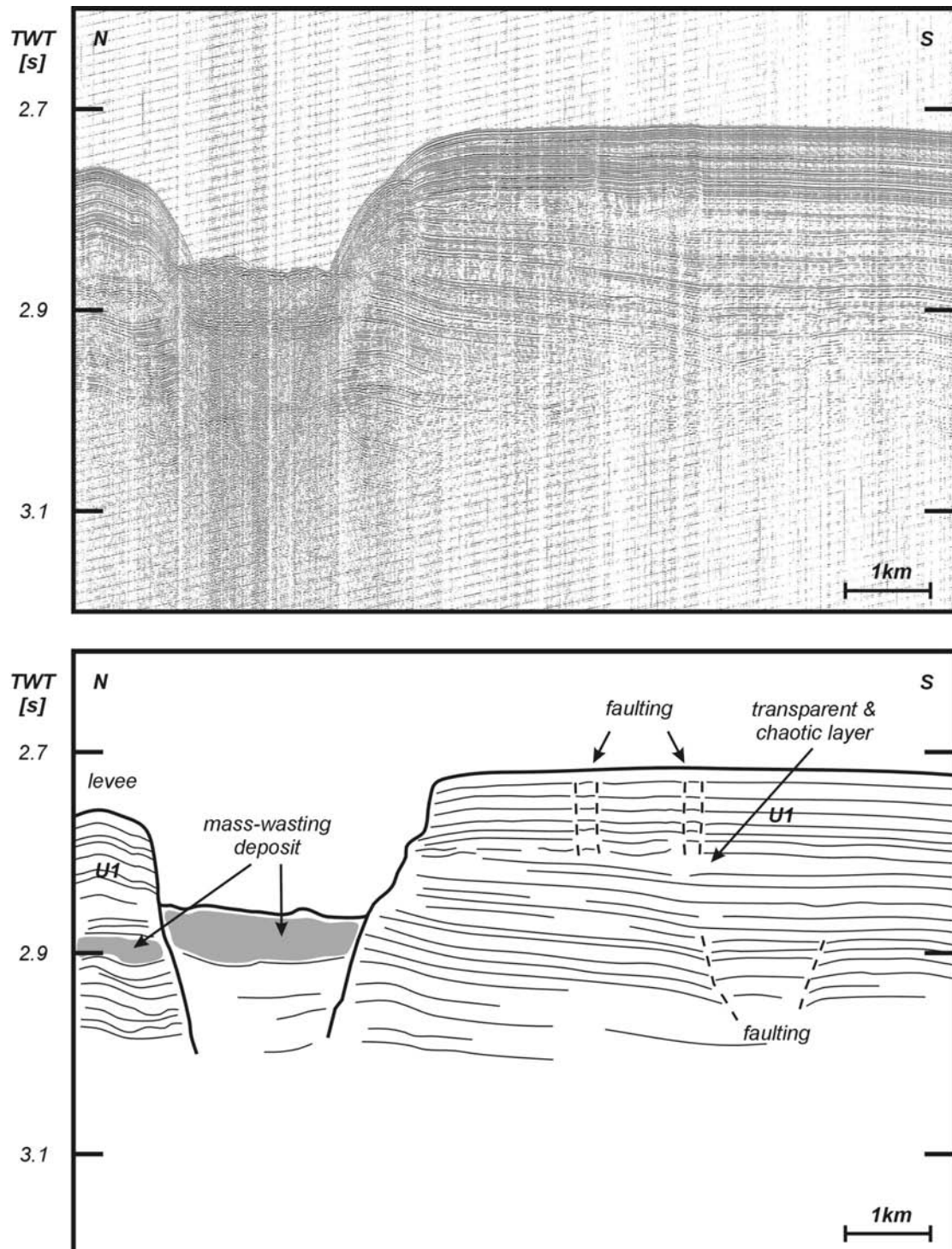


**Figure 7.28:** P99003: lowermost cross-section of the Bilbo channel featuring large mass-wasting deposits. Along the southern flank, presumed faulting is observed. The uppermost layer seems to be rooted on a transparent and chaotic layer, which might be a possible sliding plane.

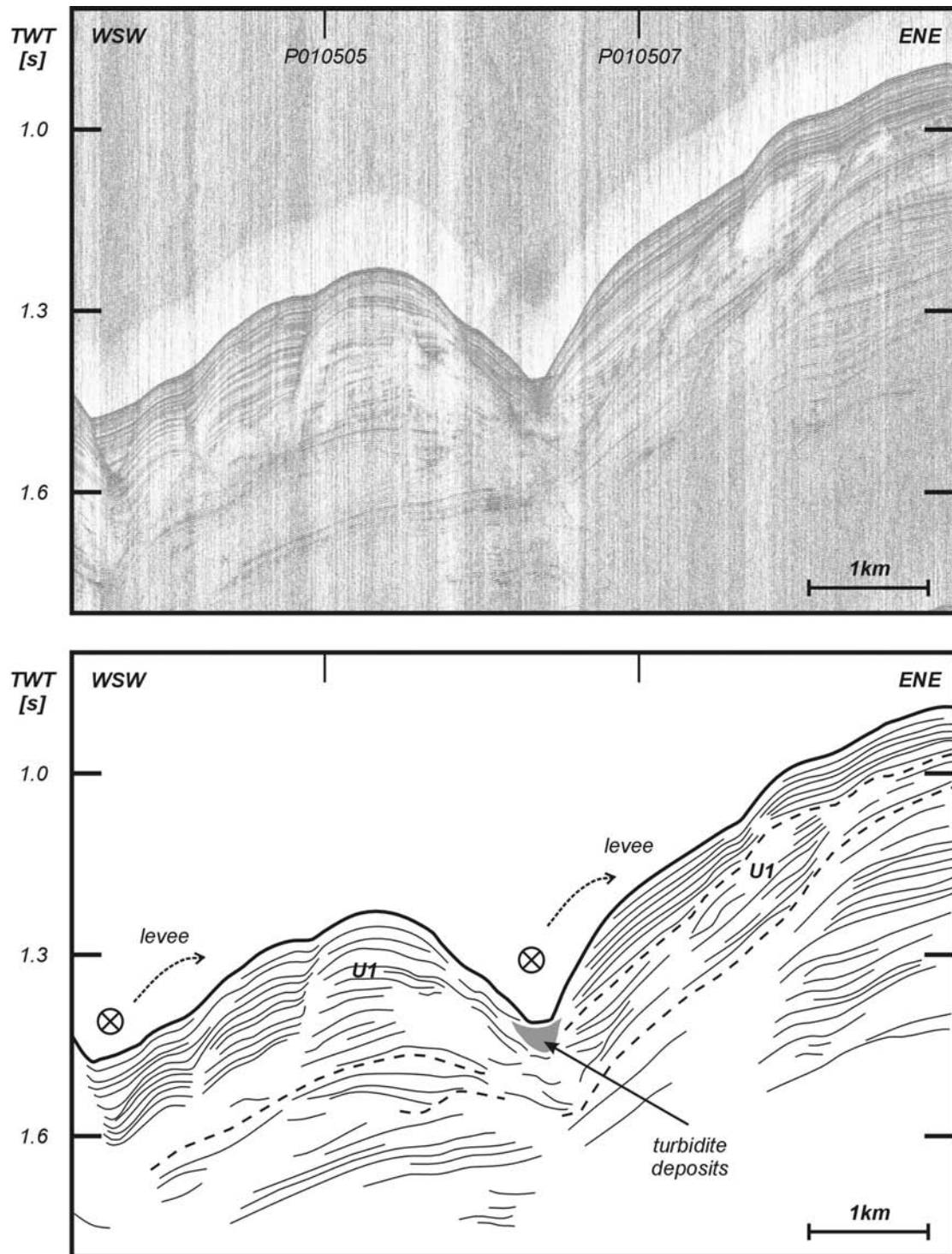


**Figure 7.29:** P030509: profile along the intra-channel area, cross-cutting secondary channels with turbidite deposits on the channel floor.

### 7.2.3 Secondary channels in between the Bilbo and Frodo channels

The 4 to 5 km broad area between the Bilbo and Frodo channels also is characterized by the presence of two secondary channels and associated features (Fig. 7.15). Previous sections already highlighted that a predominantly undisturbed, hemipelagic sedimentation occurred in this area. Along its edges, it is disturbed by sometimes large slump scars.

A first channel is presented in figures 7.17, 7.20 and 7.29. It has a predominant N315° direction and flows into the Bilbo channel under a slope angle of approximately 3°. This V-shaped channel is about 4 km long and widens from 0.5 to 1.5 km downslope. Compared to the Bilbo channel, its flanks are relatively smooth and intact, like a Kings channel (Fig. 7.15). Profile P010507 (Fig. 7.17) shows this channel has been cut in a depression between the Bilbo and Frodo channels. It has initially been filled with chaotic deposits. However, at about 1.4 ms TWT, a channel can be inferred with the construction of a levee on its right-hand side (at the NNW). A downslope running profile (Fig. P030509) confirms this and shows mass-wasting deposits (turbidites?) on the channel floor. Another, broader, less pronounced channel is observed on the WSW part of this profile.

Along the northern flank of the Frodo channel, a small, parallel secondary channel is observed (Fig. 7.23). It is only 2.4 km long, 800 m wide and it slopes under an angle of 2°, ending along the steep Frodo channel flank (Figs. 7.15 and 7.16). However, figure 7.23 clearly shows a broad levee has been built along its right-hand side (at the NNW), together with inferred turbidite deposits. Moreover, at its western extremity, it crosses the inferred vertical disturbance along the northern Frodo channel flank (Figs. 7.16 and 7.25). This might suggest that this feature could also be a buried levee of this secondary channel. Unfortunately, more data is needed to reveal the true nature of this feature.

### 7.2.4 Clues for the recent sedimentary history; core MD01-2464

In order to discover the nature of the deposits and to study the recent sedimentary history of the Bilbo channel floor (at 1014 m) an 18 m long piston core\* was taken at the intersection of profiles P010507 (Fig. 7.17) and P99006 (Fig. 7.19), located on figure 7.16. Unfortunately, the core was bent and a flow-in occurred from 10 m downward. Therefore, only the upper 9 m of core MD01-2464 were studied. This core dominantly consists of grayish brown to dark grey silty clay with frequent sulphide specks, nannofossil and occasional fine sand. Visible layers of silt and fine sand were found at the core top, with abundant foraminifers and nannofossil. Other silty to fine sand layers were observed from 60 to 80 cm, 190 to 200 cm and 240 to 280 cm.

The physical properties (Fig. 7.30) and the grainsize characteristics (Fig. 7.31) of this core allow to identify three main facies in a muddy, bioturbated hemipelagic background sediment (Fig. 7.32j, k and l): (1) fine-grained turbidites, (2) contourites and (3) hemipelagites with IRD.

---

\* 'Pour la petite histoire', the successful recovery of this interesting core was the only good event that happened on the day it was taken: 11/09/2001...

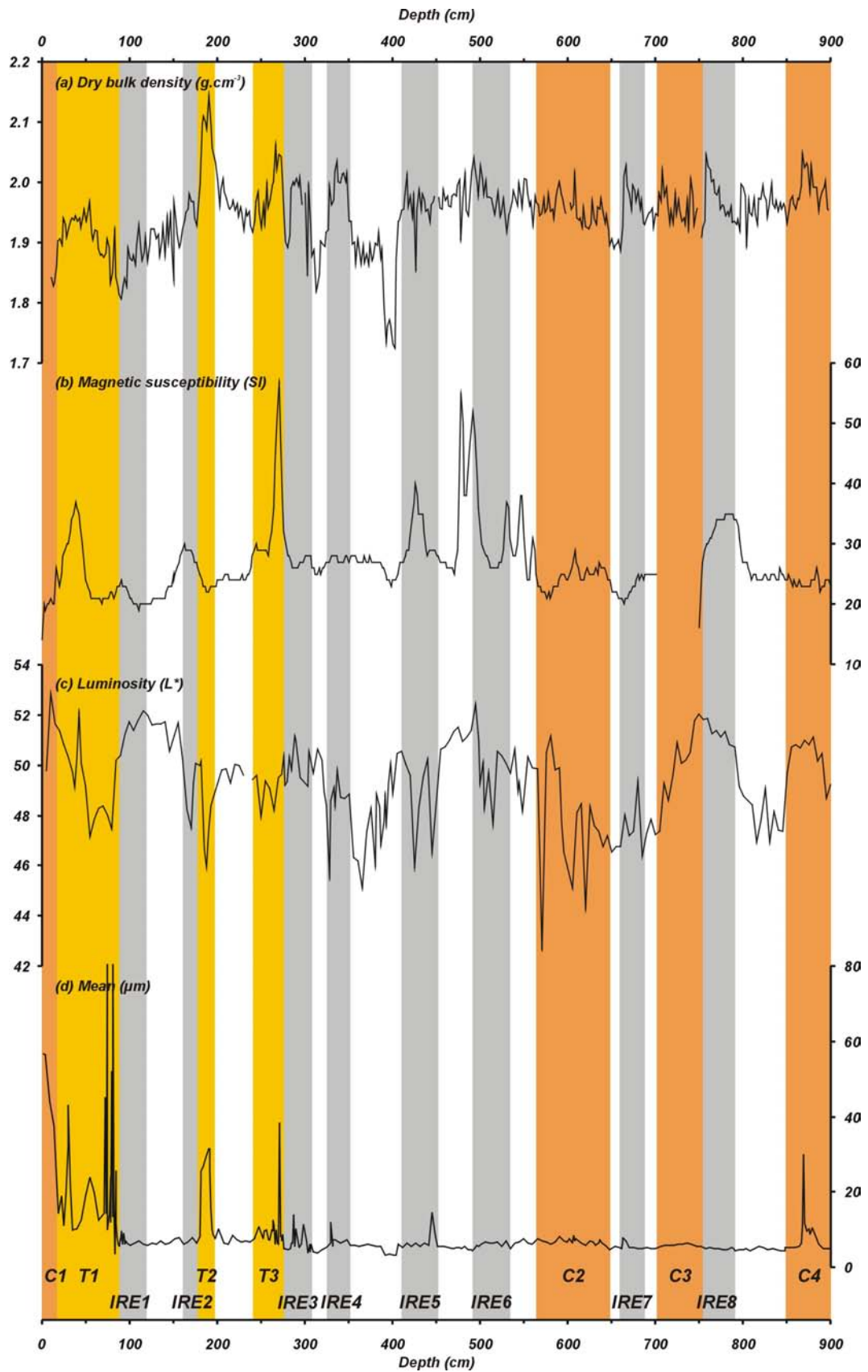


**Figure 7.30:** Physical properties of core MD01-2464 with (a) dry bulk density ( $\text{g}\cdot\text{cm}^{-3}$ ), (b) magnetic susceptibility (SI), (c) luminosity ( $L^*$ ) and (d) mean grainsize ( $\mu\text{m}$ ). The intervals containing contourites (C), turbidites (T) and ice-rafting episodes (IRE) are indicated.

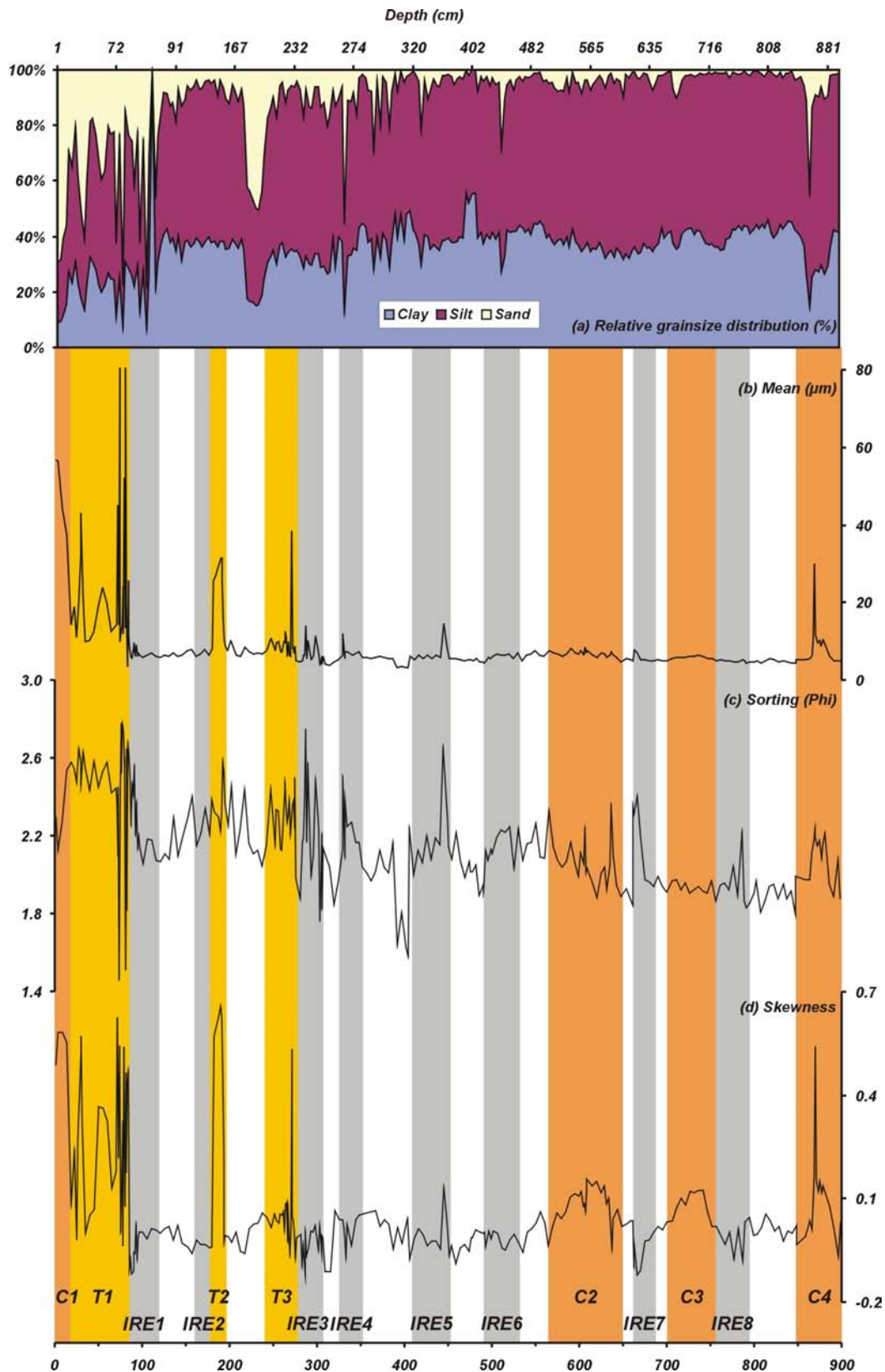


**Figure 7.31:** Grainsize characteristics of core MD01-2464 with (a) relative grainsize distribution (%), (b) mean grainsize ( $\mu\text{m}$ ), (c) sorting ( $\phi$ ) and (d) skewness. The intervals containing contourites (C), turbidites (T) and ice-rafting episodes (IRE) are indicated.

#### 7.2.4.1 Fine-grained turbidites

Visual observations already revealed the occurrence of three sandy intervals in the upper 3 m of the core. The exact limits of these intervals were set on figures 7.30 and 7.31; T1 (19-87 cm), T2 (180-195), T3 (242-274). They are characterized by elevated values in mean grainsize (from 40 up to 80  $\mu\text{m}$ ), a strong positive skewness, sharp rises in dry bulk density, a darker sediment colour and (at least at T3 and partly T1) a higher magnetic susceptibility. Only the base of T1 and T3 shows a relatively better sorting. The grainsize distribution curves in these coarser intervals are the only ones to show a pronounced coarse mode at about 100  $\mu\text{m}$  (Figs. 7.32a, b, e and f). The X-ray radiographies show a lighter (denser) facies always overlying a bioturbated, greyer facies with frequent small IRD (Figs. 33a, b and c). The X-ray facies of T2 shows the presence of convoluted lamina (Fig. 33c).

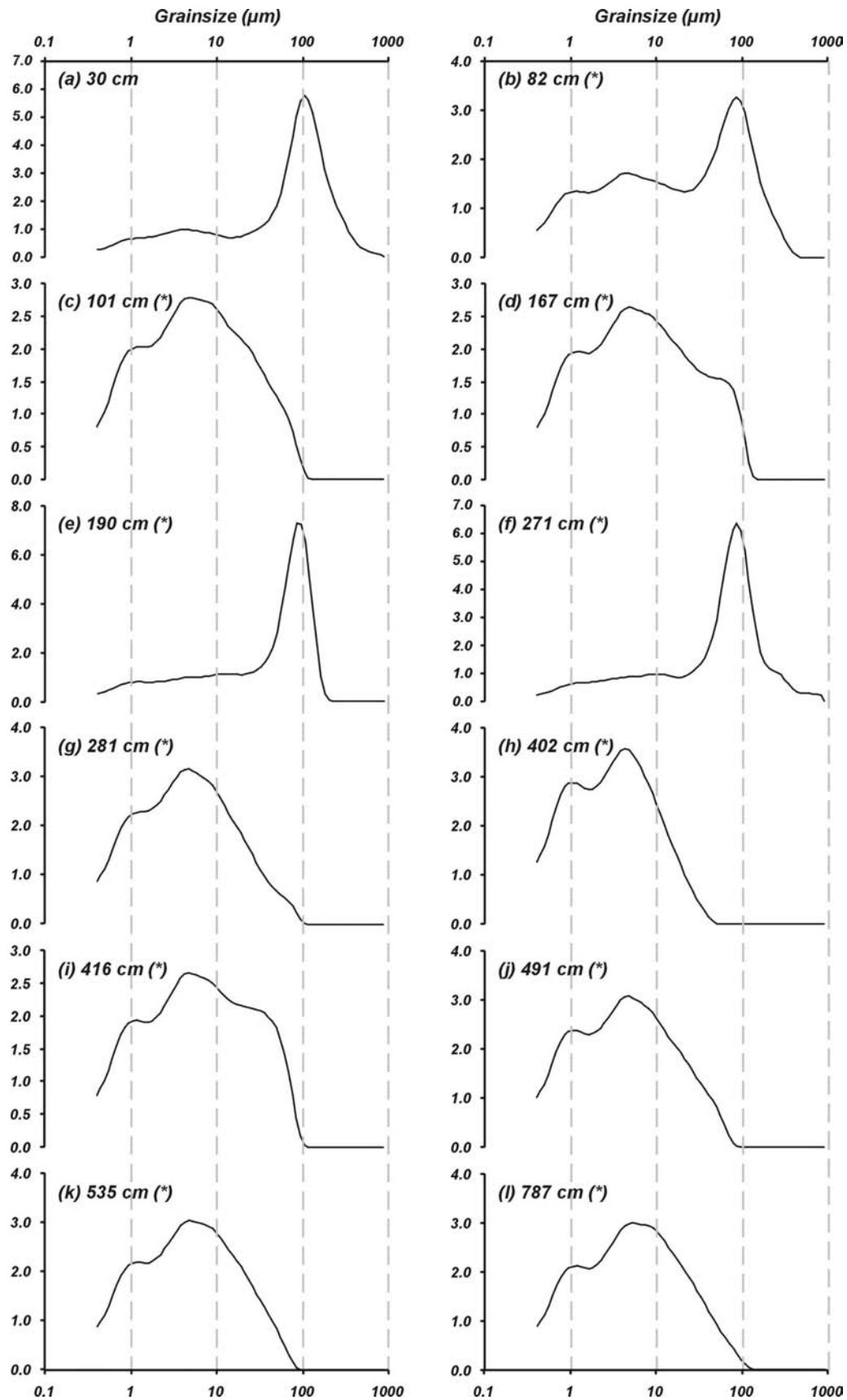
According to the classification proposed by Stow & Piper (1984) and Shanmugam (2000), these intervals might be interpreted as fine-grained turbidites, deposited by low-density turbidity currents. The observed features indicate the presence of divisions T<sub>1</sub> to T<sub>5</sub>, ranging from silty-sandy convolute laminations over thin, regular silty lamination towards graded mud (Fig. 7.34). The coarse base of the standard Bouma division is not observed, which is a common feature in fine-grained turbidites, called a base-cut-out sequence (Stow & Piper, 1984).

Figure 7.33a on the other hand shows a very chaotic T1 interval with several lamina and also bioturbations. Since normal turbidites usually do not show bioturbation, which is only restricted to the graded mud at the top (Gonthier *et al.*, 1984; Stow & Piper, 1984), this might indicate that this initial turbidite deposit might have been reworked by bottom currents during a later stage [Stow, 2002 #41. This will be further discussed in the next section.

#### 7.2.4.2 Contourites

According to the current state-of-the-art by Stow *et al.* (2002), a total of four intervals of possible muddy to silty contourites can be observed in this core; C1 (0-19 cm), C2 (565-648 cm), C3 (706-757 cm) and C4 (848-896 cm). On the X-ray radiographies, all intervals are bioturbated throughout, especially with *Mycelia* (Figs. 7.33a and f). They all have an elevated sand content, most of them are relatively better sorted than the turbidite intervals and they have a pronounced and broad fine skewness (Fig. 7.31). The grainsize distribution curves do not show a large difference with the surrounding background sediment, displaying a nicely graded silty mud (Fig. 7.31). Intervals C1 and C4, however, were not straightforward to be interpreted.

The lower boundary of interval C1 was difficult to trace, probably because the underlying fine-grained turbidite was reworked by bottom currents. However, from 19 cm, there seems to be a better sorting, suggesting that this upper part of the core could be a sandy contourite, as observed in the Belgica mound province. This also is consistent with the observations of Tudhope & Scoffin (1995), who attributed the presence of rippled, moderately-sorted fine sand to reversing bottom currents in these upper channels.



**Figure 7.32:** Grainsize distribution curves (%) of specific locations in core MD01-2464. Samples marked with (\*) are located on the X-ray sections in figures 7.33.

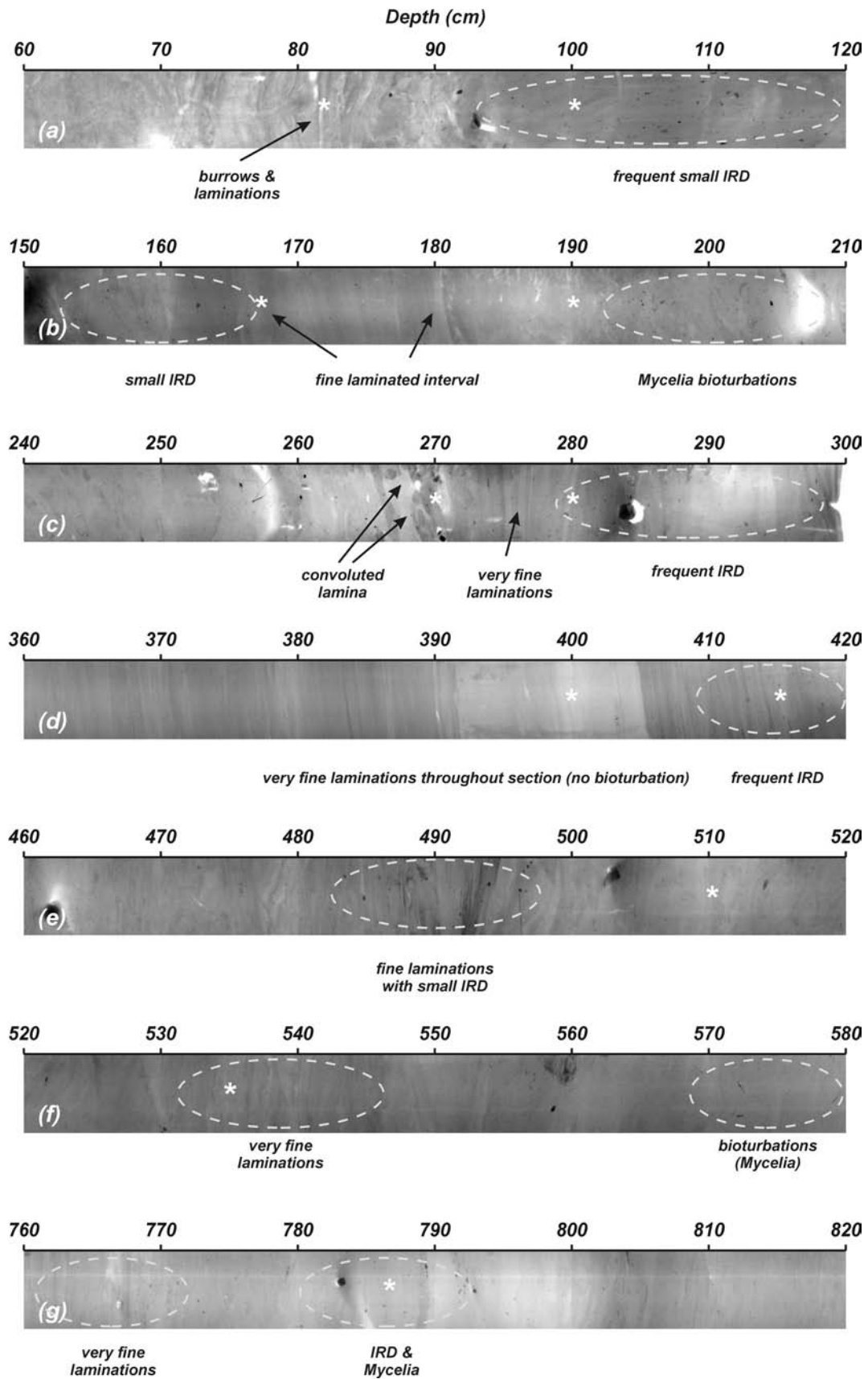


**Figure 7.33:** SCOPIX X-ray visualizations of specific intervals observed in core MD01-2464. The positions of grainsize distribution curves in figure 7.32 are indicated with “\*”.

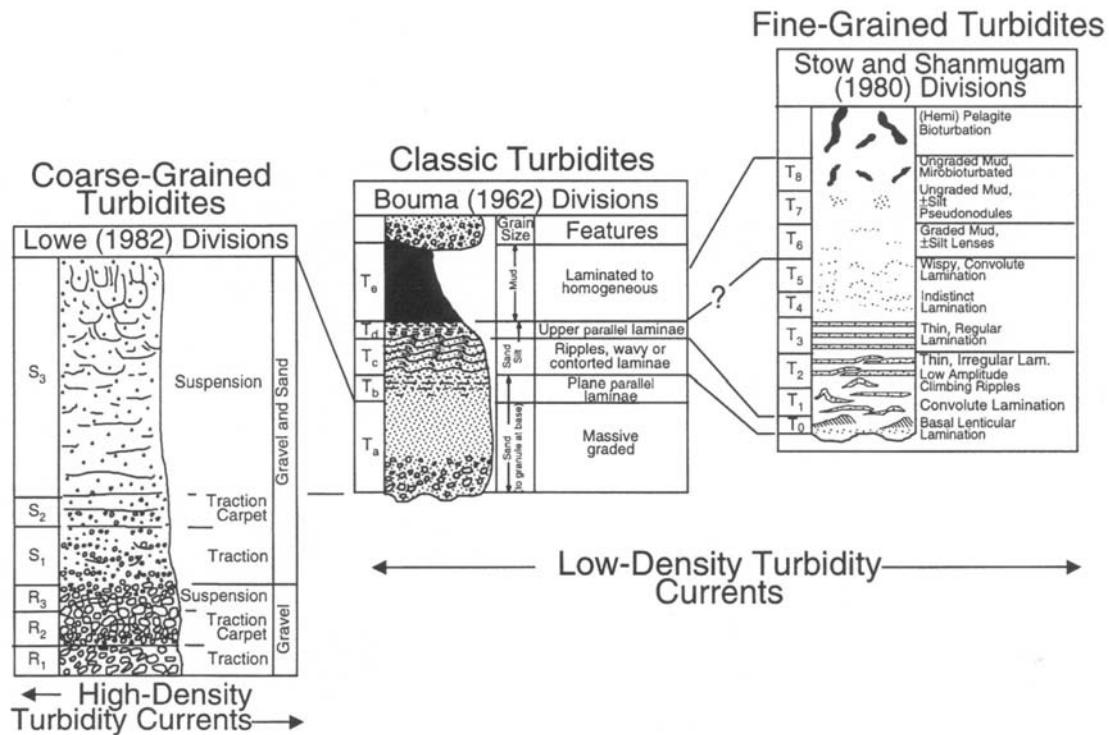


**Figure 7.34:** Existing vertical facies models of (1) coarse-grained turbidites, (2) classic turbidites (also known as the Bouma sequence), and (3) fine-grained turbidites, according to Shanmugam (2000).

The mean and skewness of interval C4 suggests a turbidite, but the grain size analysis and X-ray radiographies only show a reverse graded sandy silt with occasional fine (silty ?) laminations and bioturbation, characteristic of contourites (Stow *et al.*, 2002). Therefore, this interval could be interpreted as a silty contourite or possibly, as T1, as a bottom-current reworked turbidite.

#### 7.2.4.3 Hemipelagites with IRD

Up to 8 intervals were observed where an elevated dry bulk density (Fig. 7.30), X-ray radiographies (Fig. 7.33) and grain size distribution curves (Figs. 7.32c, d, g, i and l) suggest a sometimes finely laminated and bioturbated hemipelagic sedimentation with frequent small IRD; IRE1 (91-121 cm), IRE2 (157-180 cm), IRE3 (274-306 cm), IRE4 (329-352 cm), IRE5 (406-451 cm), IRE6 (496-530 cm), IRE7 (661-690 cm) and IRE8 (757-795 cm). The grain size distribution curves of these intervals (Figs. 7.32c, d, g and i) clearly show a silty-sandy component on top of the mud mode, which is reflected by very poorly sorted values and most of the time a negative or coarse skewness (Fig. 7.31). Some of these intervals are associated to an elevated magnetic susceptibility, suggesting that in this deeper environment indeed again LIS-sourced IRD can be observed. Moreover, the characteristics of IRE5, which is followed by an interval of low density and very fine laminations (Figs. 7.30 and 7.33d), are very similar to IRE5 in cores MD99-2327 and MD01-2449. The zone of very low density between 386 and 406 cm is also characterized by a low magnetic susceptibility and relatively well sorted fine silty clay (Fig. 7.32h). A similar structureless clay facies was observed by Zaragosi *et al.* (2001) in a core on Meriadzek terrace. It has been observed in several deep environments, caused by selective hydrotroilite staining. Such a facies is associated with supplies rich in

organic matter and could be due to high sedimentation rates or anoxic bottom water conditions. However, no particular structures or grain size variations can be associated with these layers.

#### **7.2.4.4 Last glacial sedimentary processes in the Bilbo channel**

The variety and succession of sedimentary processes observed in core MD01-2464 can bring more insight in the working and development of the Bilbo channel. However, it should be noted that the present available information does not allow to construct a reliable chronostratigraphy. However, some general suggestions can be made. First of all, a tentative correlation might be made between IRE5 in this core and those in cores MD99-2327 and MD01-2449. If this is true, the three turbidites are located in the glacial MIS2, which confirms that only during glacial lowstands turbidite currents were active in this channel system. Moreover, as observed in the Belgica mound province, the transition towards the recent climatic warm period can be coupled with higher benthic currents, even within these channels. As a consequence, already deposited sand sheets were remobilized, creating the rippled sandy seafloor as observed by Tudhope & Scoffin (1995). Such a sand sheet on the channel floor might thus very well be bottom-current reworked turbidites. In the lower part of the core, the presence of three muddy to silty contourites can be inferred. Since they have been deposited prior to IRE5 and 6, it might be assumed they have been deposited during interglacial times. Again, by analogy with core MD99-2327, these warmer periods might indeed be associated with stronger bottom currents. The presence of IRE7 and 8 however, present a problem, which could be explained by the suggestion that during interglacial periods, the Irish shelf was not completely ice free. The present available information of this core is very promising, but calls for a stronger time-frame and further analysis.

#### **7.2.5 Sedimentary processes of the Gollum channels**

The observed morphologies and seismic stratigraphy of the upper parts of the Bilbo and Frodo channels yield more insight in the past and present sedimentary processes which have influenced the development of this channel system. As the Kings channel system, the Gollum channel system most probably initiated as a canyon system, cut by the Late Pliocene RD1 erosion event into the underlying U2 unit. In early Quaternary times, these canyons were important conduits for the transfer of sediment from the shelf to the deep marine basin. As suggested by Leeder (1999), this mainly happened during (glacial) sea-level lowstands. In a classic deep-sea fan configuration, such submarine canyons commonly grade downslope into channels and gradually continue into depositional fans (Einsele, 1992; Weaver *et al.*, 2000). These downslope channels are more U-shaped in profile and have depositional elements such as levees and aggradational floors (Weaver *et al.*, 2000).

The present-day appearance of the upper part of the Bilbo and Frodo channels is rather U-shaped, but the overall architecture and the governing sedimentary processes such as slumping are similar to typical canyon processes. Also Weaver *et al.* (2000) noted that the GCS plan view rather resembles a tributary canyon system. Their large flanks however seem to be mainly built by hemipelagic sedimentation, rather than overflow of currents on the one hand and bedrock erosion on the other hand. Therefore, this upper part of the GCS is interpreted as a transition from canyon to channel. As already suggested by Leeder (1999), the

orientation of such a channel system might be controlled by faults, although only morphological evidence can be found in favour of this theory.

The core data in this part of the channel also confirm the idea that the channel system activity was confined to glacial lowstands. Moreover, the encountered sediments in this core, combined with the architecture of the channel floor (Figs. 7.17 and 7.19) illustrate a typical canyon or upper slope channel infill. According to Stow & Piper (1984), such an environment is commonly filled by muddy sediments rather than coarse-grained facies. As illustrated on the seismic profiles, much of this fill comprises slumps and debrites as well as mud turbidites and hemipelagites in a rather chaotic vertical sequence. Moreover, according to the definitions of Prather (2003) this setting can be compared with a typical perched slope fill. This is one of the important accommodation types, encountered along slopes, which can be an essential element in influencing the distribution, quality and architecture of submarine hydrocarbon reservoirs.

All these characteristics add to the view of Weaver *et al.* (2000) who compared the Madeira Distributary Channel System (MDCS) to the Gollum channel system. Both the MDCS canyons and GCS upper channels do not reach back to the shelf edge and rarely extend downslope. It is believed that both were formed during previous sea-level lowstands, on slopes of predominantly about 3°. However, in both systems, a subtle decrease in seafloor gradient exerts a dramatic control on the slope processes. After a change from 3° to a gradient of about 1°, the incision fades away into a leveed channel system which usually bifurcates further downstream into distributaries of a submarine fan (Bouma, 2000). The recent observations of Akhmetzhanov *et al.* (2003) on the Porcupine Abyssal Plain indeed support the idea of the development of a submarine fan at the downslope end of the main Gollum channel.

Associated to such deep-sea channel systems, the occurrence of turbidite sediment waves is not uncommon (Weaver *et al.*, 2000; Wynn *et al.*, 2000; Nakajima & Satoh, 2001). These mudwaves typically have crests parallel or subparallel to both the channel margins and the topographic contours of the levee backslope. According to Wynn & Stow (2002), they are formed under unconfined fine-grained turbidity currents, associated to channel levees on slopes between 0.1° and 0.7°. The westernmost seismic profiles perfectly illustrate such an environment, where the presence of such waves can be inferred. However, they are observed on only one seismic profile and need further investigation.

### 7.3 Summary

The few available seismic profiles and a narrow strip of multibeam bathymetry allowed to shed more light on the origin, development and sedimentary processes observed in the Gollum and Kings channel systems. Especially the stratigraphy of the KCS allowed to infer a late Pliocene origin for the creation of these channel systems. This RD1 erosion event, coupled to the onset of the modern oceanographic conditions, removed a substantial part of the earlier deposits sediments and created large downslope elongated depressions.

In the Gollum channel area, these canyons evolved into a large submarine fan channel system. On the upper slope, the channels are deep and serve as by-pass

region for sediment transfer. The course of these channels might have been influenced by faults and smaller, secondary channels are also present. A change in seafloor gradient makes the transition to a less deep channel with sediment levees, evolving downslope into one deep-sea channel, feeding distributaries on the Gollum deep-sea fan. The main activity of this system is located during glacial times with episodic turbidity currents and mass-wasting. During interglacial times, enhanced bottom currents could rework the channel floor deposits. This also strengthens the idea that only this system is located directly downstream of a (still undiscovered) feeding glacial fluvial system located on the Irish mainland shelf, similar to the systems along the Celtic-Armorican margin. The GCS is a fine example of a fine-grained turbidite system offering an interesting study area for research of perched slope reservoirs and the study of deep-sea sediment waves.

The Kings channels are broader and, in contrast with GCS, the evolution and construction of the channel flanks is more readily influenced by the governing downslope flowing currents. Moreover, inside the large Aragorn channel, a separate turbidite levee has been constructed. The smoother KCS might thus be affected by a less turbulent sedimentary environment compared with the GCS and was possibly also affected by a gentle northward flowing bottom current. This might also explain why the KCS does not connect downstream with a feeder channel, since most of the deposition occurs on the upper slope. This might have led to higher sediment stress during Middle to Late Pleistocene times, causing frequent mass-wasting, as observed upslope of the Denethor area. However, especially the very irregular morphology of this area, lying also downstream of the large Kings channels, calls for further investigation which might yield more information concerning the nature, development and past sedimentary processes of the KCS.

All these observations fit into the glacially influenced margin model of Weaver *et al.* (2000) with dominant canyon and channel processes along the Iberian to Southern Rockall margin, which is known to be near the southern limit of the Quaternary ice cover. Many of these canyons and channels were largely inactive during interglacials, resulting in a slow and hemipelagic sedimentation as the ice is far from the shelf (Siegert 2001). During glacial times, more material was transported to the channel heads, under a lower sea level.

## References

- Akhmetzhanov, A. M., Kenyon, N. H., Ivanov, M. K. & Cronin, B. (2003) The Continental Rise West of Porcupine Seabight, Northeast Atlantic. In: *European margin sediment dynamics: side-scan sonar and seismic images* (Ed. by J. Mienert and P. P. E. Weaver), Springer-Verlag, Heidelberg, 187-192.
- Berthois, L. & Brenot, R. (1966) Existence d'une flexure continentale parcourue par un réseau hydrographique, au Sud-Ouest de l'Irlande. *Comptes Rendus de l'Académie des Sciences Paris, Série II a*, **263**, 1297-1299.
- Beyer, A., Schenke, H. W., Klenke, M. & Niederjasper, F. (2003) High resolution bathymetry of the eastern slope of the Porcupine Seabight. *Marine Geology*, **198**, 27-54.
- Bouma, A. H. (2000) Coarse-grained and fine-grained turbidite systems as end member models: applicability and dangers. *Marine and Petroleum Geology*, **17**, 137-143.
- Droz, L., Auffret, G. A., Savoye, B. & Bourillet, J. F. (1999) L'éventail profond de la marge Celtique: stratigraphie et évolution sédimentaire. *Comptes Rendus de l'Académie des Sciences Paris, Série II a*, **328**, 173-180.
- Einsele, G. (1992) *Sedimentary basins: evolution, facies and sediment budget*. Springer-Verlag, Berlin Heidelberg, 628 pp.
- Faugères, J.-C., Stow, D. A. V., Imbert, P. & Viana, A. R. (1999) Seismic features diagnostic of contourite drifts. *Marine Geology*, **162**, 1-38.
- Gonthier, E., Faugères, J.-C. & Stow, D. A. V. (1984) Contourite facies of the Faro Drift, Gulf of Cadiz. In: *Fine Grained Sediments, Deep-Water Processes and Facies* (Ed. by D. A. V. Stow and D. J. W. Piper), London, Geological Society Special Publication, **15**, 275-291.
- Kenyon, N. H., Belderson, R. H. & Stride, A. H. (1978) Channels, canyons and slump folds between South-West Ireland and Spain. *Oceanologica Acta*, **1**(3), 369-380.
- Kenyon, N. H., Cronin, B., Wheeler, A., Satur, N. & Zaragosi, S. (1998) The Southern Porcupine Seabight: Gollum Channel System. In: *Cold water carbonate mounds and sediment transport on the Northeast Atlantic margin* (Ed. by N. H. Kenyon, M. K. Ivanov and A. M. Akhmetzhanov), UNESCO, Paris, IOC Technical Series, **52**, 54-58.
- Leeder, M. (1999) *Sedimentology and Sedimentary basins: from Turbulence to Tectonics*. Blackwell Science Ltd., Oxford, 592 pp.
- Locat, J. & Lee, H. J. (2002) Submarine landslides: advances and challenges. *Canadian Geotechnical Journal*, **39**, 193-212.
- McCann, T., Shannon, P. M. & Moore, J. G. (1995) Fault patterns in the Cretaceous and Tertiary (end syn-rift, thermal subsidence) succession of the Porcupine Basin, offshore Ireland. *Journal of Structural Geology*, **17**(2), 201-214.
- Mulder, T. & Cochonat, P. (1996) Classification of offshore mass movements. *Journal of Sedimentary Research*, **66**(1), 43-57.
- Nakajima, T. & Satoh, M. (2001) The formation of large mudwaves by turbidity currents on the levees of the Toyama deep-sea channel, Japan Sea. *Sedimentology*, **48**, 435-463.
- Prather, B. E. (2003) Controls on reservoir distribution, architecture and stratigraphic trapping in slope settings. *Marine and Petroleum Geology*, **20**, 529-545.
- Rice, A. L., Billet, D. S. M., Thurston, M. H. & Lampitt, R. S. (1991) The Institute of Oceanographic Sciences Biology programme in the Porcupine Seabight: background and general introduction. *Journal of the Marine Biological Association of the United Kingdom*, **71**, 281-310.
- Shanmugam, G. (2000) 50 years of the turbidite paradigm (1950s-1990s): deep-water processes and facies models—a critical perspective. *Marine and Petroleum Geology*, **17**, 285-342.
- Siegert, M. (2001) *Ice Sheets and Late Quaternary Environmental Change*. Wiley, Chichester, 231 pp.
- Stow, D. A. V. (1994) Deep sea processes of sediment transport and deposition. In: *Sediment Transport and Depositional Processes* (Ed. by K. Pye), Blackwell Scientific Publications, Oxford, 257-291.

- Stow, D. A. V., Faugères, J.-C., Howe, J. A., Pudsey, C. J. & Viana, A. R. (2002) Bottom currents, contourites and deep-sea sediment drifts: current state-of-the-art. In: *Deep-Water Contourite Systems: Modern Drifts and Ancient Series, Seismic and Sedimentary Characteristics* (Ed. by D. A. V. Stow, C. J. Pudsey, J. A. Howe, J.-C. Faugères and A. R. Viana), Geological Society, London, *Memoirs*, **22**, 7-20.
- Stow, D. A. V. & Piper, D. J. W. (1984) Deep-water fine-grained sediments: facies models. In: *Fine Grained Sediments, Deep-Water Processes and Facies* (Ed. by D. A. V. Stow and D. J. W. Piper), London, Geological Society Special Publication, **15**, 611-646.
- Tudhope, A. W. & Scoffin, T. P. (1995) Processes of sedimentation in Gollum Channel, Porcupine Seabight: submersible observations and sediment analyses. *Transactions of the Royal Society of Edinburgh: Earth Sciences*, **86**, 49-55.
- Van Rooij, D. (1999) Lithologie des délestages glaciaires (niveaux de Heinrich) de l'Eperon de Goban (Atlantique Nord-Est). D.E.A. thesis, Université de Bretagne Occidentale. *Université de Bretagne Occidentale*, Brest, 57 pp.
- Weaver, P. P. E., Wynn, R. B., Kenyon, N. H. & Evans, J. (2000) Continental margin sedimentation, with special reference to the north-east Atlantic margin. *Sedimentology*, **47**, 239-256.
- Wheeler, A., Cronin, B., Kenyon, N. H., Satur, N., Sautkin, A. & Devoy, R. J. (1998) Channel architecture and activity in the Gollum Channel, Porcupine Seabight. In: *Geosphere-biosphere coupling: Carbonate Mud Mounds and Cold Water Reefs* (Ed. by B. De Mol), UNESCO, Paris, IOC Workshop Report, **143**, 30-31.
- Wheeler, A. J., Kenyon, N. H., Ivanov, M. K., Beyer, A., Cronin, B., McDonnell, A., Schenke, H. W., Akhmetzhanov, A. M., Satur, N. & Zaragosi, S. (2003) Canyon Heads and Channel Architecture of the Gollum Channel, Porcupine Seabight. In: *European margin sediment dynamics: side-scan sonar and seismic images* (Ed. by J. Mienert and P. P. E. Weaver), Springer-Verlag, Heidelberg, 183-186.
- Wynn, R. B. & Stow, D. A. V. (2002) Classification and characterisation of deep-water sediment waves. *Marine Geology*, **192**, 7-22.
- Wynn, R. B., Weaver, P. P. E., Ercilla, G., Stow, D. A. V. & Masson, D. G. (2000) Sedimentary processes in the Selvage sediment-wave field, NE Atlantic: new insights into the formation of sediment waves by turbidity currents. *Sedimentology*, **47**, 1181-1197.
- Zaragosi, S., Auffret, G. A., Faugères, J.-C., Garlan, T., Pujol, C. & Cortijo, E. (2000) Physiography and recent sediment distribution of the Celtic Deep-Sea Fan, Bay of Biscay. *Marine Geology*, **169**, 207-237.
- Zaragosi, S., Eynaud, F., Pujol, C., Auffret, G. A., Turon, J.-L. & Garlan, T. (2001) Initiation of the European deglaciation as recorded in the northwestern Bay of Biscay slope environments (Meriadzek Terrace and Trevelyan Escarpment): a multi-proxy approach. *Earth and Planetary Science Letters*, **188**, 493-507.

## Chapter VIII: Summary and conclusion

This present study has shown that the eastern slope of the Porcupine Seabight, already known for its remarkable mound provinces, is a most interesting microcosm from the sedimentological as paleoceanographic points of view as well. A wide range of geophysical and sedimentological techniques allowed to evaluate the local importance of bottom currents throughout the Upper Paleogene to recent times, as well as the influence of, and interplay with other deep-water sedimentary processes. Moreover, the shaping of the Quaternary deposits was substantially influenced by the very irregular paleobathymetry, largely controlled by the mounds. The assessment of the environmental impact of these two aspects also allowed to better fathom the development and fate of the deepwater coral banks on this part of the margin. This chapter will summarize the main results of this study in terms of its initial objectives. As a conclusion, a general Late Cenozoic development model of this part of the margin will be proposed. Although this study allowed to contribute to a better understanding of this part of the NE Atlantic domain, it also has identified several questions and problems that call for further investigation, which will be briefly discussed as future perspectives.

### 8.1 Main results

#### 8.1.1 Geophysical characterization of Neogene-Quaternary deposits

The tools provided for this study mainly allowed to focus on the nature and characteristics of the Quaternary deposits of seismic unit U1. Throughout the entire study area, the sedimentary environment has been largely dominated by a dynamic bottom current environment and by the paleotopography of the underlying unit U2. From the northern part of the Belgica mound province towards the southern Gollum channel and Goban Spur, a highly irregular discontinuity has been observed, attributed to the Late Pliocene RD1 erosion event.

Since its opening, the Atlantic domain has known several turnovers in oceanic circulation leading to extensive erosion. The geophysical signatures of Middle Eocene to Pliocene deposits on this part of the slope indeed show a variable environment, with the installation of classic elongated sediment drifts, associated to a north to northwest flowing bottom current. Especially unit U3 shows that on the assumed backslope of these sediment drifts, large fields of bottom current sediment wave fields have been established. However, the RD1 event is locally very pronounced and it removed a very large part of these underlying deposits, preventing a full understanding of their depositional history. RD1 has been coupled to the amplified ice growth of the Northern hemisphere and marks the start of a period where the episodic growth and decay of continental ice sheets will influence climatic, sea-level and hydrodynamic conditions.

During this erosion event, the basis of all major channel systems on the eastern slope of the Porcupine Seabight has been created. The Arwen and Celeborn-Galadriel channels have been created by a strong south-north directed current, while the Kings and Gollum channel system were created by downslope flowing currents. During the Quaternary, these channels remained the pathways of these

currents, although the seismic characteristics suggest that the vigour of these currents seems to have decreased.

In the Belgica mound province, the unique geographic and hydrodynamic setting was responsible for the deposition of a sediment drift system along both sides of the Arwen channel. The seafloor of this area is characterized by sediment remobilization, observed as gravel lag in the channels and sand waves, sand ribbons and striations in between the coral banks. A first sediment drift body is bound at its right-hand side by the Arwen channel and displays the typical aggradation-progradation of a drift levee towards the channel. Some evidence suggests a possible tectonic control that might have influenced the morphology and sedimentation of these channels. Between the channel and the mounds, a very complex zone of sediment waves and levees suggests the combined action of the broad northward flowing current coming from the channel (locally enhanced by the presence of the steeper mound ridges) and the downslope running turbidite gullies. The sedimentary environment around these mounds is influenced by contour currents with variable strength and by turbidite deposits at the foot of the mounds. Within the central part of the Belgica mound province, a small confined mounded contourite drift is deposited in a relatively narrow passage between coral banks and a steep scarp created by the RD1 erosion event.

South of the Belgica mounds, the evolution and construction of the flanks of the broad Kings channels (KCS) are more readily influenced by downslope flowing currents. Moreover, inside the large Aragorn channel, a separated turbidite levee has been constructed. This KCS is thought to be affected by periodic turbidite currents, possibly already weakened by the inferred northward flowing bottom current system. Since most of the deposition occurs on the upper slope, this might also explain why the KCS does not connect downstream with a feeder channel. An inferred higher sediment stress during Middle to Late Pleistocene times might have caused frequent mass-wasting.

The Gollum channel system (GCS) shows similarities with a submarine fan channel system. On the upper slope, the channels are deep and serve as by-pass region for downslope fine-grained sediment transfer. The course of these channels may have been tectonically influenced. A change in the seafloor gradient marks the transition to a less deep channel with sediment levees, evolving downslope into one deep-sea channel, feeding distributaries on the Gollum deep-sea fan. The main channel deposits are turbidites and mass-wasting deposits. This study also strengthens the idea that this system is located directly downstream of a (still undiscovered) feeding glacial fluvial system located on the Irish mainland shelf, similar to the systems along the Celtic-Armorican margin. Moreover, the architecture of the upper GCS is a fine example of a perched slope accommodation zone.

### **8.1.2 A study of paleoclimatologic and paleoceanographic changes**

A SE to NW transect of five long cores has demonstrated the variability and distribution of BIIS-sourced IRD in the Porcupine Seabight. Two cores located on the eastern slope of the Porcupine Seabight almost exclusively contain BIIS-sourced material. Six ice-rafting events (IRE) were described and can be compared with the North Atlantic Heinrich Events. These regional events carry a very strong BIIS signature with mainly sands originating from Devonian and Carboniferous

sandstones. Only a limited influence of Laurentide icebergs was found. The abundance of the IRD record shows a millennial-scaled disintegration of the BIIS from 25 ka onwards with distinct ice-rafting pulses about 17.4 and 15 ka BP. A comparison with cores on the Celtic margin and in the northern part of the Porcupine Seabight shows a decreasing importance of the BIIS-derived IRD and an increase of LIS-derived IRD when moving towards a more distal position from the Irish mainland.

Three other cores located in the northern part of the Porcupine Seabight, on the other hand, do show the presence of LIS-sourced IRD. This might confirm that BIIS-sourced icebergs released along the western side of Ireland probably were transported by a southward surface current along the Irish and Celtic shelf edges. Therefore, the position of cores MD99-2327 and MD01-2449 is ideal to study BIIS variability. They contain only a minimum of non-BIIS material due to probable grounding about the Connemara region and Goban Spur.

### **8.1.3 A sedimentological study of recent glacial and interglacial deposits**

As was observed in the geophysical study, the cores also contain a record of a very dynamic sedimentary environment. All cores from the Belgica mound province and core MD01-2449 (located in the KCS) show that the glacial deposits were characterized by variable bottom currents, creating a muddy contourite facies in which several peak current episodes could be distinguished. Moreover, core MD99-2327, located on the small mounded drift, seems to contain an amplified record of this bottom current variability. The presence of a massive sandy contourite between 1500 and 2625 cm suggests that during interglacial times the bottom current regime is similar as the present day situation. However, during the transition from isotope stage 5 to stage 4, the accumulating ice volumes of the pan-Atlantic ice sheets were responsible for a global sea-level drop and the distribution of the MOW in the Eastern Atlantic was drastically diminished. Since the presence of the MOW is vital to the local vigorous hydrodynamic environment, the activity of the glacial bottom currents became reduced. However, evidence of periodic current reactivation, coupled with warmer periods and the increase of epibenthic foraminifers, suggests enough MOW sporadically entered the Porcupine Seabight in order to shortly enhance the bottom current production. The glacial deposition of muddy contourites with a strong ice-rafted sand component is influenced by turbidite deposits at the foot of the mounds.

A similar conclusion can be made from a core within one of the Gollum channel heads. During glacial times (especially during the last glacial maximum), turbidity currents were active due to a lowered sea-level. These fine-grained turbidites were deposited in a hemipelagic background sediment with IRD. During interglacial times, reversing bottom currents were active in this channel, creating muddy-silty contourites or even reworking the glacial turbidite deposits.

## **8.2 Conclusion: a Late-Cenozoic development model of the eastern Porcupine Seabight, SW of Ireland**

The earliest record in this development model goes back to the Middle Eocene. A combination of tectonic and climatic events, such as the onset of the Antarctic Bottom Water regime, was responsible for the Middle Eocene RD4 erosion event on the eastern slope of the Porcupine Seabight. The seismic characteristics of the strata deposited on this unconformity already suggest the presence of bottom currents in this part of the basin during the upper Eocene. These poorly documented deposits have an early Late Oligocene upper boundary, related with a deep erosion event related with the initiation of the Antarctic glaciation (RD3). The overlying unit U3 generally shows a similar situation. However, a large zone of strata onlapping on the lower boundary of U3 is observed, sharing similarities with well-studied North Atlantic sediment drifts. Moreover, downslope of a break in the paleo-slope and in a narrow zone of constant depth, another large zone of probably eastward migrating sediment waves is observed, inferring a N to NW flowing bottom current on this part of the slope during the Early Miocene. In the lower Middle-Miocene, the introduction of the Norwegian Sea Water in the North Atlantic Ocean was responsible for a margin-wide erosion of this sediment drift.

After this RD2 erosion event, a locally very thick acoustically transparent unit U2 with yet unknown lithology was deposited over the entire slope. A change in seismic facies near the inferred top of this unit is believed to represent the Miocene-Pliocene boundary, similar to seismic sections on Goban Spur. Due to a major change in oceanographic conditions, the large-scale RD1 erosion event was responsible for the removal of a large part of unit U2 and has cut very deeply into unit U3 and U4 during the Late Pliocene along the entire slope. During this erosion event, the main pathways of the large, present-day channels were determined. In the southern part of the basin, the steep upper slope has been intersected by large canyons. More to the north, an inferred south-north directed current has created a terrace-like paleotopography with the base of the Arwen channel as its deepest point. However, some evidence suggests that a possible tectonic control might have influenced the morphology and sedimentation of all these channels systems.

Subsequent to the Late Pliocene erosion, corals began to settle on topographic irregularities in the palaeobathymetry at the eastern side of the Arwen channel. The coral banks were built spectacularly fast in a period from the Late Pliocene to the middle Early Pleistocene when the adjacent areas experienced non-deposition. They are located in a zone within the influence of a complex system of enhanced currents, which is believed to be the main driving force of the controls in their development. However, in the southern part of the study area, three newly discovered Enya mounds are observed rooting on a cut-and-fill facies. Although there seems to be a substantial environmental control by currents, the presence of pockmarks does suggest the influence of fluid seepage.

This very turbulent episode also marked the start of the glacial-interglacial cycles and their effects on the deep-water circulation. In the Gollum and Kings channel area, this was characterized by an enhanced supply of terrigenous material, building a Gollum deep-sea fan complex. The Kings channels were also affected by turbidity currents, but here no connection to a deep-sea fan was established. Moreover, both systems are believed having been active during glacial lowstands,

while during interglacial times there was a mainly hemipelagic sedimentation environment with local effects of bottom currents. In general, high sedimentation rates have led to the deposition of a very thick upper slope sedimentary unit. Along the channel flanks, this might have led to mass-wasting. On the other hand, major slumping inferred on Goban Spur might also link this to a Middle Pleistocene enhancement of climatic variability.

Towards the northern part of the study area, however, the sedimentation rates decrease and the geometry of the Quaternary unit becomes more variable, indicating a larger influence of bottom currents. This means that, in contrast with previous suggestions, the sediments transported through and deposited in the Gollum and Kings channels are not significantly redistributed over the entire Porcupine Seabight. The main area of sediment mobilization and redistribution is found in the Belgica mound province, where sediment drift bodies were deposited in association with the Arwen channel and the coral banks. Moreover, plenty of evidence is found of an interplay between contouritic and turbiditic processes. Within the central part of the Belgica mound province, the sedimentation only started around the early Middle Pleistocene. A small confined mounded contourite drift was deposited in a narrow passage between coral banks and a scarp in the underlying paleotopography. The enhanced variability between interglacial and glacial periods also induced lithological variability with the deposition of respectively sandy and muddy contourites. This might also be read in the vertical variations in seismic amplitudes along this contourite drift.

### **8.3 Future perspectives**

In addition to the main results of this study, several gaps in our knowledge and other problems were identified. They have been grouped below into four (promising) topics, forming an outline of future research.

#### **8.3.1 Advanced understanding of PSB paleoceanography**

The results of the study of the offshore record of BIIS variability only allowed to unveil a small part of the recorded paleoceanographic changes in the Porcupine Seabight. The signals observed in cores MD99-2327 and MD01-2449 are unique and might contain valuable information concerning the variability of the Southern dome of the British-Irish Ice Sheet. An advanced understanding of this topic necessitates a very high-resolution (cm-scaled) analysis of these cores, together with detailed planktonic and benthic foraminiferal isotope data and a decent  $C^{14}$  age constraint. Moreover, a detailed geochemical study (Sr/Nd) of the lithological component of the cores could yield more exact information on the sources of the ice-rafted material. A similar high-resolution study of the long cores on the northern part of the PSB should bring more information about the presence and distribution of BIIS- and LIS-sourced IRD, explaining the reason of their absence on the high margin. It could also bring more insight in the surface paleocirculation patterns during the last glacial periods.

The present-day hydrodynamic environment is thought to be under a strong influence of the MOW. A further understanding of currents on this part of the slope asks for more current-meter deployments and high-resolution modelling. Moreover, the possible link of enhanced benthic currents with a higher abundance of

epibenthic foraminifers in a warmer climate should be further investigated. This would allow the development of a new benthic current proxy and a marker of the influence of the MOW. Also, the use of the (already valuable) sortable silt index in areas with enhanced ice-rafted material should be further investigated. It was also demonstrated that the sortable silt index is no longer applicable when sand is being remobilized, which calls for a new benthic current proxy in a sandy environment.

The encountered variability of benthic currents in core MD99-2327 is very interesting and calls for confirmation. A more advanced lithological and clay mineralogical study of the inferred sandy contourite unit is needed to better understand the characteristics and origin of this deposit. It would yield very valuable information in the contourite paradigm and could bring new insights in the occurrence of the potentially economically interesting deep-water massive sands. Ideally, an effort should be made to duplicate this sedimentary record along the flank of the small mounded drift, together with very high-resolution seismic data.

### 8.3.2 Fine-tuning of the Cenozoic margin stratigraphy

The studies of the Goban Spur transect and the stratigraphy of the Belgica mound province has also indicated several hiatuses in our knowledge of sedimentary processes and the record of large oceanographic turnovers in this area. Both are interesting areas to study past sedimentary processes and can be a key to understand large-scale regional unconformities. However, the latter can only be accomplished by a renewed study of site DSDP 548 or deep drilling through a well documented site in the central Belgica mound province (proposed in IODP 573 Full).

On Goban Spur, a further high-resolution seismic study of the paleo slide-scar could yield more information about its relation to Neogene climate changes. The inferred sediment drift and waves on this part of the margin could also add valuable information to the already large catalogue of bottom-current deposits.

A further study of units U3 and U4 (with a more powerful seismic tool) can also contribute to our knowledge of the onset of the bottom current regime in the Porcupine Seabight. A significant amount of information can be obtained by inferring the exact position and migration direction of the sediment waves of these units. Only more (pseudo-3D) seismic data, with profiles acquired under different orientations, can correctly infer the real sediment wave migration direction.

Finally, all discussed channel systems seem to have been affected by possibly reactivated Mesozoic faults. Therefore, a study of deep seismic profiles would have to yield more information about this possible structural control.

### 8.3.3 Quaternary sedimentary processes

The detailed study of unit U1 rises as many questions as answers. The main problem is the lack of time control of the important RD1 discontinuity, which lies at the base of the coral banks, sediment drift deposits, the base of the alongslope channels and the base of the Gollum and Kings channels. Therefore, several drill sites will be needed to pinpoint exact constraints on its age. From this point of view (and several others), the described small mounded contourite drift might be an interesting drill site. Up to now, the geometry of this body was only studied by NE-SW oriented profiles. Moreover, core data has yielded possibly a spectacular impact of paleoclimate changes on the sedimentation with muddy contourites during glacial

times and sandy contourites in interglacial times. This lithological variability induced by Quaternary climate changes might also be read in the vertical changes of seismic amplitudes throughout this entire seismic section. The only way to confirm this is to drill through such a contourite mound. At the same time, this can yield information on the timing of the RD1 event, mound growth, nature of U2 and onset of sedimentation in this confined basin.

An interesting area for the study of interacting sedimentary processes is located between the Arwen channel axis and the coral banks. This possible interplay between turbiditic and contouritic processes, calls for more high-resolution seismic data and core material.

The few profiles over the Gollum and King channel area clearly point out that this area deserves a further study. As on Goban Spur, the Denethor area will be ideal to study the relationship between mass-wasting and climate changes. The GCS area will be interesting to study, in an indirect way, the variability of glaciations on the British Isles, providing the discovery of a possible ancient fluvial system towards the ancient channel heads of the GCS. Moreover, the upper slope yields interesting study sites for present-day reservoir analogues, such as the identified perched slope configuration. The preliminary results of a core on this site call for a detailed study, further deciphering the interplay between contourites, turbidites and ice-rafting throughout the Quaternary. Finally, the downslope area of this system yields the presence of sediment waves and also control by creep, which should be further identified.

#### **8.3.4 On the origin of the coral banks...**

In this study, not much information was added to previous studies. The role of unit U2 in the development of the coral banks is fairly well known, but still the lithology of this unit, which could also be a factor for the attraction of coral larvae, is unknown. This evidently needs drilling, but on several locations this unit is only covered with a small Quaternary layer, which allows long coring.

The present-day dominating relationship between enhanced bottom currents and coral bank settling has been very well demonstrated in the Belgica mound province. However, the Enya mounds clearly point out that an additional internal (hydrocarbon) influence can not be ruled out. Therefore, it should become a key point of study, focussing on a detailed mapping of these new mounds and their relationship to the underlying discontinuity and the overlying pockmarks. Deeper seismic profiles should further make constraints on the role of deep faults as a conduit for the seepage. Long cores should be taken to confirm the contouritic nature of the associated drift, but also to establish the source of the pockmarks through geochemical analysis of the pore waters and the possible gas content.



## Uitgebreide Nederlandse samenvatting

### 1 Inleiding

De geleidelijke verschuiving van de petroleumindustrie naar diepwater-domeinen heeft een sterke groei veroorzaakt in de wetenschappelijke interesse naar sedimentaire systemen waar bodemstromingen een belangrijke rol spelen (Faugères *et al.*, 1999). Dank zijn hun grote reservoircapaciteiten, hebben turbidietssystemen altijd al een speciale aandacht gekregen (Stow & Johansson, 2000; Bouma, 2000; Shanmugam, 1997). Recente studies tonen echter aan de belangrijkheid van contourietafzettingen niet mag worden onderschat. Zowel turbidiet- (hellingafwaarts) als contouriet- (langs de helling) stromingen kunnen goed gesorteerde, grofkorrelige evenals fijnkorrelige sedimenten afzetten (Stow & Mayall, 2000; Stow & Piper, 1984; Gonthier *et al.*, 2003). De geofysische en lithologische karakteristieken van deze afzettingen kunnen echter heel vergelijkbaar zijn en liggen vaak aan de oorzaak van (heel dure) verkeerde interpretaties (Viana *et al.*, 1998; Faugères *et al.*, 1999).

Hoewel het onderzoek betreffend deze problematiek al bezig is sinds de jaren 60, is er nog steeds een grote nood aan goed ontwikkelde criteria om deze contourieten van andere diepwater afzettingen te onderscheiden (Stow & Johansson, 2000; Stow *et al.*, 2002a; Shanmugam, 2000; Rebesco & Stow, 2001). Daarenboven worden, grotendeels door recente technologische ontwikkelingen, jaarlijks andere en kleinschaligere variëteiten van deze afzettingen ontdekt (Faugères *et al.*, 1999; Rebesco & Stow, 2001). Het is dan ook van groot belang om de koppeling tussen klimaat, bodemwatercirculatie en de afzettingsprocessen van deze sedimentdriften te begrijpen, alhoewel dit niet altijd zo eenvoudig blijkt te zijn (Faugères & Stow, 1993; Rebesco & Stow, 2001). Zulke studies vereisen een multidisciplinaire aanpak, aangezien deze afzettingen niet ondubbelzinnig kunnen worden geïnterpreteerd aan de hand van maar één enkele techniek (Faugères *et al.*, 1999).

Een dergelijk samenspel van sedimentaire processen lijkt aanwezig te zijn langs de oostelijke helling van de Porcupine Seabight (Fig. 1.1). Deze amfiteater-vormige inham ten zuidwesten van Ierland is in feite de oppervlakte-expressie van het onderliggende diepe Porcupine Bekken. Dit bekken is een geaborteerde rift van de proto-Noord Atlantische oceaan, opgevuld met tot 10 km dikke Mesozoïsche en Cenozoïsche afzettingen (Masson & Miles, 1986; Moore & Shannon, 1991). De evolutie van dit bekken kan worden samengevat in drie grote episodes (Fig. 2.3): een Paleozoïsche syn-rift fase, een overheersende Jura fase van rifting en een Laat-Krijt tot recente periode van thermische subsidentie (Ziegler, 1982; Shannon, 1991; Moore & Shannon, 1995; McDonnell & Shannon, 2001).

Dank zij de speciale positie van de Porcupine Seabight langs de Atlantische rand en zijn bijzondere geologische achtergrond, wordt het onwaarschijnlijk geacht dat de intensieve thermo-halien gedreven bodemstromingen van de "Global Conveyor Belt" in dit bekken voorkomen. Aan de andere kant, suggereren hydrologische modellen en enkele stromingsmetingen de aanwezigheid van versterkte bodemstromingen in een beperkte zone tussen 500 en 1000 m waterdiepte (White, *in press*; New *et al.*, 2001; Rice *et al.*, 1991). Side-scan sonar en videobeelden tonen eveneens bodemstructuren die duiden op intense bodemstromingen in dit gedeelte

van het bekken (Chachkine & Akhmetzhanov, 1998; Kenyon *et al.*, 1998; Wheeler *et al.*, submitted). Sinds het midden van de jaren 90 heeft het Porcupine Bekken uitgebreide wetenschappelijke belangstelling gekregen door de aanwezigheid van speciale diep-water habitats (Henriet *et al.*, 1998; De Mol *et al.*, 2002; Huvenne *et al.*, 2003; Wheeler *et al.*, in press). Zo werden verscheidene provincies koraalbanken ontdekt en beschreven, zoals de Belgica mound provincie langs de oostelijke helling en de Hovland en Magellan mound provincies langs de noordelijke helling (Henriet *et al.*, 1998; De Mol *et al.*, 2002; Huvenne *et al.*, 2003). Voorlopige studies van het Belgica mound gebied suggereerden dat de geometrie van de meest recente sedimentlichamen werd beïnvloed door de aanwezigheid van bodemstromingen met een variabele intensiteit. Er werd voorgesteld dat de sedimenten die de koraalbanken omsluiten kunnen worden geïnterpreteerd als sedimentdriften (De Mol *et al.*, 2002; Henriet *et al.*, 2003).

Vele auteurs beschouwen deze sedimentdriften als ideale doelwitten voor paleoceanografische en paleoklimatologische studies (Joseph *et al.*, 2002; Llave *et al.*, 2001; Rebesco & Stow, 2001; Bianchi & McCave, 2000; McCave *et al.*, 1995; Stow & Lovell, 1979). Een beter begrijpen van de werking van deze sedimentdriften zou een beter inzicht kunnen teweeg brengen in de mogelijke relatie tussen de koraalbanken, de sedimentdriften en de veranderingen in het paleoklimaat. Er is echter zeer weinig gekend betreffende de regionale Kwartaire stratigrafie van het Porcupine Bekken, vooral door het ontbreken van lange, hoge-resolutie boringen. Toch is dit bekken gelegen in een ideale proximale positie voor de studie van de evolutie en de variabiliteit van de Ierse component van de Brits-Ierse ijskap (BIIS). Tot op heden is de beschikbare informatie grotendeels gebaseerd op studies aan land (Bowen *et al.*, 2002; Dowling & Coxon, 2001; McCabe *et al.*, 1998) en van werk in bekkens en op hellingen ten noorden (Knutz *et al.*, 2002b; Richter *et al.*, 2001; Armishaw *et al.*, 2000) en ten zuiden van Ierland (Auffret *et al.*, 2002; Zaragosi *et al.*, 2001; Grousset *et al.*, 2000; Scourse *et al.*, 2000; Hall & McCave, 1998; Auffret *et al.*, 1996).

Verder naar het zuidelijke gedeelte van de Porcupine Seabight, werd door Berthois & Brenot (1966) het Gollum kanalen systeem ontdekt, gelegen tussen de shelf break en de Porcupine Abyssale Vlakte. Kenyon (1987), Rice *et al.* (1991) en Wheeler *et al.* (2003) beschreven al de belangrijke rol van turbidieten en afglijdingen in dit kanalsysteem. Zijn oorsprong, verleden en huidige werking is echter niet goed gekend. Dit kanalsysteem zou een belangrijke bron kunnen geweest zijn van detritisch materiaal in het Porcupine Bekken tijdens glaciële laagstanden.

Langs de oostelijke helling van de Porcupine Seabight kunnen dus twee soorten sedimentaire omgeving worden onderscheiden, op een relatief kleine afstand van elkaar. Aan de ene kant is er een hemipelagische sedimentatie beïnvloed door bodemstromingen (sediment drift), terwijl aan de andere kant binnen het Gollum kanalen systeem hoofdzakelijk turbidietstromingen en afglijdingen de sedimentatie zouden domineren. Daarom is het nodig om de afzettingsprocessen en hun onderlinge interacties te bestuderen en te verstaan, door het gebruik van zowel sedimentologische als geofysische technieken. Het Porcupine Bekken biedt een ideaal natuurlijk laboratorium voor deze doeleinden.

Deze studie zal dan ook het belang van bodemstromingen tijdens de Neogene evolutie van de oostelijke helling van de Porcupine Seabight trachten te evalueren, evenals de invloed en het samenspel van andere diepwater-sedimentaire processen

zoals turbidieten. De aanwezigheid en de ligging van de koraalbanken bieden tegelijkertijd een ideale gelegenheid om het gedrag van de versterkte bodemstromingen te bestuderen, evenals hun impact op de sedimentatie in gebieden met een onregelmatige bathymetrie.

Meer bepaald heeft dit onderzoeksproject zich toegespitst op vier hoofdpunten:

1. **Een geofysische karakterisatie van Neogene en Kwartaire afzettingen** op de oostelijke helling van de Porcupine Seabight. Zeer hoge-resolutie éénkanaals seismische profielen, multibeam bathymetrie en side-scan sonar beelden werden gebruikt om de *geometrie* en de *opbouw* van de sedimentlichamen rond en hun *interactie* met de Belgica mounds te bestuderen. Bovendien is ook de *structuur*, *werking* en *evolutie* van het Gollum kanalsysteem onderzocht.
2. **Een sedimentologische studie van recente glaciale en interglaciale afzettingen** werpt een nieuw zicht op de aard, karakteristieken en de kortetermijn variabiliteit van een verscheidenheid aan sedimentaire processen in het Belgica mound gebied (contourieten) en het Gollum kanalsysteem (turbidieten).
3. **Een studie van paleoklimatologische en paleoceanografische veranderingen** laat toe in te schatten hoe de werking van de BIIS werd opgeslagen in het sedimentaire archief en in welke mate deze en andere globale paleoklimatologische gebeurtenissen de sedimentaire omgeving heeft beïnvloed. Vandaar is de beschikbaarheid en de toepasbaarheid van enkele goed gekende *paleoceanografische proxies geëvalueerd* en *heringeschat*.
4. **Een Laat-Cenozoïsch ontwikkelingsmodel van de Oostelijke Porcupine Seabight** is voorgesteld, die de resultaten van de vorige drie hoofdpunten integreert. Dit model tracht meer informatie te bieden betreffende de “eerste dagen” van de genese van de koraalbanken. Door een vergelijkende studie laat dit toe om de aard, oorsprong en evolutie van de afzettingen in de Porcupine Seabight beter te begrijpen.

## **2 De sedimentaire diep-water registratie van BIIS variabiliteit**

Het studiegebied is relatief dicht gelegen nabij het Ierse vasteland, waarop tijdens de Kwartaire ijstijden een relatief grote ijskap was gelegen (Fig. 4.6). De groei en het (periodische) afsmelten van zulke ijskap zal de paleoceanografie van de nabij gelegen sedimentaire bekkens beïnvloeden. De best gekende voorbeelden zijn hier de *Heinrich Events* (HE), veroorzaakt door de destabilisatie van de pan-Atlantische ijskappen. De karakteristieken van de sedimentaire registratie van deze gebeurtenissen laten het toe om relatieve dateringen te geven aan diepzeekernen in het NE Atlantische domein (Bond *et al.*, 1992; Broecker *et al.*, 1992; Chi & Mienert, 1996; Grousset *et al.*, 1993; Knutz *et al.*, 2001; Richter *et al.*, 2001). Recente observaties suggereren echter dat de destabilisatie van de Brits-Ierse ijskap wel eens zijn eigen invloed zou kunnen hebben gehad op de *ice-rafting events* (IRE) langs de noordwest Europese rand (Auffret *et al.*, 2002; Grousset *et al.*, 2000; Scourse *et al.*, 2000).

## 2.1 Kenmerken en verdeling van IRD in de Porcupine Seabight

Er werd een opmerkelijk verschil opgetekend in de verdeling van *ice-rafted debris* (IRD) langs een zuidoost-noordwest transect van vijf lange kernen. De sedimentaire geschiedenis van kernen MD99-2327 en MD01-2449 toont een zeer atypische situatie, waar BIIS IRD (hoofdzakelijk zandkorrels van Ierse Devoon en Carboon zandstenen) lijkt te overheersen. Deze regionale IRE delen niet helemaal dezelfde karakteristieken met de typische Noord-Atlantische *Heinrich Layers* (HL). Gelijkaardige kenmerken met de HL hebben aan de andere kant wel degelijk bijgedragen in de herkenning van de IRE: het hoge percentage aan de planktonische foraminifeer *N. pachyderma s.*, een verhoogde dichtheid en de karakteristieken van de radiografieën. De herkenning en de interpretatie van deze IRE is wegens verschillende redenen echter niet vanzelfsprekend.

Vooraf het ontbreken van de anomalieën in de magnetische susceptibiliteit maakte het erg moeilijk om deze gebeurtenissen op te sporen. Dit kan vooral worden uitgelegd door de mineralogische en geochemische samenstelling van de IRD (Fig. 4.8 en 4.14). De invloed van het detritisch carbonaat is duidelijk hoger en kan belangrijk genoeg zijn om kleurveranderingen te introduceren ter hoogte van de IRE (Fig. 4.11). Daarenboven zijn er maar weinig gesteenten langs de Ierse westkust die genoeg magnetisch materiaal bevatten om een significante anomalie in de magnetische susceptibiliteit te veroorzaken. De structuur van IRE1, 2, 3 en 4 doet denken aan de verschillende IRD pulsen die werden geobserveerd in typische NE Atlantische HL door Auffret *et al.* (2002), Grousset *et al.* (2000) en Grousset *et al.* (2001). Deze HE bevatten een centrale piek bestaande uit Laurentide materiaal, gevolgd en voorafgegaan door een IRE met een Europese bron. Zulk een structuur zou ook kunnen worden herkend in IRE3, 4 en mogelijks ook 5. Dit zou kunnen betekenen dat de middelste piek materiaal zou kunnen bevatten van de vroegere Noord-Amerikaanse Laurentide ijskap (LIS). Samengevat, suggereren de IRD karakteristieken van deze twee kernen dat, behalve voor IRE5, deze allemaal een Ierse oorsprong hebben.

De IRE geobserveerd in de andere drie kernen, gelegen langs de noordelijke rand van het bekken, vertonen wel gelijkenissen met de typische HL. Aangezien er echter nog geen studie werd uitgevoerd naar de korrelgrootteverdeling en de lithologische en micropaleontologische samenstelling, dienen deze interpretaties met voorzichtigheid te worden behandeld. Niettemin suggereert de variabiliteit van de magnetische susceptibiliteit een sterke invloed van LIS IRD.

Deze verdeling zou kunnen worden verklaard door het lokale systeem van oppervlaktestromingen tijdens het laatste glaciaal maximum (LGM). Hall & McCave (1998) stelden een algemene zuidwest gerichte oppervlakte stroming voor langs de Keltische rand. Dit werd bevestigd door Knutz *et al.* (2001) en Grousset *et al.* (2001) die een zuidwaardse drift suggereerden voor ijsbergen afkomstig van het westen van Ierland. Tezamen met de huidige gegevens, kan er worden voorgesteld dat de BIIS ijsbergen bijna onmiddellijk onderhevig waren aan deze zuidwaardse drift en bijgevolg hun produkten enkel langs de oostelijke rand van het Porcupine Bekken af hebben gezet. Waarschijnlijk heeft enkel een minimum aan BIIS IRD de sites in het noordelijke gedeelte van de Seabight bereikt. Aan de andere kant, tonen de drie lokale kernen typische HL afzettingen. In het ondiepe Connemara gebied, hebben seismische data de aanwezigheid aangetoond van omploegingen door vastgelopen

ijsbergen (Games, 2001; Mathys, 2001). Gezien de fysische eigenschappen van de IRD in dit gebied, lijkt het aanvaardbaar dat deze ijsbergen ook wel eens een oorsprong kunnen hebben gehad in Noord-Amerika, Groenland of zelfs IJsland en Scandinavië. Een gelijkaardige situatie werd ook geobserveerd bij Goban Spur, waar (Scourse *et al.*, 2000) een grotere LIS IRD aanvoer heeft geobserveerd dan die van BIIS. Hier werd ook het vastlopen en *in situ* smelten van grote LIS ijsbergen verondersteld langs deze rand. Tesamen met de voorgestelde zuidwaartse drift van de BIIS ijsbergen, kan dit mogelijks verklaren waarom er zeker tijdens marien isotopen stadium 2 (MIS2, 12-24 ka) bijna geen LIS IRD werd afgezet langs de oostelijke helling; ofwel liepen ze vast nabij Connemara of Goban Spur, ofwel werden ze ook meegenomen door de zuidwaartse drift. In ieder geval is dit gedeelte van de helling geschikt om de variabiliteit van de BIIS te bestuderen.

## 2.2 Gevolgen voor de BIIS-variabiliteit

Na het herkennen en interpreteren van de IRE, werd een voorlopig ouderdomsmodel voor de kernen MD99-2327 en MD01-2449 opgesteld, die toeliet de sedimentatiesnelheden en de sedimentaire fluxen te berekenen (Fig. 4.22). Dit staat toe om voorzichtig de variabiliteit van de BIIS, zoals geregistreerd in de sedimenten van de Porcupine Seabight, te bestuderen en ze te vergelijken met goed bestudeerde kernen van de Keltische rand (Auffret *et al.*, 2002).

Tijdens het veronderstelde MIS4 (59-74 ka) werd een relatief minimum aan IRD geobserveerd (Fig. 4.7, 4.8 en 4.99) met gematigd lage sedimenttoevoer (Fig. 4.22). Daarom wordt in deze periode met een dalende zeespiegel een gestaag groeiende BIIS verondersteld (Auffret *et al.*, 2002; Labeyrie *et al.*, 1987). Een verhoging aan de toevoer van IRD lijkt te beginnen rond 62 ka, rond IRE6. Alle hierop volgende toevoer van terrigene deeltjes (IRD) kan worden toegeschreven aan een waarschijnlijk millennium-schalige destabilisatie van de BIIS (Fig. 4.9). Tijdens MIS3 (24-59 ka) volgen alle IRE (3-6) heel dicht op elkaar (4.16). Dit suggereert dat tijdens deze periode geen andere grote processen van sediment toevoer moeten actief zijn geweest buiten de toevoer van IRD, hemipelagische regen en een beperkte laterale aanvoer van sediment door bodemstromingen. De lichte stijging van sedimentatiesnelheden en IRD-toevoer rond 45 ka (Fig. 4.22) illustreert een verdere expansie van de Europese ijskappen en een daarop volgende toevoer van detritisch materiaal (Auffret *et al.*, 2002). Een bescheiden piek in de waarden van de totale sedimentaanvoer zou kunnen gekoppeld worden aan een pré-LGM deglaciatie tussen 25 en 37 ka, eerder al beschreven door Bowen *et al.* (2002).

Aan het begin van MIS2 (12-24 ka) stijgen de sedimentatiesnelheden echter drastisch (Fig. 4.9, 4.15 en 4.22). Deze episode weerspiegelt een hogere variabiliteit van de BIIS, met meer IRD-toevoer dan enkel IRE1 en 2. Dit zou evenwel een registratie kunnen zijn van een millennium-schalige desintegratie van de BIIS. Grousset *et al.* (2001) hadden eerder al snelle 1-2 ka cycli vermeld bij Europese ijskappen om de gebeurtenissen die de Heinrich Layers voorafgaan en volgen, te kunnen voeden. Bovendien hadden McCabe & Clark (1998) op landsecties eerder al belangrijke oscillaties in de BIIS ontdekt tijdens deze laatste deglaciatie. Dit onderlijnt nogmaals dat de BIIS een langlevend fenomeen was die zich gedroeg al een mobiele en hoog-gevoelige ijskap (Bowen *et al.*, 2002). De Ierse binnenlandse ijskappen begonnen aan een snelle uitbouw na 30 ka, met een maximale omvang rond 24 en 20 ka (Richter *et al.*, 2001). Volgens Bowen *et al.* (2002) heeft deze ijskap

zich definitief teruggetrokken van de shelf rond 25 ka. De koude excursies tijdens IRE1 en 2 zijn dan ook heel uitgesproken in de NPS (Fig. 4.11). Vooral de op het eerste gezicht afwijkende dateringen (in vergelijking met Auffret *et al.* (2002)) voor deze twee gebeurtenissen doen denken dat ze een eerder lokale betekenis hebben en dus meer gekoppeld zijn aan de geschiedenis van de BIIS. Verschillende bronnen vermelden inderdaad twee belangrijke uitbreidingen van de BIIS lang de shelfrand (met daaropvolgende destabilisaties) van 26 tot 18 ka en rond 15 ka (Dowling & Coxon, 2001; Knutz *et al.*, 2002a), wat overeenkomt met de ouderdommen van respectievelijk IRE2 en IRE1. Bowen *et al.* (2002) en McCabe & Clark (1998) suggereerden zelfs een belangrijke deglaciatie van de zuidelijke BIIS rond 17.4 ka, wat zeer goed de  $\delta^{18}\text{O}$  smeltwater pieken na IRE2 verklaart.

### **3 Een stratigrafisch kader voor de oostelijke Porcupine Seabight**

Hoewel deze studie een grote dataset aan hoge-kwaliteits seismische data ter beschikking had, was er geen voldoende ouderdomscontrole van de Paleogene en Neogene afzettingen binnen het bekken. Eerder werd reeds aangetoond dat de basis van de koraalbanken gelegen is op een discontinuïteit (De Mol *et al.*, 2002; Huvenne *et al.*, 2003), van dewelke ouderdom en aard belangrijke informatie zou kunnen verlenen betreffende de initiële kolonisatie van deze koralen en de ontwikkeling van deze mounds. Een betere ouderdomscontrole van deze discontinuïteiten kan ook een vergelijking mogelijk maken van de lokale verantwoordelijke hydrodynamische gebeurtenissen met de heersende (paleo)oceaanografische gebeurtenissen op een grotere (wereldwijde) schaal.

Eerder uitgevoerde studies (McDonnell & Shannon, 2001) brachten deze discontinuïteiten, binnen de Paleogene-Neogene Connaught Megasequentie van het Porcupine Bekken, in verband met de stratigrafie voorgesteld door Stoker *et al.* (2001) voor het nabijgelegen Rockall Trough-bekken. McDonnell & Shannon (2001) erkenden echter ook dat door het ontbreken van vitale Neogene ouderdomsbeperingen een gedetailleerde correlatie tussen de twee bekkens heel speculatief is.

Volgens Pearson & Jenkins (1986) kan een lokale circulatie al een belangrijke invloed uitoefenen op de Cenozoïsche stratigrafische sequenties. Er kan inderdaad vermoed worden dat de bijzondere lokatie van Porcupine Seabight, evenals de nabijheid van de Kwartaire BIIS, de lokale bodemwatercirculatie en de diepmariene erosieve gebeurtenissen kan hebben beïnvloed. De meest nabijgelegen bron om dit te bestuderen is gelegen op Goban Spur (Fig. 5.1). DSDP boring 548 werd hier gebruikt als een kalibratie en werd onderzocht aan de hand van twee loodrecht kruisende zeer hoge-resolutie éénkanaals-seismische profielen. De op deze seismische profielen waargenomen discontinuïteiten werden succesvol gekoppeld aan de lithologische eenheden en hiaten in boring 548.

Deze studie toont echter aan dat de Paleogene tot Neogene stratigrafie van de diepere Rockall Trough niet noodzakelijk volledig toepasbaar is langs de ganse NW Europese rand. Vandaar dat het stratigrafische kaderwerk voorgesteld door Stoker *et al.* (2001) en toegepast door McDonnell & Shannon (2001) voor het Porcupine Bekken is aangepast in een nieuwe, regionale chronostratigrafie, gebaseerd op de observaties langs de DSDP boring 548 op Goban Spur. Dit stond de definiëring toe van enkele belangrijke erosieve gebeurtenissen of regionale discontinuïteiten. Verder

vertonen deze hoge-resolutie data de aanwezigheid van afzettingen en structuren die oorspronkelijk nog niet beschreven werden in de DSDP 548-verslagen (de Graciansky *et al.*, 1984).

Tijdens het Kwartair werden twee belangrijke paleoklimatologische en erosieve gebeurtenissen beschreven: de Midden Pleistocene Revolutie en een Laat Pliocene RD1 gebeurtenis. Beide zijn gekoppeld aan reorganisaties in het globale klimaatsysteem en worden verantwoordelijk geacht voor erosie en afglijdingen. Er werd eveneens een veld van sedimentgolven waargenomen.

RD2 is een vroeg-Midden Miocene discontinuïteit langs de ganse rand en kan worden gekoppeld aan de snelle uitbreiding van de Antarctische ijskap en het opstarten van de huidige oceanische circulatie met intensieve bodemstromingen. Een subtiele discontinuïteit werd waargenomen tussen de Miocene en Pliocene afzettingen, waarschijnlijk gekoppeld aan de Messiniaanse zeespiegeldaling. RD3 verwijst naar een vroege Laat Oligocene, diepe erosieve gebeurtenis, te wijten aan de aanzet van de Antarctische glaciatie. RD4 is een slecht gedocumenteerd Midden Eocene hiaat, veroorzaakt door een combinatie van tektonische en klimatologische gebeurtenissen, zoals de aanzet van de circulatie van het Antarctische bodemwater (AABW). De diepst waargenomen discontinuïteit RD5 staat in verband met het openen van de Noorwegen-Groenland zee en de instroom van koud bodemwater in het Noord-Atlantische domein tijdens het Onder Paleoceen.

#### **4 Seismische stratigrafie van de Belgica mound provincie**

Het beschikbare netwerk van hoge-resolutie seismische profielen staat toe om het regionale seismisch stratigrafische kaderwerk van de Belgica mound provincie te bespreken in een gebied tussen 51°00'N - 51°40'N en 11°20'W - 12°10'W, in waterdiepten tussen 200 en 1500 m (Fig. 6.1). In dit gebied kunnen vier belangrijke seismische eenheden (U4 to U1) worden onderscheiden, gescheiden door drie regionale discontinuïteiten (RD1 tot RD3). Van zowel sedimentologisch als paleoceanografisch oogpunt kan dit gebied als een unieke omgeving in het Noord Atlantische domein worden beschouwd.

##### **4.1 Aanzet van een laat-Paleogene sedimentaire drift**

De weinige profielen die de karakteristieken van eenheid U4 illustreren, suggereren gelijkenissen met grote Noord-Atlantische sedimentdriften (Stow *et al.*, 2002; Faugères *et al.*, 1999). Deze worden meestal afgezet op een erosieve discontinuïteit en tonen een hellingopwaartse migratie. Meer bepaald worden ze regelmatig geassocieerd met velden van grote sedimentgolven (Masson *et al.*, 2002; Howe, 1996). Zulke fijnkorrelige sedimentgolven hebben dikkere afzettingen langs de stroomopwaarts gerichte zijde, wat zowel een stroom- als hellingopwaartse migratie veroorzaakt (Flood & Shor, 1988; Howe, 1996; Wynn & Stow, 2002). De relatie tussen de oriëntatie van de sedimentgolven en de stromingsrichting is echter niet eenvoudig en kan evenwel een schuine migratie toelaten (Wynn & Stow, 2002). Vandaar dat een noordoostelijke migratie binnen eenheid U4 kan wijzen op een noord- tot noordwestelijke stroming.

De ondergrens van deze eenheid is een Midden Eocene RD4 discontinuïteit. Doorheen het late Eoceen en het vroege Oligoceen werd hierop een verlengde

sediment drift afgezet. Tegen het vroege Laat Oligoceen veroorzaakte een algemene zeespiegeldaling de RD3 erosieve discontinuïteit die de Paleogene U4 lagen afsneed.

## 4.2 Vroeg-Neogene sedimentgolven

De meeste U3 lagen weerspiegelen een rustige hemipelagische sedimentaire omgeving. Stratigrafisch gelijkaardige reflectoren, waargenomen op industriële seismische profielen, werden geïnterpreteerd als Vroeg tot Midden Mioceen afzettingen (A. McDonnell, pers. comm.). Op het bovenste gedeelte van de helling, tussen 1.2 tot 1.5 s TWT diepte, verschijnen echter oostelijk tot oost-zuidoostelijk migrerende sigmoïdale afzettingen (Fig. 6.17). Deze zone is gelegen ten zuidwesten van een andere zone, gekarakteriseerd door een noordoostelijk prograderende onlap. Volgens de definities van (Faugères *et al.*, 1999), (Rebesco & Stow, 2001) en (Stow *et al.*, 2002), en naar analogie met de interpretatie van eenheid U4, kan dit worden beschouwd als een begraven verlengde sedimentdrift. Vooral de onlap configuratie langs zijn ondergrens deelt gelijkenissen met de Lofoten drift, beschreven door (Laberg *et al.*, 2002). Alhoewel de geometrie en de migratierichting van deze sedimentlichamen maar werd geschat aan de hand van loodrecht kruisende profielen (Fig. 6.29), kunnen ze worden vergeleken met hellingopwaarts klimmende sedimentgolven. Ediger *et al.* (2002) beschreef een gelijkaardige reeks hellingopwaarts migrerende sedimentgolven, afgezet onder een tegenovergestelde bodemwaterstroming (Fig. 6.29). Dit impliceert de aanwezigheid van een waarschijnlijk Vroeg-Mioceen noord- tot noordwestelijke bodemstroming langs dit gedeelte van de helling. Jammer genoeg werden de meeste U3-afzettingen geërodeerd tijdens het vroege Midden Mioceen, wat een volledig verstaan van de algehele ontwikkeling van deze afzettingen tegenwerkt.

## 4.3 Eenheid U2

Deze eenheid wordt gekenmerkt door een bijna akoestisch transparant seismisch facies en heeft een beperkte laterale uitgestrektheid (Fig 6.30). De westelijke zijde van deze eenheid wordt abrupt beëindigd door een steile wand. Vandaar helt de bovengrens zachtjes en golvend naar beneden. Langs het dikke, zuidoostelijke uiteinde van deze eenheid, vertonen enkele profielen een zuidwaarts hellende discontinuïteit onder de bovengrens van U2. Deze werd opgevuld door een zogenaamde *cut-and-fill* geometrie. Dit suggereert een kleinschalige erosieve gebeurtenis, veroorzaakt door een gerichte en intensieve stroming, gevolgd door een hoog-energetische opvulling.

Alhoewel geen lithologische informatie beschikbaar is over deze eenheid, suggereren zijn distributie en seismisch facies dat het hier gaat over zeer homogene sedimenten. Een reeks interne reflectoren met hoge amplitude zou mogelijks kunnen wijzen op post-depositionele diagenese of een episode zonder afzetting. Het akoestisch transparante karakter van deze eenheid lijkt te verdwijnen naar jongere afzettingen langs de oostelijke bovengrens. Recente waarnemingen op zeer hoge-resolutie seismische profielen van het RCMG lang de DSDP 548 boring op Goban Spur, suggereert dat deze verandering verwant kan zijn met de overgang van het Mioceen naar het Pliocene. Volgens McDonnell & Shannon (2001) werd deze periode gekenmerkt door een diepmariene sedimentatie met de ontwikkeling van een sedimentdrift-lichaam. Een gebrek aan informatie over de geometrie en verspreiding van deze eenheid, door een grootschalige erosie, laat echter niet toe dit te bevestigen.

#### 4.4 RD1 discontinuïteit

Na de afzetting van eenheid U2 was een belangrijke verandering in het oceanografisch regime verantwoordelijk voor een grootschalige erosieve gebeurtenis lang de ganse helling van de Porcupine Seabight. Dit Laat-Pliocene hiaat kan worden geïnterpreteerd als de reïntroductie van het MOW in de NE Atlantische Oceaan en ook als de belangrijker wordende glaciële-interglaciële invloed op de diepwater circulatie (Stow, 1982; Pearson & Jenkins, 1986). Deze RD1 discontinuïteit verwijderde een groot gedeelte van eenheid U2 en liet een zeer onregelmatige terrasachtige paleotopografie achter. Dit suggereert dat deze erosieve gebeurtenis ook verschillende episodes kende. Deze diepe insnijdingen in eenheden U2 en ook U3 zorgden voor de ontwikkeling van zuid-noord gerichte ruggen met steile flanken, die ook nog altijd zichtbaar zijn in de hedendaagse topografie (Fig. 6.6 en 6.30). RD1 heeft ook de basis uitgeschuurd van de Arwen, Celeborn en Galadriel kanalen en snijdt soms diep in Laat-Paleogene afzettingen. Vandaar dat dit uitgebreide erosieve oppervlak grotendeels samenvalt met de bovengrens van eenheid U3.

#### 4.5 Invloed van de Laat-Pliocene omgeving op de groei van koraalbanken

De positie, morfologie en distributie van de Belgica mounds werd eerder al uitvoerig bestudeerd en besproken door De Mol (2002). Deze studie kan echter drie nieuwe mounds toevoegen aan het reeds uitgebreide bestand. Deze Enya mounds werden ontdekt tijdens de Porcupine-Belgica 2003 campagne en zijn gelegen langs de zuidelijke rand van het studiegebied (Fig. 6.30). Ze zijn eveneens gelegen op een dikke U2 eenheid, langs de rand van het eerder beschreven *cut-and-fill* facies. Eén mound is tot 100 ms TWT hoog en ongeveer 800 m breed, begraven onder 50 ms TWT sediment. De andere twee, kleinere mounds zijn beide rond 75 ms TWT hoog en 400 m breed, begraven onder ongeveer 100 ms TWT sediment.

De observaties van deze studie voegen niet veel toe aan die van De Mol (2002) die de Belgica mounds interpreteerde als koraalbanken. Deze studie laat wel toe om de mogelijke invloed van de Laat-Pliocene omgevingsfactoren op de ontwikkeling van de koraalbanken te bespreken. Freiwald *et al.* (1999) en De Mol (2002) wezen er reeds op dat de bouwers van deze koraalbanken, meestal *Lophelia pertusa* en *Madrepora oculata*, verkiezen zich te vestigen op een hard substraat op een verheven ondergrond. Ze hebben sterke bodemstromingen nodig om genoeg nutriënten te verkrijgen, maar ook om zichzelf te vrijwaren van begraving. Op deze manier is enkel en alleen al de aanwezigheid van deze mounds een aanwijzing van (sterke) bodemstromingen na de Laat-Pliocene erosie.

De multibeam kaart (Fig. 6.7) toont dat de Belgica mounds voorkomen in een nauw bathymetrisch interval tussen 700 en 1000 m waterdiepte, opgelijnd als contour-parallelle ruggen. De meeste observaties bevestigen dat de basis van de mounds gelegen is aan een steile flank of een topografische onregelmatigheid in eenheid U3 of U2. Meer bepaald liggen de U3 sedimentgolven meestal rechtstreeks onder de koraalbanken. Recente modellen, gecombineerd met enkele stromingsmetingen en side-scan sonar beelden tonen aan dat de Belgica mound provincie vandaag gelegen is in een gebied dat werd beïnvloed door versterkte stromingen (Pingree & Le Cann, 1989; Pingree & Le Cann, 1990; Rice *et al.*, 1991; New *et al.*, 2001; Akhmetzhanov *et al.*, 2001; White, submitted). Het lijkt er dus op dat sinds het begin van het Neogeen dit gedeelte van de helling onder invloed stond

van versterkte bodemstromingen. Meer bepaald zijn de steile U2 flanken en de veronderstelde harde substraten (bijvoorbeeld de top van de sigmoïdale afzettingen) ideale doelwitten om gekoloniseerd te worden door koudwater koralen. Dit, tesamen met de invloed van krachtige bodemstromingen, zou grotendeels de aanzet van de groei van de koraalbanken geholpen hebben (De Mol *et al.*, 2002).

## 5 Kwartaire sedimentaire processen

De Laat-Pliocene, erosieve RD1 discontinuïteit werd veroorzaakt door het opstarten van moderne oceanografische omstandigheden in de Noord-Atlantische Oceaan (Pearson & Jenkins, 1986; Schnitker, 1986), wanneer de glaciaal-interglaciaal cycli een uitgesproken invloed begonnen uit te oefenen op de productie van het *North Atlantic Deep Water* (NADW), het *Antarctic Bottom Water* (AABW) en het *Norwegian Sea Outflow Water* (NSW). Deze veranderingen hebben geleid tot de variabiliteit van de thermo-haliene circulatie, wat de opbouw en evolutie van de goed bestudeerde sedimentdriften langs de Atlantische randen heeft beïnvloed (Stow, 1982; Faugères *et al.*, 1993). De Belgica mound province is echter gelegen in een relatief kleine inham in deze Noord-Atlantische rand en lijkt niet beïnvloed te zijn door de diepwatercirculatie. Desondanks is er een ingewikkeld oceanografisch regime van versterkte stromingen langs een smalle zone op de helling (Rice *et al.*, 1991). Meer bepaald, werden er tijdens en na RD1 enkele topografische elementen gevormd onder invloed van deze bodemstromingen: (1) de onregelmatige paleotopografie met de steile flanken, ingesneden in beide eenheden U2 en U3, en (2) de Belgica mounds. In dit gedeelte zal, tezamen met de invloed van bodemstromingen, de belangrijkheid van beide elementen worden besproken betreffende de afzetting van de meest recente eenheid U1.

### 5.1 De Arwen & Celeborn-Galadriel kanalen

De basis van deze zuid-noord geörienteerde kanalen werd uitgegraven tijdens de Laat-Pliocene erosie. De Kwartaire sedimentaire structuren tonen aan dat ze evenwel een weg bleven vormen voor bodemstromingen. Aan hun zuidelijke uiteinden zijn deze kanalen dieper en minder bedekt met sedimenten. Dit suggereert de aanwezigheid van een krachtige stroming die afzetting voorkomt. In het noorden worden deze kanalen breder, minder diep en bevatten ze meer sedimenten. De stroming is minder krachtig, maar de vorm van een kanaal is nog altijd aanwezig. Uiteindelijk wijkt het ganse kanaal af naar het noorden en wordt minder diep. De noordwaartse contourstroming is dus als het ware tegen de oostelijke helling van de Seabight geplakt, waar het wordt gedwongen hellingopwaarts te klimmen, intensiteit te verliezen en te verdwijnen. Niettemin kan de bijdrage van hellingafwaarts gerichte stromingen niet worden uitgesloten. Langs dit kanaal werd er een dikke (ongeveer 200 tot 300 ms TWT) levee-eenheid uitgebouwd door lagen die progressief eindigen met een onlap of downlap configuratie, naarmate ze het kanaal naderen. De geometrie van zulke sedimentlichamen deelt meerdere gelijkenissen met drift levees en geassocieerde grachtkanalen, typisch voor de meeste afgescheiden, verlengde sedimentdriften (Fulthorpe & Carter, 1991; Faugères *et al.*, 1999; Stow *et al.*, 2002).

## 5.2 Sedimentaire variabiliteit aan de voet van de mounds

Tussen de kanalen en de mounds is de sedimentaire omgeving beïnvloed door bodemstromingen. Grote, onregelmatige sedimentgolven en levee-afzettingen doen veronderstellen dat er een interactie bestaat tussen contour-parallelle stromingen aan de voet van de mounds en de hellingafwaarts lopende kanaaltjes. Dit verklaart ook de afname van de dikte van eenheid U1 op deze plaats. Aan de andere kant, lijkt het alsof eenheid U1 aan de noordoostelijke en zuid-zuidoostelijke zijde van de mounds wordt afgedamd. Hier gedragen de mounds zich als een barrière, waarachter de Kwartaire sedimenten zich hebben opgestapeld. Dit suggereert dat (1) de stromingen minder krachtig zijn hellingopwaarts van de mounds, (2) de sedimentlading van turbidietstromingen doeltreffend wordt gestopt door de mounds of (3) de sedimentatie enkel wordt toegestaan aan de oostelijke, zijzijde van de mounds. De bodemstroming langs de flank van de mounds, gelegen aan de zijde van de kanalen, lijkt sterker te zijn, zoals wordt geïllustreerd door de turbidieten in kern ENAM-9905. Volgens Faugères *et al.* (1993) en Faugères *et al.* (1999) kunnen steile hellingen (in dit geval de flanken van de mounds) een versterking van de stromingen veroorzaken, verantwoordelijk voor de ontwikkeling van subtiele grachten rond obstakels. In dit geval wordt zulk een depressie gevonden langs de (steile) zuidwestelijke zijde van de mounds. Bovendien worden de mounds begrensd door kleinere kanaaltjes. De meeste kanaaltjes zijn eerder lokaal en lijken enkel de zeebodem dichtbij de mounds te beïnvloeden. Soms wordt zo'n kanaaltje aan de NNW zijde begrensd door een kleine, convexe en lichtjes prograderende levee (Faugères *et al.*, 1999). Dit wordt echter niet waargenomen aan de SSE zijde van de mound, waar eerder aggradatie gebeurt. In het algemeen kunnen deze kanaaltjes geïnterpreteerd worden als kleine turbidietkanaaltjes (Fig. 6.58), verantwoordelijk voor het afzetten van turbidieten aan de voet van een mound. Bij turbidietstromingen in het noordelijke halfmond wordt meestal een levee opgebouwd aan de rechterhandzijde van deze stroming (Faugères *et al.*, 1999). In dit geval is de aanwezigheid van een mound aan deze zijde net een beperkende factor, die de opbouw van een levee verhindert. De invloed van een eventuele noordwaarts gerichte stroming in de vorming van de kanaaltjes ten zuiden van de mound kan echter niet worden uitgesloten. Deze bodemstromingen kunnen wel het lokale karakter van deze kanaaltjes uitleggen. Aan de lager gelegen gedeelten van deze kanaaltjes is de energie van deze noordwaarts gerichte bodemstromingen sterker. Bijgevolg zal deze het hellingafwaarts getransporteerde materiaal opnemen en verdelen over een vervlakte zeebodem langs de voet van de mounds. Dit kan gezien worden als mobiele zanden, waargenomen in de top van kern ENAM-9905 en de side-scan sonar beelden.

## 5.3 Laat Kwartaire variabiliteit van de hydrodynamische omgeving

Vele observaties in en rond de Belgica mounds duiden op een hedendaagse zeer actieve hydrodynamische omgeving. Een boxcore staal van de MD99-2327 site bevestigt de aanwezigheid van een kwartsrijk, door de stroming gesorteerd foraminiferenrijk zand, wat geïnterpreteerd kan worden als een zandige contouriet.

Vele parameters wijzen erop dat kern MD99-2327 bestaat uit contourieten. De glaciële eenheid voldoet aan de vele voorwaarden van het modderige contouriet facies, gedefinieerd door Faugères *et al.* (1984), Rebesco & Stow (2001) en Stow *et al.* (2002). Deze eenheid bestaat hoofdzakelijk uit een siliciklastische, fijnkorrelige

kleiige silt (Fig. 6.63). Voorzichtigheid is echter geboden aangezien een belangrijk gedeelte van het aanwezige silt en zand afkomstig kan zijn van *ice-rafting*. Enkel sporadisch werden primaire sedimentaire structuren gevonden, want het grootste gedeelte van de kern is structuurloos. De X-straalbeelden bevestigen een uitvoerige bioturbatie met *planolites*, *mycelia* en *chondrites* omwoelingen (Fig. 6.64).

De grote verstrooiing van de stabiele zuurstof- en koolstof-isotopen data wijst erop dat de meeste van de foraminiferen werden herwerkt. Alle analyses tonen aan dat de aard en karakteristieken van de beide interglaciale eenheden (MIS1 en 5) gelijkaardig zijn, wat erop kan wijzen dat ze door eenzelfde sedimentair proces werden afgezet. Met andere woorden waren de sedimentaire en hydrodynamische omgeving in beide tijden gelijkaardig. De meeste zandige contourieten worden geobserveerd in een morfotektonisch speciale omgeving, waar ze een mengeling zijn van terrigene en biogene deeltjes die eveneens abrasie en fragmenten van bioklasten vertonen (Faugères & Stow, 1993; Stow *et al.*, 2002). Zeer dikke, structuurloze grofkorrelige afzettingen zoals deze zijn uiterst zeldzaam in deze soort omgeving en kunnen volgens Stow & Mayall (2000) geklasseerd worden als een diepwater massief zand (DWMS). De algemene karakteristieken van zulke DWMS werden gedefinieerd door Stow & Johansson (2000) en komen overeen met de karakteristieken van de MIS5 sedimenten. Het zijn slecht tot matig gesorteerde zanden en ze tonen een hoge graad van herwerking. Voorbeelden van zandige contourieten zijn zeldzaam en worden meestal gevonden in morfologisch en hydrodynamisch speciale gebieden met variabele stromingen (Habgood *et al.*, 2003; Stow & Johansson, 2000). In het algemeen, is de tot nu toe gerapporteerde grootte van een zandige contouriet of DWMS zelden groter dan 1 m (Stow & Johansson, 2000). Binnen deze morfologische en sedimentaire context is de aanwezigheid van een 10 m dikke zandige contouriet dan ook uniek.

Alhoewel geen eenvoudige globale invloed van het klimaat op de activiteit van bodemstromingen kan worden gevonden, is het aannemelijk dat de overgang van zandige naar modderige contourieten gekoppeld kan worden aan paleoklimatologische gebeurtenissen. Recente waarnemingen van Akhurst *et al.* (2002) beschrijven ook de aanwezigheid van zandige contourieten op de helling van de Hebriden tijdens interglacialen en interstadialen, gekoppeld aan een versterkte bodemstromingactiviteit. Tegelijkertijd erkenden ze ook dat tijdens ijstijden de activiteit van deze bodemstromingen minder intens is.

Aangezien de versterkte stromingen in de Belgica mound provincie sterk afhankelijk is van de aanwezigheid van het *Mediterranean Outflow Water* (MOW) (De Mol *et al.*, 2002; New *et al.*, 2001; White, submitted), lijkt het aannemelijk dat tijdens ijstijden het stromingsregime sterk verzwakt was. De verminderde uitstroom van het MOW was toen enkel beperkt tot de Golf van Cadiz en penetreerde niet verder in het Atlantische domein (Schönfeld & Zahn, 2000). De variabiliteit binnen de glaciële contouriet is echter minder duidelijk. De meeste *peak current events* (PCE) lijken gelijktijdig te zijn met warmere perioden voor en na een IRE. Deze gebeurtenissen zijn ook gerelateerd aan een verhoogd voorkomen van enkele benthische foraminiferen zoals *U. mediterranea* en *P. ariminensis*. In kern MD99-2327 worden maximale aantallen van deze species waargenomen tijdens de warme perioden MIS5 en MIS1. Schönfeld (2002) en Schönfeld & Zahn (2000) deelden deze species al eerder in bij de epibenthische groep, die grotendeels afhankelijk is van snelstromend water in een kern van MOW. Tijdens warmere klimatologische

perioden (interstadialen), zou de zeespiegel iets hoger kunnen zijn, meer bepaald na een pan-Atlantische *ice-rafting event*. Dit zou een verhoogde MOW productie met zich kunnen hebben meegebracht, zodat het ook verder in de Atlantische Oceaan kon, om zo kleinere pulsen van versterkte stromingen teweeg te brengen in de Porcupine Seabight.

#### 5.4 Small mounded drifts

De sedimentologische studie van kern MD99-2327 toonde reeds aan dat het sedimentlichaam, gelegen tussen de mounds en de steile flanken van eenheid U2, een contouriet drift is (Fig. 6.59). Het vertoont vele gelijkenissen met de welgekende contouriet drift systemen, zoals een stromingafwaartse verlenging, sub-regionale discontinuïteiten en sub-parallelle gematigde tot lage-amplitude reflectoren met geleidelijke veranderingen in seismisch facies (Faugères *et al.*, 1999; Rebesco & Stow, 2001; Stow *et al.*, 2002). De beste vergelijking kan worden gemaakt met de Sumba drift, waar door een laterale verandering in stromingssnelheid, modderige contourieten werden afgezet in het centrale gedeelte en zandige contourieten langs de flanken (Reed *et al.*, 1987). De aard van de bathymetrische randvoorwaarden, die verantwoordelijk zijn voor de versnelling van deze diepe stromingen, zijn echter helemaal verschillend. Daar waar de Sumba drift en andere *beperkte* driften worden aangetroffen in een tektonisch gecontroleerde setting, wordt in dit geval de interactie tussen stromingen en bathymetrie bepaald door een combinatie van een turbulente sedimentaire geschiedenis met verscheidene fazen van erosie en de koraalbanken.

Gebaseerd op een voorlopig ouderdomsmodel en de dikte van de contouriet drift, kan de ouderdom van deze drift worden geschat op 1.2 Ma. In het algemeen wordt verondersteld dat de afzetting van de drift mound begon ergens tijdens het midden van het Vroege Pleistoceen, terwijl de ondergrens van U1 een veronderstelde Laat Pliocene ouderdom heeft. Dit betekent dat tussen het begin van de ontwikkeling van de koraalbanken en de afzetting van de contouriet drift, er een belangrijke periode was zonder sedimentatie (Fig. 6.73a en 6.73b). Deze periode laat genoeg tijd over voor de “start-up” fase van de koraalbanken. Zulke periode werd door De Mol *et al.* (2002) vereist, zodoende dat de koralen zich konden vestigen op het harde en onregelmatige RD1 substraat in een omgeving van versterkte stromingen (Fig. 6.73c). Vanuit een paleoceanografisch oogpunt kan ervan worden uitgegaan dat een contourietische sedimentatie goed en wel op gang was getrokken tijdens een belangrijke klimatologische verandering binnen het Pleistoceen. De Midden Pleistocene Revolutie (MPR, ~940-640 ka) wordt aanzien als het begin van de toename van het gemiddelde globale ijsvolume en een toenemende amplitude van de 100 ka klimatologische cycli (Hernandez-Molina *et al.*, 2002; Raymo *et al.*, 1997). Door deze MPR werden de pulsaties tussen glaciale en interglaciale periodes meer uitgesproken en kunnen ze aan de basis liggen van zowel de start van afwisselend modderige en zandige contourietafzetting in het Belgica mound gebied, als van de variaties van de akoestische amplitudes binnen de seismische eenheid U1.

Aangezien de aanwezigheid van versterkte stromingen strikt gebonden is aan de interactie tussen de lokale morfologie en hydrologie, kunnen we besluiten dat de aanwezigheid van een contourietdrift zeer lokaal en uniek is, afhankelijk van een aantal geologische, klimatologische, biologische en hydrodynamische variabelen. Daarom gaan we ervan uit dat het vinden van een even belangrijke afzetting buiten de Belgica mound provincie niet evident is. De Kwartaire sedimenten in andere

mound provincies zoals de Hovland en Magellan mound provincie, werden afgezet in een omgeving van zwakkere stromingen en kunnen beschouwd worden als gewone sedimentdriften (De Mol *et al.*, 2002; Huvenne *et al.*, 2002).

### 5.5 De Enya mound drift

In dit gebied vertoont de morfologie van de zeebodem een 4 km lang, duidelijk zuid-noord gericht verlengd kanaal met een breedte van ongeveer 500 m (Fig. 6.68). Ten westen van dit kanaal kan een convexe, verlengde morfologie worden geobserveerd. Op de seismische profielen is dit convexe sedimentlichaam gelegen tussen mounds en een steile flank in de bovengrens van eenheid U2. Boven de mounds toont het overliggende sedimentpakket een convergentie van reflectoren, wat wijst op de invloed van stromingen. Dit bevestigt dat in een zulke omgeving de U1 sedimentatie begon na de installatie van de plaatselijke koraalbanken.

Een bijkomend element zou echter meer informatie kunnen geven betreffende het ontstaan van de Enya mounds. Op seismische profielen en side-scan sonar beelden (Figs. 6.68 and 6.72), kunnen pockmarks worden geobserveerd. Volgens Huvenne (2003) bedraagt de gemiddelde diameter van deze pockmarks rond de 140 m, wat relatief groot is (Paull *et al.*, 2002). Pockmarks zijn krater-achtige depressies, gevonden in fijnkorrelige, zachte sedimenten. In het algemeen, worden ze gevormd door opwaartse fluïda migratie doorheen de sedimenten. Deze fluïda zijn meestal gas of zelfs poriënwater (Hovland & Judd, 1988; Jensen *et al.*, 2002; Paull *et al.*, 2002). De aanwezigheid van deze pockmarks in deze specifieke zone verwijst duidelijk naar een zeer gerichte *fluid seepage*. Volgens Paull *et al.* (2002) komen de meeste pockmarks voor boven grote koolwaterstofprovincies. Alhoewel in dit gedeelte van het Porcupine Bekken de aanwezigheid van koolwaterstoffen nog niet volledig kon worden aangetoond, veronderstellen Croker & Shannon (1995) en Johnston *et al.* (2001) de aanwezigheid van reservoir in waarschijnlijk diepe Permo-Trias zandstenen. Zodoende kunnen de pockmarks gekoppeld worden aan het lekken van thermogeen gas uit deze mogelijke reservoirs. Aan de andere kant is het ten minste merkwaardig dat deze mounds voorkomen boven een *cut-and-fill* facies die eerder werd beschreven in eenheid U2. In de Magellan mound provincie, beschreef Huvenne (2003) ook de aanwezigheid van mounds boven een gelijkaardig facies. Dit werd echter eerder geassocieerd met de expulsie van biogeen gas en poriënwater, gekoppeld aan de snelle, hoog-energetische afzettingen van het *cut-and-fill* facies. Zowel de rol van thermogeen gas, poriënwater en biogeen gas kan niet worden uitgesloten bij de Enya mounds. Het steile, zuidwaarts hellende erosieve oppervlak onder deze Enya mounds zou eventueel een soort geleidingsvlak kunnen zijn voor de migratie van deze fluïda.

In ieder geval kan de aanwezigheid van de Enya mounds worden gekoppeld aan zowel de aanwezigheid van een dynamische hydrologische omgeving als fluïda migratie. Alhoewel de rol van fluïda migratie altijd werd verondersteld voor de Porcupine mounds (Henriet *et al.*, 2001), werd hun rol in de ontwikkeling van de Belgica koraalbanken nog niet volledig aangetoond (De Mol, 2002). Alle observaties wijzen erop dat de ontwikkeling van de Belgica mounds eerder kan worden toegeschreven aan omgevingsfactoren zoals stromingen (De Mol, 2002; Kenyon *et al.*, 2003; Huvenne, 2003). Daarom kunnen de waarnemingen in het Enya mound gebied als een uniek samenspel kunnen worden beschouwd tussen de invloed van stromingen aan de ene kant en fluïda migratie aan de andere kant.

## 6 Structuur en ontwikkeling van het Gollum kanalen systeem

### 6.1 Aanwijzing voor de ontwikkeling van de Kingskanalen

De waarnemingen in de Kingskanalen wijzen erop dat de erosie, verantwoordelijk voor het insnijden van deze brede kanalen, heeft plaats gevonden voor de afzetting van eenheid U1 en na de afzetting van U2. Vandaar dat het aannemelijk lijkt dat dit werd veroorzaakt door de Laat-Pliocene RD1 gebeurtenis. Hierdoor werden grote, hellingsafwaarts gerichte depressies ingesneden. Sommige elementen wijzen ook op de invloed van mogelijke syn-sedimentaire breuken. De hedendaagse loop van deze kanalen lijkt strikt de baan te volgen die werd uitgesneden door de RD1 erosie. Tijdens het Kwartair was echter de sterkte van deze hellingafwaartse stromingen heel wisselvallig. Ten eerste vertoont het bovenste gedeelte van het Theoden kanaal verschillende episodes van insnijding of verplaatsing van de stroming. Ten tweede illustreert de aanwezigheid van een grote levee in het Aragorn kanaal dat naar recente tijden toe, enkel een relatief minder intense turbidietstroming actief was. Behalve langs de noordelijke flank van het Aragorn kanaal, is de sedimentatie aan de andere flanken aanzienlijk beïnvloed door deze turbiditeitstromingen. Ze groeiden tezamen met de afzettingen in de kanalen, als hun geassocieerde levee. Buiten het bereik van deze stromingen werden redelijk dikke hemipelagische sedimenten afgezet op een dikke U2 eenheid langs de bovenste helling van de Aragorn, Boromir en Faramir kanalen.

Niet enkel turbiditische processen werden waargenomen in dit gebied. Langs steilere hellingen wijzen oude afglijdingsvlakken op frequente, volumineuse destabilisaties. Alhoewel maar weinig data beschikbaar is in dit Denethor gebied, lijkt de Kwartaire sedimentaire omgeving beïnvloed te zijn door insnijdingen en afglijdingen. Zoals op Goban Spur, suggereert dit een drastische fase van hellingsinstabiliteiten binnen het Pleistoceen. Waarschijnlijk heeft een combinatie van een sterk hydrodynamisch regime met turbidietstromingen, veranderende Pleistocene zeespiegels, een overgeërfde onregelmatige paleotopografie en een verhoogde sediment druk geleid tot regelmatige destabilisaties in het Pleistoceen. Er zijn echter meer seismische profielen en kernen nodig om de Neogene ontwikkeling van dit gebied volledig te verstaan.

### 6.2 Sedimentaire processen in de Gollum kanalen

Zoals de Kingskanalen, is het Gollum kanalen systeem (GCS) waarschijnlijk begonnen als een canyon systeem, ingesneden door de Laat-Pliocene RD1 gebeurtenis. In het vroeg-Kwartair waren deze canyons belangrijke geleiders voor de sedimenttransfer van de shelf naar het diepmariene bekken. Zoals werd gesuggereerd door Leeder (1999), heeft dit vooral plaats gevonden tijdens (glaciale) zeespiegel laagstanden. In een klassieke diepzee fan configuratie, gaan deze submariene canyons geleidelijk over naar kanalen en een depositionele fan (Einsele, 1992; Weaver *et al.*, 2000).

Het huidige aanzicht van het bovenste gedeelte van deze kanalen is eerder U-vormig, maar de algemene opbouw en de heersende sedimentaire processen zoals afglijdingen zijn gelijkaardig aan wat in canyons wordt waargenomen. Weaver *et al.* (2000) hadden eerder al de plattegrond van de GCS vergeleken met die van een dendritisch canyon systeem. De hoge flanken van deze kanalen lijken hoofdzakelijk

opgebouwd te zijn door een hemipelagische sedimentatie, eerder dan de *overspill* van turbidietstromingen of actieve erosie. Daarom kan dit bovenste gedeelte van het GCS geïnterpreteerd worden als een overgang van canyon naar kanaal. De oriëntatie van zulk kanalsysteem kan ook beïnvloed worden door breuken, alhoewel alleen enkele morfologische elementen deze theorie kunnen steunen.

De sedimentaire inhoud van kern MD01-2464 bevestigt de hypothese dat dit kanalsysteem enkel actief was tijdens glaciële laagstanden. De sedimenten van deze kern illustreren, tezamen met de seismische opbouw van de kanaalbodem (Fig. 7.17 en 7.19), een typische opvulling van kanalen gelegen op de bovenste helling. Volgens Stow & Piper (1984) worden in een zulke omgeving normaal gezien modderige sedimenten in plaats van grofkorrelige afzettingen afgezet. De seismische profielen tonen inderdaad dat de kanaalbodem is opgevuld met de producten van afglijdingen en debrieten, maar dus ook met modderige turbidieten en hemipelagieten in een eerder chaotische verticale sequentie. Volgens de definitie van Prather (2003) kan zulke setting worden vergeleken met een typische *perched* (hangende) helling opvulling. Dit is één van de belangrijke accommodatie types op de helling, die een essentieel element kunnen zijn in het beïnvloeden van de distributie, kwaliteit en opbouw van submariene koolwaterstoffenreservoirs.

Al deze waarnemingen dragen bij aan de visie van Weaver *et al.* (2000) die het *Madeira Distributary Channel System* (MDCS) vergelijkt met het Gollum kanalen systeem. Zowel de MDCS canyons en de bovenste kanalen van de GCS reiken niet tot aan de shelfrand en komen zelden hellingafwaarts. Beide systemen werden gevormd tijdens zeespiegellaagstanden op hoofdzakelijk hellingen van 3°. Daarenboven zorgt een subtiele afname in de zeebodemgradiënt voor een belangrijke invloed op de hellingsprocessen. Na een verandering van 3° naar 1°, maken de ingesneden kanalen plaats voor een kanalsysteem met levees die stroomafwaarts verder vertakt over een submariene fan. De recente waarnemingen van Akhmetzhanov *et al.* (2003) op de Porcupine Abyssale Vlakte ondersteunt inderdaad de hypothese van de ontwikkeling van een submariene fan aan het einde van het Gollum kanaal.

Zulke diepzee kanalsystemen worden meestal ook vergezeld door de aanwezigheid van turbiditische sedimentgolven (Weaver *et al.*, 2000; Wynn *et al.*, 2000; Nakajima & Satoh, 2001). Deze *mudwaves* hebben typisch toppen parallel of subparallel aan de kanaalranden en de topografische contouren van de achterzijde van de levee. Volgens Wynn & Stow (2002) worden deze afgezet door niet-begrensde fijnkorrelige turbiditische stromingen. De diepst gelegen profielen tonen inderdaad een ideale omgeving voor de afzetting van zulke sedimentgolven. Ze werd echter op één profiel waargenomen, wat vraagt om meer onderzoek.

## **7 Conclusie: een Laat-Cenozoïsch ontwikkelingsmodel van de oostelijke Porcupine Seabight, ten zuidwesten van Ierland**

De vroegst mogelijke gegevens in dit model komen uit het Midden Eoceen. Een combinatie van tektonische en klimatologische gebeurtenissen, zoals de start van het AABW regime, was verantwoordelijk voor een Midden Eocene RD4 erosie langs de oostelijke helling van de Porcupine Seabight. De seismische karakteristieken van deze afzettingen wijzen op de aanwezigheid van

bodemstromingen in het Boven Eoceen. Deze slecht gedocumenteerde afzettingen hebben een vroege Laat-Oligocene bovengrens, gekoppeld aan een diepe erosieve gebeurtenis door de initiatie van de Antarctische glaciatie (RD3). De overliggende U3 eenheid vertoont een gelijkaardige situatie. Aan de andere kant, werd er een grote zone van onlap op de U3 ondergrens waargenomen, dewelke vele karakteristieken deelt met de Noord-Atlantische sedimentdriften. Meer bepaald werd hellingafwaarts van een onderbreking in de paleohelling, in een beperkte zone van een constante diepte, er een grote zone van waarschijnlijk oostwaarts migrerende sedimentgolven waargenomen. Dit suggereert dat op dit gedeelte van de helling er tijdens het Onder-Mioceen een N- tot NW-gerichte bodemstroming aanwezig was. Tijdens de onderste helft van het Midden Mioceen was de introductie van het *Norwegian Sea Water* in de Noord Atlantische Oceaan verantwoordelijk voor de erosie van deze sedimentdrift.

Na deze RD2 erosie, werd over de ganse helling een lokaal heel dikke, akoestisch transparante eenheid U2 afgezet, met een nog ongekennde lithologie. Een verandering in het seismische facies nabij de top van deze eenheid wordt verondersteld de Mioceen-Pliocene grens te zijn, zoals op Goban Spur. Door een grote verandering in oceanografisch regime, was de grootschalige Laat-Pliocene RD1 erosie verantwoordelijk voor het verwijderen van een groot gedeelte van eenheden U2, U3 en zelfs U4. Tijdens deze gebeurtenis werd de loop van de grote, hedendaagse kanalen vastgelegd. In het zuidelijke gedeelte van het bekken werd de steile helling ingesneden door canyons. Naar het noorden toe heeft een verondersteld zuid-noord gerichte stroming een terras-achtige paleotopografie ingesneden, met de as van het Arwen kanaal als zijn diepste punt. Er zijn eveneens elementen die wijzen op een mogelijke tektonische invloed op de loop, morfologie en sedimentatie van al deze kanalsystemen.

Volgend op deze Laat-Pliocene erosie, begonnen koralen zich te vestigen op topografische onregelmatigheden langs de oostelijke zijde van het Arwen kanaal. De koraalbanken werden relatief snel gebouwd in een periode van het Laat Pliocene naar het midden Vroeg Pleistoceen, wanneer er in de naburige omgeving geen sedimenten werden afgezet. Ze zijn gelegen in een zone die beïnvloed is door een ingewikkeld systeem van versterkte stromingen. In dit geval zijn deze stromingen de belangrijkste drijfveer die de ontwikkeling van de mounds controleert. In het zuidelijke gedeelte van dit studiegebied werden drie nieuwe Enya mounds waargenomen boven een *cut-and-fill* facies. Alhoewel er een belangrijke invloed lijkt geweest te zijn door stromingen, doet de aanwezigheid van pockmarks sterk denken aan de invloed van fluïda migratie.

Deze zeer turbulente periode is ook het begin van uitgesproken glaciaal-interglaciaal cycli en hun invloed op de diepwater circulatie. In de Gollum en Kingskanalen werd dit gekenmerkt door een verhoogde toevoer van terrigeen materiaal, die het Gollum diepzee fan complex hebben opgebouwd. De Konigskanalen werden ook beïnvloed door turbiditeitstromingen, maar hier kan er geen verbinding worden gemaakt met een diepzee fan. Beide systemen leken enkel actief te zijn geweest tijdens glaciële laagstanden, terwijl tijdens interglaciële periodes er hoofdzakelijk een hemipelagische sedimentaire omgeving was, met lokale invloeden van bodemstromingen. In het algemeen hebben hoge sedimentatiesnelheden ertoe geleid dat een zeer dikke eenheid werd opgebouwd langs de bovenste helling. Langs de flanken van deze kanalen, kan dit uiteindelijk geleid hebben tot afglijdingen. Aan de andere kant werden grote (gelijktijdige?)

afglijdingen op Goban Spur in verband gebracht met een Midden Pleistocene versterking van de variabiliteit van het klimaat.

In het noordelijke gedeelte van het studiegebied nemen de sedimentatiesnelheden echter af en wordt de geometrie van de Kwartaire eenheid heel variabel, wat een verhoogde invloed van bodemstromingen betekent. Dit betekent ook dat, in tegenstelling tot eerdere suggesties, de sedimenten die vervoerd werden door de Gollum en Kingskanalen, niet beduidend werden herverdeeld over de ganse Porcupine Seabight. De mobilisatie en herverdeling van sediment is echter beduidend hoger in de Belgica mound provincie, waar sedimentdriften werden afgezet in relatie met het Arwen kanaal en de koraalbanken. Er is zelfs genoeg bewijs gevonden van een ingewikkelde samenwerking tussen contouritische en turbiditische processen. In het centrale gedeelte van het Belgica mound gebied is de sedimentatie enkel maar begonnen tijdens het vroege Midden Pleistoceen. Een kleine, beperkte contourietdrift werd afgezet in een nauwe doorgang tussen koraalbanken en een steile flank in de paleotopografie. De versterkte variabiliteit tussen de interglaciale en glaciële periodes veroorzaakten ook een lithologische variabiliteit met de afzetting van respectievelijk zandige en modderige contourieten. Dit kan ook worden gelezen in de verticale variaties van de seismische amplitudes binnen deze contouriet drift.

## Referenties

- Akhmetzhanov, A. M., Kenyon, N. H., Nielsen, T., Habgood, E., Ivanov, M. K., Henriët, J.-P. & Chachkine, P. (2001) Deep-sea bottom current depositional systems with active sand transport on the north-eastern Atlantic Margin. In: *Geological Processes on Deep-Water European Margins* (Ed. by M. K. Ivanov and S. Bourriak), pp. 14-15. Moscow State University, Moscow/Mozhenka, Russia.
- Akhurst, M. C., Stow, D. A. V. & Stoker, M. S. (2002) Late Quaternary glacial contourite, debris flow and turbidite process interaction in the Faroe-Shetland Channel, NW European Continental Margin. In: *Deep-Water Contourite Systems: Modern Drifts and Ancient Series, Seismic and Sedimentary Characteristics* (Ed. by D. A. V. Stow, C. J. Pudsey, J. A. Howe, J.-C. Faugères and A. R. Viana), Geological Society, London, *Memoirs*, 22, 73-84.
- Armishaw, J. E., Holmes, R. W. & Stow, D. A. V. (2000) The Barra Fan: A bottom-current reworked, glacially-fed submarine fans system. *Marine and Petroleum Geology*, 17, 219-238.
- Auffret, G. A., Pujol, C., Baltzer, A., Bourillet, J. F., Müller, C. & Tisot, J. P. (1996) Quaternary sedimentary regime on the Berthois Spur (Bay of Biscay). *Geo-Marine Letters*, 16, 76-84.
- Auffret, G. A., Zaragosi, S., Dennielou, B., Cortijo, E., Van Rooij, D., Grousset, F. E., Pujol, C., Eynaud, F. & Siegert, M. (2002) Terrigenous fluxes at the Celtic margin during the last glacial cycle. *Marine Geology*, 188, 79-108.
- Bond, G., Heinrich, H., Broecker, W. S., Labeyrie, L. D., McManus, J., Andrews, J. T., Huon, S., Jantschik, R., Clasen, S., Simet, C., Tedesco, K., Klas, M., Bonani, G. & Ivy, S. (1992) Evidence for massive discharges of icebergs into the North Atlantic ocean during the last glacial period. *Nature*, 360, 245-249.
- Bowen, D. Q., Phillips, F. M., McCabe, A. M., Knutz, P. C. & Sykes, G. A. (2002) New data for the Last Glacial Maximum in Great Britain and Ireland. *Quaternary Science Reviews*, 21, 89-101.
- Broecker, W. S., Bond, G., Klas, M., Clark, E. & McManus, J. (1992) Origin of the Northern Atlantic's Heinrich Events. *Climate Dynamics*, 6, 265-273.
- Chachkine, P. & Akhmetzhanov, A. M. (1998) Subbottom currents on the Porcupine Margin study by side-scan sonars. In: *Geosphere-biosphere coupling: Carbonate Mud Mounds and Cold Water Reefs* (Ed. by B. De Mol), UNESCO, Paris, IOC Workshop Report, 143, 30.
- Chi, J. & Mienert, J. (1996) Linking physical property records of Quaternary sediments to Heinrich events. *Marine Geology*, 131, 57-73.
- Croker, P. F. & Shannon, P. M. (1995) The petroleum geology of Ireland's offshore basins: introduction. In: *The Petroleum Geology of Ireland's Offshore Basins* (Ed. by P. F. Croker and P. M. Shannon), Geological Society, London, Special Publication, 93, 1-8.
- de Graciansky, P. C., Poag, C. W., Cunningham, R., Loubere, P., Masson, D. G., Mazzullo, J. M., Montadert, L., Müller, C., Otsuka, K., Reynolds, L. A., Sigal, J., Snyder, S. W., Townsend, H. A., Vaos, S. P. & Waples, D. (1984) Initial Reports of the Deep Sea Drilling Project. U.S. Government Printing Office, Washington.
- De Mol, B. (2002) Development of coral banks in Porcupine Seabight (SW Ireland): A multidisciplinary approach. Ph.D. thesis, Department of Geology and Soil Science. Ghent University, Gent, 363 pp.
- De Mol, B., Van Rensbergen, P., Pillen, S., Van Herreweghe, K., Van Rooij, D., McDonnell, A., Huvenne, V., Ivanov, M., Swennen, R. & Henriët, J.-P. (2002) Large deep-water coral banks in the Porcupine Basin, southwest of Ireland. *Marine Geology*, 188, 193-231.
- Dowling, L. A. & Coxon, P. (2001) Current understanding of Pleistocene temperate stages in Ireland. *Quaternary Science Reviews*, 20, 1631-1642.
- Ediger, V., Velegrakis, A. F. & Evans, G. (2002) Upper slope sediment waves in the Cilician Basin, northeastern Mediterranean. *Marine Geology*, 192, 321-333.
- Faugères, J.-C., Gonthier, E. & Stow, D. A. V. (1984) Contourite drift molded by deep Mediterranean outflow. *Geology*, 12, 296-300.

- Faugères, J.-C., Mézerais, M. L. & Stow, D. A. V. (1993) Contourite drift types and their distribution in the North and South Atlantic Ocean basins. *Sedimentary Geology*, 82, 189-203.
- Faugères, J.-C. & Stow, D. A. V. (1993) Bottom-current-controlled sedimentation: a synthesis of the contourite problem. *Sedimentary Geology*, 82, 287-297.
- Faugères, J.-C., Stow, D. A. V., Imbert, P. & Viana, A. R. (1999) Seismic features diagnostic of contourite drifts. *Marine Geology*, 162, 1-38.
- Flood, R. D. & Shor, A. N. (1988) Mud waves in the Argentine Basin and their relationship to regional bottom circulation patterns. *Deep-Sea Research*, 35(6), 943-971.
- Freiwald, A., Wilson, J. B. & Henrich, R. (1999) Grounding Pleistocene icebergs shape recent deep-water coral reefs. *Sedimentary Geology*, 125, 1-8.
- Fulthorpe, C. S. & Carter, R. M. (1991) Continental-shelf progradation by sediment-drift accretion. *Geological Society of America Bulletin*, 103, 300-309.
- Games, K. P. (2001) Evidence of shallow gas above the Connemara oil accumulation, Block 26/28, Porcupine Basin. In: *The Petroleum Exploration of Ireland's Offshore Basins* (Ed. by P. M. Shannon, P. Haughton and D. Corcoran), Geological Society, London, Special Publication, 188, 361-373.
- Grousset, F. E., Cortijo, E., Huon, S., Hervé, L., Richter, T. O., Burdloff, D., Duprat, J. & Weber, O. (2001) Zooming in in Heinrich layers. *Paleoceanography*, 16(3), 240-259.
- Grousset, F. E., Labeyrie, L. D., Sinko, J. A., Cremer, M., Bond, G., Duprat, J., Cortijo, E. & Huon, S. (1993) Pattern of ice-rafted detritus in the glacial North Atlantic. *Paleoceanography*, 8(2), 175-192.
- Grousset, F. E., Pujol, C., Labeyrie, L. D., Auffret, G. A. & Boelaert, A. (2000) Were the North Atlantic Heinrich events triggered by the behavior of the European ice sheets? *Geology*, 28(2), 123-126.
- Habgood, E., Kenyon, N. H., Masson, D. G., Akhmetzhanov, A. M., Weaver, P. P. E., Gardner, J. & Mulder, T. (2003) Deep-water sediment wave fields, bottom current sand channels and gravity flow channel-lobe systems: Gulf of Cadiz, NE Atlantic. *Sedimentology*, 50, 483-510.
- Hall, I. R. & McCave, I. N. (1998) Glacial-interglacial variation in organic carbon burial on the slope of the N.W. European Continental Margin. *Progress in Oceanography*, 42, 37-60.
- Henriet, J.-P., De Mol, B., Pillen, S., Vanneste, M., Van Rooij, D., Versteeg, W., Croker, P. F., Shannon, P. M., Unnithan, V., Bouriak, S., Chachkine, P. & The Porcupine-Belgica 97 Shipboard Party. (1998) Gas hydrate crystals may help build reefs. *Nature*, 391, 648-649.
- Henriet, J.-P., De Mol, B., Vanneste, M., Huvenne, V., Van Rooij, D. & the "Porcupine-Belgica" 97, a. s. p. (2001) Carbonate mounds and slope failures in the Porcupine Basin: a development model involving past fluid venting. In: *The Petroleum Exploration of Ireland's Offshore Basins* (Ed. by P. M. Shannon, P. Haughton and D. Corcoran), Geological Society, London, Special Publication, 188, 375-383.
- Hovland, M. & Judd, A. G. (1988) Seabed pockmarks and seepages, impact on geology, biology and the environment. Graham & Trotman Ltd., London, 293 pp.
- Howe, J. A. (1996) Turbidite and contourite sediment waves in the northern Rockall Trough, North Atlantic Ocean. *Sedimentology*, 43, 219-234.
- Huvenne, V. A. I. (2003) Spatial geophysical analysis of the Magellan carbonate build-ups and the interaction with sedimentary processes: key to a genetic interpretation? Ph.D. thesis, Department of Geology and Soil Science. Ghent University, Gent, 285 pp.
- Huvenne, V. A. I., De Mol, B. & Henriet, J.-P. (2003) A 3D seismic study of the morphology and spatial distribution of buried coral banks in the Porcupine Basin, SW of Ireland. *Marine Geology*, 198, 5-25.
- Jensen, J. B., Kuijpers, A., Bennike, O., Laier, T. & Werner, F. (2002) New geological aspects for freshwater seepage and formation in Eckernförde Bay, western Baltic. *Continental Shelf Research*, 22, 2159-2173.

- Johnston, S., Doré, A. G. & Spencer, A. M. (2001) The Mesozoic evolution of the southern North Atlantic region and its relationship to basin development in the south Porcupine Basin, offshore Ireland. In: *The Petroleum Exploration of Ireland's Offshore Basins* (Ed. by P. M. Shannon, P. Haughton and D. Corcoran), Geological Society, London, Special Publication, 188, 237-263.
- Kenyon, N. H. (1987) Mass-wasting features on the continental slope of Northwest Europe. *Marine Geology*, 74, 57-77.
- Kenyon, N. H., Akhmetzhanov, A. M., Wheeler, A. J., van Weering, T. C. E., de Haas, H. & Ivanov, M. K. (2003) Giant carbonate mud mounds in the southern Rockall Trough. *Marine Geology*, 195, 5-30.
- Kenyon, N. H., Ivanov, M. K., Akhmetzhanov, A. M. & New, A. L. (1998) The current swept continental slope and giant carbonate mounds to the West of Ireland. In: *Geosphere-biosphere coupling: Carbonate Mud Mounds and Cold Water Reefs* (Ed. by B. De Mol), UNESCO, Paris, IOC Workshop Report, 143, 24.
- Knutz, P. C., Austin, W. E. N. & Jones, E. J. W. (2001) Millennial-scaled depositional cycles related to British Ice Sheet variability and North Atlantic paleocirculation since 45 kyr B.P., Barra Fan, U.K. margin. *Paleoceanography*, 16(1), 53-64.
- Knutz, P. C., Hall, I. R., Zahn, R., Rasmussen, T., Kuijpers, A., Moros, M. & Shackleton, N. J. (2002a) Multidecadal ocean variability and NW European ice sheet surges during the last deglaciation. *Geochemistry Geophysics Geosystems*, 3(12), 1077, doi:10.1029/2002GC000351.
- Knutz, P. C., Jones, E. J. W., Austin, W. E. N. & van Weering, T. C. E. (2002b) Glacimarine slope sedimentation, contourite drifts and bottom current pathways on the Barra Fan, UK North Atlantic margin. *Marine Geology*, 188, 129-146.
- Laberg, J. S., Vorren, T. O. & Knutsen, S.-M. (2002) The Lofoten Drift, Norwegian Sea. In: *Deep-Water Contourite Systems: Modern Drifts and Ancient Series, Seismic and Sedimentary Characteristics* (Ed. by D. A. V. Stow, C. J. Pudsey, J. A. Howe, J.-C. Faugères and A. R. Viana), Geological Society, London, Memoir, 22, 57-64.
- Labeyrie, L. D., Duplessy, J. C. & Blanc, P. L. (1987) Variations in mode of formation and temperature of oceanic deep waters over the past 125,000 years. *Nature*, 327, 477-482.
- Masson, D. G., Howe, J. A. & Stoker, M. S. (2002) Bottom-current sediment waves, sediment drifts and contourites in the northern Rockall Trough. *Marine Geology*, 192, 215-237.
- Mathys, M. (2001) Hoge-resolutie geofysische studie van gasmigratie in oppervlakkige mariene sedimenten ter hoogte van olie- en gasreservoirs, Porcupine Bekken (SW Ierland). M.Sc. thesis, Department of Geology and Soil Science. Ghent University, Gent, 157 pp.
- McCabe, A. M. & Clark, P. U. (1998) Ice-sheet variability around the North Atlantic Ocean during the last deglaciation. *Nature*, 392, 373-377.
- McDonnell, A. & Shannon, P. M. (2001) Comparative Tertiary stratigraphic evolution of the Porcupine and Rockall basins. In: *The Petroleum Exploration of Ireland's Offshore Basins* (Ed. by P. M. Shannon, P. Haughton and D. Corcoran), Geological Society, London, Special Publication, 188, 323-344.
- Moore, J. G. & Shannon, P. M. (1995) The Cretaceous succession in the Porcupine Basin, offshore Ireland: facies distribution and hydrocarbon potential. In: *The Petroleum Geology of Ireland's Offshore Basins* (Ed. by P. F. Croker and P. M. Shannon), Geological Society, London, Special Publication, 93, 345-370.
- Nakajima, T. & Satoh, M. (2001) The formation of large mudwaves by turbidity currents on the levees of the Toyama deep-sea channel, Japan Sea. *Sedimentology*, 48, 435-463.
- New, A. L., Barnard, S., Herrmann, P. & Molines, J.-M. (2001) On the origin and pathway of the saline inflow to the Nordic Seas: insights from models. *Progress in Oceanography*, 48, 255-287.
- Paull, C., Ussler III, W., Maher, N., Rehder, G., Lorenson, T. & Lee, H. (2002) Pockmarks off Big Sur, California. *Marine Geology*, 181, 323-335.

- Pearson, I. & Jenkins, D. G. (1986) Unconformities in the Cenozoic of the North-East Atlantic. In: North Atlantic Palaeoceanography (Ed. by C. P. Summerhayes and N. J. Shackleton), Geological Society, London, Special Publication, 21, 79-86.
- Pingree, R. D. & Le Cann, B. (1989) Celtic and Armorican slope and shelf residual currents. *Progress in Oceanography*, 23, 303-338.
- Pingree, R. D. & Le Cann, B. (1990) Structure, strength and seasonality of the slope currents in the Bay of Biscay region. *Journal of the Marine Biological Association of the United Kingdom*, 70, 857-885.
- Rebesco, M. & Stow, D. A. V. (2001) Seismic expression of contourites and related deposits: A preface. *Marine Geophysical Researches*, 22(5-6), 303-308.
- Rice, A. L., Billet, D. S. M., Thurston, M. H. & Lampitt, R. S. (1991) The Institute of Oceanographic Sciences Biology programme in the Porcupine Seabight: background and general introduction. *Journal of the Marine Biological Association of the United Kingdom*, 71, 281-310.
- Richter, T. O., Lassen, S., van Weering, T. C. E. & de Haas, H. (2001) Magnetic susceptibility patterns and provenance of ice-rafted material at Feni Drift, Rockall Trough: implications for the history of the British-Irish ice sheet. *Marine Geology*, 173, 37-54.
- Schnitker, D. (1986) North-east Atlantic Neogene benthic foraminiferal faunas: tracers of deep-water palaeoceanography. In: North Atlantic Palaeoceanography (Ed. by C. P. Summerhayes and N. J. Shackleton), Geological Society, London, Special Publication, 21, 191-203.
- Schönfeld, J. (2002) Recent benthic foraminiferal assemblages in deep high-energy environments from the Gulf of Cadiz (Spain). *Marine Micropaleontology*, 44, 141-162.
- Schönfeld, J. & Zahn, R. (2000) Late Glacial to Holocene history of the Mediterranean Outflow. Evidence from benthic foraminiferal assemblages and stable isotopes at the Portuguese margin. *Palaeogeography, Palaeoclimatology, Palaeoecology*, 159, 85-111.
- Scourse, J. D., Hall, I. R., McCave, I. N., Young, J. R. & Sugdon, C. (2000) The origin of Heinrich layers: evidence from H2 for European precursor events. *Earth and Planetary Science Letters*, 182, 187-195.
- Shannon, P. M. (1991) The development of Irish offshore sedimentary basins. *Journal of the Geological Society of London*, 148, 181-189.
- Stoker, M. S., van Weering, T. C. E. & Svaerdborg, T. (2001) A mid- to late Cenozoic tectonostratigraphic framework for the Rockall Trough. In: *Petroleum Exploration of Ireland's offshore basins* (Ed. by P. M. Shannon, P. Haughton and D. Corcoran), Geological Society, London, Special Publication, 188, 411-438.
- Stow, D. A. V. (1982) Bottom currents and contourites in the North Atlantic. *Bull. Inst. Géol. Bassin d'Aquitaine*, 31, 151-166.
- Stow, D. A. V., Faugères, J.-C., Howe, J. A., Pudsey, C. J. & Viana, A. R. (2002) Bottom currents, contourites and deep-sea sediment drifts: current state-of-the-art. In: *Deep-Water Contourite Systems: Modern Drifts and Ancient Series, Seismic and Sedimentary Characteristics* (Ed. by D. A. V. Stow, C. J. Pudsey, J. A. Howe, J.-C. Faugères and A. R. Viana), Geological Society, London, *Memoirs*, 22, 7-20.
- Stow, D. A. V. & Johansson, M. (2000) Deep-water massive sands: nature, origin and hydrocarbon implications. *Marine and Petroleum Geology*, 17, 145-174.
- Stow, D. A. V. & Mayall, M. (2000) Deep-water sedimentary systems: New models for the 21st century. *Marine and Petroleum Geology*, 17, 125-135.
- Weaver, P. P. E., Wynn, R. B., Kenyon, N. H. & Evans, J. (2000) Continental margin sedimentation, with special reference to the north-east Atlantic margin. *Sedimentology*, 47, 239-256.
- Wheeler, A. J., Beyer, A., Freiwald, A., de Haas, H., Huvenne, V. A. I., Kozachenko, M. & Olu-Le Roy, K. (submitted) Morphology and Environment of Deep-water Coral Mounds on the NW European

- Margin. In: *Modern Carbonate Mound Systems: A window to Earth History* (Ed. by J.-P. Henriet and C. Dullo), Springer-Verlag, Heidelberg.
- Wheeler, A. J., Kenyon, N. H., Ivanov, M. K., Beyer, A., Cronin, B., McDonnell, A., Schenke, H. W., Akhmetzhanov, A. M., Satur, N. & Zaragosi, S. (2003) Canyon Heads and Channel Architecture of the Gollum Channel, Porcupine Seabight. In: *European margin sediment dynamics: side-scan sonar and seismic images* (Ed. by J. Mienert and P. P. E. Weaver), Springer-Verlag, Heidelberg, 183-186.
- White, M. (submitted) The hydrographic setting for the carbonate mounds of the Porcupine Bank and Sea Bight. In: *Modern Carbonate Mound Systems: A window to Earth History* (Ed. by J.-P. Henriet and C. Dullo), Springer-Verlag, Heidelberg.
- Wynn, R. B. & Stow, D. A. V. (2002) Classification and characterisation of deep-water sediment waves. *Marine Geology*, 192, 7-22.
- Zaragosi, S., Eynaud, F., Pujol, C., Auffret, G. A., Turon, J.-L. & Garlan, T. (2001) Initiation of the European deglaciation as recorded in the northwestern Bay of Biscay slope environments (Meriadzek Terrace and Trevelyan Escarpment): a multi-proxy approach. *Earth and Planetary Science Letters*, 188, 493-507.
- Ziegler, P. A. (1982) *Geological Atlas of Western and Central Europe*. Shell Internationale Petroleum Maatschappij B.V., Amsterdam, 130 pp.

